



François Roure
Ammar A. Amin
Sami Khomsi
Mansour A.M. Al Garni *Editors*

Lithosphere Dynamics and Sedimentary Basins of the Arabian Plate and Surrounding Areas



Frontiers in Earth Sciences

Series editors

J.P. Brun, Rennes, France

O. Oncken, Potsdam, Germany

H. Weissert, Zürich, Switzerland

W.-C. Dullo, Kiel, Germany

More information about this series at <http://www.springer.com/series/7066>

François Roure · Ammar A. Amin
Sami Khomsi · Mansour A.M. Al Garni
Editors

Lithosphere Dynamics and Sedimentary Basins of the Arabian Plate and Surrounding Areas

 Springer

Editors

François Roure
Geosciences
IFPEN
Rueil-Malmaison Cedex
France

Ammar A. Amin
Faculty of Earth Sciences
King Abdulaziz University
Jeddah
Saudi Arabia

and

Tectonic Group
Utrecht University
Utrecht
The Netherlands

Sami Khomsi
Faculty of Earth Sciences
King Abdulaziz University
Jeddah
Saudi Arabia

Mansour A.M. Al Garni
Department of Physical Geology
Faculty of Earth Sciences
King Abdulaziz University
Jeddah
Saudi Arabia

ISSN 1863-4621
Frontiers in Earth Sciences
ISBN 978-3-319-44725-4
DOI 10.1007/978-3-319-44726-1

ISSN 1863-463X (electronic)
ISBN 978-3-319-44726-1 (eBook)

Library of Congress Control Number: 2016951663

© Springer International Publishing AG 2017

This work is subject to copyright. All rights are reserved by the Publisher, whether the whole or part of the material is concerned, specifically the rights of translation, reprinting, reuse of illustrations, recitation, broadcasting, reproduction on microfilms or in any other physical way, and transmission or information storage and retrieval, electronic adaptation, computer software, or by similar or dissimilar methodology now known or hereafter developed.

The use of general descriptive names, registered names, trademarks, service marks, etc. in this publication does not imply, even in the absence of a specific statement, that such names are exempt from the relevant protective laws and regulations and therefore free for general use.

The publisher, the authors and the editors are safe to assume that the advice and information in this book are believed to be true and accurate at the date of publication. Neither the publisher nor the authors or the editors give a warranty, express or implied, with respect to the material contained herein or for any errors or omissions that may have been made.

Printed on acid-free paper

This Springer imprint is published by Springer Nature
The registered company is Springer International Publishing AG
The registered company address is: Gewerbestrasse 11, 6330 Cham, Switzerland

Foreword



On behalf of King Abdulaziz University (KAU), it gives me pleasure to introduce this important book dealing with the Geology of the Arabian world and circum-Arabian geology. This book edited by Prof. F. Roure (IFPEN, Paris, France) and Prof. A.A. Amin, M.A. Al-Garni and S. Khomsi (the three from KAU, Jeddah, Saudi Arabia) illustrates the importance of international scientific cooperation and constitutes an important achievement made by the Faculty of Earth Sciences at KAU. I want to acknowledge here the pertinent efforts made by the editors as well as the importance of this book as a vector for better understanding the Geology of the Arabian world. The different authors of the valuable chapters of this book present very innovative and up-to-date researches in their fields of expertise with a wide range of geological topics covering different themes: petroleum/reservoirs potentialities, geodynamics, sedimentary basins modeling, geophysics and structural geology.

I would like to acknowledge Springer for giving this opportunity within its regional geology series, thus ensuring a wide dissemination of these various chapters.

I congratulate all the editorial teams involved in this work and we are proud of such an international platform in which KAU will be also involved again in the future.

I hope every reader will enjoy the insightful scientific facts which this book is containing.

Prof. Abdulrahman O. Al-Youbi

Contents

Part I Lithosphere Architecture

- Crustal and Upper Mantle Structures Beneath the Arabian Shield and Red Sea** 3
Abdullah Al Amri, K. Abdelrahman, M.O. Andreae and M. Al-Dabbagh

Part II Reservoirs, Conduits and Fluids

- Architectural and Hydraulic Characteristics of Fault Zones in the Mesozoic Carbonate Formations of Central and Eastern Saudi Arabia** 33
Mohamed Al Mahmoud

- Optimal Aquifers and Reservoirs for CCS and EOR in the Kingdom of Saudi Arabia: An Overview** 51
Marwan Jaju, Fadi Henri Nader, François Roure and Liviu Matenco

- Tectonostratigraphic Study of Carbonate Breccias (Calcuturbidites) in the Upper Triassic Baluti Formation (Northern Iraq): New Insights on Tethyan Geodynamics** 67
Sa'ad Z.A. Kader Al-Mashaikie

Part III Tectonic Styles: From Rifts and Salt Tectonics to Foreland Inversions and Thrust Tectonics

- Structural and Stratigraphic Architecture of the Corinth Rift (Greece): An Integrated Onshore to Offshore Basin-Scale Synthesis** 89
Sébastien Rohais and Isabelle Moretti

- Styles of Salt Tectonics in the Sab'atayn Basin, Onshore Yemen** 121
Gabor Tari, Rudi Dellmour, Emma Rodgers, Chloe Asmar, Peter Hagedorn and Adel Salman

- The Effect of the Palmyra Trough and Mesozoic Structures on the Levant Margin and on the Evolution of the Levant Restraining Bend** 149
Ramadan Galhyani, Jean-Marc Daniel, Catherine Homberg, Fadi Henri Nader, Romain Darnault, Jean-Marie Mengus and Eric Barrier

- Tectonic Style and Structural Features of Alpine-Himalayan Orogeny in Central Arabia** 173
Abdullah O. Bamousa, Abdullah M. Memesh, Saleh M. Dini and Ali A. Al-Zahrani

Fast-Track 2D Seismic Processing While Drilling to Ameliorate Foothills Exploration and Optimize Well Trajectory: An Example from the Central Kurdistan Region of Iraq	187
François Sapin, Hassan Allouche, Grégoire Sterbecq, Bertrand Chevallier and Boerre Eriksen	

About the Editors



François Roure was trained at the ENS in St-Cloud in France. He got his Ph.D. at Paris VI University in 1979 and his “thèse d’état” in 1984 at the same university, dealing the geodynamic evolution of the North American Cordillera in northern California and Oregon during the Mesozoic. After 4 years spent with CNRS (1980–1984), he joined the French Institute of Petroleum (IFP) in 1984, and was still senior geosciences advisor at IFP Energies nouvelles (<http://www.ifpenergiesnouvelles.fr>), the current name of former IFP, from 2000 to 2016, extraordinary professor at the University of Utrecht, the Netherlands, from 2012 to 2016, and member of the CNE2 (French assessment board for research and

the studies into the management of radioactive waste and materials, <http://www.cne2.fr>) from 2010 to 2016. Together with Magdalena Scheck-Wenderoth from GFZ, François was also leading from 2005 till 2015 the Task Force 6 on Sedimentary basins from the International Lithosphere Program (ILP, with support from IUGS and IUGG, <http://www.scl-ilp.org/>).

Until 1995, his main research topic was the crustal architecture of the Alps and Pyrenees (Ecos program), and the petroleum systems of foreland fold-and-thrust belts in the Apennines, Carpathians, Albania, Sicily, Alaska and Venezuela.

After a sabbatical year spent at the USGS in Menlo-Park, California (1994–1995), François initiated numerous international joint industry projects for reservoir appraisal (SubTrap, Sub-thrust reservoir appraisal) in the Himalayan foothills in Pakistan, in sub-Andean basins in Venezuela and Colombia, as well as in the North American Cordillera (Mexico and Canadian Rockies). More recently, he was also involved in the study of the crustal architecture of the Northern Emirates and North Algeria (Tellian and offshore domains).

- Charles Jacob prize from the French Academy of Sciences (1996)
- Distinguished Lecturer for the AAPG (1998)
- Alfred Wegener prize from the EAGE (2010)
- André Dumont medal from Geologica Belgica (2012)



Ammar A. Amin professor of Geological Hazards got his Ph.D. at East Anglia University, UK August 1994.

Since 2010, he works as Dean of the faculty of Earth Sciences, King Abdulaziz University (KAU), Jeddah, Saudi Arabia. During his career in KAU he had involved in several administrative and academic positions. He worked as vice dean for development, vice dean for postgraduate studies, head of geoengineering department, KAU Supervisor General of the Co-supervision of Graduate Studies, Chairman of KAU Central Laboratories.

Currently in addition to his responsibility as Dean, he is a member of several important committees such as KAU Scientific Council and KAU Council.

Professor Ammar collaborated with major institutions within Saudi Arabia and the globe on earth sciences studies, academic development, accreditation, scientific donations, communities services programs, e-learning and female co-supervision of graduate studies.

He also has experience in engineering geology for roads, bridges, dams, tunnels, environmental regulations and evaluating disaster plans, environmental geological hazards and cracks resulting from the melting of ground limestone.

His main research interests include geological hazards, environmental risks, groundwater hazards, site selection of solid waste disposal, designating sustainable landfill, geotechnical hazard associated with desert environment, causes of land subsidence, karst hazard and crustal subsidence due to groundwater.



Sami Khomsi got his Ph.D. at Tunis University in 2004 and his HDR (Habilitation à Diriger des Recherches) in the same university in 2015.

Since 2011, he works in the Department of Petroleum Geology and Sedimentology, in the faculty of Earth Sciences, King Abdulaziz University, Jeddah, Saudi Arabia. He worked also in different universities in Tunisia and France. Past employment within academia (research and teaching) and industry in the upstream activities: exploration, sites survey, prospects evaluation and professional expert training (field trip leader for professionals, coaching of geoscientists, etc.) in basin analysis involving basin modeling, structural analysis and balanced cross sections. Sami collaborated with major oil companies in Eastern Maghreb on field studies, structural analysis of fold-thrust structures, subsurface reservoir characterizations and seismic interpretations. He also has experience in geophysical methods involving fast processing and interpretation of seismic reflexion sections in terms of structural geology-investigation- evaluation of plays, characterization of fractured reservoirs and subsurface mapping.

His main research interests include geometry, kinematics and dynamics of fold-thrust systems and foreland basins in North Africa Middle East and the Mediterranean realm, fractured reservoir analogues, applying structural analysis and subsurface techniques in the characterisations of drillable structures and structural evaluation of traps using regional cross sections at large scale as well as structural subsurface based on regional seismic reflection profiles in different basins.



Prof. Dr. Mansour A.M. Al Garni received a BS (1993) in Geophysics from King Abdulaziz University (KAU), Saudi Arabia, an MS (1996) in Geophysics from Colorado School of Mines (CSM), Golden, Colorado, USA, and a Ph.D. (2001) in Geophysics from Texas A&M University (TAMU), College Station, Texas, USA. In 1993, he worked as a geophysicist at the Ministry of Petroleum and Mineral Resources, United States Geological Survey, Jeddah, Saudi Arabia, and as a demonstrator of geophysics at KAU, where in 2002 he became Assistant Professor of Geophysics. He has been promoted to Associate Professor of Geophysics in 2006 and promoted to Full Professor

of Geophysics in 2010. Furthermore, he has been assigned as the chairman of geophysics department (2003–2011), vice dean (2014), and vice dean for graduate studies and scientific research (2015–Now). His research interests are controlled-source electromagnetic induction, electrical methods, gravity and magnetic methods, near-surface applied geophysics, forward and inverse modeling, environmental and engineering geophysics, environmental site characterization, ground penetrating radar, hydrogeophysics, and mining geophysics: theory, data

processing and interpretation. Professor Al-Garni has reviewed a lot of academic works and has been in many committees including those of M.Sc. and Ph.D. examinations. His remarkable efforts in the establishment and development of various projects were reflected in valuable academic and professional successes and achievements. He has conducted more than 15 research projects, the most recent of which involved EM, DC resistivity, SP, IP, and magnetic methods for mineral exploration in the Arabian Shield. He has published more than 50 research articles in international indexed and refereed journals. In 2015, Prof. Al-Garni joined the AJGS as Associate Editor responsible for evaluating submission in the fields of theoretical and applied exploration geophysics. Professor Al-Garni has been listed in the “Marquis Who’s Who in the World” as one of the world’s foremost achievers in the field of geophysics in the 28th Edition (2011).

Editorial

François Roure
Geosciences, IFPEN
Rueil-Malmaison Cedex, France
Francois.Roure@bluema.com

and

Tectonic Group, Utrecht University
Utrecht, The Netherlands

Ammar A. Amin
Faculty of Earth Sciences
King Abdulaziz University, Jeddah, Saudi Arabia
aamin@kau.edu.sa

Sami Khomsi
Faculty of Earth Sciences
King Abdulaziz University, Jeddah, Saudi Arabia
skhomsi@kau.edu.sa

Mansour A.M. Al Garni
Department of Physical Geology
Faculty of Earth Sciences
King Abdulaziz University
Jeddah, Saudi Arabia
maalgarni@kau.edu.sa

This volume of *Frontiers in Earth Sciences* series focusing on the lithosphere dynamics and sedimentary basins of the Arabian Plate and surrounding areas, is an initiative of the Task Force 6 of the International Lithosphere Program, an international network dedicated to the study of sedimentary basins (Roure et al. 2010).

Summary of Former Activities of the ILP Task Force on Sedimentary Basins and Perspectives

The ILP Task Force 6 on sedimentary basins was initiated in 2005 in order to assist the international community of Earth Sciences involved in the study of asthenospheric and deep lithospheric/crustal processes to (1) interact with other scientists involved in the study of sedimentary basins, and to promote collaborative projects integrating surface and deep processes to regional case studies, (2) organize yearly international meetings involving attendees from universities, public research institutes and the industry, and (3) provide support for young scientists (PhD and postdoctorants) to participate in the activities of this international network.

From 2005 to 2014, the ILP Task Force 6 was driven by François Roure at IFPEN (Rueil-Malmaison, France) and Magdalena Scheck-Wenderoth at GFZ (Potsdam, Germany). The first international conference during this period was hosted by IFPEN in Rueil-Malmaison (France) in 2005, focusing on thrust belts and foreland basins, with local support from the French and Spanish geological societies (SGF and SGE) and proceedings (Lacombe et al. 2007) published by Springer in the *Frontiers in the Earth Sciences* series initiated in collaboration with other European geological societies.

In 2006, the yearly conference of the ILP Task Force 6 was organized by Canadian colleagues at Laval University in Québec, focusing on the geology and geodynamics of circum-Polar basins from both the northern (sub-Arctic basins) and southern (sub-Antarctic basins) hemispheres. The conference included a forum discussion between North American (Canada, Alaska, Greenland), Russian, West European (Denemark, Norway and Germany) and Australian geological surveys, academy as well as participants from the industry on frontier exploration in the Arctic, as well as a field trip downtown Québec and its surroundings (Lavoie and Kirkwood 2006). Scientific outcomes of the conference were published in a Canadian journal, the *Bulletin of Canadian Petroleum Geology* (Kirwood et al. 2010).

The 2007 meeting of this ILP Task Force was organized in Marrakech (Morocco) in association with the AAPG (American association of petroleum geology), the MAPG and ONHYM (Moroccan association of petroleum geology and national Moroccan exploration company, respectively), aiming at the study of vertical motion in the Atlas Mountains and adjacent offshore basins at the junction between the Mediterranean and Central Atlantic margins. A field trip was also organized by university colleagues in the Atlas Mountains (Taki et al. 2007). Main scientific results presented during this conference were published in a special issue of *Tectonophysics* (Bertotti et al. 2009).

We crossed again the Atlantic in 2008 to reconvin in Ensenada in Baja California in Mexico, close to the US border, with a joint-meeting with other ILP teams involved in the study of geohazards. This conference was hosted by CICESE (Centro de Investigacion cientifica y de educacion superior de Ensenada, Baja California), involving also the Mexican institute of petroleum (IMP) and the Mexican union of geophysics (Union Geoffisica Maxicana) who edited an abstract and program volume (Delgado-Argotte et al. 2008). The conference benefited also from an excellent field trip dedicated to the opening of the Gulf of California (Suarez-Vidal 2008).

Thanks to a strong support from the Ministry of Energy of Abu-Dhabi, the 2009 conference of the ILP Task Force 6 was held in the Emirates, in Abu-Dhabi, addressing for the time for ILP discussions between universities and industry on lithosphere dynamics and sedimentary basins of the Arabian Plate. BGS (British Geological Survey) and the university of Al Ain organized two successful field trips in the Emirati foothills near Al Ain and in the Dibba Zone and Semail ophiolite in Fudjeirah (Ellison et al. 2009; Fowler et al. 2009). Pr. Al Amri was kind enough to invite the Task Force to edit a first ILP Topical issue of the *AJGS* by then (Roure et al. 2010), whereas Springer published a book compiling another set of chapters presented at the conference (Al Hosani et al. 2010).

We came back to Europe in Albania for the 2010 ILP Task Force conference, hosted in Tirana by the Polytechnic university, the main focus being the local geodynamics and geohazards, Albania providing a unique natural laboratory for the study of active tectonics and further couplings with sedimentary processes and fluid rocks interactions. Two field trips were organized in the Ionian Basin and Peri-Adriatic depression in the south, and the Kruja and Krasta zones and Mirdita ophiolite in the north (Durmishi et al. 2011a, b). Main scientific results presented during the meeting were published in a special issue of the *Italian Journal of Geosciences* (Roure et al. 2013).

We moved to South Africa in 2011, with dedicated ILP sessions at the Geosynthesis conference organized in Cape Town by SAGA and the Geological Society of South Africa (GSSA). This was an opportunity for German teams to share preliminary results of their SAMPLE program on the architecture and geodynamic evolution of conjugate margins of the South Atlantic with other scientists from local countries, and for French teams to do the same

for scientific outcomes of the Topo-Africa project, main scientific results presented in Cape Town being included in a special issue of *Tectonophysics* (Scheck-Wenderoth et al. 2013).

Thanks to the support of Geoscience Australia, the national geological survey, IUGS and IUGG, the ILP Task Force 6 on sedimentary basins benefited from a dedicated room and specific sessions on compressional, transform and passive margins during the entire length of the World International Congress held in Brisbane in 2012. Main results on hyperextended margins presented during the congress were subsequently published in a dedicated memoir of the Geological Society of London (Gibson et al. 2015).

Back to France to discuss on the geodynamics and sedimentary basins of the Mediterranean and its surrounding countries, the 2013 meeting of the Task Force was hosted in Marseille by the CEREGE team (Aix-Marseille university), with support once again from the SGF who published the main scientific results presented during the meeting in a special issue of the *Bulletin* (Séranne et al. 2015). Worth mentioning, the local organizers guided also an exciting field trip combining onshore and marine tour, documenting the Paleogene inversions of the Alpine foreland in Provence (Floquet and Lamarche 2013).

Our target for 2014 was to come back to the Middle-East and Arabian Plate, and we were lucky enough to get the full support from the Faculty of Earth Sciences of King Abdulaziz university to host our last yearly meeting in Jeddah. Despite the fact that we could get over 100 registrants and more than 140 abstract contributions dealing for the second time on the lithosphere dynamics and sedimentary basins of the Arabian Plate and its surroundings, we had to cancel this international event at the last minute, due to delays in the delivery of visas for foreign participants. Fortunately, we could still get the full support from the Saudi Society of Earth Sciences and Springer to edit this book published in the *Frontiers in Earth Sciences* series, as well as second ILP Topical issue of the *AJGS* (Khomsi et al. 2016), in order to still keep the benefit of the scientific presentations initially scheduled for this conference.

From 2005 to 2014, the ILP Task Force 6 on sedimentary basins was also present on a yearly basis with dedicated sessions at the EGU in Vienna, which resulted also in the publication of numerous special issues from *Tectonophysics* and *Marine and Petroleum geology* (Scheck-Wenderoth et al. 2009, 2010a, b; Gaullier et al. 2013).

Since 2015, this ILP Task Force is now driven by Liviu Matenco (Tectonic Group, Utrecht university, the Netherlands) and Fadi H. Nader (IFPEN, Rueil-Malmaison, France). They coordinated with colleagues from the Tokyo university the last meeting held in Japan in 2015, dealing with circum-Pacific island arcs and back-arc systems. The Task Force on sedimentary basins will contribute in 2016 to a joint-task forces meeting in Clermont-Ferrand, France, and has longer term plans for conferences in the Eastern Mediterranean (Cyprus) and around the world to still address yearly meetings on lithosphere dynamics and sedimentary basins. They will for sure come back in a near future in the Middle-East for a third conference on the Arabian Plate.

Scientific Topics Addressed in this Book

This book on the Arabian Plate and surrounding areas comprises a set of 9 papers combined into three different parts, dealing successively with the (I) lithosphere architecture, (II) reservoirs, conduits and fluids, and tectonic styles (III).

Part I is made up of a very comprehensive and original paper by Abdullah Al Amri et al. on the crustal and upper mantle structures beneath the Arabian Shield and the Red Sea, providing an updated data base on lateral lithosphere thickness variations and heterogeneities within the western border of the Arabian Plate.

Part II comprises 3 papers aiming at the study of potential reservoirs, fluid transfers and fluid-rock interactions. The first of them is actually a duplicate of an excellent synthesis already published in a regular issue of the *AJGS* in 2015, by Mohamed Al Mahmoud from Aramco, on the tectonic conduits controlling the overall vertical fluid transfers in Mesozoic carbonates of Central and Eastern Saudi Arabia. The second paper of this chapter by Marwan Jaju et al. is also included in the companion 2016 ILP Topical issue of the *AJGS*, and provides

a regional synthesis of sandstone and carbonate reservoirs from the Arabian Platform in the Kingdom of Saudi Arabia, with the aim to differentiate among them saline aquifers which could be used for long-term CO₂ sequestration, from fresh water aquifers which must be preserved for agriculture and other societal uses, as well as some specific hydrocarbon-bearing reservoirs that would deserve specific EOR (enhanced oil recovery) techniques for improving the recovery of heavy oil. The last paper of this chapter, by Sa'ad Kader Al-Mashaikie, describes for the first time carbonate breccias (calciturbidites) in the Upper Triassic Baluti Formation in northern Iraq, outlining their significance in the overall geodynamic evolution of the former Tethyan margin, and their long-living diagenetic evolution and reservoir potential.

Part III is dedicated to case studies depicting the various structural styles expressed in the Arabian plate but also in two nearby sectors of the Mediterranean. For instance, the paper by Sébastien Rohais and Isabelle Moretti is an attempt to correlate offshore and onshore synrift sedimentary series preserved in the Corinth rift in Greece, and constitutes an excellent analogue for more mature rifts systems and relatively young passive continental margins of the Red Sea and Aden, where coeval series and potential reservoirs are still poorly understood because they are deeply buried beneath the salt. In the second paper of this chapter, also included in the companion 2016 ILP Topical issue of the AJGS, Gabor Tari et al. provide excellent seismic profiles and structural cross-sections documenting the overall geometry of halokinetic structures in a Mesozoic rift basin onshore Yemen. In the next paper, Ramadan Galhyani et al. have performed sand box experiments to better understand the fault pattern in onshore Lebanon and adjacent Mediterranean offshore in the vicinity of the Levant fault, in a tectonically complex domain where this major transcurrent neotectonic feature is dissecting the former Palmyra basin. Far field effects of the Arabian-Eurasian collision are also discussed by Abdullah Bamoussa and al. in their paper, which aims at documenting both thick- and thin-skinned foreland inversion features in Central Arabia. Last but not least, the last paper of the volume by François Sapin et al. shows the benefit of enhanced 2D seismic processing for better imaging the complex structures of prospects of the Zagros foothills in the Central Kurdistan region of Iraq, which constitutes a prerequisite to optimize well trajectory.

Acknowledgements

We would like to thank here Pr. Abdullah Al Amri, the Saudi Society of Earth Sciences and the King Abdulaziz university as well as Abdullah Baamour for their constant support and help. Thanks also to ILP, Magdalena Scheck-Wenderoth and Sierd Cloetingh, BGS, John Ludden and Tim Pharaoh for initial support and sponsorship when preparing a second ILP conference in the Middle-East, and to the SGF (French geological society), Isabelle Cojan, Jean-Jacques Jarrige, Solange Chaimbault, Sébastien Garnaud and Cécile Lamey, for keeping trace of the website and registration process for the 2014 conference, and endless iterations with registrants after cancelation of the meeting.

References

- Al Hosani K, Ellison R, Lokier S, Roure F (eds) (2010) Lithosphere dynamics and sedimentary basins: The Arabian Plate and analogues. ILP Abu-Dhabi 2009, New Frontiers in Earth Sciences, Springer
- Bertotti G, Teixell A, Frizon de Lamotte D, Charroud M (2009) The geology of vertical movements of the lithosphere. ILP Marrakech 2007, Special issue, Tectonophysics 475:1–200
- Delgado-Argotte L, Ortuño-Arzate F, Martín-Barajas A, Pedrin I, Suarez-Vidal F (2008) ILP joint task forces meeting, Ensenada, Mexico. Abstracts and program, GEOS, Boletín Informativo de la Unión Geofísica Mexicana 28(1):1–69
- Durmishi G, Fundo A, Meshi A, Muceku B, Onuzi K (2011a) Kruja Zone, Makaresh and Kruja structures, Krasta-Cukali Zone and Mirdita ohiolite. ILP Tirana 2011, Pre-Conference field trip, Field Trip Guide, Polytechnic univ. of Tirana and SGF
- Durmishi G, Fundo A, Meshi A, Muceku B, Onuzi K (2011b) Ionian-Sazani zones and Peri-Adriatic depression. ILP Tirana 2011, Post-Conference field trip, Field Trip Guide, Polytechnic univ. of Tirana and SGF

- Ellison R, Phillips ER, Styles MT (2009) A geotraverse across the late Cretaceous fold and thrust belt of the UAE: From ophiolite to platform margin. ILP Abu Dhabi 2009, Guide for Dibba Zone field excursion, p 31
- Floquet M, Lamarche J (2013) Mesozoic basin dynamics and polyphase tectonic inversion in the Pyrenean and Alpine forelands. ILP Marseille 2013, Field trip guide, Cerege and SGF
- Fowler AR, Abdelghany O, Abu Saima M, Ellison R (2009) Carbonate sedimentology, stratigraphy and structures of the Tertiary foreland basin, Al Ain area, UAE. ILP Abu Dhabi 2009, Field trip guide, p 16
- Gaullier V, Basile C, Roure F, Scheck-Wenderoth M (eds) (2013) Basin dynamics, Special issue, *Tectonophysics* 591:1–210
- Gibson G, Manatschal G, Roure F (eds) (2015) Sedimentary basins and crustal processes at continental margins: from modern hyper-extended margins to deformed ancient analogues. ILP Brisbane 2012, Geological Society, London, Special publication, 413, p 350
- Khomsis S, Al Garni M, Amin A, Roure F (2016) Arabian Plate: Lithosphere dynamics, sedimentary basins and georesources. ILP Topical issue, *Arabian J Geosci*, in press
- Kirkwood D, Malo M, Lavoie D, et Osadetz K (2010) Tectono-stratigraphic events at continental margins and their significance for hydrocarbon resources: an introduction to a set of thematic papers from the International Lithosphere Programme, Québec City Workshop. ILP Québec City 2006, *Bull Can Petrol Geol* 58(1):1–2. doi:[10.2113/gscpgbull.58.1.1](https://doi.org/10.2113/gscpgbull.58.1.1)
- Lacombe O, Lavé O, Roure F, Vergés J (eds) (2007) Thrust belts and foreland basins: From fold kinematics to hydrocarbon systems. ILP Rueil-Malmaison 2005, *Frontiers in Earth Sciences*, Springer, p 492
- Lavoie D, Kirkwood D (2006) The early Paleozoic margin of Eastern Laurentia: Transition from a passive margin to a tectonically active margin. ILP Québec 2006, Field trip guide, Laval Univ. and Geological Survey of Canada
- Roure F, Cloetingh S, Scheck-Wenderoth M, Ziegler P (2010) Achievements and challenges in sedimentary basin analysis: a review. In: Cloetingh S, Negendank G (eds) *New Frontiers in integrated Solid Earth Sciences*. International year of Planet Earth, Springer. doi:[10.1007/978-90-481-2737-5-5](https://doi.org/10.1007/978-90-481-2737-5-5)
- Roure F, Scheck-Wenderoth M, Gahnoog A, Pharaoh T, guest editors (2010) Arabian plate: Lithosphere dynamics, sedimentary basins and geohazards. ILP Abu-Dhabi 2009, Special issue, *Arab J Geosci* 3(4, 3):327–329. doi:[10.1007/s12517-010-02213](https://doi.org/10.1007/s12517-010-02213)
- Roure F, Scheck-Wenderoth M, Muska K, Nazaj S, guest editors (2013) Dynamics and active processes: the Albanian natural laboratory and analogues. ILP Tirana 2011 Special issue, *Italian J Geosci* 132
- Scheck-Wenderoth M, Bayer U, Roure F, guest editors (2009) Progress in understanding sedimentary basins. ILP Task Force, Special issue, *Tectonophysics* 470(1–2):1–194
- Scheck-Wenderoth M, Bayer U, Roure F, guest editors (2010a) The link between shallow and deep processes in sedimentary basins. ILP Task Force, Special issue, *Mar Pet Geol* 27:563–730
- Scheck-Wenderoth M, Roure F, Bünge, Glasmacher U, guest editors (2013) Progress in understanding South Atlantic margins. ILP Cape Town 2010, Special issue, *Tectonophysics* 604:1–296
- Scheck-Wenderoth M, Roure F, Corver M, guest editors (2010b) Thematic set on the implication of basin dynamics on petroleum systems. Special issue, *Mar Pet Geol* 28(4):861–958
- Séranne M, Lamarche J, Agosta F, guest editors (2015) Lithosphere dynamics of sedimentary basins: The circum-Mediterranean basins and analogues. ILP Marseille 2013, Special issue, *Bull Soc Géol France*, 186 (4–5)
- Suarez-Vidal (2008) Field trip log: Gulf of California rift system: Laguna Salada-Valle Chico-San Felipe, Baja California, Mexico. *GEOS, Boletín Informativo de la Unión Geofísica Mexicana* 28(1):57–69
- Taki Z, Frizon de Lamotte D, Saddiqi O (2007) Vertical movements, coeval continental deposits and active tectonics along the northern border of the High Atlas. ILP Marrakech 2007, Field trip guide

Part I
Lithosphere Architecture

Crustal and Upper Mantle Structures Beneath the Arabian Shield and Red Sea

Abdullah Al Amri, K. Abdelrahman, M.O. Andreae, and M. Al-Dabbagh

Abstract

The Arabian Shield and Red Sea region is considered one of only a few places in the world undergoing active continental rifting and formation of new oceanic lithosphere. We determined the seismic velocity structure of the crust and upper mantle beneath this region using broadband seismic waveform data. We estimated teleseismic receiver functions from high-quality waveform data. The raw data for RF analysis consist of 3-component broadband velocity seismograms for earthquakes with magnitudes $M_w > 5.8$ and epicentral distances between 30° and 90° . We performed several state-of-the-art seismic analyses of the KACST and SGS data. Teleseismic P- and S-wave travel time tomography provides an image of upper mantle compressional and shear velocities related to thermal variations. We present a multi-step procedure for jointly fitting surface-wave group-velocity dispersion curves (from 7 to 100 s for Rayleigh and 20 to 70 s for Love waves) and teleseismic receiver functions for lithospheric velocity structure. The method relies on an initial grid search for a simple crustal structure, followed by a formal iterative inversion, an additional grid search for shear wave velocity in the mantle and finally forward modeling of transverse isotropy to resolve surface-wave dispersion discrepancy. Inversions of receiver functions have poor sensitivity to absolute velocities. To overcome this shortcoming we have applied the method of Julia et al. (Geophys J Int 143:99–112, 2000), which combines surface-wave group velocities with receiver functions in formal inversions for crustal and uppermost mantle velocities. The resulting velocity models provide new constraints on crustal and upper mantle structure in the Arabian Peninsula. While crustal thickness and average crustal velocities are consistent with many previous studies, the results for detailed mantle structure are completely new. Finally, teleseismic shear-wave splitting was measured to estimate upper mantle anisotropy. These analyses indicate that stations near the Gulf of Aqabah display fast orientations that are aligned parallel to the Dead Sea Transform Fault, most likely related to the strike-slip motion between Africa and Arabia. The remaining stations across Saudi Arabia yield statistically the same result, showing a consistent pattern of north-south oriented fast directions with delay times averaging about 1.4 s. The uniform anisotropic signature across Saudi Arabia is best explained by a combination of plate and density driven flow in the asthenosphere. By combining the northeast oriented flow associated with absolute plate motion with the northwest oriented flow associated with the channelized Afar plume along the Red Sea, we

A. Al Amri (✉) · K. Abdelrahman · M.O. Andreae ·
M. Al-Dabbagh
Geology and Geophysics Department, King Saud University,
Riyadh, Saudi Arabia
e-mail: alamri.geo@gmail.com

M.O. Andreae
Biogeochemistry Department, Max Planck Institute for Chemistry,
Mainz, Germany

© Springer International Publishing AG 2017

F. Roure et al. (eds.), *Lithosphere Dynamics and Sedimentary Basins of the Arabian Plate and Surrounding Areas*, Frontiers in Earth Sciences, DOI 10.1007/978-3-319-44726-1_1

obtain a north-south oriented resultant that matches our splitting observations and supports models of the active rifting processes. This explains why the north-south orientation of the fast polarization direction is so pervasive across the vast Arabian Plate. Seafloor spreading in the Red Sea is non-uniform, ranging from nearly 0.8 cm/a in the north to about 2 cm/a in the south. The Moho and LAB are shallowest near the Red Sea and become deeper towards the Arabian interior. Near the coast, the Moho is at a depth of about 22–25 km. Crustal thickening continues until an average Moho depth of about 35–40 km is reached beneath the interior Arabian Shield. The LAB near the coast is at a depth of about 55 km; however, it also deepens beneath the Shield to attain a maximum depth of 100–110 km. At the Shield-Platform boundary, a step is observed in the lithospheric thickness where the LAB depth increases to about 160 km. This study supports multi plume model, which states that there are two separated plumes beneath the Arabian Shield, and that the lower velocity zones (higher temperature zones) are related to volcanic activities and topographic characteristics on the surface of the Arabian Shield. In addition, our results suggest a two-stage rifting history, where extension and erosion by flow in the underlying asthenosphere are responsible for variations in LAB depth. LAB topography guides asthenospheric flow beneath western Arabia and the Red Sea, demonstrating the important role lithospheric variations play in the thermal modification of tectonic environments.

Keywords

Crustal • Upper mantle • Structures • Arabian Shield • Red Sea

Introduction

The Arabian Peninsula presents several interesting seismological problems. On the west, rifting in the Red Sea has split a large Precambrian Shield. Active rifting is responsible for the geometry of the plate margins in the west and southwest. To the south, similar rifting running in a more east-west direction through the Gulf of Aden has separated the Arabian Peninsula from Africa. In the northwest, the Gulf of Aqabah forms the southernmost continuation of the Dead Sea transform. The northern and northeastern boundaries of the Arabian Plate are areas of continental collision, with the Arabian Plate colliding with the Persian Plate.

King Saud University (KSU) and King Abdulaziz City for Science and Technology (KACST) operate the seismic networks in Saudi Arabia since 1985 (Al-Amri and Al-Amri 1999a, b). Both networks feature the Boulder Real Time Technologies (BRTT) Antelope system, however the networks operate independently. Data is collected and transmitted in real time to the central processing facilities in Riyadh. Events are automatically detected and located and waveforms are excerpted for later analysis, while continuous data are archived. The KACST network features 37 stations (26 BB STS-2 and 11 SP sensors). The system uses the IASP91 earth model to locate events. Figure 1 shows all events with magnitude greater than 5.5 recorded by the KACST stations between 2000 and 2004. Events we had access to are shown in red. The large number of new events in the proper distance range for S and SKS splitting analysis

are sufficient to allow us to investigate patterns of splitting parameters with arrival direction and determine whether more complex anisotropic models are required below the Red Sea Rift. In 2005, The Saudi Geological Survey (SGS) began operating the national seismographic network in Jeddah, Saudi Arabia. Recently, it consists of more than 120 broadband stations (Nanometrics Trillium broadband seismometers, 24-bit digitizers, GPS receivers, and VSAT transceivers) distributed across the Arabian Shield.

The Saudi Arabian Broadband Deployment (SABD, Vernon et al. 1996) provided the first data set of broadband recordings in this region. This deployment consisted of 9 broadband three-component seismic stations along a similar transect to an early seismic refraction study (Mooney et al. 1985; Gettings et al. 1986; Mechie et al. 1986). Data from the experiment resulted in several studies and models of the seismic structure of the Arabian Shield (Sandvol et al. 1998a, b; Mellors et al. 1999; Rodgers et al. 1999; Benoit et al. 2003; Al-Amri et al. 2004; Al-Damegh et al. 2004). These studies provided new constraints on crustal and upper mantle structure. The crustal model of the western Arabian Platform shows a little higher P-velocity for the upper crust in the Shield than in the Platform and the crustal Platform seems to have a greater thickness than the Shield by about 3 km. The Moho discontinuity beneath the western Arabian Platform indicates a velocity of 8.2 km/s of the upper mantle and a 42 km MOHO depth (Al-Amri 1998a, b, 1999a, b).

Generally, the crustal thickness in the Arabian Shield area varies from 35 to 40 km in the west adjacent to the Red Sea

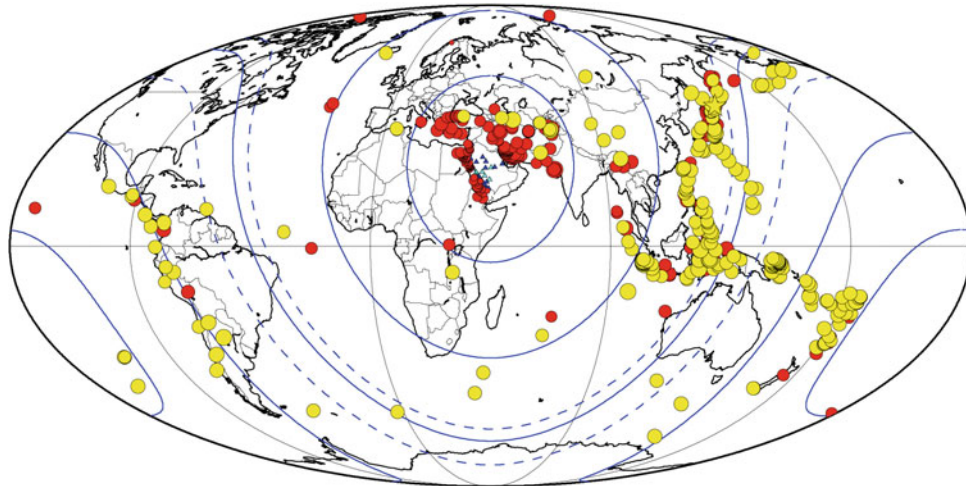
Teleseismic events with $M > 5.5$ between 2000-2004

Fig. 1 Map of the world centered on the Red Sea showing events recorded by KACST and SGS broadband stations between 2000 and 2001 (*red*) and 2002–2004 (*yellow*). Events outside the first contour (30°) are at teleseismic distances and all have magnitude >5.5 . Some

events within the 30° contour have magnitudes <5.5 . Many of the *red* events (2000–2001) in the western Pacific subduction zones are hidden beneath the more recent events (*yellow*)

to 45 km in central Arabia (Sandvol et al. 1998a, b; Rodgers et al. 1999). Not surprising the crust thins nears the Red Sea (Mooney et al. 1985; Gettings et al. 1986; Mechie et al. 1986). High-frequency regional S-wave phases are quite different for paths sampling the Arabian Shield than those sampling the Arabian Platform (Mellors et al. 1999; Sandvol et al. 1998a, b). In particular the mantle Sn phase is nearly absent for paths crossing parts of the Arabian Shield, while the crustal Lg phase is of extremely large amplitude. This may result from an elastic propagation effect or extremely high mantle attenuation and low crustal attenuation occurring simultaneously, or a combination of both.

The Red Sea is a region of current tectonic activity where continental lithosphere is being ruptured to form oceanic lithosphere, as the opening of the Red Sea split the Arabian-Nubian Shield. While much work has been done to understand the uplift and volcanism of the Arabian Shield, little is known about the structure of the underlying upper mantle. The Arabian Shield consists of at least five Precambrian terranes separated by suture zones (Schmidt et al. 1979). During the late Oligocene and early Miocene, the Arabian Shield was disrupted by the development of the Red Sea and Gulf of Aden rifts, and from the mid-Miocene to the present, the region experienced volcanism and uplift (Bohannon et al. 1989). The uplift and volcanism are generally assumed to be the result of hot, buoyant material in the upper mantle that may have eroded the base of the lithosphere (Camp and Roobol 1992). However, details about the nature of the upper mantle, such as its thermal and compositional state, are not known.

Saudi Arabia and the Red Sea Rift zone offer an excellent environment in which to study the seismic anisotropy

associated with rifting and extension. Several different types of models have been proposed to explain how continental rifting in the Red Sea developed. The passive rifting model assumes simple shear conditions, where extensional stresses are accommodated on large-scale detachment planes extending through the entire lithosphere below the rift. Flow beneath the rift is parallel to the direction of extension as the underlying asthenosphere is passively upwelled, which would predict a rift-perpendicular ϕ . The active rifting model involves thinning of the lithosphere by flow in the underlying asthenosphere and requires the presence of hot, ascending material (Camp and Roobol 1992; Ebinger and Sleep 1998; Daradich et al. 2003). In this case, local convection may lead to more complicated flow patterns and therefore more complex anisotropy at depth. Several studies have suggested that these two end-member models may not be mutually exclusive; rifting in the Red Sea may have been initiated by far-field collision and passive processes, followed by more recent active processes associated with a mantle plume (Camp and Roobol 1992; Ebinger and Sleep 1998; Daradich et al. 2003).

Several previous studies have examined the anisotropic characteristics in the vicinity of the Red Sea Rift and show a fairly consistent pattern. Using eight PASSCAL stations across the Arabian Shield, Wolfe et al. (1999) performed shear-wave splitting analysis and found δt of 1.0–1.5 s and ϕ oriented approximately north-south. Using receiver functions, Levin and Park (2000) found evidence for a more complex anisotropic structure beneath the PASSCAL station RAYN consisting of two dipping layers at depth, but again with a resultant ϕ oriented north-south. Further north, Schmid et al. (2004) and Levin et al. (2006) examined splitting

at several stations near the Gulf of Aqabah and the Dead Sea Transform Fault, where they found average δt of about 1.3 s and ϕ slightly east of north, with some evidence for a more complex, two-layer anisotropic model. However, each of these studies was somewhat limited in their station distribution and data availability. Hansen et al. (2006) presented a more comprehensive analysis of the anisotropic signature along the Red Sea and across Saudi Arabia by analyzing shear-wave splitting recorded by stations from three different seismic networks. This is the largest, most widely distributed array of stations examined across Saudi Arabia to date. They demonstrated that the north-south orientation of the fast polarization direction is not just valid at isolated sites on the Arabian Shield, but extends throughout the whole of Arabia.

In this paper, we extend previous efforts to determine crustal and lithospheric mantle structure under the Arabian Shield and Red Sea by applying an improved method for inverting receiver functions and shear wave group velocity (SWGv) measurements. We apply this technique to a number of stations that sample the complexity of tectonic environments and provide new constraints on structure.

While there have been many studies of this topic using a wide variety of techniques, many questions about the structure of the Arabian Peninsula remain unanswered. A thorough understanding of the seismic structure and wave propagation characteristics of the region must be established before we can proceed to assess seismic hazard. We implemented several types of analysis to seismic data recorded by KACST and SGS seismic networks. These analyses include:

- teleseismic P- and S-wave travel time tomography;
- teleseismic receiver functions for crustal structure;
- teleseismic receiver functions for upper mantle discontinuity structure;
- teleseismic shear-wave splitting; and
- regional and far-regional surface waveform modeling.

Together these analyses result in a unified model of the structure and physical state of the lithosphere beneath the Arabian Shield and Red Sea. The dense station spacing and excellent quality of the KACST and SGS data allow for very detailed resolution of the structures.

Seismotectonics and Seismic Structures

The Arabian Peninsula consists of a single tectonic plate, the Arabian Plate. It is surrounded on all sides by active plate boundaries as evidenced by earthquake locations. Figure 2 shows a map of the Arabian Peninsula along with major tectonic features and earthquake locations. The active tectonics of the region is dominated by the collision of the Arabian Plate with the Eurasian Plate along the Zagros and

Bitlis Thrust systems, rifting and seafloor spreading in the Red Sea and Gulf of Aden. Strike-slip faulting occurs along the Gulf of Aqabah and Dead Sea Transform fault systems. The great number of earthquakes in the Gulf of Aqabah poses a significant seismic hazard to Saudi Arabia. Large earthquakes in the Zagros Mountains of southern Iran may lead to long-period ground motion in eastern Saudi Arabia.

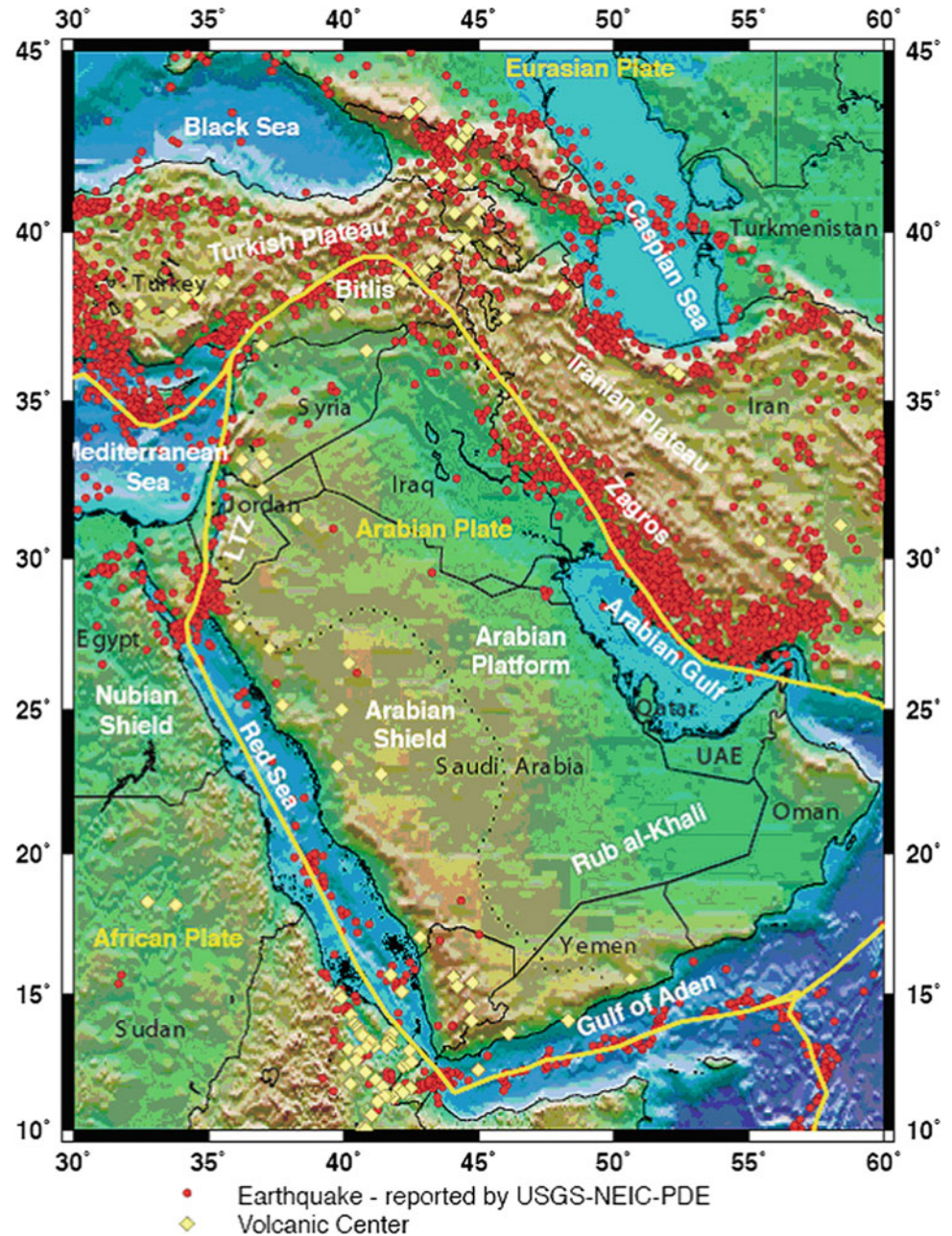
The two large regions, associated with the presence or absence of sedimentary cover, define the large-scale geologic structure of the Arabian Peninsula. The Arabian Platform (eastern Arabia) is covered by sediments that thicken toward the Arabian Gulf. In contrast, the Arabian Shield has no appreciable sedimentary cover, with many outcrops of bedrock. Figure 3 shows the sediment thickness, estimated from compiled drill hole, gravity, and seismic reflection data (Seber et al. 1997). The Arabian Shield consists of at least five Precambrian terranes separated by suture zones (Schmidt et al. 1979). During the late Oligocene and early Miocene, the Arabian Shield was disrupted by the development of the Red Sea and Gulf of Aden rifts, and from the mid-Miocene to the present, the region experienced volcanism and uplift (Bohannon et al. 1989). The uplift and volcanism are generally assumed to be the result of hot, buoyant material in the upper mantle that may have eroded the base of the lithosphere (Camp and Roobol 1992). However details about the nature of the upper mantle, such as its thermal and compositional state, are not known. Volcanic activity (the Harrats) is observed on the Arabian Shield (Fig. 2). This is likely related to the opening of the Red Sea and mantle asthenospheric upwelling beneath western Arabia (e.g. Camp and Roobol 1992).

The northwestern regions of Saudi Arabia are distinct from the Arabian Shield, as this region is characterized by high seismicity in the Gulf of Aqabah and Dead Sea Rift. Active tectonics in this region is associated with the opening of the northern Red Sea and Gulf of Aqabah, as well as a major continental strike-slip plate boundary.

The Dead Sea transform system connects active spreading centers of the Red Sea to the area where the Arabian Plate is converging with Eurasia in southern Turkey. The Gulf of Aqabah in the southern portion of the rift system has experienced left-lateral strike-slip faulting with a 110 km offset since the early Tertiary to the present. The seismicity of the Dead Sea transform is characterized by both swarm and mainshock-aftershock types of earthquake activities. The instrumental and historical seismic records indicate a seismic slip rate of 0.15–0.35 cm/year during the last 1000–1500 years, while estimates of the average Pliocene-Pleistocene rate are 0.7–1.0 cm/year.

Historically, the most significant earthquakes to hit the Dead Sea region were the events of 1759 (Damascus), 1822 (Aleppo), and of 1837; 1068 (Gulf of Aqabah area) caused deaths of more than 30,000 people. Ben Menahem (1979) indicated that about 26 major earthquakes ($6.1 < ML < 7.3$)

Fig. 2 Map of the Arabian Peninsula and surrounding regions. Major geographic and tectonic/geologic features are indicated. Plate boundaries are indicated by *yellow lines*. Earthquakes and volcanic centers are shown as *red circles* and *yellow diamond*, respectively



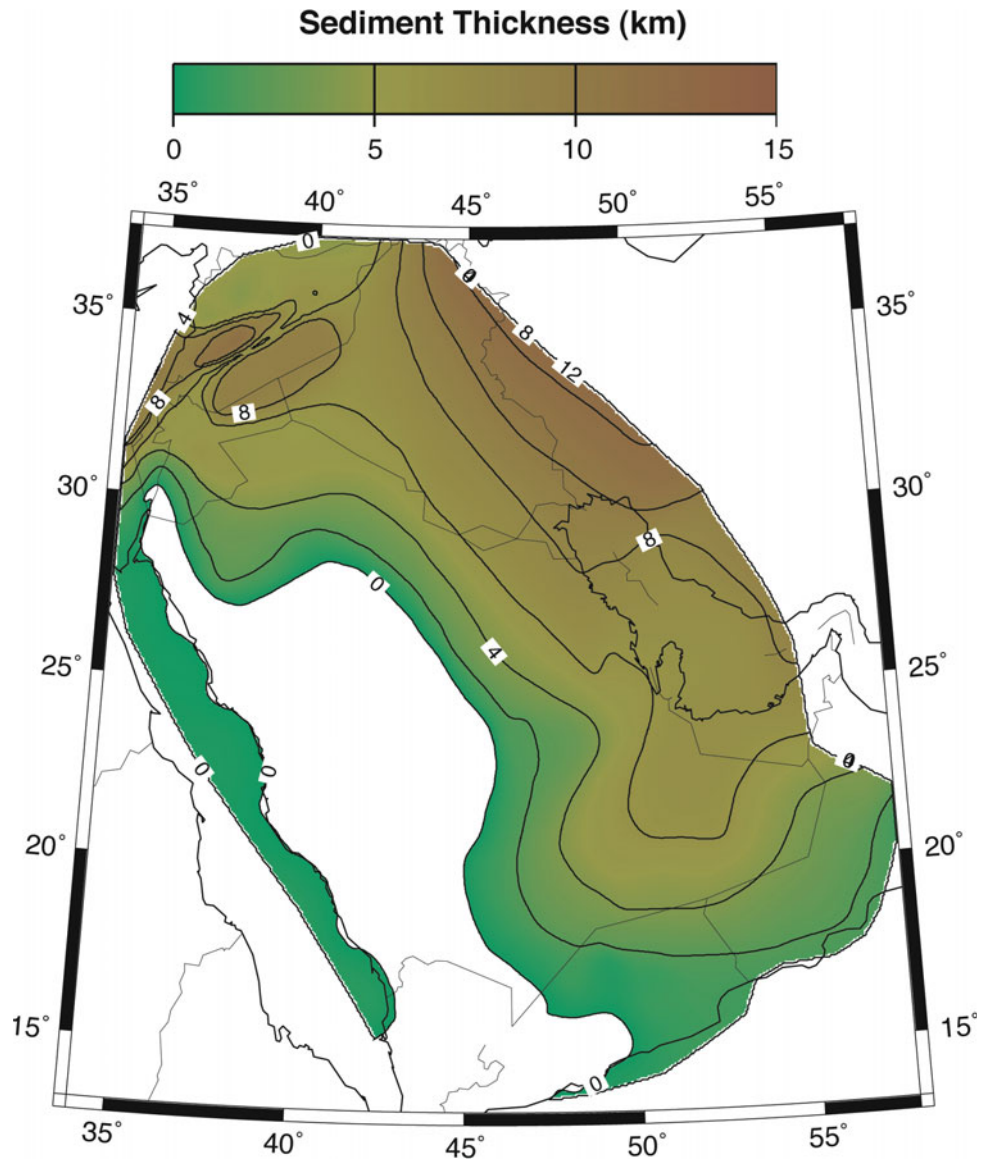
occurred in southern Dead Sea region between 2100 B.C. and 1900 A.D. In 1980 and 1990, the occurrence of earthquake swarms in 1983, 1985, 1991, 1993 and 1995 in the Gulf of Aqabah clearly indicates that this segment is one of the most seismically active zones in the Dead Sea transform system. Earthquake locations provide evidence for continuation of the faulting regime from the Gulf northeastward inland beneath thick sediments, suggesting that the northern portion of the Gulf is subjected to more severe seismic hazard compared to the southern portion (Al-Amri et al. 1991).

To the south, the majority of earthquakes and tectonic activity in the Red Sea region are concentrated along a belt

that extends from the central Red Sea region south to Afar and then east through the Gulf of Aden. There is little seismic activity in the northern part of the Red Sea, and only three earthquakes have been recorded north of latitude 25°N. Instrumental seismicity of the northern Red Sea shows that 68 earthquakes ($3.8 < m_b < 6.0$) are reported to have occurred in the period from 1964 to 1993.

Historically, about 10 earthquakes have occurred during the period 1913–1994 with surface-wave (M_s) magnitudes between 5.2 and 6.1. Some of these events were associated with earthquake swarms, long sequences of shocks and aftershocks (the earthquakes of 1941, 1955, 1967 and 1993).

Fig. 3 Sediment thickness of the Arabian Plate, estimated from compiled drill hole, gravity, and seismic reflection data



The occurrence of the January 11, 1941 earthquake in the northwest of Yemen ($M_s = 5.9$) with an aftershock on February 4, 1941 ($M_s = 5.2$), the earthquake of October 17, 1955 ($M_s = 4.8$), and the 1982 Yemen earthquake of magnitude 6.0 highlight the hazards that may result from nearby seismic sources and demonstrate the vulnerability of northern Yemen to moderate-magnitude and larger earthquakes. Instrumental seismicity of the southern Red Sea shows that 170 earthquakes ($3.0 < m_b < 6.6$) are reported to have occurred in the period 1965–1994. The historical and instrumental records of strong shaking in the southern Arabian Shield and Yemen (1832; 1845; 1941; 1982 and 1991) indicate that the return period of severe earthquakes that affect the area is about 60 years (Al-Amri 1995).

The Arabian Plate boundary extends east-northeast from the Afar region through the Gulf of Aden and into the Arabian

Sea and Zagros fold belt. The boundary is clearly delineated by teleseismic epicenters, although there are fewer epicenters bounding the eastern third of the Arabian Plate south of Oman. Most seismicity occurs in the crustal part of the Arabian Plate beneath the Zagros folded belt (Jackson and Fitch 1981). The Zagros is a prolific source of large magnitude earthquakes with numerous magnitude 7+ events occurring in the last few decades. The overall lack of seismicity in the interior of the Arabian Peninsula suggests that little internal deformation of the Arabian Plate is presently occurring.

Seismic structure studies of the Arabian Peninsula have been varied, with dense coverage along the 1978 refraction survey and little or no coverage of the aseismic regions, such as the Empty Quarter. In 1978, the Directorate General of Mineral Resources of Saudi Arabia and the U.S. Geologic Survey conducted a seismic refraction survey aimed at

determining the structure of the crust and upper mantle. This survey was conducted primarily in the Arabian Shield along a line from the Red Sea to Riyadh. Reports of crust structure found a relatively fast-velocity crust with thickness of 38–43 km (Mooney et al. 1985; Mechie et al. 1986; Gettings et al. 1986, Badri 1991). The crust in the western shield is slightly thinner than that in the eastern shield. Mooney et al. (1985) suggested that the geology and velocity structure of the Shield can be explained by a model in which the Shield developed in the Precambrian by suturing of island arcs. They interpret the boundary between the eastern shield and the Arabian Platform as a suture zone between crustal blocks of differing composition.

Surface waves observed at the long-period analog stations RYD (Riyadh), SHI (Shiraz, Iran), TAB (Tabriz, Iran), HLW (Helwan, Egypt), AAE (Addis-Ababa, Ethiopia) and JER (Jerusalem) were used to estimate crustal and upper mantle structure (Seber and Mitchell 1992; Mokhtar and Al-Saeed 1994). These studies reported faster crustal velocities for the Arabian Shield and slower velocities for the Arabian Platform. The Saudi Arabian Broadband Deployment (Vernon and Berger 1997; Al-Amri et al. 1999) provided the first data set of broadband recordings from this region. This deployment consisted of 9 broadband three-component seismic stations along a similar transect to an early seismic refraction study (Mooney et al. 1985; Gettings et al. 1986; Mechie et al. 1986). Data from the experiment resulted in several studies and models (Sandvol et al. 1998a, b; Mellors et al. 1999; Rodgers et al. 1999; Benoit et al. 2003). These studies provided new constraints on crustal and upper mantle structure. The crustal model of the western Arabian Platform shows a little higher P-velocity for the upper crust in the Shield than in the Platform, and the crustal Platform seems to have a greater thickness than in the Shield by about 3 km. The Moho discontinuity beneath the western Arabian Platform indicates a velocity of 8.2 km/s of the upper mantle and a 42 km Moho depth (Al-Amri 1998a, b, 1999a, b). Julià et al. (2003) presented velocity models for the same stations, combining RF with surface wave dispersion data to invert for structure. Al-Damegh et al. (2005) calculated RF's for the Arabian Plate for permanent broadband stations in Saudi Arabia (Al-Amri and Al-Amri 1999a, b) and Jordan (Rodgers et al. 2003).

Methodology

We improved our understanding of the crustal structures and upper mantle of the Red Sea and the Arabian Shield by using broadband waveform data from the KACST, RAYN/GSN (Fig. 4) and SGS Digital Seismic Networks. This paper includes standard seismological investigations as well as newly developed techniques as follows:

Data Collection and Validation

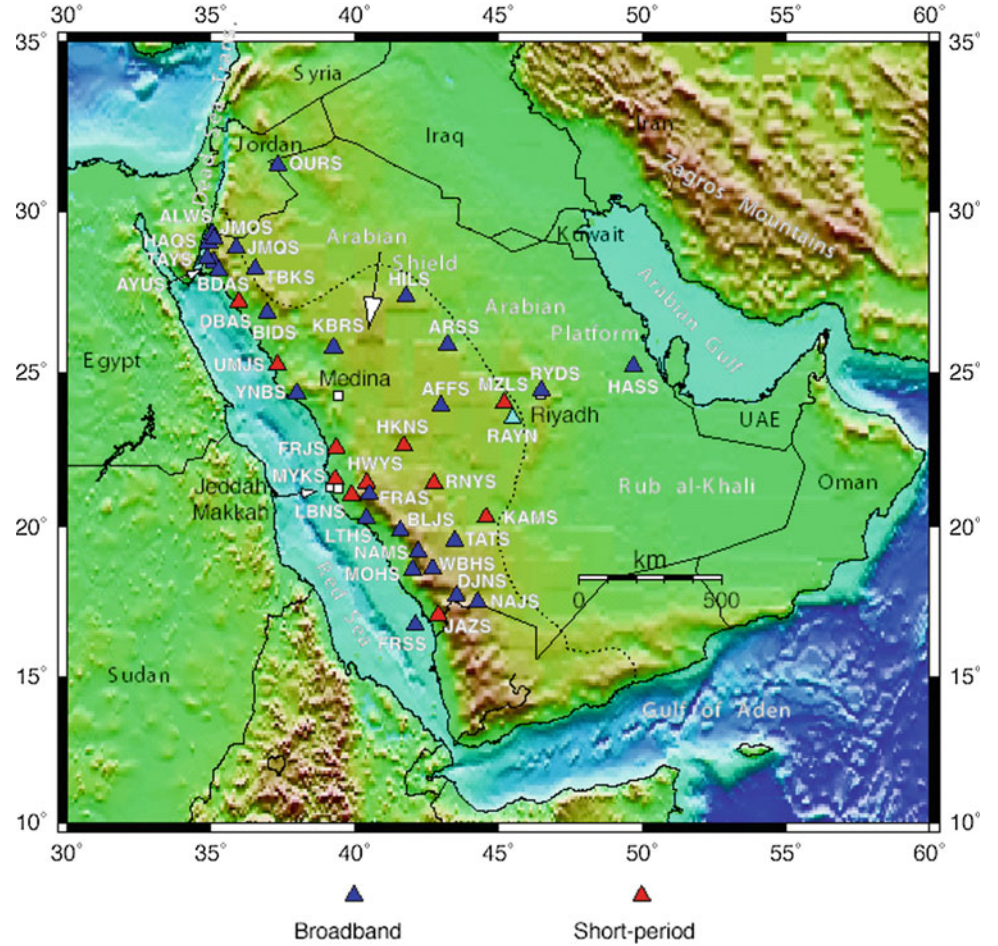
The investigators wrote software to extract waveform data. This software facilitated the extraction and exchange of seismic waveform and parameter data. In order to validate the station timing and instrument response we performed comparisons of timing and amplitudes of P-waves for large teleseismic events at the KACST and SGS stations with the Global Seismic Station RAYN. This station has well calibrated timing and instrument response. The relative arrival times of teleseismic P-waves at the KACST stations can be accurately measured by cross-correlating with the observed waveforms at RAYN and correcting for distance effects. Absolute amplitudes of teleseismic P-waves at the KACST, SGS and RAYN stations were measured by removing the instrument response, gain, and band-pass filtering.

This study also considered many events and computed average travel time and amplitude residuals relative to a globally averaged one dimensional earth model, such as IASP91. Although there were deviations between the timing and amplitudes of the KACST and SGS P-waves from the predictions of the iasp91 model (because of lateral heterogeneity), the tests were useful to identify which stations might have timing and/or instrument calibration problems.

Teleseismic Travel Time Tomography

A number of tomographic methods are available for using P- and S-wave travel time delays to image upper mantle velocity variations (e.g., Thurber 1983; VanDecar 1991; Evans and Achauer 1993). We used these methods to image relative velocity variations in the upper mantle beneath the Arabian Shield. An example of the results we obtained is provided by a recent study by Benoit et al. (2003) of upper mantle P-wave velocity structure under the Arabian Shield. In this study, P-wave travel time residuals were determined from the SABD dataset using the multi-channel cross correlation (MCCC) method of VanDecar and Crossen (1990) and then modeled using the inversion method of VanDecar (1991). The MCCC method of VanDecar and Crossen (1990), which makes use of the waveform coherency that is found across a regional network, involves three steps. First, the data is band-passed filtered between 0.5 and 5 Hz. A cross correlation is then computed for all possible pairs of stations to find the relative arrival times, and finally a least squares optimization scheme is applied to the arrival times to minimize inconsistencies in the data. The uncertainties in the relative P-wave travel times obtained from the SABD dataset are about 0.1 to 0.15 s. After computing the travel time residuals, they were inverted for P-wave slowness and earthquake relocations. The inversion searches for the smoothest model with the least amount of structure that will

Fig. 4 Map of the stations from the KACST digital seismic network and RAYN/GSN



match the data. The inversion is linear and minimizes both spatial gradients and model roughness using a conjugate gradient scheme. Root mean square (rms) and variance reduction (VR) for each model are calculated as a measure of misfit according to the following expressions:

$$rms = \sqrt{\frac{N_{max}}{N}} \sqrt{\frac{\sum_{i=1}^N w_i (obs_i - theor_i)^2}{N}};$$

$$VR = \left\{ 1 - \frac{\sum_i (obs_i - theor_i)^2}{\sum_i obs_i^2} \right\} 100\%$$

where N is the number of selected periods for Love or Rayleigh wave dispersion at a given station (typically, we consider 11 discrete periods spanning from 20 to 70 s for Love waves, and 20 discrete periods spanning from 7 to 100 s for Rayleigh waves), and N_{max} is the number of periods for Rayleigh wave dispersion. The factor $\sqrt{\frac{N_{max}}{N}}$ is then a normalization factor, which equalizes the relative

significance of rms results for Love and Rayleigh wave dispersion, given the fact that less data points are available for Love waves. The parameter w_i is defined as $1/e$ (where e is the error of each point in surface wave dispersion curves) and is a relative weight of each velocity measurement in the dispersion. If there is a large misfit at only period of the group velocity dispersion, the above expression for rms would significantly impact the result. However, the above expression for variance reduction would not significantly penalize the result. Therefore, variance reduction is a more appropriate measure of misfit than rms for waveforms (receiver functions) with a much larger number of points than in discrete dispersion measurements, where it is important to fit the character of the waveform. The rms and VR expressions are used in combination as criteria for selecting and plotting small percentages of the best models.

Overall, even though the resulting models consisting of a 3-layer crust and a half space are in many cases too simplistic, we note that some excellent matches of the data by the synthetics were found, particularly in cases when only receiver function or only surface wave data (either Love or Rayleigh wave dispersion) are considered.

Receiver Functions

The use of P-wave receiver functions to infer the existence of major crustal and upper mantle discontinuities has become a standard technique in seismology. These methods are described elsewhere (e.g., Langston 1979; Owens et al. 1984; Ammon 1991) and consist of deconvolving the vertical P-wave component from the radial (and possibly tangential) component to expose P-to-S converted waves in the P-wave coda. The timing and amplitude of these conversions are then modeled or incorporated in inversion algorithms to infer S-wave velocity models and the depth to the discontinuities. We performed P-wave receiver function studies for some stations of the network. To image crustal structure, we combined the receiver functions with surface wave dispersion measurements out to 30 s using the joint receiver function/surface wave inversion method of Julia et al. (2000). This method, then, provides a simple way to control trade-offs between fitting the receiver functions and the dispersion curves (normalized by the data uncertainty and number of points), and also the trade-off between fitting the data and model smoothness. Both smoothness and weighting parameters are estimated empirically, after running a suite of inversions.

The combination of receiver functions with surface wave dispersion measurements allowed us to place tight constraints on average crustal S velocities and Moho depths.

Teleseismic Shear Wave Splitting

The most abundant and highly anisotropic upper mantle mineral, olivine, develops preferred lattice orientations when deformed in the dislocation creep regime (Karato 1998). For large strains, the olivine axes become parallel to the direction of shear. Therefore, measurements of seismic anisotropy can be used to investigate mantle deformation. While seismic anisotropy has been studied in several diverse tectonic settings, its interpretation in many cases is still enigmatic. No tectonic environment has been more difficult to understand than rift zones. Since Hess' (1964) pioneering study of anisotropy in ocean basins, it has been expected that extension should align fast directions of olivine parallel to the rifting direction through shear in the lithosphere or asthenosphere. However, recent studies of seismic anisotropy from SKS splitting in the Basin and Range (Savage et al. 1990), the Rio Grande Rift (Sandvol et al. 1992), the Baikal Rift (Gao et al. 1997), and an area adjacent to the Red Sea Rift Zone (Wolfe et al. 1999; Hansen et al. 2006) have not found extension-parallel fast directions. This

suggests that flow in the asthenosphere is not completely driven by surface tectonics.

The anisotropic signature beneath continental rift zones can provide important constraints on the mechanism of extension. For example, a passive model of continental rifting, where the entire lithosphere is extended below the rift, would be expected to produce a lattice preferred orientation (LPO) of olivine aligned parallel to the direction of extension. Active rifting involving thinning of the lithosphere through small-scale convection might result in more complex flow and therefore more complicated LPO alignments, depending on the details of the small scale convection. In addition to LPO developed during mantle flow, alternative models for seismic anisotropy beneath rift zones include fossil LPO frozen into the lithosphere during a previous tectonic event and the alignment of magmatic cracks. These magma-filled cracks are expected to align themselves perpendicular to the east compressive stress direction, resulting in rift-parallel fast polarization directions. This mechanism is analogous to extensive dilatancy anisotropy, where parallel alignment of vertical, fluid-filled microcracks in the crust produces anisotropy. It has been suggested as the dominant cause of anisotropy beneath the Rio Grande and East African Rifts (Gao et al. 1997).

Results of previous research found a fast polarization direction parallel to the Red Sea Rift's spreading, by modeling far-regional surface waves (Schwartz et al. 2000). That study estimated crustal and upper mantle velocity structures for the Red Sea Rift Zone that were derived by modeling regional and far-regional body and surface waveforms. The best-fit model had a 17 km thick crust with anomalously low upper mantle velocities ($V_p = 7.7$ km/s) underlain by a significant low velocity zone. Velocity models that fit the radial and vertical waveforms are unable to accurately predict the Love wave on the transverse component. Including 3–4 % faster SH than SV velocities in the upper mantle replicates the Love wave and points to a fast anisotropic polarization axis parallel to the rift's spreading direction. These results are in direct contradiction to the SKS splitting results of Wolfe et al. (1999) and require further investigation of the anisotropic structure beneath the Red Sea Rift zone to understand its origin and relationship to the geodynamic processes involved in continental rifting.

Here we used the KACST data set to address this very important problem. Specifically, we measured teleseismic shear wave splitting in S and SKS phases recorded by 26 broadband stations of the KACST network that border the Red Sea in Saudi Arabia. The S and SKS splitting parameters were analyzed for the possibility of lateral variations in anisotropic structure and dipping symmetry axes. Dipping

symmetry axes were not considered in any of the previous studies of rift zone anisotropy, but may be able to reconcile the apparent difference in fast polarization directions obtained from body and surface waves for the Red Sea Rift Zone. Regional and far-regional surface waves from moderate sized events in the Red Sea region recorded by all available stations in the area were modeled to increase the surface wave observations and confirm or refute our previously obtained extension-parallel fast propagation direction. The S, SKS, and surface wave anisotropy results were combined in an attempt to construct a consistent model for mantle flow beneath this rift zone.

The study of Wolfe et al. (1999) as well as most shear-wave splitting studies concentrate on the SKS phase and average individual splitting measurements (fast polarization directions and delay times) made from events at various back-azimuths to obtain station averages. SKS is the favored phase because it passes through the liquid outer core and any effects of source-side splitting are obliterated due to its complete conversion to compressional motion in the outer core. This property of outer-core-traversing waves renders them very powerful to study receiver side anisotropy. The tendency to average individual splitting parameters is primarily due to the relatively small number of observations at each station (since SKS phases alone are favored) and large measurement errors. Averaging splitting parameters implicitly assumes that the anisotropy is adequately described by a single anisotropic region of hexagonal symmetry with the olivine axes oriented horizontally, thus implying horizontal flow. This may not always be a valid assumption, so rather than averaging individual splitting parameters obtained from different events to produce station averages, we analyzed the dependence of splitting parameters on arrival directions. This allowed us to determine: 1) if waves from different directions sample different anisotropic regions; and 2) if the anisotropic medium has a symmetry that is more general than hexagonal with a horizontal symmetry axis.

Although S phase splitting is more difficult to interpret than SKS, since its splitting could have occurred anywhere along its propagation path, the inclusion of S phases greatly increases the range of available incidence angles and back azimuths and allows interpretation of individual splitting measurements. We incorporate S-wave splitting in this study and remain aware of the possibility of source-side anisotropy for the S phases. We however, preferably analyzed S phases from deep focus events to minimize this effect. We used the horizontal velocity traces to obtain the splitting parameters. For SKS phases we rotated and shifted the two components to find those parameters (polarization direction, phi and delay time) that minimize the energy on the transverse component and render the particle motion most linear, that

is, we minimized the smallest eigenvalue of the covariance matrix. For S we used this covariance method. Measurement errors were estimated by the commonly used F test method.

Regional and Far-Regional Surface Wave Modeling

While knowledge of the velocity structure of northeastern Africa is important for understanding its tectonic development, progress has historically been hindered by both a lack of large African earthquakes and the sparseness of seismic stations at regional distance from seismic sources. Although large African earthquakes are still quite rare, station coverage in the area of the Red Sea Rift is now sufficient for regional waveform modeling of relatively pure paths traversing the Red Sea. We tested and refined our previously derived model of the crust and upper mantle structure beneath the Red Sea Rift zone through waveform modeling at regional and far-regional distances. Events with high signal to noise with known focal mechanisms were culled to insure that the data possess distinct compressional, shear, and surface wave arrivals. Processing and modeling of the data were done following procedures used by Rodgers and Schwartz (1998) and Rodgers et al. (1999) and include: (1) deconvolution of the station response to ground displacement; (2) initial band-pass filtering between 5 and 100 s; (3) rotation of horizontal components to the great-circle coordinates; and (4) application of a grid-search algorithm to determine crustal and mantle parameters that best-fit both the surface and body waves in the period ranges between 20 and 100 s.

Modeling surface and body waves together provides better constraints upon the crustal and upper mantle structure than modeling selected portions of the seismograms because it includes information about the surface wave group and phase velocities plus the body wave arrival times and their relative amplitude to the surface waves. Using a range of velocity and layer thickness parameters, a suite of models is created and synthetic reflectivity seismograms (Randall 1994) generated for each. The best parameters are chosen by calculating a normalized least-squares misfit between the data and synthetic components. Initial iterations focus on constraining the crustal velocities and thickness through fitting the absolute timing, amplitude, and dispersion of the Love and Rayleigh surface wave packets. Later iterations involve varying lid and upper mantle thickness and gradients, allowing shear velocity to increase independently of the P/SV velocity structure if necessary to fit the transverse and radial component surface waves and the P and S body wave arrivals and amplitudes.

Data Analysis and Results

Teleseismic Travel Time Tomography

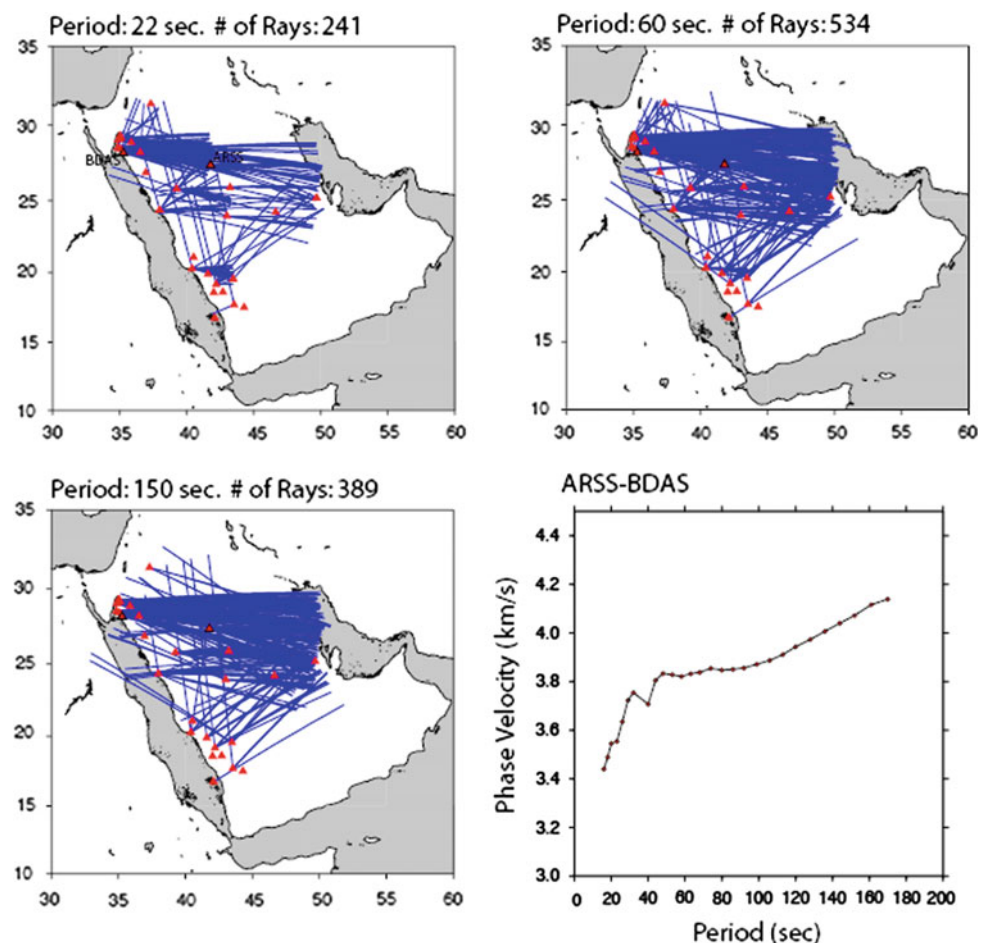
We determined detailed models of compressional and shear velocities of the crust and upper mantle down to about 400 km using teleseismic receiver functions and P- and S-wave travel time tomography. The state of strain in the upper mantle was determined from teleseismic shear wave splitting. Deep receiver functions were sampled for the upper mantle transition zone discontinuities at 410 and 660 km. The resulting models provided new constraints on tectonic models of the rupturing of continental lithosphere and the source of volcanism in the Arabian Shield.

Rayleigh wave dispersion curves were measured using the array methods of Menke and Levin (2002) as shown in Fig. 5. The figure shows path coverage for three period bands centered at 22, 60 and 150 s. The fourth panel shows the Rayleigh wave dispersion curve for the inter-station path between KACST station (ARSS) and BDAS in Ethiopia. The coverage is quite good for this data set (Park et al. 2005).

In this study, the tomographic inversion method uses a multi-channel cross-correlation (VanDecar and Crossen 1990) to find the optimal set of relative delays between teleseismic P-wave arrivals at the entire KACST network. Tomography requires many crossing ray paths in order to isolate the locations of velocity anomalies below the network. The method uses an iterative non-linear ray-tracing algorithm to allow for ray-bending 3-D structure. For the P-wave model, we used 401 earthquakes resulting in 3416 ray paths with P- and PKP-wave arrivals. The majority of the events are located in the western Pacific Rim between back azimuths of 15 and 150 degrees, but the events are distributed over a wide range of back azimuths (Fig. 6a). The waveforms were filtered with a zero-phase two-pole Butterworth filter between 0.5 to 2 Hz, and relative P-wave travel time residuals were computed (Park et al. 2005).

For the S-wave model, we used 201 earthquakes resulting in 1602 ray paths with S- and SKS-wave arrivals. Although the total number of rays for the S-wave model is half of the rays for the P-wave model, the event distribution shows better coverage of back azimuths (Fig. 6b). The signal processing procedures for S-wave are exactly same as for

Fig. 5 Rayleigh wave dispersion curves for three period bands centered at 22, 60, and 150 s. The fourth panel shows the Rayleigh wave dispersion curve for the inter-station path between KACST station ARSS and BDAS in Ethiopia



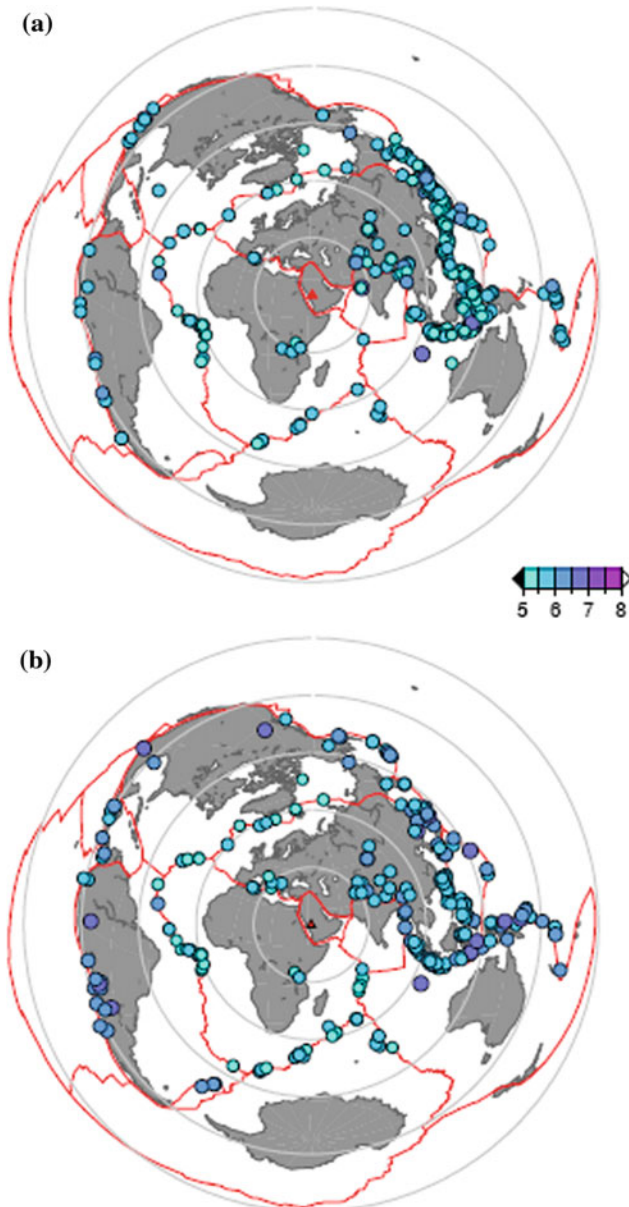


Fig. 6 The distribution of earthquakes for **a** P-wave (3416 rays from 401 events) and **b** S-wave (1602 rays from 201 events) events plotted by the equal distance projection. The color scale indicates the magnitude of each event, the *red solid lines* show plate boundaries, and each circle represents a 30° distance interval from the center of KACST seismic array

P-wave data, but traces are filtered with a lower frequency band (0.04 to 0.1 Hz) and relative arrival time residuals are computed by the multi-channel cross-correlation (MCCC) method with a fifteen-second time window (Park et al. 2005).

The resulting tomographic images of upper mantle structure at depths of 100–400 km are shown in Fig. 7. P-wave velocities vary by $\pm 2\%$ beneath Arabia where

slower velocities than average are generally beneath the Arabian Shield and faster than average velocities beneath the Arabian Platform. However, a striking feature is the low velocities extending through the upper mantle beneath the eastern edge of the Arabian Shield (beneath Riyadh). This feature can be seen in the cross-sections shown in Fig. 8.

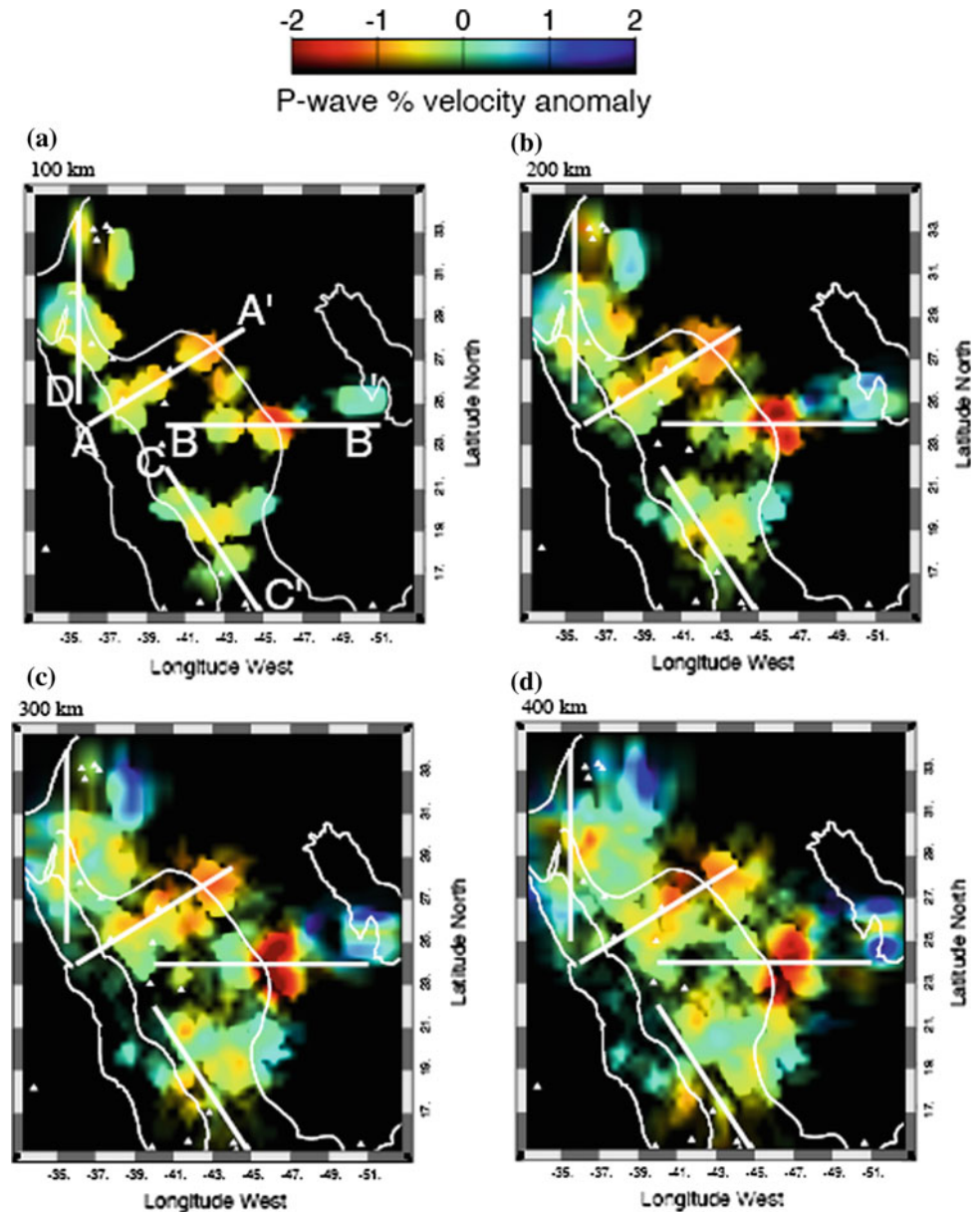
For comparison, we show the upper mantle P-wave velocity model of Benoit et al. (2003) in depth slice and cross-section view in Figs. 9 and 10, respectively. That study used data from the 9 station IRIS-PASSCAL Saudi Broadband Deployment (Vernon et al. 1996). In fact, the sampling is complementary, with the PASSCAL data covering north-south and northeast-southwest trending zones across the Arabian Shield beneath the stations. As can be seen in Figs. 9 and 10, the resolution and lateral extent of the area imaged using the Saudi Arabian Broadband Deployment (SABD) data sets are quite limited.

Resolution Tests

To test the resolution of our P- and S-wave model, we produced a synthetic checkerboard model consisting of 100 km diameter spheres with $\pm 5\%$ slowness anomalies placed at 100, 400, and 700 km depths (Figs. 11 and 12). Ray paths through a 1-D reference mode as defined by the IASP91 (Kennett and Engdahl 1991) are used, and noise is added to the synthetic travel-times as a Gaussian residual time error with a standard deviation of 0.02 and 0.04 s for the P- and S-wave data, respectively. Figures 11 and 12 show the recovered structure from the checkerboard test for P- and S-wave velocity perturbations, respectively. The input spheres are retrieved below 200 km depth (Fig. 11 e–h for P-wave tomography and Fig. 12 e–h for S-wave tomography), and the amplitudes of the slowness anomalies are recovered at $\sim 20\%$ of the input anomaly. Since the spacing of seismic stations is sparse, and the ray paths of teleseismic body-waves are incident vertically near the surface, the velocity perturbations set at 100 km depth were recovered with very small anomaly values in our model. However, the cross-section images of P- and S-wave models show that the patterns of the retrieved models are reliable between 200 km and 400 km depth (Figs. 11g, h and 12g, h).

Generally speaking, we would suggest that low velocities beneath the Gulf of Aqabah and southern Arabian Shield and Red Sea at depths below 200 km are related to mantle upwelling and seafloor spreading. Low velocities beneath the northern Arabian Shield below 200 km may be related to volcanism. The low-velocity feature near the eastern edge of the Arabian Shield and western edge of the Arabian Platform could be related to mantle flow effects near the interface of lithosphere of different thickness.

Fig. 7 P-wave velocities in the upper mantle at depths of **a** 100, **b** 200, **c** 300 and **d** 400 km depths. Velocities are plotted with the color scale as the relative perturbation to the average one-dimensional background model. The locations of cross-sections through the model are indicated by the white lines



Modeling of Surface Wave Dispersion

In this study we applied a new method to simultaneously fit receiver function and surface wave group velocity data (Tkalcic et al. et al. 2005). The method involves a combination of grid search, iterative inversions, and forward modeling to simultaneously explain the surface wave dispersion (from 7 to 100 s for Rayleigh and 20 to 70 s for Love waves) and teleseismic RF observations at the broadband stations in the Arabian Peninsula. For the grid search, we used a database of pre-calculated theoretical receiver functions and dispersion curves, which allowed us to significantly reduce the computing time and investigate a wide range of structural models. We initially fit receiver functions and shorter periods of the

observed dispersion curves with the structure within the crust and immediately beneath the crust. We then used an additional grid search to characterize the lithospheric lid and low velocity zone in the upper mantle, fixing the crustal structure and fitting longer period dispersion curves. The method proved to be robust and could be applied in the cases where little a priori knowledge exists about the crustal structure. Additionally, as a result of the “step by step” approach to recover the structure starting from the “top” and ending with the “bottom” of the model, the multi-step method revealed how mantle velocity variations and transverse isotropy is needed to simultaneously fit all available data.

We apply this technique to a number of stations that sample the complexity of tectonic environments and provide

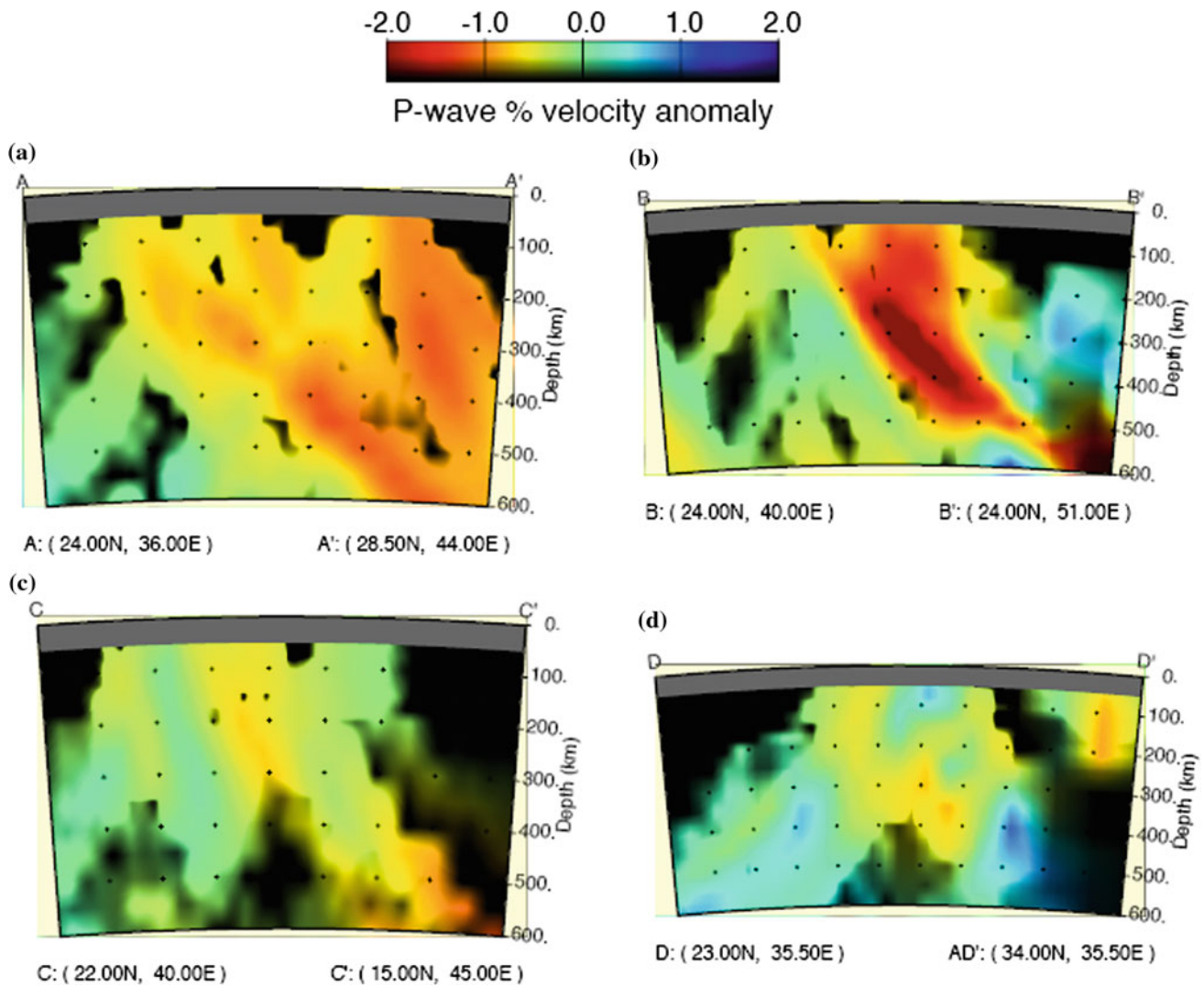


Fig. 8 Cross-sections through the upper mantle tomography model: **a** A-A' across the northern Arabian Shield; **b** B-B' across the shield-platform boundary; **c** C-C' along the southern Red Sea coast (Asir Province); and **d** D-D' along the Gulf of Aqabah and the Dead Sea Rift

new constraints on structure. Figures 13, 14, 15, and 16 illustrate the final fit to the data and our best models for stations ARSS, BLJS, NAMS, and YNBS, respectively. In the following, we discuss the features of these models.

Station **ARSS** (Fig. 13) is located on the eastern edge of the Arabian shield. Our final model has a 40 km thick crust and a relatively pronounced Moho, with a thin lithospheric lid extending 10 km below the Moho. No transverse isotropy is needed to explain simultaneously the RFs and surface-wave dispersion data. It appears that the lithospheric lid thickens significantly and that the slight transverse isotropy does not exist at ARSS.

The velocity structure for station **BLJS** (Fig. 14) is characterized by shallow low velocities, normal crustal velocities, and a Moho depth of 38 km. The mantle is characterized by a thin lid and decreasing velocities, and up

to 5 % anisotropy ($v_{SV} > v_{SH}$). These results are consistent with the nearby station, NAMS.

We observe a strong contrast in the velocity at the Moho for station **NAMS** (Fig. 15). The crustal thickness of 41 km is in agreement with the estimate of Al-Damegh et al. (2005). The mid-crustal structure is characterized by a transition from slow to fast shear-wave speeds (exceeding 4 km/s) and a sudden drop of velocities at about 23 km depth by 0.6 km/s. The lithospheric lid of about 20 km thickness, overlaying a broad low-velocity zone that extends to about 140 km depth, is a well-pronounced feature in the upper mantle.

Station **YNBS** (Fig. 16) lies in the northern part of the Red Sea coast. YNBS is a station with considerably thinner crust (28 km) compared to other stations modeled in this report, but is consistent with the results of Al-Damegh et al.

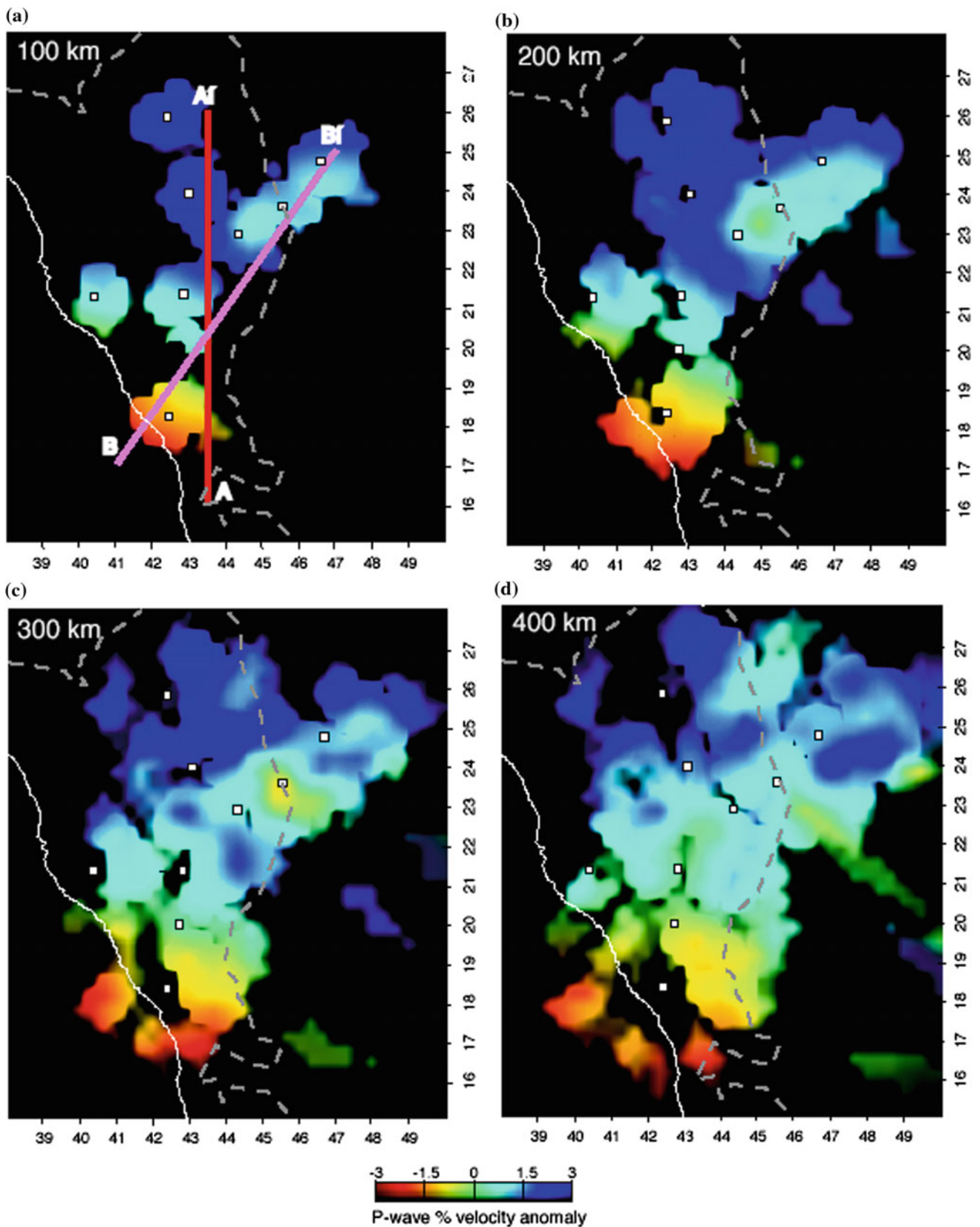
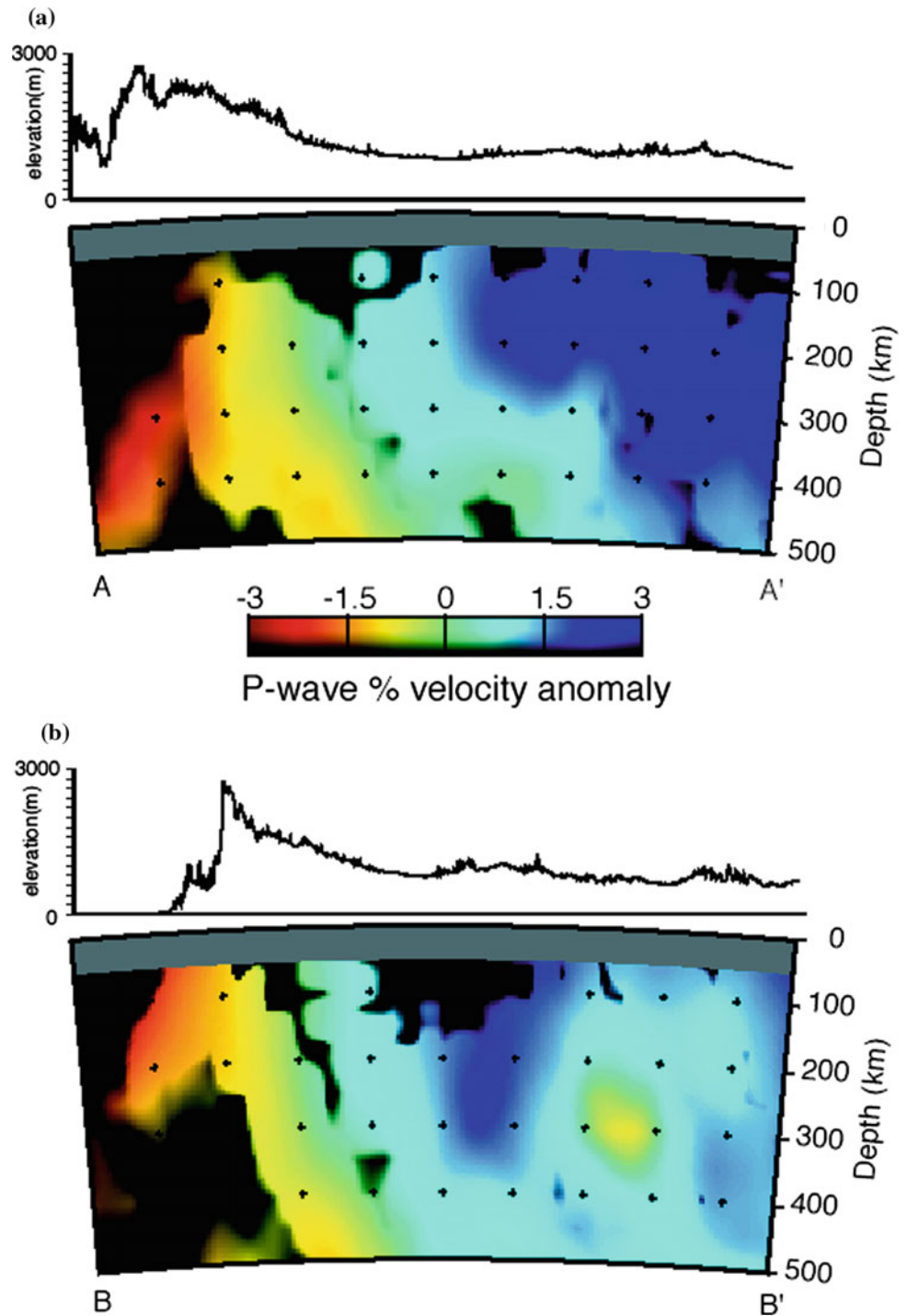


Fig. 9 Tomographic model of Benoit et al. (2003). P-wave velocities in the upper mantle at depths of **a** 100, **b** 200, **c** 300 and **d** 400 km depths. Velocities are plotted with the color scale as the relative

perturbation to the average one-dimensional background model. The locations of cross-sections through the model are indicated by the red lines

Fig. 10 Cross-sections through the upper mantle tomography model: **a** A-A' north-south section across the Arabian Shield and **b** B-B' southwest-northeast section from the Red Sea across the Arabian shield to the Arabian platform



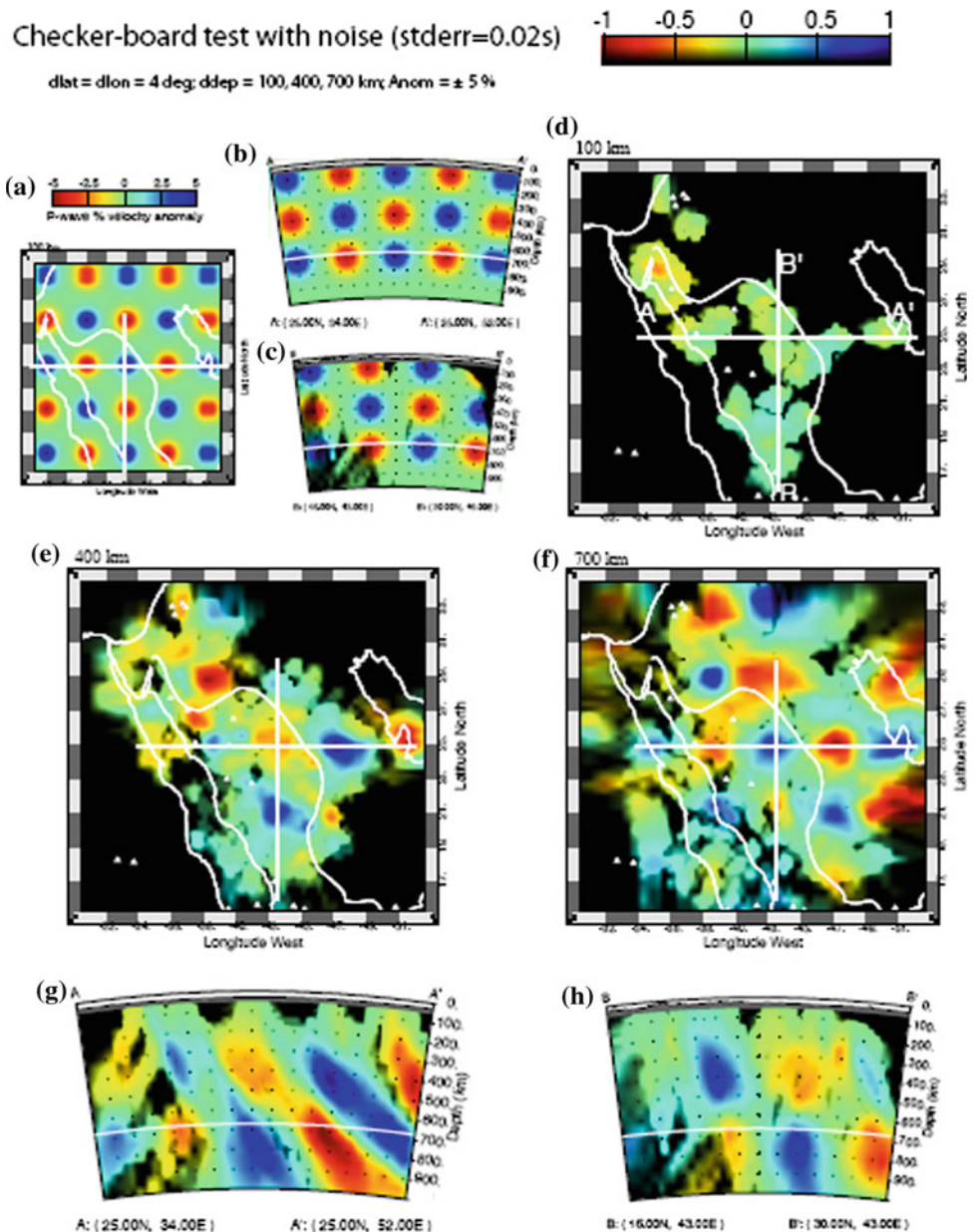
(2005). The mantle velocity is low (4.2 km/s on average), and no lithospheric lid could be observed in the final model (although a strong v_{SH} lid is required). The sign of anisotropy is thus opposite from the sign modeled for stations BLJS and NAMS in the southern part of the Red Sea.

We suggest that low velocities beneath the Gulf of Aqabah and southern Arabian Shield and Red Sea at depths below 200 km are related to mantle upwelling and seafloor

spreading. Low velocities beneath the northern Arabian Shield below 200 km may be related to volcanism. The low velocity feature near the eastern edge of the Arabian Shield and western edge of the Arabian Platform could be related to mantle flow effects near the interface of lithosphere of different thickness.

The resulting velocity models beneath the Arabian Peninsula provide new constraints on crustal and upper

Fig. 11 Synthetic checker-board resolution test for the inverted P-wave model. **a** shows the 100 km depth profile of the input model, and **b, c** show the cross sections located on **(a)**. 100 km diameter spheres defined by Gaussian functions across their diameter of $\pm 5\%$ peak velocity anomaly are distributed in layers of depth 100, 400 and 700 km. **d, e, f** are the 100, 400 and 700 km depth profiles inverted from the input model, and **g, h** are the cross-sections



mantle structure. This study shows an average crustal thickness of the Arabian shield of 36 km for the stations used in this study. Three layers can be deduced from the final velocity model, which is consistent with models reported by Al-Amri et al. (2004).

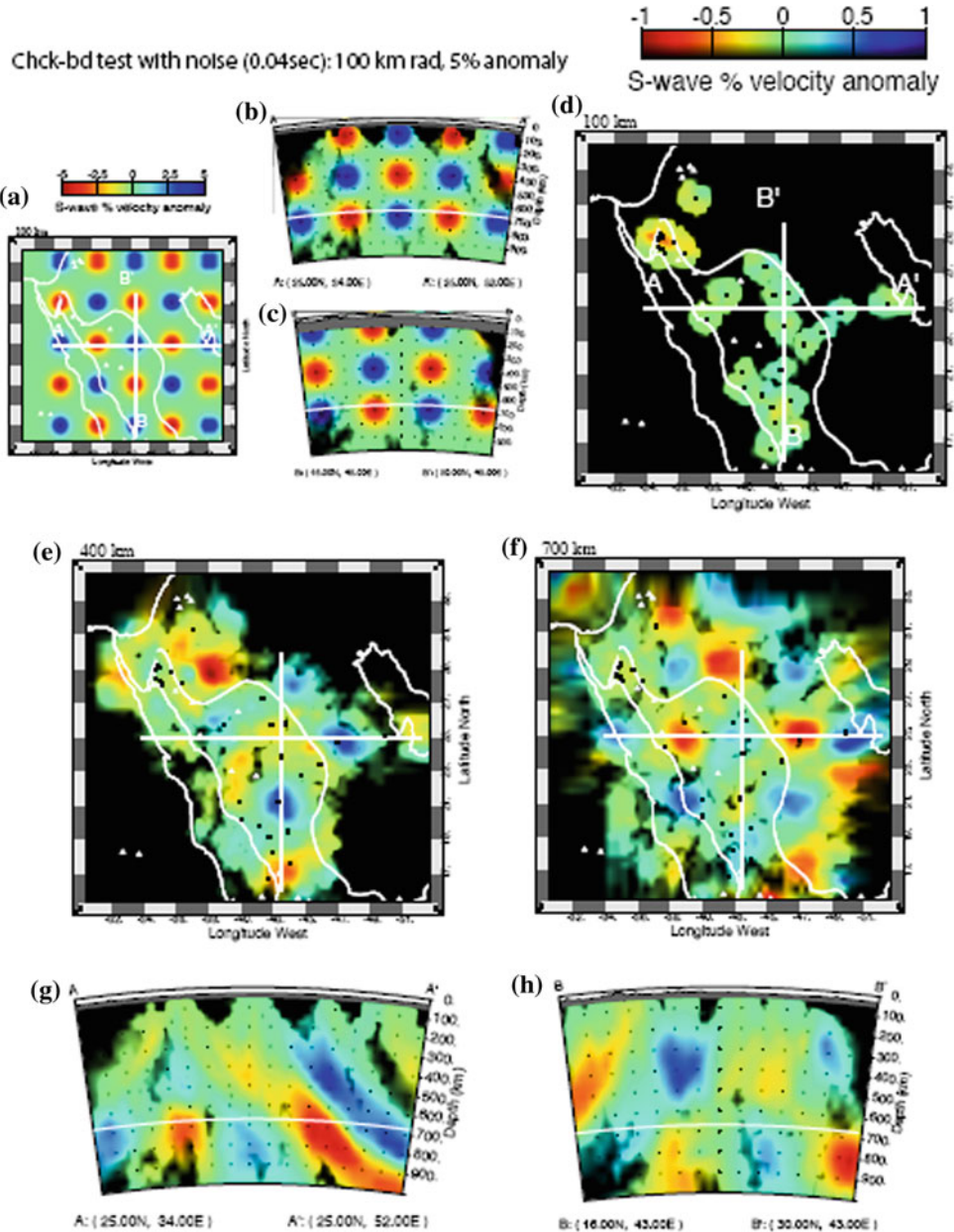
Generally speaking, the results for crustal structure are consistent with previous studies, where applicable. The new results for the lithosphere suggest that the mantle lithosphere is thin and the LVZ is significant near the Red Sea, where rifting is active. The mantle lid thickens away from the Red Sea in the Arabian interior. Furthermore, our results indicate the presence of polarization anisotropy in the lithospheric upper mantle, in the vicinity, as well as farther away from the Red Sea. Our modeling suggests $v_{SV} > v_{SH}$ in the

southern part of the Red Sea, consistent with vertical flow, and $v_{SH} > v_{SV}$ in the northern part of the Red Sea and the continental interior, as is commonly reported in the continents.

Mantle Anisotropy from Shear-Wave Splitting

Seismic anisotropy in the earth causes wave motions in different directions to travel at different speeds. For shear-waves, this can lead to bi-refringence, where different polarizations travel at different speeds. Furthermore, anisotropy can cause motions with one polarization to couple into other polarizations. The SKS phase is widely used to study

Fig. 12 Synthetic checker-board resolution test for the inverted S-wave model. **a** shows the 100 km depth profile of the input model, and **b, c** show the cross sections located on **(a)**. 100 km diameter spheres defined by Gaussian functions across their diameter of $\pm 5\%$ peak velocity anomaly are distributed in layers of depth 100, 400 and 700 km. **d, e, f** are the 100, 400 and 700 km depth profiles inverted from the input model, and **g, h** are the cross-sections

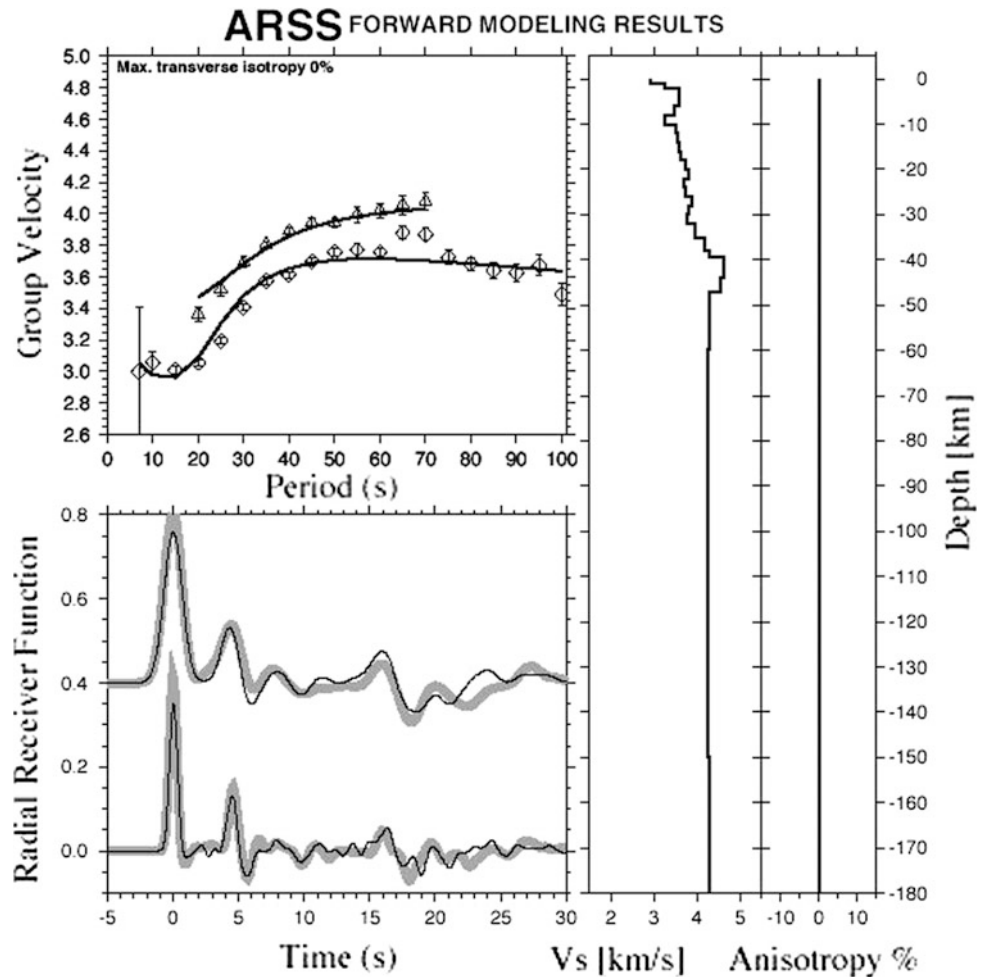


anisotropy because it emerges from the outer core as purely a radially polarized wave. Splitting of the SKS phase occurs when the radially polarized shear wave encounters a zone of anisotropy. One then observes SKS energy on the transverse component of motion, unexpected in an isotropic earth model. The two waves arrive at the station with a relative time shift proportional to the amount of anisotropy and the thickness of the anisotropic layer. The SKS data are processed to estimate the direction of the fast-axis of the anisotropic layer and the delay time. Hansen et al. (2006) have processed a set of waveforms from several stations in the KACST network. They show clear SKS splitting due to seismic anisotropy. In total, they used 135 events including

247 records of SKS phases, 12 records of SKKS phases, and 52 records of S phases. The splitting parameters from different events at each station were averaged to find an overall resultant, shown in Fig. 17. In general, the stations display a north-south oriented ϕ with an average δt of 1.4 s, similar to the findings of previous studies throughout the area (Wolfe et al. 1999; Levin and Park 2000; Schmid et al. 2004; Levin et al. 2006).

The splitting observations at the Gulf of Aqabah stations can be best explained by a one-layer model, whose ϕ is oriented parallel to the Dead Sea Transform. Most of the splitting parameter observations across Saudi Arabia are very consistent. The observed north-south ϕ is not oriented

Fig. 13 Forward modeling of velocity and anisotropy structure in the upper mantle from love and Rayleigh wave group dispersion for the ARSS station. The model shows the final fit to the data and no transverse isotropy is needed to simultaneously fit all available data



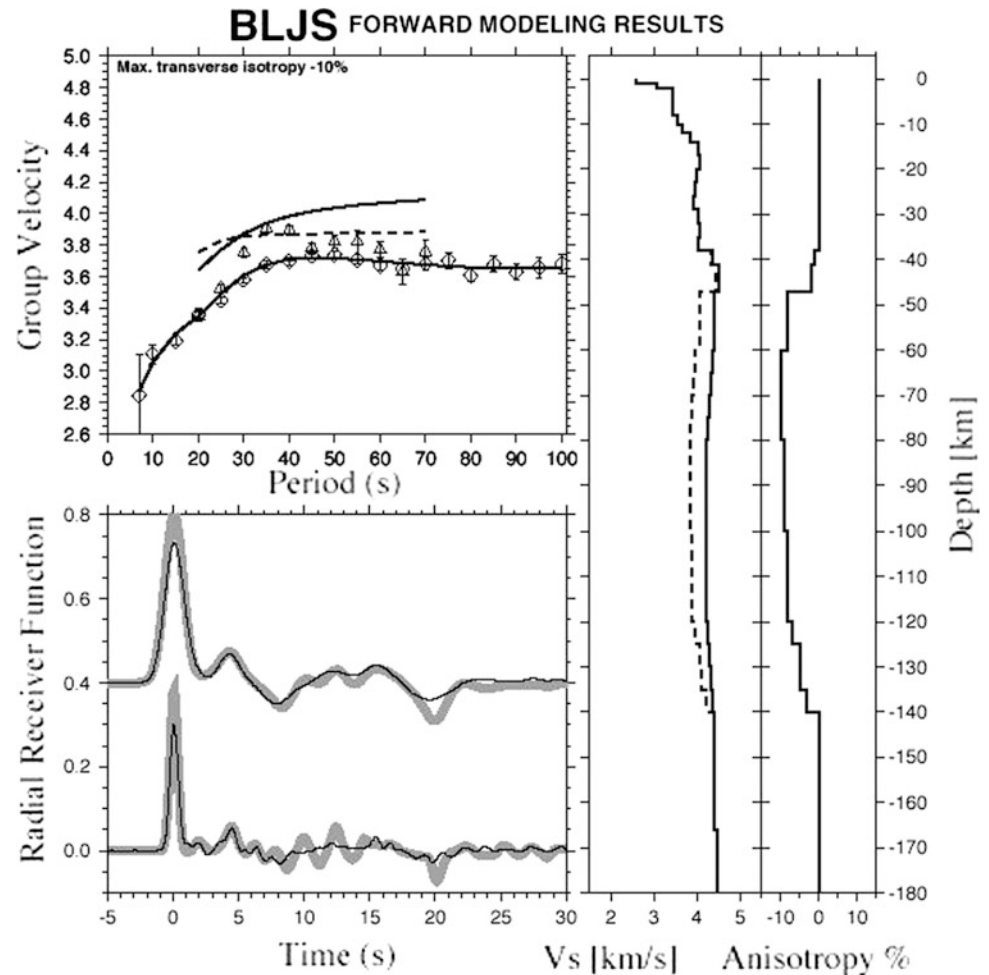
perpendicular to the Red Sea Rift and therefore does not support a passive rifting model. Also, the orientation of φ is at least 30° different from the reported absolute plate motion direction. It is possible that the anisotropic signature obtained could be the result of fossilized anisotropy in the lithosphere, where φ is aligned parallel to the northerly strike of accreted terranes and sutures dating back to the Proterozoic assembly of the Arabian platform (Stoeser and Camp 1985).

The results of Hansen et al. (2006) indicate a fairly consistent fast polarization direction of N20-25°W with delay times ranging between 0.75 and 1.2 s. This direction is similar but about 20° more westerly than the north-south fast polarization direction reported by Wolfe et al. (1999) from a temporary network of broadband sensors deployed over a much more spatially limited region of the Arabian Shield. The results of Hansen et al. (2006) extend and confirm their interpretation of a fairly homogeneous anisotropic fabric throughout the shield. However, Wolfe et al. (1999) could not discriminate between different interpretations of their dominantly north-south fast polarization directions. The

mechanisms that they considered included fossil anisotropy associated with formation of the Proterozoic Arabian lithosphere and modern mineral alignment caused by asthenospheric flow associated with the present northward motion of the Arabian Shield or with an Ethiopian mantle plume.

Generally, this study suggests that the observed splitting parameters are the result of a complex interaction of mantle flow in the asthenosphere. Shear caused by the absolute plate motion, which is directed approximately 40° east of north at about 22 mm/y (Fig. 18), may affect the alignment of mantle minerals. However, it has also been suggested that flow radiating from the mantle plume beneath Afar is channeled towards the Red Sea Rift (Ebinger and Sleep 1998), which is oriented approximately 30° west of north. Assuming that the strain caused by the plume flow is comparable to that of the plate motion, we can combine these two flow orientations, similar to the vector approach of Silver and Holt (2002). This gives an overall resultant that is oriented with a north-south alignment (Fig. 18). Our preferred interpretation of the slightly more westerly, and Red Sea Rift parallel, fast directions we obtained is the alignment of magma filled

Fig. 14 Forward modeling of velocity and anisotropy structure in the upper mantle from Love and Rayleigh wave group dispersion for the BLJS station. The model shows the final fit to the data and up to 5 % anisotropy ($V_{sv} > V_{sh}$)



cracks that form perpendicular to the least compressive stress direction resulting in rift-parallel fast-polarization directions. This mechanism has been suggested as the dominant cause of anisotropy beneath other rift zones.

Seismic tomography models have shown that the upper mantle beneath the western portion of the Arabian Shield is anomalously slow, with velocities increasing towards the continental interior (Debaille et al. 2001; Benoit et al. 2003). These observations are attributed to thermal differences beneath Saudi Arabia and indicate a much hotter mantle beneath the Red Sea than beneath the interior of the shield, which is consistent with plume flow directed beneath the rift. Surface wave and receiver function analysis shows that there is a change from vertical flow in southwest Saudi Arabia to horizontal flow further north, also consistent with the presence of channelized flow from the mantle plume (Tkalcic et al. 2005). Daradich et al. (2003) demonstrated that the higher elevations along the Red Sea Rift and the overall tilt of the Arabian plate result from viscous stresses associated with large-scale mantle flow from the Afar plume. In addition, Schilling et al. (1992) found isotopic evidence for

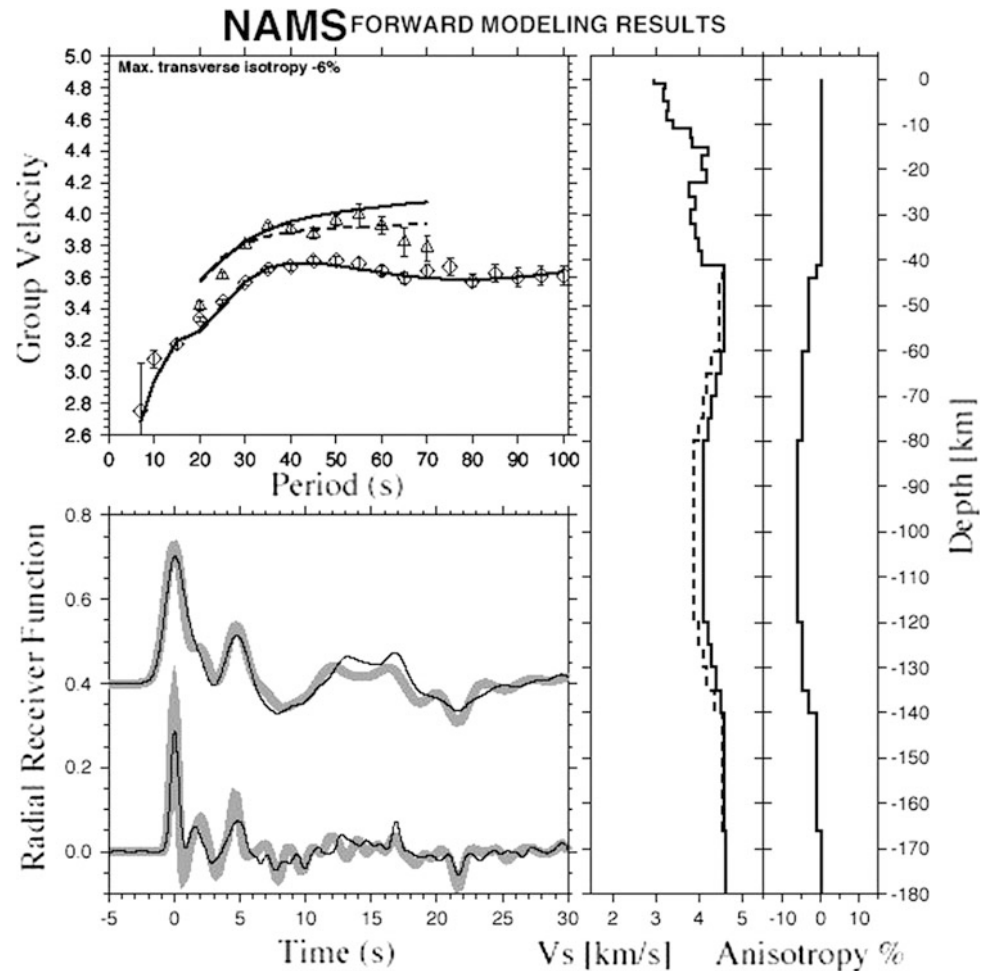
mantle mixing between a depleted asthenosphere and plume flow in Saudi Arabia, supporting the idea that an interaction of flows is occurring at depth. This combination of both plate and density driven flow can explain the observed anisotropic signature and is consistent with an active rifting model.

Discussion and Conclusions

Teleseismic data recorded on broadband instruments from four different seismic arrays were used in this study. The largest array of instruments used is the KACST and SGS seismic networks. To supplement the coverage, we also analyzed data recorded by the eight IRIS-PASSCAL Saudi Arabian Broadband Array stations, which operated from November 1995 to March 1997, RAYN/GSN data, data from two stations deployed in Jordan, and data recorded by two stations in the UAE.

S-waves with high signal-to-noise ratios were selected from earthquakes with magnitudes larger than 5.7 in a distance range of 60° to 85° . Waveforms were first rotated from

Fig. 15 Forward modeling of velocity and anisotropy structure in the upper mantle from love and Rayleigh wave group dispersion for the NAMS station. The model shows the final fit to the data. A broad transverse isotropy coinciding with the low velocity zone in the mantle is required with V_{sv} exceeding V_{sh} by 6 %

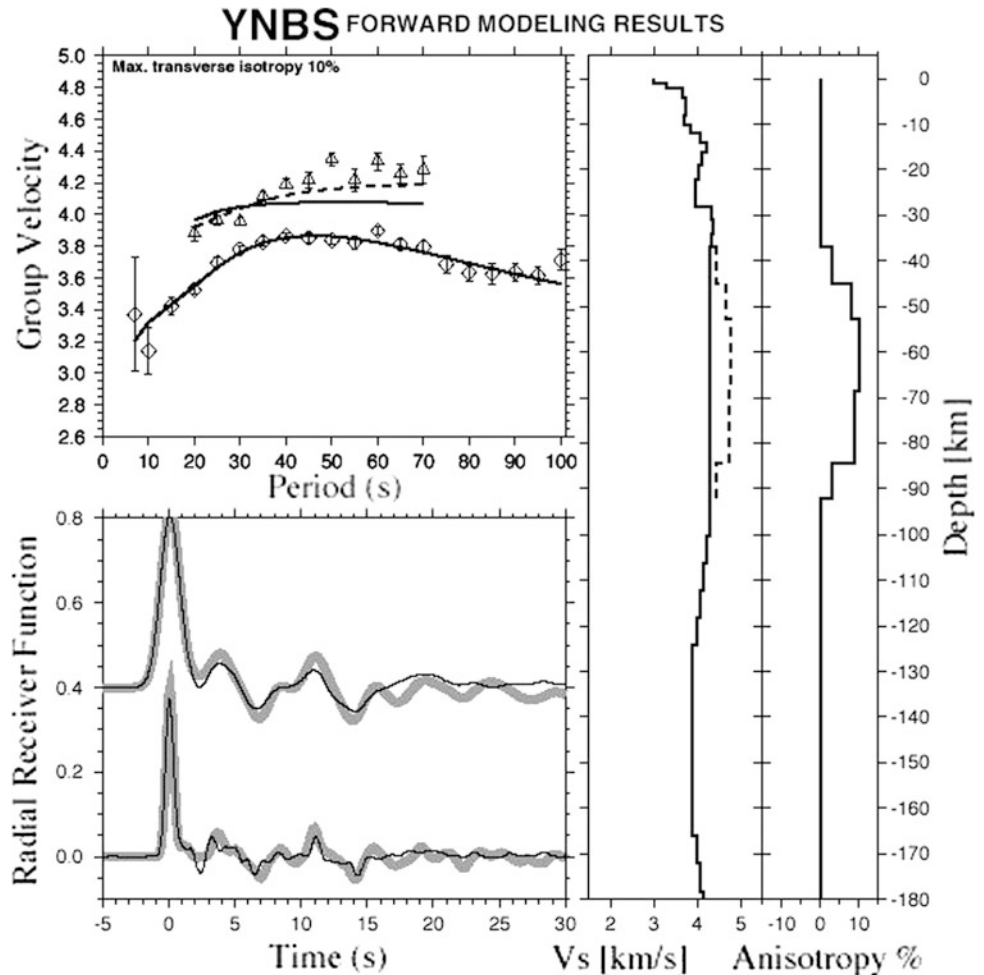


the N-E-Z to the R-T-Z coordinate system using the event's back-azimuth and were visually inspected to pick the S-wave onset. The three-component records were then cut to focus on the section of the waveform that is 100 s prior to the S-wave onset and 20 s after. To more clearly detect Sp conversions, the cut R-T-Z data must be further rotated around the incidence angle into the SH-SV-P coordinate system and deconvolved. This second rotation is critical because if an incorrect incidence angle is used, noise can be significantly enhanced and major converted phases may become undetectable. A subroutine was developed, based on the approach of Sodoudi (2005), which rotates the cut R-T-Z seismograms through a series of incidence angles, from 0° to 90° in 3° increments, to create a set of quasi-SV and quasi-P data. Each quasi-SV component is then deconvolved from the corresponding quasi-P component using *Ligorria and Ammon's* iterative time domain method, which creates an SRF. To make the SRFs directly comparable to PRFs, both the time axes and the amplitudes of the SRFs must be reversed. Using this approach, 31 different SRFs, corresponding to the 31 different incidence angles examined, are created for each event at a given station.

To limit our examination to the true P-SV components and their corresponding receiver function, we found the incidence angle that minimizes the direct S-wave energy on the P-component. On the time-reversed receiver functions, the direct S arrival is at 0 s. Therefore, we are only interested in the receiver function whose mean amplitude is closest to zero at zero time. A second subroutine was developed to examine all the generated receiver functions for a given event and determine which record best meets this criterion. The P-SV components and the corresponding receiver function with the appropriate incidence angle are retained, and the remaining records are discarded.

Once receiver functions were generated for all events at an examined station, a move-out correction was applied to the receiver functions to correct for variations in distance between events. Again, to make the SRFs directly comparable to PRFs, we used a reference slowness of 6.4 s/deg. Each individual receiver function is then visually inspected and compared to previously determined PRFs at the same station to identify the Moho phase. Only SRFs that display a clear Moho conversion at the appropriate time are used for further analysis. These records were then stacked to obtain a

Fig. 16 Forward modeling of velocity and anisotropy structure in the upper mantle from love and Rayleigh wave group dispersion for the YNBS station. The model shows the final fit to the data. A strong transverse isotropy is found (8 % of $V_{sh} > V_{sv}$)



better signal-to-noise ratio for the weaker LAB phase (Lithosphere/Asthenosphere Boundary).

It should be noted that a similar approach to that outlined above was also used to examine SKS arrivals. In this case, we examined earthquakes with magnitudes larger than 5.6 in a distance range from 85° to 120° . However, it was discovered that the SKS arrivals do not generate clear Sp conversions given their steeper angles of incidence. Therefore, further examination of SKS receiver functions was not pursued.

Synthetic receiver functions were generated using the reflectivity method to match the amplitude and timing of both the Moho and LAB conversions on the stacked SRFs. Using the programs "icmod" and "respknt", the responses of an incoming S-wave to different three-layer velocity models were generated. These synthetic responses were then processed using the same approach outlined previously to obtain the synthetic SRFs. The amplitude and timing of the phases on the real and synthetic receiver functions were matched by adjusting the crustal, upper mantle, and lower mantle velocities as well as the depth of the Moho and the

LAB. While these values varied from station to station, the average crustal and upper mantle S-wave velocities needed to fit the Moho amplitude were about 3.6 and 4.5 km/s, respectively. These are similar to the S-wave velocities used to fit the Moho amplitude on the SANDSN PRFs. To fit the LAB amplitude, an average lower mantle velocity of about 4.2 km/s is required. In all cases, a default Poisson's ratio of 0.25 was used.

It should be noted that the average shear velocities and default Poisson's ratio used to generate the synthetics differ from those found by waveform modeling. Rodgers et al. (1999) reported average crustal S-wave velocities of 3.7 and 3.5 km/s and average upper mantle S velocities of 4.3 and 4.55 km/s for the Arabian Shield and Platform, respectively. In addition, the reported Poisson's ratio in the Arabian Shield mantle was 0.29, while in the Platform it was 0.27. Testing revealed that the waveform modeling velocities did not fit the SRF phase amplitudes as well, but the timing of the phases only changed by a few tenths of a second. Therefore, the difference in shear velocities only leads to a few kilometers difference in depth. However, the timing of

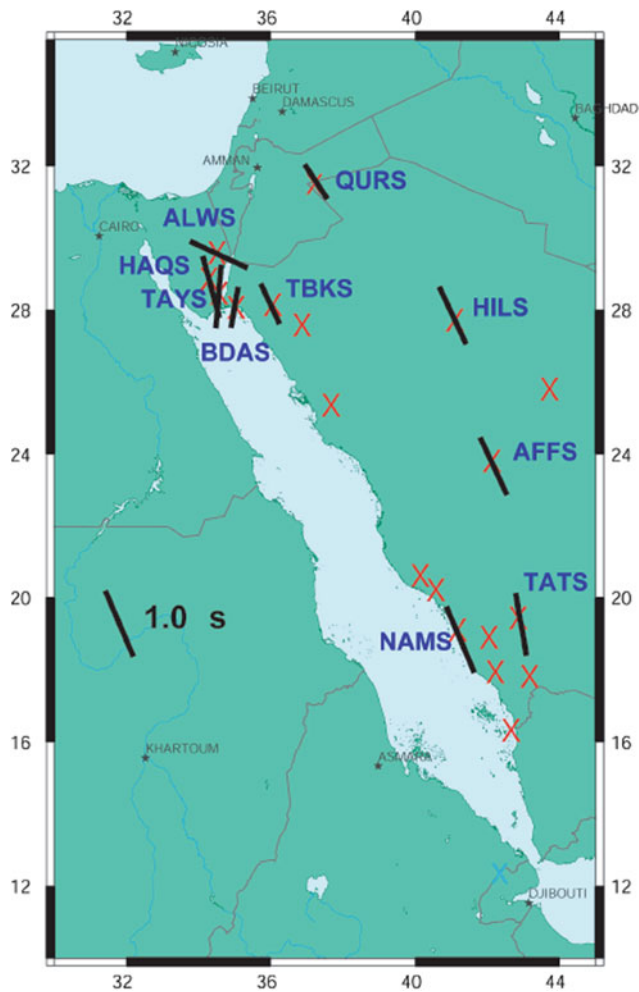


Fig. 17 SKS splitting parameters for several KACST stations. *Red crosses* indicate station locations with too few SKS splitting parameters to determine a meaningful average. The direction of the *black bar* indicates the average direction of fast polarization and its length is scaled by the delay time between the fast and slow waves. Most stations east of the Red Sea Rift show consistent northwesterly fast directions with some complications arising in the vicinity of the Dead Sea

the phase conversions is more dependent on the Poisson's ratio. Larger Poisson's ratios, such as those suggested by the waveform modeling, results in earlier arrivals and hence shallower depths. Several tests were performed to examine how much the Moho and LAB depths changed when using the Shield and Platform Poisson's ratio values. Based on the amount of variation observed, the reported Moho and LAB depths are accurate to within 5 and 10 km, respectively.

Seafloor spreading in the Red Sea is non-uniform, ranging from nearly 0 cm/year in the north to about 2 cm/year in the south. Given the configuration of stations, we focused our examination along profile AA', which extends from the southern Red Sea Rift axis inland to station HASS (Fig. 19). This allowed us to examine the most extensively rifted portion of the lithosphere as well as the structure beneath

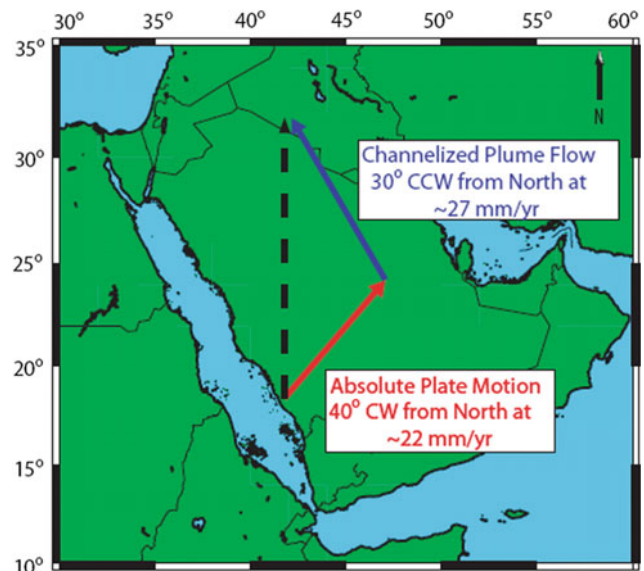


Fig. 18 Vector analysis of plate motion (*red arrow*) coupled with channelized upwelling flow (*blue arrow*) beneath Saudi Arabia. If we estimate that absolute plate motion is oriented N40E at a rate of 22 mm/year and that channelized hotspot flow is oriented approximately N30W, then the rate of hotspot flow needed to obtain a north-south resultant (*black dashed arrow*) is ~ 27 mm/year

both the Arabian Shield and Platform. However, for comparison, we also examined the more northern profile BB', which extends from the northern rift axis across the Arabian Shield to station ARSS.

Similar to profile AA', the Moho and LAB along BB' are shallowest near the Red Sea and become deeper towards the Arabian interior. Near the coast, the Moho is at a depth of about 22–25 km. Crustal thickening continues until an average Moho depth of about 35–40 km is reached beneath the interior Arabian Shield. The LAB near the coast is at a depth of about 55 km; however, it also deepens beneath the Shield to attain a maximum depth of 100–110 km. These boundary depths are comparable to those at similar distances along profile AA' (Hansen et al. 2007).

The lithospheric structure along profile BB' was also tested by comparing its predicted gravity signature to data collected by the GRACE satellites (Fig. 20). The same density values for the Arabian Shield used in the examination of profile AA' were employed. In addition, since profile BB' has fewer stations and therefore fewer constraints, we set the lithospheric thickness beneath the rift axis to be similar to that on profile AA' and examined if the calculated gravity signature is consistent with the recorded data. Small-scale recorded gravity observations can be matched very well by slightly adjusting the Moho and LAB boundaries (within the estimated error). Broad-scale gravity observations are also fitted well by a shallow asthenosphere beneath the Red Sea. These results demonstrate that while

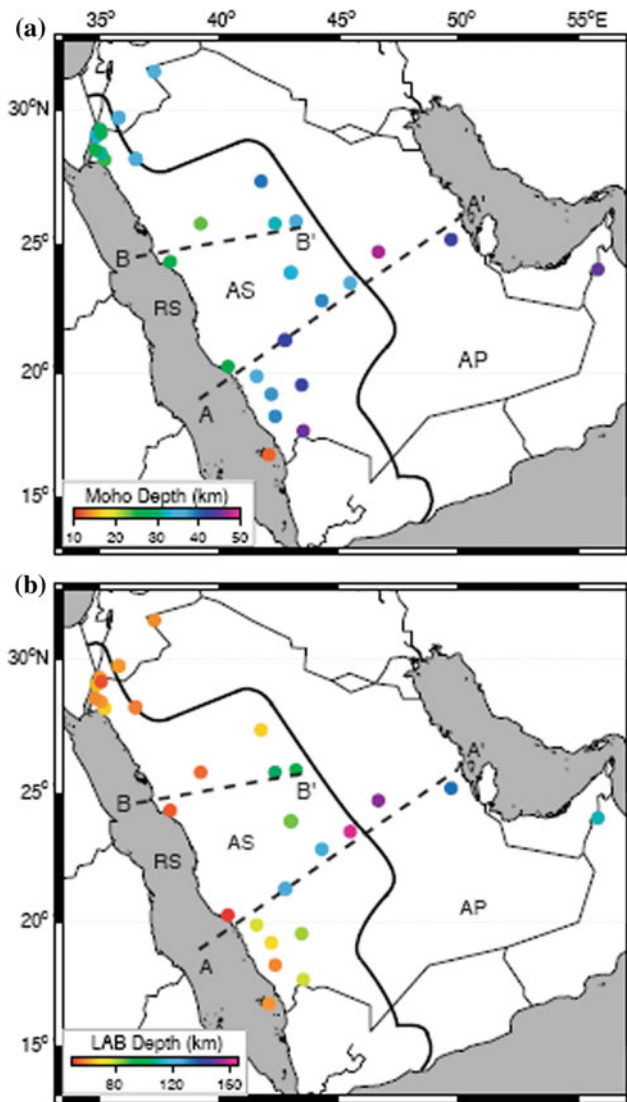


Fig. 19 Maps showing the boundary depths beneath Arabia. The colored circles show the **a** Moho and **b** LAB depths beneath individual stations, where warmer colors indicate shallower depths than cooler colors. The solid line marks the boundary between the Arabian shield (AS) and the Arabian Platform (AP) while the two dashed lines mark the locations of cross-sectional profiles AA' and BB'. The shallow (40–60 km) LAB along the Red Sea coast and Gulf of Aqabah thickens (80–120 km) toward the interior of shield with a step (20–40 km) across the Shield-Platform boundary (Hansen et al. 2007)

seafloor spreading is not as developed in the northern Red Sea, the lithosphere has still been thinned and eroded by rifting processes (Hansen et al. 2007).

Crustal Structures

Al-Amri et al. (2004) performed a grid search using travel time data sets: (a) Pn and Pg, and (b) Pn, Pg, and Sg. In order to select a single velocity model to be representative of the

paths sampled, they made use of the results of a seismic refraction study (El-Isa 1990; Seber et al. 1997). Their grid search results with the thicker crusts (28–30 km) are consistent with these earlier studies. The preferred model has a crustal thickness of 28 km for the Gulf of Aqabah (Table 1).

Earlier work with waveform data from the 1995–1997 Saudi Arabian Broadband Deployment by the University of California, San Diego (UCSD), and King Saud University resulted in models for the Arabian Platform and Arabian Shield (Rodgers et al. 1999). In that study, Love and Rayleigh wave group velocities were modeled to estimate average one-dimensional seismic velocity models of the two main geologic/tectonic provinces of Saudi Arabia. A grid search was used to quickly find a range of models that satisfactorily fit the dispersion data, then this range of models was explored to fit the three-component broadband (10–100 s) waveforms. The resulting models revealed significant differences between the lithospheric structures of the two regions (Tables 2 and 3).

To check the validity of the Arabian Platform model, we measured Rayleigh and Love wave group velocities for a number of regional events from the Zagros Mountains and Turkish-Iranian Plateau. Paths from these events to the SANDSN stations sample the Arabian Platform.

Generally, we would suggest that low velocities beneath the Gulf of Aqabah and southern Arabian Shield and Red Sea at depths below 200 km are related to mantle upwelling and seafloor spreading. Low velocities beneath the northern Arabian Shield below 200 km may be related to volcanism. The low-velocity feature near the eastern edge of the Arabian Shield and western edge of the Arabian Platform could be related to mantle flow effects near the interface of lithosphere of different thickness.

The results for crustal structure are consistent with previous studies, where applicable. New results for the lithosphere suggest that the mantle lithosphere is thin and the LVZ is significant near the Red Sea, where rifting is active. The mantle lid thickens away from the Red Sea in the Arabian interior. Furthermore, our results indicate the presence of polarization anisotropy in the lithospheric upper mantle, in the vicinity as well as farther away from the Red Sea. Our modeling suggests $v_{SV} > v_{SH}$ in the southern part of the Red Sea, consistent with vertical flow, and $v_{SH} > v_{SV}$ in the northern part of the Red Sea and the continental interior, as is commonly reported in the continents. The Moho appears to be gradational, but the crustal thickness does not exceed 40 km, which is consistent with the v_p/v_s analysis and inconsistent with a grid search analysis for receiver functions fits only. The mantle velocities are consistent with stable continental values.

Teleseismic shear-wave splitting along the Red Sea and across Saudi Arabia reveals that the stations in the Gulf of Aqabah display fast orientations that are aligned parallel to

Fig. 20 Topography, gravity signature, and lithospheric structure along cross-sectional profile AA'. **a** Topography along the profile plotted with a 32× vertical exaggeration (V.E.). The sediment thickness is shown by the grey shaded areas.

b Comparison of the observed gravity data from the GRACE satellites (*black dots*) and the calculated gravity (*grey line*) resulting from the structural model shown in **c**. The S-wave velocities (V_s) in km/s and densities (ρ) in g/cm^3 of each layer are listed (Hansen et al. 2007)

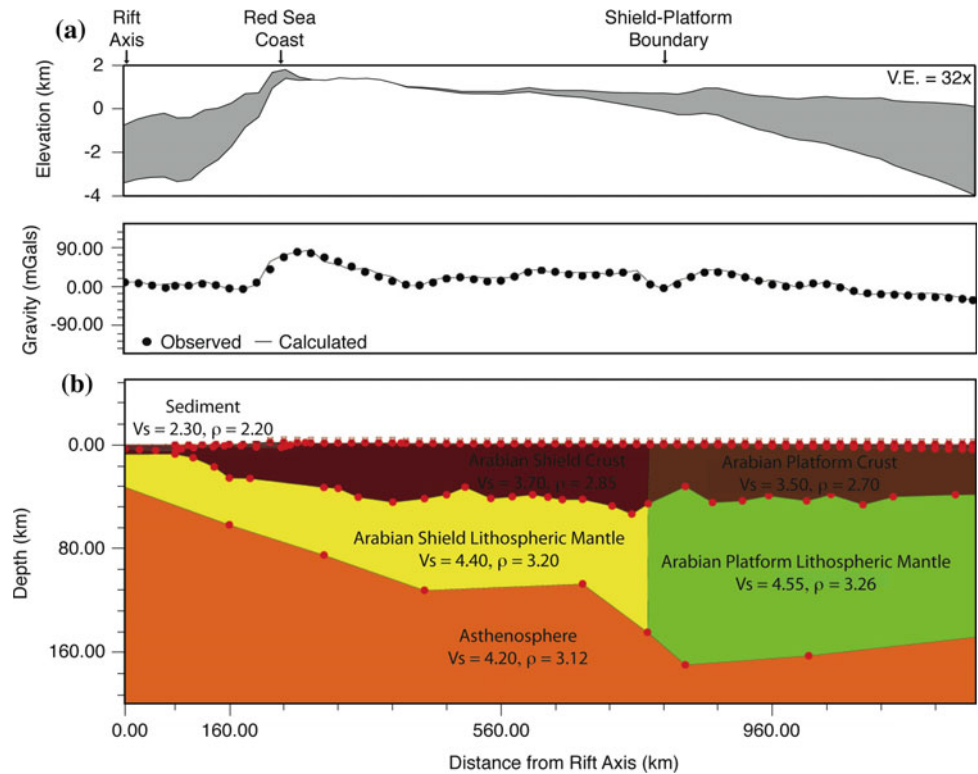


Table 1 Velocity model for the gulf of aqabah/dead sea region (V_P and V_S are the P- and S-wave velocities, respectively)

Depth (km)	Thickness (km)	V_P (km/s)	V_S (km/s)
0	2	4.50	2.60
2	5	5.50	3.18
7	10	6.10	3.52
17	11	6.20	3.60
28	∞	7.80	4.37

Table 2 Velocity model for the Arabian shield region

Depth (km)	Thickness (km)	v_p (km/s)	v_s (km/s)
0	1	4.0	2.31
1	15	6.20	3.58
16	20	6.80	3.93
36	∞	7.90	4.30

Table 3 velocity model for the arabian platform region

Depth (km)	Thickness (km)	v_p (km/s)	v_s (km/s)
0	4	4.00	2.31
4	16	6.20	3.64
20	20	6.4	3.70
40	∞	8.10	4.55

the Dead Sea Transform Fault. However, our observations across Saudi Arabia show a consistent pattern of north-south oriented fast directions with delay times averaging about 1.4 s. While fossilized anisotropy related to the Proterozoic assembly of the Arabian Shield may contribute to our

observations, we feel that the anisotropic signature is best explained by a combination of plate-motion and density driven flow in the asthenosphere. Shear caused by the absolute plate motion, which is directed approximately 40° east of north at about 22 mm/year, may affect the alignment

of mantle minerals. Combining the northeast oriented flow associated with absolute plate motion with the northwest oriented flow associated with the mantle plume beneath Afar generates a north-south oriented resultant that matches our splitting observations.

Acknowledgments The authors would like to express their thanks and gratitude to KACST (Project AR-23-40) and DSFP for funding this work. We would like also to extend our sincerest thanks to Drs. S. Hansen, A. Rodgers, A. Nyblade, H. Tkalci and Y. Park for their valuable support.

References

- Al-Amri AM (1995) Preliminary seismic hazard assessment of the southern Red Sea region. *J Europ earthq Eng* 3:33–38
- Al-Amri AM (1998a) The crustal structure of the western Arabian platform from the spectral analysis of long-period P-wave amplitude ratios. *Tectonophysics* 290:271–283
- Al-Amri AM (1998b) The crustal structure of the western Arabian platform from the spectral analysis of long-period P-wave amplitude ratios. *Tectonophysics* 290:271–283
- Al-Amri AM (1999a) The crustal and upper-mantle structure of the interior Arabian platform. *Geophys J Int* 136:421–430
- Al-Amri AM (1999b) The crustal and upper-mantle structure of the interior Arabian platform. *Geophys J Int* 136:421–430
- Al-Amri MS, Al-Amri AM (1999a) Configuration of the seismographic networks in Saudi Arabia. *Seism Res Lett* 70:322–331
- Al-Amri M, Al-Amri A (1999b) Configuration of the seismographic networks in Saudi Arabia. *Seism Res Lett* 70:322–331
- Al-Amri AM, Schult FR, Bufe CG (1991) Seismicity and aeromagnetic features of the Gulf of Aqabah (Elat) region. *J Geophys Res* 96:20179–20185
- Al-Amri AM, Mellors R, Vernon F (1999) Broadband seismic noise characteristics of the Arabian shield. *Arab J Sci Eng* 24(2A):99–113
- Al-Amri A, Rodgers A, Alkhalifah T (2004) Improving seismic hazard assessment in Saudi Arabia using earthquake location and magnitude calibration. In: *Proceedings of the third symposium on scientific research and technological development outlook in the Arab world*. Riyadh, Saudi Arabia
- Al-Damegh K, Sandvol E, Al-Lazki A, Barazangi M (2004) Regional seismic wave propagation (Lg and Sn) and Pn attenuation in the Arabian Plate and surrounding regions. *Geophys J Int* 157:775–795
- Al-Damegh K, Sandvol E, Barazangi M (2005) Crustal structure of the Arabian plate: new constraints from the analysis of teleseismic receiver functions. *Earth Planet Sci Lett* 231:177–196
- Ammon CJ (1991) The isolation of receiver effects from teleseismic P waveforms. *Bull Seism Soc Am* 81:2504–2510
- Badri M (1991) Crustal structure of central Saudi Arabia determined from seismic refraction profiling. *Tectonophysics* 185:357–374
- Ben-Menahem A (1979) Earthquake catalogue for the Middle East (92 BC–1980 AD). *Boll Geofisica Teor Appl* 21:245–310
- Benoit M, Nyblade A, VanDecar J, Gurrrola H (2003) Upper mantle P wave velocity structure and transition zone thickness beneath the Arabian shield. *Geophys Res Lett* 80. doi:10.1029/2002GL016436
- Bohannon RG, Naeser CW, Schmidt DL, Zimmerman RA (1989) The timing of uplift, and rifting peripheral to the Red Sea: a case for passive rifting? *J Geophys Res* 94:1683–1701
- Camp VE, Roobol MJ (1992) Upwelling asthenosphere beneath western Arabia and its regional implications. *J Geophys Res* 97:15255–15271
- Daradich A, Mitrovica J, Pysklywec R, Willett S, Forte A (2003) Mantle flow, dynamic topography, and rift-flank uplift of Arabia. *Geology* 31:901–904
- Debayle E, Lévêque JJ, Cara M (2001) Seismic evidence for a deeply rooted low-velocity anomaly in the upper mantle beneath the northeastern Afro/Arabian continent. *Earth Plan Sci Lett* 193:423–436
- Ebinger C, Sleep N (1998) Cenozoic magmatism throughout east Africa resulting from impact of a single plume. *Nature* 395:788–791
- El-Isa ZH (1990) Lithospheric structure of the Jordan-Dead Sea transform from earthquake data. *Tectonophysics* 180:29–36
- Evans JR, Achauer U (1993) Teleseismic velocity tomography using the ACH-method: theory and application to continental scale studies. *Seismic tomography: theory and practice*. Chapman and Hall, London, pp 319–360
- Gao S, Davis P, Liu H, Slack P, Rigor A, Zorin Y, Mordvinova V, Kozhevnikov V, Logatchev N (1997) SKS splitting beneath continental rift zones. *J Geophys Res* 102:22781–22797
- Gettings M, Blank H, Mooney W, Healey J (1986) Crustal structure of southwestern Saudi Arabia. *J Geophys Res* 91:6491–6512
- Hansen S, Schwartz S, Al-Amri A, Rodgers A (2006) Combined plate motion and density-driven flow in the asthenosphere beneath Saudi Arabia: Evidence from shear-wave splitting and seismic anisotropy. *Geology* 34(10):869–872
- Hansen S, Rodgers A, Schwartz S, Al-Amri A (2007) Imaging ruptured lithosphere beneath the Red Sea and Arabian Peninsula. Accepted for publication in *earth and planetary science letter*
- Jackson J, Fitch T (1981) Basement faulting and the focal depths of the larger earthquakes in the Zagros mountains (Iran). *Geophys J R Astron Soc* 64:561–586
- Julia J, Ammon CJ, Herrmann RB, Correig AM (2000) Joint inversion of receiver function and surface wave dispersion observations. *Geophys J Int* 143:99–112
- Julia J, Ammon CJ, Herrmann RB (2003) Lithospheric structure of the Arabian Shield from the joint inversion of receiver functions and surface-wave group velocities. *Tectonophysics* 371:1–21
- Karato SI (1998) Seismic anisotropy in the deep mantle, boundary layers and the geometry of mantle convection. *Pure Appl Geophys* 151:565–587
- Kennett B, Engdahl ER (1991) Travel times for global earthquake location and phase identification. *Geophys J Int* 105:429–465
- Langston CA (1979) Structure under mount rainier, Washington, inferred from teleseismic body waves. *J Geophys Res* 84:4749–4762
- Levin V, Park J (2000) Shear zones in the proterozoic lithosphere of the Arabian shield and the nature of the Hales discontinuity. *Tectonophysics* 323:131–148
- Levin V, Henza A, Park J, Rodgers A (2006) Texture of mantle lithosphere along the dead sea rift: recently imposed or inherited? *Phys Earth Planet Inter* (in press)
- Mechie J, Prodehl C, Koptschalitsch G (1986) Ray path interpretation of the crustal structure beneath Saudi Arabia. *Tectonophysics* 131:333–351
- Mellors RJ, Camp VE, Vernon FL, Al-Amri AMS, Gharib A (1999) Regional waveform propagation in the Arabian Peninsula. *J Geophys Res* 104:20221–20235
- Menke W, Levin V (2002) Anomalous seaward dip of the lithosphere-asthenosphere boundary beneath northeastern USA detected using differential-array measurements of Rayleigh waves. *Geophys J Int* 149:414–422
- Mokhtar T, Al-Saeed M (1994) Shear wave velocity structures of the Arabian Peninsula. *Tectonophysics* 230:105–125
- Mooney W, Gettings M, Blank H, Healy J (1985) Saudi Arabian seismic refraction profile: a travelttime interpretation of crustal and upper mantle structure. *Tectonophysics* 111:173–246

- Owens TJ, ZandL G, Taylor SR (1984) Seismic evidence for ancient rift beneath the Cumberland plateau, Tennessee: a detailed analysis of broadband teleseismic P waveforms. *J Geophys Res* 89:7783–7795
- Park Y, Nyblade A, Rodgers A, Al-Amri A (2005) Tomographic imaging of upper mantle P-and S-wave velocity heterogeneity beneath the arabian peninsula. UCRL-TR-214906
- Randall G (1994) Efficient calculation of complete differential seismograms for laterally homogeneous earth models. *Geophys J Int* 118:245–254
- Rodgers A, Schwartz SY (1998) Lithospheric structure of the Qiangtang Terrane, northern Tibetan Plateau, from complete waveform modeling: evidence for partial melt. *J Geophys Res* 103:7137–7152
- Rodgers A, Walter W, Mellors R, Al-Amri A, Zhang Y (1999) Lithospheric structure of the Arabian shield and platform from complete regional waveform modeling and surface wave group velocities. *Geophys J Int* 138:871–878
- Rodgers AJ, Harris D, Ruppert S, Lewis JP, O’Boyle J, Pasyanos M, Fandi Abdallah AQ, Al-Yazjeen T, Al-Gazo A (2003) A broadband seismic deployment in Jordan. *Seism Res Lett* 74:374–381
- Rodgers A, Tkalcic A, Nyblade A, Park A, Schwartz S, Hansen S (2005) Upper mantle structure beneath the Arabian Shield and Red Sea. Unpublished report, LLNL
- Sandvol E, Ni J, Ozalaybey S, Schlue J (1992) Shear-wave splitting in the rio grande rift. *Geophys Res Lett* 19:2337–2340
- Sandvol E, Seber D, Barazangi M, Vernon F, Mellors R, Al-Amri A (1998a) Lithospheric seismic velocity discontinuities beneath the Arabian shield. *Geophys Res Lett* 25:2873–2876
- Sandvol E, Seber D, Calvert A, Barazangi M (1998b) Grid search modeling of receiver functions: implications for crustal structure in the Middle East and North Africa. *J Geophys Res* 103:26899–26917
- Savage MK, Silver PG, Meyer RP (1990) Observations of teleseismic shear wave splitting in the Basin and range from portable and permanent stations. *Geophys Res Lett* 17:21–24
- Schilling J, Kingsley R, Hanan B, McCully B (1992) Nd-Sr-Pb isotopic variations along the Gulf of Aden: evidence for Afar mantle plume—continental lithosphere interaction. *J Geophys Res* 97:10927–10966
- Schmid C, van der Lee S, Giardini D (2004) Delay times and shear wave splitting in the Mediterranean region. *Geophys J Int* 159:275–290
- Schmidt DL, Hadley DG, Stoeser DB (1979) Late Proterozoic crustal history of the Arabian Shield, southern NaJd province, Kingdom of Saudi Arabia, evolution and mineralization of the Arabian-Nubian Shield. *IAG Bull* 3:41–58
- Schwartz SY, Rodgers A, Russell S (2000) Crustal and upper mantle structure beneath northeast Africa and the Red Sea Rift Zone. In: Ryerson FJ, Cook KH, Tweed J (eds) Institute of geophysics and planetary physics, annual report. Lawrence Livermore National Laboratory
- Seber D, Mitchell B (1992) Attenuation of surface waves across the Arabian Peninsula. *Tectonophysics* 204:137–150
- Seber D, Vallve M, Sandvol E, Steer D, Barazangi M (1997) Middle east tectonics: applications of geographical information systems (GIS). *GSA Today* 1–5
- Silver P, Holt W (2002) The mantle flow field beneath Western North America. *Science* 295:1054–1057
- Sodoudi F (2005) Lithospheric structure of the Aegean obtained from P and S receiver functions. Ph.D. Thesis, Freie Universitat Berlin
- Stoeser D, Camp V (1985) Pan-African microplate accretion of the Arabian shield. *Geol Soc Am Bull* 96:817–826
- Thurber CH (1983) Earthquake locations and three-dimensional crustal structure in the Coyote Lake area, central California. *J Geophys Res* 88:8226–8236
- Tkalcic H, Pasyanos M, Rodgers A, Gok R, Walter W, Al-Amri A (2005) A multi-step approach in joint modeling of surface wave dispersion and teleseismic receiver functions: Implications for lithospheric structure of the Arabian Peninsula, UCRL-TR-214906
- VanDecar JC (1991) Upper mantle structure of the Cascadia subduction zone from non-linear teleseismic travel time inversion, Ph.D. thesis, Univ. of Wash., Seattle
- VanDecar JC, Crossen RS (1990) Determination of teleseismic relative phase arrival times using multi-channel cross-correlation and least-squares. *Bull Seismol Soc Am* 80:150–161
- Vernon F, Berger J (1997) Broadband seismic characterization of the Arabian Shield, Final Scientific Technical Report, Department of Energy Contract No. F 19628-95-K-0015, 36 pp
- Vernon F, Mellors R, Berger J, Edelman A, Al-Amri A, Zollweg J, Wolfe C (1996) Observations from regional and teleseismic earthquakes recorded by a deployment of broadband seismometers in the Saudi Arabian shield. *EOS Trans AGU* 77(46):478
- Wolfe CJ, Vernon FL, Al-Amri A (1999) Shear-wave splitting across western Saudi Arabia: The pattern of mantle anisotropy at a Proterozoic shield. *Geophys Res Lett* 26:779–782

Part II
Reservoirs, Conduits and Fluids

Architectural and Hydraulic Characteristics of Fault Zones in the Mesozoic Carbonate Formations of Central and Eastern Saudi Arabia

Mohamed Al Mahmoud

Abstract

Reservoir pressure data in central and eastern Saudi Arabia reveals the presence of two normally-pressured (NPR 1 and NPR 2) and two overpressured (OPR 1 and OPR 2) regimes. The NPR 1 comprises the sequence from the Saq through the lower Jilh Formations, from outcrops to 15,000 ft below ground. The NPR 2 comprises the sequence from the upper Jilh through the Dammam Formations and extends from outcrops to 14,000 ft. The OPR 1 comprises the sequence from the Saq through the Khuff Formations at depths from 12,000 to 19,000 ft. Overpressures in the OPR1 are a result of reduced porosity and permeability, and gas generation from the Qusaiba shale. The OPR 2 comprises the lower Jilh Formation at depths between 10,000 and 13,000 ft. Compaction and/or hydrocarbon charging from the Qusaiba shale could be the reason for overpressures in the OPR 2. The NPR 1, NPR 2, and OPR 1 are divided into pressure systems by stratigraphic seals, but these are locally breached by unconformities or faults forming local anomalies. Geothermal gradients illustrate shallow and deep thermal regimes (STR and DTR) separated by a high thermal conductivity zone (HTCZ). The STR extends from land surface to 8000 ft, with low and high gradients in the up-dip and down-dip areas, respectively. The DTR extends from 10,000 to 19,000 ft, with no differences in gradients between the up-dip and down-dip areas. The HTCZ lies between 8000 and 10,000 ft, with low gradients.

Keywords

Pressure regimes • Arabian Basin • Saudi Arabia

Introduction

The subsurface fluid environments are characterized by measurable physical and chemical properties such as fluid pressures, temperatures, and chemical composition. Characterization of these properties can provide useful concepts in the exploration and development of oil, gas, and water resources. For example, characterization of fluid pressures or compositions in a sedimentary sequence leads to identifying

communication and/or compartmentalization of reservoirs and aquifers which is important information for decisions related to drilling of exploration and development wells.

Oil and gas exploration, along with water well drilling in central and eastern Saudi Arabia (Fig. 1) since the 1930s, has resulted in a wealth of data on the subsurface rock and fluid properties. Fluid pressure, temperature, water salinity, hydrocarbon source rocks, reservoirs, and seals are some of the important data collected from the deep and shallow well drilling. Oil and gas wells provided data on reservoir pressures, temperatures and water salinity in both shallow and deep reservoirs. However, such data is conventionally used to characterize reservoirs at depths greater than 6000 ft and only at an oilfield scale. Data from water wells are normally used to study aquifers at regional scales. Studies of Saudi

The full citation and reference to the original article published in AJGS.

M. Al Mahmoud (✉)
Dhahran Geological Consulting, Dhahran, Saudi Arabia
e-mail: al_mahmoudmj@yahoo.com

© Springer International Publishing AG 2017

F. Roure et al. (eds.), *Lithosphere Dynamics and Sedimentary Basins of the Arabian Plate and Surrounding Areas*, Frontiers in Earth Sciences, DOI 10.1007/978-3-319-44726-1_2



Fig. 1 Regional geological map of central and eastern Saudi Arabia

Arabian aquifers provided regional hydraulic head, salinity and water temperature maps for most of the major aquifers from ground surface to depths of about 6000 ft (MAW 1984).

The present study utilizes all available fluid and geologic data from shallow and deep wells to define and characterize the thermal and pressure regimes and systems in central and eastern Saudi Arabia for the first time. It also provides an original insight to the factors that controlled the evolution of the subsurface pressures and temperatures in central and eastern Saudi Arabia.

The subsurface fluid pressures can be characterized in terms of their distribution on the stratigraphic sequence in which they exist. The patterns of pressure distribution are commonly referred to as pressure regimes, systems, or compartments. These terms have been used inconsistently in the literature (e.g. Law and Spencer 1998; Swarbrick and Osborne 1998). In this paper, they are used as defined below:

A *pressure regime* includes a stratigraphic sequence that constitutes one fluid environment of either normal pressure or overpressure and which is **completely** separated from other regimes by a competent stratigraphic seal at the basin scale.

A *pressure system* is a subclass of the pressure regime; it includes a reservoir or group of reservoirs contained between two stratigraphic seals within a pressure regime, but these

seals are locally breached and the pressure systems are locally in hydraulic communication with each other. The pressure system should have a pressure range that can be segregated in pressure/depth plots from pressure ranges for other systems in the same pressure regime.

A *pressure compartment* is a block of a single-reservoir pressure system which is characterized by one pressure/depth gradient and is separated from other blocks by a permeability barrier such as a fault or lateral change in lithofacies.

This classification of subsurface pressures is totally based on observations of the present-day pressure patterns which, likely, could have not been persistent throughout geologic time. Therefore, the classification presented here represents only the present-day status of the cumulative evolution of subsurface pressures.

The rate of increase in temperature with depth below land surface is referred to as the geothermal gradient. The global model for geothermal gradients excludes the shallow zone from land surface to an approximate depth of 100 ft where geothermal gradient is highly affected by the diurnal and seasonal changes in air temperature. Below this zone, the geothermal gradient averages 1 °C (1.8 °F) for every 100 ft (Walton 1970; Ward, 1975; Freeze and Cherry 1979; Todd 1980). This geothermal gradient could change from one area

to another due to variations in subsurface heat transfer. On a global scale, the geothermal gradients evolve as a result of the flow of heat from the deep layers of the earth towards its surface. Heat is transferred from deeper layers of the earth by conduction through the rock material and by convection through the fluids contained in the rocks with the conduction being the dominant mechanism (Freeze and Cherry 1979).

The heat capacity of water is more than four times that of the average matrix component of sedimentary rocks (Deming 1994). Therefore, regional heat transfer in sedimentary basins is profoundly affected by the groundwater flow in aquifers (Majorowicz 1987). Field studies (e.g. Majorowicz and Jessop 1981; Chapman et al. 1981) and theoretical studies (e.g. Hitchon 1984; Luheshi and Jackson 1986; Person and Garven 1989) have revealed that moving fluids are capable of transferring a large amount of heat over long distances which can cause significant disturbance in the thermal regimes of sedimentary basins. The general pattern of heat distribution in sedimentary basins constituting regional aquifers is that the heat dissipates in the up streams of aquifers by the flow of relatively cold groundwater from recharge areas, and increases in the down streams of aquifers towards discharge areas (Diao et al. 2004). This pattern could be locally disturbed by cross-flow between deep and shallow aquifers. Therefore, heat may increase above normal in relatively shallow aquifers due to up-ward flow of hotter water from deep aquifers or vice versa. From this perspective, the coupling between groundwater flow and heat transfer emphasizes the significance of utilizing groundwater flow indicators such as water pressure and salinity data in defining and characterizing thermal regimes in sedimentary basins and explaining anomalies in such regimes.

Stratigraphic Setting

Lithostratigraphic Sequences

The Phanerozoic sedimentary sequence of Saudi Arabia consists of more than 25,000 ft of sandstone and carbonate rock units with subordinate shale and anhydrite ranging in age from Cambrian to Recent (Powers et al. 1966). The Paleozoic formations generally consist of siliciclastic units, whereas the Mesozoic and Cenozoic formations consist mainly of carbonate and anhydrite, with minor shale and sandstone units in the Middle Cretaceous (Fig. 2). The lithological characteristics of the Phanerozoic sequence are relatively consistent throughout central and eastern Saudi Arabia. The outcrops of the Phanerozoic rock units make curved belts flanking the eastern margin of the Arabian Shield (Fig. 1). In the subsurface, all Phanerozoic formations generally dip at 1°–2° towards the northeast, east and

southeast following the Arabian Shield basement rocks' configuration.

The Paleozoic rocks consist mainly of a massive sequence of continental to shallow marine siliciclastics transgressing to carbonates (Khuff Formation) towards the Mid-Late Permian (Fig. 2). The total thickness of this sequence ranges from approximately 8000 ft in the basinal areas to about 2000 ft on the uplifted areas where significant erosion occurred (Pollastro 2003). The sandstone units have relatively high porosity and permeability on the western areas near the outcrops forming prolific regional aquifers. Towards deeper areas in the east, the porosity and permeability decrease due to compaction and further deteriorate due to quartz cement and diagenetic illite formation (Carney et al. 2002; Franks and Zwingmann 2010; Arouri et al. 2010). The Paleozoic sandstone units are the primary targets for oil in central Arabia and sweet gas in eastern and northwestern Saudi Arabia. The Paleozoic shale units generally act as regional seals for the underlying sandstone aquifers and hydrocarbon reservoirs (Fig. 2).

The Mesozoic sequence consists in its lower part of the Sudair shale and the Jilh and Minjur carbonates and sandstone. In the middle part, it consists of carbonate units with subordinate shale and anhydrite represented by the sequence from the Marrat through Buwaib Formations. In the upper part, it consists of the sandstone of the Biyadh and Wasia Formations which are capped by the carbonate of the Aruma Formation (Fig. 2). Oil and water wells drilled through the Mesozoic formations show that the carbonate and sandstone units act as regional and sub-regional aquifers and oil reservoirs, whereas the shale and anhydrite units act as regional seals.

The Cenozoic sequence consists mainly of carbonate units with subordinate marl, shale and anhydrite units (Fig. 2). The carbonate units are extremely porous and permeable forming regional prolific aquifers in eastern Saudi Arabia. They also constitute secondary oil reservoirs offshore in the Arabian Gulf. The subordinate marl, shale and anhydrite units act as regional top seals to the underlying carbonate units.

Unconformities

The sedimentary sequence of Saudi Arabia constitutes several regional unconformities of which the most significant and aerially extensive are the Pre-Unayzah, pre-Marrat, pre-Aruma, and pre-Neogene unconformities (Fig. 2). Except for the pre-Marrat unconformity, which was caused by the global marine regression of the Early Jurassic (Haq and Al-Qahtani 2005), all these major unconformities are a result of uplift and erosion during tectonic events. This uplifting had caused differential erosion of the underlying

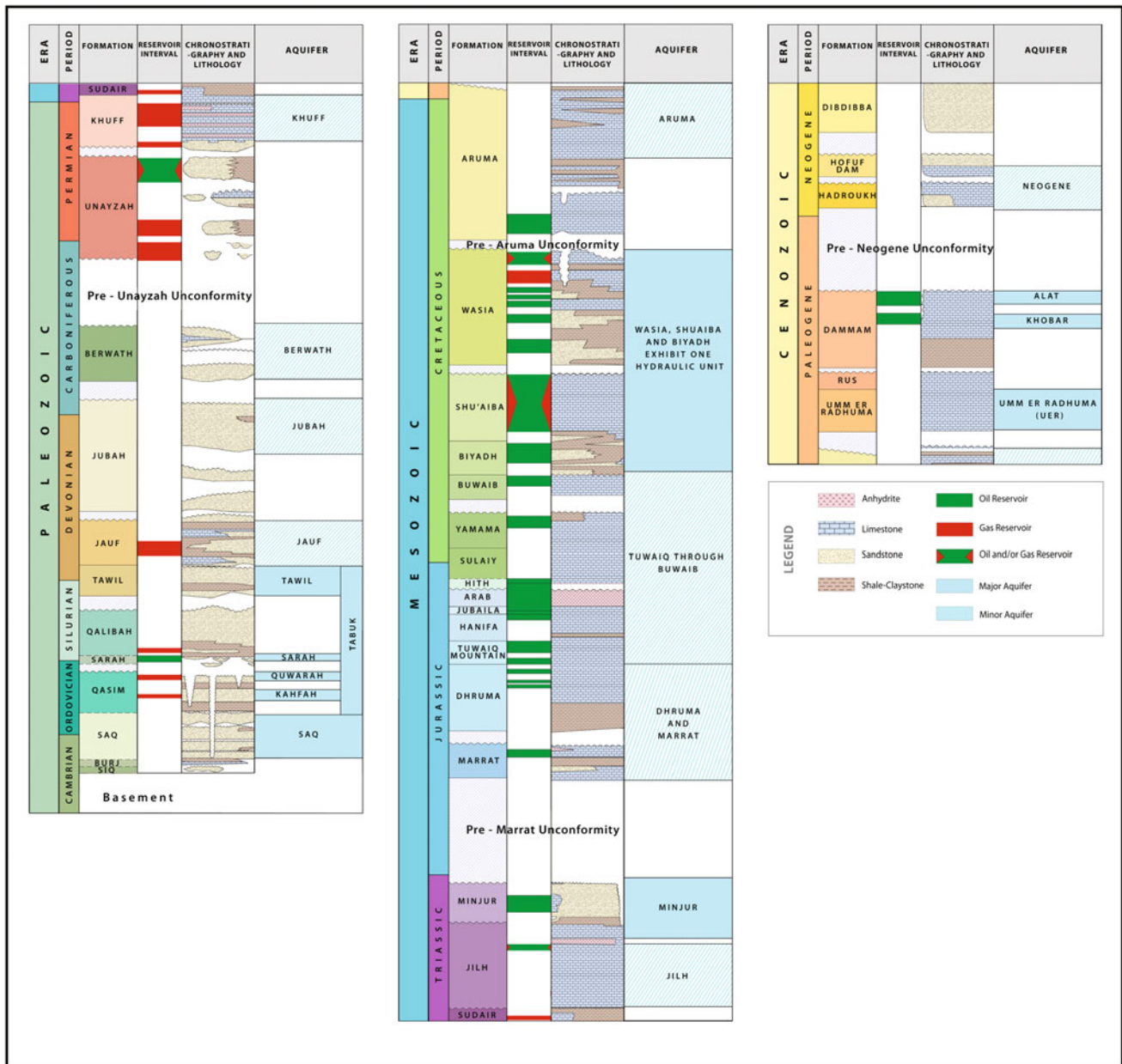


Fig. 2 Stratigraphic column of central and eastern Saudi Arabia showing the oil and gas reservoirs, and major and minor aquifers

rock units with the maximum erosion over major anticlines such as the Ghawar Anticline (e.g. Al-Laboun 1988; McGillivray and Hussein 1992).

The unconformities play important roles in the development of the hydrocarbon and aquifer systems of eastern Saudi Arabia. For example, they form hydrocarbon traps flanks of anticlines such the Jauf gas play on the flanks of the Ghawar anticline (Wender et al. 1998). They also cause cross-formational flow of groundwater in aquifers (BRGM 1977).

Stratigraphic Seals

Geologic data from oil and gas fields and from aquifers provided valuable information on stratigraphic units acting as top seals for hydrocarbon traps and aquifer systems. These seals are mainly shales in the Paleozoic and Cretaceous siliciclastic sequences, anhydrite within the Mesozoic carbonate sequence, and anhydrite, marl, and shale units in the Cenozoic sequence (Fig. 2).

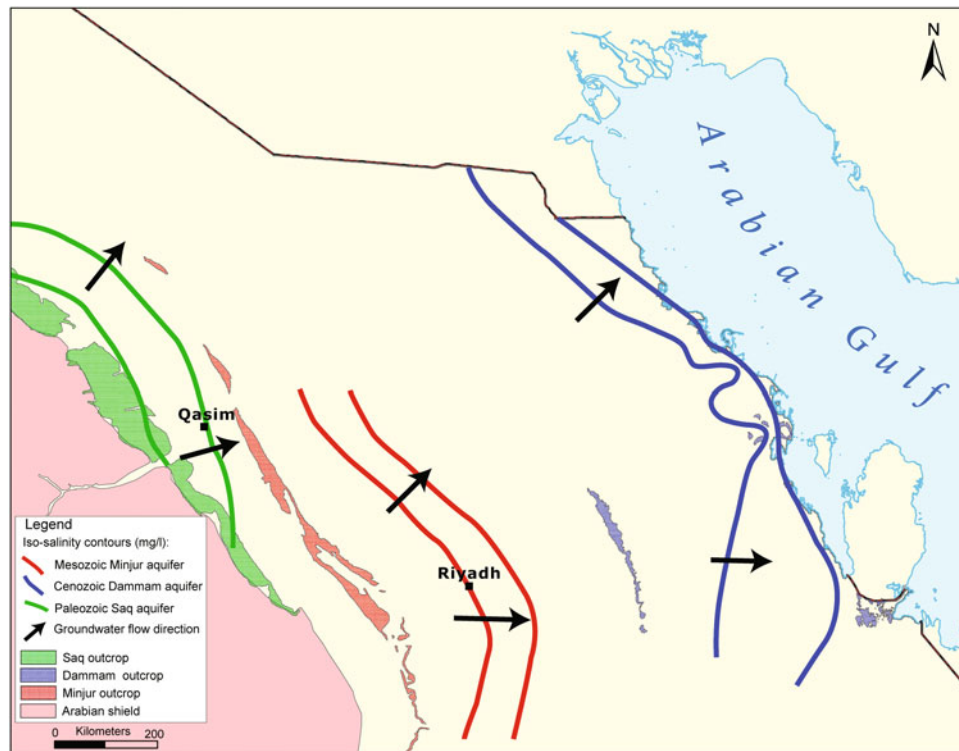


Fig. 3 Regional water salinity and groundwater flow in central and eastern Saudi Arabia (modified after MAW 1984)

In the Paleozoic section, seals include the Ordovician Hanadir and Ra'an shale members of the Qasim Formation, the Silurian Qusaiba shale member of the Qalibah Formation, the Devonian D3B shale unit of the Jauf Formation, and the impermeable lower carbonate unit of the Permian Khuff Formation. These units are known to act as effective top seals for different aquifers near the outcrops (MAW 1984 as well as for the oil and gas reservoirs in central and eastern Saudi Arabia (Konert et al. 2001).

In the Mesozoic section, seals include the Lower Triassic Sudair shale, the Middle Triassic Jilh Dolomite, the anhydrite units of the Arab-D, Arab-C, and Arab-B members of the Jurassic Arab Formation, the Hith Anhydrite, and the Late Cretaceous Lower Aruma Shale. Beside these, other shale and argillaceous carbonate units are known to act as local seals in some oil fields (e.g. Alsharhan and Kendall 1986; MAW 1984).

The regional stratigraphic seals in the Cenozoic sequence are known from hydrogeologic studies of the Tertiary aquifers (e.g. ITALCONSULT 1969; BRGM 1976; BRGM 1977). These seals include the Middle to Upper Paleocene argillaceous carbonate in the lower part of the Umm er Radhuma Formation, the Lower Eocene anhydrite and marls of the Rus Formation, and the Middle Eocene Midra and Saila shale Members of the Dammam Formation as well as

the marl units in the Khobar and Alat Members of the Dammam Formation.

Structural Setting

All formations in central and eastern Arabia dip towards the east and northeast at an angle ranging between 1° and 3° (Powers et al. 1966). This gentle dip is dissected by several major anticlines such as the Ghawar and Khurais which typically extend in a more or less north-south direction. Seismic data show that basement rock faults exist underneath these anticlines. Seismic data show that the vertical displacement on these faults is mainly in the Paleozoic sequence. However, wireline and image logs for some horizontal wells show faults with relatively small vertical displacements (<50 ft) in the Jurassic and Cretaceous formations.

The present day structural elements of central and eastern Saudi Arabia are a result of several tectonic phases through which the central and eastern Saudi Arabia went during the Phanerozoic time (Powers et al. 1966; McGillivray and Husseini 1992; Wender et al. 1998; Al-Husseini 2000). The onset of the basement faults took place in the Late Precambrian when the Arabian Plate was subjected to east-west

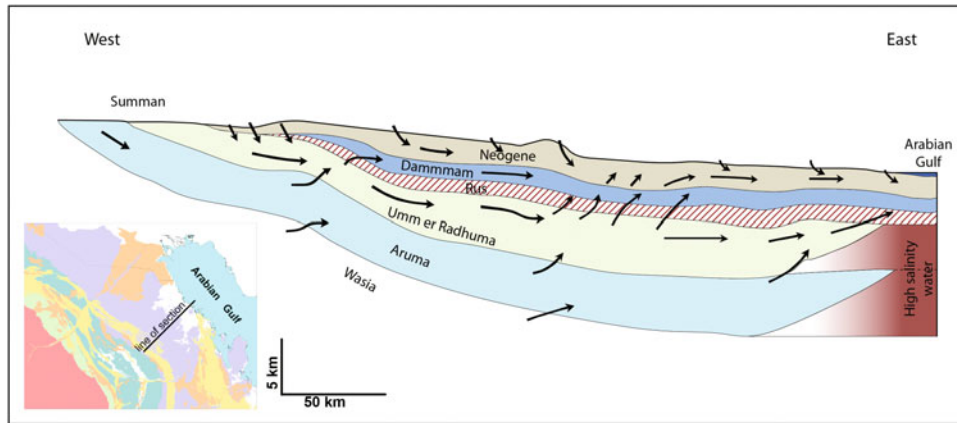


Fig. 4 Regional hydrogeologic cross-section through the Upper Cretaceous and Tertiary aquifers of eastern Saudi Arabia showing the down-dip and cross-formation flow (modified after Bakwicz et al. 1982)

compressive stresses (Al-Husseini 2000). Reactivations of these faults during the alternating tectonic phases of the Phanerozoic resulted in the evolution of anticlines, unconformity surfaces associated with uplifting, and faulting of the overlying sedimentary formations.

Hydrogeologic Setting

The Phanerozoic stratigraphic column of central and eastern Saudi Arabia constitutes 7 major and more than 10 minor aquifers (Fig. 2). Numerous hydrogeologic studies (e.g. Naimi 1965; ITALCONSULT 1969; B.R.G.M. 1976; 1977) covered the Paleozoic aquifers only in central Arabia and the Mesozoic and Cenozoic aquifers in eastern Saudi Arabia. The Paleozoic aquifers are very deep in eastern Saudi Arabia, therefore, they were not targeted by the hydrogeologic studies which focused only on water resources. Aquifer maps from the hydrogeologic studies have shown a general decrease in hydraulic head and an increase in water salinity from the outcrop belt in the west to the deeper areas in the east, following the regional structural dip. This relationship between the regional dip and the hydraulic head and salinity trends indicate that the aquifers are dominated by gravity flow. Figure 3 shows regional trends of groundwater salinity in selected aquifers illustrating the regional flow directions from the outcrops in the west towards the deeper areas in the east. The hydrogeologic studies have also shown that the seals separating the aquifers are generally leaky and the regional groundwater flow is towards the Arabian Gulf (Fig. 4).

Aquifer studies by the Ministry of Agriculture and Water indicate that the meteoric water recharge during the Pleistocene-Holocene at the outcrops has differentially flushed the aquifers (Edgell 1996). It is likely that the differential flushing is due to the spatial variation in aquifer

permeability. The flushing with Pleistocene-Holocene meteoric water has reached to as deep as 7000 ft in the vicinity of the Ghawar field (Stenger et al. 2003). The

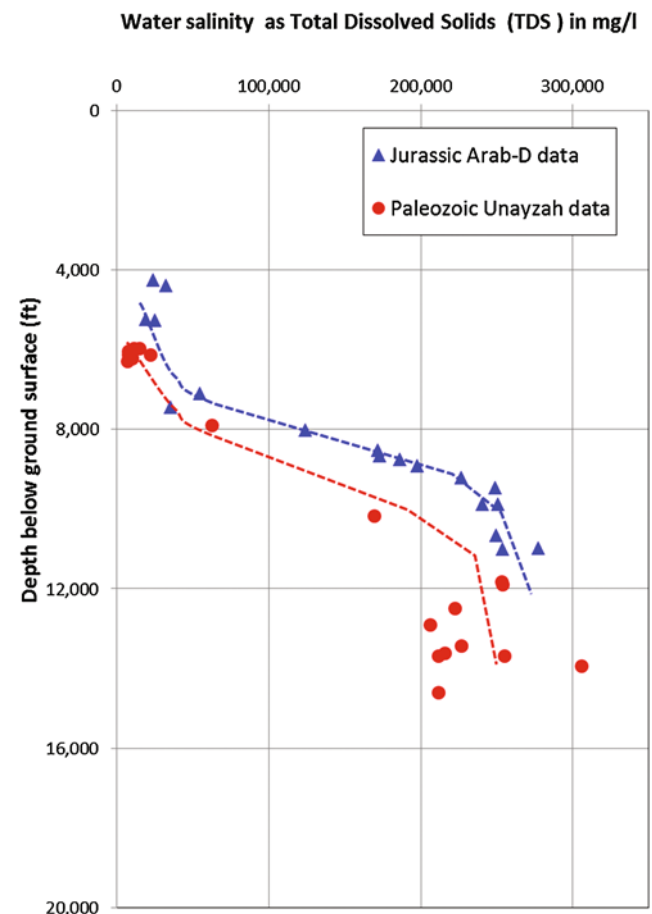


Fig. 5 Groundwater salinity variation with depth in the Arab-D and Unayzah reservoirs of central and eastern Saudi Arabia

salinity data from two aquifers (the Jurassic Arab-D and Paleozoic Unayzah) show that the relatively low salinity water has reached to depths around 8000 ft which suggests that the meteoric water flushing could have reached to that depth (Fig. 5). Below 8000 ft, the water salinity starts to increase sharply to as high as 250,000 mg/l at 10,000 ft. Below 10,000 ft, the salinity does not significantly increase with depth likely because that the formations contain connate water which is super-saturated with salts and not flushed with the meteoric water.

Hydrocarbon Systems

The hydrocarbon province of central and eastern Saudi Arabia constitutes two major petroleum systems; the Paleozoic and Jurassic petroleum systems (Pollastro 2003). Each system includes regionally extensive source rock facies and

multi reservoirs and seals pairs. A relatively minor hydrocarbon system exists in the Triassic lower Jilh Formation (Jenden et al. 2004).

Geochemical studies by Abu-Ali et al. (1991) concluded that the Paleozoic System was sourced primarily from the “hot” shale in the basal Qusaiba Member of the Silurian Qaliba Formation. Basin modeling indicates that the Qusaiba “hot” shale has been generating hydrocarbons since the mid-Cretaceous time (Abu-Ali and Littke 2005). Gas generation from the Qusaiba “hot” shale, which started in the Cretaceous, dominates in eastern Saudi Arabia whereas oil generation is in relatively small areas in central Saudi Arabia (Abu-Ali and Littke 2005). Main reservoirs in the Paleozoic system exist in the sequence above the source rock, specifically in the Khuff, Unayzah, and Jauf Formations (Fig. 2). The regional seal of the Paleozoic system is the Triassic Sudair shale, which completely separates it from the overlying Mesozoic systems (Konert et al. 2001). The Silurian

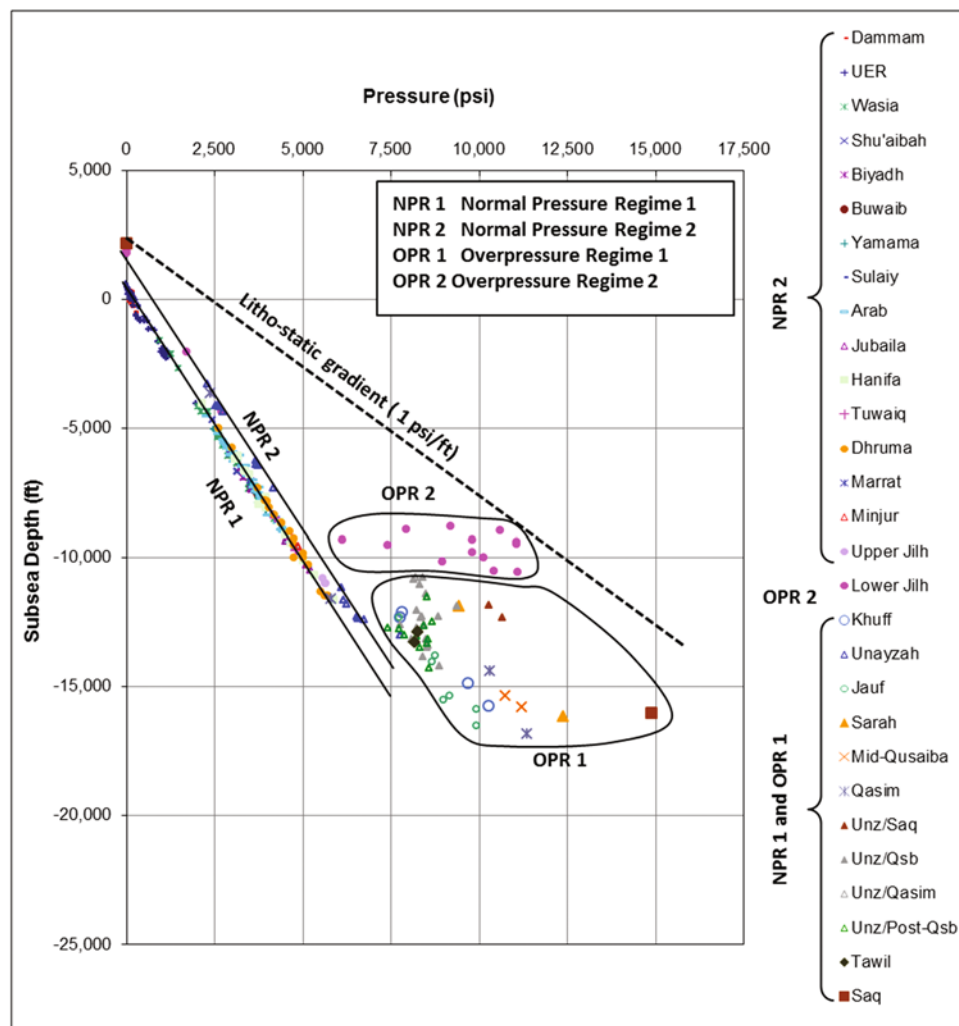


Fig. 6 Pressure/depth plot for all reservoirs in central and eastern Saudi Arabia

Qusaiba “hot” shale forms the main source and ultimate seal to the secondary sub-Qusaiba reservoirs in the Silurian Sarah Formation (Al-Husseini 1991).

The prolific Jurassic oil system of Saudi Arabia constitutes two organic-rich intervals of carbonate mudstones in the Tuwaiq and Hanifa Formations as source rocks (Ayres et al. 1982). Porous carbonate facies forming reservoir units along with anhydrites or argillaceous carbonates forming sealing units exist in the Dhurma, Tuwaiq, Hanifa, Arab, and Hith Formations. The Jurassic reservoirs constitute the main oil producing units in Saudi Arabia. Oil reservoirs also exist in the Cretaceous and Tertiary Formations (Fig. 2), and they are charged mainly from the Jurassic source rocks (Alsharhan and Nairn 1994).

Pressure and Thermal Regimes and Systems

Pressure Regimes and Systems

Pressure and static water level data from more than 220 oil, gas or water wells were used to study the pressure patterns in the sedimentary sequence of central and eastern Saudi Arabia. The static water level data represents pre-production aquifer water levels and are considered as pressures with value of zero at the depth they were measured. The reservoir extrapolated pressure data were obtained from drill-stem test reports. The whole data set covers 25 reservoirs ranging in age from Cambrian to Eocene.

The subsurface fluid pressures in central and eastern Saudi Arabia can be characterized based on the relative magnitudes of pressures and their relationship with their stratigraphic position. The fluid pressures can be classified into pressure regimes, systems, and compartments as defined earlier. Pressure regimes and systems in a basin can be identified and characterized using pressure/depth plots whereas pressure compartments can be identified using either pressure/depth plots or pressure maps.

A regional pressure-depth plot (Fig. 6) allows for classification of 4 pressure regimes named as Normal Pressure Regime 1 (NPR1), Normal Pressure Regime 2 (NPR 2), Overpressure Regime 1 (OPR 1), and Overpressure Regime 2 (OPR 2).

The NPR 1 comprises the sequence from the Cambro-Ordovician Saq Formation through the Lower part of the Triassic Jilh Formation (below the Jilh Dolomite). All reservoirs in this regime are characterized by normal pressures from the outcrops in central Arabia at an average elevation of 2000 ft above sea level to as deep as 13,000 ft below sea level (15,000 ft below ground surface). Within the NPR2, there are slight differences in pressures suggesting the presence of leaky seals between these reservoirs. Al-Aswad and Al-Bassam (1997) reported that the sandstone aquifers within the Paleozoic (NPR 2) are separated from each other by aquitards (leaky shale units). Similar to NPR 1, the identification of the pressure systems within NPR 2 requires an integrated hydrogeologic mapping of the aquifers.

The NPR 2 comprises the stratigraphic sequence from the Triassic Upper Jilh (above the Jilh Dolomite) through the

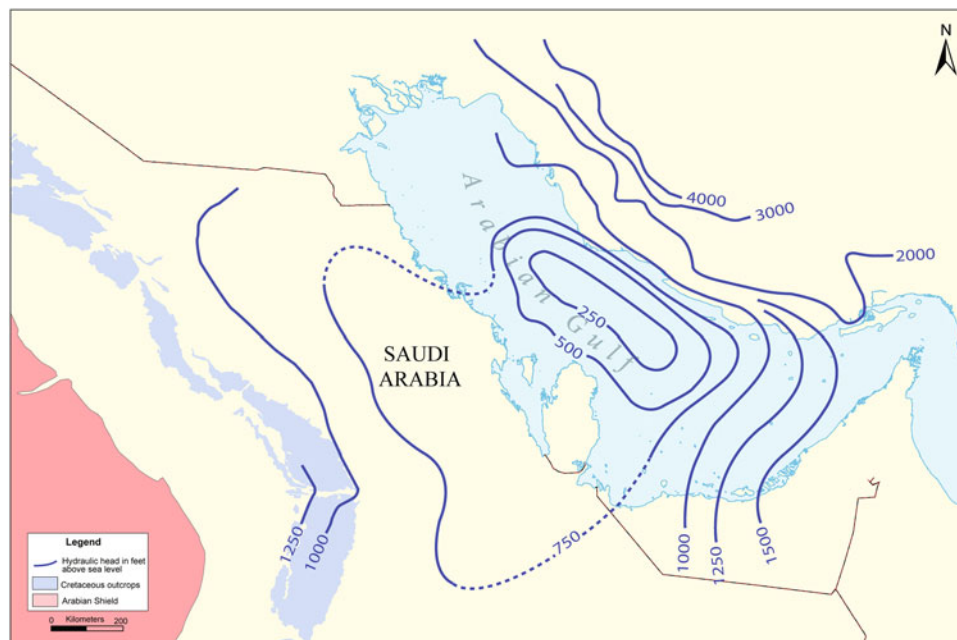


Fig. 7 Regional hydraulic head map of the Cretaceous aquifers (compiled and modified from Pelissier et al. (1980) and Naimi (1965))

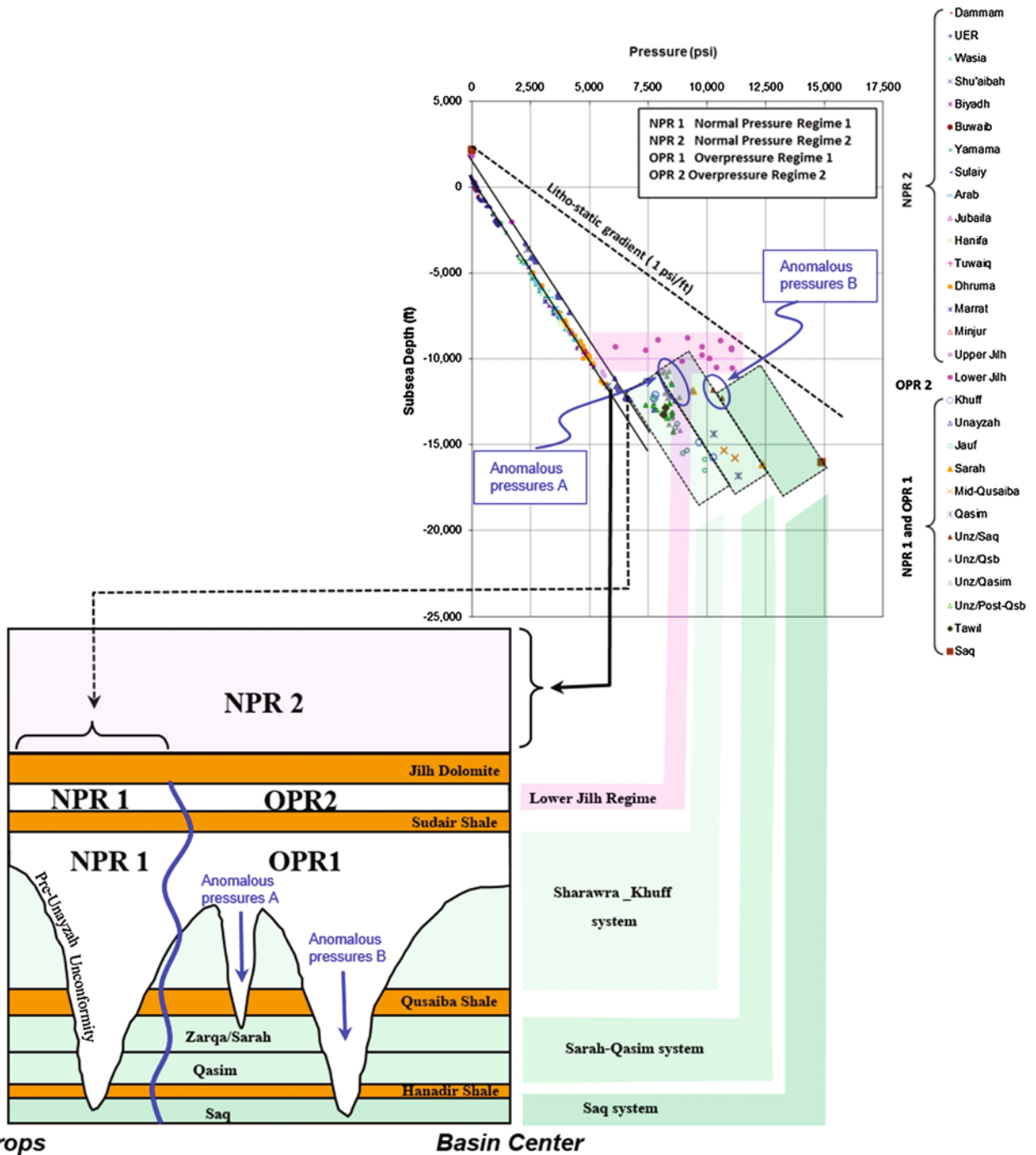


Fig. 8 Pressure/stratigraphy relationship in central and eastern Saudi Arabia

Tertiary Dammam Formation. The linear variation of pressure with depth indicates a normally-pressured sequence from the ground level at an elevation of 2000 ft above sea level to as deep as 12,000 ft below sea level (14,000 ft below ground surface). Geographically, this regime extends from the formation outcrops in central Arabia to the Arabian Gulf in the east. It is likely that this regime also extends into

western Iran as suggested by the potentiometric surface map of the Cretaceous aquifers (Fig. 7). The average pressure gradient of NPR1 is calculated at approximately 0.48 psi/ft. Slight differences in pressure between reservoirs are noticeable in this regime. These differences are due to the presence of leaky seals between the reservoirs as confirmed by several hydrogeologic studies such as ITALCONSULT

(1969), and BRGM (1977). Therefore, the NPR 1 constitutes several pressure systems that can be identified only through an integrated hydrogeological mapping of aquifers in this regime.

NPR 1 and NPR 2 have similar pressure gradients (approximately 0.48 psi/ft), but they are totally separate from each other indicating the presence of a regional stratigraphic seal between the two regimes. From the pressure distribution on the stratigraphic units (Fig. 6), the seal between NPR1 and NPR2 exists in the middle of the Jilh Formation and is likely to be the dense Jilh Dolomite; possibly with some of the underlying shale in the lower Jilh. Both regimes are hydraulically connected to the outcrops and have been continuously recharged with meteoric water since the Pleistocene age (Edgell 1996).

The first overpressure regime (OPR 1) comprises the sequence from the Cambro-Ordovician Saq Formation through the Triassic lower Jilh Formation at depths ranging from approximately 10,000 ft to more than 17,000 ft below sea level (12,000 ft to more than 19,000 ft below land surface). The OPR 1 and NPR 2 overlap with each other in the depth range from 10,000 to 13,000 ft below sea level (12,000–15,000 ft below ground surface). This overlap is attributed to spatial variations in reservoir porosity and permeability in this interval as will be discussed later in this paper.

The substantial differences in pressures within the OPR1 have made it easy to classify it into 3 main pressure systems separated by locally breached seals. These systems are named here the Saq, Sarah-Qasim, and Sharawra-Khuff systems. The seals separating these pressures systems, from bottom up, are the Hanadir and Qusaiba shales. The upper system (Sharawra-Khuff) is separated from the overlying OPR 2 by the 700 ft thick Sudair shale. Seals exist within each pressure system, but due to relatively small differences in pressures, they can only be recognized on oil field and well scales using well test data. The pressure increases from shallower to deeper systems with a pressure range of 1500–2000 psi for each system (Fig. 8). The pressures in all systems are well below the average litho-static gradient of 1 psi/ft (Fig. 6) suggesting that the leakage through the seals between these systems is not due to overpressure-related fracturing. However, this does not exclude the possibility of seal leaking through overpressure-related fracturing in the past if the paleo-pressures had exceeded the litho-static gradient at any geologic time. In areas where the seals are substantially or totally eroded by the Pre-Unayzah unconformity, the Unayzah reservoir of the Sharawra-Khuff system overlies either the Sarah-Qasim system or the Saq system. Pressures in the Unayzah reservoir at these areas become closer to the underlying pressure system

(Anomalous Pressures A and B in Fig. 8). The Unayzah pressures in these areas are considered anomalies in the Sharawra-Khuff pressure system and are associated with anomalies in the reservoir temperatures as will be illustrated later. Due to the absence of local heat generation sources such as igneous intrusions or radioactive mineral concentrations in the Unayzah reservoir, the local high temperature anomalies are considered to be indicators for local fluid communication with deeper systems. Therefore, the Unayzah pressure anomalies, in the areas where the underlying seals are eroded, are a result of high pressure-high temperature water flow from the underlying systems; i.e. the Sarah-Qasim or Saq systems.

Figure 6 shows that the OPR 2 comprises only the lower part of the Triassic Jilh Formation at depths between 8000 ft and 11,000 below sea level (10,000 and 13,000 ft below ground surface). The data for this regime span a wider range of pressures than any other sequence. It is obvious from the pressure/depth relationship that this regime is isolated from both the overlying OPR1 and underlying NPR 2 by strong seals. The OPR 2 is isolated from the underlying OPR 1 by the regionally extending thick Sudair shale. The OPR2 is separated from the overlying NPR 2 by the non-porous extensive Jilh Dolomite, possibly, with some of the shale and anhydrite units at the upper part of the lower Jilh sequence.

Overpressure Generation Mechanisms

Several possible mechanisms have been proposed for the generation of reservoir over-pressures in the subsurface, e.g. the compaction of rapidly deposited sediments, gas generation, and generation of extra-water volumes by mineral transformation such as gypsum to anhydrite (Law and Spencer 1998; Swarbrick and Osborne 1998). In old basins, the dominant mechanism for generating overpressure is the fluid volume expansion resulting from gas generation (Law and Spencer 1998).

Basin modeling by Abu Ali and Littke (2005) indicates that the present-day gas generation window for the Qusaiba source rock in central and eastern Saudi Arabia starts at a depth of about 12,000 ft. It is also interesting that the porosity and permeability of the Paleozoic sandstones are significantly reduced at depths exceeding 12,000 ft due to cementation with quartz overgrowth and illite (Carney et al. 2002; Franks and Zwingmann 2010). This is the same depth at which the OPR 1 starts which indicates that the gas generation aided by the reduced porosity and permeability of the reservoirs are the likely factors involved in generating overpressures in the OPR 1. It is thought that the reduction

of porosity and permeability in the Paleozoic reservoirs acted on retarding the upward gas migration which have resulted in the generation of overpressures at depths below 12,000 ft. NPR 2 is continuous from the ground surface to a depth of approximately 15,000 ft in some areas with an overlap with OPR 2 in the range 12,000–15,000 ft. This overlap is likely related to spatial variations in the reservoir porosity and permeability in the interval between 12,000 and 15,000 ft. In areas where relatively high porosity and permeability exist below 12,000 ft, the upward gas migration is less restricted which prevents the evolution of overpressures. Therefore, the overlap between the NPR 2 and OPR 1 in the interval 12,000–15,000 ft is attributed to lateral variations in reservoir porosity and permeability within this interval.

The OPR 2, in the lower Jilh Formation, shows an extremely wide range of overpressures (Fig. 6) over a small interval of depth which suggests a domination of isolated pockets of overpressured reservoirs. The mixed facies of carbonates, shales, and anhydrites and the quick lateral variations of these facies form a suitable geologic

environment for the development of isolated compartments with wide range of overpressures. Compaction and/or hydrocarbon generation along with the quick facies changes in the lower Jilh Formation could be the main reason for the generation of the overpressures in the lower Jilh Formation.

Spatial Distribution of Overpressures

The wide overlap zone (12,000–15,000 ft) between the NPR 1 and OPR 1 indicates that accurate mapping of the overpressures in the subsurface requires the availability of data with sufficient geographic distribution for all reservoirs in the OPR 1. The limitations of data with the variability in overpressure ranges in the OPR 1 make it difficult to generate pressure distribution maps for the OPR 1. Most of the data available to this study is for the Unayzah reservoir; therefore, it was possible to map the overpressure distribution only for the Unayzah reservoir (Fig. 9).

The Unayzah reservoir pressure generally increases towards the east following the regional dip of the Arabian platform (Fig. 9). Moreover, the pressure gradients vary across faults indicating reservoir compartmentalization by the faults...

As highlighted before, that the presence of relatively high porosity and permeability in the Unayzah Formation within the depth interval 12,000–15,000 ft would make the upward gas migration less restricted which results in preventing the evolution of overpressures in this interval. Therefore, the boundary between OPR 1 and NPR 2 is located down-dip from the top of the gas generation at 12,000 ft (Fig. 9).

Thermal Regimes

Figure 10 shows a plot of Bottom Hole Temperature (BHT) data from wire line logs versus True Vertical Depth at which the temperature was measured. Some data scattering is seen in the temperature/depth plot. Never the less, the data available to this study in its present format is relatively good enough to investigate the general trends in geothermal gradients.

Figure 10 shows that there are two main thermal regimes: a shallow thermal regime (STR) and a deep thermal regime (DTR) in central and eastern Saudi Arabia. STR and DTR are separated from each other by a high thermal conductivity zone (HTCZ) with low geothermal gradient in the depth range between 8000 and 10,000 ft below ground surface. Based on the relative magnitude of temperature in the wells, both thermal regimes are classified into low-temperature wells and high-temperature wells with an overlap zone. The low-temperature wells are located westward and up-dip of

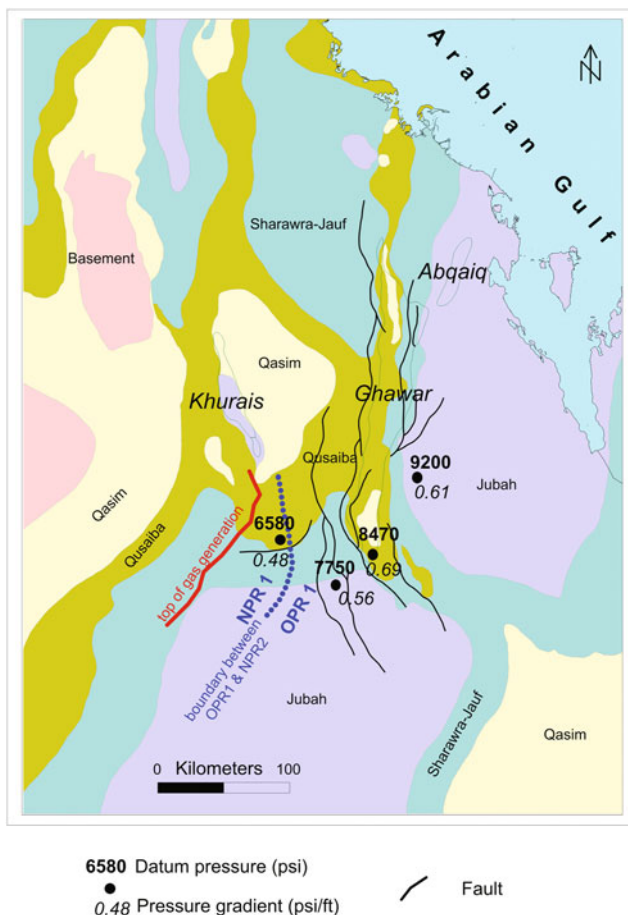


Fig. 9 Unayzah reservoir datum pressures and pressure gradients showing compartmentalization by faults

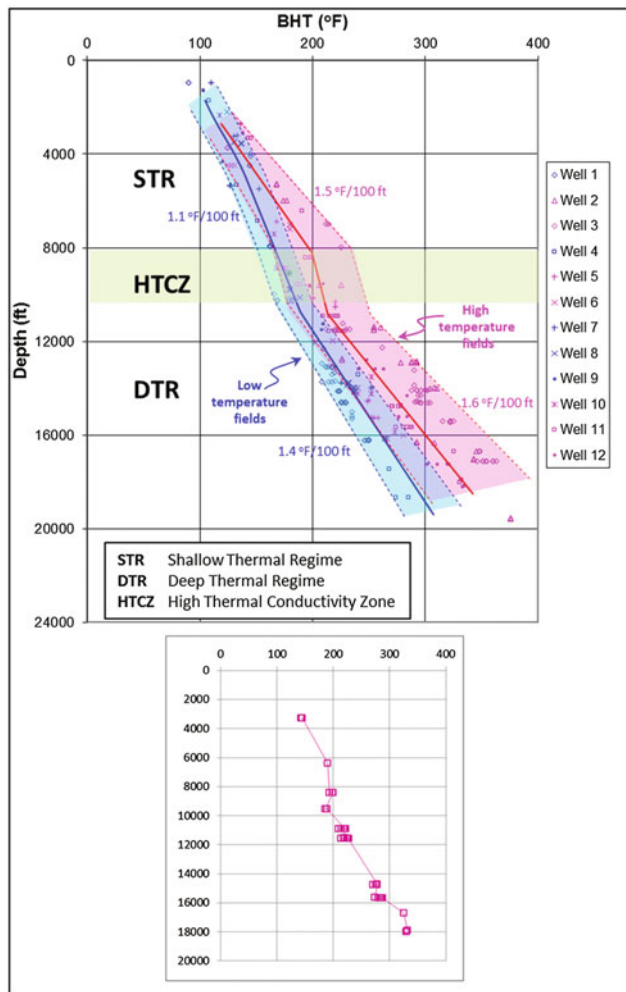


Fig. 10 Temperature/depth plot for selected wells in central and eastern Saudi Arabia with an extracted plot for well 11 showing the details of temperature changes with depth

the high-temperature wells with an overlap zone between the two (Figs. 10 and 11).

The STR extends from the ground surface to about 8000 ft below ground surface (about 6000 ft below sea level). The temperature in this regime increases from about 90 °F at 1000 ft below ground surface to about 220 °F at 8000 ft below ground surface. The average geothermal gradients for the low-temperature and high-temperature wells in this regime are 1.1 and 1.5 °F/100, respectively.

The DTR extends from approximately 10,000 ft to more than 19,000 ft below ground surface (about 8000–16,000 ft below sea level). The temperature of this regime increases from as low as 180 °F at 10,000 ft below ground surface to more than 370 °F at 19,000 ft below ground surface. The average geothermal gradients for the low-temperature and high-temperature wells in this regime are 1.4 and 1.6 °

F/100 ft, respectively. The DTR has a relatively wider range of lateral variations in temperatures than in the STR.

The HTCZ lies 8000 and 10,000 ft below ground surface (about 6000 and 8000 ft below sea level). Geothermal gradients across the HTCZ are very low indicating a relatively high heat conductivity zone. The HTCZ is less obvious in the low-temperature wells suggesting that there is a cooling effect from the STR in these wells. The cooling may be attributed to the aquifer flushing by the cold meteoric water through the outcrops.

The depths of the boundaries between the thermal regimes (Fig. 10) are comparable to the depths at which the water salinity gradients change (Fig. 5). This suggests that the pattern of geothermal gradients in these thermal regimes is very much related to the fluid environment rather than to the rock matrix. Also, the geothermal gradient in the low-temperature wells changes from 1.1 °F/100 ft in the STR to 1.5 °F/100 ft in the DTR indicating a cooling effect in the up-dip areas of the aquifers close to the recharge areas. On the other hand, high-temperature wells show a smaller difference between the geothermal gradients for the STR and DTR (1.4 °F/100 in the STR to 1.6 °F/100 in the DTR) which indicates a much less effect of cooling in these wells. This pattern of variations in geothermal gradients is in line with the general pattern of heat transfer observed in gravity-dominated groundwater flow basins. At the edges of these basins, the geothermal gradient and surface heat flow are depressed by the downward moving water (Deming 1994; Diao et al. 2004). In the deeper parts of the basin where the groundwater can only move upward, higher geothermal gradients and higher heat transfer to surface exist. Mid-way between the highest and lowest elevations of the basin, groundwater flow is largely horizontal and the effect on temperature is minimal.

Anomalies in the Pressure and Thermal Systems

Anomalies in reservoir pressures and temperatures have been observed in the NPR2 and OPR1 at several locations. For example, BRGM (1977) showed anomalously high temperature, hydraulic head, and salinity in the Neogene, and Dammam aquifers in the middle of the Ghawar anticline. BRGM 1977 interpreted these anomalies to be caused by the upward flow of hotter and higher pressure water from the Early Tertiary Umm er Radhuma aquifer into the Late Tertiary Dammam and Neogene aquifers through the area where the Middle Tertiary sealing Rus Formation is eroded by the pre-Neogene unconformity (Fig. 12).

The present study reveals anomalously high temperatures and pressures in the Unayzah reservoir in southern Ghawar (Fig. 13). In this case the water flows upward from the

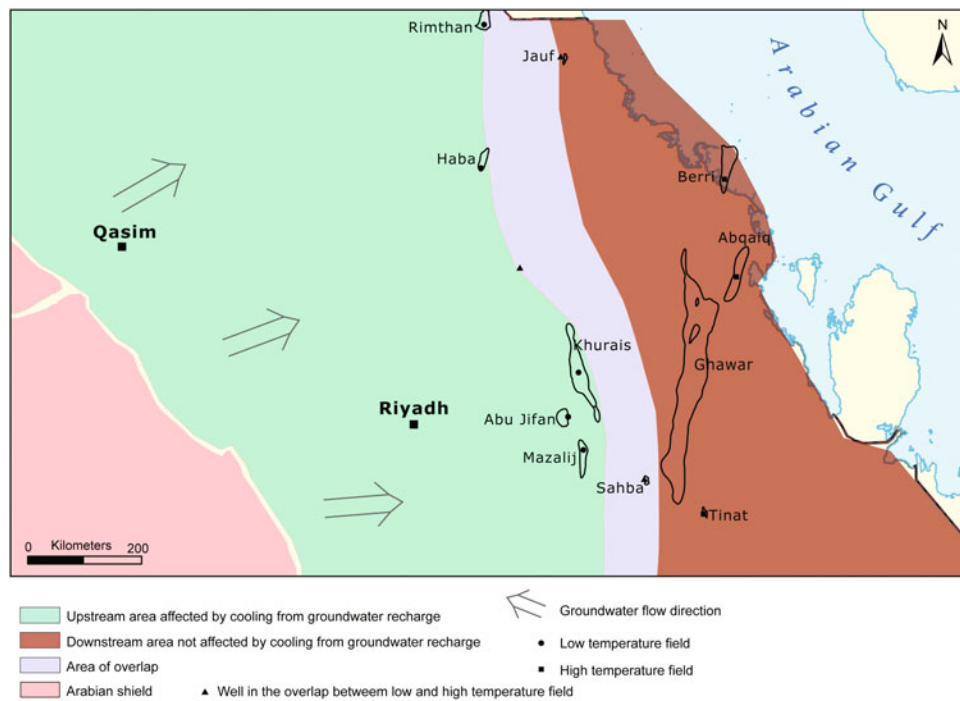


Fig. 11 Low and high temperature areas of central and eastern Saudi Arabia

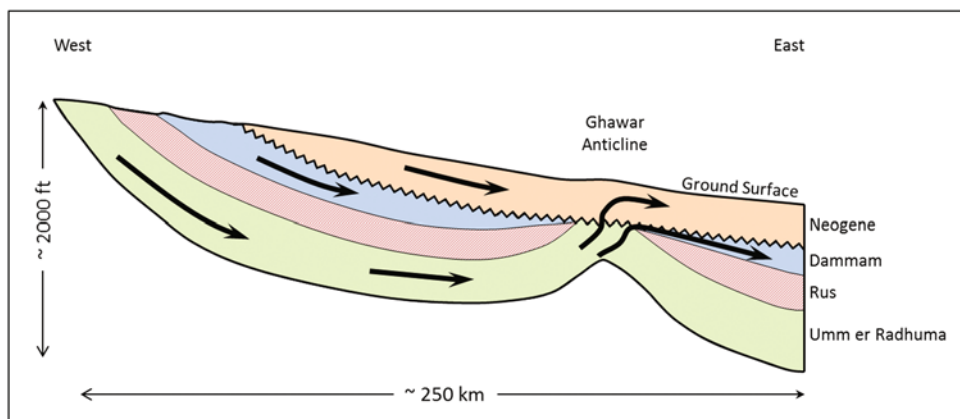


Fig. 12 Regional schematic cross-section through eastern Saudi Arabia showing the groundwater cross-formation flow in the Ghawar anticline (drawn from the concept by BRGM 1977)

Qasim Formation into the Unayzah reservoir in the area where the Qusaiba sealing shale is eroded and the Ordovician Saq-Qasim section is subcropping underneath the Unayzah.

Another anomalously high temperature is also obvious in the Unayzah reservoir at the Muradhaf, Mihwaz, and Dilam areas (Fig. 14). Here, the Qusaiba shale is not eroded, and the anomalous temperatures are associated with faults

(Fig. 14). It is believed that in these areas, the water flows upward from the Qasim Formation to the Unayzah reservoir through the fractured damage zones surrounding the fault core zones. Fault damage zones typically act as conduits for vertical fluid flow whereas fault core zones act as barriers to fluid flow (Caine et al. 1996).

From the above examples of anomalous pressure and temperature areas, it is apparent that cross-seal water flow

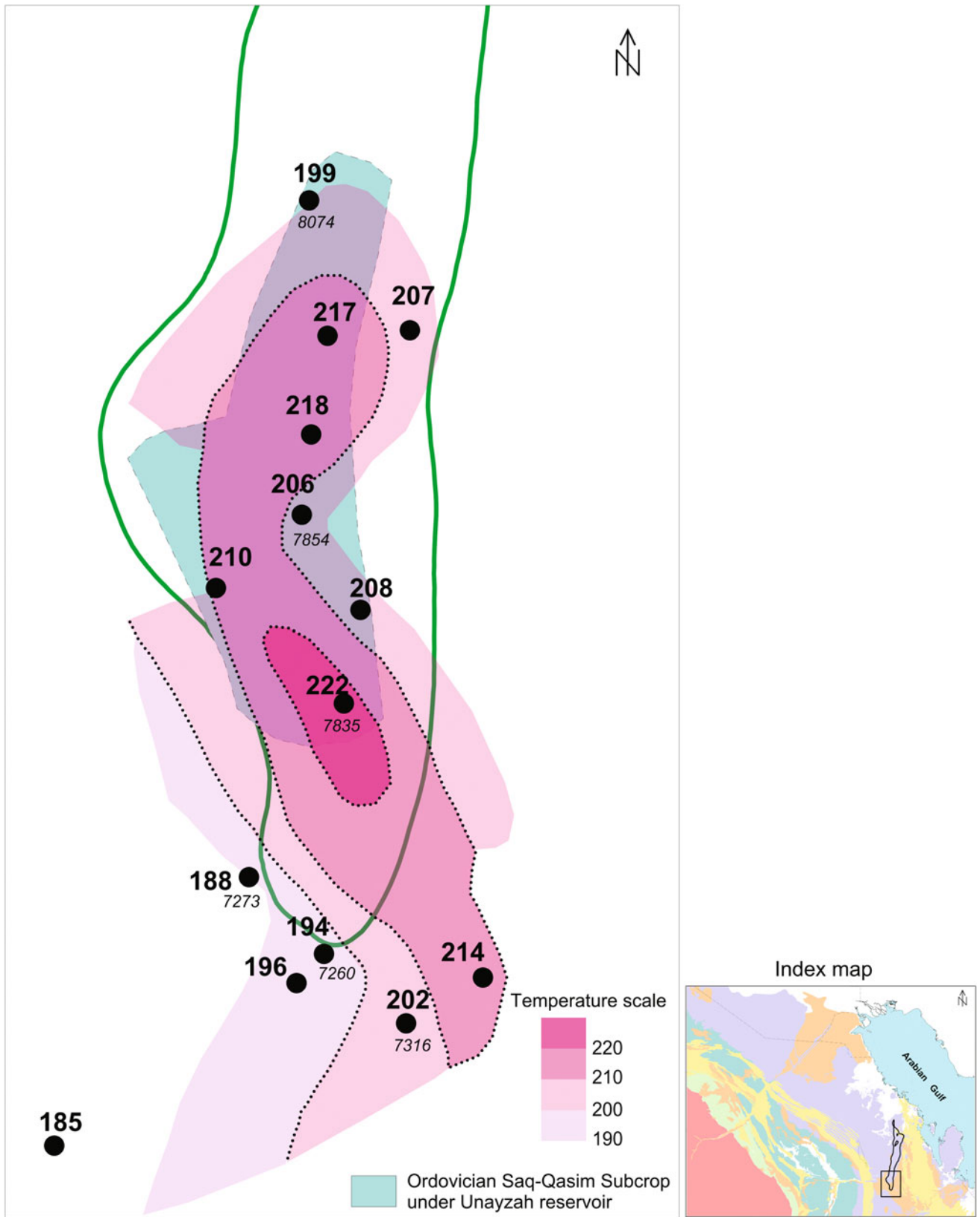


Fig. 13 Map of the Unayzah reservoir in South Ghawar showing an increase of temperature and pressure towards the Saq-Qasim subcrop area

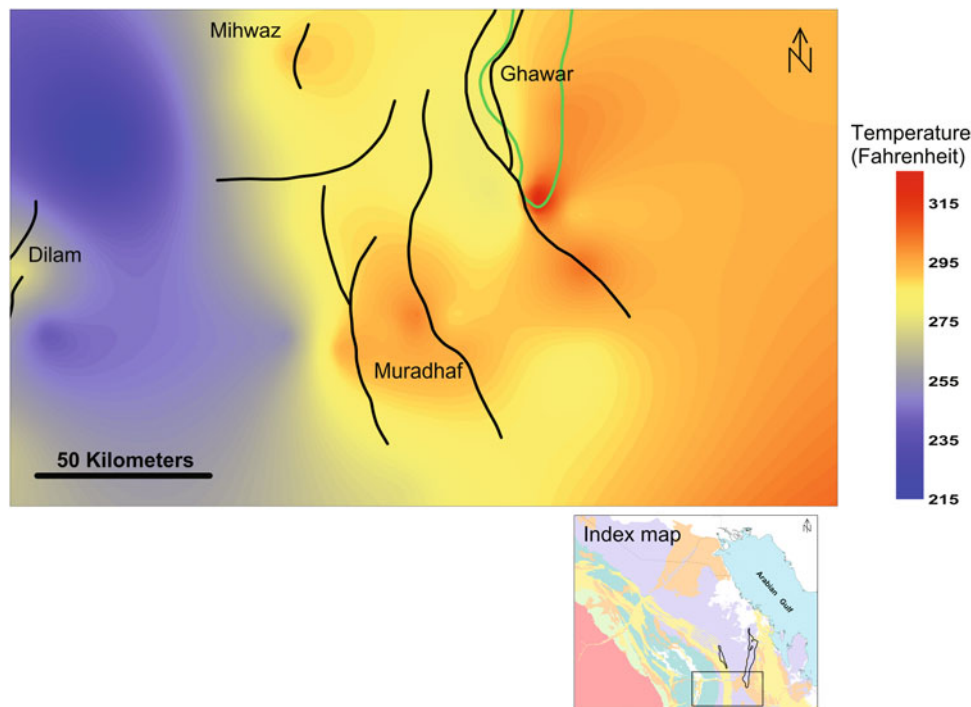


Fig. 14 Temperature map for the Unayzah reservoir in central and eastern Saudi Arabia showing the anomalously high temperatures associated with faults near Muraddaf, Mihwaz, and Dilam

could take place in two geologic settings: in areas where the sealing formations are eroded, and in areas where the fault damage zones act as conduits for the cross-seal flow. It is also possible that the two geologic settings coexist in one area.

An Integrated Thermo-Pressure Model

The main characteristics of pressure and thermal patterns in the sedimentary sequence of central and eastern Saudi Arabia are summarized in the 2-D model shown in Fig. 15. The model illustrates, schematically, the distribution of the pressure and thermal regimes and systems along with groundwater flow directions and salinity distribution. It also shows the anomalies in the geothermal gradients associated with breaching of seals within individual regimes.

The sedimentary sequence of central and eastern Saudi Arabia constitutes primarily aquifers that are separated from each other by stratigraphic seals; mainly shales in the Paleozoic sequence and anhydrites or shales in the Mesozoic and Cenozoic sequences. With the exception of the Sudair shale and Jilh Dolomite, these seals are known to be locally breached causing cross-aquifer flow to exist throughout

central and eastern Saudi Arabia. The Sudair shale acts as a strong seal that separates the Paleozoic aquifers and petroleum system from the Mesozoic aquifers and petroleum system. The regionally dense Jilh Dolomite formed an upper seal for the overpressure regime in the lower Jilh Formation.

The whole sedimentary sequence of central and eastern Saudi Arabia has been recharged with meteoric water since the Pleistocene. Regionally, the meteoric water formed relatively fresh water zone in the shallow areas (<8000 ft). Also, it has resulted in lower geothermal gradients in the upstream areas. The gas generation from the Silurian Qusaiba Shale which started in the Late Cretaceous has resulted in the generation of an overpressured system in the Paleozoic sequence at the deep areas of central and eastern Saudi Arabia.

Unconformities and faults are obviously important geologic factors in characterizing pressure systems. Unconformities and faults cutting through seals create opportunities for hydraulic communication between pressure systems allowing for the generation of local pressure and temperature anomalies. Faults could play double action role; their damage zones act as vertical conduits for cross-seal flow between pressure systems, and their core zones could act as seals forming different pressure compartments within individual pressure systems.

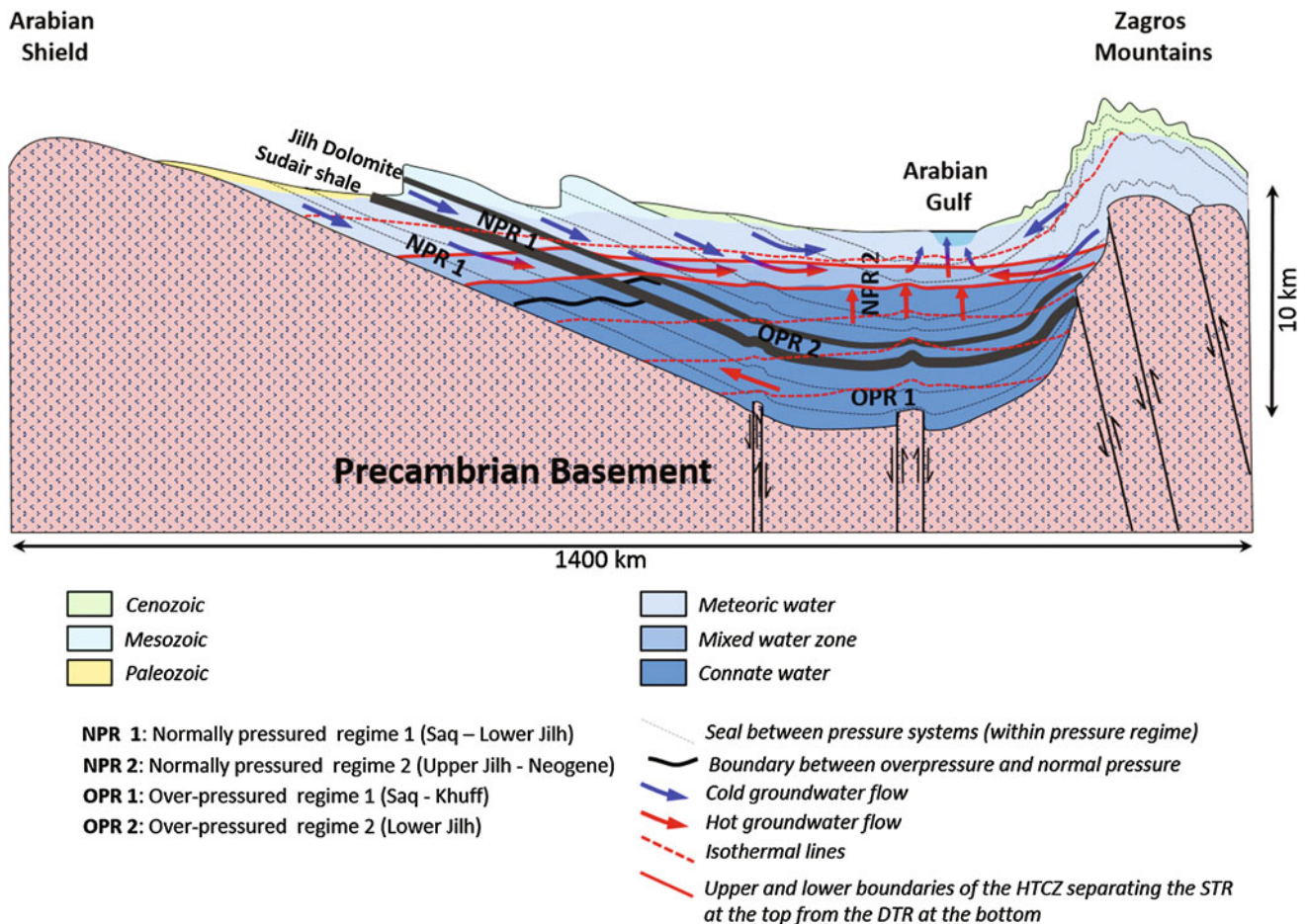


Fig. 15 Regional 2-D model illustrating the pressure regimes and systems, thermal gradients, groundwater flow and salinity in central and eastern Saudi Arabia

Conclusions

Pressure and thermal regimes and systems in the sedimentary sequence of central and eastern Saudi Arabia have been defined for the first time. The pressure regimes which are totally separated from each other by stratigraphic seals include:

- (1) Normally pressured regime (NPR2) in the sequence from the Cambro-Ordovician Saq Formation through the Lower part of the Triassic Jilh Formation (below the Jilh Dolomite). This regime extends from the formation outcrops at ground surface to as deep as 15,000 ft.
- (2) Normally pressured regime (NPR2) in the sequence from the Triassic Upper Jilh (above the Jilh Dolomite) through the Tertiary Dammam Formations. This regime extends from the formation outcrops at ground surface to as deep as 14,000 ft.
- (3) Overpressured regime (OPR1) in the sequence from the Cambro-Ordovician Saq Formation through the Triassic Khuff Formation at depths ranging from approximately

12,000 to more than 19,000 ft. This regime constitutes 3 main pressure systems; named here as the Saq, Sarah-Qasim, and Sharawra-Khuff systems. These systems are separated from each other by seals that are breached locally by unconformities or faults resulting in local hydraulic communication.

- (4) Overpressured regime (OPR2) in the lower part of the Triassic Jilh Formation at depths between 10,000 and 13,000 ft.

The thermal regimes include:

- (1) Shallow thermal regime (STR) that extends from the ground surface to depths around 8000 ft. This regime exhibits low geothermal gradient in the up-dip areas and normal geothermal gradient in the down-dip areas.
- (2) Deep thermal regime (DTR) that extends from approximately 10,000 ft to more than 19,000 ft. This regime exhibits normal geothermal gradients in both the up-dip and down-dip areas.

- (3) High thermal conductivity zone (HTCZ) in the depth range between 8000 and 10,000 ft.

Several factors are thought to have controlled the evolution of the pressure and thermal regimes and systems in the sedimentary sequence of central and eastern Saudi Arabia. The most important of these factors are the reservoir flushing with meteoric water during the Pleistocene-Holocene, gas generation in the Paleozoic sequence since the Cretaceous, porosity and permeability reduction with depth, and the regional stratigraphic and structural settings of the area.

Acknowledgments The author would like to thank Saudi Aramco for permission to publish this paper. Also, thanks go to Sedat Inan and Abdulkadir Afifi from Saudi Aramco for reviewing the paper and making constructive comments. Thanks are also extended to the anonymous reviewers for their helpful comments. Finally, the author appreciates the drafting efforts by Salma Zahrani from Saudi Aramco.

References

- Abu-Ali MA, Franz UA, Shen J, Monnier F, Mahmoud MD, Chambers TM (1991) Hydrocarbon generation and migration in the Paleozoic sequence of Saudi Arabia. SPE Middle East Oil Show Bahrain paper 21376:345–356
- Abu-Ali M, Littke R (2005) Paleozoic petroleum systems of Saudi Arabia: a basin modeling approach. *GeoArabia* 10(3):131–168
- Al-Aswad AA, Al-Bassam AM (1997) Proposed hydrostratigraphical classification and nomenclature: application to the Paleozoic in Saudi Arabia. *J Afr Earth Sci* 24(4):497–510
- Al-Husseini MI (1991) Potential petroleum resources of the Paleozoic rocks of Saudi Arabia. In: Thirteenth world petroleum congress, Buenos Aires. Topic 1, recently discovered and potential petroleum resources, 11 p
- Al-Husseini, MI (2000) Origin of the Arabian Plate Structures: Amar Collision and Najd Rift, *GeoArabia* 5(4):527–542.
- Al-Laboun AA (1988) The distribution of carboniferous—Permian siliciclastic rocks in the greater Arabian Basin. *Geol Soc Am Bull* 100(3):362–373
- Alsharhan AS, St C, Kendall C (1986) Precambrian to Jurassic rocks of Arabian gulf and adjacent areas: their facies, depositional setting, and hydrocarbon habitat. *AAPG Bull* 70(8):977–1002
- Alsharhan AS, Nairn AEM (1995) Tertiary of the Arabian gulf: sedimentology and hydrocarbon potential, in Elsevier, 1995. *Paleogeogr, Paleoclimatol, Paleocol* 114:369–384
- Arouri KR, Van Laer PJ, Prudden MH, Jenden PD, Carrigan WJ, Al-Hajji AA (2010) Controls on hydrocarbon properties in a paleozoic petroleum system in Saudi Arabia: exploration and development implications. *AAPG Bull* 94(2):163–188
- Ayres MG, Bilal M, Jones RW, Slentz LW, Tartir M, Wilson AO (1982) Hydrocarbon habitat in main producing areas, Saudi Arabia. *AAPG Bull* 66(1):1–9
- Bakiewicz W, Milne DM, Noori M (1982) Hydrogeology of the Umm Er Radhuma aquifer, Saudi Arabia, with reference to fossil gradients. *Q J Eng Hydrogeol* 15:105–126
- BRGM (1976) Hydrogeological investigations of the Wasia Aquifer in the Eastern Province of Saudi Arabia, final report and appendices, vol 2, Ministry of Saudi Arabia, Riyadh
- BRGM. (1977) Al-Hassa development groundwater studies and program, vol 4, Ministry of Agriculture and Water, Riyadh
- Caine JS, Evans JP, Forster CB (1996) Fault zone architecture and permeability structure. *Geology* 24(11):1025–1028
- Carney S, Hill S, Franks SG (2002) Petrophysical characterization of lower Paleozoic Reservoirs of Saudi Arabia: an insight into factors controlling reservoir quality (abstract). In: AAPG international convention, Cairo, Egypt, 27–30 October 2002
- Chapman DS, Clement MD, Mase CE (1981) Thermal regime of the Escalante Desert, Utah, with an analysis of the new castle geothermal system, *J Geophys Res* 86(B12):11735–11746
- Deming D (1994). Overburden rock, temperature and heat flow. In: Magoon LB, Dow WG (eds) *The petroleum system—from source to trap*. AAPG memoir 60, Chapter 9, pp. 165–186
- Diao N, Li Q, Fanq Z (2004) Heat transfer in ground heat exchangers with groundwater advection. *Int J Therm Sci* 43:1203–1211
- Edgell HS (1996) Aquifers of Saudi Arabia and their geological framework. *Arab J Sci Eng*, vol 22, Number IC. King Fahd University of petroleum and Minerals, pp. 3–31
- Franks SG, Zwingmann H (2010) Origin and timing of the late diagenetic illite in the Permian-carboniferous Unayzah sandstone reservoirs of Saudi Arabia. *AAPG Bull* 94(8):1133–1159
- Freeze RA, Cherry JA (1979) *Groundwater*. Prentice-Hall Inc, Englewood Cliffs, NJ 604 p
- Haq BU, Al-Qahtani AM (2005) Phanerozoic cycles of sea-level change on the Arabian platform. *GeoArabia* 10(2):127–160
- Hitchon B (1984) Geothermal gradients, hydrodynamics and hydrocarbon occurrences, Alberta, Canada. *AAPG Bull* 68:713–743
- ITALCONSULT (1969) Water and agricultural development studies for area IV, Final report, geohydrology. Ministry of Agriculture and Water, Riyadh 80 p
- Jenden, P.D., A. A. Al-Hajji, W. J. Carrigan, A. S. Ahmed, and M. A. Abu-Ali, 2004, Petroleum Potential of the Triassic System, Saudi Arabia (Abstract), GEO 2004 Conference, Bahrain
- Konert G, Al-Hajri SA, Al Naim A, Afifi AM, Groot K de, Droste HJ (2001) Paleozoic stratigraphy and hydrocarbon habitat of the Arabian Plate. In: Downy MW, Threet JC, Morgan WA (eds) *Petroleum provinces of the twenty-first century*. AAPG Memoir 74:483–515
- Law BE, Spencer CW (1998) Abnormal pressures in hydrocarbon environments, Chapter 1. In: Law BE, Ulmishek GF, Slavin VI (eds) *Abnormal pressures in hydrocarbon environments*, AAPG memoir 70
- Luheshi MN, Jackson D (1986) Conductive and convective heat transfer in the sedimentary basins. In: Burrows J(ed) *Proceedings of the 1st IFP exploration research conference; thermal modeling in sedimentary basins*, Caracans, France, pp. 219–234.
- Majorowicz JA, Jessop AM (1981) Regional heat flow in the Western Canadian basin. *Tectonophysics* 41:209–239
- Majorowicz JA (1987) The controversy over the significance of the hydrodynamic effect on heat flow in the Prairies basin. In: Beck AE, Garven G, Stegena L (eds) *Hydrogeological regimes and their subsurface thermal effects*, geophysical monograph 47, vol 2. IUGG, pp. 101–118
- MAW (Ministry of Agriculture and Water) (1984) *Water Atlas of Saudi Arabia*. Water Resources Development, Riyadh 272 p
- McGillivray JG, Hussein MI (1992) The Paleozoic petroleum geology of Central Arabia. *AAPG Bull* 76:1473–1490
- Naimi AI (1965) The groundwater of Northeastern Saudi Arabia. In: Fifth arab petroleum congress, Cairo, 24 p
- Person M, Garven G (1989) Hydrogeologic constraints on the thermal evolution of the Rhine Graben. In: Beck AE, Garven G, Stegena L (eds) *Hydrogeological regimes and their subsurface thermal effects*, geophysical monograph 47, vol 2. IUGG, pp. 35–58

- Pelissier J, Hedayati AA, Abgrall E, Plique J (1980) Study of hydrodynamic activity in the Mishrif fields offshore Iran. *J Pet Technol* 32(6):1043–1052
- Pollastro RM (2003) Total petroleum systems of the Paleozoic and Jurassic, greater Ghawar uplift and adjoining provinces of Central Saudi Arabia and Northern Arabian-Persian Gulf, U.S. geological survey bulletin 2202-H, 100 p
- Powers RW, Ramirez LF, Redmond CD, Elberg EL Jr (1966) Geology of the Arabian Peninsula: sedimentary geology of Saudi Arabia, U. S. geological survey professional paper 560-D, 147 p
- Stenger B, Pham T, Al-Afaleg N, Lawrence Paul (2003) Tilted original oil/water contact in the Arab-D reservoir, Ghawar field, Saudi Arabia. *GeoArabia* 8(1):9–42
- Swarbrick RE, Osborne MJ (1998) Mechanisms that generate abnormal pressures: an overview, Chapter 2. In Law BE, Ulmishek GF, Slavin VI (eds) *Abnormal pressures in hydrocarbon environments*, AAPG memoir 70
- Todd DK (1980) *Groundwater hydrology*. John Wiley and Sons, New York 535 p
- Walton WC (1970) *Groundwater resource evaluation*. McGraw-Hill Kogakusha, Tokyo 664 p
- Ward RC (1975) *Principles of hydrology*, 2nd edn. McGraw-Hill Book Company (UK), Limited, England 367 p
- Wender LE, Bryant JW, Dickens MF, Neville AS, Al-Moqbel AM (1998) Paleozoic (Pre-Khuff) hydrocarbon geology of the Ghawar area, Eastern Saudi Arabia. *GeoArabia* 3(2):273–302

Optimal Aquifers and Reservoirs for CCS and EOR in the Kingdom of Saudi Arabia: An Overview

Marwan Jaju, Fadi Henri Nader, François Roure, and Liviu Matenco

Abstract

An overview on the tectono-stratigraphic framework of the Arabian plate indicates obvious differences between two distinct areas: the hydrocarbon-prolific sector and non-hydrocarbon-prolific sector. These differences resulted from the interplay of a variety of factors; some of which are related to the paleo-geographic configuration (eustatic sea level fluctuations, climatic conditions, and salt Basins), others to differential subsidence (burial) and structural inversions. During the Paleozoic, the regional compression was caused by far field effects of the Hercynian orogeny. This led to major folded structures in central and eastern Saudi Arabia (e.g., Ghawar anticline). During the Mesozoic, the most important tectonic factor was the stretching of the crust (extension), accompanied with the increase in temperature, resulting in an increase of the accommodation space, and thicker sedimentary successions. Regional unconformities are mostly found where folded structures are dominant, and they acted as a carrier systems for the accumulation of hydrocarbon and groundwater. A good understanding of the stratigraphy and tectonic evolution is, thus, required to develop Carbon Capture and Storage (CCS) and to design efficiently enhanced oil recovery (EOR) in both sectors. Oil and gas reservoirs offer geologic storage potential as well as the economic opportunity of better production through CO₂-EOR. The world greatest hydrocarbon reservoirs mainly consist of Jurassic carbonate rocks, and are located around the Arabian Basin (including the eastern KSA and the Arabian Gulf). The Cretaceous reservoirs, which mainly consist of calcarenite and dolomite, are located around the Gotnia salt Basin (northeast of KSA). Depleted oil and gas fields, which generally have proven as geologic traps, reservoirs and seals, are ideal sites for storage of injected CO₂. Each potential site for CO₂-EOR or CCS should be evaluated for its potential storage with respect to the containment properties, and to ensure that

The full citation and reference to the original article published in AJGS.

M. Jaju (✉)
School of Geosciences, University of Aberdeen, Aberdeen,
AB24 3UE, UK
e-mail: marwan.jaju@gmail.com

F.H. Nader · F. Roure
Geosciences, IFPEN, 1–4 Avenue de Bois-Préau,
92852 Rueil-Malmaison Cedex, France

F. Roure
Tectonic Group, Utrecht University, Utrecht, The Netherlands

L. Matenco
Department of Earth Sciences, Utrecht University,
Utrecht, The Netherlands

conditions for safe and effective long term storage are present. The secured deep underground storage of CO₂ implies appropriate geologic rock formations with suitable reservoir rocks, traps, and impermeable caprocks. Proposed targets for CCS, in the non-hydrocarbon-prolific sector, are Kharij super-aquifer (Triassic), Az-Zulfi aquifer (Middle Jurassic), Layla aquifer (Late Jurassic), and Wasia aquifer (Middle Cretaceous). Proposed targets for EOR are Safaniya oil field (Middle Cretaceous) (Safaniya, Wara and Khafji reservoirs), Manifa oil field (Las, Safaniya and Khafji reservoirs) (Late Jurassic), and Khuff reservoir (Late Permian-Early Triassic) in central to eastern KSA.

Keywords

Tectono-stratigraphy • Hydrocarbon/non-hydrocarbon—prolific sectors • Paleoclimate • EOR & CCS • Arabian plate • KSA

Introduction

The Arabian plate extends from the eastern Mediterranean region to the western Zagros thrust zone, and comprises the whole Arabian Peninsula. It is enclosed by latitude 13° and 38°N and longitudinal 35° and 60°E. The Arabian plate is subdivided in distinct geologic domains; i.e., the Arabian Shield in the west, the Arabian platform into the Center and the Arabian Gulf in the east. The study area covers the Kingdom of Saudi Arabia (KSA), which constitutes most of the Arabian plate (Fig. 1).

A comprehensive literature review of previous work and the general geology of the KSA were first conducted. It covered issues related on the geodynamics, tectonics, stratigraphy, paleoclimate, sea-level variations, hydrogeology, hydrostratigraphy, petroleum systems, and petro-physical properties of the rock formations, (i.e., Powers et al. 1966; Beydoun 1991; Cole et al. 1994; Stump and Van Der Eem 1995; Alsharhan and Naim 1997; Aswad and Al-Bassam 1997; Al-Bassam et al. 2000; Sharland et al. 2001; Zeigler 2001; Le-Nindre et al. 2003; Pollastro 2003; Haq and Al-Qahtani 2005; Bell and Spaak 2007; and Rahman and Khondaker 2012).

In order to summarize and analyze the vast wealth of available information, 12 synthetic lithostratigraphic columns were compiled representing the main oil productive and non-oil productive sectors (Fig. 2). Eight sites are located between the Tabuk area in the northwest and Ash-Sharawarh in the southwest across Wajid area (Figs. 1 and 2). The four other sites are located between Safaniyah in the northeast and Oman in the southeast, and include the Ghawar area (Figs. 1 and 2).

Geo-sequestration of CO₂ is burdened with systematic risks, which relates to the geological characteristics of the site, nature and efficiency of reservoirs, underlying and overlying impervious formations, and the prevailing fluid-flow regimes (Kaldi 2008; Barkto et al. 2009; Taglia 2010). Understanding the links between tectonics and

stratigraphy, throughout a large, geological time-scale, is believed to help in defining such major factors (listed above) that affects the success of CO₂ underground storage and eventually, associated EOR.

First, a stratigraphical model is proposed including most of aquifers and reservoirs in the study area (i.e., the KSA). Then, we identify, in this contribution, the potential rock units suitable for long term application of CO₂ sequestration and reservoirs which could be used for enhanced oil recovery (EOR), in order to reduce anthropogenic greenhouse gases, and their effects on global climate change.

Geological Setting

Based on generalized plate-scale chronostratigraphy charts, unconformities, sea level variation, climate and the paleogeographic location of the plate across geological times, the impacts of paleoclimate and tectonic activity on depositional environments and hydrocarbon evolution can be highlighted. The Paleozoic rock series have been characterized, accordingly, through two distinct cycles.

During an early Paleozoic cycle (Cambrian—Ordovician—Silurian), the Arabian plate was first located near the equatorial line in the Cambrian time, resulting in a relatively warmer climate, and an increase in the accommodation space due to induced sea level variation. This coincided with rifting, extension, at the northern Gondwana margin (Konert et al. 2001) (Fig. 3). In the Ordovician, the Arabian plate drifted towards the south latitudes and that coincided with several tectonic pulses. Consequently, collision tectonics led to major uplifts (e.g., Oman), and affected considerably sedimentary and facies patterns (Otterdoom et al. 1999; Al-Jallal and Al-Sharhan 2005) (Fig. 4). The Arabian plate continuously moved toward the South Pole until it reached the latitude of 55° (Konert et al. 2001). Here, the paleoclimate witnessed an expansion of major continental ice sheets in Ashgillian time, and the effects of late Ordovician

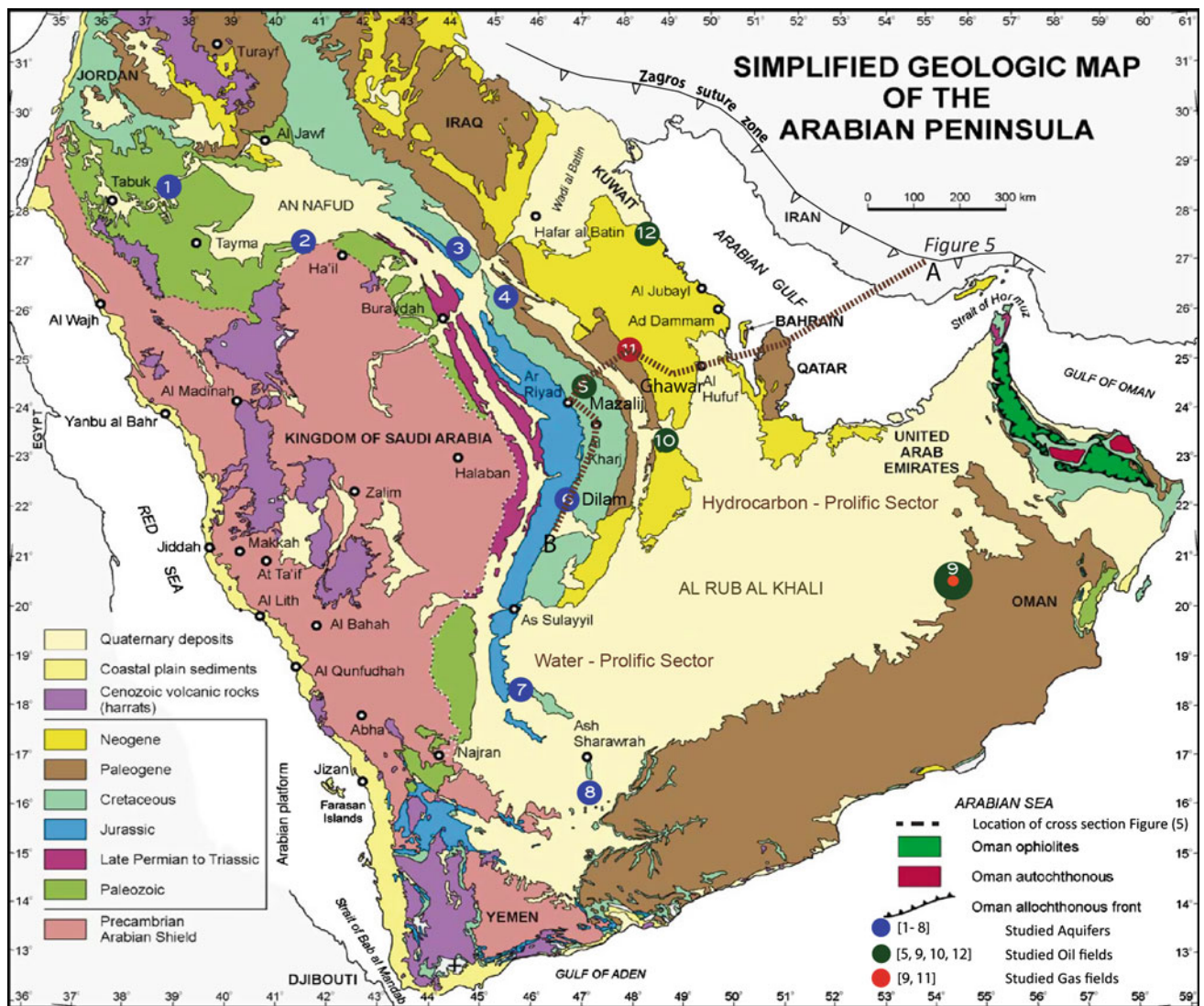


Fig. 1 Simplified geological map of the Arabian Peninsula, showing the studied hydrocarbon wells, aquifers and the regional cross section a–b of Fig. 5 location. After Le Nindre et al. (2003)

glaciations (El-Ghali 2005), which reached eastward, from Jordan through western Saudi Arabia (McClure 1978). This remained until the Silurian, when the whole plate returned to the equatorial line. It was accompanied with the increase in temperature, resulting in deglaciation and sea level rise, consequently source rock (hot shale) deposited in anoxic conditions (McClure 1978).

The late Paleozoic cycle (Carboniferous—Permian—Early Triassic), started with a remarkable event of erosion and non-deposition driven by the propagation of far field compressional stresses through the area, the “Hercynian event”. The Arabian plate moved again toward the South Pole and the paleoclimate started to control the plate-scale depositional processes. Glaciations spanned the Late Carboniferous and ended with return to the equatorial

line associated with increased temperatures in the late Permian—early Triassic, coincident with slab pull in the south-facing subduction zone (Konert et al. 2001) (Fig. 3).

Throughout the Mesozoic, the stratigraphic architectures and geometries confined within the Arab Basin, resulted from the sea level fluctuations, due to the effects of eustatic changes or relative uplift and subsidence in the vicinity of the Arabian Arch. Besides, the petroleum systems within this Basin (and the hydrocarbon—prolific sector) are pretty much influenced by such stratigraphic configuration. During the middle Jurassic to early Cretaceous times, the axial zone of the Arabian plate underwent subsidence in both prolific and non-prolific sectors, leading to sea level rise and marine sedimentation covering large areas of the Arabian plate (Fig. 4).

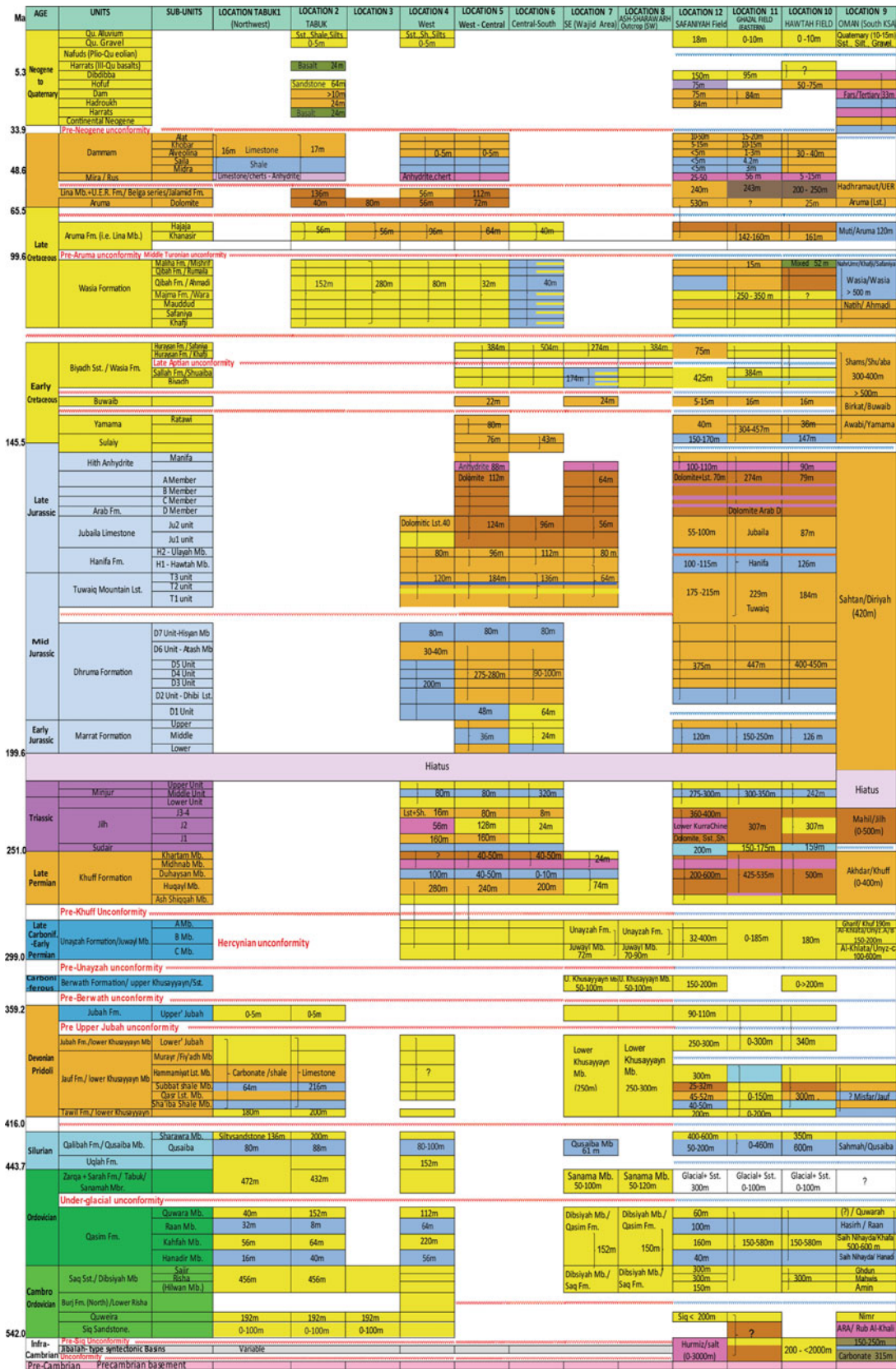


Fig. 2 Twelve synthetic lithostratigraphic columns, representative of the main hydrocarbon productive and non-hydrocarbon productive sectors in the Arabian plate. The main unconformities in both sectors are illustrated. Data compiled from Morton (1959), Powers et al. (1966), McClure (1978), Murriss (1980), Wilson (1981), Bazanti (1988),

Cole et al. (1994), Stump and Van Der Eem (1995), Al-Sharhan, and Narin (1995, 1997), Cagatay et al. (1996), Oterdoom (1999), Jones and Stump (1999), Al-Shayea (2000), Pollastro (2003) and Al-Ramadan et al. (2004)

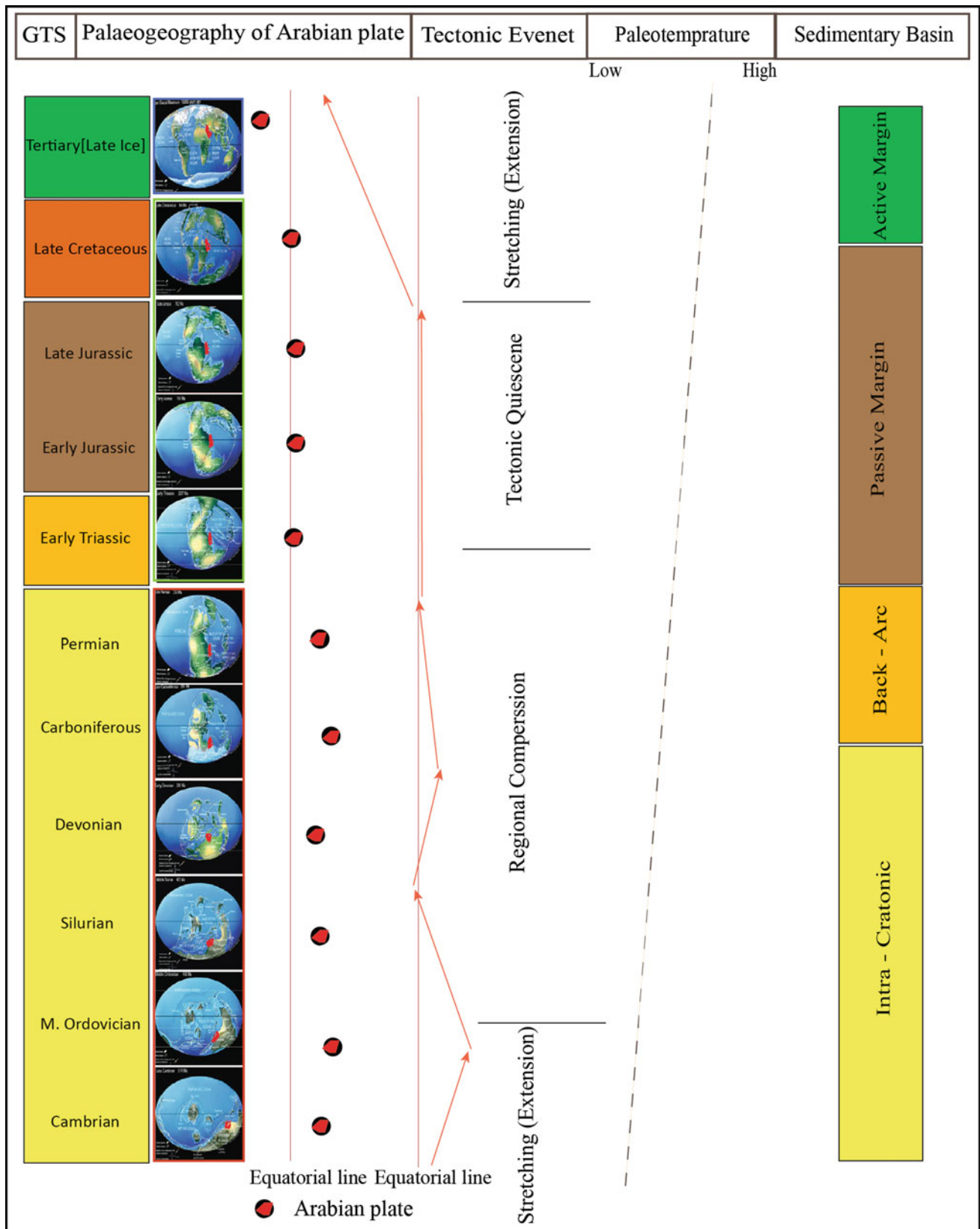
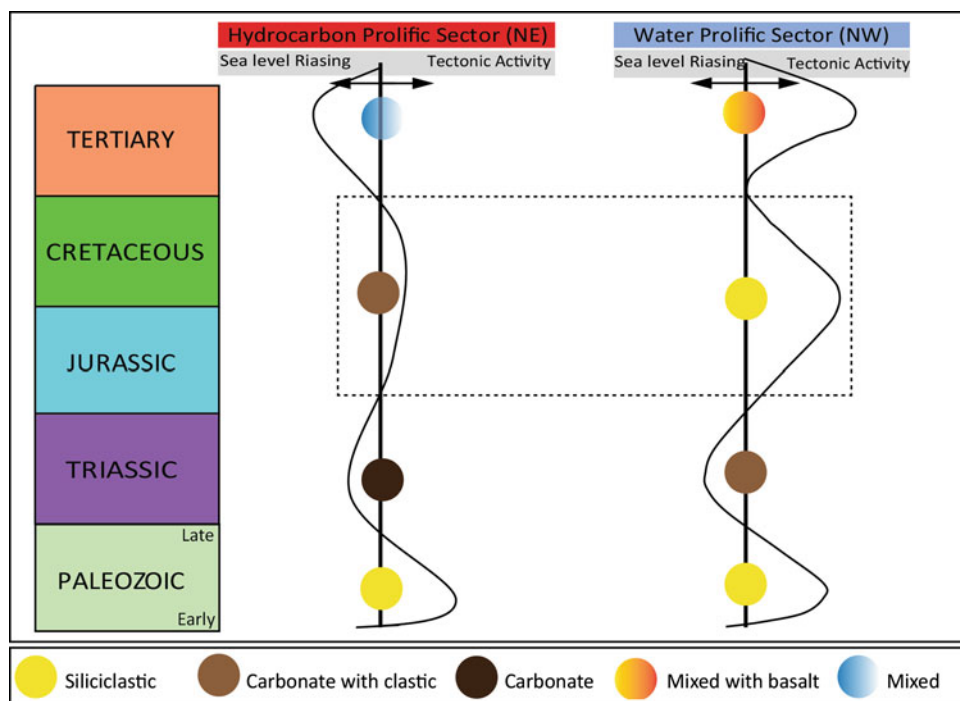


Fig. 3 Conceptual composite Fig. showing the tectonic drifting of the Arabian plate and Paleoclimate. Modified from Brown (1972) and Scotese (1998)

Fig. 4 Conceptual figure shows the impact of the tectonic activity and the eustatic sea level variations on the Arabian plate evolution across geological times



From early to middle Cretaceous, continuous subsidence in the Arabian arch occurred in the hydrocarbon-prolific sector, whereas the Arabian Arch was reactivated and uplifted towards the west in the non-prolific sector. This led to a local sea level fall and deposition of siliciclastic (marine and non-marine series) (Figs. 2 and 4).

Accordingly, there are obvious differences in the tectonic evolution between prolific and non-prolific areas, which could be illustrated through the presence of distinct structural features. In the prolific area (eastern margin of the Arabian Gulf), there are wide spreading of faults due to extension and subsidence, whereas in the western part, uplift structure are dominant and that can be observed by the difference in topography between these two areas. In addition, the thicknesses of the sediments may reflect the related tectonic events, which increase toward the eastern part of Saudi Arabia, and that could be due to the continuing subsidence and deposition, mostly without breaks and evidenced by a decrease of the number of unconformities, whereas in the western part, most of the geological rock formations are thinner, with relatively high amount of unconformities (Figs. 2 and 5).

Water Dominant Sector (Non-Hydrocarbon Prolific Area)

In the eastern part of Saudi Arabia, where hydrocarbon accumulations are rather lacking, aquifers are mainly Paleogene in age (Bakiewicz et al. 1982), i.e., the Umm Er

Radhuma and Dammam formations. The Rub'Al-Khali embayment province hosts also such aquifers (Edgell 1987a). In northwestern Saudi Arabia, the major aquifer-hosting, tectono-sedimentary Basins are the Tabuk Basin, the Wadi as Sirhan Basin, the Widyan Basin margin and the northeastern interior homocline (Edgell 1987a, b) (cf., Figure 1).

Al-Aswad and Al-Bassam (1997) have divided the deeper Paleozoic rock series into eight basic aquifer units separated from each other by aquitards. The hydrostratigraphical units of the Mesozoic-Cenozoic in Saudi Arabia overly the Sudair mega-aquitard (Al-Bassam et al. 2000), and the classification proposed by the latter authors was based on the inherent properties of the sedimentary rocks, namely the porosity, permeability, presence of aquitard, thickness and areal extent. Accordingly, based on the combination of large amounts of hydrogeological data from previous published articles and unpublished work, we present a summarized hydrostratigraphical chart of the Arabian plate (Fig. 6).

Hydrocarbon Dominant Sector

The major Paleozoic reservoirs of central Arabia are sandstones of the Devonian Jauf and Permian Unayzah formations. Further to the east, in the Arabian Gulf region, the main Paleozoic reservoirs are made up of carbonates of the Upper Permian Khuff formation. Other reservoirs include clastics of pre-Qusaiba sequence that are fault-bounded and sourced laterally by down-faulted Qusaiba shale member.

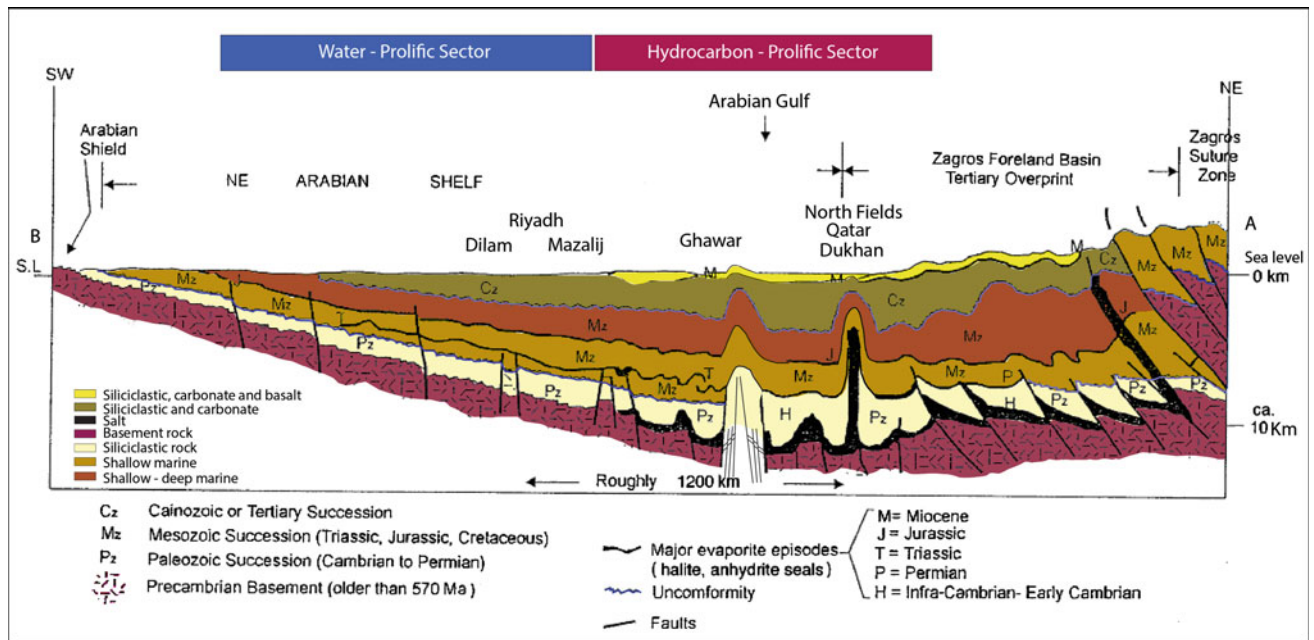


Fig. 5 Schematic section from Zagros suture zone—to Arabian Gulf—to Arabian shield. Modified from Beydoun (1998) and Konert et al. (2001). For location see Fig. 1

These reservoirs are characteristically affected by silica cementation, which decreases their flow properties (Jones and Stump 1999).

Many of the Ordovician sandstone reservoirs are sealed by the overlying Lower Silurian Qusaiba shale. The Devonian Jauf sandstone reservoir is sealed by a very distinctive shaly unit called (D3B) in the Ghawar field (Pollastro 2003). The impermeable anhydrite, carbonate rocks and shale beds of the Khuff formation and/or equivalent unit, also constitute a major regional seal for the central Arabia, Qusaibah Paleozoic sequence. Basal Khuff strata form the top seal to the Permian Unayzah reservoir in Ghawar field.

Traps are mostly structural and related to basement block faulting, tectonic salt movement and deformation (halokinesis) as well as wrench faulting (Pollastro 2003) (Fig. 7). Generally, in Saudi Arabia and Iraq the direction of hydrocarbon migration is toward the west (Cole et al. 1994) (Fig. 5).

The best and most prolific Mesozoic reservoirs occur in the Upper Jurassic Arab formation; especially Arab C and D members, where bulk rock porosity averages 25 % and permeability exceeds 100 md (Edgell 1987a, b). Seal units for the carbonate rock reservoirs of the major Arab formation are made up of anhydrite beds of the upper part of the Arab and Hith formations (Murriss 1980). Other known reservoirs include the porous carbonate-rock units within the Hanifa and Tuwaiq Mountain formations (Koepnick et al.

1995). During the middle Cretaceous, regressive sandstones, which are prolific hydrocarbon reservoirs (Wara, Safaniya, Khafji) of the Wasia group, were deposited. They are sealed by Rumailah member which consists of limestone, and Ahmadi member which consists of shale of the Wasia formation.

Long Term CO₂ Sequestration

The major factors that are believed to influence the sequestration of CO₂ as (CCS) in aquifers are: lithology, storage coefficient, transmissivity, porosity, permeability, thickness, depth, TDS, reservoir type, and hydro-stratigraphical units (Table 1). Most of these factors were documented and compiled from previously published work during this study, allowing the characterization of the best candidate aquifers with respect to geological sequestration (discussed below).

With respect to prospective geological CO₂ sequestration for EOR within producing oil/gas fields in the prolific sector, many issues should be taken into account; such as the source of CO₂, chemistry of water, hydrocarbon miscible activity, original oil in place (% OOIP), depth, dip of the layer, initial pressure, saturation pressure, fracture pressure, and temperature. CO₂ displacement processes are highly sensitive to pressure, reservoir type, wetness, heterogeneity, and oil density (API) (i.e., Barkto et al. 2009).

Chronostratigraphic Units			Lithostratigraphic Units	Hydrostratigraphic Units			
System	Age/Ma	Series	Formation Member	Aquifer	Super Aquifer	Aqua Group	Aqua system
NEOGENE	67	MIOCENE & PLIOCENE	HOFUF	HOFUF	MESO -	RUB'AL - KHALI	AD - DAHNA'A - AQUASYSTEM
			DAM	HASA AQUIFER	HARADH SUPER - AQUIFER		
PALEOGENE	67	EOCENE	HARDUK			RUB'AL - KHALI	AD - DAHNA'A - AQUASYSTEM
			DAMMAM				
CRETACEOUS	140	PALEOCENE	RUS	UER AQUIFER		RUB'AL - KHALI	AD - DAHNA'A - AQUASYSTEM
			UMM ER RADHUMA				
CRETACEOUS	140	CAMPANIAN	ARUMA	ARUMA	MESO - AQUIFER	RUB'AL - KHALI	AD - DAHNA'A - AQUASYSTEM
			WASIA	WASIA AQUIFER	KHURAI SUPER - AQUIFER		
CRETACEOUS	140	CENOMANIAN	BIYADH	BIYAYADH AQUIFER		RUB'AL - KHALI	AD - DAHNA'A - AQUASYSTEM
			BUWAIB				
CRETACEOUS	140	APTIAN	YAMAMA		BUWAIB MESO - AQUITARD	RUB'AL - KHALI	AD - DAHNA'A - AQUASYSTEM
			SULAIY				
JURASSIC	204	UPPER	HITH		LAYLA AQUIFER	RUB'AL - KHALI	AD - DAHNA'A - AQUASYSTEM
			ARAB				
JURASSIC	204	UPPER	JUBAILA		LAYLA AQUIFER	RUB'AL - KHALI	AD - DAHNA'A - AQUASYSTEM
			HANIFA				
JURASSIC	204	MIDDLE	TUWAYQ MOUNTAIN	TUWAYQ	MESO -	RUB'AL - KHALI	AD - DAHNA'A - AQUASYSTEM
			DHRUMA	AZ ZULFI AQUIFER			
TRIASSIC	250	LOWER	MARAT	MURAT	MESO - AQUITARD	RUB'AL - KHALI	AD - DAHNA'A - AQUASYSTEM
			MINJUR	AL SUWAIDI AQUIFER	KHARJ		
TRIASSIC	250	MIDDLE	JILH	JA'LAH	SUPER - AQUIFER	RUB'AL - KHALI	AD - DAHNA'A - AQUASYSTEM
				SHAMASIYAH			
PERMIAN	290	LOWER	SUDAIR	SUDAIR	MEGA -	RUB'AL - KHALI	AD - DAHNA'A - AQUASYSTEM
					AQUITARD		
CARBONIF.	360	UPPER	KHUFF	KHUFF AQUIFER		RUB'AL - KHALI	AD - DAHNA'A - AQUASYSTEM
			UNAYZAH	UNAYZAH AQUITARD	RAFHAH SUPPER - AQUIFER		
DEVONIAN	375	UPPER	JUBAH	BADANAH AQUIFER		RUB'AL - KHALI	AD - DAHNA'A - AQUASYSTEM
			HAMMAMIYAT				
DEVONIAN	385	MIDDLE	SUBBAT	SUBBAT	MESO - AQUITARD	RUB'AL - KHALI	AD - DAHNA'A - AQUASYSTEM
			QASR	QASR AQUIFER			
DEVONIAN	410	LOWER	SHA'BA	SHA'IBA AQUITARD	JALAMID	RUB'AL - KHALI	AD - DAHNA'A - AQUASYSTEM
			TAWIL		SUPER - AQUIFER		
SILURIAN	440	UPPER	AR'AR	AR'AR AQUIFER		RUB'AL - KHALI	AD - DAHNA'A - AQUASYSTEM
			SHARAWRAH				
ORDOVICIAN	460	UPPER	QUSAIBA	QUSAIBA	MEGA - AQUITARD	RUB'AL - KHALI	AD - DAHNA'A - AQUASYSTEM
			SARAH	TAYMA AQUIFER			
ORDOVICIAN	505	LOWER	QUWARAH		HAIL	RUB'AL - KHALI	AD - DAHNA'A - AQUASYSTEM
			RA'AN	RAAN AQUITARD	SUPER - AQUIFER		
CAMBRIAN	570	UPPER	KAHFAH	KAHFAH AQUIFER		RUB'AL - KHALI	AD - DAHNA'A - AQUASYSTEM
			HANADIR	HANADIR	MESO - AQUITARD		
CAMBRIAN	570	LOWER	SAJIR	SAJIR AQUIFER		RUB'AL - KHALI	AD - DAHNA'A - AQUASYSTEM
			RISHA	RISHA AQUIFER	S A Q SUPER - AQUIFER		
PROTEROZOIC BASEMENT				ARABIAN	SHIELD	AQUIFUGE	NAJD - AQUASYSTEM

Fig. 6 The Hydrostratigraphical units of Paleozoic, Mesozoic and Cenozoic of Saudi Arabia. Modified from Edgell (1987a, b, 1990), Al-Aswad and Al-Bassam (1997), Al-Bassam et al. (2000) and BRGM (1985)

Fig. 7 Schematic representation of the major petroleum systems of the Arabian Plate. Compiled From Ayres et al. (1982), Benedyczak and Al-Towailib (1984), Al-Marjeby and Nash (1986), Al-Husseini (1991), Abu-Ali et al. (1999), McGillivray and Husseini (1992, 1999), Fox and Ahlbrandt (2002), Al-Ghamdi et al. (2008), Arouri et al. (2009) and IFP-EN unpublished data (2011)

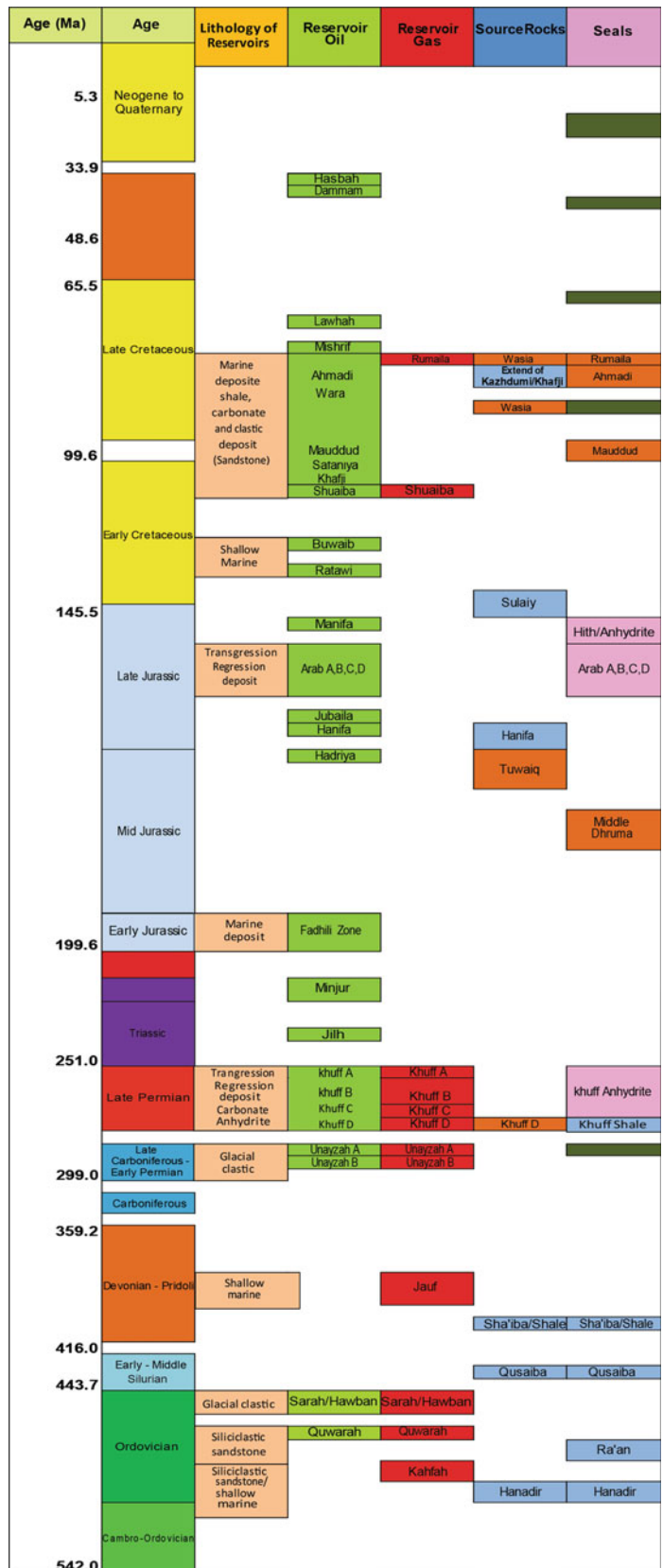


Table 1 Main hydrogeological units and their assessed factors (hydrostratigraphical properties) for CO₂ sequestration. Data compiled from *Different sources* Saudi geological survey report, sa./21936 and BRGM (1985)

Litho-Stratigraphic Units	Comment	Transmissivity m ² /sec	Storage Coefficient	TDS mg/l	Area Expolated	Source	Water Quality	Porosity%	Permeability m d m/s
Harrats Aquifer		15× 10 ⁻³ (NW) 40× 10 ⁻³ (SE)	1×10 ⁻² 3×10 ⁻² 2× 10 ⁻³	2000	varies	Edgell,H.S, 1990			
Hofuf Meso-Aquitard									
Hasa Aquifer	Haradh Super-Aquifer	1 × 10 ⁻² to 3 × 10 ⁻⁶	1 × 10 ⁻² to 2.6 × 10 ⁻⁵	1000 - 35.000	Hasa, Coastal Belt and Wadi Mijah	AL-BASSAM et al., 2000	Fair to Good Quality Water		
Rus Aquifer		7 × 10 ⁻³ - 0.62	10 ⁻³ to 5×10 ⁻¹	900 - 10.000 Av. 2257	Hasa, Haradh	Alyamani, M.S et al., 2005	Enriched in Na ⁺ ,Ca ²⁺ ,Mg ²⁺ ,Cl ⁻ and SO ₄ ²⁻ Mineralization increases with depth (Cl ⁻), Na ⁺		4×10 ⁻⁵ 1,1× 10 ⁻³
Aruma Meso-Aquitard									
Wasia Aquifer	Khurais Super-Aquifer	1.5 × 10 ⁻² to 3 × 10 ⁻⁴	2 × 10 ⁻² to 3 × 10 ⁻⁴	400 - 1550	Khrais, Wadi Dawasir and kharj		Water quality is good near the outcrop (mainly calcium & sulphate) but decreases with depth as the NaCl content increases.	10-29% in Wadi as Sirhan Basin	In Safaniya field 0.5 - 2700
Biyadh Aquifer									
Buwaib MesoAquitard									
Layla Aquifer		1.6 × 10 ⁻³ to 5×10 ⁻³	1 × 10 ⁻⁴	720 - 5000	Layla Wadi Hanifa & Yamama	AL-BASSAM et al., 2000		10-29% In Central Hanifa Av. 17% in Eastern S-30 (Av. 13.25 Arab Fm in Eastern	1.1 1-1000
Tuwaiq MesoAquitard									
Az-Zulfi Aquifer		1 × 10 ⁻² to 1.6 × 10 ⁻²	1 × 10 ⁻³	2400 - 4850	Az - Zulfi	AL-BASSAM et al., 2000	Poor Quality Water		
Marrat Meso-Aquitard									
Al-Suwaidi Aquifer	Kharij Super-Aquifer	7.2 × 10 ⁻³ 1.7 × 10 ⁻³	1.3 × 10 ⁻⁴	1000 - 4100	Riyad, Karj, Sudair and Washem	AL-BASSAM et al., 2000	Mineralization (Cl and Na) increasing with depth. Lower sandstone generally of poorer quality. In Riyadh area Good Quality		1×10 ⁻⁵ to 13×10 ⁻⁵
Jahrah Aquifer									
Shamsiyah Aquifer									
Sudair Mega-Aquitard									
Khuff Aquifer		53 × 10 ⁻³ AV.(0.6 × 10 ⁻³)	0.19 0.72 × 10 ⁻⁴	5000	varies areas	BRGM(1985)	Poor Quality Water	3% - > 20% in North Safaniyah	500-2000 in Central
Unayzah Aquifer	RAFHAH Super Aquifer							9.7-20%	13-2498
Badanah Aquifer		8×10 ⁻⁶ to 1.7 × 10 ⁻⁵	1 × 10 ⁻²	500-1500	varies Wadyan Basin margin	Wood-Mackenzie	Moderate to Good Quality	30% at depth of 4260 m	8×10 ⁻⁶ to 1.7×10 ⁻⁵
Subbat MesoAquitard									
Qasr Aquifer	Jalamid Super Aquifer	< 1,0 × 10 ⁻³ 2×10 ⁻²	2 × 10 ⁻³	300	JAUFI	BRGM (1985)	Good Quality Water	2-15%	8.5 × 10 ⁶
Qusaiba Aquifer									
Arar Aquifer		0.1 × 10 ⁻³ to 23.0 × 10 ⁻⁴	0,01 × 10 ⁻⁴ to 2 × 10 ⁻⁴	<1000 to <500	JAUFI-SAKAKAH and North AL-QASIM		Moderate to Good Quality	Rawil Aquifer 10-20% in Tabuk Basin	2×10 ⁻⁵ 13×10 ⁻⁵
Qusaiba MegaAquitard									
Tayma Aquifer	Hail Super-Aquifer	0.6 × 10 ⁻³ to 3.5 × 10 ⁻³	1.4 × 10 ⁻⁴ to 6.8 × 10 ⁻⁴	<1500	VARIOUS AREA	BRGM (1985) AL-WATBAN (1976)			
Ra'an Aquifer									
Kahfah Aquifer		0.07× 10 ⁻³ to 2,1 × 10 ⁻³	0,8 × 10 ⁻⁴ to 6,7 × 10 ⁻⁴		Tabuk Area	BRGM (1985) ALWATBAN(1976)		8-20% in Tabuk Basin	7×10 ⁻⁶ 1,6×10 ⁻⁵
Hanadir Meso-Aquitard									
Sajir Aquifer									
Risha Aquifer	Saq Super-Aquifer	27 × 10 ⁻³ to 18.7 × 10 ⁻³	0.01 - 0.04 1 × 10 ⁻⁴ to 20 × 10 ⁻⁴	420-630 (NW) (TABUK Area) 300-1000 Various Areas	VARIOUS AREAS	PARSONS BASIL (1969)	Fresh Water and Safe for irrigation Chloride and Sulphate are the dominant anions Calcium and Sodium are the dominant cations.	10-25%	13×10 ⁻⁵ (Saq vicinity) 6×10 ⁻⁴ TO 9,0×10 ⁻⁴ (Al-Qasim Area) 3,5×10 ⁻⁴ TO 9,0×10 ⁻⁶ (Tabuk Area)

Climatic Implications and Economic Perspectives

Due to continuously rising global demand for energy, the consumption of fossil fuels is expected to rise through 2035, leading to greater CO₂ emissions (International Energy Agency 2011), CCS technology offers the opportunity to reduce emissions while maintaining a role for fossil fuels in national energy portfolios. The CCS technology has the potential to reduce CO₂ emissions from a coal or natural gas-fuelled power plant by as much as 90 % (Finkenrath 2011); hence it could provide efficient means for significant reductions of CO₂ emissions.

Besides, oil produced by CO₂-EOR projects can be considered to be relatively less carbon releasing than oil produced by standard techniques (Taglia 2010). Consequently, whether CO₂ sequestration is applied through CCS projects into aquifers or as CO₂-EOR procedures in old producing fields, the net results are a decrease in anthropogenic greenhouse gases and a globally more economic and cleaner energy production.

Discussion

The main objectives of this study is to highlight the significance of understanding the tectono-stratigraphic and paleoclimatic evolutions on selecting sites for carbon capture and storage (CCS), and to provide a first-hand inventory of potential targets for CCS and CO₂-EOR in the Kingdom of Saudi Arabia (KSA). The KSA possesses mature oil and gas fields, which have trapped hydrocarbon for millions of years. They may provide excellent choices for CO₂ underground sequestration. Besides, EOR can be achieved by pumping CO₂ in some depleting reservoirs, resulting in an economic approach for improving production and decreasing greenhouse gases emissions. Still, some of the deep lying aquifers with low quality groundwater can be also used for CCS, under vast, unpopulated regions (such as the Rub' Al-Khali region).

According to a generalized geological review of the KSA, an easternmost prolific sector and an adjacent westward non-prolific sector have been defined (see above). For instance, obvious changes in thicknesses and lithologies are observed in these two sectors as Saudi Arabia were affected by far-field effects of the Hercynian orogeny.

The non-hydrocarbon—prolific sector belongs to a zone which remained tectonically stable from early Cambrian till late Ordovician. It is characterized by deposition of clastics formations (Siq, Quweria, and Saq sandstones, as well as Qasim (transgressive-regressive cycles)).

During late Ordovician, two glaciations episodes affected the Arabia plate, represented by the Zarqa and Sarah formations (McClure 1978; Bell and Spaak 2007).

Then a new period of increasing temperature due to the move of the Arabian plate toward the equatorial position (Fig. 3). The deposition of the Tawil formation during early Devonian consists of continental clastic sandstone, and middle-late Devonian is recorded by the Jauf formation which consists of carbonate and shale. It was then followed by the late Devonian Jubah formation (Jones and Stump 1999) (Fig. 2).

Paleozoic carbonate rocks are rare, and in general sandstone is the dominant lithology in the rock formations toward the south (Rub'Al-Khali region). The thicknesses of the Paleozoic formations are almost twice larger in the hydrocarbon-prolific sector (compared to those in the non-prolific sector), which matches with the general north-eastward trend of thickening and tilting (Beydoun 1991, 1998) (Fig. 5). During the Permian, the northern and eastern margins of the plate were affected by rifting (inducing a rise of the asthenosphere) as well as a general increase in surface temperature caused by warmer climatic conditions (Murriss 1980; Konert et al. 2001). By mid-Permian time an eperic carbonate platform was established. Evaporites are present in the central part of the KSA and towards the northeast. Clastic material was mainly derived from the erosion of the western hinterland, with local supplies from the east in the high Zagros (Murriss 1980).

During Early Triassic, hot arid conditions are prevailed over the whole Basin. A coeval increase in clastic influx from the western hinterland is evident. The climate became less arid and there was apparently a relative drop in sea level, caused either by eustatic lowering of the sea level or a rise of the Arabian Arch (Fig. 4). During the Jurassic, high sedimentation rates characterized the transgressive limestone deposits of the Marrat formation (Figs. 3 and 8). A gradual return to more humid climate occurred in the Early Cretaceous (Fig. 3). This led to the disappearance of evaporite from the sedimentary records. The regional sea level dropped, and ramp type deposition prevailed. Whereas the clastic influx was still limited, and restricted to the far southwestern part of Arabia. It was followed by a period of increasing clastic influx represented by the Biyadh formation, which occupied the area from the central-west to the southwestern parts of the Saudi Arabia (Powers et al. 1966). Clastic influx restricted carbonate production. It was followed by the deposition of the Wasia formation (sandstone with shale), whereas toward the northeast (hydrocarbon-prolific sector) this formation consists mainly of transgressive carbonate and evaporite deposits (Fig. 8).

Differential sea level variations between two sectors is suggested resulting from the re-uplift of the axial zone of the Arabian Arch from early to middle Cretaceous. Hence, a local apparent sea level fall has affected this area (including most of the non-prolific sector) (Fig. 4). In the northeastern area, the subsidence of the Arch was continuous. It started in



Fig. 8 Simplified stratigraphic sections and sea level variations representing the northwestern and northeastern sectors of the Arabian plate, respectively. Modified from Sharland et al. (2001) and Haq and Al-Qahtani (2005)

the middle Jurassic and spanned through middle Cretaceous times, leading to relative sea level rise. With the prevailing humid climatic conditions, different lithologies are observed for the same chronostratigraphic units in the Cretaceous, as we move from west to east across the Arabian Basin. For instance, the Wasia/Sakaka formation in the northwest are characterized by clastic sandstones deposited on a proximal shelf environment, whereas the same chronostratigraphic unit is made up of relatively deeper carbonate intrashelf facies in the northeast (Fig. 8). Furthermore, the overlying Aruma formation (Late Cretaceous), is mainly made up of sandstone in the Tabuk area (northwest of KSA), and grades laterally to carbonate rocks to the northeast, where it accumulates hydrocarbon instead of water as in the Tabuk area (Fig. 8).

The Paleozoic times are supposed to be of lower overall temperatures and higher humidity than the Mesozoic (Konert et al. 2001). This seems to remain undifferentiated across Arabia. During the Mesozoic, slightly different paleoclimatic conditions appear to have been established in the eastern and western margins of Saudi Arabia; towards the west, temperatures seem to have been lower and a higher humidity prevailed, invoking considerable erosion and weathering.

The Paleozoic rock aquifers have relatively low TDS (mostly lower than 1500 mg/l) with lower porosity and permeability values compared to those of the Mesozoic units (Ahmed and Abderrahman 2008; *Saudi geological survey report sa./21936*) (Table 1). Accordingly, the major proposed targets for CCS in the non-prolific regions are Kharij super-aquifer (Triassic), Az-Zulfi aquifer (Middle Jurassic), Layla aquifer (Late Jurassic), and lastly, the Wasia aquifer (Middle Cretaceous).

Extensive studies on the reservoirs properties in the KSA have been achieved for hydrocarbon exploration (e.g., Magara et al. 1992; Sail et al. 1998; Koepnick et al. 1995; Hussain et al. 2006; Sahin et al. 2007; Macrides and Neves 2008), compiled the results of these studies with the present geological assessments resulted into proposition of the best targets for EOR (i.e., Safaniya oil field (Middle Cretaceous) (Safaniya, Wara and Khafji reservoirs), Manifa oil field (Las, Safaniya and Khafji reservoirs) (Late Jurassic), and Khuff reservoir (Late Permian-Early Triassic)) in central to eastern the Kingdom of Saudi Arabia.

Unconformities across the Arabian plate constitute an important factor for CO₂ storage, because most of them act as a lateral carrier systems which allow higher circulations of fluid (water, gas and oil). The present study has identified 12 major unconformities (Fig. 2).

Conclusions

- This study recognized hydrocarbon-prolific sector (mainly reservoirs area) in the northeastern, eastern and central parts of KSA and non-hydrocarbon-prolific sector (mainly aquifers areas) in the western parts of KSA.
- The Paleozoic rock sequences are affected by far field Hercynian orogeny. Relatively thinner rock units with clastics as dominant sediments, prevailed. The Mesozoic rock sequence is affected by extension. Relatively thicker, less unconformities, a smaller number of reservoirs, mainly carbonate sediment, and a relatively higher numbers of seals. It was a period of relative tectonic quiescence, mainly controlled by an increase of temperature and sea level rises.
- The main differences in lithology between the two sectors across the Arabian plate is driven by tectonic inversion operating in the axial part of the central Arabian Arch, which induced uplift and erosion in the western (non-hydrocarbon-prolific sector), and relative subsidence in the eastern (hydrocarbon-prolific sector). This is evidenced by the lithology variation of the Wasia formation in the two sectors.
- Proposed targets for CCS, in the non-prolific sector, are Kharij super-aquifer (Triassic), Az-Zulfi aquifer (Middle Jurassic), Layla aquifer (Late Jurassic), and Wasia aquifer (Middle Cretaceous).
- Proposed targets for EOR are Safaniya oil field (Middle Cretaceous) (Safaniya, Wara and Khafji reservoirs), Manifa oil field (Las, Safaniya and Khafji reservoirs) (Late Jurassic), and Khuff reservoir (Late Permian-Early Triassic) in central to eastern KSA.

References

- Abu-Ali MA, Rudkiewicz JLL, McGillivray JG, Behar F (1999) Paleozoic petroleum system of central Saudi Arabia. *GeoArabia* 4 (3):321–336
- Al-Ahmadi ME (2009) Hydrogeology of the Saq aquifer Northwest of Tabuk, Northern Saudi Arabia. *J King Abdulaziz Univ Earth Sci* 20 (1):51–66
- Al-Aswad AA, Al-Bassam AM (1997) Proposed hydrostratigraphical classification and nomenclature: application to the Paleozoic in Saudi Arabia. *J Afr Earth Sci* 24(4):497–510
- Al-Bassam AM, Al-Dabbagh ME, Hussein MT (2000) Application of a revised hydrostratigraphical classification and nomenclature to the Mesozoic and Cenozoic succession of Saudi Arabia. *J Afr Earth Sci* 30(4):917–927
- Al-Ghamdi A, Tello R, Al-Bani F (2008) Collaboration breeds success in the Khurais mega-project in Saudi Arabia. *SPE 120798-MS*:1–9

- Al-Husseini MI (1991) Potential petroleum resource of the phanerozoic rocks of Saudi Arabia. *SPE* 24101:1–12
- Al-Jallal A, Al-Sharhan AS (2005) Arabia and gulf. In: Selley R, Cocks R, Plimer I (eds) *Encyclopedia of geology*. Elsevier, pp 140–152
- Al-Marjebly A, Nash D (1986) A summary of the geology and oil habitat of the Eastern Flank hydrocarbon province of South Oman. *Mar Petrol Geol* 3:306–314
- Al-Ramadan KA, Hussain M, Imam B, Saner S (2004) Lithologic characteristics and diagenesis of the Devonian Jauf sandstone at Ghawar field. Eastern Saudi Arabia. *Mar Petrol Geol* 2:1221–1234
- Al-Sharhan AS, Narin AEM (1995) Tertiary of the Arabian gulf: sedimentology and hydrocarbon potential. *Paleogeography* 114:369–384
- Al-Sharhan AS, Narin AEM (1997) Sedimentary basins and petroleum geology of the middle east. Elsevier Science B.V., Amsterdam, The Netherlands, pp 1–942
- Al-Shayea NA (2000) Inherent heterogeneity of sediment in Dhahran, Saudi Arabia—a case study. *Eng Geol* 56:305–323
- Arouri KR, Al-Saleh SH, Al-Hilal ZM (2009). Residual oil as a tool in migration and filling history analysis of petroleum reservoir, Ghazal Field, Saudi Arabia. *Org Geochem* 40:617–627
- Ayres MG, Bilal M, Jones RW, Slentz LW, Tartir M, Wilson AO (1982) Hydrocarbon Habitat in main producing areas, Saudi Arabia. *AAPG Bull* 66(1):1–9
- Bakiewicz W, Milne DM, Noori M (1982) Hydrogeology of the Umm Er Radhuma aquifer, Saudi Arabia, with reference to fossil gradients. *Q J Eng Geol Lond* 15:105–126
- Barkto K, Al-Shobaili Y, Gagnard P, Warlick M, Ba Im A (2009) Drill cutting re-injection (CRI) assessment for the Manifa field: an environmentally safe and coast-effective drilling waste management strategy. *SPE* 126077:1–11
- Bazanti MS (1988) Sand production model for Safaniya field, Saudi Arabia. *SPE* 19035:1–21
- Bell A, Spaak P (2007) Gondwana glacial events and their influence on petroleum system in Arabia. *AAPG Int Conf* 1–4
- Benedyczak C, Al-Towailib AA (1984) Offshore sandstone reservoir perforating practices used in Saudi Arabia. *J Petrol Technol* 0149-2136/84/0091-1497. *AIM*:1511–1516
- Beydoun ZR (1991) Arabian plate hydrocarbon geology and potential—a plate tectonic approach. *Am Assoc Petrol Geol Bull Stud Geol* 33:1–77
- Beydoun ZR (1998) Arabia plate oil and gas: why so rich and so prolific. *Episodes* 21(2):1–8
- Brown GF (1972) Tectonic map of the Arabian Peninsula. Ministry of petroleum and mineral resources. Directorate general of mineral resources, Saudi Arabia, Map AP-2
- Cagatay MN, Saner S, Al-Saiyed I, Carrigan W (1996) Diagenesis of the Safaniya sandstone member (mid-cretaceous) in Saudi Arabia. *Sediment Geol* 105:221–239
- Cole GA, Abu-Ali MA, Aoudeh SM, Carrigan MJ, Chen HH, Colling EL, Gwathney WJ, Al-Hajji AA, Halpen HI, Jones PJ, Al-Sharidi SH, Tobey MH (1994) Organic geochemistry of the Paleozoic petroleum system of Saudi Arabia. *Energy Fuels* 8: 1425–1442
- Edgell HS (1987a) Geology of studied areas. In: KFUPM ground water resources evaluation in Saudi Arabia, King Fahd University of petroleum and minerals, KFUPM Press, Dhahran, pp 24–77
- Edgell HS (1987b) Regional stratigraphic relationships of Arabia in exploration for oil and gas. In: Short course on hydrocarbon exploration, KFUPM Press, Dhahran, pp 1–44
- Edgell HS (1990) Geological framework of Saudi Arabia groundwater resources. *J King Abdulaziz Univ Earth Sci* 3:267–286
- El-Ghali M (2005) Depositional environments and sequence stratigraphy of paralic glacial, paraglacial and postglacial upper ordovician siliciclastic deposits in the Murzuq basin, SW Libya. *Sediment Geol* 177:145–173
- Finkenrath M (2011) Cost and performance of carbon dioxide capture from power generation. International Energy Agency
- Fox JE, Ahlbrandt TS (2002) Petroleum geology and total petroleum systems of the Widyan basin and interior platform of the Saudi Arabia and Iraq. *US Geol Surv Bull* 2202-E:1–26
- Haq BU, Al-Qahtani AM (2005) Phanerozoic cycles of sea-level change on the Arabian platform. *GeoArabia* 10(2):127–159
- Hussain M, Hassan WM, Abdulraheem A (2006) Controls of Grian-size distribution on geomechanical properties of reservoir rock—a case study: Cretaceous Khafji member, Zuluf field, offshore Arabin gulf. *J Marpetgeo* 23:703–713
- Hussain M, Ahmed SM, Abderrahman W (2008) Cluster analysis and quality assessment of logged water at an irrigation project, eastern Saudi Arabia. *J Environ Manag* 86(2008):297–307
- International Energy Agency (2011) World energy outlook factsheet—how will global energy markets evolve to 2035
- Jones PJ, Stump TE (1999) Depositional and tectonic setting of the lower Silurian hydrocarbon source rock facies, Central Saudi Arabia. *Am Assoc Petrol Geol Bull* 83:314–332
- Kaldi JG (2008) Geosequestration of CO₂. *Am Assoc Petrol Geol* 4: 1–3
- Koepnick RB, Lowell EW, Kompanick GS, Al-Shammery MJ, Al-Amoudi MO (1995) Sequences stratal geometries and burial-related microporosity development controls on performance of the Hadriya reservoir (upper Jurassic) Berri field, Saudi arabia. In: Al-Husseini MI (ed) *Geok-94, middle east petroleum geosciences conference*. Gulf Petrol, Manama, Bahrain 2: 615–623
- Konert G, Afifi AM, Al-Hajri SA, Droste HJ (2001) Paleozoic stratigraphy and hydrocarbon habitat of the Arabian plate. *GeoArabia* 6: 407–442
- Le-Nindre Y-M, Vaslet D, Le-Metour J, Bertrand J, Halawani M (2003) Subsidence modeling of the Arabian platform from Permian to paleogene outcrops. *Sediment Geol* 156:263–285
- Macrides CG, Neves FA (2008) Lithology estimation from a multicomponent 3D–4D OPC gulf. *GeoArabia* 1:15–33
- Magara K, Khan MS, Sharief FA, Al-Khatib HN (1992) Log-derived reservoir properties and porosity preservation of Upper Jurassic Arab formation in Saudi Arabia. *Mar Petrol Geol* 10:352–363
- McClure HA (1978) Early paleozoic glaciation in Arabia. *Paleogeogr Paleocl Paleocool* 25:315–326
- McGillivray JG, Husseini MI (1992) The paleozoic petroleum geology of central Arabia. *APPG Bull* 76(10):1473–1490, 17 Figs
- Ministry of Agriculture and Water (1984) Water Atlas of Saudi Arabia, Riyadh, Saudi Arabia, 1–112
- Morton DM (1959) The geology of Oman. In: 5th world petroleum congress. Section 1, pp 1–14
- Morris RJ (1980) Middle east: stratigraphic evolution and oil habitat. *Am Assoc Petrol Geol Bull* 64(5):597–618, 25 Figs
- Oterdoom WH, Worthington M, Partington M (1999) Petrological and tectonostratigraphic evidence for a mid-ordovician rift pulse on the Arabian Peninsula. *GeoArabia* 4:467–500
- Pollastro RM (2003) Total petroleum systems of the paleozoic and Jurassic, greater Ghawar uplift and adjoining provinces of central Saudi Arabia and Northern Arabian-Persian gulf *US Geol Surv Bull* 2202-H:1–100
- Powers RW, Ramirez LF, Redmond CD, Elberg EL (1966) Sedimentary geology of Saudi Arabia, U.S.G.S. prof. paper 560-D, pp 1–147
- Rahman SM, Khondaker AN (2012) Mitigation measures to reduce greenhouse gas emission and enhance carbon capture and storage in Saudi Arabia. *Renew Sustain Energy Rev.* 16:2446–2460
- Sahin A, Ali AZ, Saner S, Menouar H (2007) Permeability anisotropy distributions in an upper Jurassic carbonate reservoir, eastern Saudi Arabia. *J Petrol Geol* 30(2):147–158

- Sail IA, Abdulla HM, Magara K (1998) Lith-statistical study of both the Jurassic and cretaceous type section in Saudi Arabia. *J King Abdulaziz Univ Earth Sci* 1:61–85
- Saudi geological survey: stratigraphy of the phanerozoic rocks of Saudi Arabia. Faculty of KSU.sa./21936
- Scotese CR (1998) Quick time computer animations, Paleomap project: Department of Geology, University of Texas at Arlington
- Sharaf MA, Hussein MT (1996) Groundwater quality in the Saq aquifer, Saudi Arabia. *Hydrol Sci* 41(5):638–696
- Sharland PR, Archer R, Casey DM, Davies RB, Hall SH, Heward AP, Horbury AD, Simmons MD (2001) Arabian plate sequences stratigraphy. *GeoArabia Special Publication 2*, Gulf Petrolink, Manama, Bahrain, pp 1–371
- Stump TE, Van Der Eem JG (1995) The stratigraphy, depositional environments and periods of deformation of the Wajid outcrop belt, southwestern Saudi Arabia. *J Afr Earth Sci* 21(3):421–441
- Taglia P (2010) Enhanced oil recovery (EOR)—petroleum resources and low carbon fuel policy in the Midwest
- Wilson AO (1981) Jurassic Arab—C and D carbonate petroleum reservoirs, Qatif field, Saudi Arabia. *SPE*:171–178

Tectonostratigraphic Study of Carbonate Breccias (Calciturbidites) in the Upper Triassic Baluti Formation (Northern Iraq): New Insights on Tethyan Geodynamics

Sa'ad Z.A. Kader Al-Mashaikie

Abstract

This study aims at describing the sedimentology and geodynamics of the Upper Triassic Baluti Formation from north Iraq. During Late-Triassic period, rift tectonic movement started to spread the Neo-Tethys Ocean in northwest of Gondwana super continent. Intracratonic basins were created where carbonate sediments were deposited in a ramp setting and were interbedded with evaporite near the paleo shore line. The evolution of the rift spreading induced the deposition of polygenetic carbonate breccia and slumps the transition from the ramp to deeper margins. Several types of brecciated sediments are observed in the Baluti Formation. Slump carbonate breccias are arranged in calciturbidite succession and are interbedded with lithic sandstone and thick shale, and sometimes fragmented shales. Along rift-related fault zones, tectonic breccia was formed. Karstic carbonate breccia type was formed due to the dissolution of evaporites and collapse of the cavities roofs, forming another type of carbonate breccia in the Baluti Formation. Tectogenic-diagenetic breccia was formed due to intense dissolution of the carbonate fragments resulting in a late diagenetic breccia. The circulations of fluids through fault zones led to partial dissolution, dolomitization, dedolomitization, micritic-recrystallization and calcitization processes. The fault systems which resulted from the continuous geodynamic evolution of the rift induced the formation of these various types of carbonate breccias in the Late Triassic period.

Keywords

Polygenetic breccia • Baluti formation • Intracratonic basin • Rift movement • Geodynamic evolution • Late triassic

Introduction

The Baluti Formation is composed of calciturbidite successions interbedded with various types of carbonate breccias. The study of these rocks is important to reconstruct the paleo depositional environments and consequently the geodynamic evolution of the Baluti Basin. Previous studies consisted in field notes referring only to the collapse type of breccias from the type locality listed in

the Stratigraphic Lexicon of Iraq (i.e., Bolton 1955; Dunnington 1958; Bellen et al. 1959; Buday 1980; Jassim and Goff 2006; Aqrabi et al. 2010).

The Rhaetian (Upper Triassic) Baluti Formation is cropping out in the highly folded zone parallel to the Zagros Thrust Zone of north and northeast Iraq. The sedimentological characteristics of this formation have been investigated during our study in the Gulley Derash Valley in Jabal Gara Mountain, southeast of Amadiya city in the northern part of Iraq (Fig. 1). The type locality of the Baluti Formation is situated at about 10 km west of the study area. Continuous deposition e.g., lack of significant discontinuities characterizes the local stratigraphic succession.

S.Z.A. Kader Al-Mashaikie (✉)
Department of Earth Sciences, College of Sciences, Baghdad
University, Al-Jadriyah, Baghdad, Iraq
e-mail: geozakee13@yahoo.com

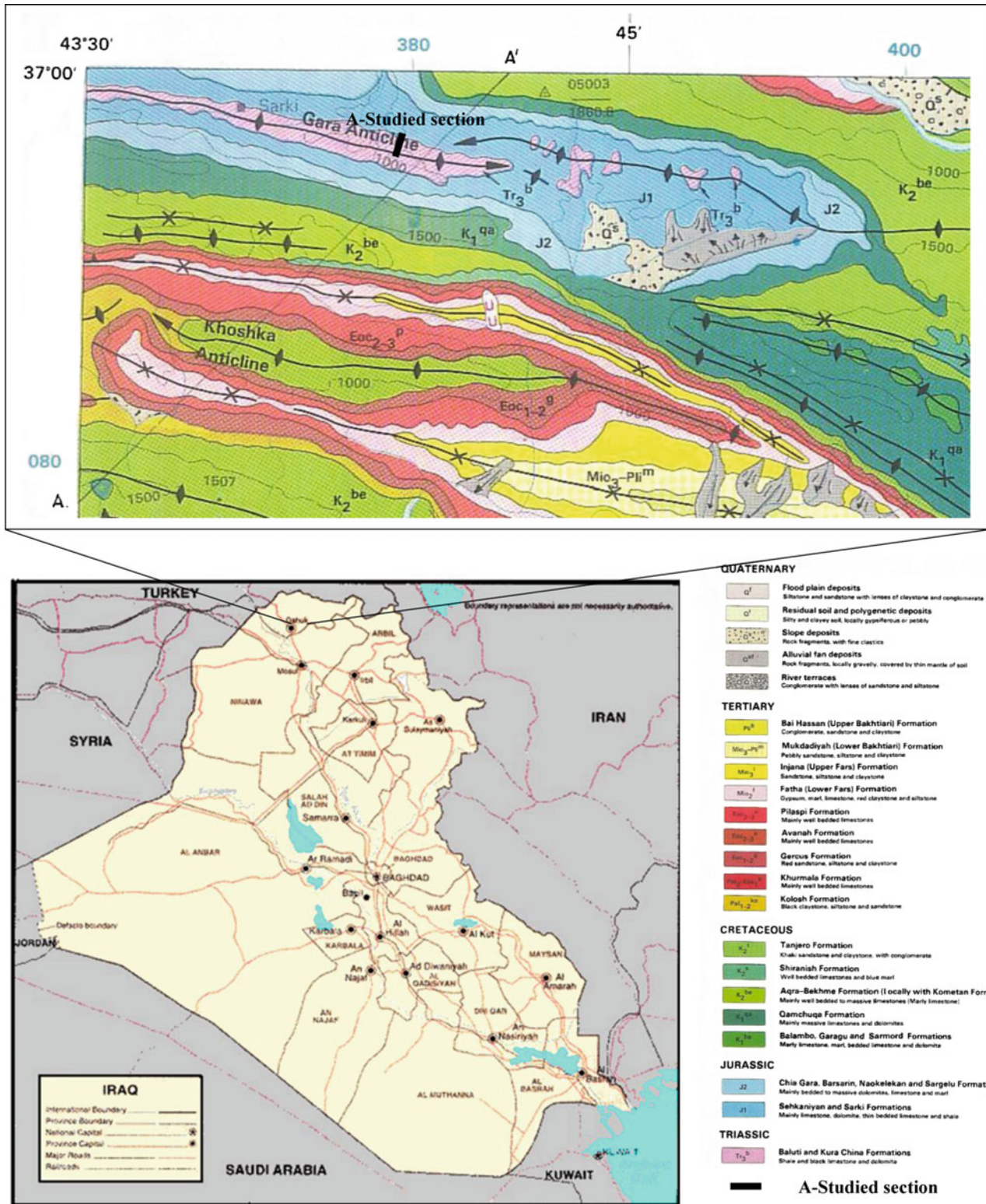


Fig. 1 Location and geological map of the Gulley Derash area shows different exposed geological units. The heavy black line refers to the studied section

The aim of this paper is to define a geodynamic model for the Late Triassic basin accounting also for its sedimentary infill and coeval paleo depositional environments. This paper discusses for the first time the type, origin and tectonostratigraphic evolution of the carbonate breccias/calcuturbidite rocks of the Late Triassic in northern Iraq. The Baluti Formation is subject below to systematic, bed-scale lithologic analysis. Moreover, detailed investigation and discussion were carried out for the types and origin of the carbonate breccias as well as the tectonostratigraphic evolution of the Baluti basin in the Upper Triassic Period.

Geologic Setting

The Baluti Formation constitutes a poorly defined stratigraphic unit, which was introduced by Wetzel (1950) and amended by Bellen et al. (1959). They were sited that the Baluti Formation is comprised 60 m of green and grey shales with decimetric beds made up of thin bedded dolomitic, silicified and oolitic limestones and recrystallization breccias. In NE Iraq the Baluti Formation crops out in the Ranya area (Bolton 1955), and in the Serwan gorge SE of Halabjah city, where two shale units similar to the Baluti Formation crop out. In other areas of Iraq a unit made up of limestone, anhydrite and subordinate shales is usually referred to as the Baluti Shale Formation (Bellen et al. 1959; Ditmar and the Iraqi-Soviet Team 1971) but it lacks the high proportion of shale seen in the outcrops in Gully Derash area. Its status as a separate Formation is thus questionable (Jassim and Goff 2006; Aqrabi et al. 2010).

In the subsurface the Baluti Formation shows variable thicknesses. It was identified in wells; Jabal Kand-1 (61 m), Khlessia-1 (22 m), Atshan-1 (40 m) and W Kifl-1 (46 m). In well Dewan-1, the unit was not identified, being either included within the lower Kurra Chine Formation or the Butmah Formation. The Baluti Formation thins westwards as indicated in the drilled wells. Both lower and upper contacts are conformable (Bellen et al. 1959) except in well Tharthar-1 (Jassim and Goff 2006; Aqrabi et al. 2010).

The age of the Baluti Formation was determined as Rhaetian from its stratigraphic position between the proved Upper Triassic Kurra Chine Formation and the overlying Sarki Formation (Liassic) (Bellen et al. 1959). It was deposited in lagoonal/evaporitic and estuarine environments (Jassim and Goff 2006). Equivalent formations in W Iraq may be eroded. Buday (1980) assumed that the Zor Hauran Formation is tentatively correlatable with the Baluti Formation. This formation may be equivalent also to the "Mulussa-F" unit in the Palmyride and SE Syria (Brew et al. 1999; Jassim and Goff 2006).

The studied section lies in a narrow valley in the core of the Jabal Gara anticline. No similar zone composed of

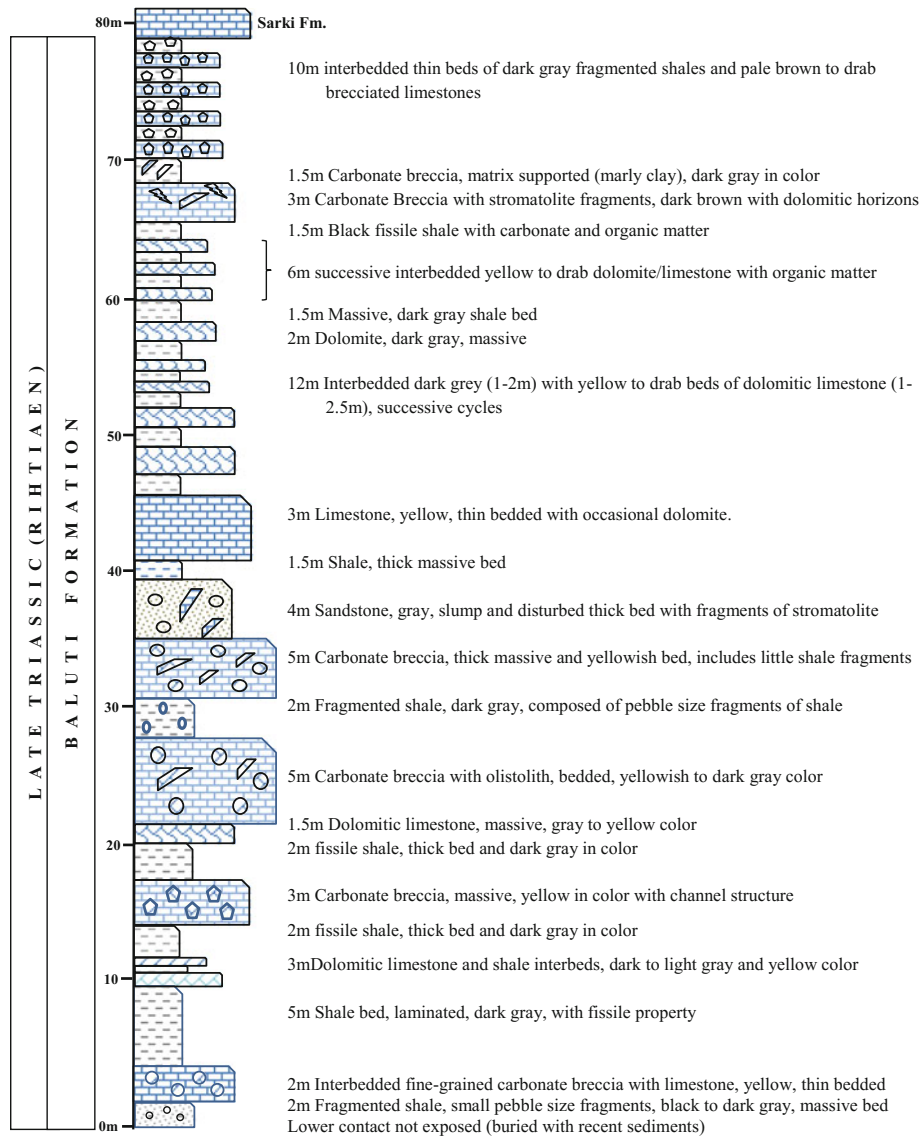
dolomite-limestone breccia was previously recorded in Rhaetian series (Fig. 2). In the Gully Derash Valley the lower contact of the Baluti Formation with the underlying Kurra Chine Formation is covered with valley deposits, while its upper limit is gradational and exposed in the downstream valley. The lateral changes in the breccia zone cannot be observed due to sediments cover, especially along the younger fault zones. Large, more or less well preserved dolomite blocks occur in the breccia units, and are best interpreted as olistoliths. The stratigraphic position of the Baluti Formation can only be established on the basis of superpositional relationships. This is evident from out crop data that the Baluti beds are situated between underlying Kurra Chine and overlying Sarki Formations.

Characteristics of the Breccias

Field observations show that the Baluti Formation is composed of dolomite-limestone carbonate breccias, shales, fragmented shale and debris flow deposits of calciturbidite successions (Plates 1 and 2). Breccia fragments are varying in size, the most common grains being 1–10 cm in diameter, while in some parts of the brecciated zone, decimeter-sized fragments are present, and even blocks of less than meter in size e.g., olistolith (Plate 1) are also present. Some of these fragments are rounded due to the possible slump transport.

Several types of carbonate breccias were identified in the Baluti Formation both in the field observations and petrographic analysis outlining complex and polygenetic origin. This results in great variability of the observed lithofacies. All of the carbonate breccia successions are characterized by the important influence of late-diagenetic processes, which were associated with intense tectonic disintegration. Therefore, the entire breccia successions are defined as tectogenic-diagenetic breccia. However, the brecciated zone reveals spatial relics of former syndepositional breccia, which have been widely impacted by subsequent and post depositional tectonic activity. Fuchtbauer and Richter (1983) and later Vlahovic et al. (2002) defined a specific nomenclature to describe various types of carbonate breccias, such as tectonic breccia, stylolite breccia, collapse breccia, slump breccia, and debris flow breccias. According to this nomenclature each type of carbonate breccias identified in the Baluti Formation is discussed below.

Tectonic breccia was formed by tectonic disintegration of different rock types occurs very close to major fault zones. This type of breccia is of limited surficial and subsurface extension. Petrography of this breccia shows highly fractured micrite and dolomicrite. The fractures usually trend parallel to two directions and are filled with spary calcite with little dolomite crystals (Plate 3c, d).



LEGEND

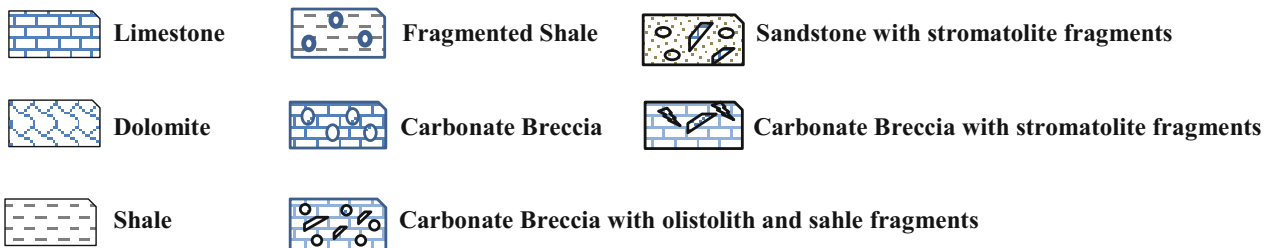
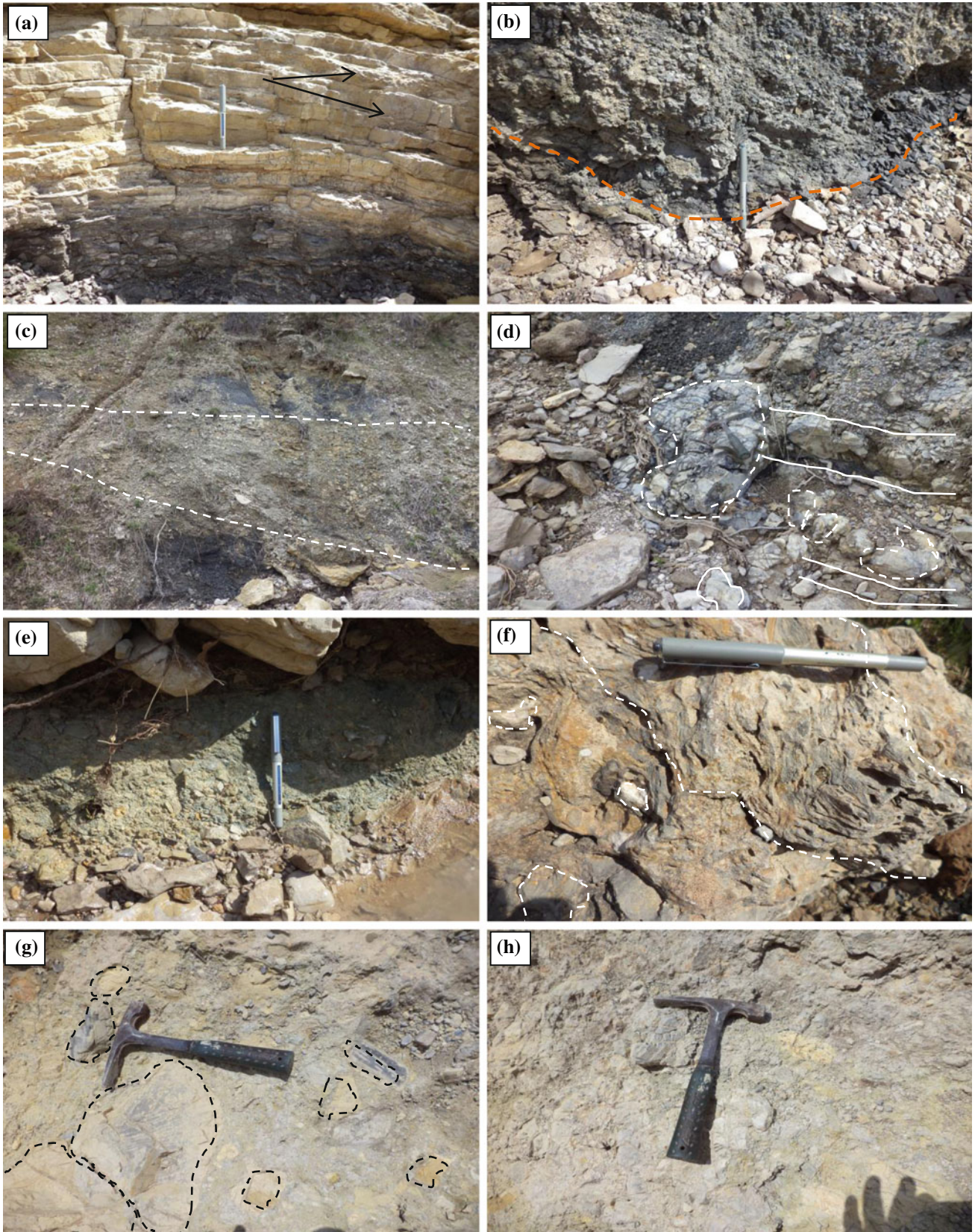


Fig. 2 Stratigraphic log of the Baluti Formation shows different lithological units in Gulley Derash Valley

Plate 1 Field photographs show lithological units of Baluti Formation includes the carbonate breccias. **a** Thin-bedded calciturbidite succession where the arrows refer to pebble sized carbonate breccia. The succession overlies laminated fissile black shale bed with undulated surface (pencil = 10 cm). **b** Black fragmented shale bed composed of pebble angular shale fragments cemented with black shale with undulated lower surface (*dotted red line*) (pencil = 10 cm). **c** Successive beds of carbonate breccias interbedded with channeled fragmented shale. The thickness of the channeled fragmented shale is 1.25 m in the right side of the photo. **d** Carbonate breccias include olistolith clasts (*white dotted lines*) show faint bedded succession (hammer = 30 cm). **e** Fine-grained breccia composed of pebble-sized fragments of carbonate and shales supported with clay matrix (pencil = 10 cm). **f** Dark brown stromatolite fragments in carbonate breccias and supported with carbonate material (pencil = 10 cm). **g** Carbonate breccia composed of variable sizes and shapes carbonate clasts embedded in marly carbonate materials (hammer = 30 cm). **h** Thick gray bed of disturbed and slumped sandstone, which was identified in turbidite succession (hammer = 30 cm)



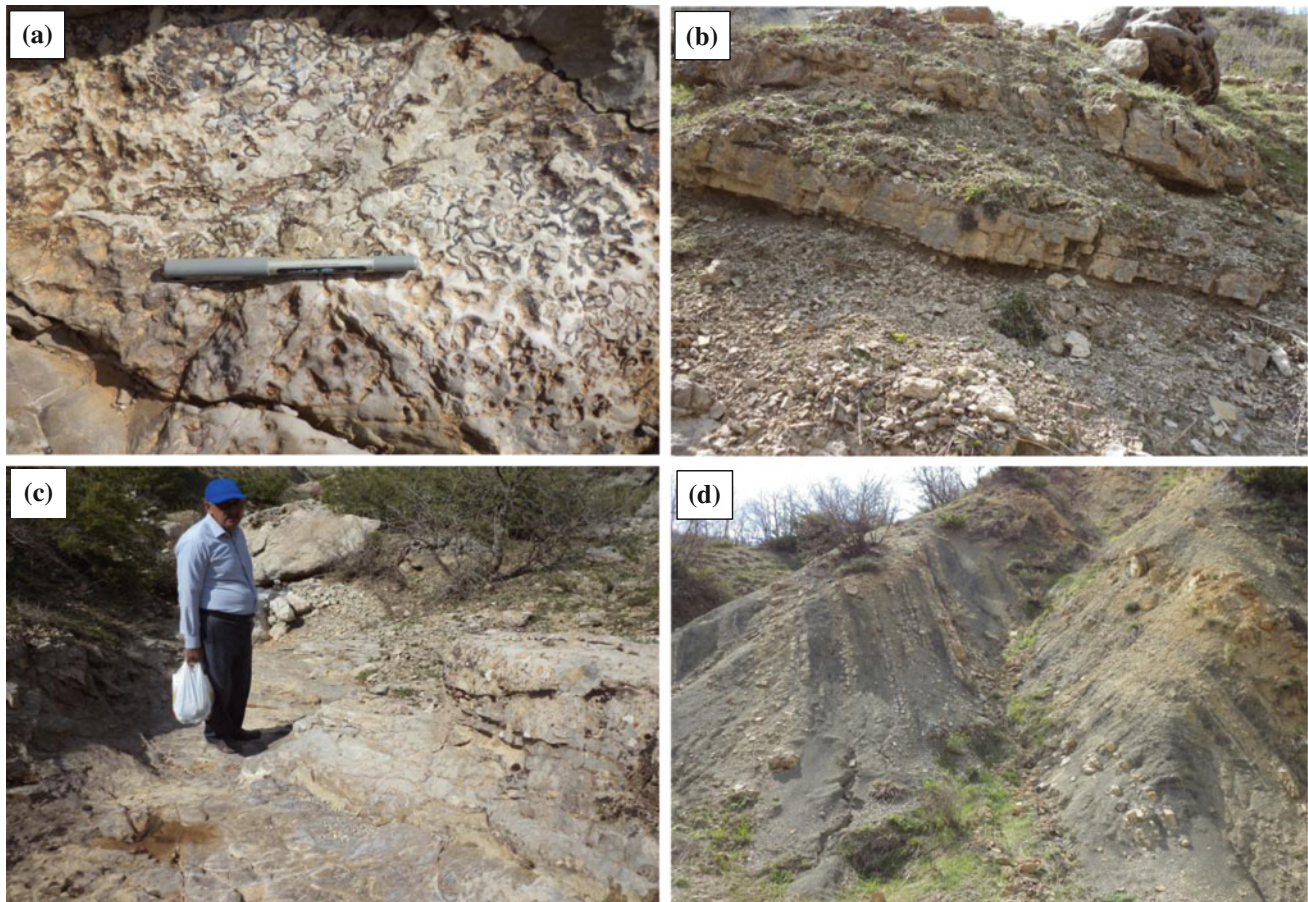


Plate 2 Field photographs show lithological units of Baluti Formation includes the carbonate breccias. **a** Fossiliferous limestone fragment as olistolith includes pelecypods and gastropods fossils (pencil = 10 cm). **b** Interbedded brecciated carbonate beds with gray shales arranged in calciturbidite succession. Note that the thickness of the beds are not uniform with undulated surface (thickness of carbonate bed is about

0.75 m). **c** Channeled carbonate bed overlies fragmented carbonate bed, which were recognized in calciturbidite succession (person long = 1.7 m). **d** Successive interbeds of brecciated and fragmented carbonate beds with fissile and fragmented shale horizons in calciturbidite sequence (the whole succession is about 12–15 m thick)

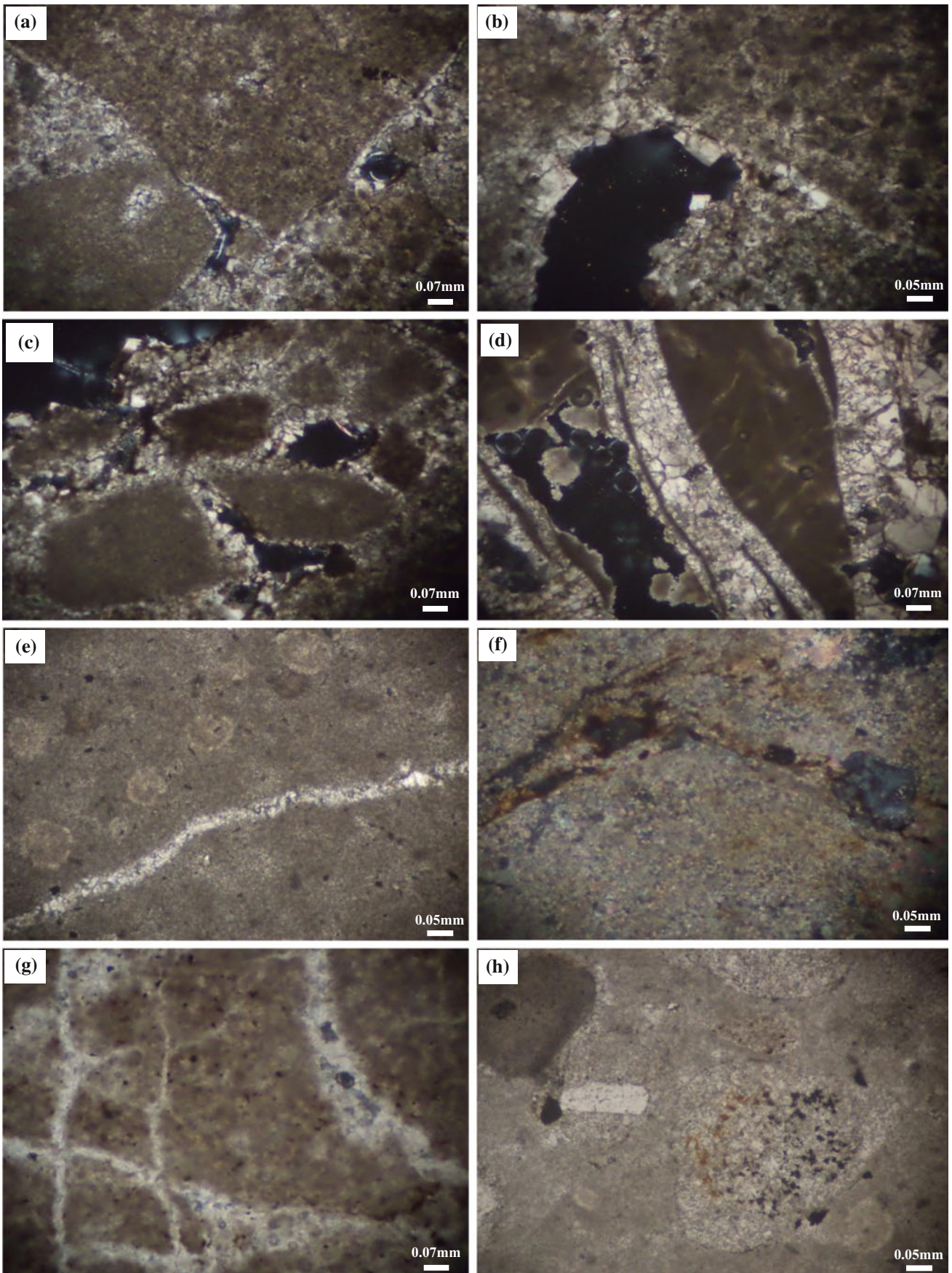
Stylolitization breccia shows more or less intense stylolites around individual breccia fragments. Most of stylolites are filled by brown to dark brown organic matters with local authigenic quartz (Plate 3f).

Collapse breccia is characterized by a mixture of different fragments originated from adjacent beds (which were rotated during their reworking, therefore resulting in much lower fitting) as well as variable proportions of other fragments, finely-crushed matrix and cement fills the remaining open spaces (Plate 1a, c, g). Collapse breccias are much more common near major tectonic feature, but have been usually subsequently diagenetically altered.

Slump breccia is composed of various sizes of carbonate fragments ranging from 0.1 to 0.3 m. Larger clasts are rare. Two types of slump breccias have been identified in the Baluti Formation i.e., clast supported breccia and carbonate matrix supported breccia. These two type of breccia have been observed in the field together with dolomitized olistolith (Plate 1d, e, g).

Debris flow breccia is formed by submarine slump of ramp deposits of various lithologies mainly carbonates and shales under the influence of turbidity currents and due to tectonic movement e.g., rifting, earthquakes. The debris fragments are supported by a carbonate matrix composed

Plate 3 Photomicrographs show the petrographic characteristics, composition and texture of carbonate breccias in Baluti Formation. **a** Angular breccia fragments composed of dolomite and supported with dolomite matrix (CNx25X). **b** Intergranular recrystallized dolomite around pore space shows dissolution of edges of brecciated fragments (CNx40X). **c** Crushed dolomite fragments supported with partially recrystallized dolomites around pore spaces and present influence of dissolution on the edges of the grains (CNx25X). **d** Calcitization of formerly dolomites rocks present in faulted fractured zone characterized by high pore spaces content (CNx25X). **e** Limestone micrite groundmass shows calcisphere fossils and vein composed of spary calcite crystals (CNx40X). **f** Intergranular contacts of breccia fragments characterized by stylolitization and shows authigenic quartz with organic matters (CNx40X). **g** Fractured dolomicrite grains filled with spary calcite (CNx25X). **h** Dolomicrite pelletal grains show partial replacement with calcite. Note authigenic quartz in the mid left of the photo (CNx40X)



basically of small carbonate clasts with calcite and dolomite cement. The lithoclast is range in sizes from 0.1 to 0.3 m in diameter (Plate 1h).

Petrographic study shows that the breccia is dominantly composed of dolomite fragments, with variable amounts of

limestone; authigenous quartz aggregates, pyrite and mostly calcite microspar to spar cement (Plates 3 and 4). Dolomite fragments are characterized by various textural types. Besides the most common homogenous crypto and micro-crystalline textures, pelletal dolomicrite and dolosparite

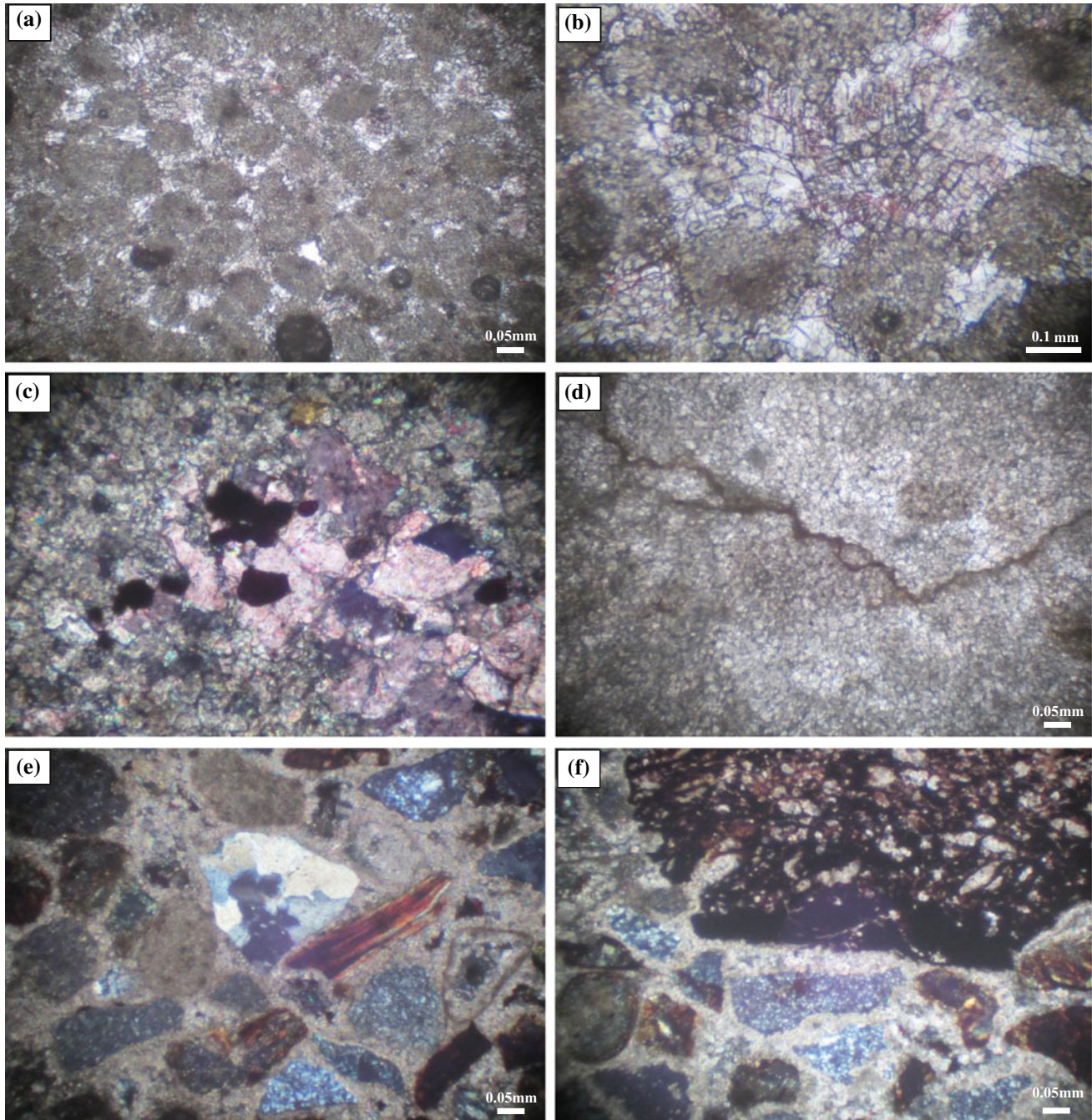


Plate 4 Photomicrographs show mineralogical composition and textures of different lithological units of Baluti Formation (All carbonate thin sections are stained with Alizarin Red). **a** Pelletal dolomites supported with dolosparite crystals with inter-crystalline pore spaces (CNx40X). **b** Pelletal dolomites cement with dolosparite and spary calcite crystals (CNx100X). **c** Crystalline dolomites surrounded spary calcite with pyrite crystals (CNx100X). **d** Micro crystalline dolomite

show relics of pelledolomite and stylolite filled with organic matter (CNx40X). **e** Lithic arenite type sandstone shows different varieties of lithic fragments; carbonate, chert and metamorphic types with polycrystalline quartz in the mid of the photo (CNx40X). **f** Large intrabasinal pebble size grain (dark brown) of very fine sandstone to mudstone was identified in lithic arenite sandstone. Note majority of chert fragments with minor carbonates (CNx40X)

types are identified, indicating early to late diagenetic origin (Plates 3a–c and 4d). Corrosion of fragments is clearly visible in thin sections, especially by obvious centripetal calcification. This process gradually progrades from tectonic fissures surrounding the fragments towards the interior of the grains (Plate 1c). Intergranular contacts are frequently stylolitized entrapping organic materials and authigenic quartz (Plates 3f and 4d). Authigenic quartz druses are mostly composed of hypidiomorphic crystals of variable size.

The cement and matrix of the dolomite-limestone breccia are mostly composed of calcite microspar. Younger tectonic fractures and some solution cavities are completely cemented by mosaic spary calcite.

In infrequent, undolomitized limestone relics, algae, calcispheres (Plate 3e) and planktonic bivalves have been observed without chronostratigraphic significance.

Facies Associations

Sedimentary facies in the Baluti Formation have been studied at outcrop scale and on thin-sections. Facies and lithofacies were identified on the basis of lithology, bounding surfaces, primary physical sedimentary structures, and bioclastic or fossil composition and formational process as listed in Table 1. Trace fossils are not observed in the studied section and thus are not utilized in lithofacies segregation. Carbonate classification by Dunham (1962) and modified by Embry and Klovan (1971) has been used here. The identification and classification of facies types followed Burchette and Wright 1992; Walker and James (1998), Einsele (2000), Posamentier and Walker (2006) and James and Dalrymple (2010).

The specific interpretation for the depositional environments requires the consideration of facies associations as discussed later. Facies associations in the Baluti Formation are interpreted as deposited in deeper marine margins (i.e., below storm wave base). Facies associations are discussed in order of their occurrence (from bottom to the top); (1) FA1 hemipelagic turbidites, (2) FA2 debris flow, and (3) FA2 slump turbidite/debrites.

FA1 Hemipelagic Turbidites

Planar laminated, black, calcareous, silty shale overlain with successive graded thin bedded fine-grained, matrix supported carbonate breccia with erosional base overlain and grading to carbonate mudstone (Plate 1a). These deposits vary from thin bedded and slightly convoluted. Rare current ripples were observed with undulated and scoured lower surface of the beds characterizing the lower surface of black fragmented shale bed (Plate 1b). The bioclastic detritus in

these lithofacies consists of low percentages (<5 %) of planktonic pelecypods shells, some being disarticulated, with scattered organic matter. Intraclasts are primarily made up of planar bedded, fine-pebbly intraclasts grains. Most clasts are oriented roughly concordant to bedding. These are overlain by fragmented black shale composed basically of fine pebble-sized fragments of shale supported by clay matrix (Plate 2b), and massive cloudy dotted very fine crystalline dolomite (mudstone) with patches of organic matter including cavities and vugs. The upper beds consist of successive interbedded fragmented dark gray shale, 1–1.5 m thick, with carbonate debrites. Clasts are relatively equal in size (10–15 cm scale), grain-supported with 1–1.5 m thick beds. Carbonate beds reveals submarine channel structure (Plate 1c). The thickness of these beds reaches up to 8 m.

FA2 Debris Flow

This type of deposits comprises matrix-supported olistolith-intraclast bearing debrites (Plate 1d) grading upward to rudstone-grainstone dolomite (Plate 2b). These deposits vary from massive or structureless to convolute beds. Rare current ripples are observed in this association. Other physical sedimentary structures are not observed. The bioclastic detritus that are identified in these lithofacies consists of algae, planktonic bivalves, calcisphere, gastropods and organic detritus with rounded phosphatic grains (Plate 2a). Large intraclasts are present as olistoliths, and are composed primarily of planar bedding silty dolomitic/calcareous wackestone in packstone/rudstone matrix (Plate 2c). Most clasts are oriented roughly concordant to bedding. However rare examples are oriented oblique or perpendicular to bedding. Intraclasts consist primarily of silty, dolomitic and calcareous wackestone.

FA3 Slump Turbidite/Debrites

This facies association comprises matrix supported carbonate breccia of small and large clasts cf., 3–0.5 m (Plate 1g), rippled laminae of carbonate and organic matter, bioclasts including large stromatolitic fragments (Plate 1f), calcisphere, algae and organic detritus, pellets of micritic and dolomitic composition, which grades upwards to sandstone beds (Plate 1h). The sandstone facies comprises thick disturbed beds, which are slightly convoluted, lithic, medium to fine-grained, well sorted and composed mainly of carbonate and metamorphic lithic fragments with little quartz and feldspar grains. The sandstone beds grades upward in-to thick bed of massive shale including shaley clasts. This facies association is capped by thick dolomite beds, which are composed of structureless microcrystalline dolomite.

Table 1 Facies types of the Baluti Formation in the Gully Derash Valley in Amadiya area arranged from bottom to top of the studied section

Facies	Thick (m)	Lithology	Characteristics	Processes
F1	~ 2	Laminated/fissile shale	Planar laminated, black, calcareous, silty shale. 0.5–15 cm thick laminates	Hemipelagic
F2	1–1.5	Carbonate turbidite	Successive graded-laminated/thin bedded fine-grained carbonate breccia (composed of fine pebbles, matrix supported); erosional base overlain and graded to planktonic pelecypod (<5 %) carbonate mudstone	Hemipelagic & low concentration turbidity currents
F3	1	Fragmented shale	Fragmented black colored shale composed of fine pebble-sized fragments of shale supported with clay matrix	Turbidity currents
F4	1	Dolomite	Massive cloudy dotted very fine crystalline dolomite (mudstone) with patches of organic matter; includes cavities and vugs	Hemipelagic/pelagic sedimentation
F5	10	Successive fragmented shale/carbonate debrites	Thick fragmented dark gray shale, 1–1.5 m thick, interbedded with carbonate debrites, clasts are relatively equal in size (10–15 cm) scale, clasts oriented-concordant to bedding, grain-supported, beds 1–1.5 m thick. Carbonate bed reveals submarine channel structure	High-concentration turbidity currents/debris flow
F6	5	Olistolith bearing Debrites matrix-supported	Intraclasts of planer bedding silty dolomitic/calcareous wackestone in packstone/rudstone matrix, clasts vary in size from mm to m scale, clasts randomly oriented, quartz sand, scattered silt-sized, well rounded phosphatic grains, sorting poor, beds 3–5 m thick	.debris flow/turbidites
F7	3–5	Bioclastic/Rudstone-grainstone, dolomite	Bedded, massive, Moderately sorted, grainstone; cloudy dolomite dominated by bioclastic detritus –10 %, pellets, intraclasts, algae, planktonic bivalves, calcisphere, gastropods and organic detritus common; beds several dm to more than 0.3 m thick	High-concentration turbidity currents/debris flow
F8	6	Carbonate breccia/matrix supported	Large & small clasts cf., 0.5–2 cm; rippled laminae of carbonate & organic matter; bioclastic large fragments of stromatolite, calcisphere & algae, pellets of micrite & dolomite; organic detritus, grades upwards to sandstone	High-concentration turbidity currents/debris flow
F9	4	Slump disturbed sandstone	Thick/thin bedded, some beds show disturbance & convolution, lithic, fine-grained, well sorted; composed mainly of carbonate & metamorphic lithic fragments	High-concentration turbidity currents
F10	2	Shale	Thick, massive, gray colored shale, include shale clasts (cf., 10 cm to 0.5 m), of the same composition	Low-concentration turbidity currents
F11	1–2	Dolomite	Microcrystalline dolomite, structureless; small patches of crystalline calcite	Hemipelagic/pelagic sedimentation
F12	1–2	Carbonate breccia/grain-supported	Intraclasts of angular carbonate and shale small fragments (size 2–3 cm), support with clay matrix	High-concentration turbidity currents/debris flow
F13	5	Fossiliferous & dolomitic limestone	Thick & thin bedded; channeled, scoured, rippled & undulated surfaces; gastropods, pelecypods, brecciated beds	debris flow/turbidites

These beds are characterized by scoured bedding planes or bedsets resulted from current action.

Interpretation of Depositional Model

Three depositional systems are proposed below for the Baluti Formation. These are based on facies types and associations, which constitute the depositional model. These depositional systems are discussed from bottom to top.

Slope Turbidites/Hemipelagic System

The sharp-based, normally thin beds of carbonate breccias grading to carbonate dolomitic mudstone that comprise FA1 are interpreted to have been deposited by turbidity currents in medial to distal slope settings (Fig. 3a). This is supported by the underlying fragmented and laminated fissile black shale with scoured contact. Turbidity currents are gravity-driven sediment flows that maintain grain dispersion in the flow and

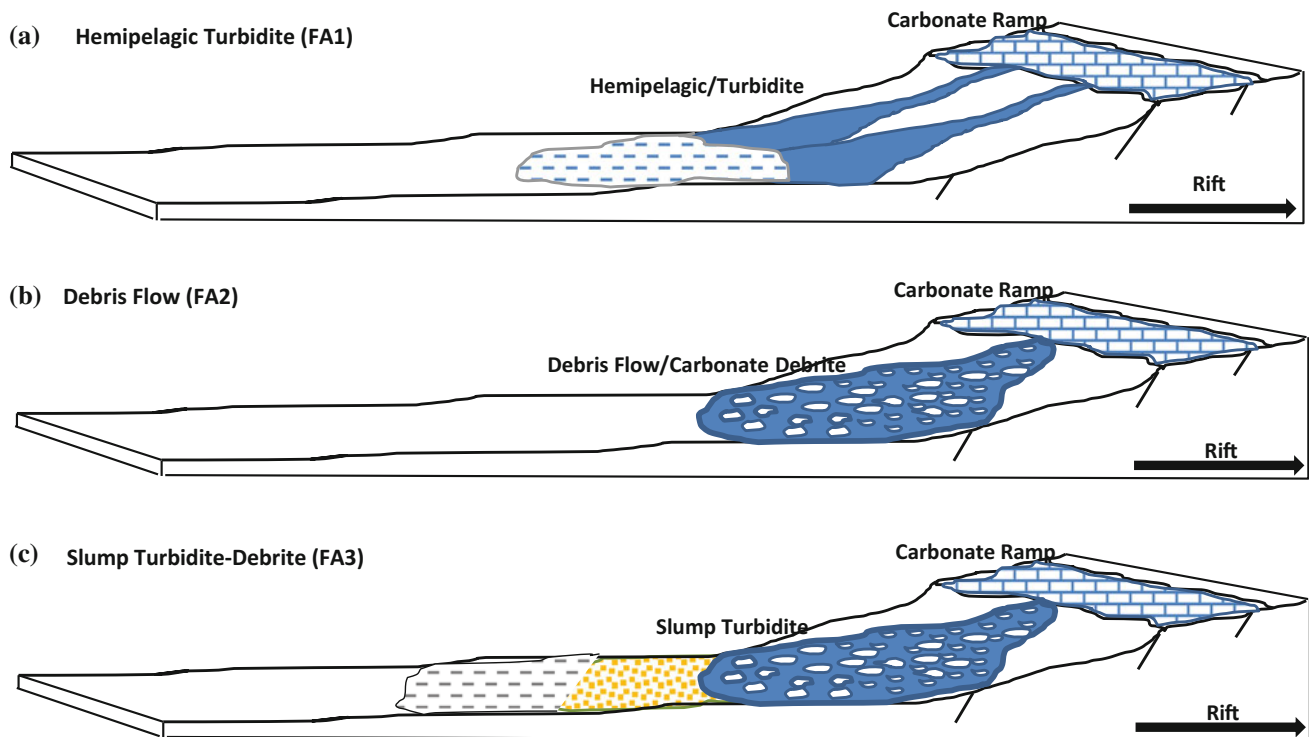


Fig. 3 Schematic diagram discuss the depositional model of the Baluti Formation. **a**, **b** and **c** represents the depositional systems of the formation, each one refers to the main facies association

suspended sediment resulted in a gravity differential between the current and the ambient water (i.e., Middleton and Hampton 1976; Lowe 1982; Stow 1986; Walker 1992; Middleton 1993; Martinsen 1994; Mulder and Cochonat 1996).

Turbidity currents rework and transfer the coarse and fine clastic and carbonate material from shallow to deep marine settings (Eberli 1991a, b; Haak and Schlager 1985). The FA1 turbidites record the transport of invertebrate taxa that normally inhabited shallow water to medial/distal slope settings. The presence of sharp-based tabular beds, normally graded laminasets/beds, plane parallel laminae, bimodal grain-size distribution and partial Bouma sequences in FA1 are diagnostic characteristics of calcareous turbidites (Eberli 1991a, b; Haak and Schlager 1985). Evidence of scour or undulating surfaces was also observed with rare current ripples. Coarse-grained, poorly sorted, variably graded beds may indicate a transport mechanism intermediate between true turbidity current (grains supported by fluid turbulence) and debris flow (grains supported by grain-grain interaction; i.e., Creveallo and Schlager 1980).

Chert nodules are common in calcareous turbidites, due to secondary silicification during lithification, likely sourced from siliceous skeletal debris transported in the turbidity current (Eberli 1991a, b). As evidenced by examples from FA1, calcareous turbidites are typically poorly sorted compared to siliciclastic ones. This is due to both poor sorting in

the source area as well as variable bulk densities and hydraulic qualities for similar sized grains (Rusnak and Nesteroff 1964; Eberli 1991a, b). Siliciclastic turbidites are most commonly associated with turbidite fan complexes. However calcareous turbidites have much more widespread distribution as source materials are more or less evenly distributed along many carbonate shelves/platforms margins (Eberli 1991a, b).

FA2 Debris Flow System

Carbonate breccias, such as those in facies association FA2, occur in a broad range of depositional settings, most commonly seaward of the shelf-slope margin (i.e., James and Mountjoy 1983; Eberli 1991a, b; Coniglio and Dix 1992). Evidence of reworking (fair-weather or storm) is absent in the Baluti Formation and thus, it is interpreted to be deposited below the zone of storm reworking. The massive to slightly convolute bedded bioclastic rudstone and matrix-supported intraclast breccia includes olistoliths, which are interpreted to reflect deposition by debris flows in distally steepened carbonate ramp settings (sensu Read 1985) (Fig. 3b). These debris flow deposits (i.e., debrites sensu Stow 1984, 1986) are the product of slope failure of both coherent (firm/cemented cf., olistolith) and incoherent (loose

cf., carbonate matrix and cement) carbonate deposits in more proximal settings and subsequent basin ward transport via sediment gravity flows (Burchette and Wright 1992; Playton and Kerans 2002).

Evidence that the sediment was supported by fluid turbulence (i.e., graded beds) is lacking and thus these deposits are not interpreted as turbidites. Absence of a clay mineral matrix suggests that these deposits may result from a combination of grain flow and debris flow processes (Middleton and Hampton 1976). However beds in this facies association look more like debrites than grain flow deposits. Large and small intraclasts occur as abundant isolated, blocks 'floating' in a bioclastic rudstone matrix (Plate 1d, g).

Petrographic analyses of clasts and matrix confirm that both are derived from deposits of similar composition providing evidence of early submarine cementation. The presence of out-sized 'floating' blocks cf., olistolith (Walker and James 1998; Einsele 2000; James and Dalrymple 2010) provides evidence for sudden, in situ freezing of a sediment mass rather than particle-by particle sedimentation that characterizes traction deposits (Hampton 1972; Middleton and Hampton 1976). Individual sediment gravity flow freeze when the driving stress decreases to a point less than that necessary to propel the flow (Middleton and Hampton 1976).

Large out-sized clasts may be transported within turbidity flows at the interface between pseudo laminar inertia-flow layer and an overlying faster moving turbulent layer. These deposits are usually characterized by either normal grading or a combination of inverse and normal grading, as well as flute casts on bed soles and physical sedimentary structures consistent with deposition by turbidity currents (Postma et al. 1988). These features are lacking in facies association FA2 and thus the breccia beds are interpreted as debrites rather than turbidites. Debrites in the study interval occur as a stacked succession of decimeter to more than meter scale beds characterized by primarily massive internal structure and crude clast grading. They are thus interpreted to occur from several discrete debris flow events rather than from progressive, incremental accretion.

FA3 Slump Turbidite/Debrites System

Deposition of individual beds and bedsets of FA3 occurred under similar conditions to those in FA1 and FA2. However; FA3 beds exhibited clear evidence of post-depositional sediment remobilization. Despite mass movement, physical sedimentary structures are well-preserved and thus this facies association is interpreted as successions of submarine slump associated with high density turbidity currents (Fig. 3c). The presence of planktonic bivalve, calcisphere, rare radiolaria and rich organic detritus refers to deep marine

setting (Flügel 1982; Scholle and Scholle 2003). The graded matrix-supported carbonate breccias of FA3 are interpreted to have been deposited in a distal turbidite slope setting, associated with slumping of sediment laden to deeper margins (Lowe 1982; Reading 1986; Walker and James 1998; Einsele 2000; James and Dalrymple 2010). The carbonate sediments were accumulated in a slope of carbonate ramp. They were subsequently slumped under the action of turbidity currents with gravity-driven flow. Suspended sediments resulting from gravity differential between the current and the ambient water (i.e., Middleton and Hampton 1976; Lowe 1982; Reading 1986; Middleton 1993; Mulder and Cochonat 1996; Walker and James 1998; Einsele 2000; James and Dalrymple 2010) allowed to transport the coarse clastic, clasts and carbonate material from shallow to deeper margins (Eberli 1991a, b; Haak and Schlager 1985). The turbidites in FA3 show disturbance in internal nature of the beds due to slump of sediments e.g., coarser and finer materials in high density turbidity currents (Lowe 1982). The presence of normally graded upwards, bimodal grain-size distribution and partial or almost complete Bouma sequences in FA3 are diagnostic characteristics of siliciclastic-calcareous turbidites (Eberli 1991a, b; Haak and Schlager 1985; Walker and James 1998; Einsele 2000). Evidence of scour or erosion with sharp-based beds was observed in the lower surface of the beds. Coarse-grained, poorly sorted and graded beds may indicate intermediate transport mechanism between true turbidity currents and debris (Creveallo and Schlager 1980). This is evidenced from FA3, calcareous turbidites cf., carbonate breccias, which are poorly sorted compared to overlying siliciclastic cf., disturbed sandstone and shale beds.

Tectonogenic/Diagenetic Relationships

As aforementioned, several types of carbonate breccias were identified both during field works and in thin-sections, basically related to tectonic activities. Within these types of breccia, elements of all other types are encompassed in some places, and are more or less overprinted by important polyphase diagenetic alterations. Tectonic-diagenetic breccia is a collective designation for rocks of brecciated appearance formed as a result of the diagenetic alteration of in situ rocks affected by intense tectonics. It was noticed that in some of the studied rocks, evidence of specific causes of brecciation is still visible e.g., tectonic crushing, rock collapse from the roof of paleo cavities or stylolitization. Worth to mention, most of the identified brecciated rocks are composite, thus comprising a mix of three characteristic types, the slump type, faulted fractured zone type and in situ brecciation characterized by very short distance of transported breccia fragments in the case of collapse origin.

In northern Iraq in the Baluti Formation, syn and post depositional faults occurred in the carbonate ramp during the main rifting episode and subsequent post-rift thermal subsidence of the basin. The faulted areas became fractured zones forming carbonate breccia (Fig. 3). The porous nature of faulted rocks become zones of high circulation of solutions and accordingly karstification formed due to dissolution of evaporates, inducing the formation of collapse breccias. The circulation of saturated saline solutions was responsible to early and late diagenesis, dolomitization, calcitization and micritization processes. The main active factor controlling all diagenetic processes is the tectonic activities, which are associated with continuous rifting and subsidence.

The carbonate debrite, debris flows with oilstoliths and associated fragmented shales resulted from slumping of competent and incompetent sediments and were most probably associated with lava flows related to intracratonic fracturing and widening of the Late Triassic rift basin in North Iraq.

The poorly sorted carbonate fragments preserved large percentages of pore spaces that permit the solution to circulate and affect the rocks and/or sediments by various diagenetic processes (Plate 3a–d). The most important in this case are the dissolution and corrosion as well as dolomitization of carbonate fragments that lead to increase the percentage of pore spaces by secondary dissolution and mineral transformation. The inverse cementation process lead to decrease the pore spaces (Plate 4a–d).

The rock succession of peritidal early-diagenetic and/or syn-sedimentary dolomite and limestone fragments of the early-diagenetic and/or syn-depositional dolomites are commonly characterized by relics of cryptalgal lamination indicative of formation by early-diagenetic dolomitization in peritidal (supratidal) conditions (Plate 5d).

Interbedded shallow subtidal limestones were subsequently gradually dolomitized into late-diagenetic dolomite during the late-diagenetic phase, which is characterized by mosaic structure of hypidiomorphic dolomite crystals. No

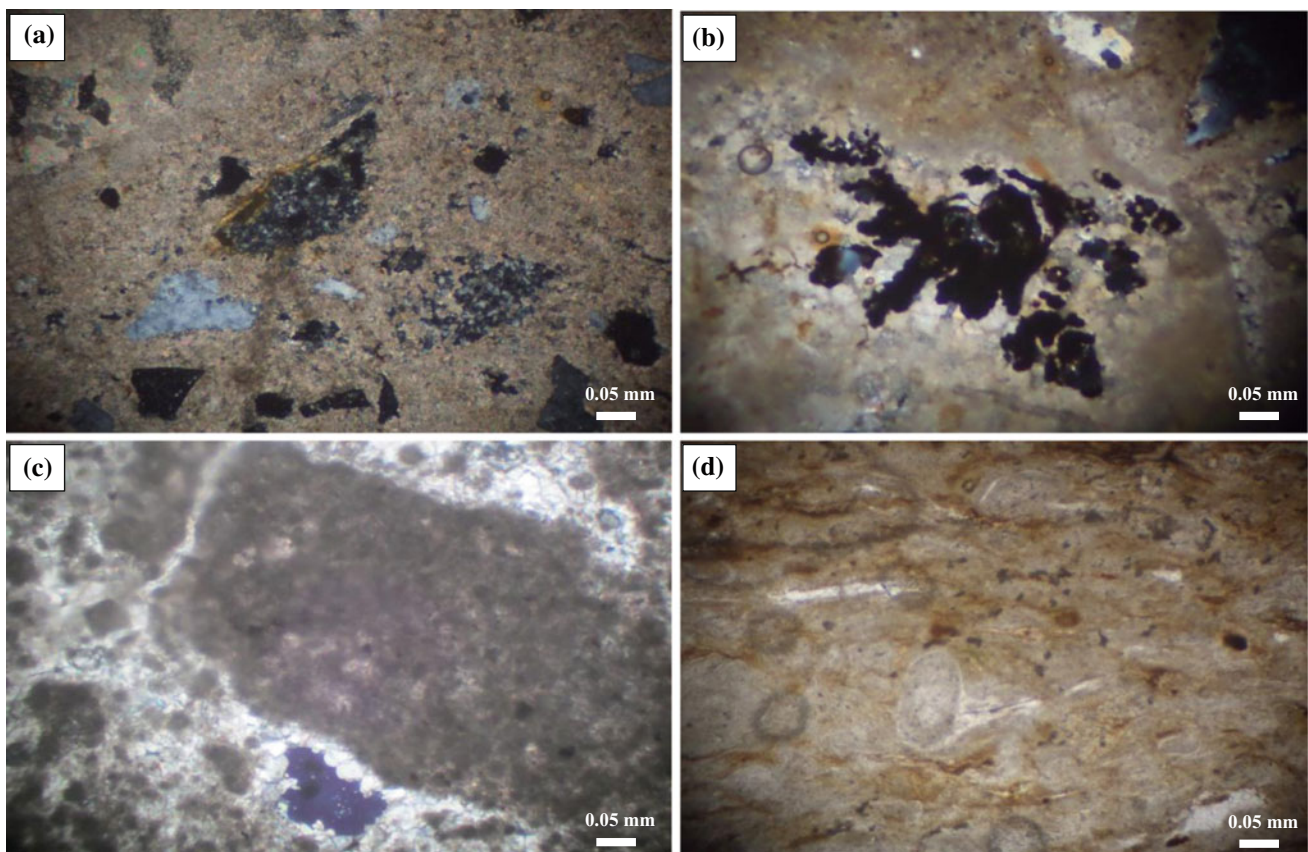


Plate 5 Photomicrographs show mineralogical composition and textures of different lithological units of Baluti Formation (All carbonate thin sections are stained with Alizarin Red) (all photomicrographs are CNx40X). **a** Authigenic quartz aggregate and crystals are embedded with dolomitic groundmass, note the late-diagenetic calcite in the upper left corner of the photo. **b** Peloidal, calcite, probably microbial

branching growths that formed in association with basaltic pillow lavas. **c** Dolomitic breccia fragment are surrounding with crushed dolomite grains with microspar cement and pores. **d** Relics of cryptalgal lamination with peloides indicate formation by early-diagenetic dolomitization in peritidal margin

similar successions have been described in previous literatures, neither in underlying deposits nor in the overlying rocks.

It is very important to investigate the origin of breccia types that resulted from polygenetic processes and diagenetic changes. In another analogous case, breccias are mainly controlled by the presence of specific lithologies (dolomites), which are surrounded by rocks of different composition (predominantly limestones) including diagenetic quartz horizons.

During Tertiary, the entire rock successions in the study area were affected by quite intense post-sedimentary tectonics. Tectonic contraction during Cretaceous in the High Zagros, and propagated forelandward in the Outer Zagros during the Neogene, with episodic episodes of foreland basin inversion since the Upper Cretaceous, the later accounting for local reactivation of former Triassic normal faults associated with the Baluti Formation. However, because dolomite rocks are much more prone to tectonic disintegration than limestones (Handin and Hager 1957) alternation of early-diagenetic and late-diagenetic dolomites are even more intensely fractured than the surrounding limestones. The zones around major faults are even completely crushed, resulting greatly enhanced permeability (Plates 3a, c, d and 5c). Further diagenetic changes took place under conditions where limestone comprises the stable and dolomite the unstable phase. Highly fractured and permeable dolomite rocks enable circulation of chemically aggressive pore solutions, causing partial dissolution and/or diagenetic changes of the rock fragments, since these solutions are oversaturated with calcite and under saturated with dolomite. The chemical composition of pore waters derived from the thick Mesozoic overburden, were characterized by relatively high concentration in calcium, hydrogen and carbonate ions inducing intense dissolution and stylolitization of limestones intervals during tectonic stress phases. Dissolution by meteoric waters rich in CO₂ occurred also in more surficial deposits.

Relatively aggressive fluids caused partial dissolution of dolomite rocks and important allochemical late-diagenetic processes of calcitization (dedolomitization) and late-diagenetic silicification (Plate 5a), which were amplified by the relatively large reactive surfaces of tectonically, disintegrated dolomites. These processes induced important changes of mineral and chemical composition of the original rocks.

Dissolution of dolomite rock along the tectonic fault, fissures and joints caused formation of varying sizes of corrosional voids (Plate 5c), significant widening of fissures and joints, as well as corrosion and rounding corners of dolomite fragments (Plate 3c–d). Therefore, in zones of intense circulation, many grains became rounded, a process which was formerly misinterpreted as a result of transport.

Very important diagenetic processes are affected by recrystallization of matrix and cement and coeval development of calcite in the pore spaces, fissures and fractures as a result of oversaturation of pore solutions with respect to calcium carbonate, followed by gradual replacement of dolomite by calcite e.g., dedolomitization (Plate 3c, d).

It is important to conclude that rounding of fragments is a special result in intense tectonic zones. Polyphase calcitization process formed several neocalcite minerals of various composition e.g., calcite to Fe-calcite, which was caused by polyphase tectonics and variable chemical composition of pore solutions.

Another important allochemical diagenetic process (of lesser extent) formed late-diagenetic silicification of dolomites and dedolomites e.g., calcite, and the neocalcite was formed the matrix and cement (Plates 3f and 5a).

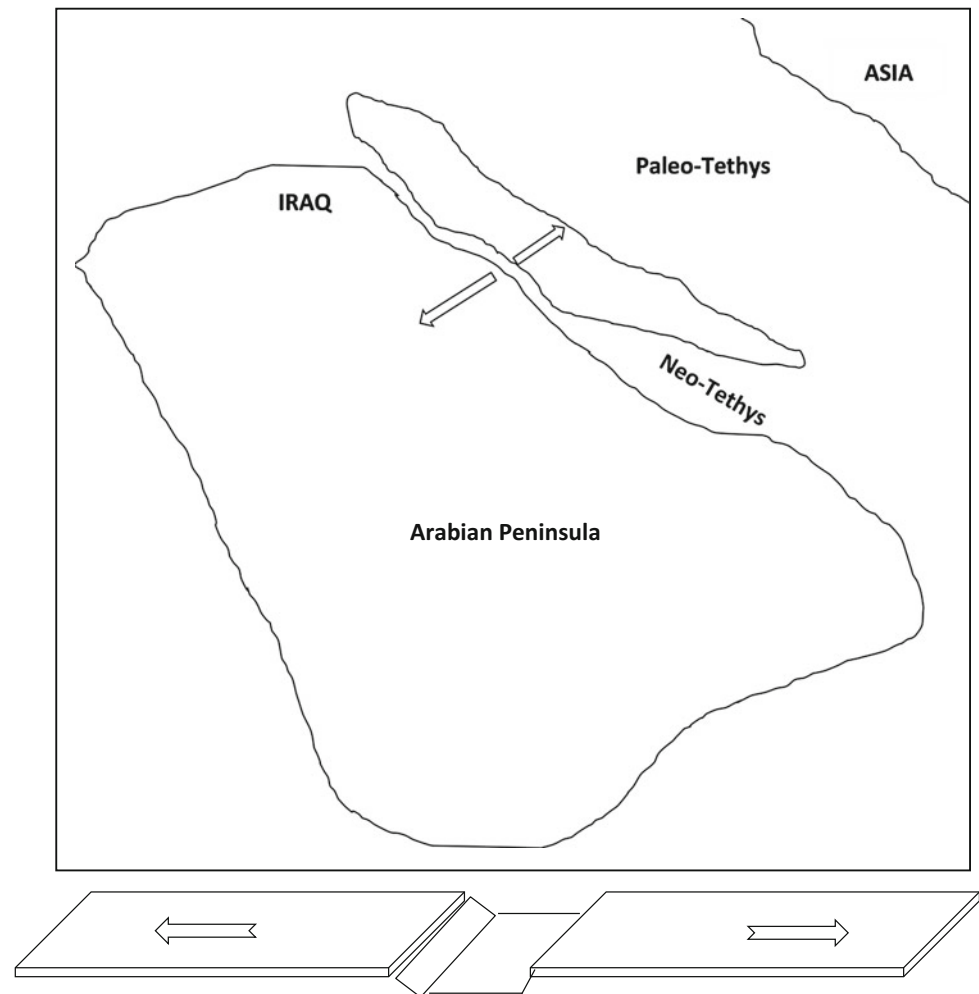
Diluted silicic acid solutions were gradually replacing carbonate minerals, which is unstable under weak acidic pH conditions and/or deeper margins. Silicification reveals microcrystalline and/or rarely crypto crystalline quartz aggregates within the dolomite fragments or within the calcitized matrix. Silicification constitutes a later process than the main calcitization phase despite the fact that a limited younger phase of calcite crystallization occurred. The most probable source of the excess silica was coming from the older formations. These were formed by late diagenetic silicification of limestones caused by the aeolian input of dust and/or volcanic ash.

The tectonic porosity formed due to brecciation is very important in evaluating the reservoir quality in petroleum exploration. In Iraq, the Baluti Formation was not encountered in the drilled oil wells in southern, middle and northern Iraq. The tectonic diagenetic processes are more effective in subsurface than in outcropped rocks. Intense dissolution, dolomitization and new pore spaces generation. We thus assume that Triassic breccias may constitute an excellent reservoir in the subsurface in prospect which could have been charged by hydrocarbons. The petrographic study reveals that some Triassic horizons constitute also a potential source rock with up to 2–4 % of organic matters content, which could constitute a local source to charge the associated Baluti reservoir beds.

Insights on Geodynamics

Geodynamic evolution of the Baluti Formation was developed through several stages, consistent with tectono-stratigraphic evolution in the Late Triassic rift basin (Fig. 4). The successive stages discussed below from the onset of opening of the Neo-Tethys Ocean in the Upper Permian.

Fig. 4 Paleogeographic map of the Upper Permian-Lower Triassic in Iraq shows the first stage of rift to form intracratonic basin in passive continental margin



Upper Permian-Lower Triassic (Start Opening of the Neo-Tethys)

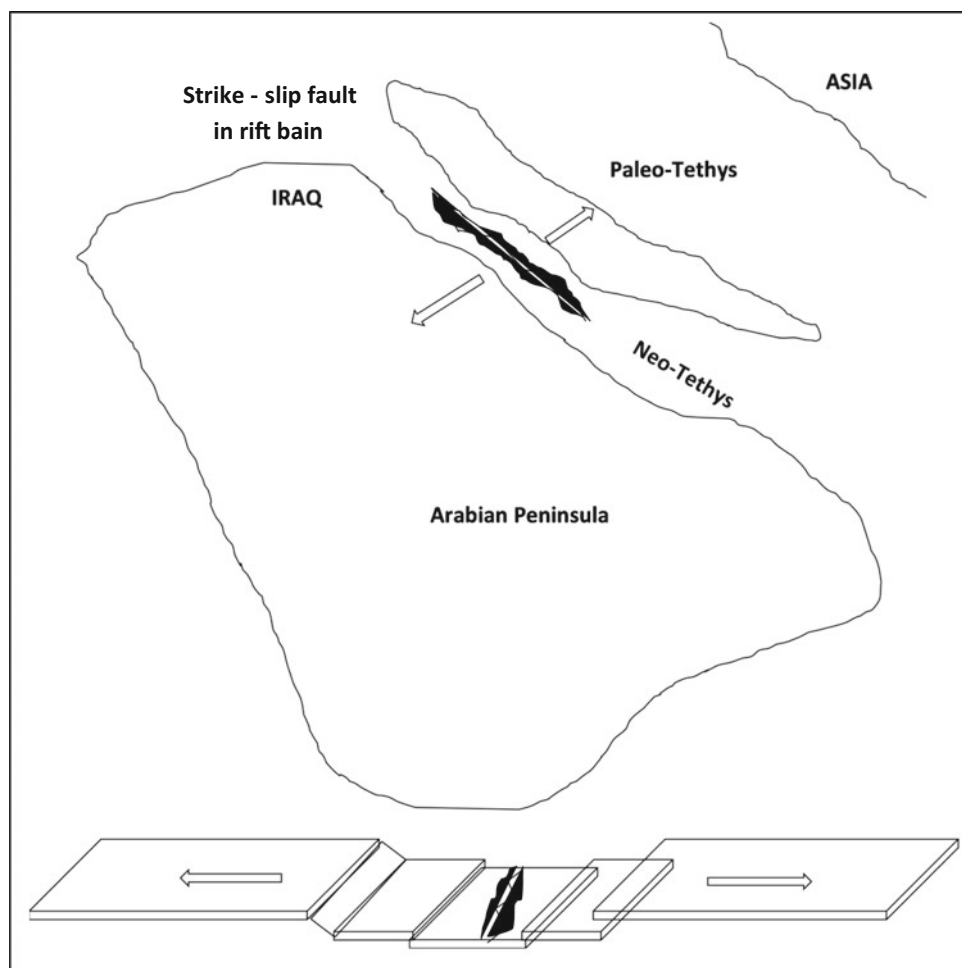
From the field observation in the Guley Derash Valley, Jabal Gara Mountain and northern parts of Iraq and southern parts of Turkey (at the border with Iraq) the pre Mesozoic substratum of the Zagros foreland is made up of crystalline Precambrian basement rocks and its overlying Paleozoic sedimentary cover (Al-Laboun 1986). These areas comprise a part of Sanadaj-Sirjan Zone (Szabo and Kheradpir 1978; Ricou 1994). The Neo-Tethys Ocean started to open in the Late Permian time in the north and northeastern parts of the Arabian Peninsula inducing the progressive development of passive margins (Setudahnia 1978; Murriss 1980). The narrow continental margin in north Iraq was splitting from Arabian Plate (Fig. 4). As noted by Altiner (1984, 2000), a detailed analysis of the successive microfacies of the Permian carbonate sequences of the Arabian Platform effectively suggest that they formed a single giant Upper Permian carbonate platform along the northern margins of the Gondwana supercontinent.

During Early Triassic time the Neo-Tethys Ocean was progressively widened inducing the splitting of the former platform into narrower conjugate continental margins along the northern and eastern sides of the Arabian plate, developing above the break-up unconformity. The Mesozoic passive margin megasequence was subsequently deposited during post-rift episodes of thermal subsidence (Garfunkel and Derin 1985; Guiraud and Bellion 1995; Shinaq 1996).

Middle Triassic-Upper Triassic (Carnian-Norian) (Extensional Tectonics)

Progressive extension still occurred during Mid-Late Triassic time around the northern and eastern margins of the Arabian Plate including northern Iraq (Figs. 4 and 5). This idea is evidenced and supported by the occurrence of alkali basalts in three localities near the border with Iraq e.g., in Bitlis Massif of Turkey (Perincek 1980), as well as near the Zagros suture zone associated with the Triassic Avroman and Bis-toun carbonates in NE Iraq/SE Iran (Szabo and Kheradpir

Fig. 5 Paleogeographic map of the Middle-Late Triassic (Carnian-Norian) in Iraq shows the progressive opening in the intracratonic basin



1978; Guiraud and Bellion 1995; Jassim and Goff 2006; Aqrabi et al. 2010). Many of these exotic carbonates have been interpreted as the cover of volcanic sea mounts during rift extension (Haq et al. 1988; Pillevuit et al. 1997; Haq and Al-Qahtani 2005). Various subsidence movements occurred in the Mesopotamian (Iraq) Basin in the Middle-Upper Triassic time being characterized by evaporate deposits. Locally euxinic basinal carbonates were restricted in restricted environment. These sediments were partly deposited during a second Triassic infilling-subsidence event (Fig. 5). The early Carnian 'Saharan salinity crisis' is a clear indication of a sea-level lowstand at 223 Ma (Haq and Al-Qahtani 2005).

In Iraq, the limestone/dolomite/evaporite series of the Kurra Chine Formation underlying the Baluti Formation represents, (like the Middle Triassic Geli Khana), a succession of shoaling-upward, and shallow-water to inner-neritic, euxinic, to near-shore deposits.

These depositional systems supports the suggestion of Le Métour et al. (1995) who reported a second phase of Neo-Tethyan extensional tectonics in the eastern part of the Arabian Platform during this time interval. This caused the drowning of the northeastern margin, and localized volcanic

activity on the continental slope as accounted for by the local rocks succession. Powers et al. (1966), Szabo and Kheradpir (1978), Le Nindre et al. (1990), Guiraud and Bellion (1995) and Zegler (2001) precised the impact of Triassic extension on the geology, sedimentology and the tectonics of the Arabian Plate including Iraq.

These authors indeed suggested that during Late Triassic, second stage of rift subsidence caused renewed thinning in the Arabian crust accounting for volcanic activity in the former continental slope of northern Iraq at a stage still pre-dating of the accretion of oceanic crust in the Neo-Tethys. The Late Triassic basin in northern Iraq was occupied by shallow-marine carbonates, interbedded with multiple evaporite intervals.

Concurrent with Neo-Tethys extensional rifting in the eastern Mediterranean, pillow lavas, continental sands, deep-water radiolarites and limestones were deposited. The facies and faunal distribution in Late Carnian to Rhaetian rock in northern Iraq allowed the distinction of continental platform and reef and deeper-marine slump facies. These lithotypes are consistent with the data reported by Hirsch (1992) and Hirsch et al. (1995).

Upper Triassic, Rhaetian (Progressive Extensional Stage, Carbonate Ramp)

In Upper Triassic (Rhaetian) time the rate of subsidence on the northern Arabian Plate increased, whereas relatively uniform marginal marine clastics, evaporites and shallow water lagoonal and inner and outer ramp carbonates were deposited. The late Permian to early Jurassic sequences is equated with the Arabian Plate Megasequence AP6 (Sharland et al. 2001).

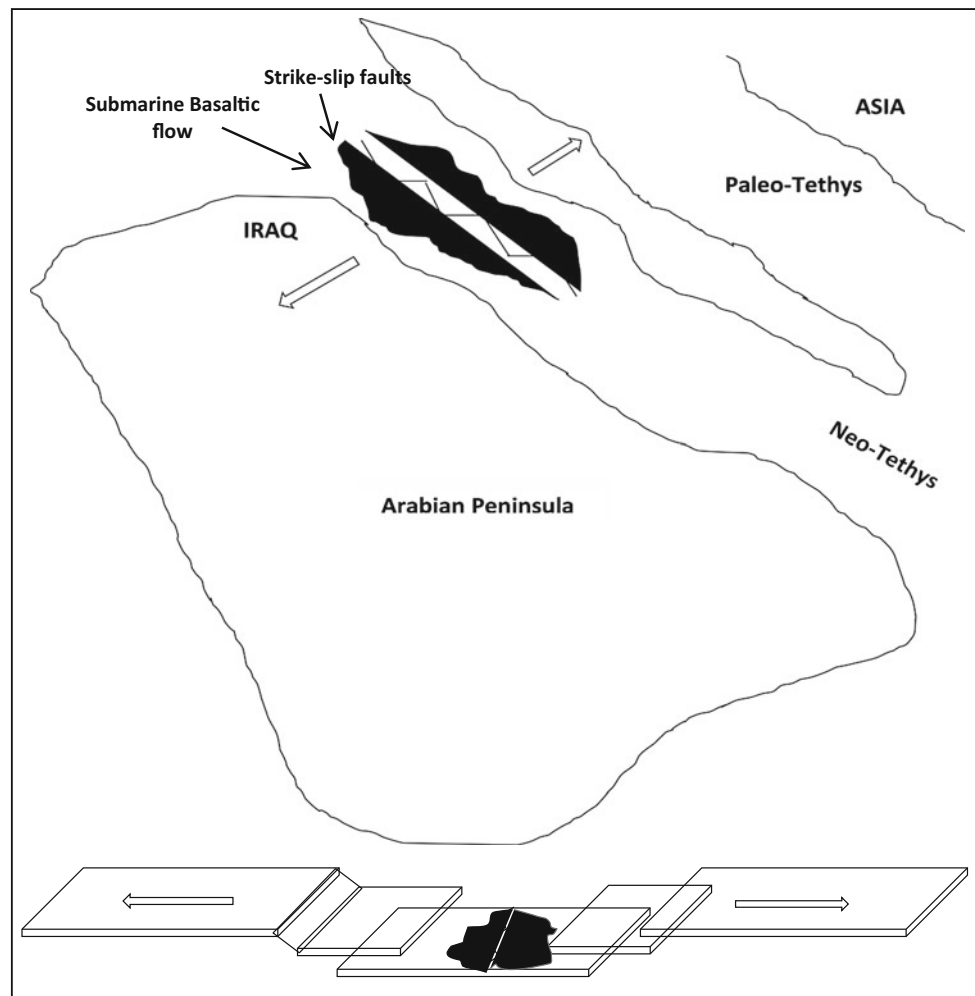
In this study, field observations and petrographic examination suggest that during the sedimentation of the Baluti Formation, volcanic eruptions and/or sub-marine lava flows were emplaced within the basin (Fig. 6). This is evident from the presence of a well-developed laminated and contorted stromatolite (loferite). Moreover, calcitic probably microbial branching growth (Plate 5b) have been described in close association with basaltic pillow lava, which erupted at that time within the basin. The microbes grew atop glassy,

zeolitic pillow rings. These shrub-like growths were later encased in spary calcite cement (Scholle and Scholle 2003).

In later time, the Baluti Formation and its lateral equivalents were deposited in northern Iraq. Rocks of the Kurra Chini rest conformable on top of the Baluti Formation, while the Rhaetian and Hettangian series are missing in most other part of the Arabian Plate. This is most probably due to the fact that rift and post-rift thermal subsidence still occurred in the north and northeastern Iraq e.g., Baluti Basin, preserving small horsts and grabens below sea level. This is confirmed by the slight differences in the thicknesses of the formation from one location to another in the out-cropping areas.

The facies distribution seems to have been controlled by deep-seated tectonic inherited from the first Permian extensional episode. In general, the Hakkari area of southeastern Turkey at the border with Iraq, directly north of the studied area belongs to the transition from the peri-Gotnia Basin to the Tethys. The sedimentary succession started there with limestone/dolomite subsequently recording episodes of

Fig. 6 Paleogeographic map of the Late Triassic-Rhaetian in Iraq shows the progressive stage of rift in basin



emersion and intense weathering before grading again into agitated shallow-marine, shelf-marginal carbonates.

Field observations of the Baluti Formation show evidences of slumping sediments in the whole succession. Carbonate debris flows, calciturbidite successions, carbonate breccia and debrites include carbonate olistolith clasts, thus confirming the idea of slumping from the ramp into hemi-pelagic-pelagic margins by Arc and Yilmaz (1990) report similar evidences with the slumping of carbonates in the Mardin district at the border with northern Iraq, thus suggesting that the Baluti deposits extend as well to southern Turkey.

Hirsch and Picard (1988) report also extrusive volcanic basalts, which are related to intracratonic fracturing that was probably associated with the opening of the eastern Mediterranean.

A Permo–Triassic oceanic seaway separating continental fragments from the northern margin of Gondwana was proposed by Szabo and Kheradpir (1978), Catalano et al. (1992) and Stampfli (2015) to explain the Late Permian–Early Triassic deep-water faunas of Sicily. However, the field and geochemical evidence supports rifting throughout the eastern Mediterranean only from the Middle-Late Triassic onward (e.g., Sengör et al. 1980; Robertson 1988).

The present eastern Mediterranean and its easterly continuation into the Bitlis and Zagros oceans began its opening mainly during the Carnian-Norian interval. This opening marked the birth of Neo-Tethys behind the Cimmerian continent which, at that time, started to separate from northern Gondwana-Land. Rifting tectonic in the north Iraq took place from Late Permian? to Mid Triassic time, being followed by continental break-up in the Late Triassic.

Rifting processes, leading to sea-floor spreading were characterized by a sequence of events: transtensive phase of extension with syn-rift volcanism; simple shear extension accompanied by lithospheric thinning and asthenospheric up-welling and thermal uplift of the rift shoulder and asymmetric volcanism.

Conclusion

Late Triassic carbonate breccias have been studied in details for the first time herein Iraq. Late Triassic deposits are present in most parts of the Neo-Tethys Ocean. Carbonate platform deposits of the Baluti Formation in Iraq are characterized by intense dolomitization and recrystallization of limestone relics, which needs excess of magnesium for intense early-late diagenetic dolomitization. Magnesium was provided by early diagenetic dolomites as a consequence of the formation of extensive tidal flats during relative sea level changes. However, dolomite-carbonate breccias are present only in some places in north and northeast Iraq. The

formation of dolomite-limestone breccia is clearly indicative of two main controlling factors; (a) Presence of specific lithologies, distinct from adjacent units, (b) Occurrence of narrow zones of intense tectonic activity.

Combination of both factors enabled the intense disintegration of rocks and lead to significant influence of poly-phase diagenetic processes. Based on the presence of dolomite-limestone breccias in the Baluti Formation their composition and structural-textural characteristics, as well as relevant of the complex tectonic and diagenetic processes to their formation, the following main conclusions may be drawn:

- (1) The investigated sequence of carbonate breccia represents a continuous Late Triassic succession in the core of Gara Anticline.
- (2) The first group of carbonate breccias i.e., the slump and debris flow breccias are of sedimentary, intrabasinal origin. As such, they formed by synsedimentary slump due to tectonic phases contemporaneous to the opening of Neo-Tethys Ocean.
- (3) The second group of carbonate breccias i.e., the tectonic, stylolization and collapse breccias is of polyphase tectogenic-diagenetic origin. They formed by collapse of roof forming cavities and major fault zones that allowed intense circulation of solutions and coeval diagenetic processes.

This kind of genetic interpretation is also partly or completely applicable for breccias for some other stratigraphic levels in the Neo-Tethys carbonate platform system of Iraq. In these cases the interrelation of intense tectonics and specific lithologies are also obvious in areas where tectogenic diagenetic dolomite breccia can be found i.e., in the area of Jabal Gara Mountain where good examples have been recognized.

The rifting, subsidence and resulted faulting are factors controlling various types of identified breccias. The related fault zones are responsible for circulation of saturated saline solution, which lead to various diagenetic processes.

Evidences of slumped sediment from carbonate ramp to deeper margin were induced by the rift tectonics and associated fault system, coeval with the local extrusion of basaltic lava flows in the basin floor.

References

- Al-Laboun AA (1986) Stratigraphy and hydrocarbon potential of the Paleozoic succession in both Tabuk and Widyan basins, Arabia. *Am Assoc Pet Geol Mem* 40:373–397
- Altiner D (1984) Upper Permian foraminiferal biostratigraphy in some localities of the Taurus Belt. In: Tekeli O, Gönüoğlu MC

- (eds) *Geology of the Taurus Belt*. MTA Ankara, Turkey, pp 255–268
- Altiner D (2000) Upper permian foraminiferal biofacies belts in Turkey: palaeogeographic and tectonic implications. In: Bozkurt E, Winchester JA, Piper JDA (eds) *Tectonics and magmatism in Turkey and the surrounding areas*. geological society, London, Special Publication 173, pp 83–96
- Agrawi AM, Goff CJ, Horbury DA, Sadoone NF (2010) *The petroleum geology of Iraq*. Scientific Press, UK, p 424
- Arac M, Yilmaz E (1990) Facies analysis of Bakuk formation (Cudi group) in the south of Petroleum district XII, southeast Turkey. In: *Proceedings of the 8th Petroleum congress of Turkey*, Ankara, pp 281–289
- Bellen RCV, Dunnington HV, Wetzel W, Morton DM (1959) *Lexique stratigraphique international, Asie Fasc. 10a*, Centre Natl. Recherche Sci. Paris, Iraq, p 333
- Bolton CMG (1955) *Geological map-Kurdistan series, scale 1:100,000 sheet K4 Ranya*. Site. Inv. Co. Report, Library, No. 276, Baghdad
- Brew G, Litak R, Barazangi M, Sawaf T (1999) Tectonic evolution of northeast Syria: Regional implications and hydrocarbon prospects. *GeoArabia* 4:289–318
- Buday T (1980) The regional geology of Iraq, Volume 1, Stratigraphy and paleontology. In: Kassab IM, Jassim SZ (eds) *Directorate general of geological survey and minerals*, p 445 (in collaboration with staff members and experts of the State Organization for Minerals, Baghdad)
- Burchette TP, Wright VP (1992) Carbonate ramp depositional systems. *Sediment Geol* 79:3–57
- Catalano R, Di Stefano P, Kozu RH (1992) New data on Permian and Triassic stratigraphy of western Sicily. *Neues Jahrb Geol Paliiontol Abh* 184:25–61
- Coniglio M, Dix GR (1992) Carbonate slopes. In: Walker RG, James NP (eds) *Facies models: response to sea level change*, St. Johns, Newfoundland: Geological Association of Canada, pp 349–373
- Cowie JW (1986) Guidelines for boundary stratotypes. *Episodes* 9:78–82
- Crevello D, Schlager W (1980) Carbonate debris sheets and turbidites, Exuma sound, Bahamas. *J Sediment Petrol* 50:1121–1148
- Ditmar V, Iraqi-Soviet Team (1971) Geological conditions and hydrocarbon prospects of the Republic of Iraq (Northern and Central parts). Manuscript report, INOC Library, Baghdad
- Dunham RJ (1962) Classification of carbonate rocks according to their depositional texture. In: Ham WE (ed) *Classification of carbonate rocks*: Tulsa, OK, American association of petroleum geologists, memoire, vol 1, pp 108–121
- Dunnington HV (1958) Generation, migration, accumulation and dissipation of oil northern Iraq. In: Weeks GL (ed) *Habitat of oil, a symposium*, Amer. Assoc. Pet. Geol., Tulsa
- Eberli GP (1991a) Carbonate turbidite sequences deposited in rift-basins of the Jurassic Tethys ocean (eastern Alps, Switzerland). *Sedimentology* 34:363–388
- Eberli GP (1991b) Calcareous turbidites and their relationship to sea-level fluctuations and tectonism. In: Einsele G, Ricken WA, Seilacher A (eds) *Cycles and events in stratigraphy*, Springer-Verlag, Dortmund, pp 320–359
- Einsele G (2000) *Sedimentary basins, evolution, facies and sediment budget*, Springer Verlag, Berlin, p 628
- Embry AF, Kolvan JE (1971) Late Devonian reef tract on northeastern bank island, N.W.T. *Bull Can Pet Geol* 19:730–781
- Flügel E (1982) *Microfacies analysis of limestones*. In: (trans: Christenson K), Springer-Verlag, Berlin, Heidelberg, New York, book, p 633
- Fuchtbauer H, Richter DK (1983) Relations between submarine fissures, internal breccias and mass flows during Triassic and earlier rifting periods. *Geol Rundsch* 72(1):53–66
- Garfunkel Z, Derin B (1985) Permian-Early Mesozoic tectonism and continental margin formation in Israel and its implication for the history of the Eastern Mediterranean. *Geol Soc Lond Spec Publ* 17:187–201
- Guiraud R, Bellion Y (1995) Late Carboniferous to recent geodynamic evolution on the West Gondwana, cratonic, Tethyan margins. In: Nairin EM, Ricou LE, Vrilyneck B, Decourt J (eds) *The ocean basins and margins. The Tethys ocean*, vol 8, Plenum Press, New York, pp 101–124
- Haak AB, Schlager W (1985) Compositional variations in calciturbidites due to sea-level fluctuations, late quaternary, Bahamas. *Geol Rundsch* 78:477–486
- Hampton MA (1972) The role of subaqueous debris flow in generating turbidity currents. *J Sediment Petrol* 42:775–793
- Handin J, Hager RV (1957) Experimental deformation of sedimentary rocks under confining pressure. *Bull Am Assoc Petrol Geol* 41:1–50 (and 42, 2897–2934)
- Haq UB, Al-Qahtani AM (2005) Phanerozoic cycles of sea-level changes on the Arabian platform. *GeoArabia* 10(2):1–34
- Haq BU, Hardenbol J, Vail PR (1988) Mesozoic and cenozoic chronostratigraphy and cycles of sea-level change. In: Wilgus CK, Hastings BS, Kendall CGS, Posamentier H, Van Wagoner J, Ross CA (eds) *Sea-level changes: an integrated approach*. Society of economic paleontologists and mineralogists, special publication, vol 42, pp 71–108
- Hirsch F (1992) Circum Mediterranean Triassic eustatic cycles. *Israeli J Earth Sci* 40:29–33
- Hirsch F, Picard L (1988) The Jurassic facies in the Levant. *J Pet Geol* 11(3):277–308
- Hirsch F, Flexer A, Rosenfeld A, Yellin-Dror A (1995) Palinspastic and crustal setting of the Eastern Mediterranean. *J Pet Geol* 18(2):149–170
- James PN, Dalrymple WR (2010) *Facies models 4*. GEOText 6, Canadian sedimentology research group, geological association of Canada, p 586
- James NP, Mountjoy EW (1983) Shelf-slope break in fossil carbonate platforms—an overview. In: Stanley DJ, Moore GT (eds) *The shelf-break critical interface on continental margins*, society of economic paleontologists and mineralogists. Special publication, Tulsa, vol 33, pp 189–206
- Jassim SZ, Goff JC (2006) *Geology of Iraq*. Dolin Prague and Moravian Museum, Brno, Czech Republic, p 341
- Le Métour J, Michel JC, Béchennec F, Platel JP, Roger J (1995) *Geology and mineral wealth of the sultanate of Oman*. Ministry of Petroleum and Minerals, Directorate General of Minerals, Oman, p 285
- Le Nindre YM, Manivit J, Vaslet D (1990) *Géodynamique et paléogéographie de la plateforme Arabe du Permien au Jurassique; histoire géologique de la bordure occidentale de la plateforme Arabe*, vol 2. French Bureau de Recherches Géologiques et Minières, document 192, p 280
- Lowe DR (1982) Sediment gravity flow: II. Depositional models with special reference to the deposits of high-density turbidity currents. *J Sed Pet* 52:279–297
- Martinsen OJ (1994) Mass movements. In: Maltman A (ed) *The geological deformation of sediments*, Chapman and Hall, London, pp 127–165
- Middleton GV (1993) Sediment deposition from turbidity currents. *Ann Rev Earth Planet Sci* 21:89–114
- Middleton GV, Hampton MA (1976) Subaqueous sediment transport and deposition by sediment gravity flows. In: Stanley DJ, Swift DJP (eds) *Marine sediment transport and environmental management*. John Wiley and Sons, New York, pp 197–218
- Mulder T, Cochonot P (1996) Classification of offshore mass movements. *J Sediment Res* 66:43–57

- Murris RJ (1980) Middle East stratigraphic evolution and oil habitat. *Am Assoc Pet Geol Bull* 64:597–618
- Perincek D (1980) Volcanics of Triassic age in Bitlis metamorphic rocks. *Bull Geol Soc Turkey* 23:201–211
- Pillevuit A, Marcoux J, Stampfli G, Baud A (1997) The Oman exotics: a key to the understanding of the Neo-Tethyan geodynamic evolution. *Geodin Acta Paris* 10:209–238
- Playton TE, Kerans C (2002) Slope and toe-of-slope deposits from a late Wolfcampian tectonically active carbonate ramp margin. In: Dutton SP, Ruppel SC, Hentz TF (eds) Gulf coast association of geological societies and gulf coast section SEPM; technical papers and abstracts. *Trans Gulf Coast Assoc Geol Soc* 52:811–820
- Posamentier HW, Walker RG (2006) Facies models revisited. In: Crossey LJ, McNeill DS (eds) SEPM special publication 84, Tulsa Oklahoma, USA, p 527
- Postma G, Nemeč W, Klinsphen KL (1988) Large floating clasts in turbidites: a mechanism for their emplacement. *Sediment Geol* 58:47–61
- Powers RW, Ramirez LF, Redmond CD, Elberg LE (1966) Geology of the Arabian Peninsula: sedimentary geology of Saudi Arabia. US geological survey, professional paper 560D, p 147
- Read JF (1985). Carbonate platform facies models. *Am Assoc Pet Geol Bull* 69:1–21
- Reading HG (1986) *Sedimentary environments and facies*, 2nd edn. Blackwell Scientific Publications, Oxford, London, Edinburgh, p 615
- Ricou LE (1994) Tethys reconstructed; plates, continental fragments and their boundaries since 260 Ma from Central America to South-eastern Asia. *Geodin Acta Paris* 7(4):169–218
- Robertson AFH (1988) Mesozoic-Tertiary tectonic evolution of the Easternmost Mediterranean area: integration of marine and land evidences. *Proc Ocean Drill Progr Sci Res* 160:723–782
- Rusnak GA, Nesteroff WD (1964). Modern turbidites: terrigenous abyssal plain versus bioclastic basin. In: Miller RL (ed) *Papers in marine geology*, MacMillan, New York, pp 488–507
- Scholle PAD, Scholle U (2003) A color guide to the petrography of carbonate rocks: grains, textures, porosity, diagenesis. *AAPG Mem* 77:459
- Sengor AMC, Yilmaz Y, Ketin I (1980) Remnants of a pre-Late Jurassic ocean in the northern Turkey: fragments of Permian-Triassic Palaeo-Tethys? *Geol Soc Am Bull* 91:599–609
- Setudahnia A (1978) The Mesozoic Sequence in South-West Iran and adjacent areas. *J Pet Geol* 1:3–42
- Sharland PR, Archer R, Casey DM, Davies RB, Hall SH, Heward AP, Horbury D, Simmons MD (2001) Arabian plate sequence stratigraphy. *GeoArabia*, Special publication 2, Bahrain. 371 pp and 3 enclosures
- Shinaq R (1996) Subsurface Triassic sediments in Jordan: Stratigraphic and depositional characteristics, & hydrocarbon potential. *J Pet Geol* 19:57–76
- Stampfli GM (2015) Tethyan oceans. <http://sp.lyellcollection.org/>
- Stow DAV (1984) Anatomy of debris-flow deposits. In: Hay WW, Sibuet JC et al (eds) Initial reports deep sea drilling project 75, U.S. Govt. Print. Office, Washington, DC
- Stow DAV (1986) Deep clastic systems. In: Reading HG (ed) *Sedimentary environments and facies*, revised edn. Blackwell, London, pp 399–444
- Szabo F, Kheradpir A (1978) Permian and Triassic stratigraphy, Zagros Basin, South-West Iran. *J Petrol Geol* 1(2):57–82
- Vlahovic I, Tisljar J, Fucek L, Ostric N, Prtoljan B, Velic I, Maticec D (2002) The origin and importance of the dolomite-limestone breccia between the Lower and Upper Cretaceous deposits of the Adriatic carbonate platform: An example from Cicarija Mt. (Istria, Croatia). *Geol Croat* 55(1):45–55
- Walker RG (1992) Turbidites and submarine fans. In: Walker RG, James NP (eds) *Facies models: response to sea level change*. Geological Association of Canada, St. Johns, Newfoundland, pp 239–263
- Walker J, James A (1998) Facies models in response to sea level changes. *Canada geosciences, Geotext-1*, Geological Association of Canada, p 454
- Wetzel R (1950) Stratigraphy of Amadia region. MPC report No. IR/WR 12. Manuscript report, GEOSURV, Baghdad
- Ziegler MA (2001) Late Permian to Holocene paleofacies evolution of the Arabian Plate and its hydrocarbon occurrences. *GeoArabia* 6 (3):445–504

Part III

**Tectonic Styles: From Rifts and Salt Tectonics to
Foreland Inversions and Thrust Tectonics**

Structural and Stratigraphic Architecture of the Corinth Rift (Greece): An Integrated Onshore to Offshore Basin-Scale Synthesis

Sébastien Rohais and Isabelle Moretti

Abstract

The overall rifting history of the Corinth basin in Greece is still debated due to (1) the lack of deep wells to constrain the offshore domain, (2) sparse dating available onshore and (3) the only few integrated basin-scale studies covering both offshore and onshore data providing an homogeneous overview of its stratigraphic architecture. This paper provides an update to the structural and stratigraphic architecture of the Corinth rift through the results of field mapping, geological and structural map synthesis, outcrop stratigraphic characterization and seismic sequence stratigraphic correlations. A comparison with the surrounding basins to extrapolate ages and a correlation between onshore stratigraphic architecture and offshore seismic stratigraphy in the Corinth rift are proposed to establish time lines of the key stages during the rift evolution, and its relationship with the previous Hellenic compressive phase and the Aegean back-arc opening eastward. The rift history can be subdivided into two major syn-rift phases. A Syn-rift 1 including (a) the rift initiation at around 5.3 Ma with continental to lacustrine sediments deposited in km-scale isolated depocenters. (b) The rift widening (ca. 5.3–3.0 Ma) combined with a rift propagation from east to west. First marine incursions were recorded along the Corinth Isthmus. At that time, the rift was still subdivided into numerous 2–10 km-wide depocenters controlled by active faults where continental to lacustrine deposits occurred. The depocenters progressively grew and became linked. (c) The Syn-rift 1 “climax” (ca. 3.0–2.6 Ma) with 15–25 km-long fault segments subdivided the rift into 5–10 km wide fault blocks. Sedimentation was characterized by thick alluvial fans and large Gilbert-type deltas along the active fault segments and a starved basin along the basin axis. Marine connection with the Mediterranean Sea was dominantly established through the Corinth Isthmus. (d) The Syn-rift 1 phase ended with a basinward fault migration phase (ca. 2.6–0.8 Ma) characterized by a progressive demise of the rift border fault and a rapid forced regressive trend recorded by the large Gilbert-type deltas. Bathymetry continued to increase along the basin axis. An additional phase of rifting (Syn-rift 2) ensued, and was characterized by the Peloponnesus margin uplift combined with an increase of both tectonic and total subsidences in the basin axis (ca. 0.8 Ma to present day). The depositional profile was shorter than during the previous stages, the rift progressively narrowed and the sedimentation rate strongly increased in the depocenter. The short lived duration of each phase and the peculiarity of the present phase are discussed in relation to the inherited

S. Rohais (✉)

Direction Géosciences, IFPEN, 1 et 4 Avenue de Bois-Préau,
92852 Rueil-Malmaison Cedex, France
e-mail: sebastien.rohais@ifpen.fr

I. Moretti

Département Exploration et Géosciences, ENGIE EPI, 1 Place
Samuel de Champlain, 92930 Paris La Défense Cedex, France

© Springer International Publishing AG 2017

F. Roure et al. (eds.), *Lithosphere Dynamics and Sedimentary Basins of the Arabian Plate and Surrounding Areas*, *Frontiers in Earth Sciences*, DOI 10.1007/978-3-319-44726-1_5

structures and relative influence of the far field stress changes within the global context of the Hellenic subduction.

Keywords

Corinth rift • Syn-rift • Stratigraphic architecture • Fault • Structural evolution • Back-arc • Seismic stratigraphy

Introduction

The Corinth rift, one of the most active extensional seismic zone in the world, provides both onshore early rift sedimentary fill exposed in spectacular outcrops along its southern margin, and offshore active rift basin fill illustrated by numerous seismic profiles. The Corinth rift with its impressive outcrops has attracted geoscientists attention since the nineteenth century (Philipson 1890). From the beginning of the XXth century, the authors already proposed an evolution of poly-phased rift (Desperet 1913), but the sedimentological and stratigraphic studies were poorly developed. During the 50–60s, the research themes were mainly focused on the evolution of the Hellenides chain and its quaternary deposits. Most of the interpretation proposed have been significantly updated but the dataset, stratigraphic and structural frameworks that were established at this period of time deeply marked the second major generation of researchers of the 70–80s who were interested in the Pliocene-Quaternary deposits, faults and basin dynamic, and geodynamic reconstruction of Greece (e.g. Keraudren 1970, 1971, 1972; Dufaure 1975; Dufaure et al. 1979; Jacobshagen et al. 1978; Le Pichon and Angelier 1979). Since 1980, significant insights were made in sedimentology and structural geology in the Corinth rift through the development of new interpretations in these areas (Kontopoulos and Doutsos 1985; Collier 1988; Doutsos and Piper 1990; Collier and Dart 1991). In parallel, the geodynamic context of the Aegean domain was better constrained (e.g. Tselentis and Makropoulos 1986; Doutsos et al. 1988; Jolivet et al. 1994). However, the relationship between the Corinth rift and the Aegean extensive domain remained poorly constrained, as well as the controlling mechanism onto the rift extension. These issues have been a major research line starting from the 90s (e.g. Rigo et al. 1996; Roberts and Koukouvelas 1996; Sorel 2000; Westaway 2002; Nyst and Thatcher 2004; Zelt et al. 2004). Meanwhile, sedimentological studies were focused on Gilbert-type fan deltas and their integration into a tectono-stratigraphic model for rift basins (e.g. Ori et al. 1991; Poulimenos et al. 1993; Dart et al. 1994; Gawthorpe et al. 1994; Zelilidis and Kontopoulos 1996; Zelilidis 2003). Since 2000, the scientific debate on the Gulf of Corinth has intensified with major issues and potential controversies on a

very large number of scientific debates. Major scientific challenges have been firstly addressed regarding the location of the active fault system, the relationship between seismicity and fault geometry, the inherent seismic risks, geohazards and monitoring, especially since the Corinth Rift Laboratory has been installed in its western part for more than 15 years (e.g. Bernard et al. 1997; Moretti et al. 2002; Avallone et al. 2004; Bernard et al. 2006; McNeill et al. 2007; Pik and Marty 2009; Hadler et al. 2011, 2013; Console et al. 2015; Chouliaras et al. 2015; Kapetanidis et al. 2015). A second main domain of interest was focused on the faults and rift dynamics (Goldsworthy and Jackson 2001; Goldsworthy et al. 2002; Micarelli et al. 2003, Leeder et al. 2003, 2008; Causse et al. 2004; McNeill et al. 2005; Benedicto et al. 2008; Bell et al. 2009; Taylor et al. 2011; Ford et al. 2013; Charalampakis et al. 2014; Beckers et al. 2015; Nixon et al. 2016; Hemelsdael and Ford 2016). Models for extension and integration into the Aegean geodynamic setting still continue to be a major challenge for the Corinth rift (Briole et al. 2000; Doutsos et al. 2000; Xypolias and Doutsos 2000; Goldsworthy et al. 2002; Westaway 2002; Moretti et al. 2003; Leeder et al. 2003, 2012; Zelt et al. 2004; Flotté et al. 2005; McNeill et al. 2005; Kokkalas et al. 2006; Papanikolaou et al. 2009; Skourtsos and Kranis 2009; Jolivet et al. 2010a, b) Following the extension model issues, i.e. detachment fault versus early core-complex versus multi-phased planar normal faults, numerous studies were dedicated to the influence of inherited structure on rift development and dynamic (Exadaktylos et al. 2003; Ghisetti and Vezzani 2004, 2005; Le Pourhiet et al. 2003, 2004; Mattioni et al. 2006). In addition, geomorphological studies have also been carried out to better characterize the overall structural pattern and basin dynamic (Zelilidis 2000; Palyvos et al. 2007; Rohais et al. 2007a, Maroukian et al. 2008; Tsodoulos et al. 2008; Demoulin et al. 2015). The connection between the Gulf of Corinth sea and the surrounding seas has also animated numerous debates for the most recent syn-rift deposits (Perissoratis et al. 2000; Kershaw and Guo 2003; Moretti et al. 2004; Kershaw et al. 2005; Portman et al. 2005; Rohais et al. 2007b). Finally, one of the most challenging ongoing issue is the age of the syn-rift fill, including both offshore seismic stratigraphy and onshore stratigraphic architecture (Stefatos et al. 2002; Sachpazi et al. 2003;

Clement et al. 2004; Ford et al. 2007; Rohais et al. 2007b; Lykousis et al. 2007; Sakellariou et al. 2007; Bell et al. 2009; Taylor et al. 2011; Leeder et al. 2012; Nixon et al. 2016). For example, if the Upper Group (ca. 0.8 Ma to present) has been studied in detail, the offshore stratigraphic architecture of the full syn-rift packages has never been interpreted at high resolution using sequence stratigraphy concepts.

The result of these numerous studies is a large dataset from both onshore and offshore, covering the western to easternmost parts of the rift. Nevertheless, the limiting factor to progress in the quantification of fault activity, strain dynamics, rifting timing, erosion versus sedimentation versus uplift dynamic, and geomorphological processes is the availability of a consistent and relevant chronostratigraphic framework at basin scale within an updated structural pattern and absolute ages constraints. All these issues can benefit from timeline correlations between onshore to offshore sequences (north to south) and along the outcrops from west to east as well as the integration of previous dating (e.g. Collier and Dart 1991; Danatsas 1989, 1994; Ford et al. 2007; Rohais et al. 2007b; Leeder et al. 2008, 2012).

In this paper, we propose onshore to offshore correlations and seismic sequence stratigraphy correlations based on newly acquired data and including an update of previous works, basin-scale cross sections and geological mapping. The comparison with surrounding basins and unification of absolute dating into the basin-scale stratigraphic architecture provide the opportunity to propose a synthetic review of the Corinth rift evolution and its integration within the geodynamic setting.

Geodynamic Setting

The Corinth rift is located in the Mediterranean area where complex geodynamic domains are interacting and boundary condition changes are extremely fast. The convergence between Africa and Europe led to the formation of the Hellenides chain composed of NW-SE overlapping fronts and of the Hellenic subduction zone (Fig. 1). The present day deformation regime is spatially evolving from continental collision (Alps, Dinarides and Hellenides), to the oceanic subduction (Hellenic arc) through transform fault systems accommodating differential gradient rate (Fig. 1), such as the Kephallonia Fault (e.g. Kiliias et al. 2002; Royden and Papanikolaou 2011). To the east, back-arc basins developed in the Aegean sea since the Eocene and a major plate boundary NE-SW now subdivides this domain; the North Anatolian Fault (NAF, Fig. 1). The current slab geometry of the subducting plate deduced from tomographic data show an anomaly eastward (below Turkey) that is interpreted as slab tear by Jolivet et al. (2015). Westward, below the Peloponnese, it has been proven that the slab is

rather flat (see Leeder and Mack 2007 and reference within) with a smooth ramp geometry between 30° and 10° with dip increasing (up to 45°) beneath the Saronic Gulf. The subducting lithosphere is supposed to be oceanic in the south and continental north from the Kephallonia Fault, however the dip of the subducting plate in the first 100 km remains rather shallow (average 20°, Pearce et al. 2012), and another tear separates these two parts of the slab (Royden and Papanikolaou 2011).

From Eocene to Miocene, the Corinth rift area was characterized by subaqueous “fore-arc” equivalent to an accretionary prism setting as evidenced by the stacked nappes and associated turbiditic deposits (e.g. Sotiropoulos et al. 2003; Kamberis et al. 2005; Pantopoulos and Zelilidis 2014). Similarly westward, the deformation of the Apennines started in the Miocene, so relatively later compared to the Hellenides and Dinarides compression. In the Apennines, the main decollement level is the Triassic evaporitic layer and the thin-skinned style thrust belts involved the Jurassic and Cretaceous marine sequences (Ghisetti et al. 1993). On the Hellenides, the main decollement level is less clear but the Triassic evaporates known from subsurface data west of Patras, are commonly considered as the major lowest detachment level of individual overthrust sheets in the external Hellenides (Karakitsios and Rigakis 2007; Karakitsios 2013).

The first post-thrusting normal faults and extensional setting occurred around mid-Miocene in the Corinth rift area based on detailed geological mapping of extensional fault along the northern margin (Papanikolaou et al. 2009). The relationship between the Miocene normal faults (oriented ca. 160°) and the current ones in the Gulf (oriented ca. 090°) remains unclear but from that period of time, the Corinth rift area was characterized by an extensional regime up to the present day.

In this global context, many issues are still debated and a majority of the authors are currently exploring the influence and relationship between (1) the subduction plate characteristic, (2) the overriding plate heterogeneity (mainly the compressive heritage) and (3) the farfield stress changes (e.g. Kydonakis et al. 2015; Jolivet et al. 2015; Brun et al. 2016). The geodynamic mechanisms proposed in the literature to explain the origin of the Corinth rift extension are commonly accepted as combination of gravitational collapse, lithospheric thinning of the back-arc, rotation of micro blocks with respect to the propagation of the North Anatolian Fault (e.g. Moretti et al. 2003; Jolivet et al. 2010a, b).

The gravitational collapse of an over-thickened crust has been documented along the Hellenides chain (Horvath and Berckhemer 1982; Gautier et al. 1999; Jolivet 2001) and has already been discussed as a controlling mechanism on the early stages Corinth rift extension (e.g. Papanikolaou et al. 2009). Nevertheless, the cross cutting relationship between

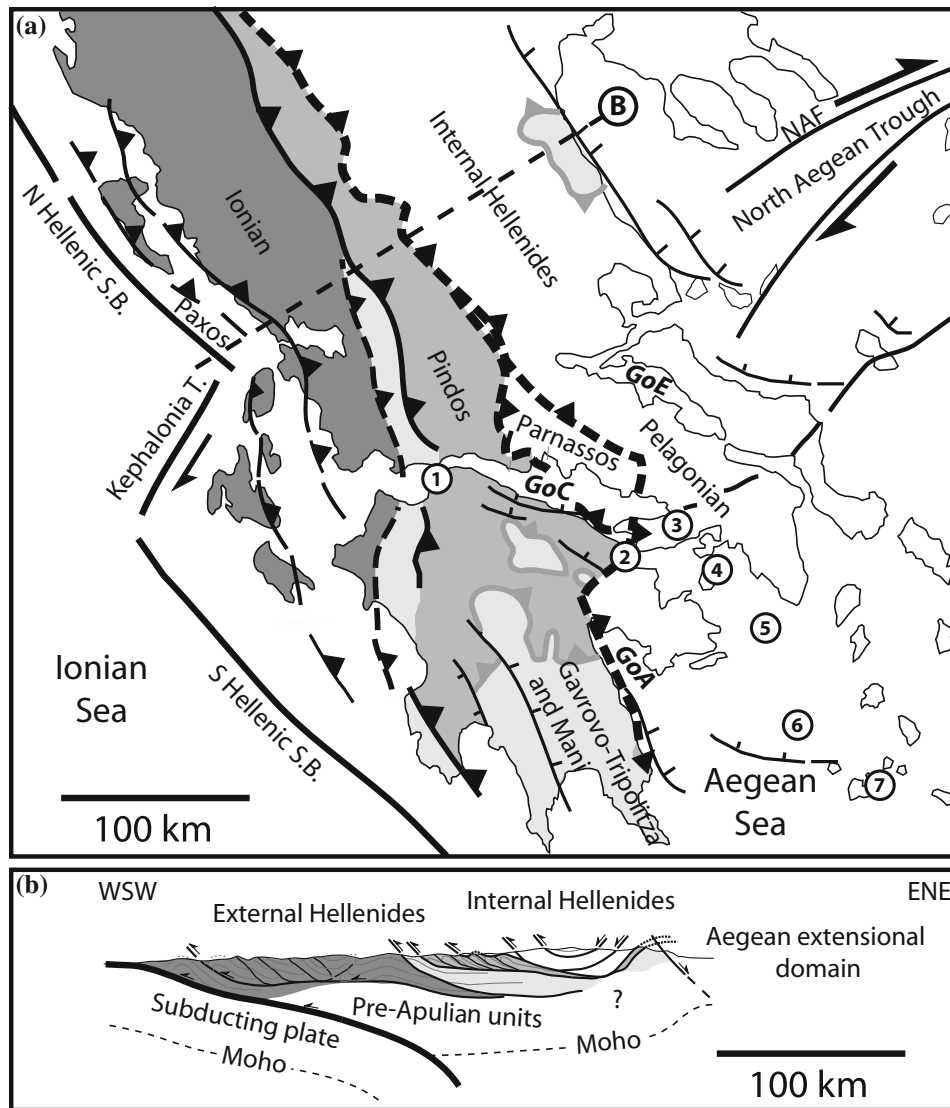


Fig. 1 **a** Geodynamic setting of the Gulf of Corinth (GoC) showing the main thrust belt structures within mainland Greece and the Peloponnese (modified from Royden and Papanikolaou 2011). The Kephalaria Transform (Kephalaria T.) separates the slowly subducting, continental foreland of the northern Hellenides with its North Hellenic Subduction boundary (N Hellenic S.B.) from the rapidly moving upper plate of the southern Hellenides with its South Hellenic Subduction boundary (S Hellenic S.B.). The Parnassos is a large shallow-water carbonate platform (upper Triassic through Cretaceous) unit from the Internal Hellenides that

lies between the Pindos and Pelagonian nappes, with deeper slope facies in its lower thrust sheets (Papanikolaou et al. 2009). Location of the main surrounding basins discussed in this paper: 1. Patras Basin, 2. Megara Basin, 3. Corinth Isthmus, 4. Aegina Island, 5. Gulf of Saronic, 6. Myrtoon Basin, 7. Mylos Island. Gulf of Argolikos (GoA) and gulf of Evvia (GoE) are also highlighted. Well DSDP 378 is located at ca. 100 km to the southeast of the Mylos Island. **b** Simplified structural cross-section across the Hellenides chain (modified from Royden and Papanikolaou 2011)

the rift architecture and the previous stacked nappes suggest another additional and dominant mechanism to promote extension.

The crustal thinning is well documented in the Aegean sea with the back-arc extension during the slab retreat (e.g. Fytikas et al. 1984; Armijo et al. 1996; Pe-Piper and Piper 2007; Jolivet and Brun 2010; Jolivet et al. 2015). This massive extension lead to the exhumation of metamorphic core complexes (Lister et al. 1984; Jolivet et al. 2015 and

reference within). Nevertheless, above a flat slab there is no space for asthenosphere between the subduction and overriding lithospheres, and consequently there is no extension and no volcanism (Martinod et al. 2010). As the Gulf of Corinth is mainly located above a flat slab (only its easternmost part corresponds to the transition between flat and steep slab geometries) and the current displacement recorded across the Gulf clearly overpass the slab retreat rate, crustal thinning by mantellic convection cannot be considered as the

dominant controlling mechanism to promote extensional stress in this area.

The rotation of micro blocks with respect to the propagation of the North Anatolian Fault (NAF, Fig. 1) is thus a major geodynamic mechanism that could have controlled extension in the Gulf of Corinth. Indeed, all the GPS data show that the Anatolian block bounded northward by the NAF, south and westward by the Hellenic subduction and eastward by the prolongation of the Levant Fault system is extruded toward the east-southeast (Dewey and Sengor 1979; Armijo et al. 1999; Goldsworthy et al. 2002; Flerit et al. 2004). The velocity of this displacement is large, around 35 cm/year, much larger than the current Hellenic subduction rate toward the west-northwest (6 cm/year). This unbalanced “convergence” should affect the Evvia-Corinth-Peloponnese area and is proposed by some authors to be the main cause of the Peloponnese uplift (Leeder and Marck 2007). Alternatively this uplift could be due to gravity changes in the subducting plate as it is documented in the Andes in front of the oceanic plateau or ridges affecting the Pacific plate (Martinod et al. 2010).

Pre-rift Fabrics and Rift Pattern

The northern and southern margins of the Gulf of Corinth are characterized by a pile of NW–SE striking nappes separated from one another by major east dipping thrust faults (Fig. 1). These nappes include the Pelagonian and the Parnassos units forming the Internal Hellenides (Fig. 1), the Pindos, the Gavrovo-Tripolitza units forming the external Hellenides (Aubouin 1959). The Ionian and the Pre-Apulian (e.g. Paxos nappe), which correspond to the western part of the Hellenic structure are not outcropping along the Corinth rift margins. The Zaroukla Unit then corresponds to low-grade metamorphic rocks (Phyllites-Quartzite) that are exposed in the Feneos depression underneath the Gavrovo-Tripolitza carbonates (Fig. 2). Each nappe consists of Mesozoic to early Tertiary pelagic sedimentary rocks, overlain by a clastic sequence of clays and turbiditic sandstones (“flysch”) that accumulated during the compressive wedge growth in front of the active nappe bounding thrust (I.F.P. and I.G.R.S. 1966; Dercourt et al. 1976). The progressively younger ages of the flysch units from NE to SW thus reflect the southwestward propagation of nappe stacking (Figs. 2 and 3).

The northern rift shoulder is mainly characterized by a well-preserved nappe stacking while the southern rift shoulder has been strongly uplifted and eroded with the occurrence of structural windows down to the low-grade metamorphic rocks of the Zaroukla Unit (Figs. 2 and 3). The nappes are separated by decollement levels which consist of shallow-dipping surfaces that can be recognized in the pre-rift series. “Detachment” is used by numerous authors to

refer to levels with large associated horizontal displacements, they are more or less thick depending of the mechanical layering of the initial sedimentary series. The strain localization in compression is known to be sometimes very efficient on over-pressured shale or salt layer and few ten of kilometers of horizontal offset may be accommodate through a thin layer with almost no deformation below (see for instance for the Zagros; Sherkati et al. 2005). It corresponds to the flat parallel part of an inverse fault and the term “detachment” is used independent of thickness, i.e. it could represent a very thin bed (flat fault plane) or a rather thick one (few hundred meters of shale for instance). Normal faults could root in the same kind of layers and the term of detachment is also used for normal faults with large horizontal offset within a given series. In the Gulf of Corinth area, three main shallow-dipping heterogeneities of that kind have been recognized in the pre-rift series: (1) the east Peloponnese detachment related to a Middle Miocene to early Pliocene post-orogenic extension (Papanikolaou and Royden 2007; Papanikolaou et al. 2009). Its northern end corresponds to the Itea–Amfissa detachment outcropping along the northern shoulder of the Corinth rift (Figs. 2 and 3). (2) The Chelmos detachment of Sorel (2000) at the contact between the Gavrovo and Zaroukla units. It is also described as the Zaroukla detachment between the Tyros beds and the Gavrovo-Tripolitza carbonates. It has been interpreted to be the most recent detachment feature acting only in the brittle crust (Jolivet et al. 2010a, b). (3) Within the Zaroukla Unit, the contact between the Phyllites-Quartzite and the Tyros beds is interpreted as an important shear zone with main pressure gap similar to the Cretan detachment (Xypolias and Doutsos 2000; Jolivet et al. 2010a, b).

Along the northern rift shoulder, these three shallow-dipping heterogeneities are around 1–2 km deep for the shallowest (East Peloponnese detachment) to 5–7 km deep for the deepest (Cretan detachment equivalent). Along the southern rift shoulder, they are 0–2.5 km (maximum) deep respectively. These heterogeneities are shallower than the depth of the seismogenic zone below the present day gulf (6–12 km, Chouliaras et al. 2015). The depth of seismogenic zone is geometrically more consistent with the main lowest detachment level of individual overthrust sheets in the external Hellenides, i.e. the Triassic evaporates at the base of the Ionian/Pre-Apulian nappes (Fig. 1).

The Moho depth beneath northern Greece and the Peloponnese follows a west to east shallowing trend resulting from pre-rift crustal thickening of the Hellenides orogeny (Fig. 1, Tiberi et al. 2001; Zelt et al. 2005; Sachpazi et al. 2007). The Moho depth beneath the Corinth rift follows a similar trend from 42 km in the west (22°E) to less than 30 km in the east (23°E), without any significant evidence for crustal thinning along the rift axis (Sachpazi et al. 2007). This thinning trend is more or less perpendicular to the

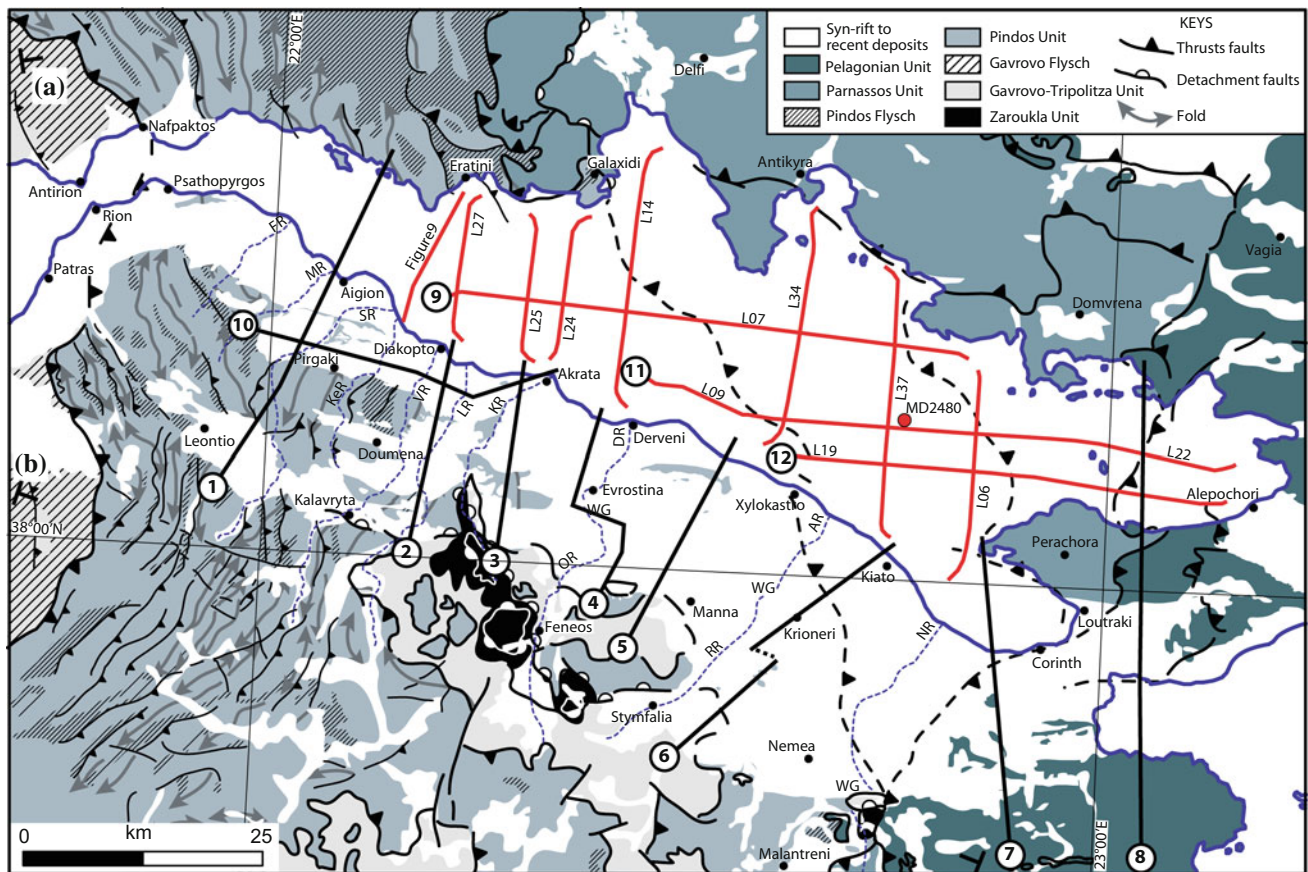


Fig. 2 Geological map of the pre-rift fabrics of the Corinth Rift (modified from Papastamatiou et al. 1962; Aronis et al. 1964; Loftus et al. 1971; Paraschoudis and Machairas 1977; Tsoflias et al. 1984; Doutsos et al. 1988; Koutsouveli et al. 1989; Bentham et al. 1991; Collier and Dart 1991; Tsoflias et al. 1993; Xypolias and Doutsos 2000; Ghisetti and Vezzani 2004, 2005; Rohais et al. 2007a; Benedicto et al. 2008; Bell et al. 2009; Jolivet et al. 2010a, b; Taylor et al. 2011; Ford et al. 2013). Red lines indicate seismic profiles from Taylor et al.

(2011). Labeled black lines indicates the cross-sections presented in Figs. 12 and 13. MD2480 stands for the Marion Dufresne's piston core (red dot). a and b correspond to the two cross-sections presented in Fig. 3. FR Finix river, MR Meganitis river, SR Selinous river, KeR Kerinitis river, VR Vouraikos river, LR Ladopotanmos river, KR Krathis river, DR Derveni river, OR Olvios river, AR Agriolagado river, RR Rethis river, NR Nemea river WG: Wind Gap

Saronic and Evvia gulfs, ca. 045° that is consistent with the Hellenic subduction trend in this area (ca. 145° westward of the Peloponnese).

Onshore Stratigraphic Architecture

There are numerous publications on the Corinth onshore basin fill (e.g. Doutsos et al. 1988; Ori 1989; Doutsos and Piper 1990; Bentham et al. 1991; Collier and Dart 1991; Rohais et al. 2007a; Ford et al. 2007). Nevertheless, the extrapolation of the most recent sedimentary subdivision along the entire margin is not straightforward, due primarily to major vertical and lateral facies changes occurred at basin scale. In addition, the Lower, Middle and Upper groups subdivision (Rohais et al. 2007a) has been extrapolated to

the western rift portion (Ford et al. 2013) mainly based on lithostratigraphic correlations, inducing laterally diachronous boundaries that are inconvenient for discussing the rift evolution. The recent publication by Leeder et al. (2012) provides an absolute age at the very base of the Mavro Gilbert-type delta (Middle Group) promoting a necessary update of the stratigraphic architecture. We thus carried out sedimentological sections and mapping all along the southern margin of the Corinth rift from the western part (Aigion) to the eastern part (Corinth Isthmus) together with a synthesis of the Hellenic geological maps (Papastamatiou et al. 1962; Aronis et al. 1964; Loftus et al. 1971; Paraschoudis and Machairas 1977; Tsoflias et al. 1984; Doutsos et al. 1988; Koutsouveli et al. 1989; Tsoflias et al. 1993) resulting in a unified basin scale geological map (Fig. 4) based on updated syn-rift succession description.

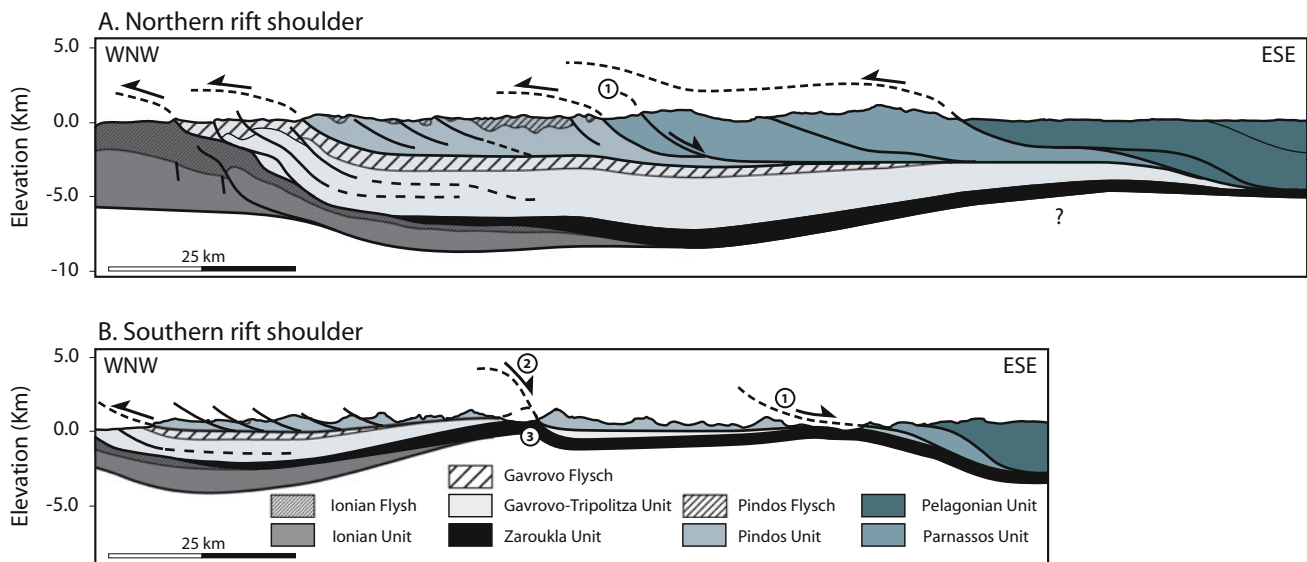


Fig. 3 Structural cross-section across the northern (A) and southern (B) rift shoulders based on the synthetic geological map presented in Fig. 2 and modified from previous works (Aubouin et al. 1963; I.F. P. and I.G.R.S. 1966; Dercourt et al. 1976; Jacobshagen et al. 1978;

Doutsos et al. 1993; Papanikolaou et al. 2009; Royden and Papanikolaou 2011; Jolivet et al. 2010a, b). 1, 2 and 3 stand for the east Peloponnesus, Chelmos and Zaroukla detachments respectively. See Fig. 2 for location

Updated Syn-rift Description

The syn-rift sedimentary fill of the southern margin is commonly subdivided into three groups (Fig. 5), i.e. the Lower, Middle and Upper groups (Rohais et al. 2007a). The correlation of the Lower Group, as well as the Lower to Middle Group transition are the biggest challenges at basin-scale, from the easternmost to the westernmost onshore side. The Krathis river corresponds to a transition area where syn-rift series present major difference in facies association from east to west (e.g. Ghisetti and Vezzani 2005; Rohais et al. 2007a; Ford et al. 2013). We had to address two main issues to homogenize the nomenclature across the Krathis river. First, we propose that the upper portion of the Lower Group (D3 of Ford et al. 2013) on the western side of the Krathis river is coeval with the Middle Group (Sequence 2 of the Killini Gilbert-type fan delta described by Rohais et al. 2008). It is the best option because the thickness variation, the relationship with the rift shoulder and the overall prograding trend are more consistent with the Middle Group stratigraphic architecture (Fig. 6). Second, we propose that the first sequence of the Middle Group (Sequence 1 of Rohais et al. 2008) is coeval with the topmost part of the Lower Group (Fig. 6). It is the best option because the aggrading trend of the Sequence 1 in the Middle Group is more consistent with the final trend described in the topmost part of the Lower Group (Rohais et al. 2007a). The Lower to Middle Group transition is now considered at the transition between D2 and D3 on the western side of the Krathis river, and at the transition between sequences 1 and 2

on the eastern side (Fig. 5c). The resulting geological map is presented in Fig. 4.

At a regional scale (Fig. 6), the Lower Group is characterized by coarse-grained alluvial to fine-grained lacustrine series with the coarse-grained facies more developed to the west (Fig. 5c). Following a brief flooding event, the Lower Group is mainly characterized by an aggrading trend (Rohais et al. 2007a). The tilted block crest onlap and the backstepping of depositional system indicate a widening of the basin that is structurally active with tilted block of 5–10 km wide. The lowermost part of the Lower Group is interpreted as a low-stand system track [equivalent to D1 of Ford et al. (2013)]. The topmost part of the Lower Group is interpreted as a transgressive system track (equivalent to D2 of Ford et al. 2013).

The transition from the Lower to Middle Group is characterized by a major landward shift and a deepening of the depositional environments (Figs. 5 and 6). In term of sequence stratigraphy, this transition corresponds to a major flooding surface rapidly followed up by a major maximum flooding surface (Rohais et al. 2007a). As previously mentioned, this surface is obvious in the outcrops along the present day shoreline where the turbidites physically related to the giant Gilbert-type deltas directly prograde onto shallow lacustrine deposits of the Lower Group (Fig. 5b). It is less obvious along the rift shoulder and the recent investigations indicate that the first maximum flooding event at the base of Sequence 1 defined by Rohais et al. (2008) is more consistently correlated with the flooding event within the Lower Group defined by Rohais et al. (2007a) (Fig. 6).

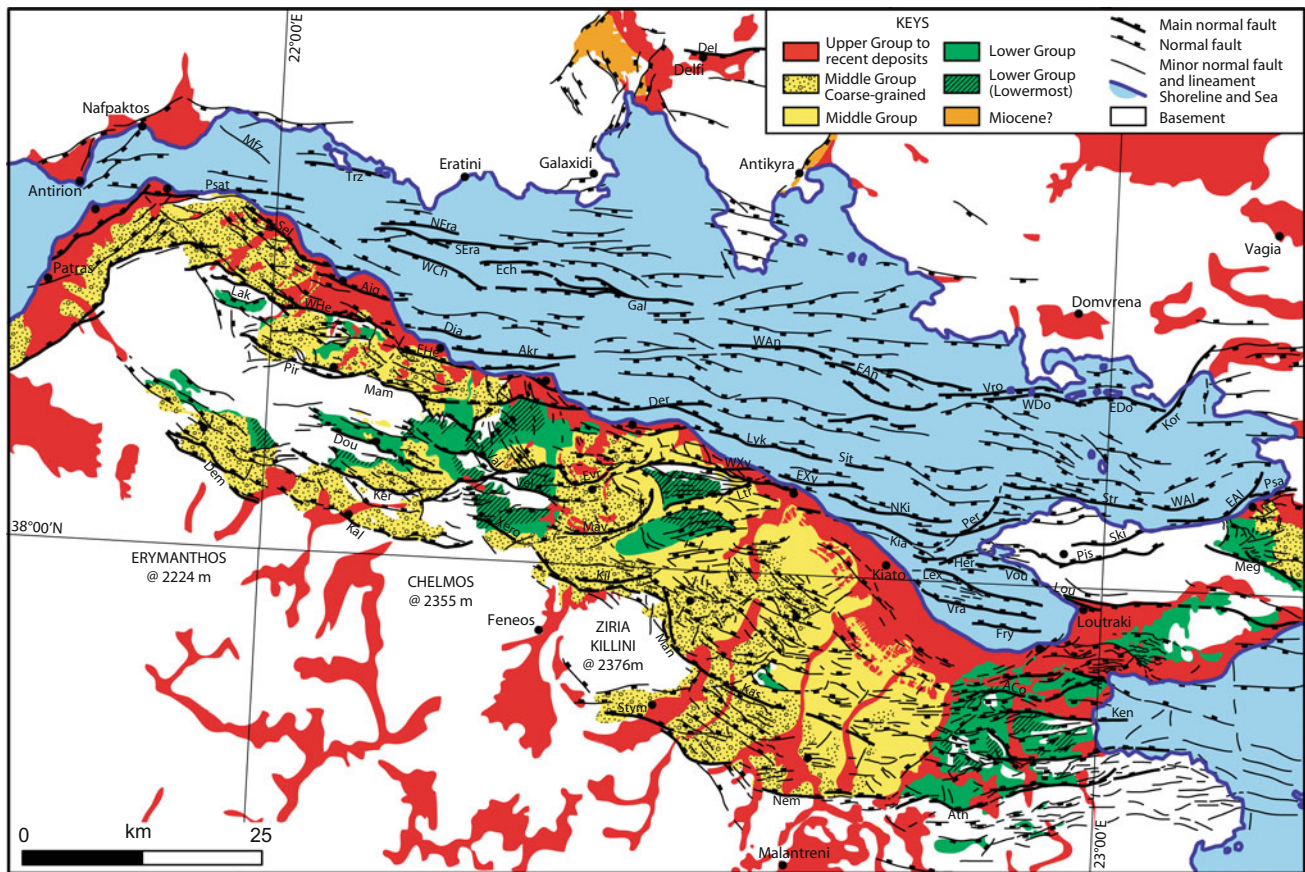


Fig. 4 Geological map of the syn-rift fill of the Corinth rift (present study and modified from Papastamatiou et al. 1962; Aronis et al. 1964; Loftus et al. 1971; Paraschoudis and Machairas 1977; Tsoflias et al. 1984; Doutsos et al. 1988; Koutsouveli et al. 1989; Bentham et al., 1991; Collier and Dart 1991; Tsoflias et al. 1993; Papanikolaou et al. 1996; Ghisetti and Vezzani 2004, 2005; Rohais et al. 2007a; Bell et al. 2009; Taylor et al. 2011; Ford et al. 2013; Nixon et al. 2016). Faults: *ACo* Accro Corinth, *Aig* Aigion, *Akr* Akrata, *Ath* Athika, *Del* Delfi, *Dem* Demestika, *Der* Derveni, *Dia* Diakopto, *Dou* Doumena, *EAl* East Alkyonides, *EAn* East Antikyra, *ECh* East Channel, *EDo* East Domvrena, *EHe* East

Heliki, *Evr* Evrostini, *EXy* East Xylokaastro, *Fry* Fryne, *Gal* Galaxidi, *Her* Heraion, *Kas* Kastraki, *Ken* Kenchreai, *Ker* Kerpini, *Kia* Kiato, *Kor* Korombili, *Lex* Lechaion, *Lou* Loutraki, *Ltr* Loutro, *Lyk* Lykopia, *Mam* Mamoussia, *Man* Manna, *Mav* Mavro, *Meg* Megara, *Mfz* Managouli, *Nem* Nemea, *NEra* North Eratini, *NKi* North Kiato, *Per* Perachora, *Pir* Pirgaki, *Pis* Pisias, *Psa* Psatha, *Psat* Psathopyrgos, *Sel* Selinous, *SEra* South Eratini, *Ski* Skinos, *Str* Strava, *Syt* Sytas, *Trz* Trizonia, *Val* Valimi, *Vra* Vrachonisida, *Vro* Vroma, *WAl* West Alkyonides, *WCh* West Channel, *WDo* West Domvrena, *WHe* West Heliki, *WXy* West Xylokaastro, *WAn* West Antikyra, *Xero* Xerovouni

The onshore Middle group comprises alluvial and Gilbert-type fan deltas that built northward into a marine or brackish body of water with laterally equivalent fine-grained distal turbidites and basal suspension deposits (Fig. 5b). Following a main aggrading trend (Sequence 1 of Rohais et al. 2008) that is hereafter considered as the Lower Group, the Middle group is characterized by three major stages of basinward progradation (Killini, Mavro and Evrostini Gilbert-type fan deltas) organized in a forced regressive trend as suggested by the geomorphologic evidence (Rohais et al. 2007a, 2008). The rift shoulder was overlapped with commonly more than 100 m of massive very proximal conglomerates. This overall organization suggest that the Killini Gilbert-type fan delta (Sequence 2) can be considered

as a highstand system track and the Mavro (and Ilias) and Evrostini Gilbert-type fan deltas as falling stage system track (Sequence 3 and 4 respectively, Fig. 6).

Transition from the Middle to Upper Group is characterized by a basinward shift that locally can reach 3 km, combined with a major forced regression ca. 400–500 m in height. In term of sequence stratigraphy, this transition corresponds to a major sequence boundary (Fig. 5a).

The onshore Upper Group consists of perched Gilbert-type fan deltas and minor local deposits such as marine terraces and slope breccias that record progressive uplift of the margin (Fig. 4). Locally, the Upper Group includes travertine and tufa deposits that could be reworked to form pebbles organized in small deltas (Fig. 5a).

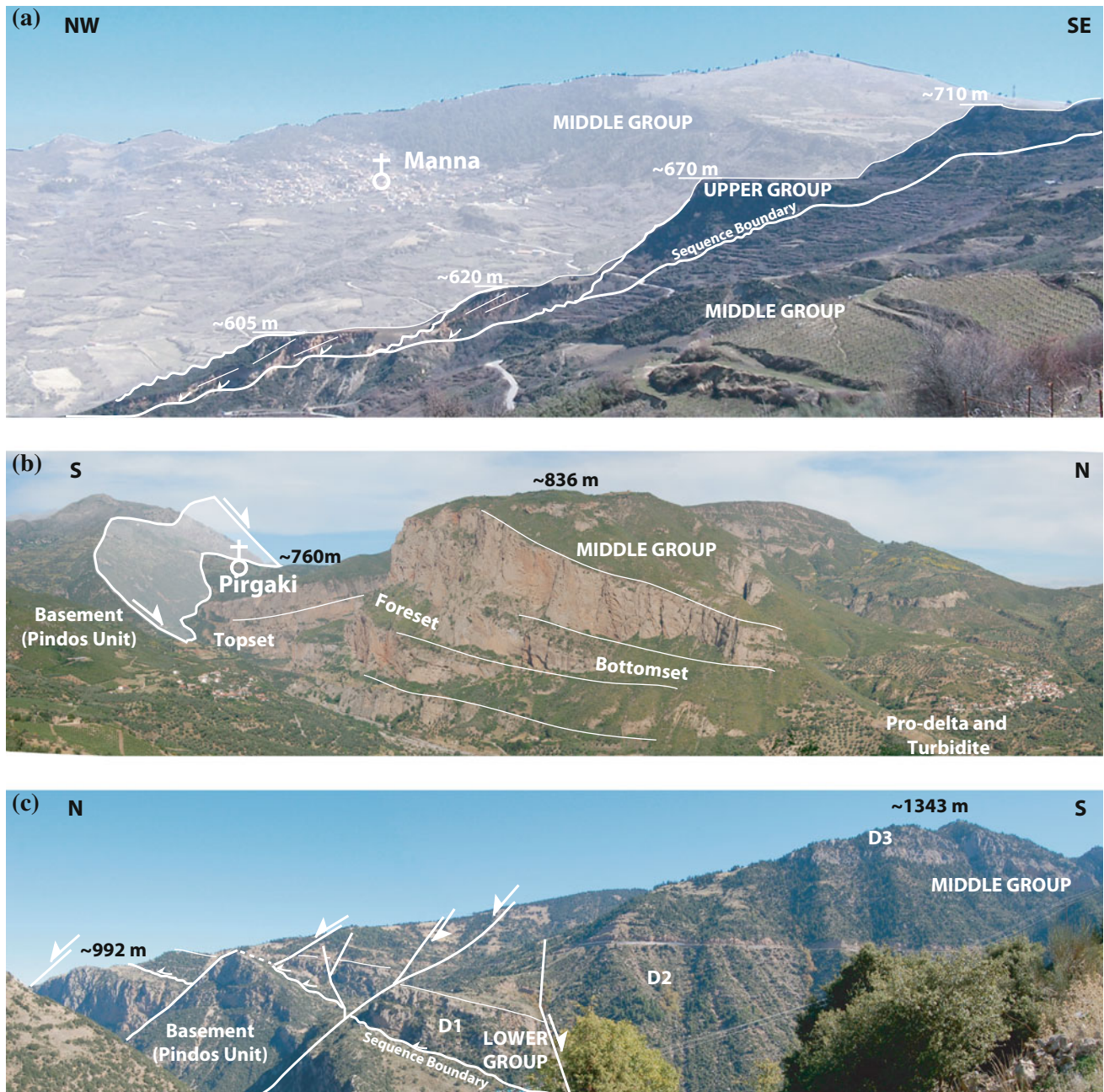


Fig. 5 Groups and stratigraphic architecture of the onshore syn-rift deposits. *A* Upper group in the Manna area with at least three major forced regressive wedges developed on the major sequence boundary between upper and middle group. *B*. Middle group with Kerinitis giant

gilbert-type delta from the Pirgaki-Mamoussia faulted block. *C*. Lower group along the Vouraikos valley with major onlap feature on the tilted block crest of the Pirgaki-Mamoussia fault

Age Model

Recent absolute dating allows us to adjust the age model. The oldest age for the lowermost deposits is Miocene (ca. 5.3 Ma) based on palynological analysis (Muntzos 1992) and ostracods studies (Danatsas 1989, 1994). This age has never been confirmed by more recent studies. The transition from Lower to Middle Group is not well constrained either.

Recent results based on ash dating indicate that the Middle group is at least 2.5 Ma old (Mavro fan delta turbidites, Leeder et al. 2012). Transition between the Lower and Middle Group could be considered at ca. 3.0–3.2 Ma following the great deepening event of Leeder et al. (2012). The last prograding stage of the Middle group is constrained to 1.1–0.7 Ma using mammalian fossils (Dercourt 1964; Symeonidis et al. 1987) and palynological studies

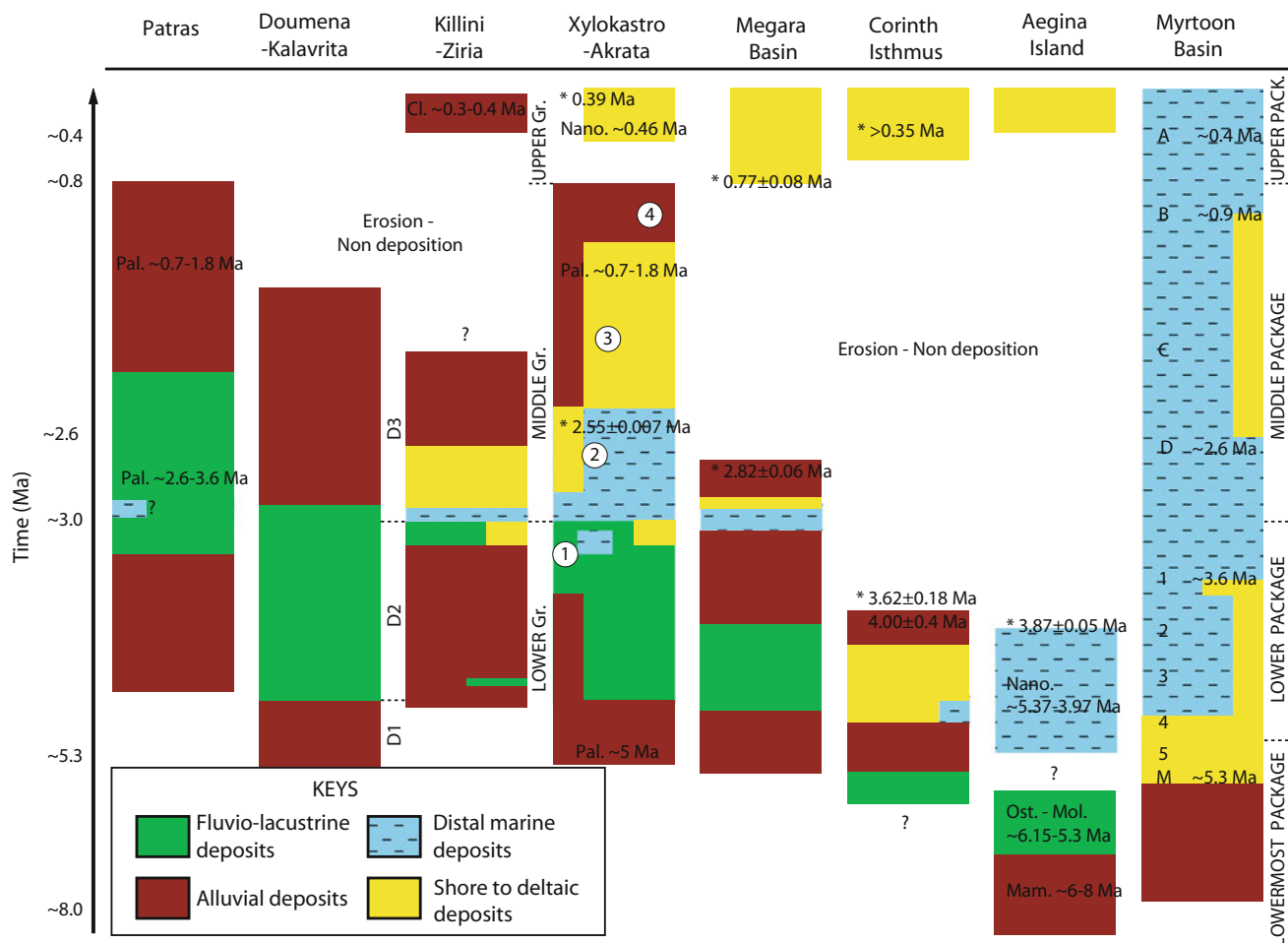


Fig. 6 Synthesis of the sedimentary fills and chronostratigraphy from the Corinth rift (rift shoulder: Killini-Ziria, southern margin onshore: Xylokastro-Akrata, Doumena-Kalavrita areas) with the Lower, middle and upper groups of Rohais et al. (2007a) correlated with D1, D2 and D3 of Ford et al. (2013) and sequences 1, 2, 3 and 4 of Rohais et al. (2008). A comparison with the surrounding basin is also provided with the Patras Basin, Megara Basin, Corinth Isthmus, Aegina Island and

Myrtoon Basin. Star (*) indicates radiometric ages, *Pal.* stands for palynological dating, *Mam.* for mammalian, *Ost-Mol* for Ostracods and mollusk, *Nano.* for nanofossils, *Cl.* for clays (indicative of specific quaternary climate setting in Greece). A–D, 1–5 and M are the main markers identified in the Myrtoon basin and calibrated to surrounding basin and well DSDP well 378 (see references within the text). See Fig. 1 for location

(Ford et al. 2007; Rohais et al. 2007b). The oldest ages for the Upper Group are 0.46–0.45 Ma in the Xylokastro area (Keraudren and Sorel 1987) and 0.307 Ma \pm 0.06 in the Akrata area (McNeill and Collier 2004). The transition between the Middle and Upper Group could thus be considered at 0.8 Ma \pm 0.1.

Offshore Seismic Stratigraphy

The syn-rift stratigraphy of the offshore Gulf of Corinth is generally subdivided into two main units (early- and late-rift sections, Fig. 7) with contrasting seismic character (e.g. Moretti et al. 2003; Sachpazi et al. 2003; Clément et al. 2004; Zelt et al. 2004; Bell et al. 2008; Taylor et al. 2011; Nixon et al. 2016). A major widespread unconformity

separates the two units (Fig. 7) and is a key horizon that has been interpreted as the Middle to Upper group transition (Ford et al. 2013). In this paper, we used the seismic data already published by Zelt et al. (2004) and Taylor et al. (2011) that are available thanks to the Marine Geoscience Data System (<http://www.marine-geo.org/>, Goodliffe and Taylor 2014).

Upper Group

The Upper Group includes large Gilbert-type fan delta, associated turbidites, channel and asymmetrical levees, distal starved basin and starved shorelines (Figs. 8 and 9). In the basin axis, where only starved deposits are dominant, changes in amplitude and frequency of reflectors were used

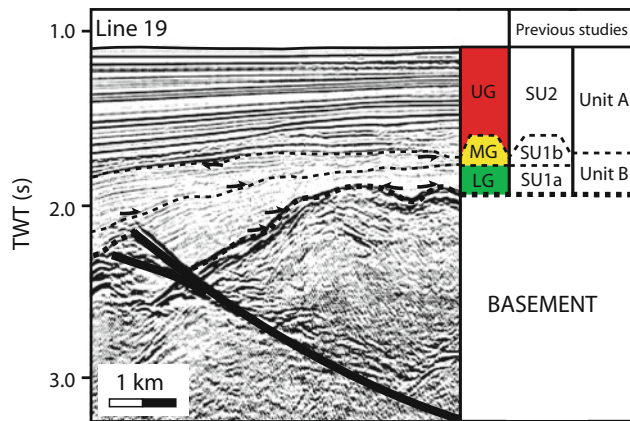


Fig. 7 Seismic stratigraphy of the Corinth rift using an extraction of seismic line 19 (see section 12 in Fig. 12 for location of the seismic window extraction). *UG* upper group, *MG* middle group, *LG* lower group are correlated with previous studies (Moretti et al. 2003; Sachpazi et al. 2003; Clément et al. 2004; Zelt et al. 2004; Bell et al. 2008; Taylor et al. 2011). Onlap features onto inherited paleotopography are highlighted at the base of the lower group. The fault (*thick black line*) is within the Lykoporia and Sytas faults trend. Transition from the lower to middle group is characterized by a major landward shift and fault stopping with downlap features onto the maximum flooding surface recording the rift climax. Major unconformity is characterized by truncation and toplap features at the base of the upper group. See Fig. 2 for location of line 19

to subdivide the stratigraphy (Sachpazi et al. 2003; Lykousis et al. 2007; Bell et al. 2008; 2009; Taylor et al. 2011; Nixon et al. 2016, Fig. 8). These seismic packages have then been calibrated with Marion Dufresne long piston cores (Moretti et al. 2004) which sampled the last lowstand (lacustrine) and most recent highstand sequences (marine). The alternating marine and lacustrine horizons in the central part of the Corinth rift have been correlated with ca. 100 kyr glacio-eustatic cycles to finally propose age estimates for each stratigraphic horizon for the past ca. 500–700 kyr (see review in Nixon et al. 2016). In these previous studies, there is a mismatch between the studies using shallow-penetration, high-resolution seismic reflection data (e.g. Perissoratis et al. 1986; Lykousis et al. 1998; Sakellariou et al. 1998; Perissoratis et al. 2000; Stefatos et al. 2002) that have been later on calibrated with long piston cores (Moretti et al. 2004; McNeil et al. 2005; Lykousis et al. 2007; Sakellariou et al. 2007; Bell et al. 2008), and the studies using marine multichannel seismic data (MCS, Brooks and Ferentinos 1984; Higgs 1988; Sachpazi et al. 2003; Taylor et al. 2011; Nixon et al. 2016). Indeed, the Marion Dufresne piston core dating (Moretti et al. 2004, Lykoussis et al. 2007) has shown that the last 13 kyr old glaciation was ca. 12 m deep in the core MD2480 and that the sedimentation rate ranged from 1 to 1.8 m/kyr in the central part of the basin for this period of

time (Figs. 4 and 8). On the MCS data, if visible it would correspond to the very first reflector (vertical seismic resolution 15–20 m). Sachpazi et al. (2003) and Taylor et al. (2011) consider that it cannot be seen and correlated the bottom of the first laminated seismic package with the 120–130 kyr glaciation. Nevertheless, some authors using the MCS data have interpreted this last glaciation at ca. 80–100 m below the present day sea floor (see review by Nixon et al. 2016). Such a thickness would imply 6–8 times a higher sedimentation rate for that period (Fig. 8), as well as inconsistent slip rates that are not in line with the results provided by the Marion Dufresne piston core. We thus consider the Upper to Middle Group transition reflector as ca. 710 kyr old (and not 620 kyr as Nixon et al. 2016), that is consistent with $0.8 \text{ Ma} \pm 0.1$.

Middle and Lower Groups

In the absence of drill-hole data, it has never been possible to properly correlate the detailed offshore early-rift section with its onshore equivalents. Re-interpretation of Line 19 published by Taylor et al. (2011) provides clear geometric clues to subdivide the early-rift section equivalent to Unit B of Bell et al. (2009) into two groups (Fig. 7). The basal portion is characterized by a fault controlled, isolated depocenter (e.g. Xylokastro, Pirgaki-Mamoussia, Galaxidi, Akrata faults). Seismic facies mainly correspond to continuous reflectors organized into an overall widening trend as suggested by the progressive onlap paleotopography features developed on top of the pre-rift basement (Fig. 7). The seismic character suggests continental to fluvio-lacustrine deposits (e.g. West et al. 2002). An upper portion, recording a progressive death of some major older syn-rift faults, a major flooding and the widening of the basin. The seismic character of the upper portion suggests gravity flow, lobes, channel-levees and distal basinal deposits (Fig. 10). These two groups share many similarities with the Lower and Middle groups onshore, respectively. Transition between these two groups is characterized by an unconformity with onlap and downlap features in the basin axis, recording a major structural rearrangement in the basin (Fig. 7). This subdivision is in line with the recent offshore seismic stratigraphy proposed by Hemelsdaël and Ford (2016) in the vicinity of Akrata (see location in Fig. 2).

The sedimentary features from the offshore Middle Group include large asymmetrical levees associated to channel and basinal deposits (Fig. 10), a very similar depositional profile as the Upper Group and present day active depositional system (Fig. 9). The large asymmetrical levee of the Upper Group is confined into the channel-levees system of the

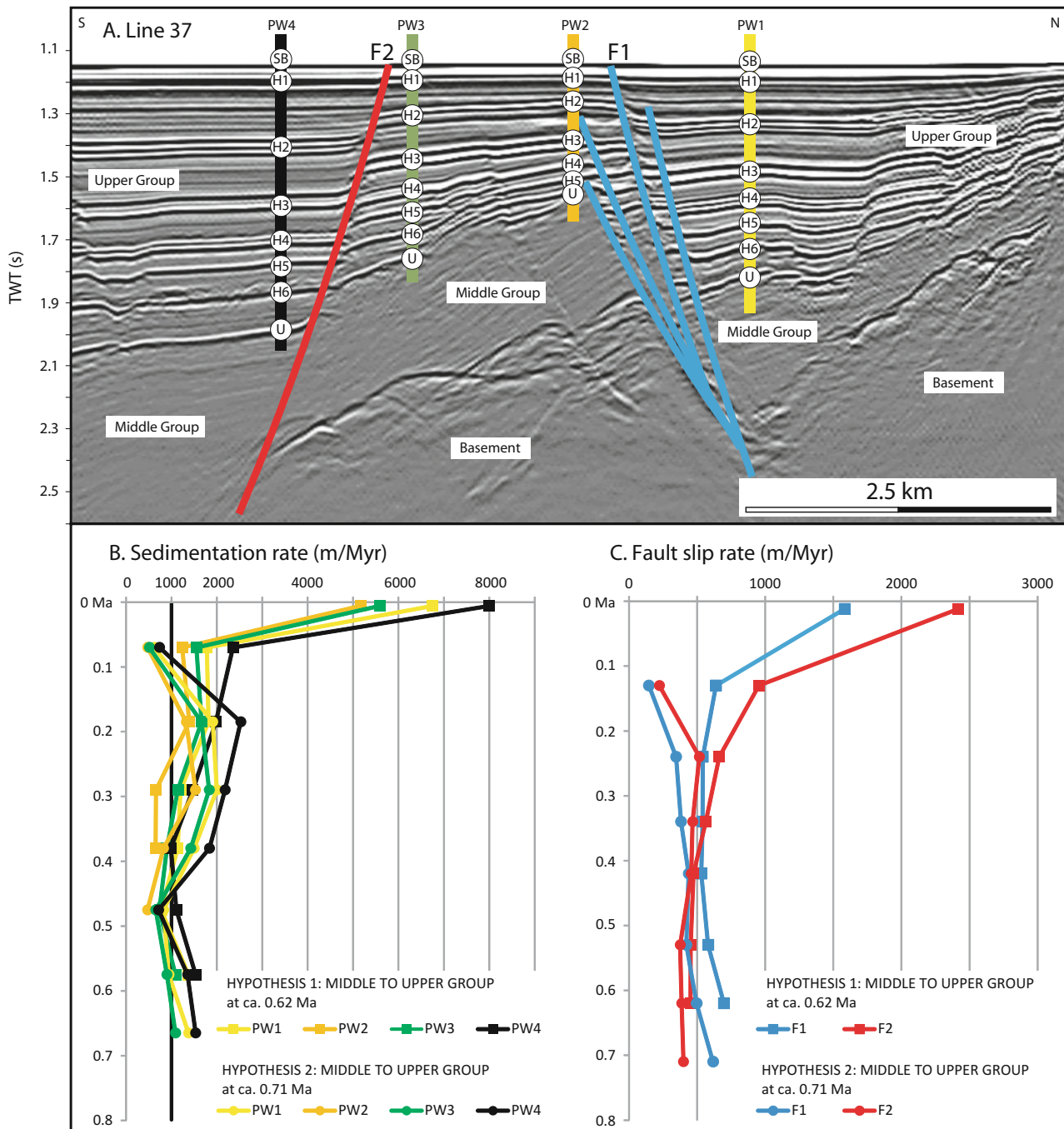


Fig. 8 A High resolution seismic stratigraphy of the upper group along the seismic line 37 (see section 6 in Fig. 12 for location of the seismic window). Seismic horizon labeling is from Nixon et al. (2016). Two hypothesis on the timing of the transition from the middle to upper group are tested to highlight their influence onto sedimentation (B) and fault slip (C) rates. Four pseudo-wells (PW) have been used to quantify

these two parameters. Time to depth conversion is from Taylor et al. (2011). Hypothesis 1 considered the transition to occur at ca. 0.62 Ma with the first seismic horizon (H1) at 0.012 Ma. Hypothesis 2 considered the transition at ca. 0.71 Ma with the first seismic horizon (H1) at 0.13 Ma. Not that the mean sedimentation rate derived from the core MD2480 is 1000 m/Myr

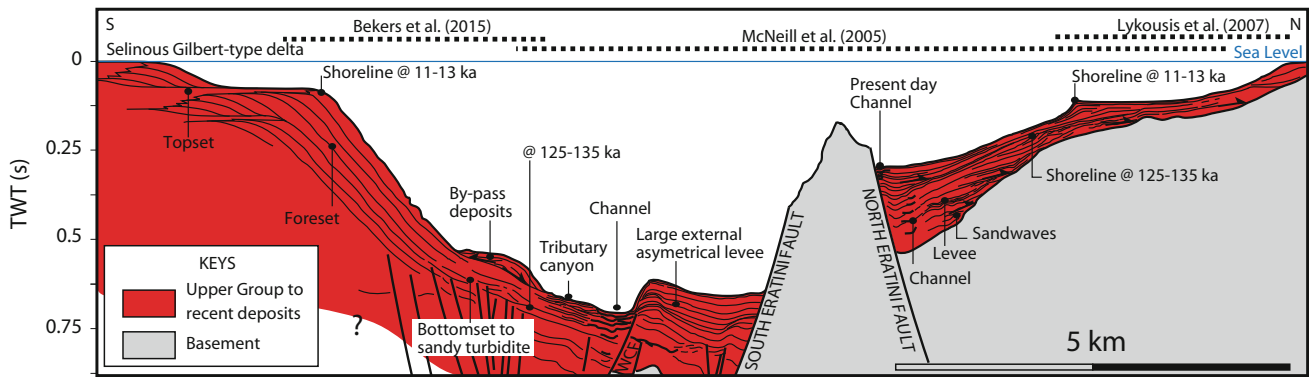


Fig. 9 Upper group depositional profile and stratigraphic architecture in the offshore basin based on shallow seismic lines (modified from Beckers et al. 2015; McNeill et al. 2005; Lykousis et al. 2007). The southern coastline is characterized by high sediment supply setting with giant Gilbert-type delta and related turbiditic systems. The northern

coastline is characterized by a starved setting where highstand system tracks are poorly preserved. Deposits along the northern coastline correspond to an alternation of very deep facies (turbidite) and shallow water sedimentary wedge interpreted as lowstand system tracks. See Fig. 2 for location

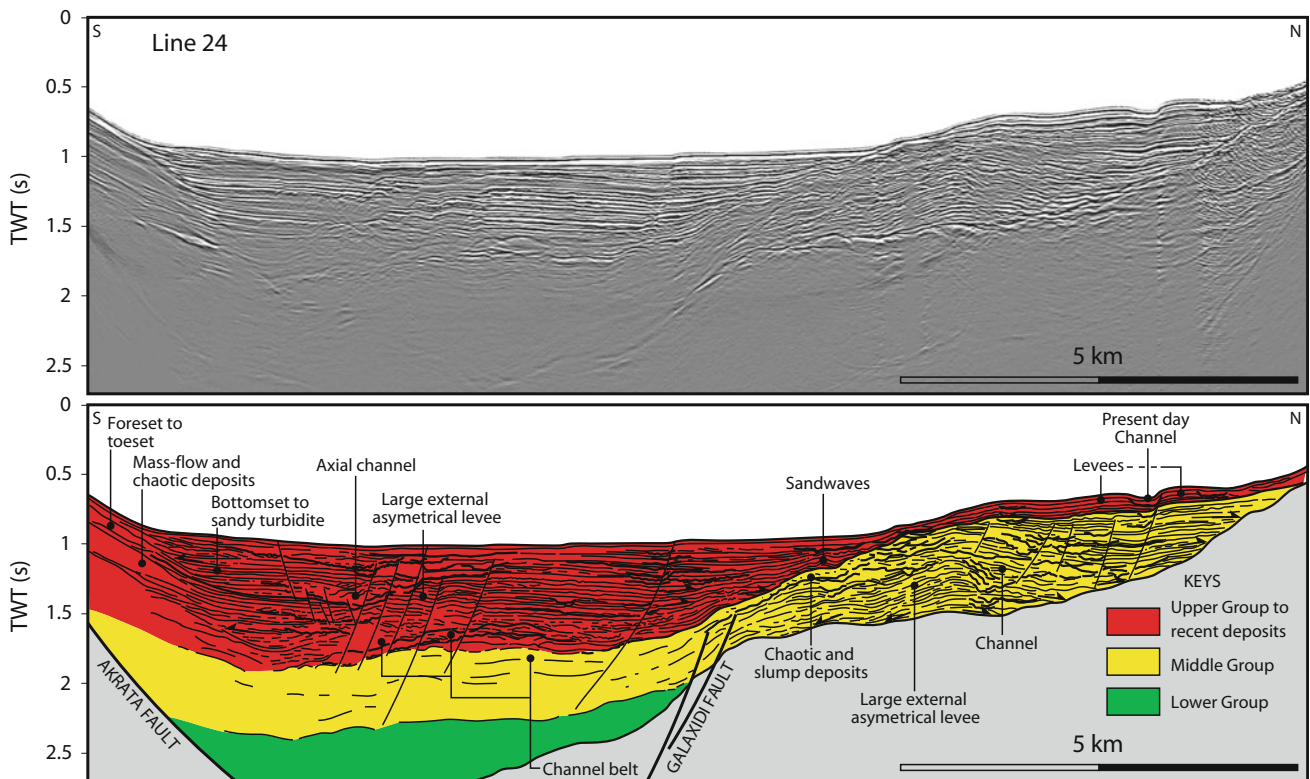


Fig. 10 Middle group architecture in the offshore basin (line 24). The footwall of the Galaxidi fault is characterized by aggradational external asymmetrical turbiditic levee. The Upper Group is restricted into the

topographic morphology induced by the turbiditic levee of the Middle Group. See Fig. 2 for location

Middle Group (Fig. 10). It indicates that the distance between the active Gilbert-type deltas and the large asymmetrical levees has been shortened between the Middle to Upper Group. It results in a progressive confinement of the sedimentary fluxes potentially related to the Galaxidi Fault activity (Fig. 10).

Comparison with Surrounding Basins

The most complete and well-constrained Tertiary sedimentary fill in the vicinity of the Corinth basin is recorded in the Myrtoon basin (Fig. 1). The seismic stratigraphy of the Myrtoon basin has already been correlated with its

surrounding basins: southern Evvia, Saronikos and Argolikos gulfs (Anastasakis and Piper 2005; Anastasakis et al. 2006), and constrained with DSDP well 378 (5°55.67'N, 25°06.97'E). Based on the main flooding event (ca. 5.3–4, 3.6–2.6 and 0.5–0.4 Ma) and the overall stratigraphic architecture (Fig. 6), its seismic stratigraphic architecture can be extrapolated to the Corinth rift passing through the Aeginea Island, Corinth Isthmus and Megara Basin where numerous other age constraints are available (Fig. 6). Three major packages can be recognized in the sedimentary fills of these surrounding basins and compare with the three main groups of the Corinth rift (Figs. 6 and 11).

Lower Group and Equivalent Strata

A lowermost package that includes (1) basal continental to fluvio-lacustrine deposits from Miocene to Lower Pliocene age (ca. 8–5.3 Ma, e.g. Rögl et al. 1991), (2) marine deposits (White Marl formation, Collier and Dart 1991) that could be correlated across towards the southeastern most part of the Corinth Isthmus of Pliocene age (ca. 5.3–4 Ma), and (3) prograding deltaic to continental deposits that were capped by volcanics at around 3.6 Ma (Collier and Dart 1991). We propose that the lowermost part of the Lower Group in the Corinth rift and Megara basin is the lateral equivalent of this lower package with more proximal depositional systems and a major coeval maximum flooding event recorded by lacustrine deposits (Fig. 6). The oldest age for the Lower Group in the Corinth rift could then be considered at ca. 5.3 Ma. This lowermost package could be interpreted as a third order lowstand system track.

A lower package that includes (1) a major marine flooding with marine evidence in the Megara Basin (Harbour Ridges Fm, Bentham et al. 1991) from Pliocene age (ca. 3.6 Ma), (2) an aggrading to backstepping trend characterized by thick marine distal deposits in the basin axis and deltaic systems along the basin margins from Pliocene age (ca. 3.6–2.6 Ma, e.g. Anastasakis et al. 2006). We propose that the topmost part of the Lower Group in the Corinth Rift basin is the lateral equivalent of this lower package with more proximal depositional systems (Fig. 6). This lower package could be interpreted as a third order transgressive system track.

Middle Group and Equivalent Strata

A middle package that includes a major prograding trend of the deltaic systems along the basin margins from Pliocene to Pleistocene age (ca. 2.6–0.9 Ma, e.g. Anastasakis et al. 2006), lasting up to a major sequence boundary. We propose that the Middle Group in the Corinth Rift is its lateral equivalent because age constraints and stratigraphic trends are very consistent (Fig. 6). This middle package could be interpreted as a third order highstand to falling stage system track.

Upper Group and Equivalent Strata

An upper package that includes (1) a flooding event following a major erosive event (time gap of 2–3 Ma in the Megara basin, Corinth Isthmus, Aeginea Island),

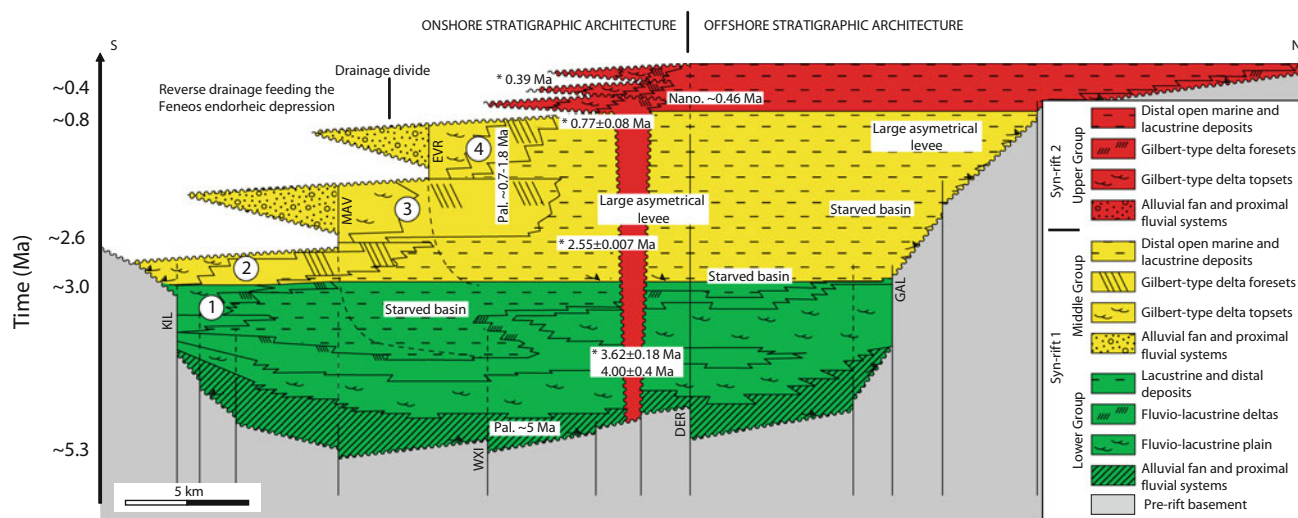


Fig. 11 Chronostratigraphic scheme of the onshore to offshore syn-rift deposits from the Corinth rift across an idealized line in the central part of the rift (Killini-Ziria, Xylokastro-Akrata to lines 14 and 34). See text

for further information about the absolute ages. 1, 2, 3 and 4 refer to sequence labeling of Rohais et al. (2008). See Fig. 4 for location

(2) terraces, breccia and perched deposits preserved along the present day uplifted margins and (3) thick marine distal deposits from Pleistocene age (ca. 0.9-present day) in the basin axis. We propose that the Upper Group in the Corinth rift is its lateral equivalent because age constraints and stratigraphic trends are also very consistent (Fig. 6). This upper package could be interpreted as a third order, early to late lowstand system track.

Rift Architecture and Subsidence

This new offshore seismic stratigraphic scheme has been used to interpret the seismic profiles of Taylor et al. (2011), in order to trace the three main groups in the offshore basin (Figs. 12 and 13). Combined with the updated onshore stratigraphy (Fig. 11), they provide good constraints to document the basin segmentation, along-strike evolution of the rift and fault geometries. These cross-sections do not illustrate the pre-rift structure.

Western Domain

The western domain is located in between Aigion and Akrata (Fig. 4). Offshore, the main faults are S-dipping faults with the South Eratini (Sera), West and East Channel faults (Wch and ECh, respectively), and N-dipping faults with the Aigion (Aig), Diakofto (Dia) and Akrata (Akr) faults (Figs. 4 and 12). Onshore, the main faults are N-dipping faults with West and East Helike (WHe and EHe, respectively), the Pirgaki-Mamoussia (Pir-Mam), the Doumena (Dou), the Demestika (Dem) and Kalavrita (Kal) faults (Figs. 4 and 12). These faults subdivide the rift into 5–8 km wide and 10–25 km long faulted blocks (Figs. 4 and 12). Most of the blocks are back tilted to the South (Fig. 12). Buried S-dipping faults are preserved in the Pirgaki-Mamoussia faulted block (Fig. 12, section 2, Ford et al. 2013). Seismicity data and structural reconstruction have shown that the main rift faults such as Pirgaki/Mamoussia and Helike faults affect both syn- and pre-rift sequences, are mainly planar over kilometers (dip 55°–60° down to 6–12 km) and root in a northward dipping seismogenic zone (Chouliaris et al. 2015).

The Lower Group is not preserved (no deposition) offshore Aigion and progressively thickened eastward (Fig. 13). The Middle Group progressively onlap the southern rift shoulder as well as the northern margin of the rift (Fig. 12, sections 1, 2 and 3). The Middle Group also onlap progressive the pre-rift basement toward the West (Fig. 13, sections 9 and 10).

In the Pirgaki-Mamoussia faulted block, the Lower Group is organized into two merging depocenters (Fig. 13, section 10). The two fault controlled Lower Group depocenters were progressively connected along the breached relay ramp between the Kerinitis and Vouraikos Gilbert-type fan delta (Fig. 13, section 10). During the Middle Group these two fault segments formed the Pirgaki-Mamoussia Fault whose maximum fault throw was located just west of the breached relay ramp (between Selinous and Kerinitis Gilbert-type deltas). The cumulative maximum throw along the Pirgaki-Mamoussia fault is still located in this area as suggested by the structural characterization provided by Micarelli et al. (2003). Finally, during the Upper Group, the fault continues to propagate eastward as proven by the relay ramp features on top of which the Akrata Gilbert-type fan delta prograded (Fig. 13, section 10). These observations are visible on the geological map where the preserved progradational Middle Group packages are localized in between tilting block crests in the Vouraikos valley (Fig. 4).

Syncline and anticline geometries are spectacularly preserved in the Doumena, the Pirgaki-Mamoussia and the Valimi fault blocks (Fig. 12, sections 1, 2 and 3, Rohais et al. 2007a; Ford et al. 2013). Combined with the evidence of depocenter migration between the Lower and Middle Group, all these observations suggest fault propagation in the Corinth rift.

Central Domain

The central domain is located in between Akrata and Xylokaastro (Fig. 4). Offshore, the main faults are S-dipping faults with the Galaxidi (Gal), West Antikyra (WAn) faults, and N-dipping faults with the Derveni (Der), Lykoporia (Lyk) faults (Figs. 4 and 12). Onshore, the main faults are N-dipping faults with the Pirgaki-Mamoussia (Pir-Mam), Valimi (Val), West Xylokaastro (WXy), Vela (Vel), Evrostini (Evr), Mavro (Mav), Xerovouni (Xer) and Killini (Kil) faults (Figs. 4 and 12). These faults subdivide the rift into 5–8 km wide and 10–25 km long faulted blocks as in the western domain (Figs. 4 and 12). Nevertheless, the basement is less exposed along the tilted block crest than in the western domain (Fig. 4). Syn-rift deposits thickness is at maximum both onshore and offshore (Fig. 12, sections 4 and 5).

Large listric faults are also documented in central part where Lower Group is dominated by fine-grained deposits and the Middle Group corresponds to thick Gilbert-type fan delta (e.g. Rohais et al. 2007a). Smaller examples are also documented in the western and eastern domains (Fig. 12, sections 2 and 6, e.g. Ford et al. 2013; Doutsos and Piper

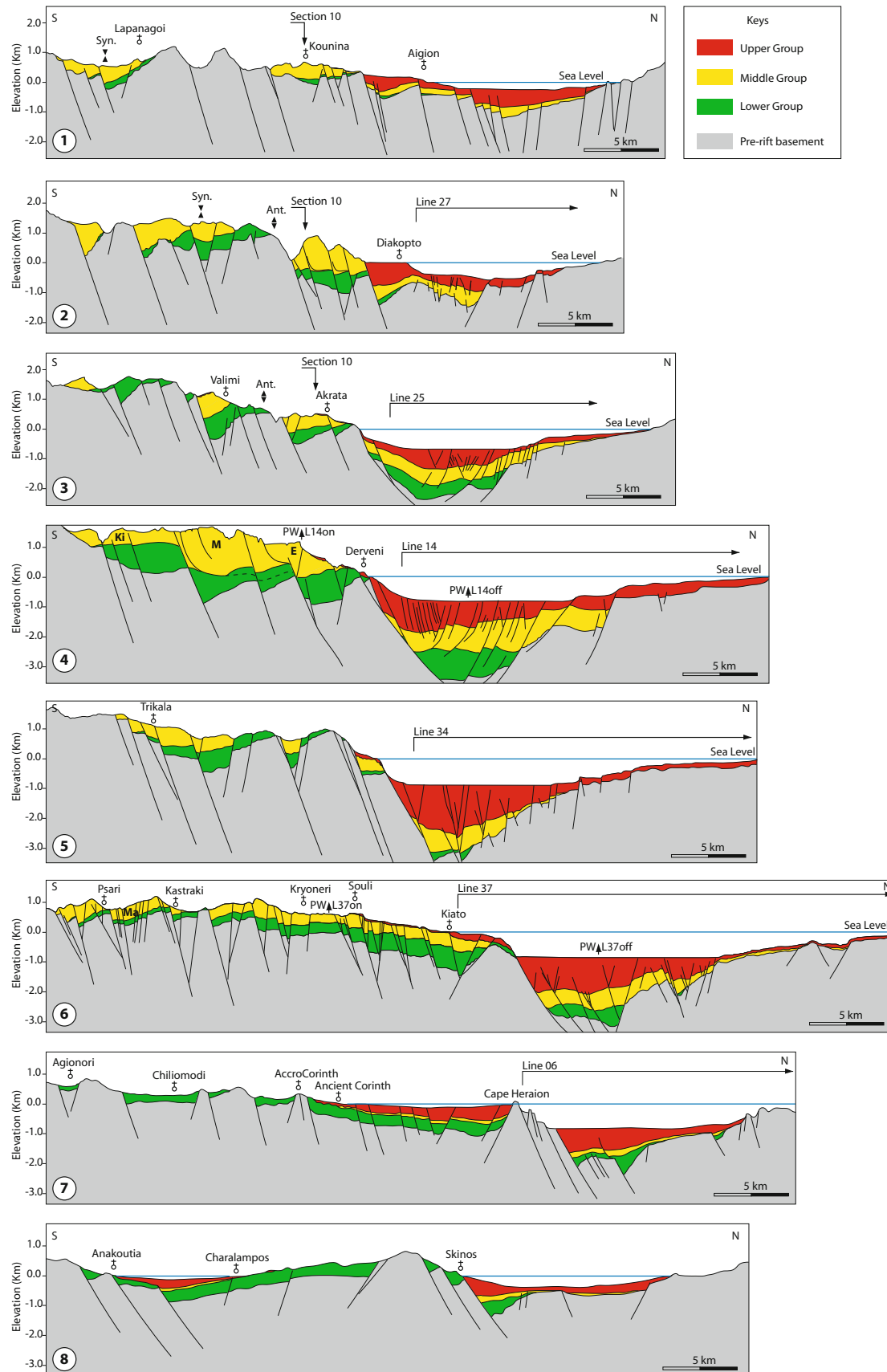


Fig. 12 N-S basin scale cross-sections of the Corinth rift showing the distribution of the main three groups based on outcrop data and seismic line interpretation. Offshore seismic lines time to depth conversions are from Taylor et al. (2011). *Syn.* Synform, *Ant.* Antiform. Giant Gilbert-type deltas: *Ki* Killini, *M* Mavro, *E* Evrostini, *Ma* Manna. See Fig. 2 for location. PW corresponds to the pseudo-wells extracted for back-stripping quantification

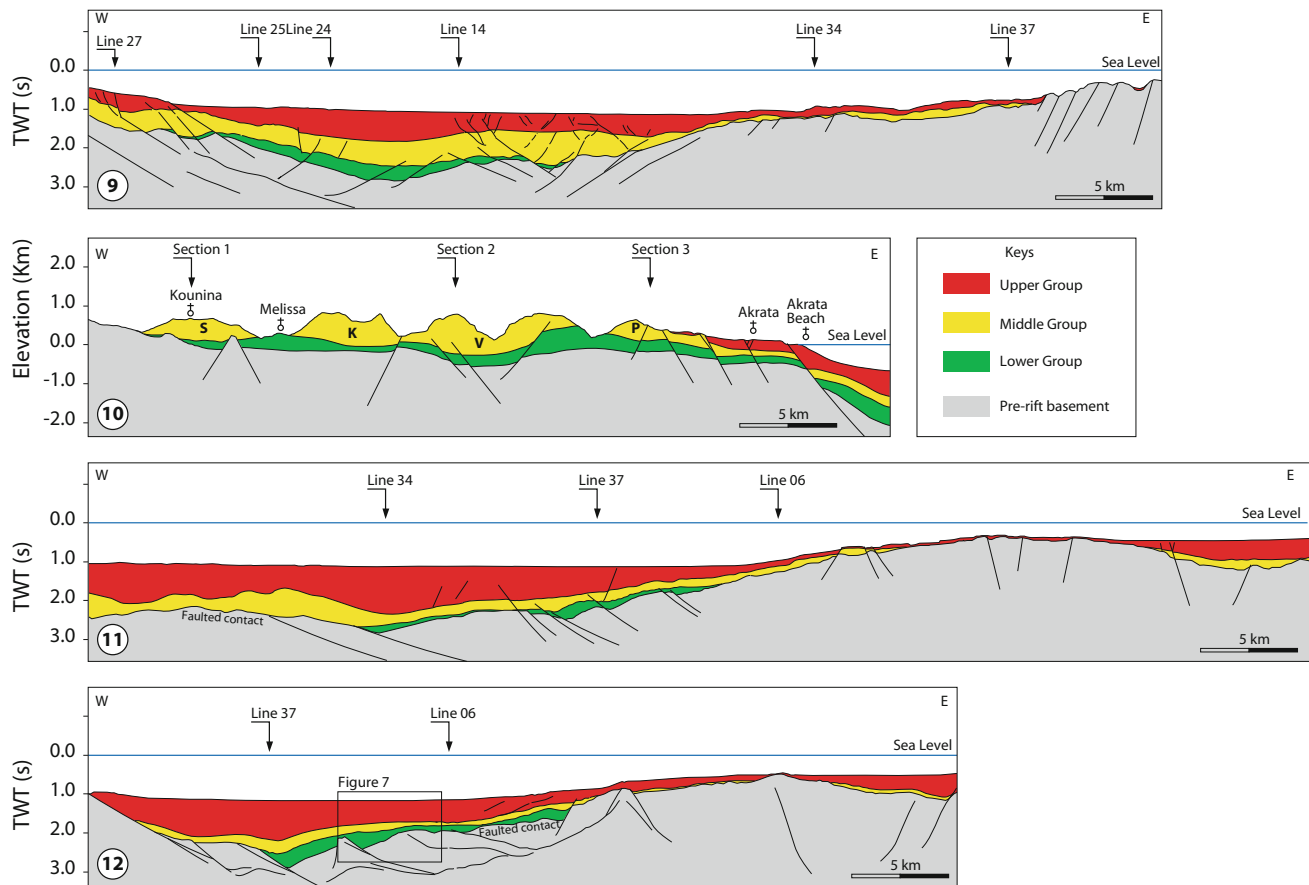


Fig. 13 W-E basin scale cross-sections of the Corinth rift showing the distribution of the main three groups based on outcrop data and seismic line interpretation. Offshore seismic lines time to depth conversions are

from Taylor et al. (2011) for the eastern part of section 10. Giant Gilbert-type deltas: *S* Selinous, *K* Kerinitis, *V* Vouraikos, *P* Platanos. See Fig. 2 for location

1990). These faults are rooted in the syn-rift deposits (Fig. 12, section 4). Four Gilbert-type deltas are structured by these faults along the southern margin: the Vouraikos, Evrostini, Mavro-Ilias and Manna deltas (Figs. 4 and 12). They are interpreted as gravity-driven listric fault initiated during the giant Gilbert-type delta progradation (Middle Group) in the footwall of some major normal fault (Figs. 4 and 12).

The Middle Group show the same distribution as in the western domain with onlap on southern rift shoulder as well as the northern margin of the rift (Fig. 12, sections 4 and 5), suggesting an overall widening of the rift from the Lower to the Middle Group. Along the present day coastline, Upper Group could be locally directly in contact with the Lower Group (Fig. 11), and in some places such as the Mavra Litharia faulted block crest (Derвени area, Fig. 12, section 4), the Upper Group is directly in contact with the pre-rift basement.

Eastern and Easternmost Domains

The eastern to easternmost domains are located from Xylokaastro to the Corinth Isthmus (Fig. 4). The easternmost domain is commonly considered as the gulfs of Alkyonides and Lechaion, the Corinth Isthmus and the Megara basin with in between the Perachora peninsula (Fig. 4, e.g. Bell et al. 2009; Taylor et al. 2011). Offshore, the main faults are S-dipping faults with the East Antikyra (EAn), Vro (Vroma), East and West Domvrena (EDo and WDo respectively), Korombili (Kor), Kiato (Kia), Heraion (Her), Vouliagmeni (Vou) and Lechaion (Lex) faults, and N-dipping faults with East Xylokaastro (EXy), Sytas (Syt), North Kiato (NKi), Strava (Str), Vrachati (Vra), Fryne (Fry), West Alkyonides (WAl) and Psatha (Psa) faults (Figs. 4 and 12). NW-dipping faults are also documented such as the Perachora (Per) and East Alkyonides (EAl) faults (Figs. 4 and 12). Onshore, the main faults are N-dipping faults with the Megara (Meg),

Skinos (Ski), Pisia (Pis), Kenchreai (Ken), Nemea (Nem) and Athikia (Ath) faults and few S-dipping faults such as the Loutraki (Lou) fault (Figs. 4 and 12). These faults subdivide the rift into 5–15 km wide and 15–30 km long faulted blocks (Figs. 4 and 12). Onshore between Kiato and the Corinth Isthmus, a large N-dipping faulted block is mainly controlled by S-dipping fault (Loutraki, Lechaion, Kiato faults, Figs. 4 and 12, sections 6 and 7). In the easternmost part of the rift, toward the Gulf of Saronic (Fig. 12, section 8), the faulted blocks are S-dipping as in the Western and Central part of the rift. The Corinth Isthmus as well as the area in between Kiato and Xylokastro thus correspond to accommodation zone or twist zones as defined by Colletta et al. (1988). The large and thin Manna Gilbert-type delta of the Middle Group is then preserved in between these two accommodation zones (Figs. 4 and 12, section 6).

Offshore, the transition between the central and eastern domains is characterized by very thin or even lack of Lower Group deposits (Fig. 13, sections 10 and 11). The Middle Group was then developed on top of the pre-rift basement with onlap geometries (Figs. 12 and 13). Paleo-high structures, such as the Cape Heraion/Perachora Peninsula and the westernmost part of the Gulf of Alkyonides are still starved in sediment with very thin and isolated preserved deposits of the Upper Group (Fig. 12, section 7; Fig. 13, sections 11 and 12). Along the Corinth Isthmus, the Upper Group is commonly in direct contact with the Lower Group suggesting strong exposure and erosion at the transition between the Middle and Upper Group (Fig. 12, sections 7 and 8).

Fault Birth and Death

Death fault can also be observed in the Corinth rift (Figs. 12 and 13). Firstly, the southern border faults (e.g. Killini, Kalavrita, Nemea faults, Figs. 4 and 12) that controlled the accommodation space during the Lower Group and the Middle Group. These faults stopped during the Middle Group as suggested by the stratigraphic architecture of the syn-rift (abandonment surface, passive onlap on rift shoulders). Secondly, small S-dipping faults along the present day shoreline which cut the main faulted block (e.g. footwall of Xylokastro, Helike, Pirgaki-Mamoussia faulted blocks see cross sections in Fig. 12). Non active S-dipping faults could also be observed offshore such as the Galaxidi fault which were active during the Lower Group deposition and almost inactive during the Middle Group as suggested by the lack of significant thickness changes across the fault (Figs. 10 and 12). And thirdly, normal faults both S- and N-dipping controlling small isolated Lower Group depocenters preserved in graben structures (e.g. south of Athikia Fault, south of Lakka fault, Fig. 4). These faults do not show any evidences of activity during the Middle Group.

Late Faults and Present Day Active Faults

The GPS data show that the present day extension is 10 mm/year in the eastern part, 14 mm/year in the central part and 15 mm/year in the western part (Avallone et al. 2004). The area affected by extension is larger than the current subsiding gulf and the southern shore is uplifted at a rate of 1 mm/year near Aigion. The present day active fault system is well described by McNeill et al. (2005), Bell et al. (2009) and Beckers et al. (2015). Offshore, the main active faults are the Aigion, Western Channel, Eratini (South and North), Trizonia, Psatopirgos faults (Figs. 4 and 12). Onshore, late and active faults are mainly documented by cross-cutting relationship with the Upper Group geomorphological features (abandonment surface, terraces, slope breccias). 20–200 m fault throws are documented on top of the Selinous, Vouraikos or Akrata Gilbert-type fan delta, i.e. in the footwall of the Helike-Akrata fault segment. 5–10 m fault throws are also documented along the Perachora peninsula.

When the sedimentary signal is missing, fault activity could also be studied by analyzing cements preserved along the fault plane (e.g. Causse et al. 2004) coupled with a structural study and by the current seismicity and GPS data. For instance, the Pirgaki fault (Rigo et al. 1996; Lyon-Caen et al. 2004) and some faults outcropping along the northern shore (Sokos et al. 2012) have been interpreted to be recently reactivated.

Subsidence and Sedimentation Rates

In a classical rift system extension and subsidence are linked. The crustal thinning in the upper crust recorded by normal faults results in tectonic subsidence. Tectonic subsidence is strengthened by the sediment loading and is finally recorded as total subsidence. The lack of apparent crustal thinning below the area affected by extension in and around the Gulf of Corinth, compared to the northern and southern border has been already mentioned (Bell et al. 2011). These two types of subsidence versus time have been computed in different parts of the rift and compared to the sedimentary signal (Table 1). The results are presented Figs. 14 and 15; Table 2 for four pseudo-wells, two offshore and two onshore respectively in the cross-sections 4 and 6 of Fig. 12 (see location in Fig. 2). The sedimentation rates are restored from the data and computed using a back-stripping program to taken into account decompaction (Fig. 14, Table 2). The subsidences, both tectonic and total, are depending on water depth hypothesis (Fig. 14). Based on the facies analysis, we have considered that the present day gulf was very shallow during sedimentation of the Lower Group (0–50 m), then quickly deepened during the Middle Group

Table 1 Input data for the back-stripping quantification (GENEX)

Pseudo-wells	Markers	Depths (m)	Paleobathymetry/Topography (m)
PW_L37on	Topography (-)		-780
	Upper Group	10	500
	Middle Group	290	50
	Lower Group	670	0
PW_L37off	Sea bottom	860	860
	Upper Group	2126	680
	Middle Group	3000	50
	Lower Group	3200	0
PW_L14on	Topography (-)		-1100
	Upper Group	10	700
	Middle Group	1700	50
	Lower Group	2500	0
PW_L14off	Sea bottom	836	836
	Upper Group	1697	680
	Middle Group	2497	50
	Lower Group	3496	0

Lithologies are kept constant with 30 % of sand, 30 % of silt, 30 % of shale and 10 % of carbonate. Crustal thickness is 40 km-thick. Four pseudo-wells (PW) has been selected, two onshore (on) and two offshore (off) along seismic line 14 and seismic line 37 (sections 4 and 6 in Fig. 12). Offshore seismic lines time to depth conversions are from Taylor et al. (2011)

(200–600 m) and finally increased smoothly during the Upper Group (600–800 m, Fig. 11, Table 1).

Results show that in the offshore (Figs. 14 and 15, Table 2), tectonic subsidence rates increased during the first syn-rift phase (Syn-rift 1 including Lower and Middle Groups) and then rapidly increased during the second syn-rift phase (Syn-rift2, Upper Group). This overall trend is demonstrated independent on the age model (Fig. 15). Onshore, the same trend were recorded with an increase of the tectonic subsidence rate by a factor two between Lower and Middle Groups (Fig. 14).

In terms of sedimentation rate, average values during the Upper, Middle and Lower groups illustrate the depocenter migration between deposition of the Middle and Upper Group (Fig. 14, Table 2). In the central part of the rift (cross-section 4, Line 14 in Fig. 12) the maximum sedimentation rate was 0.8 m/kyr located onshore during the Middle Group and then migrated in the present day during deposition of the Upper Group (Fig. 14). The highest average sedimentation rates occurred during the Upper Group eastward (1.3 m/kyr). In this eastern part, we also computed high resolution sedimentation rates based on the age model proposed for the Upper Group (Figs. 8 and 14d). Results show very high variable values (0.6–1.9 m/kyr, Fig. 14). As tectonic subsidence and slip rates along the faults (0.5 m/kyr) are relatively constant for the same period of time (Figs. 8 and 14b), it suggests high resolution variation in sediment supply during the deposition of the Upper Group. This is very consistent with the results of Collier et al. (2000) who described the influence of cold and wet winters during the two last glaciations in the Alkynoides basin (0.1 up to 0.8 m/kyr).

Stratigraphic Architecture and Rifting Scenario

The major phases recognized in the rift evolution, already well described along several portions of its southern margin (e.g. Doutsos et al. 1988; Ori 1989; Rohais et al. 2007a; Ford et al. 2013), can thus be now extrapolated at the rift scale, based on the correlation of the three main groups (Fig. 16). In the absence of drill-hole data in offshore series, the following scenario is our favorite option taking into account all the present day available data. It will have to be updated in the future as soon as an offshore well will provide a description of the offshore syn-rift fill. If the evolution of deformation seems now rather well constrained (Fig. 16), the absolute ages of some steps remain poorly constrained and these uncertainties are addressed later in the paper. Subsidence and sedimentation rates can nevertheless been quantified and discussed based on these scenario (Figs. 14 and 15, Table 2).

Syn-rift 1

Rift Initiation ca. 5.3 Ma

The Corinth rift initiation event is based on the oldest age for the lowermost deposits in the Akrata-Derveni area (Miocene —Muntzos 1992; Danatsas 1989, 1994). It is consistent with the propagation of extension from southeast to northwest with fault-controlled basin already active during early Miocene as for example the Myrtoon or Saronic basins (e.g. Anastasakis et al. 2006). It is also consistent with the Late Miocene deposits preserved along the northern shoulder of

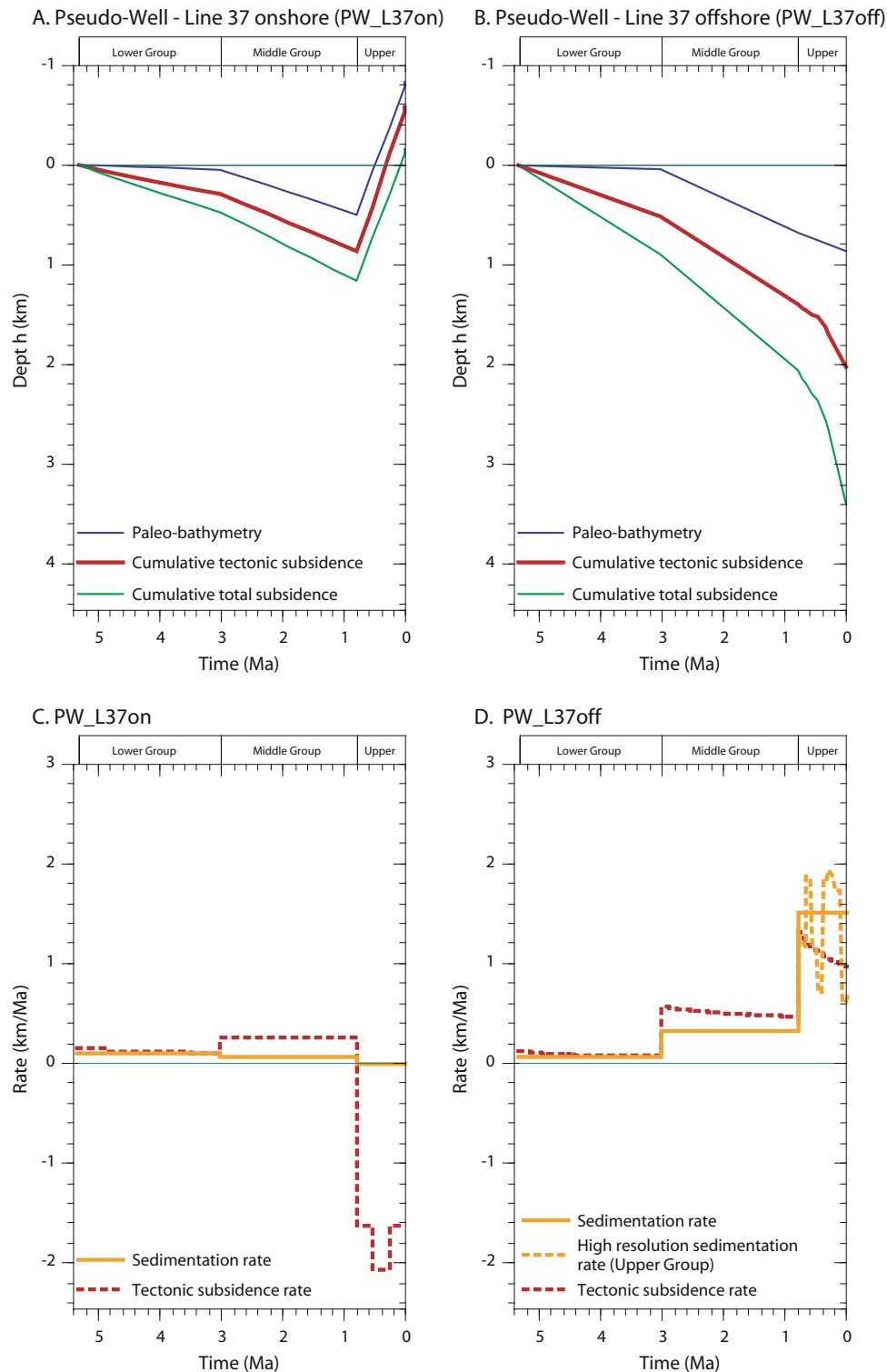


Fig. 14 Subsidence (A and B) and sedimentation rates (C and D) in two pseudo-wells on section 6 (seismic line 37), see location in Fig. 12. *Note* Sedimentation rates are deduced from the data using a back-stripping tools (GENEX). Subsidence rates are highly dependent on the water depth (shown in the figure for both onshore and offshore positions). As a comparison, sedimentation rate measured on the core MD2480 is 1 km/Myr and the maximum extrapolated in the depocenter from this point using HR shallow seismic is 1.8 km/Myr (Moretti et al. 2004; Lykoussis et al. 2007). The sedimentation rate given by Collier et al. (2000) vary along the Gulf but also versus time in a range of 0.1–0.7 km/Myr during the last 128 kyr. Uplift rate for the exhumation of the Peloponnese proposed by Doutsos et al. (2000) range from 0.7 to 1.5 km/Myr

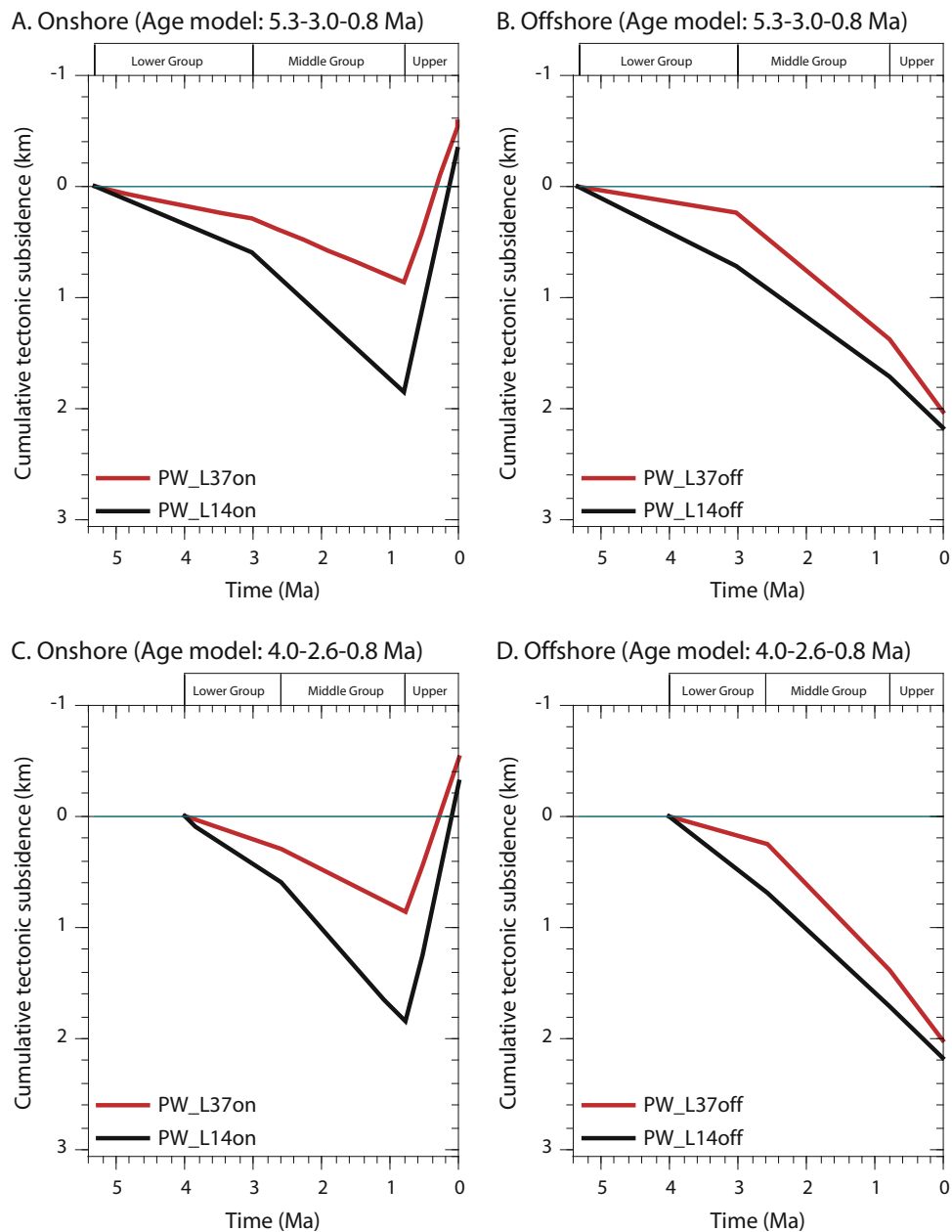


Fig. 15 Subsidence rates in four pseudo-wells (PW), two onshore (A and C) and two offshore (B and D) along seismic line 14 and seismic line 37 (sections 4 and 6 in Fig. 12). Two age models were used to test extreme scenario, with a “maximal” (A and B) versus “low” (C and D) age model. See text for further information

the rift in detachment-controlled basin (Papanikolaou et al. 2009). No volcanism has ever been documented during the initiation phase. In the Corinth rift, the rift initiation was recorded by isolated fault-controlled depocenters with alluvial to fluvial deposits, mainly preserved in the eastern and central parts of the rift that were controlled by inherited structures (Fig. 16a). The main active fault were dipping to both the north and the south (Fig. 16a).

Rift Widening ca. 5.3–3.0 Ma

The Lower Group then recorded a widening of the rift with a progressive marine flooding coming from the southeast (Corinth Isthmus, Fig. 16a). This is in line with a dramatic relative sea level rise (ca. 900 m) that has been documented around 5 Ma on Milos Island (Krijgsman et al. 1999) and the Saronic Gulf (Papanikolaou et al. 1988). The Lower Group depocenters were progressively spread toward the rift

Table 2 Tectonic subsidence and sedimentation rates in four pseudo-wells (PW), two onshore (on) and two offshore (off) along seismic line 14 and seismic line 37 (sections 4 and 6 in Fig. 12)

Age model	Group	Duration (Ma)	Tectonic subsidence (m/Myr)			Sedimentation Rate (m/Myr)				
			Onshore		Offshore		Onshore		Offshore	
"Maximal"	Upper Gr.	0–0.8	PW_L14on	–1375	PW_L14off	1214	PW_L14on	< 6	PW_L14off	1479
			PW_L37on	–1280	PW_L37off	1241	PW_L37on	< 6	PW_L37off	1515
	Middle Gr.	0.8–3.0	PW_L14on	574	PW_L14off	444	PW_L14on	530	PW_L14off	299
			PW_L37on	260	PW_L37off	399	PW_L37on	71	PW_L37off	181
	Lower Gr.	3.0–5.3	PW_L14on	256	PW_L14off	313	PW_L14on	286	PW_L14off	379
			PW_L37on	128	PW_L37off	217	PW_L37on	107	PW_L37off	227
"Low"	Upper Gr.	0–0.8	PW_L14on	–1375	PW_L14off	1214	PW_L14on	< 6	PW_L14off	1479
			PW_L37on	–1280	PW_L37off	1241	PW_L37on	< 6	PW_L37off	1515
	Middle Gr.	0.8–2.6	PW_L14on	702	PW_L14off	542	PW_L14on	648	PW_L14off	365
			PW_L37on	318	PW_L37off	488	PW_L37on	87	PW_L37off	413
	Lower Gr.	2.6–4.0	PW_L14on	420	PW_L14off	515	PW_L14on	469	PW_L14off	623
			PW_L37on	210	PW_L37off	357	PW_L37on	176	PW_L37off	126

Results are computed using a back-stripping tool (GENEX). Two age models were used to test extreme scenario, with a "maximal" versus "low" age model. See text for further information

shoulder to the south and to the west (Fig. 16a). Marine evidences are only recognized along the Corinth Isthmus (Fig. 16a). Sedimentation in merging depocenters was characterized by alluvial (west) to fluvio-lacustrine deposits. Transition toward the rift climax is characterized by an unconformity with downlap feature and starved facies in the basin axis (Fig. 11). Turbidite deposits are preserved along the Corinth Isthmus (Corinth Marl formation, Collier and Dart 1991).

Rift Climax ca. 3.0–2.6 Ma

The "rift climax" is commonly defined as the period of time when the rate of fault displacement increases markedly and sedimentation cannot keep pace with subsidence (e.g. Gupta et al. 1998). In that sense, the rift climax identification will clearly be dependent of the sediment supply delivery into the basin. Hereafter, we add to this definition a criterion on the rift width that is supposed to have reached its maximum during the rift climax. Following this definition, the Middle Group recorded the rift climax that corresponds to a major structural reorganization of the rift (Fig. 16b). Proximal depositional systems were organized in aggrading trends with thickest depocenters preserved along the rift shoulders (Fig. 16b). The basin axis was progressively starved and recorded a major increase in bathymetry (Fig. 14). The end of the rift climax is characterized by the switching-off of the major rift shoulder faults and the initiation of basinward migration of the depocenters (ca. 2.6 Ma). Syn-rift deposits include large Gilbert-type deltas to the east [Killini Gilbert-type delta, Sequence 2 of Rohais et al. (2008)] and alluvial fans to the west [D3 of Ford et al. (2013)] (Fig. 11).

Northward Fault Migration ca. 2.6–0.8 Ma

The uppermost part of the Middle Group [ca. Mavro and Evrostini Gilbert-type deltas, Rohais et al. (2008)] was then characterized by a rapid basinward progradation organized in a forced regressive trend (Rohais et al. 2007a). The progradation was combined with a northward migration of the active faults. Listric faults were also documented during this progradation where the Lower Group thickness and lithology were favorable to promote listric faulting, that is in the central and eastern segments (Doutsos and Piper 1990; Rohais et al. 2007a). The sedimentation in the present day gulf area was starved except along some fault controlled topographic feature where large asymmetrical turbiditic levees occurred (Fig. 16b). Four main channel-levee systems can be mapped, one along the Eratini-Galaxidi fault trend potentially related to the Selinous-Kerinitis-Vouraikos-Platanos Gilbert-type fan deltas, another along the Derveni-Lykoporia fault trend related to the Mavro-Evrostini-Ilias Gilbert-type fan deltas, another along the Xylokaastro-Sytas-Kiato fault trend related to the Manna Gilbert-type fan delta and a final one along the Perachora fault trend related to the Nemea Gilbert-type fan delta (Fig. 16b).

Syn-rift 2: Southern Margin Uplift, Basin Axis Rapid Subsidence ca. 0.8–Present Day

The Upper Group then recorded a major change in rift dynamics with an overall uplift of the southern margin and an acceleration of the subsidence in the basin axis where thickest depocenters were preserved (Figs. 14, 15 and 16c).

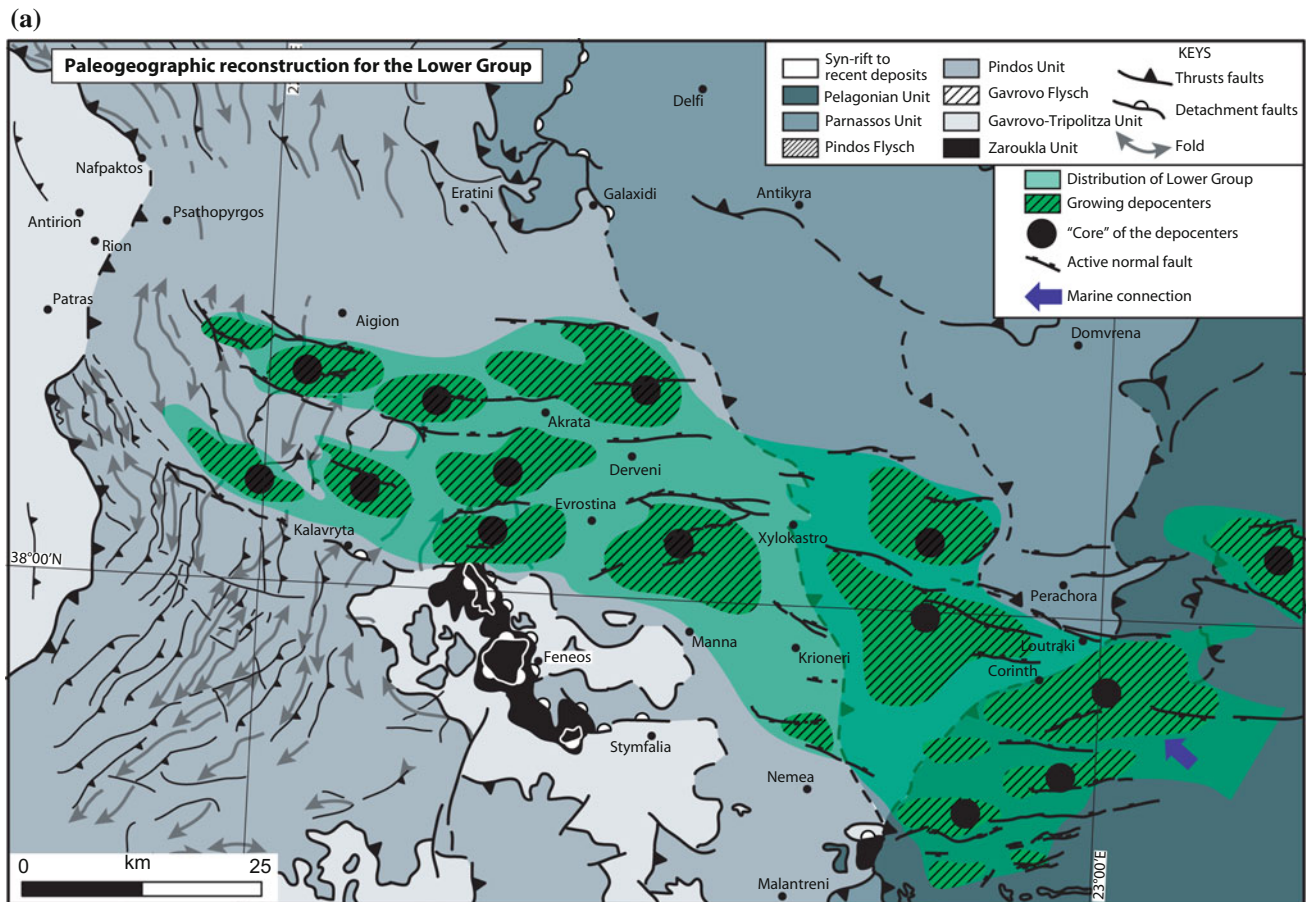


Fig. 16 Paleogeographic reconstructions for the lower (a), middle (b) and upper groups (c) that illustrate the main stages of the Corinth rift evolution. The paleogeographic map for the lower group is

superimposed onto the pre-rift fabrics to highlight the influence of inherited structures on rift initiation. See text for detailed description

Erosion processes did not balance the uplift rate in the vicinity of Feneos and Styμφαλία areas, inducing a major drop in the sediment supply from Derveni to the Corinth Isthmus (Fig. 16c). Uplift rate were in pace with erosion rate on the western part of the rift where large Gilbert-type delta prograded into the gulf (Fig. 16c). Canyon, gullies were developed along the submarine slope and fed an axial turbiditic channel associated with an asymmetrical levees (Figs. 9 and 16c). Along the Derveni-Likoporia fault trend, talus and massive deposits formed the submarine slope (Fig. 16c). In the eastern and easternmost part of the rift (Corinth Isthmus, Xylokastro to Perachora area), sedimentation was primarily characterized by shallow marine carbonate-dominated deposits (Fig. 16c). The Corinth Isthmus was forming a strait with a sill between the Corinth gulf and the Mediterranean Sea (Fig. 16c).

On the westernmost part of the rift (Fig. 16c), the Pleistocene sea level changes interacted with the Rion-Antirion sill inducing highly heterogeneous cycles of marine and lacustrine deposits with major basinward shift along the

northern margin of the gulf (e.g. Perrisoratis et al. 2000; Lykousis et al. 2007; Sakellariou et al. 2007; Fig. 9). A main structural event also occurred around ca. 0.4 Ma with truncation and onlap/downlap features (e.g. Hemelsdaël and Ford 2016) that could be coeval with a main event recognized in the Myrtoon and Saronic basins (Anastasakis and Piper 2005; Anastasakis et al. 2006). This ca. 0.4 Ma event was coeval with the oldest terraces preserved along the Corinth Isthmus ca. 0.4 Ma (e.g. Collier 1990). It indicates that from ca. 0.8 to 0.4 Ma, the southern margin was mainly subaerially exposed (sequence boundary propagation) and was then rapidly flooded by marine deposits at ca. 0.4 Ma.

Discussion

East to West Onshore Correlation

The geological map (Fig. 4) and structural cross sections (Figs. 12 and 13) presented here are an attempt to combine

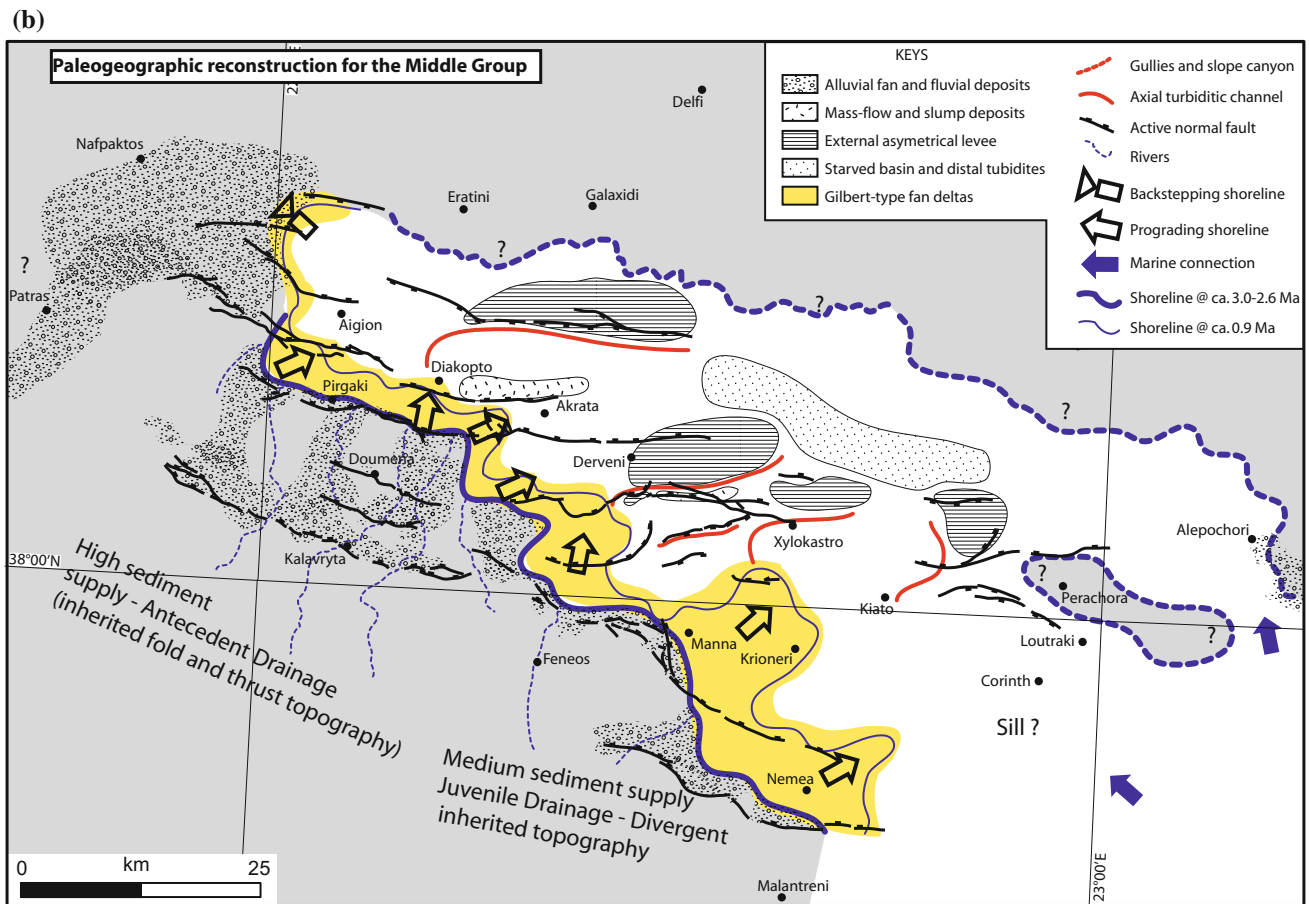


Fig. 16 (continued)

consistently all the absolute dating available in the Corinth rift with the known stratigraphic architecture of the western, central and easternmost part of the rift (and its extension into the Megara basin). We had to adjust two main points to homogenize the nomenclature between the Lower and Middle groups initially defined in the central part of the rift (Rohais et al. 2007a) rift to keep consistency with thickness variation, rift shoulder geometrical relationship and the overall stratigraphic architecture (Fig. 11). The key challenge is the terminology of deposits across the Krathis valley. The D3 unit of Ford et al. (2013) is now considered as Middle Group and the sequence 1 in the Middle Group of Rohais et al. (2008) is now considered as Lower Group. By doing so, part of what has been previously described as Lower Group in the Valimi section (Rohais et al. 2007a, b) is now considered as Middle Group (Fig. 11).

Keeping a Lower Group terminology for all the deposits preserved into the Doumena, Kalavrita, Demestika would imply that this part of the rift could have recorded an additional stage with an overall and rapid uplift dynamic that

do not fit with the stratigraphic architecture recorded in the central part of the rift (Fig. 11). In our reconstruction, the border fault dynamic was consistent from the western (Demestika-Kalavrita faults) to the easternmost part of the rift (Nemea-Athikia faults) with initiation, maximum subsidence, death and abandonment. To explain the occurrence of large alluvial fan on the western part and contemporaneous large Gilbert-type fan deltas in the central to eastern parts, we propose that sediment supply was in pace with accommodation to the west as recorded by aggradational alluvial fan and fluvial systems, while to the east, accommodation was much higher than sediment supply as recorded by a rapid increase in bathymetry and the strong gradient of the giant Gilbert-type fan deltas (Fig. 16b). The lateral variability in sediment supply along the rift shoulder could be related to the relief maturity with to the west a well-organized and mature drainage inherited from the thrusts and fold belts in the Pindos unit, while to the east exhumation along the Feneos window induced divergent juvenile drainage (Fig. 16b).

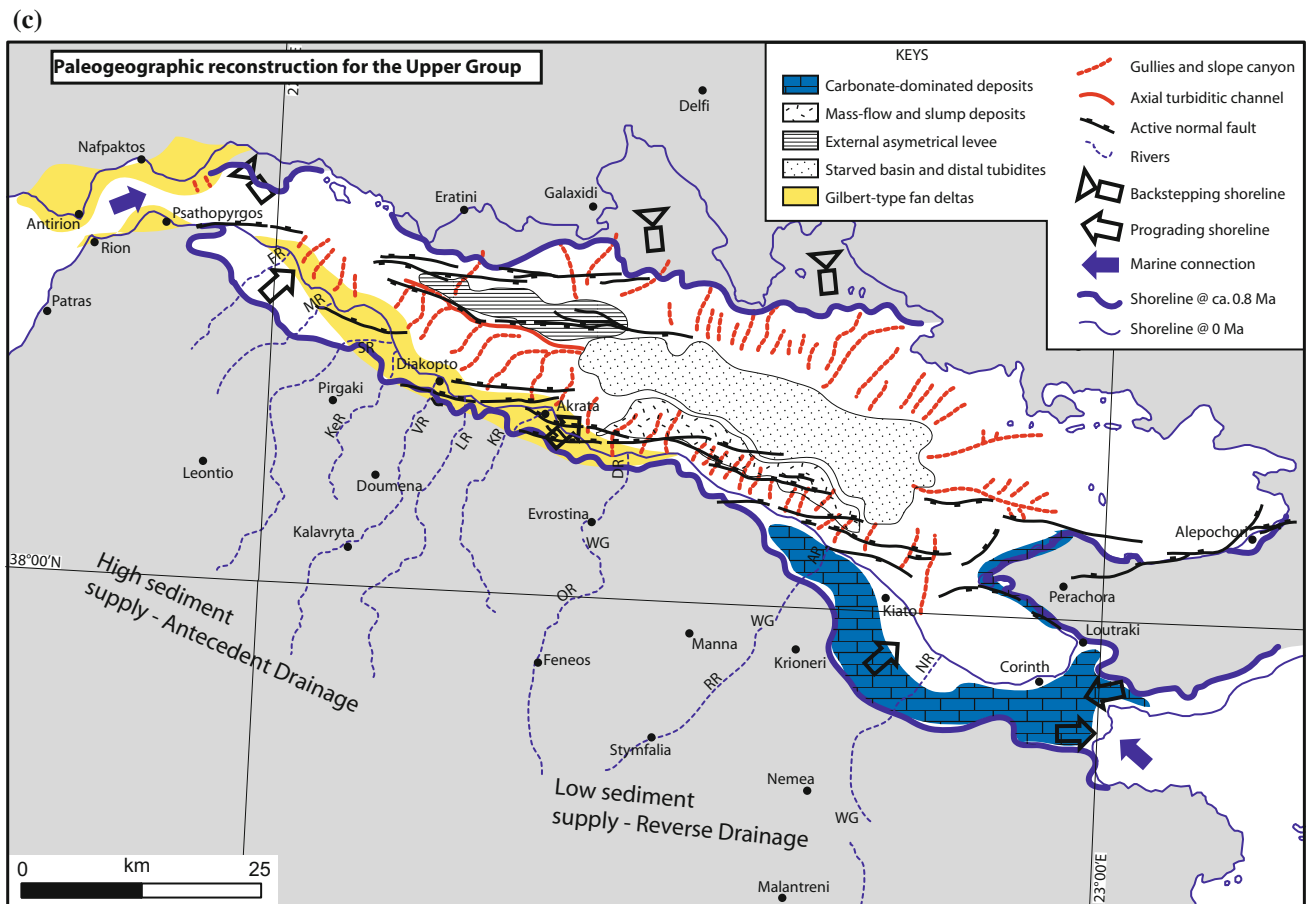


Fig. 16 (continued)

Onshore to Offshore Correlation

The correlation between offshore and onshore deposits from the Upper Group is robust based on numerous previous works and a good consistency in term of age, stratigraphic architecture and rift dynamic (e.g. Bell et al. 2009; Ford et al. 2013; Nixon et al. 2016). Age attribution is nevertheless questionable (Fig. 8). As explained previously we favor the 120 kyr glaciation for the first seismic layered package as Sachpazi et al. (2003), Lykousis et al. (2007) and Taylor et al. (2011) since the correlation with the 13 kyr glaciation lead to inconsistent sedimentation rates with the only hard data of the Marion Dufresne piston core drilled and dated in the Gulf of Corinth (Fig. 8).

The correlation for the Middle Group is less robust than for the Upper Group. The offshore stratigraphic architecture and seismic facies are very consistent with the onshore observations: bottomset, turbidite, channel-levee preserved along the Helike-Akrata, Derveni-Likoporia and Xylokastro footwalls (Figs. 10, 12 and 16). The thickness of the offshore Middle Group and the occurrence of Lower Group preserved

just above are nevertheless questionable. In the westernmost part of the rift, seismic interpretation show that there is no Lower Group preserved (section 1 in Fig. 12) or very small depocenters (section 2 in Fig. 12). In the central and eastern parts of the rift, the seismic packages preserved just below the offshore Middle Group have a different seismic signature (Fig. 7) and are only preserved in isolated depocenters (Figs. 12 and 13). In the Alkyonides and Lechaion gulfs, the geometrical relationship and the absolute dating available onshore imply that the basal portion preserved in small depocenters offshore are effectively correlated with the Lower Group (Figs. 12 and 13). We could even argue that along the present day shoreline, the outcrops of the Lower Group do not suggest any proximal relief nor catchment just few kilometer to the north (Rohais et al. 2007a). Lower Group deposits have to be preserved offshore Akrata and Kiato (Figs. 11 and 16).

Age Model

Geological mapping (Fig. 4), correlation and comparison with surrounding basins provide timelines that are the

“maximal” option (Fig. 11). Every quantification of extension rate, sediment supply or subsidence based on this age model should thus be considered as minimum rates. Without any good age constrains for the very basal part of the Lower Group, it is not clear if the rift has been initiated at 4 or 5.3 Ma. Age of transition from the Lower to Middle Group is also questionable. It occurred in between 2.6–3.6 Ma and we finally propose 3.0 Ma to split the progradation of the Middle Group into three ca. 600–800 kyr sequences. It is the most reasonable assumption used the geometrical relationship between the Mavro Gilbert-type fan delta and the Ash layer of Leeder et al. (2012). The duration of the Lower Group and Middle Group are thus ca. 2.3 and ca. 2.2 Myr respectively. A shorter duration for the Lower Group deposition, as for example a rift initiation at ca. 4 Ma or a transition between the Lower to Middle Group at ca. 3.6 Ma, would have induced inconsistent sedimentation and subsidence rates in the rift history. As the duration of the Middle Group is minimum 1.8 Myr (2.6–0.8 Myr), we could speculate that the rift initiation is at least 4.4 Ma (0.8 + 1.8 + 1.8 Myr). Age of transition from the Middle to Upper Group is also uncertain, as it has not been absolutely dated. Nevertheless, the error bars are much more smaller than for the previous ages. 0.8 Ma \pm 0.1 Myr is actually the best option to fit stratigraphic architecture, offshore seismic interpretation and marine terrace dating as previously discussed (Fig. 11). To test the “maximal” versus “low” age model, we compute the sedimentation rate and tectonic subsidence for these two extreme scenario (Fig. 15). The overall trend are still the same for these two scenario, only the relative factors between the different rates change (Table 2). A well penetrating the offshore distal deposits would provide key data to constrain the age model (e.g. McNeill et al. 2014).

Fault and Rift Dynamics

The depocenter migration and the stratigraphic architecture of the syn-rift fill provide very good field and subsurface evidence for fault growth and linkage processes, and rift propagation (Fig. 16). The main stages of rift evolution can be recognized from rift initiation, rift widening, rift climax (Syn-rift 1), as recorded by the Lower and Middle Groups. Then, the Syn-rift 2 phase was characterized by an asymmetrical basinward fault migration phase and finally a major asymmetrical margin uplift combined with a rapid subsidence in the basin axis (Upper Group). This final phase is uncommon in rift as the two end-member are (1) a rift abandonment recorded by a passive filling with aggradational shallow facies (e.g. Gawthorpe and Leeder 2000; Rohais et al. 2016), or (2) transitional sag phase characterized by

widespread subsidence and an overall tilting of the basin toward the future ocean (e.g. Chaboureaud et al. 2013; Leroy et al. 2012). However, the back-arc evolution could include an abandonment by migration of the spreading zone toward the trench (Clark et al. 2008) and also very often an inversion if the overriding plate switches from extension to compression as it has been documented in the Andes where all the Mesozoic back-arc basins have been inverted during the Tertiary (Colletta et al. 1990). If the back-arc area remains in extension, multiple extension stages are commons (Clark et al. 2008) and could result in a classical rift with several stacked syn-rift packages. An analogous stacking of several syn-rift packages is also observed along the Brazilian and African margins (e.g. Karner and Driscoll 1999; Rangel and Carminatti 2000; Lohr and Underhill 2015; Gianni et al. 2015) and is commonly interpreted as the results of major plate tectonic or boundary condition re-adjustments (e.g. Nürnberg and Müller 1991; Pángaro and Ramos 2012). In the case of the Hellenic subduction, change may come from the subducting plate or from the overriding plate velocity. On the subducting plate, at the level of the Peloponnese the heterogeneities of the subducting lithosphere covered by sediments are poorly known but westward, the main recent feature is the arrival of the Eratosthenes seamount near the trench. Effectively, Schattner (2010) proposed that the progressive closure of the entire eastern Mediterranean basin across the Cyprus, Hellenic and Calabria arcs was temporarily interrupted by the incipient Seamount (Eratosthenes) during the early- to mid-Pleistocene (ca. 1 Ma). It has induced a subduction dynamic change with structural modifications across the entire region and accentuated regional topography (Schattner 2010). This boundary condition change could thus be inferred as one of the controlling mechanisms for the most recent syn-rift package in the Corinth rift (Syn-rift 2). This is an alternative, and/or additional explanation for the strain localization across the Corinth rift primary due to the overriding plate velocity (spatial acceleration of overriding Peloponnese with respect to central Greece) that has been previously envisaged (Armijo et al. 1996 and many others) and the resulting fore-arc “pushback” and flat slab (Leeder et al. 2003, 2008).

Inherited Structure and Geodynamic

The Hellenic subduction has been active since the Eocene and extension started in the Aegean region from 30 to 35 Ma as recorded by the formation of the large Cycladic metamorphic core complexes and extensional collapse features (Lister et al. 1984; Gautier and Brun 1994; Jolivet et al. 1994; Jolivet and Faccenna 2000; Kiliyas et al. 2002). Shortening was contemporary with extension; the nappe

stacking and related turbiditic deposits preserved in the pre-rift basement indicate that the Corinth rift area was firstly a subaqueous accretionary prism from Late Eocene (45–40 Ma) to Middle Miocene. Then a rapid and widely distributed uplift event of the entire Corinth rift area occurred during Middle to Late Miocene, locally associated with detachment structures (e.g. Papanikolaou et al. 2009). At approximately 5.3 Ma, Aegean extension was then localized in series of grabens such as the Corinth rift, an event commonly attributed to the propagation of the North Anatolian Fault (McKenzie 1978; Jackson 1994; Armijo et al. 1996). A major debate is thus focused on either the Gulf of Corinth being a precursor of a future metamorphic core complex similar to those of the Cyclades or the Aegean region (Chéry 2001; Jolivet 2001; Jolivet et al. 2010a) or not (Bell et al. 2009, 2011; Ford et al. 2013).

The geometrical relationships between the rift structural pattern and pre-rift detachments are not obvious on the outcrops neither on the seismic. On the western part of the Corinth rift, block sizes, sedimentary fill and thicknesses are different from the eastern part (Figs. 12, 13 and 16), and the Moho geometry does not suggest any significant crustal thinning. The seismogenic zone recorded at depth in the western part is compatible with the brittle-ductile at the base of the Ionian/Pre-Apulian units (Figs. 1 and 3; King et al. 1985; Rigo et al. 1996). Thus, the three identified shallow detachment features do not seem to be directly related to the rift extension. In that sense, the Gulf of Corinth should better be seen as the northern termination of an aborted core complex rather than a precursor. Nevertheless, as proposed by Jolivet et al. (2010a) if rift faults are only transient features one may expect a future period of exhumation by one of the detachments or their future equivalents.

Conclusion

The present paper proposes a synthesis and update of the timing and dynamic of the Corinth rift based on field mapping, onshore to offshore stratigraphic correlation at basin scale. As presented, the proposed scenario supposed that the Lower, Middle and Upper Groups outcropping along the southern onshore margin have their equivalent offshore. Having a well offshore would definitively be a significant insight for upgrading our interpretation. The main results can be summarized as follow:

We showed that the rift initially propagated from east to west with fault growth and linkage processes. Inherited structures deeply influenced the rift dynamic from its initiation to the present day configuration, by both modulating sediment supply dynamic and structural architecture. The Corinth rift recorded a Syn-rift 1 with the common rift initiation, widening, climax phases and “late” rift stage

characterized by a basinward migration of the active faults. Syn-rift 1 correspond to the Lower and Middle Groups. A second syn-rift packages can be identified in the sedimentary basin fill with a rift narrowing and still an east to west rift propagation (Upper Group, Syn-rift 2). The stacking of two successive syn-rift packages suggest that the Corinth rift has recorded major changes in terms of boundary conditions and deformation was progressively focused. Its initiation at around 5.3 Ma and its strong reorganization at around 0.8 Ma were potentially linked to major geodynamic changes in the Aegean domain. As previously discussed, the North Anatolian Fault (NAF) propagation lead to an increase of the South-Southwest absolute Anatolian plate motion, while the slab retreat is slow (and maybe slowed by the Eratosthenes seamount), these major changes lead to the Peloponnese uplift and to the narrowing of the Gulf at ca. 0.8 Ma. By comparison to other back-arc area (see Heuret and Lallemand 2005 for a comprehensive review) one may infer that all conditions are present for a switch from an extensional phase to a compressional one. Indeed, the Gulf of Corinth is the most active seismic zone of the European Union and extension measured by GPS is still active (up to 1.5 mm/year) but in the Gulf of Saronic (Chousianitis et al. 2015) shortening is now recorded parallel to the subduction direction. The future of the area is maybe not a core complex or even neither a subsiding extensional basin.

Acknowledgments This work was funded by IFP Energies Nouvelles in the frame of the Numerical and Geological Modeling project. Brian Taylor, Laurent Jolivet and François Roure provided suitable comments on an earlier version of this paper that led to improve the manuscript. We thank Lisa Mc Neill and Dimitris Sakellariou for helpful discussions. We are very grateful to April Lloyd for post-editing the English style and grammar. We also thank the IGME, Athens, for permissions to do fieldwork for the last 12 years in the Gulf of Corinth. Finally, we thank two anonymous reviewers for helpful constructive comments and corrections of an earlier version.

References

- Anastasakis G, Piper DJW (2005) Late neogene evolution of the western South Aegean volcanic arc: sedimentary imprint of volcanicity around Milos. *Mar Geol* 215(2005):135–158
- Anastasakis G, Piper DJW, Dermitzakis MD, Karakitsios V (2006) Upper cenozoic stratigraphy and paleogeographic evolution of Myrtoon and adjacent basins, Aegean Sea, Greece. *Mar Pet Geol* 23:353–369
- Armijo R, Meyer B, King GCP, Rigo A, Papanastassiou M (1996) Quaternary evolution of the Corinth rift and its implications for the late Cenozoic evolution of the Aegean. *Geophys J Int* 126:11–53
- Armijo R, Meyer B, Hubert A, Barka A (1999) Westward propagation of the North Anatolian fault into the northern Aegean; timing and kinematics. *Geology* 27(3):267–270
- Aronis G, Panayotides GR, Monopolis D, Morikis AN, Zachos K (1964) Geological map of Greece, Delfi Sheet, scale 1:50 000. Institute of Geology and Mineral Exploration, Athens

- Aubouin J (1959) Contribution à l'étude géologique de la Grèce septentrionale: les confins de l'Épire et de la Thessalie. (These, Paris, 1958). Ann Geol Pays Hell, Ire série, vol X, 483 p
- Aubouin J, Brunn JH, Celet P, Dercourt J, Godfriaux I, Mercier J (1963) Esquisse de la Géologie de la Grèce, Fallot memorial volume, Societe Geologique de France, pp 583–610
- Avallone A, Briole P, Agatza-Balodimou AM, Billiris H, Charade O, Mitsakaki C, Nercessian A, Papazissi K, Paradissis D, Veis G (2004) Analysis of eleven years of deformation measured by GPS in the Corinth rift laboratory area. *Comptes Rendus Geosci* 336(4–5):301–311. doi:10.1016/j.crte.2003.12.007
- Beckers A, Hubert-Ferrari A, Beck C, Bodeux S, Tripsanas E, Sakellariou D, De Batist M (2015) Active faulting at the western tip of the Gulf of Corinth, Greece, from high-resolution seismic data. *Mar Geol* 360:55–69. doi:10.1016/j.margeo.2014.12.003
- Bell RE, McNeill LC, Bull JM, Henstock TJ (2008) Evolution of the offshore western Gulf of Corinth. *Geol Soc Am Bull* 120:156–178
- Bell RE, McNeill LC, Bull JM, Henstock TJ, Collier REL, Leeder MR (2009) Fault architecture, basin structure and evolution of the Gulf of Corinth rift, central Greece. *Basin Res* 21:824–855. doi:10.1111/j.1365-2117.2009.00401.x
- Bell RE, McNeill LC, Henstock TJ, Bull JM (2011) Comparing extension on multiple time and depth scales in the Corinth rift Central Greece. *Geophys J Int* 186:463–470
- Benedicto A, Plagnes V, Vergély P, Flotté N, Schultz RA (2008) Fault and fluid interaction in a rifted margin: integrated study of calcite-sealed fault-related structures (Southern Corinth margin). In: Wibberley CAJ, Kurz W, Imber J, Holdsworth RE, Collettini C (eds) The internal structure of fault zones: implications for mechanical and fluid-flow properties, vol 299. Geological Society, London, pp 257–275 (Special Publications)
- Bentham P, Collier REL, Gawthorpe RL, Leeder MR, Prossers S, Stark C (1991) Tectono-sedimentary development of an extensional basin: the Neogene Megara Basin, Greece. *J Geol Soc Lond* 148:923–934
- Bernard P, Briole P, Meyer B, Lyon-Caen H, Gomez JM, Tiberi C, Berge C, Cattin R, Hatzfeld D, Lachet C, Lebrun B, Deschamps A, Courboulex F, Larroque C, Rigo A, Massonnet D, Papadimitriou P, Kassaras J, Diagourtas D, Makropoulos K (1997) The Ms = 6.2, June 15, 1995 Aigion earthquake (Greece): evidence for low angle normal faulting in the Corinth rift. *J Seismol* 1:131–150
- Bernard P et al (2006) Seismicity, deformation and seismic hazard in the western rift of Corinth: new insights from the Corinth rift laboratory (CRL). *Tectonophysics* 426:7–30
- Briole P, Rigo A, Lyon-Caen H, Ruegg JC, Papazissi K, Mitsakaki C, Balodimou A, Veis G, Hatzfeld D, Deschamps A (2000) Active deformation of the Corinth Rift, Greece: results from repeated global positioning system surveys between 1990 and 1995. *J Geophys Res* 105:605–625
- Brooks M, Ferentinos G (1984) Tectonics and sedimentation in the Gulf of Corinth and the Zakynthos and Kefallinia channels, western Greece. *Tectonophysics* 101:25–54
- Causse C, Moretti I, Ghisetti F, Eschard R, Micarelli L, Ghaleb B, Frank N (2004) Kinematics of the Corinth Gulf inferred from calcite dating and syntectonic sedimentary characteristics. *C R Geosci* 336:281–290
- Chaboureaud AC, Guillocheau F, Robin C, Rohais S, Moulin M, Aslanian D (2013) Paleogeographic evolution of the central segment of the South Atlantic during early cretaceous times: paleotopographic and geodynamic implications. *Tectonophysics* 604:191–223
- Charalampakis M, Lykousis V, Sakellariou D, Papatheodorou G, Ferentinos G (2014) The tectono-sedimentary evolution of the Lechaion Gulf, the south eastern branch of the Corinth graben, Greece. *Mar Geol* 351:58–75. doi:10.1016/j.margeo.2014.03.014
- Chéry J (2001) Core complex mechanics: from the gulf of Corinth to the Snake Range. *Geology* 29(5):439–442
- Chouliaras G, Kassaras I, Kapetanidis V, Petrou P, Drakatos G (2015) Seismotectonic analysis of the 2013 seismic sequence at the western Corinth rift. *J Geodynam* 90:42–57. doi:10.1016/j.jog.2015.07.001
- Clark SR, Stegman D, Müller RD (2008) Episodicity in back-arc tectonic regimes. *Phys Earth Planet Inter* 171:265–279. doi:10.1016/j.pepi.2008.04.01
- Clement C, Sachpazi M, Charvis P, Graindorge D, Laigle M, Hirn A, Zafropoulos G (2004) Reflection-refraction seismics in the Gulf of Corinth: hints at deep structure and control of the deep marine basin. *Tectonophysics* 391:85–95
- Colletta B, LeQuellec P, Letouzey J, Moretti I (1988) Longitudinal evolution of the Suez rift structure (Egypt). *Tectonophysics* 153:221–233
- Colletta B, Hebrard F, Letouzey J, Werner P, Rudkiewicz JL (1990) Tectonic style and crustal structure of the Eastern Cordillera (Colombia) from a balanced cross-section. In: Letouzey J (ed) Petroleum and tectonics in mobile belts. Editions Technip, Paris, pp 81–100
- Collier REL (1988) Sedimentary facies evolution in continental fault-bounded basins formed by crustal extension: the Corinth Basin, Greece. PhD thesis, University of Leeds
- Collier REL (1990) Eustatic and tectonic controls upon quaternary coastal sedimentation in the Corinth Basin, Greece. *J Geol Soc* 147:301–314
- Collier REL, Dart CJ (1991) Neogene to quaternary rifting, sedimentation and uplift in the Corinth. *J Geol Soc Lond* 148:1049–1065
- Collier REL, Leeder M, Trout M, Ferentinos G, Lyberis E, Papatheodorou G (2000) High sedimentation yields and cool wet winters: test of last glacial paleoclimates in the northern Mediterranean. *Geology* 28:999–1002
- Console R, Carluccio R, Papadimitriou E, Karakostas V (2015) Synthetic earthquake catalogs simulating seismic activity in the Corinth Gulf, Greece, fault system, *J Geophys Res Solid Earth*, vol 120, doi:10.1002/2014JB011765
- Danatsas I (1989) Die känozoischen Ostrakoden des NW- und N-Peloponnes und ihre stratigraphische, paläoökologische und paläogeographische Bedeutung. Inaug. Diss. Münster, 171
- Danatsas I (1994) Zur Entwicklung der miozänen-altpleistozänen Ostrakoden-Fauna des Korinthis-Beckens, Griechenland. *Münster. Forsch Geol Paläont* 76:191–200
- Dart CJ, Collier REL, Gawthorpe RL, Keller JVA, Nichols G (1994) Sequence stratigraphy of (?) Pliocene-quaternary synrift, Gilbert-type fan deltas, northern Peloponnesos, Greece. *Mar Petrol Geol* 11:545–560
- Demoulin A, Beckers A, Hubert-Ferrari A (2015) Patterns of quaternary uplift of the Corinth rift southern border (N. Peloponnes, Greece) revealed by fluvial landscape morphometry. *Geomorphology* 246:188–204
- Dercourt J (1964) Contribution à l'étude géologique du secteur du Péloponnèse septentrional. PhD thesis, University of Paris, pp 1–418
- Dercourt J, De Wever P, Fleury J (1976) Données sur le style tectonique de la nappe de Tripolitza en Peloponnes septentrional (Grèce). *Bull Soc Geol Fr* 7(28):317–326
- Desperet C (1913) Observations sur l'histoire géologique pliocène et quaternaire du golfe et de l'isthme de Corinthe. CR hebdomadaire des séances de l'Académie des Sciences 156
- Dewey JF, Sengör AMC (1979) Aegean and surrounding regions: complex multiplate and continuum tectonics in a convergent zone. *Geol Soc Am Bull* 90:84–92
- Doutsos T, Piper G, Boronkay K, Koukouvelas I (1993) Kinematics of the central Hellenides. *Tectonics* 12:936–953
- Doutsos T, Piper DJW (1990) Listric faulting, sedimentation, and morphological evolution of the quaternary eastern Corinth rift,

- Greece: first stages of continental rifting. *Geol Soc Am Bull* 102:812–829
- Doutsos T, Kontopoulos N, Poulimenos G (1988) The Corinth-Patras rift as the initial stage of the continental fragmentation behind an active island arc [Greece]. *Basin Res* 1:177–190
- Doutsos T, Koukouvelas I, Poulimenos G, Kokkalas S, Xypolias P, Skourlis K (2000) An exhumation model of the south Peloponnesus, Greece. *Int J Earth Sci* 89:350–365. doi:10.1007/s005310000087
- Dufaure JJ (1975) Le relief du Péloponnèse. PhD thesis, Université Paris IV, France, p 1422
- Dufaure JJ, Bousquet B, Péchoux PY (1979) Contribution de la géomorphologie à la connaissance du Quaternaire continental grec, en relation avec la néotectonique. *Rev Géol Dynam Géog Phys* 21:29–40
- Exadaktylos GE, Vardoulakis I, Stavropoulou MC, Tsombos P (2003) Analogue and numerical modeling of normal fault patterns produced due to slip along a detachment zone. *Tectonophysics* 376:117–134
- Flerit F, Armijo R, King G, Meyer B (2004) The mechanical interaction between the propagating North Anatolian Fault and the back-arc extension in the Aegean. *Earth Planet Sci Lett* 224:347–362
- Flotté N, Sorel D, Müller C, Tensi J (2005) Along strike changes in the structural evolution over a brittle detachment fault, example of the Pleistocene Corinth-Patras rift (Greece). *Tectonophysics* 403 (2005):77–94
- Ford M, Williams EA, Malartre F, Popescu SM (2007) Stratigraphic architecture, sedimentology and structure of the Vouraikos Gilbert-type delta, Gulf of Corinth, Greece. In: Nichols GJ, Williams EA, Paola C (eds) *Sedimentary processes, environments and basins: a tribute to Peter Friend*, vol 38, pp 49–90 (Spec Publ Int Assoc Sedimentol)
- Ford M, Rohais S, Williams EA, Bourlange S, Jousset D, Backert N, Malartre F (2013) Tectono-sedimentary evolution of the western Corinth rift (Central Greece). *Basin Res* 25:3–25. doi:10.1111/j.1365-2117.2012.00550.x
- Fytikas M, Innocenti F, Manetti P, Mazzuoli R, Peccerilo A, Villari L (1984) Tertiary to quaternary evolution of volcanism in the Aegean region. *Geol Soc London Spec Publ* 17:687–699
- Gautier P, Brun JP (1994) Ductile crust exhumation and extensional detachments in the central Aegean (Cyclades and Evvia islands). *Geodin Acta* 7(2):57–85
- Gautier P, Brun JP, Moriceau R, Sokoutis D, Martinod J, Jolivet L (1999) Timing kinematics and cause of the Aegean extension: a scenario based on a comparison with simple analogue experiments. *Tectonophysics* 315:31–72
- Gawthorpe RL, Leeder MR (2000) Tectono-sedimentary evolution of active extensional basins. *Basin Res* 12(3–4):195–218
- Gawthorpe RL, Fraser AJ, Collier RELL (1994) Sequence stratigraphy in active extensional basins: implication for the interpretation of ancient basin-fills. *Mar Petrol Geol* 11(6):642–658
- Ghisetti F, Vezzani L (2004) Fault segmentation in the Gulf of Corinth (Greece) constrained by patterns of Pleistocene sedimentation. *Comptes Rendus Geosci* 336:243–249
- Ghisetti F, Vezzani L (2005) Inherited structural controls on normal fault architecture in the Gulf of Corinth (Greece). *Tectonics*, vol 24 doi:10.1029/2004TC001696
- Ghisetti F, Barchi M, Bally AW, Moretti I, Vezzani L (1993) Conflicting balanced structural section across the Central Apennines (Italy): problems and implications. In: Spencer AM (ed) *Generation, accumulation and production of Europe's hydrocarbons III*, vol 3. European Association of Petroleum Geoscience, Special Publication, pp 219–231
- Gianni G, Navarrete C, Orts D, Tobal J, Folguera A, Giménez M (2015) Patagonian broken foreland and related synorogenic rifting: the origin of the Chubut Group Basin. *Tectonophysics*. doi:10.1016/j.tecto.2015.03.006
- Goldsworthy M, Jackson J (2001) Migration of activity within normal fault systems: examples from the quaternary of mainland Greece. *J Struct Geol* 23:489–506
- Goldsworthy M, Jackson J, Haines J (2002) The continuity of active fault systems in Greece. *Geophys J Int* 148:596–618. doi:10.1046/j.1365-246X.2002.01609.x
- Goodliffe A, Taylor B (2014) Raw multi-channel seismic shot data from the Gulf of Corinth acquired during R/V Maurice Ewing expedition EW0108 (2001). *Integr Earth Data Appl (IEDA)*. doi:10.1594/IEDA/306914
- Gupta S, Cowie PA, Dawers NH, Underhill JR (1998) A mechanism to explain rift basin subsidence and stratigraphic patterns through fault array evolution. *Geology* 26:595–598
- Hadler H, Vött A, Koster B, Mathes-Schmidt M, Mattern T, Ntageretis K, Reicherter K, Sakellariou D, Willershäuser T (2011) Lechaion, the ancient harbour of Corinth (Peloponnese, Greece) destroyed by tsunamigenic impact. In: Grützner C, Pérez-López R, Fernández Steeger T, Papanikolaou I, Reicherter K, Silva PG, Vött A (eds) *Earthquake Geology and archaeology: science, society and critical facilities*. proceedings of the 2nd INQUA-IGCP-567 international workshop on active tectonics, earthquake geology, archaeology and engineering, Sept 19–24 2011, Corinth (Greece), ISBN: 978-960-466-093-3, 70–73
- Hadler H, Kissas K, Koster B, Mathes-Schmidt M, Mattern T, Ntageretis K, Reicherter K, Willershäuser T, Vött A (2013) Multiple late-Holocene tsunami landfall in the eastern Gulf of Corinth recorded in the palaeotsunami geo-archive at Lechaion, harbour of ancient Corinth (Peloponnese, Greece). *Z Geomorph* 57 (4):1–42 NF Suppl
- Hemelsdaël R, Ford M (2016) Relay zone evolution: a history of repeated fault propagation and linkage, central Corinth rift. *Basin Res*, Greece. doi:10.1111/bre.12101
- Heuret A, Lallemand S (2005) Plate motions, slab dynamics and back-arc extension. *Phys Earth Planet Inter* 149:31–51
- Higgs B (1988) Syn-sedimentary structural controls on basin deformation in the Gulf of Corinth, Greece. *Basin Res* 1:155–165
- Horvath F, Berckhemer H (1982) Mediterranean back-arc basins. In: Berckhemer H, Hsü KJ (eds) *Alpine-Mediterranean geodynamics*. *Geodynam Res* 7:609–620
- I.G.R.S.-I.F.P. (1966) *Etude Géologique de l'Épire (Grèce Nord-occidentale)*. Technip. Paris, p. 306, pl. 9
- Jackson J (1994) Active tectonics of the Aegean region. *Annu Rev Earth Planet Sci* 22:239–271
- Jacobshagen V, Durr S, Kockel F, Kopp KO, Kowalczyk G, Berckhemer H, Buttner D (1978) Structure and geodynamic evolution of the Aegean region. In: Closs H, Roeder D, Schmidt KE (eds) *Alpes, Apennines, Hellenides*. Verlagsbuchhandlung, Stuttgart, Schweizerbart'sche, pp 537–564
- Jolivet L (2001) A comparison of geodetic and finite strain pattern in the Aegean, geodynamic implications. *Earth Planet Sci Lett* 187:95–104
- Jolivet L, Faccenna C (2000) Mediterranean extension and the Africa–Eurasia collision. *Tectonics* 19(6):1095–1106
- Jolivet L, Brun JP, Gautier P, Lallemeant S, Patriat M (1994) 3D kinematics of extension in the Aegean region from the early Miocene to the present, insights from the ductile crust. *Bull Soc Geol Fr* 165(3):195–209
- Jolivet L, Brun JP (2010) Cenozoic geodynamic evolution of the Aegean region. *Int J Earth Science* 99:109–138. doi:10.1007/s00531-008-0366-4
- Jolivet L, Labrousse L, Agard P, Lacombe O, Bailly V, Lecomte E, Mouthereau F, Mehl C (2010a) Corinth rifting and shallow-dipping

- detachments, clues from the Corinth rift and the Aegean. *Tectonophysics* 483:287–304. doi:[10.1016/j.tecto.2009.11.001](https://doi.org/10.1016/j.tecto.2009.11.001)
- Jolivet L, Trotet F, Monié P, Vidal O, Goffé B, Labrousse L, Agard P, Ghorbal B (2010b) Along-strike variations of P-T conditions in accretionary wedges and synorogenic extension, the HP-LT phyllite-quartzite nappe in crete and the Peloponnese. *Tectonophysics* 480:133–148. doi:[10.1016/j.tecto.2009.10.002](https://doi.org/10.1016/j.tecto.2009.10.002)
- Jolivet L, Menant A, Sternai P, Rabillard A, Arbaret L, et al (2015) The geological signature of a slab tear below the Aegean. *Tectonophysics* 659:166–182. doi:[10.1016/j.tecto.2015.08.004](https://doi.org/10.1016/j.tecto.2015.08.004)
- Kamberis E, Pavlopoulos A, Tsaila-Monopolis S, Sotiropoulos S, Ioakim C (2005) Paleogene deep-water sedimentation and paleogeography of foreland basins in the NW Peloponnese (Greece). *Geol Carpath* 56:503–515
- Kapetanidis V, Deschamps A, Papadimitriou P, Matrullo E, Karakonstantis A, Bozionelos G, Kaviris G, Serpetsidaki A, Lyon-Caen H, Voulgaris N, Bernard P, Sokos E, Makropoulos K (2015) The 2013 earthquake swarm in Helike, Greece: seismic activity at the root of old normal faults. *Geophys J Int* 202:2044–2073
- Karakitsios V (2013) Western Greece and Ionian Sea petroleum systems. *AAPG Bull* 97(9):1567–1595
- Karakitsios V, Rigakis N (2007) Evolution and petroleum potential of western Greece. *J Petrol Geol* 30(3):197–218. doi:[10.1111/j.1747-5457.2007.00197.x](https://doi.org/10.1111/j.1747-5457.2007.00197.x)
- Karner GD, Driscoll NW (1999) Tectonic and stratigraphic development of the West African and eastern Brazilian Margins: insights from quantitative basin modelling. In: Cameron NR, Bate RH, Clure VS (eds) *The oil and gas habitats of the South Atlantic*. *Geol Soc Lond* 153:11–40 (Spec Publ)
- Keraudren B (1970) *Les formations quaternaires marines de la Grèce*. PhD thesis, *Bull Mus Anthropol Préhist Monaco* 16:5–153
- Keraudren B (1971) *Les formations quaternaires marines de la Grèce*. PhD thesis, *Bull Mus Anthropol Préhist Monaco* 17:87–169
- Keraudren B (1972) *Les formations quaternaires marines de la Grèce*. PhD thesis, *Bull Mus Anthropol Préhist Monaco* 18:223–270
- Keraudren B, Sorel D (1987) The terraces of Corinth (Greece): a detailed record of eustatic sea level variations during the last 500 000 years. *Mar Geol* 77(1–2):99–107
- Kershaw S, Guo L (2003) Pleistocene cyanobacterial mounds in the Perachora Peninsula, Gulf of Corinth, Greece: structure and applications to interpreting sea-level history and terrace sequences in an unstable tectonic setting. *Palaeogeogr Palaeoclimatol Palaeoecol* 193:503–514
- Kershaw S, Guo L, Braga JC (2005) A Holocene coral-algal reef at Mavra Litharia, Gulf of Corinth, Greece: structure, history and applications in relative sea-level change. *Mar Geol* 215:171–192
- Kiliadis AA, Tranos MD, Orozco M, Alonso-Chaves FM, Soto GI (2002) Extensional collapse of the Hellenides: a review. *Revista de la Sociedad Geológica de España* 15(3–4):129–139
- King GCP, Ouyang ZX, Papadimitriou P, Deschamps A, Gagnepain J, Houseman G, Jackson JA, Soufleris C, Virieux J (1985) The evolution of the Gulf of Corinth (Greece): an aftershock study of the 1981 earthquakes. *Geophys J R Astr Soc* 80:677–683
- Kokkalas S, Xypolias P, Koukouvelas I, Doutsos T (2006) Postcollisional contractional and extensional deformation in the Aegean region. *Spe Pap Geol Soc Am* 409:97–123
- Kontopoulos N, Doutsos T (1985) Sedimentology and tectonics of the Antirion area (Western Greece). *Bull Geol Soc Ital* 104:479–489
- Koutsouveli A, Mettos A, Tsapralis V, Tsaila-Monopolis ST, Ioakim CH, Mavrides A (1989) Geological map of Greece, Xylokastro sheet Scale 1:50 000. Institute of Geology and Mineral Exploration, Athens
- Krijgsman W, Hilgen FJ, Raffi I, Sierro FJ, Wilson DS (1999) Chronology, causes and progression of the Messinian salinity crisis. *Nature* 400:625–655
- Kydonakis K, Brun JP, Sokoutis D (2015) North Aegean core complexes, the gravity spreading of a thrust wedge. *J Geophys Res Am Geophys Union* 120(1):595–616. doi:[10.1002/2014JB011601](https://doi.org/10.1002/2014JB011601)
- Le Pichon X, Angelier J (1979) The Hellenic arc and trench system: a key to the neotectonic evolution of the eastern Mediterranean area. *Tectonophysics* 60:1–42
- Le Pourhiet L, Burov E, Moretti I (2003) Initial crustal thickness geometry controls on the extension in a back arc domain: case of the Gulf of Corinth. *Tectonics*, vol 22(4). doi:[10.1029/2002TC001433](https://doi.org/10.1029/2002TC001433)
- Le Pourhiet L, Burov E, Moretti I (2004) Rifting through a stack of inhomogeneous thrusts (the dipping pie concept). *Tectonics*, vol 23 (TC4005). doi:[10.1029/2003TC001584](https://doi.org/10.1029/2003TC001584)
- Leeder MR, Mack GH (2007) Basin-fill incision, Rio Grande and Gulf of Corinth rifts: convergent response to climatic and tectonic drivers. In: Nichols G, Williams E, Paola C (eds) *Sedimentary processes, environments and basins*. Blackwell Publishing, Malden, pp 9–28
- Leeder MR, McNeill LC, Collier REL, Portman C, Rowe PJ, Andrews JE (2003) Corinth rift margin uplift: new evidence from late quaternary marine shorelines. *Geophys Res Lett* 30(12):13–14
- Leeder MR, Mack GH, Brasier AT, Parrish RR, McIntosh WC, Andrews JE, Duermeijer CE (2008) Late-Pliocene timing of Corinth (Greece) rift-margin fault migration. *Earth Planet Sci Lett* 274:132–141. doi:[10.1016/j.epsl.2008.07.006](https://doi.org/10.1016/j.epsl.2008.07.006)
- Leeder MR, Mark DF, Gawthorpe RL, Kranis H, Loveless S, Pedentchouk N, Skourtsos E, Turner J, Andrews JE, Stamatakis M (2012) A ‘great deepening’: chronology of rift climax, Corinth rift, Greece. *Geology* 40:999–1002
- Leroy S, Razin P, Autin J, Bache F, d’Acremont E, Watremez L, Robinet J, Baurion C, Denèle Y, Bellahsen N, Lucazeau F, Rolandone F, Rouzo S, Serra Kiel J, Robin C et al. (2012) From rifting to oceanic spreading in the Gulf of Aden: a synthesis. *Arab J Geosci* 5:859–901. doi:[10.1007/s12517-011-0475-4](https://doi.org/10.1007/s12517-011-0475-4)
- Lister GS, Banga G, Feenstra A (1984) Metamorphic core complexes of cordilleran type in the Cyclades, Aegean Sea. *Greece Geol* 12:221–225
- Loftus L, Tsoflias P, Yannetakis CP (1971) Geological map of Greece, Nafaktos sheet, scale 1:50 000. Institute of Geology and Mineral Exploration, Athens
- Lohr T, Underhill JR (2015) Role of rift transection and punctuated subsidence in the development of the North Falkland Basin. *Petrol Geosci* 21:85–110. doi:[10.1144/petgeo2014-050](https://doi.org/10.1144/petgeo2014-050)
- Lykousis V, Sakellariou D, Papanikolaou D (1998) Sequence stratigraphy in the northern margin of the Gulf of Corinth: implications to upper quaternary basin evolution. *Bull Geol Soc Greece* 32:157–164
- Lykousis V, Sakellariou D, Moretti I, Kaberi H (2007) Late quaternary basin evolution of the Gulf of Corinth: sequence stratigraphy, sedimentation, fault-slip and subsidence rates. *Tectonophysics* 440:29–51
- Lyon-caen H, Papadimitriou P, Deschamps A, Bernard P, Makropoulos K, Pacchiani F, Patau G (2004) First results of the CRLN seismic network in the western Corinth Rift: evidence for old-fault reactivation. *CRG* 336:343–351. doi:[10.1016/j.crte.2003.12.004](https://doi.org/10.1016/j.crte.2003.12.004)
- Maroukian H, Gaki-Papanastassiou K, Karymbalis E, Vouvalidis K, Pavlopoulos K, Papanastassiou D, Albanakis K (2008) Morphotectonic control on drainage network evolution in the Perachora Peninsula, Greece. *Geomorphology* 102:81–92

- Martinod J, Husson L, Roperch P, Guillaume B, Espurt N (2010) Horizontal subduction zones, convergence velocity and building of the Andes. *EPSL* 299:299–309
- Mattioni L, Le Pourhiet L, Moretti I (2006) Extension through a heterogeneous crust: new insight from analogue modelling. *J Geol Soc Lond*, Special publication n° 253:213–231
- McKenzie D (1978) Active tectonics of the Alpine-Himalayan belt: the Aegean Sea and surrounding regions. *Geophys J R Astr Soc* 55:217–254
- McNeill LC, Collier REL (2004) Uplift and slip rates of the Eastern Eliki fault segment, Gulf of Corinth, Greece, inferred from Holocene and Pleistocene terraces. *J Geol Soc Lond* 161:81–92
- McNeill LC, Cotterill CJ, Henstock TJ, Bull JM, Stefatos A, Collier REL, Papatheoderou G, Ferentinos G, Hicks SE (2005) Active faulting within the offshore western gulf of Corinth, Greece: implications for models of continental rift deformation. *Geology* 33:241–244
- McNeill LC, Cotterill CJ, Bull JM, Henstock TJ, Bell R, Stefatos A (2007) Geometry and slip rate of the Aigion fault, a young normal fault system in the Western Gulf of Corinth. *Geology* 35:355–358
- McNeill L, Sakellariou D, Nixon C (2014) Drilling to resolve the evolution of the Corinth Rift, Eos. *Trans Am Geophys Union* 95 (20):170–170. doi:10.1002/2014EO200009
- Micarelli L, Moretti I, Daniel JM (2003) Structural properties of rift-related normal faults: the case study of the Gulf of Corinth—Greece. *J Geodynam* 36:275–303
- Moretti I, Delhomme JP, Comet F, Bernard P (2002) In: Schmidt-Hattenberger C, Borm G (eds) *The Corinth rift laboratory: monitoring of active faults*. *First Break* 20(2)
- Moretti I, Sakellariou D, Lykousis V, Micarelli L (2003) The Gulf of Corinth: an active half graben? *J Geodyn* 36:323–340
- Moretti I, Lykousis V, Sakellariou D, Reynaud JY, Benziane B, Prinzhofer A (2004) Sedimentation and subsidence rate in the Gulf of Corinth: what we learn from the Marion Dufresne's long-piston coring. *C R Geosci* 336:291–299
- Muntzos T (1992) Palyno- und Paläoklima-Stratigraphie der pliozänen und altpleistozänen Sedimente der nördlichen und nordwestlichen Peloponnes (Hellas). *Newslett Stratigr* 27(1–2):71–91
- Nixon CW et al (2016) Rapid spatiotemporal variations in rift structure during development of the Corinth Rift, central Greece. *Tectonics*, vol 35, doi:10.1002/2015TC004026
- Nürnberg D, Müller RD (1991) The tectonic evolution of the South Atlantic from Late Jurassic to present. *Tectonophysics* 191:27–53
- Nyst M, Thatcher W (2004) New constraints on the active tectonic deformation of the Aegean. *J Geophys Res* 109:B11406. doi:10.1029/2003JB002830
- Ori GG (1989) Geologic history of the extensional basin of the gulf of Corinth (?Miocene-Pleistocene), Greece. *Geology* 17:918–921
- Ori GG, Roveri M, Nichols G (1991) Architectural patterns in large-scale Gilbert-type delta complexes, Pleistocene, Gulf of Corinth, Greece. In: Miall AD, Tyler N (eds) *The three dimensional facies architecture of terrigenous clastic sediments and its implications for hydrocarbon discovery and recovery*. *SEPM*, pp 207–216 (Concept in Sedimentology and Paleontology)
- Palyvos N, Sorel D, Lemeille F, Mancini M, Pantosti D, Julia R, Triantaphyllou M, De Martini P (2007) Review and new data on uplift rates at the W termination of the Corinth Rift and the NE Rion graben area (Achaia, NW Peloponnesos). *Bull Soc Geol Greece* 40:412–424
- Pángaro F, Ramos VA (2012) Paleozoic crustal blocks of onshore and offshore central Argentina: new pieces of the southwestern Gondwana collage and their role in the accretion of Patagonia and the evolution of Mesozoic south Atlantic sedimentary basins. *Mar Petrol Geol* 37:162–183
- Pantopoulos G, Zelilidis A (2014) Eocene to early oligocene turbidite sedimentation in the SE Aegean (Karthos Island, SE Greece): stratigraphy, facies analysis, nannofossil study, and possible hydrocarbon potential. *Turk J Earth Sci* 23:31–52. doi:10.3906/yer-1204-8
- Papanikolaou D, Royden L (2007) Disruption of the Hellenic arc, late Miocene extensional detachment faults and steep pliocene–quaternary normal faults—or what happened at Corinth? *Tectonics* 26:TC5003 <http://dx.doi.org/10.1029/2006TC002007>
- Papanikolaou D, Lykousis V, Chronis G, Pavlakis P (1988) A comparative study of neotectonic basins across the Hellenic Arc: the Messiniakos, Argolikos and Southern Evoikos Gulfs. *Basin Res* 1:167–176
- Papanikolaou D, Logos E, Lozios S, Sideris C (1996) Geological map of Greece, Korinthos sheet, scale 1:100 000, European center on prevention and forecasting of earthquakes, earthquake planning and protection organization and tectonic committee of the geological society of Greece, Athens
- Papanikolaou D, Gouliotis L, Triantaphyllou M (2009) The Itea-Amfissa detachment: a pre-Corinth rift Miocene extensional structure in central Greece. In: van Hinsbergen DJJ, Edwards MA, Govers R (eds) *Collision and collapse at the Africa-Arabia-Eurasia subduction zone*. *Geol Soc Spec Publ* 311:293–310
- Papastamatiou I, Tataris A, Katsikatsos G, Maragoudakis N, Kallergis G, Elefteriou A, Zachos K (1962) Geological map of Greece, Galaxidion sheet, scale 1:50 000. Institute of Geology and Mineral Exploration, Athens
- Paraschoudis B, Machairas G (1977) Geological map of Greece, Amygdalea sheet, scale 1:50 000. Institute of Geology and Mining Research, Athens 1977
- Pearce FD, Rondenay S, Sachpazi M, Charalampakis M, Royden LH (2012) Seismic investigation of the transition from continental to oceanic subduction along the western Hellenic subduction zone. *J Geophys Res* 117 no. B7. <http://dx.doi.org/10.1029/2011jb009023>
- Pe-Piper G, Piper DJW (2007) Neogene back-arc volcanism of the Aegean: new insights into the relationship between magmatism and tectonics. In: Beccaluva L, Bianchini G (eds) *Cenozoic volcanism in the Mediterranean area*. Geological Society of America, pp 17–31. doi:10.1130/2007.2418(02) (Geol Soc Am Spec Paper)
- Perissoratis C, Mitropoulos D, Angelopoulos L (1986) Marine geological research at the eastern Corinthiakos Gulf. *Geol geophys Res Special Issue*, IGME, Athens 381–401
- Perissoratis C, Piper DJW, Lykousis V (2000) Alternating marine and lacustrine edimentation during late quaternary in the Gulf of Corinth rift basin, central Greece. *Mar Geol* 167:391–411. doi:10.1016/S0025-3227(00)00038-4
- Philippson A (1890) *Der Isthmus Von Korinth*, vol 25. Zeitschrift der Gesselschaft fur Erdkunde, Berlin, pp. 1–98
- Pik R, Marty B (2009) Helium isotopic signature of modern and fossil fluids associated with the Corinth rift fault zone (Greece): implication for fault connectivity in the lower crust. *Chem Geol* 266(1–2):67–75
- Portman C, Andrews JE, Rowe PJ, Leeder MR, Hoogewerff J (2005) Submarine-spring controlled calcification and growth of spectacular *Rivularia* bioherms: late Pleistocene (MIS 5e), Gulf of Corinth, Greece. *Sedimentology* 52:441–465
- Poulimenos G, Zelilidis A, Kontopoulos N, Doutsos T (1993) Geometry of trapezoidal fan deltas and their relationship to extensional faulting along the south-western active margins of the Corinth rift, Greece. *Basins Res* 5:179–192
- Rangel HD, Carminatti M (2000) Rift lake stratigraphy of the Lagoa Feia formation, Campos basin, Brazil, lake basins through space and time. *Am Assoc Petrol Geol Stud Geol* 46:225–244
- Rigo A, Lyon Caen H, Armijo R, Deschamps A, Hatzfeld D, Makioupolous K, Papadimitriou P, Kassaras I (1996) A microseismic study of the western part of the Gulf of Corinth [Greece]: implications for the large-scale normal faulting mechanisms. *Geophys J Int* 126:663–688

- Roberts GP, Koukouvelas I (1996) Structural and seismological segmentation of the gulf of Corinth fault system: implication for models of fault growth. *Annali di geofisica* XXXIX(3):619–646
- Rögl F, Bernor RL, Dermitzakis MD, Müller C, Stancheva M (1991) On the Pontian correlation in the Aegean (Aegina Island). *Newsl Stratigr* 24:137–158
- Rohais S, Eschard R, Ford M, Guillocheau F, Moretti I (2007a) Stratigraphic architecture of the Plio-Pleistocene infill of the Corinth rift: implications for its structural evolution. *Tectonophysics* 440:5–28. doi:10.1016/j.tecto.2006.11.006
- Rohais S, Joannin S, Colin JP, Suc JP, Guillocheau F, Eschard R (2007b) Age and environmental evolution of the syn-rift fill of the southern coast of the gulf of Corinth (Akrata-Derveni region, Greece). *Bull Soc Géol Fr* 178:231–243
- Rohais S, Eschard R, Guillocheau F (2008) Depositional model and stratigraphic architecture of rift climax Gilbert-type fan deltas (Gulf of Corinth, Greece). *Sediment Geol* 210:132–145. doi:10.1016/j.sedgeo.2008.08.001
- Rohais S, Barrois A, Colletta B, Moretti I (2016) Pre-salt to salt stratigraphic architecture in a rift basin: insights from a basin-scale study of the Gulf of Suez (Egypt). *Arab J Geosci* 9:317. doi:10.1007/s12517-016-2327-8
- Royden LH, Papanikolaou D (2011) Slab segmentation and late Cenozoic disruption of the Hellenic arc. *Geochem Geophys Geosyst* 12:Q03010. doi:10.1029/2010GC003280
- Sachpazi M, Clément C, Laigle M, Hirn A, Roussos N (2003) Rift structure, evolution, and earthquakes in the Gulf of Corinth, from reflection seismic images. *Earth* 216:243–257
- Sachpazi M et al (2007) Moho topography under central Greece and its compensation by Pn time-terms for accurate location of hypocenters: the example of the Gulf of Corinth 1995 Aigion earthquake. *Tectonophysics* 440:53–65
- Sakellariou D, Lykousis V, Papanikolaou D (1998) Neotectonic structure and evolution of the Gulf of Alkyonides, central Greece. *Bull Geol Soc Greece* 32:241–250
- Sakellariou D, Lykousis V, Alexandri S, Kaberi H, Rousakis G, Nomikou P, Georgiou P, Ballas D (2007) Faulting, seismic-stratigraphic architecture and late quaternary evolution of the Gulf of Alkyonides Basin-East Gulf of Corinth, Central Greece. *Basin Res* 19:273–295
- Schattner U (2010) What triggered the early-to-mid Pleistocene tectonic transition across the entire eastern Mediterranean? *Earth Planet Sci Lett* 289:539–548. doi:10.1016/j.epsl.2009.11.048
- Sherkati S, Molinaro M, Frizon de Lamotte D, Letouzey J (2005) Detachment folding in the Central and eastern Zagros fold-belt (Iran): salt mobility, multiple detachments and late basemebnt control. *JSG* 27(9):1680–1696
- Skourtsos E, Kranis H (2009) Structure and evolution of the western Corinth rift, through new field data from the Northern Peloponnese. *Geol Soc Lond Spec Publ* 321(1):119–138, doi:10.1144/SP321.6
- Sokos E, Zahradník J, Kiratzi A, Janský J, Gallovič F, Novotný O, Kostecký J, Serpetsidaki A, Tselentis G-A (2012) The January 2010 Efpalio earthquake sequence in the western Corinth Gulf (Greece). *Tectonophysics* 530–531:299–309
- Sorel D (2000) A Pleistocene and still active detachment fault and the origin of Corinth Patras rift, Greece. *Geology* 28:83–86
- Sotiropoulos S, Kamberis E, Triantaphyllou M, Doutsos T (2003) Thrust sequences in the central part of the external Hellenides. *Geol Mag* 140(6):661–68
- Stefatos A, Papatheodorou G, Ferentinos G, Leeder M, Collier REL (2002) Seismic reflection imaging of active offshore faults in the Gulf of Corinth: their seismotectonic significance. *Basin Res* 14(4):487–502. doi:10.1046/j.1365-2117.2002.00176.x
- Symeonidis N, Theodorou G, Schutt H, Velitzelos E (1987) Paleontological and stratigraphic observations in the area of Achaia and Etoloakamania W-Greece. *Ann Geol Pays Hell Athens* 38:317–353
- Taylor B, Weiss JR, Goodliffe AM, Sachpazi M, Laigle M, Hirn A (2011) The structure, stratigraphy and evolution of the Gulf of Corinth rift, Greece. *Geophys J Int* 185:1189–1219. doi:10.1111/j.1365-246X.2011.05014.x
- Tiberi C, Diament M, Lyon-Caen H, King T (2001) Moho topography beneath the Corinth Rift area (Greece) from inversion of gravity data. *Geophys J Int* 145:797–808
- Tselentis GA, Makiopoulos K (1986) Rates of crustal deformation in the Gulf of Corinth [central Greece] as determined from seismicity. *Tectonophysics* 24:55–61
- Tsodoulos IM, Koukouvelas IK, Pavlides S (2008) Tectonic geomorphology of the easternmost extension of the Gulf of Corinth (Beotia, Central Greece). *Tectonophysics* 453:211–232
- Tsoflias P, Fleury JJ, Bizon G, Stoppel D, Symeonides N, Katsikatsos G (1984) Geological map of Greece, Khalandrista sheet, scale 1:50 000. Institute of Geology and Mineral Exploration, Athens
- Tsoflias P, Fleury JJ, Ioakim CH, Mavridis AN (1993) Geological map of Greece, Derveni sheet, scale 1:50 000. Institute of Geology and Mineral Exploration, Athens
- West BP, May SR, Eastwood JE, Rossen C (2002) Interactive seismic facies classification using textural attributes and neural networks. *Lead Edge*, pp 1042–1049, Oct 2002
- Westaway R (2002) The Quaternary evolution of the Gulf of Corinth, central Greece: coupling between surface processes and flow in the lower continental crust. *Tectonophysics* 348:269–318
- Xypolias P, Doutsos T (2000) Kinematics of rock flow in a crustal-scale shear zone: implication for the orogenic evolution of the south-western Hellenides. *Geol Mag* 137(1):81–96
- Zelilidis A (2000) Drainage evolution in a rifted basin, Corinth graben, Greece. *Geomorphology* 35:69–85
- Zelilidis A (2003) The geometry of fan-deltas and related turbidites in narrow linear basin. *Geol J* 37:1–16
- Zelilidis A, Kontopoulos N (1996) Significance of fan deltas without toe-sets within rift and piggy-back basins: examples from the Corinth graben and the Meso-hellenic though, Central Greece. *Sedimentology* 43:253–262
- Zelt BC, Taylor B, Weiss JR, Goodliffe AM, Sachpazi M, Hirn A (2004) Streamer tomography velocity models for the Gulf of Corinth and the Gulf of Itea, Greece. *Geophys J Int* 159:333–346
- Zelt BC, Taylor B, Sachpazi M, Hirn A (2005) Crustal velocity and Moho structure beneath the Gulf of Corinth, Greece. *Geophys J Int* 162:257–268

Styles of Salt Tectonics in the Sab'atayn Basin, Onshore Yemen

Gabor Tari, Rudi Dellmour, Emma Rodgers, Chloe Asmar, Peter Hagedorn, and Adel Salman

Abstract

A variety of distinct salt tectonic features are present in the Sab'atayn Basin of western Yemen. Based on the interpretation of regional 2D seismic reflection data and exploration wells in the central part of the basin, an Upper Jurassic evaporite formation produced numerous salt rollers, pillows, reactive, flip-flop and falling diapirs. Due to regional extension, halokinetics began as soon as the early Cretaceous, within just a few million years after the deposition of the Tithonian Sab'atayn evaporite sequence, by formation of salt rollers. The salt locally formed salt pillows which evolved to reactive and active salt diapirs and diapiric salt walls as the result of renewed, but low-strain extension in the basin. Some of the diapiric walls further evolved into falling diapirs due to ongoing extension. As the result of a prominent extensional episode at the end of the Cretaceous many of the diapiric walls in the basin are controlled by large normal faults on their updip flanks. As the post-Cretaceous sedimentary cover is largely missing in the study area, the assumed reactivation of salt structures during the Cenozoic remains poorly constrained. The interpreted changes in the style of salt tectonics in the Sab'atayn Basin offer a better understanding of the regional-scale tectonic development of the Arabian plate during the late Jurassic and Cretaceous.

Keywords

Yemen • Salt tectonics • Seismic interpretation • Rifting • Diapirism • Fractured basement

Introduction

The Mesozoic basins of Yemen are part of a large basin system in NE Africa and the Arabian Peninsula (Fig. 1) as the result of the break-up of Gondwana during the Late Jurassic/Early Cretaceous (e.g. Redfern and Jones 1995; Beydoun 1997; Bosence 1997; As-Saruri and Sorkhabi

2014). The dominantly NW-SE orientation of these basins is inherited from the NW-SE oriented Najd Fault system of the Arabian Peninsula. This system was active as a result of extensional collapse during the late stage of the Pan-African orogeny (~620–540 Ma, e.g. As Saruri et al. 2010), and it was reactivated during several Mesozoic extensional events.

The Sab'atayn Basin is a major hydrocarbon province in western and central Yemen (e.g. As-Saruri and Sorkhabi 2014) located in the southwestern part of the Arabian Peninsula (Fig. 2). The basin itself is one of several intra-cratonic basins in Yemen where a major rifting phase ended by the end of the Jurassic (e.g. Redfern and Jones 1995; Bosence 1997; Veening et al. 2015). The first commercial field in the basin was discovered in 1984 (Fairchild 1992; Alsharhan and Nairn 1997) and the subsequent exploration efforts showed that most of the petroleum play types in this basin are related to a widespread evaporite

The full citation and reference to the original article published in AJGS.

G. Tari (✉) · R. Dellmour · E. Rodgers · C. Asmar · P. Hagedorn
OMV Exploration and Production, Trabrennstrasse 6-8,
1020 Vienna, Austria
e-mail: gabor.tari@omv.com

A. Salman
OMV Yemen, Faj Attan, Beirut Street, Hadda Zone, 15361
Sana'a, Yemen

© Springer International Publishing AG 2017

F. Roure et al. (eds.), *Lithosphere Dynamics and Sedimentary Basins of the Arabian Plate and Surrounding Areas*, *Frontiers in Earth Sciences*, DOI 10.1007/978-3-319-44726-1_6

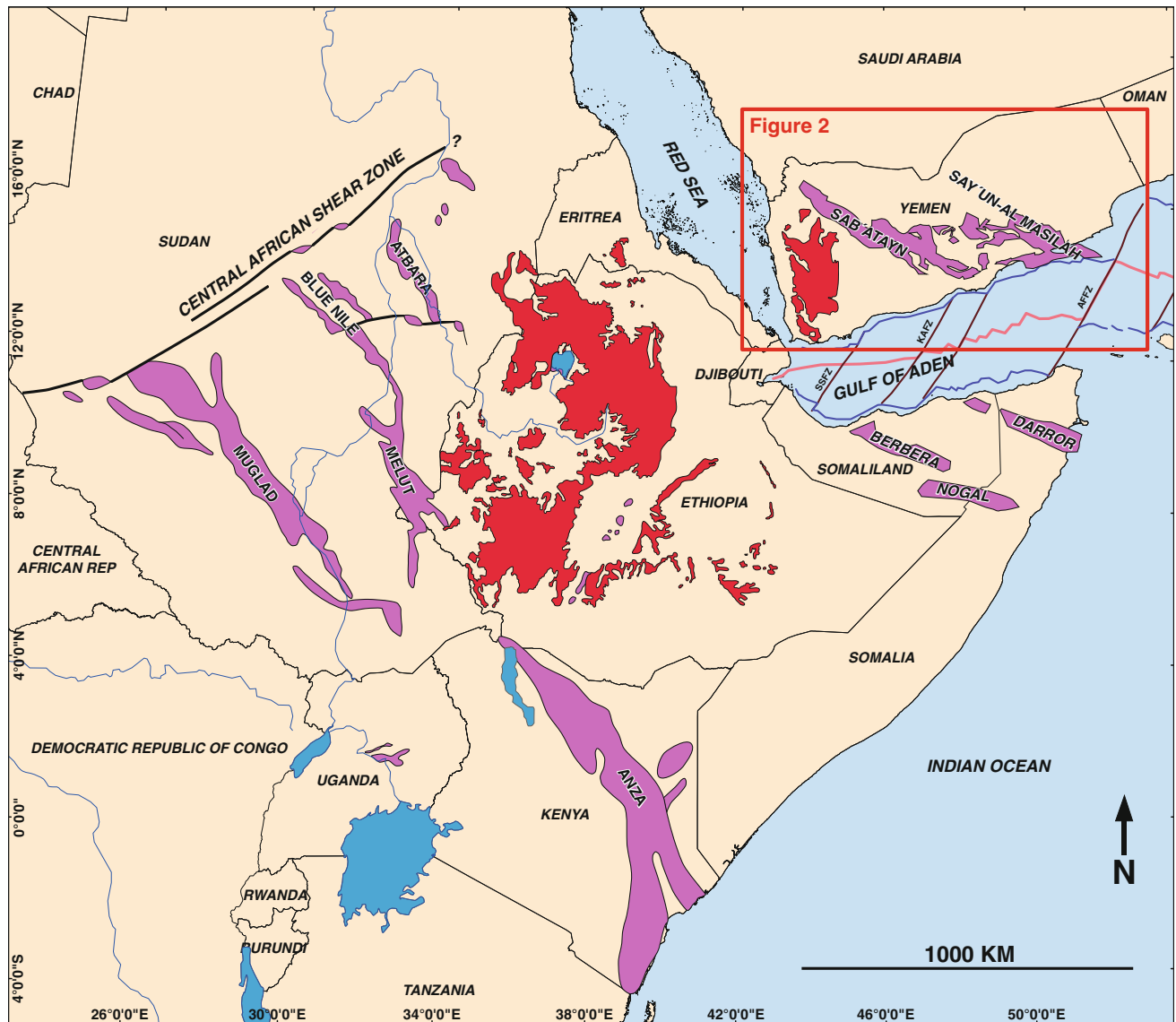


Fig. 1 Location of the Mesozoic rift basins of Yemen in the broader framework of the Arabian Peninsula and NE Africa, highlighted in magenta, compiled from Schull (1988), Bosworth (1992), Granath (2001), Guiraud et al. (2005), Fournier et al. (2010), Leroy et al. (2013) and Autin et al. (2013). Red colored areas show the extent of Miocene to Recent flood basalts possibly masking more Mesozoic grabens. In the Gulf of Aden area the abbreviations stand for: *SSFZ* Shukra El

Sheik Fracture Zone, *KAFZ* Khanshir Al Irquah Fracture Zone, *AFFZ* Alula-Fartak Fracture Zone. The location of Fig. 2 is shown by a red rectangle. Note the general NW-SE orientation of the basins changing in Yemen from NW-SE to W-E in an easterly direction. This is interpreted as the result of a change in the movement direction of the Indian Plate during Cretaceous times and the Neogene rifting of the Gulf of Aden (e.g. Bosence 1997)

unit which was deposited during the Late Jurassic (Brannan et al. 1999; Ahlbrandt, 2002; Csato et al. 2001; Csato 2005). As to general geological evolution of this previously poorly known basin, several important overviews were published since the 1990s (e.g. Beydoun 1997; Beydoun et al. 1998; As-Saruri and Sorkhabi 2014).

The Tithonian Sab'atayn Formation is a complex lithostratigraphic unit (Fig. 3) and it is considered as a sequence which is present in all the three segments of the entire Sab'atayn Basin (Fig. 1). This formation has typically several massive salt intervals in it and defines post-, intra- and

pre-salt play types in the basin (e.g. Towner and Lindsay 2000). It is generally accepted that most of the hydrocarbons in the basin were generated from pre-salt Upper Jurassic source rocks (Hakimi et al. 2011; Sachsenhofer et al. 2012; Hakimi and Abdullah 2013) in both the Sab'atayn and Masilah Basins (Fig. 2) during the Cenozoic. Also, the salt provides the ultimate seal for the pre-salt and intra-salt traps. The traps associated with the pre-salt fractured basement play (Angerer et al. 2011) are syn-rift fault blocks showing some correlation with the overlying salt structures (e.g. Tari et al. 2014). Therefore the proper understanding of salt tectonics is

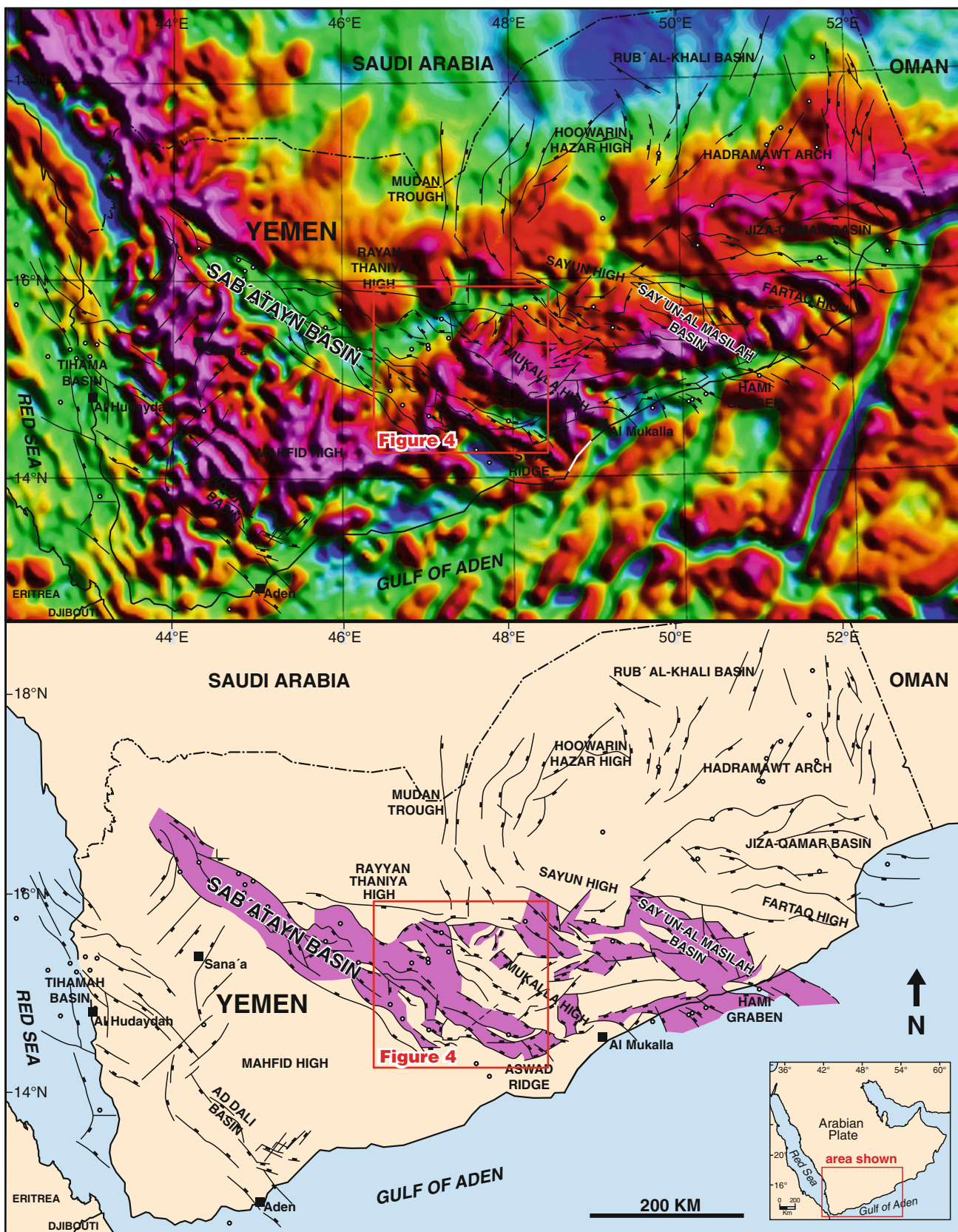


Fig. 2 Location of the Sab'atayn Basin in southwestern Yemen, in the southern part of the Arabian Peninsula. **a** Satellite-based free-air gravity map with the major faults superimposed on it. There is a good

correspondence between the major faults trends/basins and the gravity signal. **b** Major fault Mesozoic faults in Yemen with the aborted Late Jurassic rift grabens highlighted in magenta

critical for ongoing hydrocarbon exploration efforts in the Sab'atayn Basin (Hall and Le Nen 2014; Tari et al. 2014). Interestingly, there are only a few papers which show some seismic images from the Sab'atayn Basin illustrating salt tectonics (e.g. Seaborne 1996, Brannan et al. 1999; Angerer et al. 2011; Ghiglione and Iftikhar 2012; Tari et al. 2014). The aim of this paper is three-fold: (a) to provide additional seismic examples of the various salt tectonics styles in the central Shabwah segment of the Sab'atayn Basin (Fig. 4), (b) to illustrate the typical seismic interpretation challenges using vintage 2D seismic data and (c) to describe the temporal evolution of salt tectonics as the result of successive extensional, compressional and uplift periods in the basin.

Whereas Yemen has a prominent salt basin along the Red Sea coast (e.g. El-Anbaawy et al. 1992; Davison et al. 1994, 1996; Heathon et al. 1996), the present paper only addresses the salt tectonics within the Sab'atayn Basin (Figs. 2 and 3).

Geological Setting and Regional Structure

The NW-SE trending Sab'atayn Basin (Fig. 2) is one of the aborted Jurassic rift basins located in the southern part of the Arabian Peninsula with a length of about 600 km and average width of about 100 km (Redfern and Jones 1995). This rift basin system was probably even more elongated (Fig. 1), but its probable NW continuation was removed by the prominent Miocene uplift and erosion associated with the eastern rift shoulder of the Red Sea rift (Mitchell and Galbiati 1995).

The formation of the Sab'atayn Basin was interpreted by Ziegler (2001) as a consequence of an extensional phase related to the separation of India from Africa-Arabia. On a mega-regional scale, NW-SE trending Jurassic rift systems can be found not only on the Arabian Peninsula but also in East Africa, for example in Sudan, Ethiopia, Somaliland and Somalia (e.g. Schull 1988; Bosworth 1992; Ali and Watts 2015) as part of a pan-African aborted Jurassic rift system developed within Gondwana (Fig. 1).

To the SE, the Sab'atayn Basin finds its continuation across the Gulf of Aden in the Berbera Basin in Somaliland (e.g. Fournier et al. 2010; Leroy et al. 2013; Autin et al. 2013; As-Saruri and Sorkhabi 2014; Ali and Watts 2015). As the Sab'atayn Basin has a distinct Upper Jurassic evaporite succession in it, as opposed to the adjacent Masilah Basin to the east (Fig. 2), it had to have a narrow seaway connection to the Indian Ocean.

Specifically, in the southern part of the Arabian Peninsula two major tectonic periods are responsible for the structural elements of Yemen (As-Saruri and Sorkhabi 2014).

Whereas the Mesozoic rifting of the Sab'atayn Basin is relatively well constrained (e.g., Redfern and Jones 1995; Beydoun et al. 1996), the complex, poly-phase tectonics occurring during the Cenozoic is much less understood

(Huchon et al. 1991; Davison et al. 1994; Ellis et al. 1996). The sedimentary record associated with the Cenozoic opening of the Gulf of Aden and the Red Sea and the collision of the Arabian Peninsula with Eurasia is largely missing due to regional uplift and erosion in the study area (e.g. As-Saruri and Sorkhabi 2014).

Stratigraphy of the Sab'atayn Basin

There are many publications describing the various aspects of the stratigraphy in Yemen (e.g. Beydoun 1964, 1997; Jungwirth and As-Saruri 1990; Beydoun et al. 1998; Beydoun and As-Saruri 1998), but a simplified summary of the Mesozoic chrono- and lithostratigraphy of the Sab'atayn Basin is shown in Fig. 3 using the recent synthesis by As-Saruri and Sorkhabi (2014). Above a Pan-African granitic and metamorphic basement, the pre- to syn-rift deposits are represented by non-marine to shallow-marine siliciclastics (Kuhlan Formation; Beydoun et al. 1998) overlain by shallow-marine carbonates of the Shuqra Formation (Beydoun et al. 1998).

The Late Jurassic rifting in the Sab'atayn Basin resulted in the deposition of the Madbi Formation locally exceeding 1500 m in thickness (e.g. Seaborne 1996). It comprises muddy limestones and chalks with shaly horizons. An occasional rich, but low-diversity nannofossil/dinocyst assemblage suggests deposition in a relatively deep, partly restricted environment (Brannan et al. 1999). Beydoun et al. (1998) subdivided the Madbi Formation into a lower Meem Member and an upper Lam Member in the basin itself. At the same time, coarse continental sediments were deposited along the rift margins.

During the latest syn-rift (Ahlbrandt 2002) or early post-rift phase (Tari et al. 2014) the Sab'atayn Formation (Beydoun 1964) was deposited. The stratigraphic column adopted here (Fig. 3) from As-Saruri and Sorkhabi (2014) illustrates the complexity of this formation composed of sandstones, evaporites and shales. In fact, in the Sab'atayn Basin, the Sab'atayn Formation is divided into four conformably overlying members including the Yah, Seen, Alif and Safir Members (Beydoun et al. 1998). As the marine circulation in the Sab'atayn Basin became restricted, the lowermost Yah Member has the first evaporite layers in the formation (Fig. 3). The overlying Seen Member is dominated by fluvial to deltaic sands and shales. The Alif Member is the main reservoir in the Marib sector of the Sab'atayn Basin and it comprises over 90 % of recoverable oil in the basin. The overlying Safir Member consists of predominantly of halite with subordinate anhydrite layers separated by intercalated shales and sandstones with minor argillaceous, dolomite and limestone (Beydoun et al. 1998). The interbedded organic rich shales within the Safir Member are considered to be the

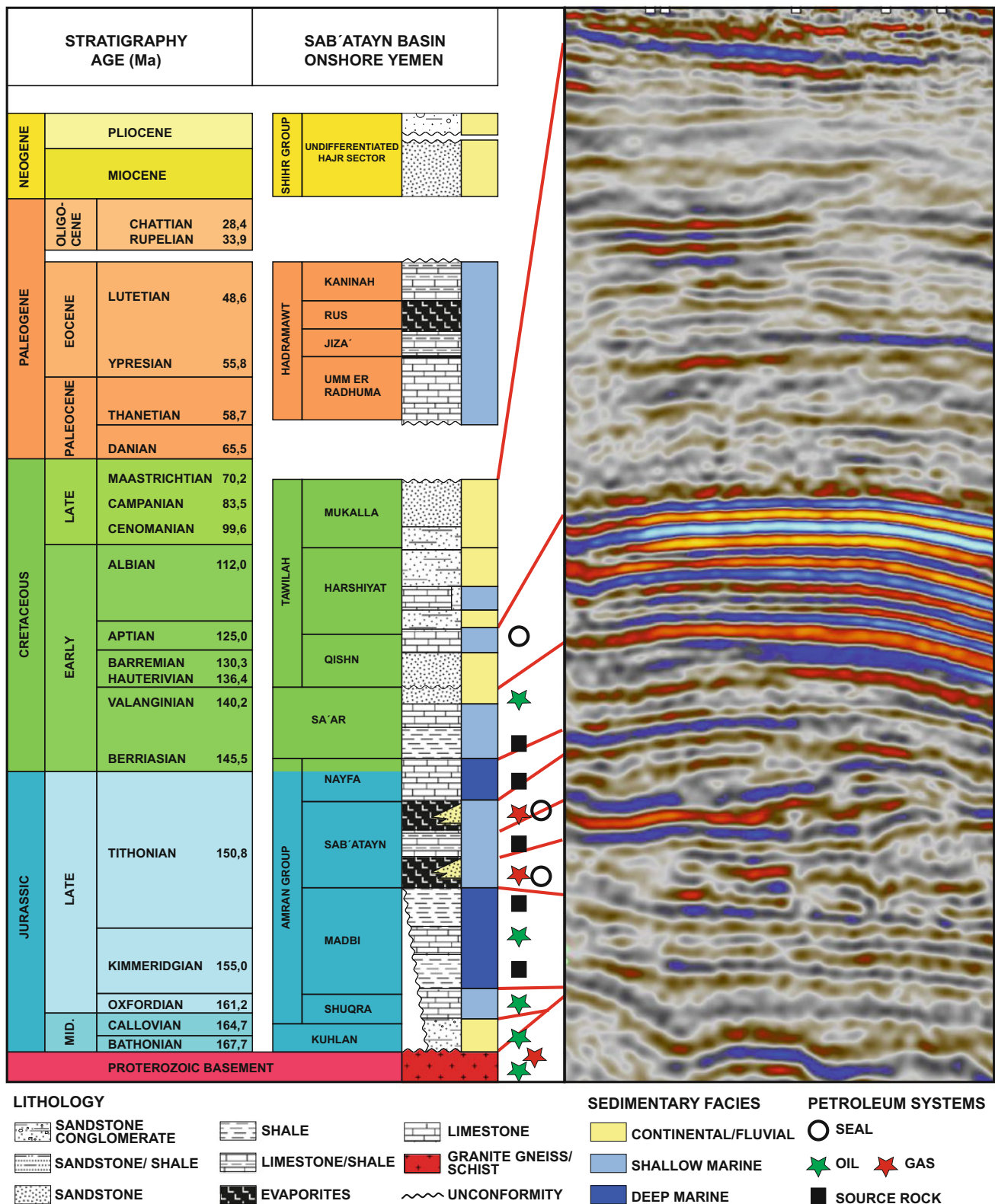


Fig. 3 Detailed stratigraphic scheme of the Sab'atayn Basin taken from As-Saruri and Sorkhabi (2014). Note that several stratigraphic nomenclature schemes were adopted by various authors, mostly following Beydoun (1964, 1997). In this work the Tithonian Sab'atayn Formation is referred to as a dominantly evaporite succession, for brevity "salt" from this point on, ranging from the base of the first evaporite bed to the top of the last one as the salt typically has several siliciclastic or carbonate intercalations. These are quite common across

the basin and the sandstones intercalated in the salt are quite important for the prolific Alif play (e.g. Towner and Lindsay 2000). Note that the salt is interpreted in this work, following Tari et al. (2014), as an early post-rift sediment (cf. Seaborne 1996; Ahlbrandt 2002). The seismic inset on the right hand-side has been modified from Tari et al. (2014) to show the correlation of the stratigraphy with the seismic facies, calibrated by the Al Nilam ST-1 well

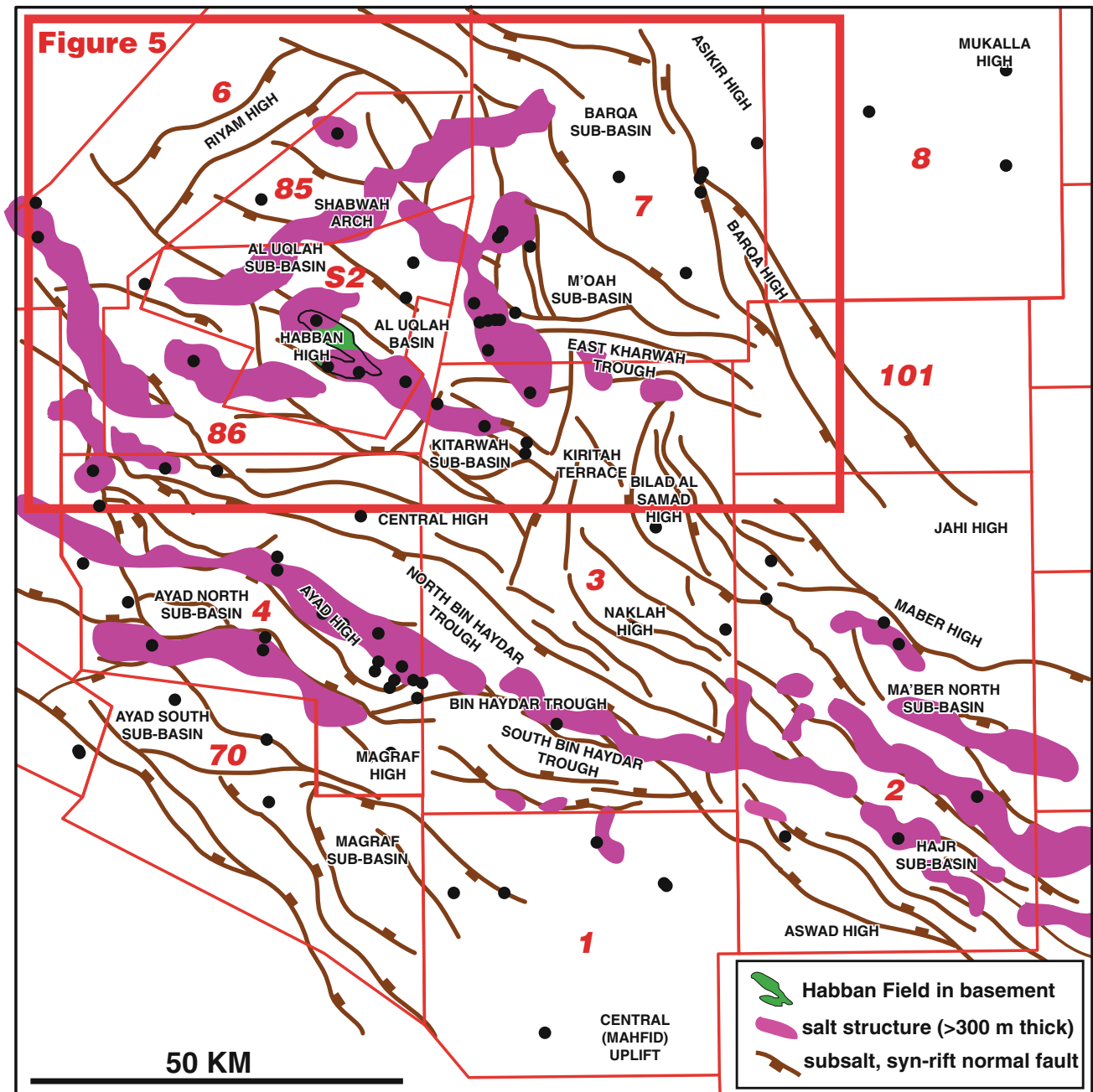


Fig. 4 Simplified structural map of the central part of the Sab'atayn Basin, slightly modified from Tari et al. (2014), with the outline of salt features (for location see Fig. 2). The location of the index map of the

study area shown in Fig. 5 is highlighted in a red rectangle. Brown lines are large rift-related normal faults depicted in a simplified center-line manner

prolific oil-prone source rock in the Marib-Shabwah Basin (Sachsenhofer et al. 2012; Hakimi and Abdullah 2013). The Safir Member also constitutes an excellent overall seal unit to the underlying Alif Member reservoir levels. Within the Safir Member there are multiple reservoir/seal pairs documented in the Alif Field (Ahlbrandt 2002).

Based on the large number of well penetrations (Figs. 4 and 5), the relative proportions of non-evaporitic lithologic

units such as neritic carbonate, coarser siliciclastic and shaly intercalations within the Sab'atayn Formation are depending on, at any location, the depositional environment within the rift basin. Anhydrite and coarse clastics are common along the basin margin whereas massive halite and neritic carbonates are more frequently drilled in the basin center (Csato 2005). The lithologic complexity of the Sab'atayn Formation is expressed by a subtle top salt and moderately defined base

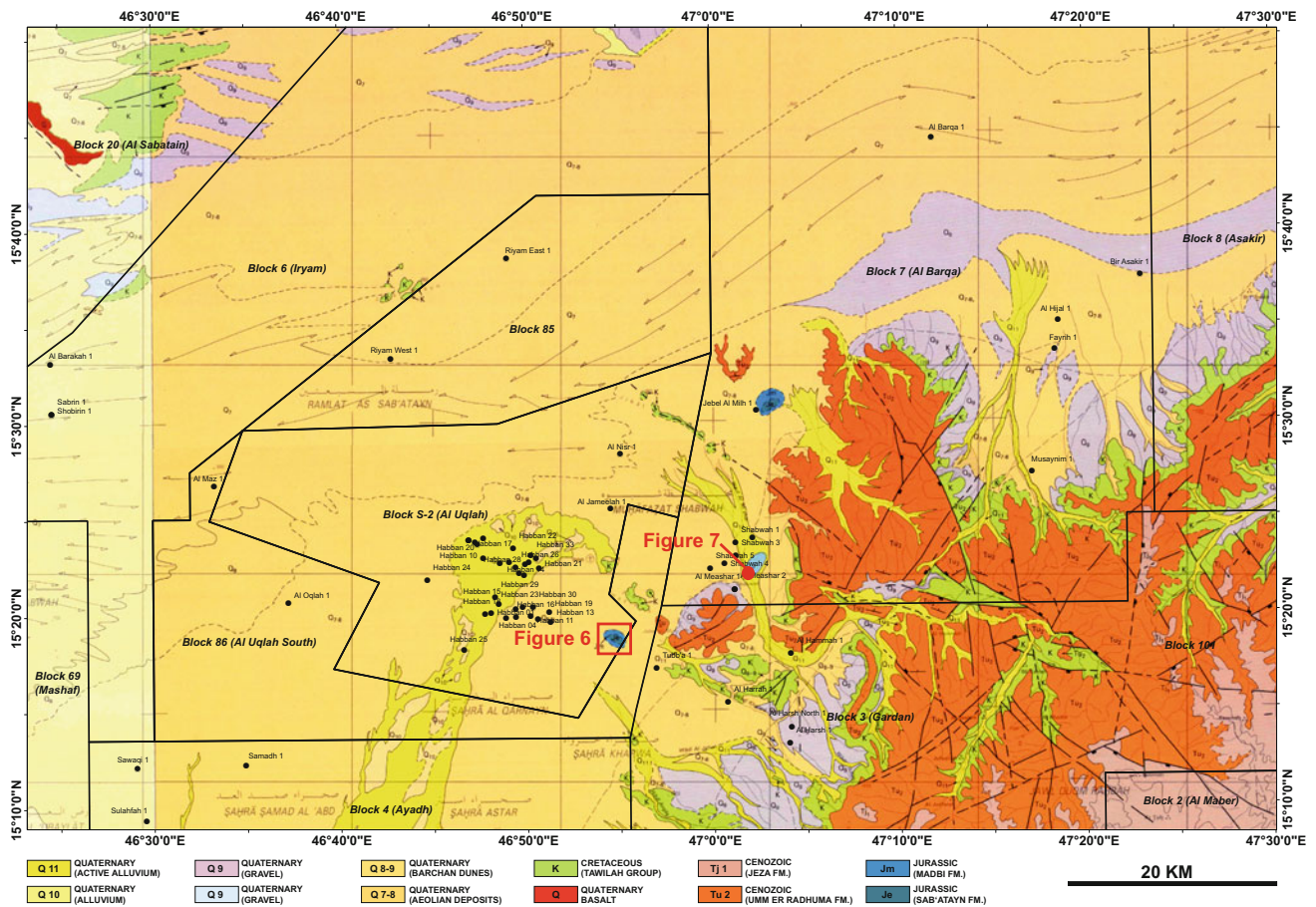


Fig. 5 Surface geology of the study area based on the 1:250,000 scale geologic maps of Yemen (sheets 15I and 15H). For location see Fig. 4

salt seismic response (Tari et al. 2014). Non-evaporitic lithologies within the Sab'atayn Formation are quite common (Fig. 3) and are quite important for the prolific Alif play (Towner and Lindsay 2000).

The internal complexity within the Sab'atayn Formation is well-illustrated by a high-resolution satellite image of one of the salt diapirs outcropping just east of the Habban Field area (Fig. 6). The complex internal structure of the diapir is expressed by intra-salt folds with subvertical axes (curtain folds). In this example the Upper Jurassic salt is interpreted to have transformed mostly to gypsum on the surface (light colors) alternating with bituminous marls and possibly “stringers” of other, non-evaporitic lithologies (dark colors). Note that the geometry of intra-salt refolded drape and curtain folds with subvertical fold axes is very characteristic for the stems of diapirs suggesting significant post-kinematic erosion in the area.

The outcrop expression of the salt within the Sab'atayn Formation (Fig. 7) is shown at another outcropping diapir near Shabwah (Fig. 5). We tentatively interpret the steep dips seen in this abandoned salt mine as the expression of dominantly vertical layering and flow fabrics within the salt.

Thus this outcrop may capture the intra-salt flow geometry to be expected in diapir stems. Similarly to the other salt diapir (Fig. 6), the lack of subhorizontal layering and flow textures characteristic for overhangs and salt tongues suggests significant post-kinematic erosion of the diapir.

The Sab'atayn Formation behaves as a mobile substratum due to its multiple evaporite layers, and therefore it will be referred to as “salt” from this point on. The present-day thickness of the Sab'atayn Formation is strongly controlled by multiple phases of salt tectonics. The original salt depositional level is often welded out and therefore prominent salt windows exist.

Regardless, Seaborne (1996) estimated its original depositional thickness as about 300 m.

The earliest Cretaceous (Berriasian-Valanginian) post-rift stage is represented by shallow to deep marine shales and limestones of the upper part of the Nayfa Formation and the overlying marine siliciclastics of the Sa'ar Formation. A major depositional hiatus occurs at the top of the Sa'ar Formation (Fig. 3), spanning about 5–6 Ma.

Above the late Valanginian unconformity, the Lower Cretaceous Qishn Formation (Hauterivian to Late Aptian)

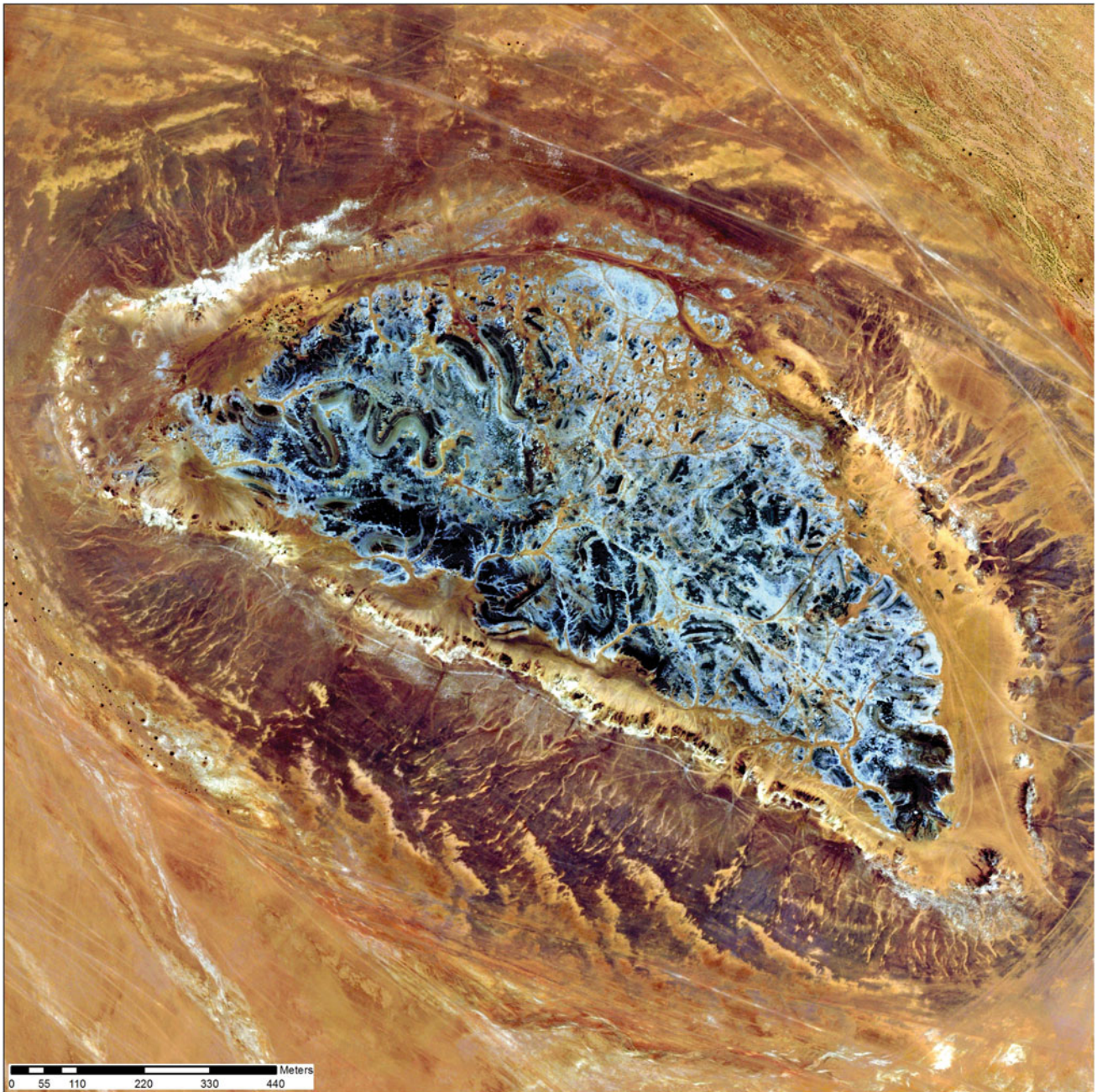


Fig. 6 High-resolution satellite image of one of the salt diapirs exposed on the surface just east of the Habban Field area, for location see Fig. 5. The Upper Jurassic salt transformed mostly to gypsum on the surface (*light colors*) alternating with bituminous marls and

limestone “stringers” (*dark colors*). The complex internal structure of the diapir is expressed by intra-salt folds with subvertical axes (curtain folds). Image courtesy of DigitalGlobe

comprising the Qishn Clastics Member and the Qishn Carbonates Member is the lowermost unit of the Tawilah Group (e.g. Leckie and Rumpel 2003). On top of the late Aptian unconformity (Fig. 3), the Albian to Late Cretaceous continental clastics (the subsurface equivalent of the Harshiyat and Mukalla Formations) were deposited. The total thickness of

the Tawilah Group reaches 1500 m (Seaborne 1996). The overlying Hadramawt Group of Paleocene to Middle Eocene age is up to 1770 m thick (Watchorn et al. 1998) although its thickness in the study area is significantly less. Sediments of the upper Cenozoic are also mostly missing in our study area due to erosion and/or non-deposition.



Fig. 7 Very steeply dipping evaporite layers at the outcropping Shabwah salt diapir, photo courtesy of Robert McDonald. The height of the outcrop is about 8 m, for location see Fig. 5. We tentatively interpret the steep dips as the expression of dominantly vertical

layering and associated flow fabrics within the salt. If correct, this outcrop captures an intra-salt flow geometry to be expected in diapir stems. In contrast, subhorizontal layering and flow textures are more typical in overhangs and salt tongues

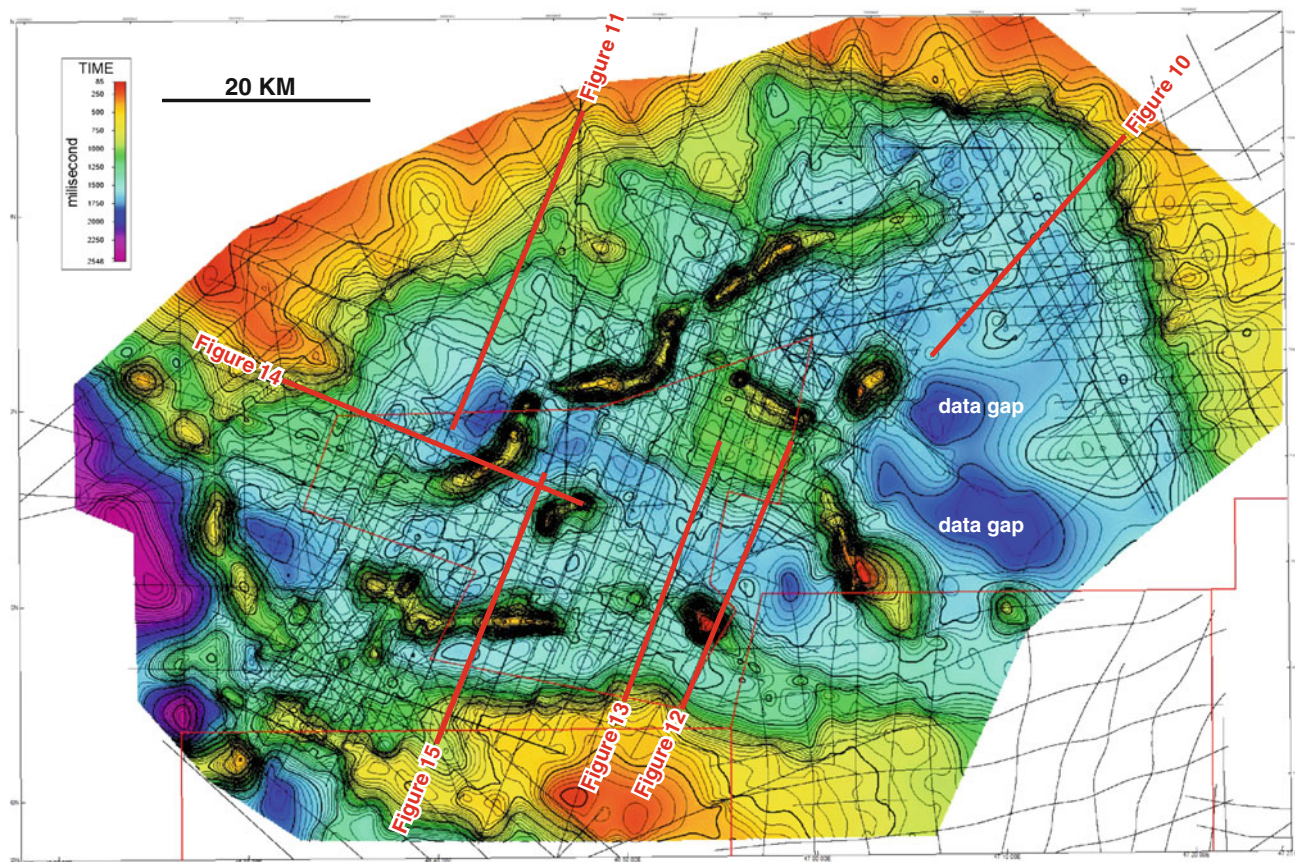


Fig. 8 Time structure map of the top salt in a segment of the central part of the Sab'atayn Basin based only on 2D seismic data interpretation. The traces of the seismic lines used for the gridding are shown as

black sticks. The grid size was 200 m using a minimum curvature algorithm with only minor smoothing applied. The location of the seismic examples shown in Figs. 10–15 are highlighted as *red lines*

Data Sets and Methodology

This study focuses on the northern part of the central Shabwah segment of the Sab'atayn Basin (Figs. 2 and 4) and uses 2D vintage seismic reflection data in an area covering about *ca.* 8000 km² (Figs. 5 and 8). As the seismic data were acquired in multiple acquisition campaigns starting in the seventies, the orientation and the length of the *ca.* 600 individual seismic profiles and the spacing of the seismic grid are highly variable and locally quite uneven (Fig. 8). The quality of the different seismic sets is also very variable depending on their vintage, compounded by the fact that about a third of the seismic profiles used in this study were reconstructed from scanned and vectorized hard-copy sections when the original data were not available in digital format. Whereas there are modern 3D seismic data sets in the study area, for example, covering the Habban Field (Angerer et al. 2011; Legrand et al. 2011; Ghiglione and Iftikhar 2012; Zabalza et al. 2012), in order to have a consistent and unbiased view across the entire area, only 2D seismic data were used in the seismic interpretation. The

seismic data were calibrated by about 60 exploration wells drilled in the broader area of the Habban Field (Fig. 5).

Mapping was done on multiple seismic horizons, corresponding to the major unconformities in the tectonostratigraphic scheme of the basin (Fig. 3). As to the time-structure of these regionally mapped horizons, only the top salt horizon is shown in a map view sense (Fig. 8), for confidentiality reasons. The time-structure map of the top salt seismic horizon was produced using a minimum curvature algorithm with a 200 × 200 m grid size, followed by minor Bartlett-type smoothing of the contours.

Seismic Expression of the Stratigraphy and Interpretation Challenges on Vintage 2D Seismic Data

The typical seismic response of the various stratigraphic units in the basin has been discussed to various degrees by Seaborne (1996), Ellis et al. (1996), Brannan et al. (1999), McDonald (2005), Angerer et al. (2011) and Tari et al.

(2014). The following overview briefly describes the seismic signature of the major stratigraphic units from bottom to top in the study area (Fig. 3).

The top crystalline basement reflector is the acoustic basement reflector as it is picked as the last coherent bright reflector at the base of the seismically imaged basin fill. The Kuhlan Formation is always very thin, i.e. 10–20 m, therefore it is below seismic resolution. The overlying Shuqra Formation, as a tight limestone unit, does not have a clear seismic expression. In contrast, the Meem member of the Madbi Formation is typically a very bright package of fairly organized reflectors in the deeper parts of the basin as it has many interbedded sandstones in a shale-dominated sequence. The transition from the Meem Member to Lam Member is very distinct and abrupt, as the Lam has very little coherent internal reflectivity being composed primarily of shales.

The salt within the Sab'atayn Formation has variable seismic signature depending on the position in the basin. If the salt is very thin (i.e. less than 100 m thick) or welded out (i.e. less than 10 m thick), there is only a bright reflector associated with it. However, if the salt is thick due to halokinetics, the seismic mapping of its top and base could become very problematic, especially on older, low-fold, poor quality vintage lines. In these cases the seismic interpretation tool, the so-called “Napoleon’s hat” geometry (Albert Bally, personal communication, *ca.* 1988) could be used to identify the position of salt on the seismic data if not clearly imaged (Fig. 9). The recognition criteria for salt in poor quality, vintage seismic data, without obvious top and base salt reflectors, is the flat-lying, isochronous strata below, arching/folding above, wedging and apparent downlapping at the edges of the “hat” (Fig. 9). Especially, the wedging between post- and pre-salt reflection packages on the flanks of salt pillows and diapirs is a useful give-away for the interpreter to properly pick the top and the base of the salt and correlate it into the central part of any salt structure. Moreover, in time-domain seismic data a velocity pull-up is very typical beneath the “hat” (Fig. 9). As the amplitude of the pull-up is the function of (a) the velocity contrast between the salt and the surrounding sediments and (b) the salt thickness, the magnitude of the pull-up could be used as an independent check of the interpreted salt thickness. The salt velocity, like in any other salt basin, scatters between 4400 and 4600 m/s in the Sab'atayn Basin.

The supra-salt Uppermost Jurassic to Lower Cretaceous Nayfa Formation has a relatively well organized reflectivity, i.e. good continuity and intermediate reflection strength. The top of the Sa'ar Formation, coinciding with the Valanginian unconformity, is typically a single bright peak reflector, which is easy to map around. Similarly, above a fairly reflective Hauterivian-Aptian sequence, the top Qishn Formation is a booming reflector corresponding to the positive impedance contrast between the Qishn carbonates and the

overlying Upper Cretaceous Harshiyat and Mukalla strata (Fig. 3). Whereas there are coherent seismic reflectors within the Tawilah Group, their poor continuity is the result of the dominant continental to coastal siliciclastic depositional patterns in this sequence.

The top of the Cretaceous sequence is a pronounced angular unconformity (Fig. 3) seen on some of the seismic sections, however, this seismic pick is typically so close to the surface that it is missing on most seismic profiles in the study area.

Salt Tectonics Styles Interpreted on 2D Seismic Reflection Data: Observations and Interpretations

The seismic examples in this section were selected to illustrate different salt tectonics styles in certain segments of the basin, from simple to more advanced cases.

A sub-regional seismic section (Fig. 10) located in the Barqa subbasin of the Sab'atayn Basin (Fig. 8) illustrates the presence of closely spaced salt-rollers involving mostly the Valanginian-Berriasian strata. All the rollers are controlled by listric faults dipping towards the basin center, to the SW. There is no evidence for growth associated with these listric faults, so deformation occurred in a single episode, mostly, but not entirely pre-dating the top Valanginian unconformity. Some compressional elements detached on top of the thin salt such as folds on the southwestern end of the section suggests the presence of a small (i.e. 30 km wide) linked system, i.e. the extension associated with the salt rollers might have been compensated by the reverse faults basinward. We have not attempted to kinematically balance this apparent linked system.

The next sub-regional 2D seismic section (Fig. 11) is located in the Al Uqlah subbasin of the Sab'atayn Basin (Fig. 8). The style of salt tectonics in this segment of the basin is more advanced, as not only the “early” salt-rollers (cf. Fig. 10) are present, involving the Berriasian-Valanginian strata, but much larger, “late” salt rollers as well, which formed at the end of Cretaceous. The base Cenozoic angular unconformity (see Fig. 2) truncates the strata on top of the late salt rollers. Note that the lateral separation between some of the rollers due to the normal faulting is such that we consider some of these features true rafts (*sensu* Duval et al. 1992). Also note that the roller in the center of the seismic line (Fig. 11) displays clear growth during the deposition of the Qishn sequence. Therefore this seismic section records three phases of salt-roller tectonics during: (a) intra-Nayfa; (b) intra-Qishn and (c) latest (or partly post?) Tawilah times.

The next sub-regional 2D seismic section (Fig. 12) is located in the Kitarwah subbasin of the Sab'atayn Basin

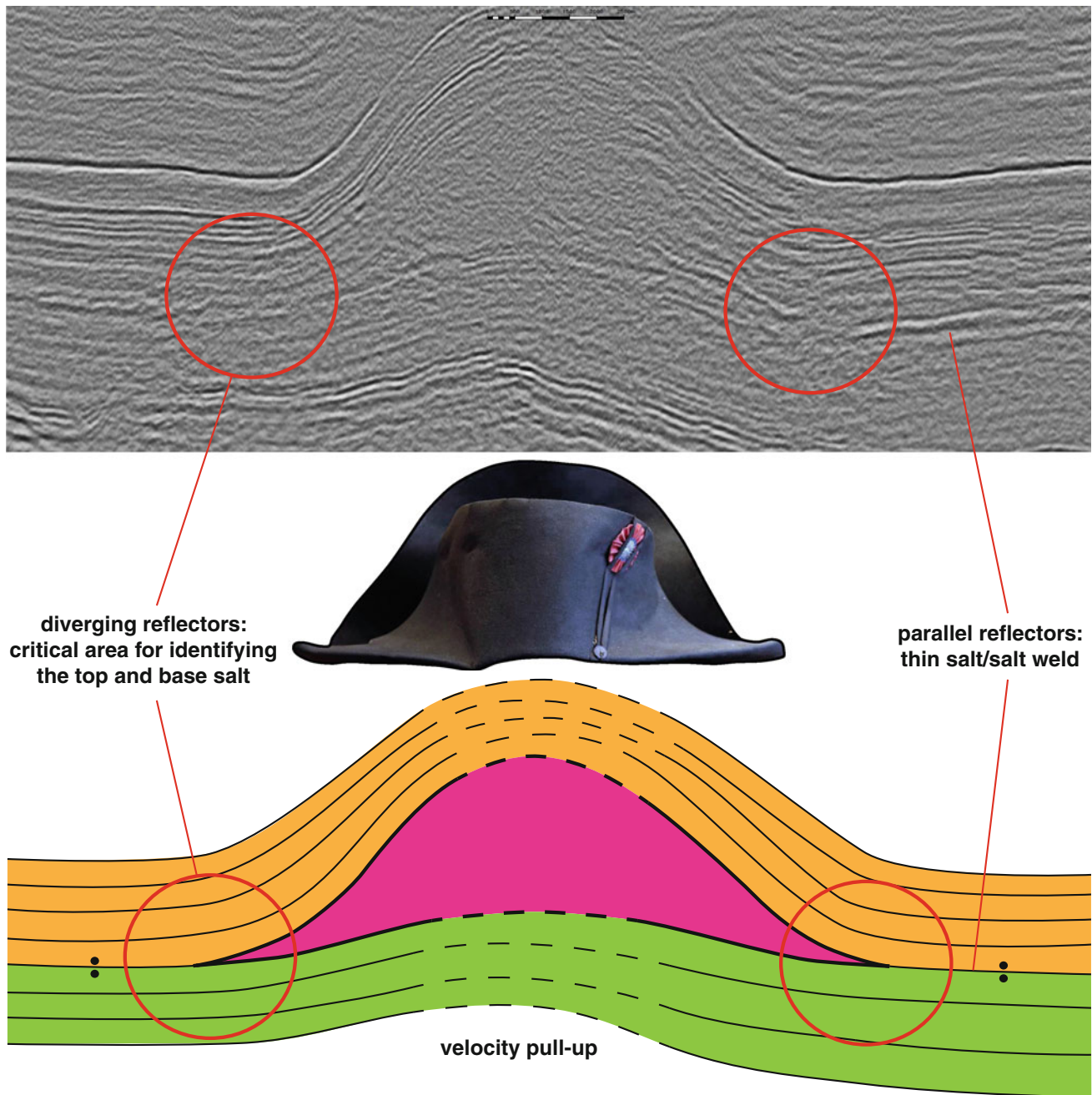


Fig. 9 The illustration of the “Napoleon’s hat” seismic interpretation concept (Albert Bally, personal communication, 1988) as an interpretation tool specifically used to identify the position of salt poorly imaged on seismic data. The recognition criteria for salt in poor quality, vintage seismic data without obvious top and base salt reflectors is the flat-lying, isopachous strata below, arching above, wedging and

apparent downlap at the edges of the “hat”. In time-domain seismic data a velocity pull-up is very typical beneath the “hat”, like in the example shown here. As the amplitude of the pull-up is the function of the salt thickness and the typical salt velocity is 4400–4600 m/s, the pull-up could be used as an independent check of the interpreted salt thickness

(Fig. 8). This seismic example is markedly different from the previous examples with a large salt diapir reaching the surface. Note the asymmetry on the flanks of the diapir, the southwestern flank being controlled by a major normal fault. The thinning of the Qishn sequence towards the diapir is interpreted as evidence for an early salt-pillow. Some

smaller normal faults on both flanks of the diapir dipping towards it record the reactive-stage growth of this salt feature sensu Vendeville and Jackson (1992a). However, the geometry of the Tawilah reflectors suggests the main rise of the diapir post-Tawilah times. As to its location, the diapir appears to be developed above an intra-basin rotated syn-rift

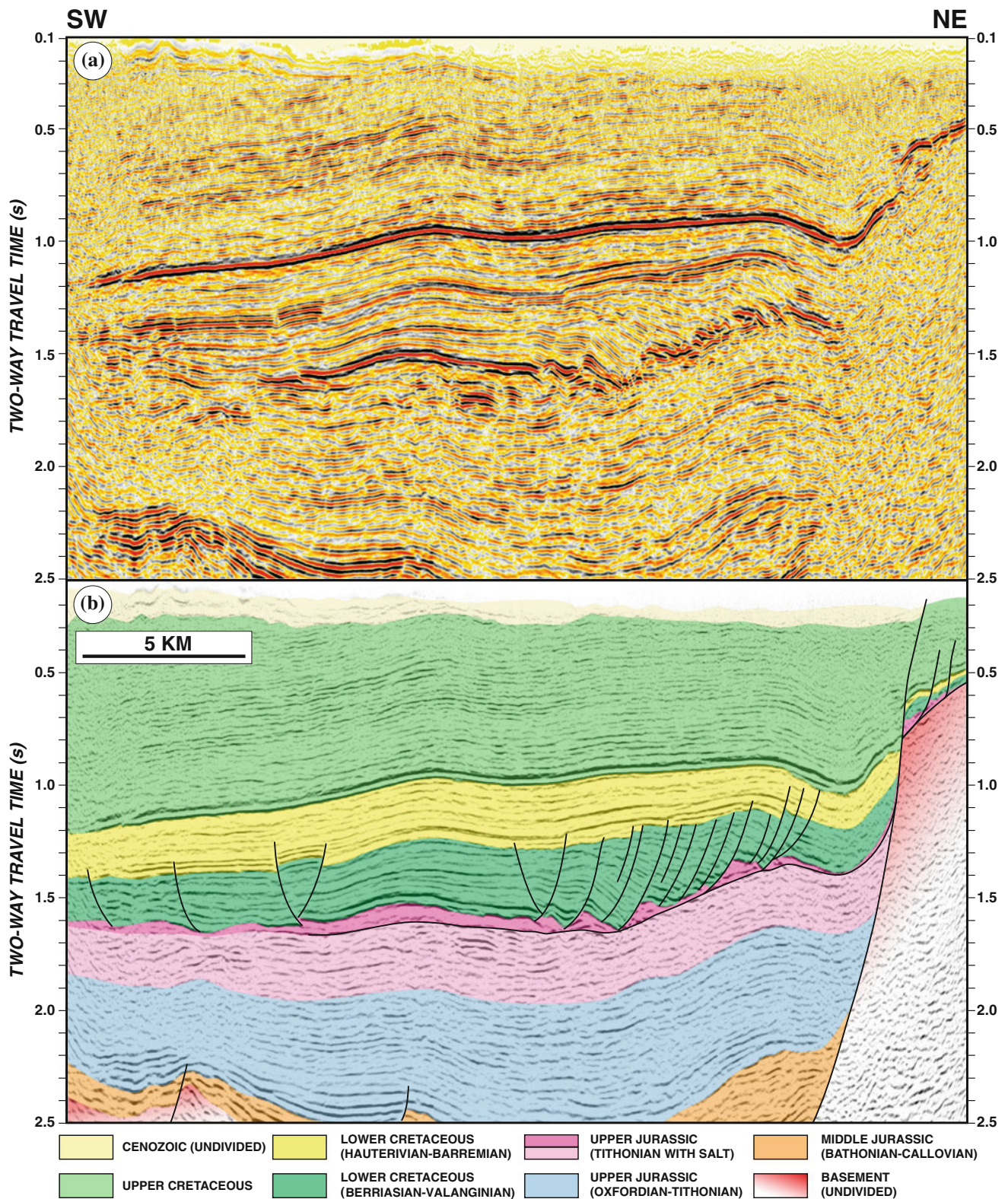


Fig. 10 **a** Sub-regional 2D seismic section located in the Barqa subbasin of the Sab'atayn Basin (see Fig. 8 for location). **b** Interpretation of the seismic data with emphasis on the salt highlighted in *magenta*. The style of salt tectonics in this segment of the basin is simple, only closely spaced salt-rollers are present involving mostly within the Berriasian-Valanginian strata

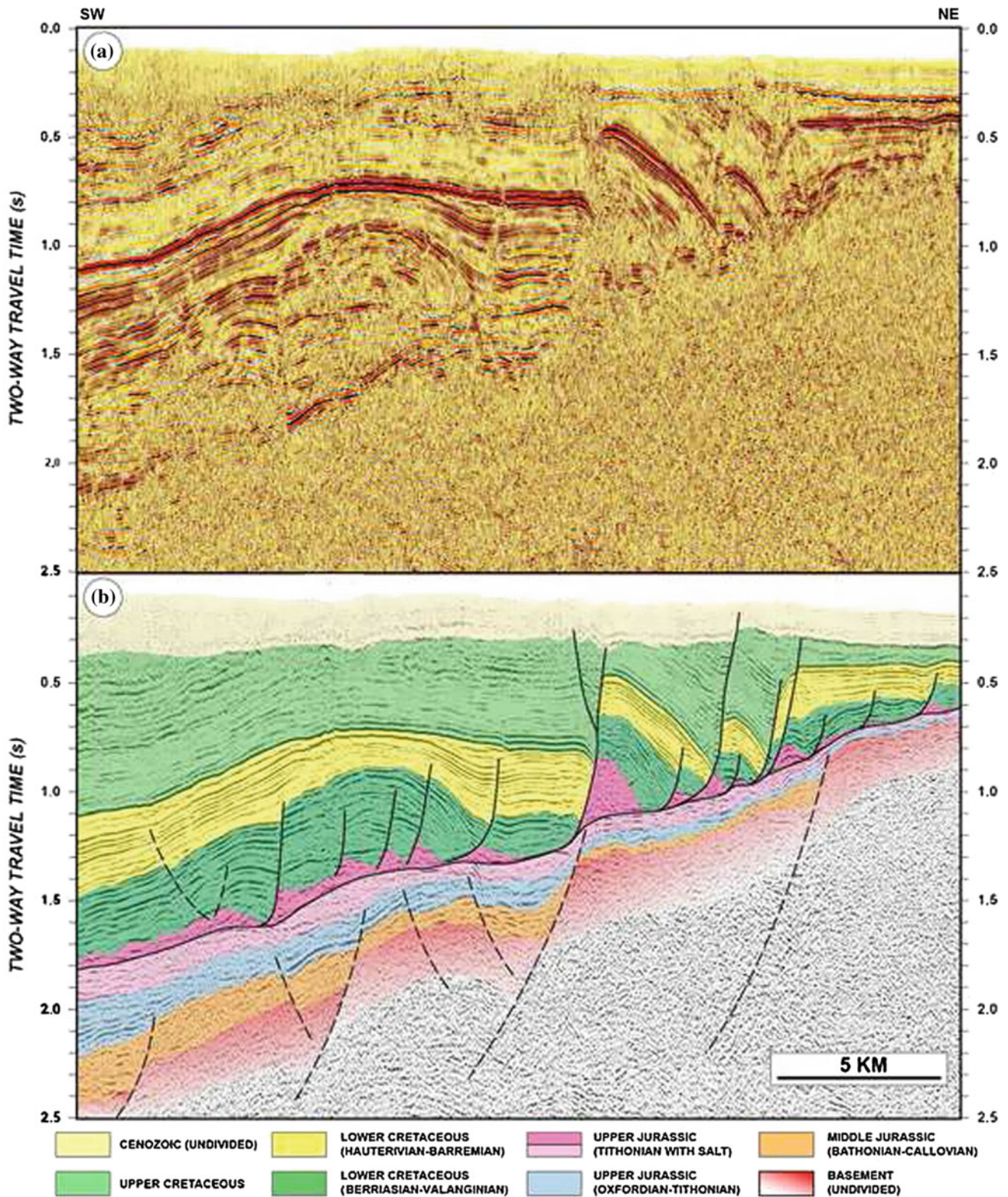


Fig. 11 a Sub-regional 2D seismic section located in the Al Uqlah subbasin of the Sab'atayn Basin (see Fig. 8 for location). b Interpretation of the seismic data, with emphasis on the salt highlighted in magenta. The style of salt tectonics in this segment of the basin is more

advanced, as not only the “early” salt-rollers are present involving the Berriasian-Valanginian strata but much larger “late” salt rollers as well, which formed at the end of Cretaceous. The base Cenozoic angular unconformity (see Fig. 2) truncates the strata on top of the salt rollers

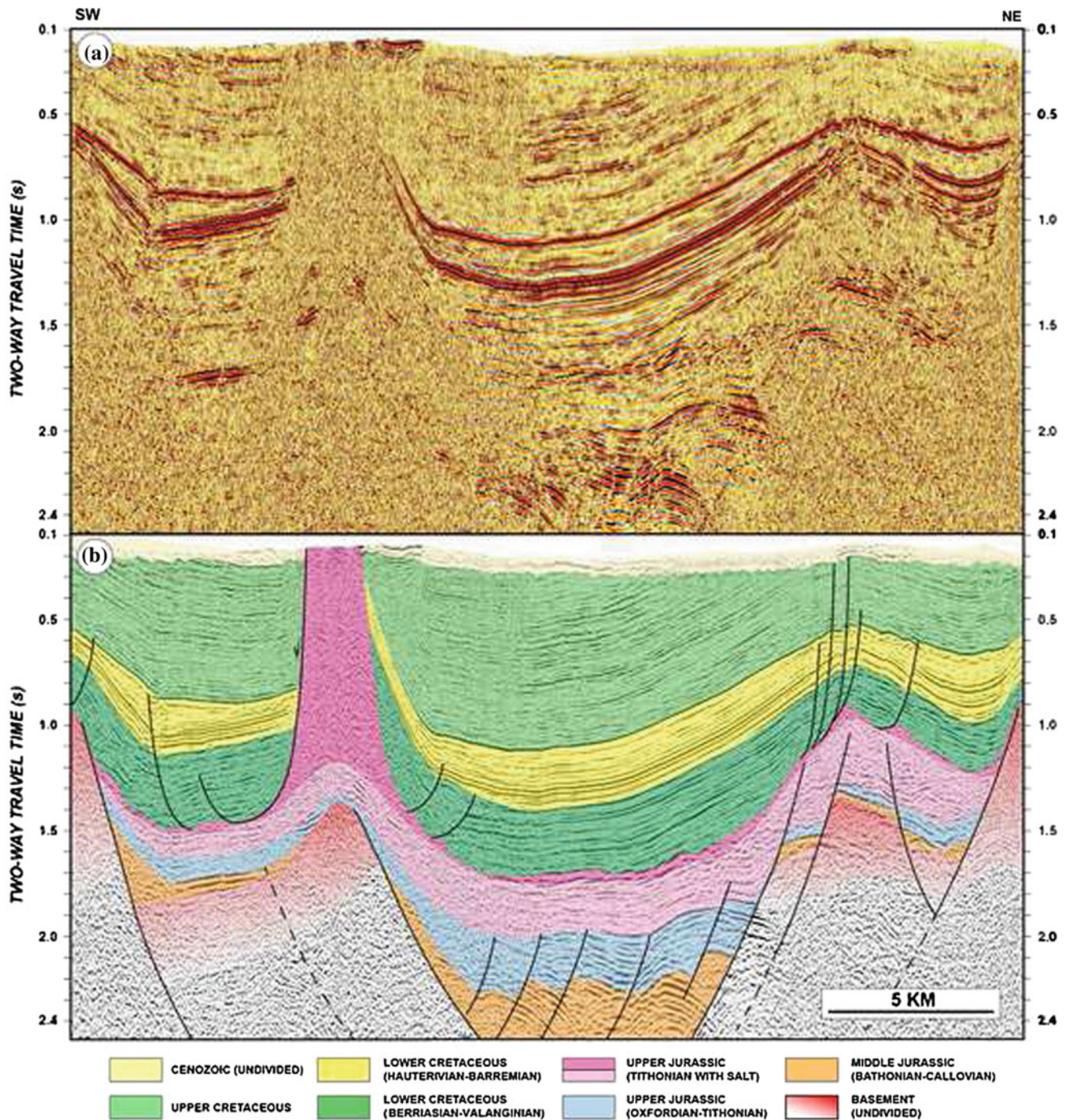


Fig. 12 a Sub-regional 2D seismic section located in the Kitarwah subbasin of the Sab'atayn Basin (see Fig. 8 for location). b Interpretation of the seismic data, with emphasis on the salt highlighted in magenta. The style of salt tectonics in this segment of the basin is

markedly different from the previous examples with a diapir reaching the surface. Note the asymmetry on the flanks of the diapir, the southwestern flank being controlled by a major normal fault

block. In this basin center location there are no salt rollers, except just a few examples.

The next 2D seismic section (Fig. 13), just 5 km to the WNW along strike (Fig. 8) shows the same diapir as in

Fig. 12, but as a falling diapir, sensu Vendeville and Jackson (1992b). The salt is welded out between the largest normal faults in the center. Just like in the example shown on Fig. 12, some smaller normal faults on both flanks of the

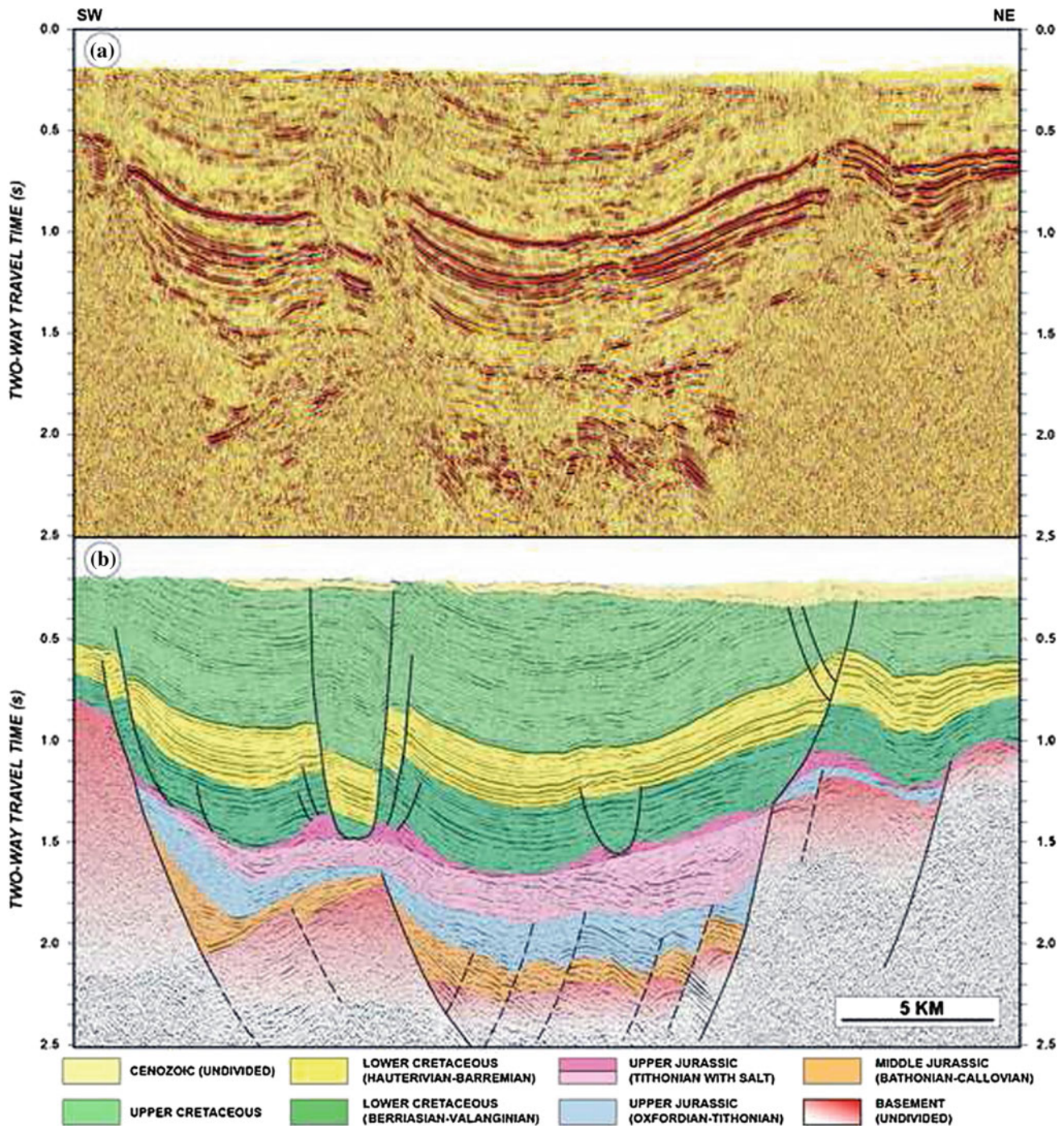


Fig. 13 a Sub-regional 2D seismic section located in the Kitarwah subbasin of the Sab'atayn Basin (see Fig. 8 for location). b Interpretation of the seismic data, with emphasis on the salt highlighted in

magenta. This line is relatively close to the example shown in Fig. 12 with a falling diapir sensu Vendeville and Jackson (1992b) as the result of an extensional period at the end of the Cretaceous

previous diapir record the reactive-stage growth of this salt feature. The total fall of the diapir occurred as the result of a distinct extensional period at the end of the Cretaceous.

The salt tectonic style seen on a sub-regional 2D seismic section (Fig. 14) located in the Al Uqlah subbasin of the Sab'atayn Basin (Fig. 8) is very similar to the one shown in

Fig. 11, despite the fact the line has a perpendicular orientation, running NW-SE. The large diapir has a marked asymmetry here as well, the northwestern flank being controlled by a major normal fault. The base Cenozoic angular unconformity (see Fig. 2) indicates the erosional removal of large portions of the Upper Cretaceous strata. Salt tectonics

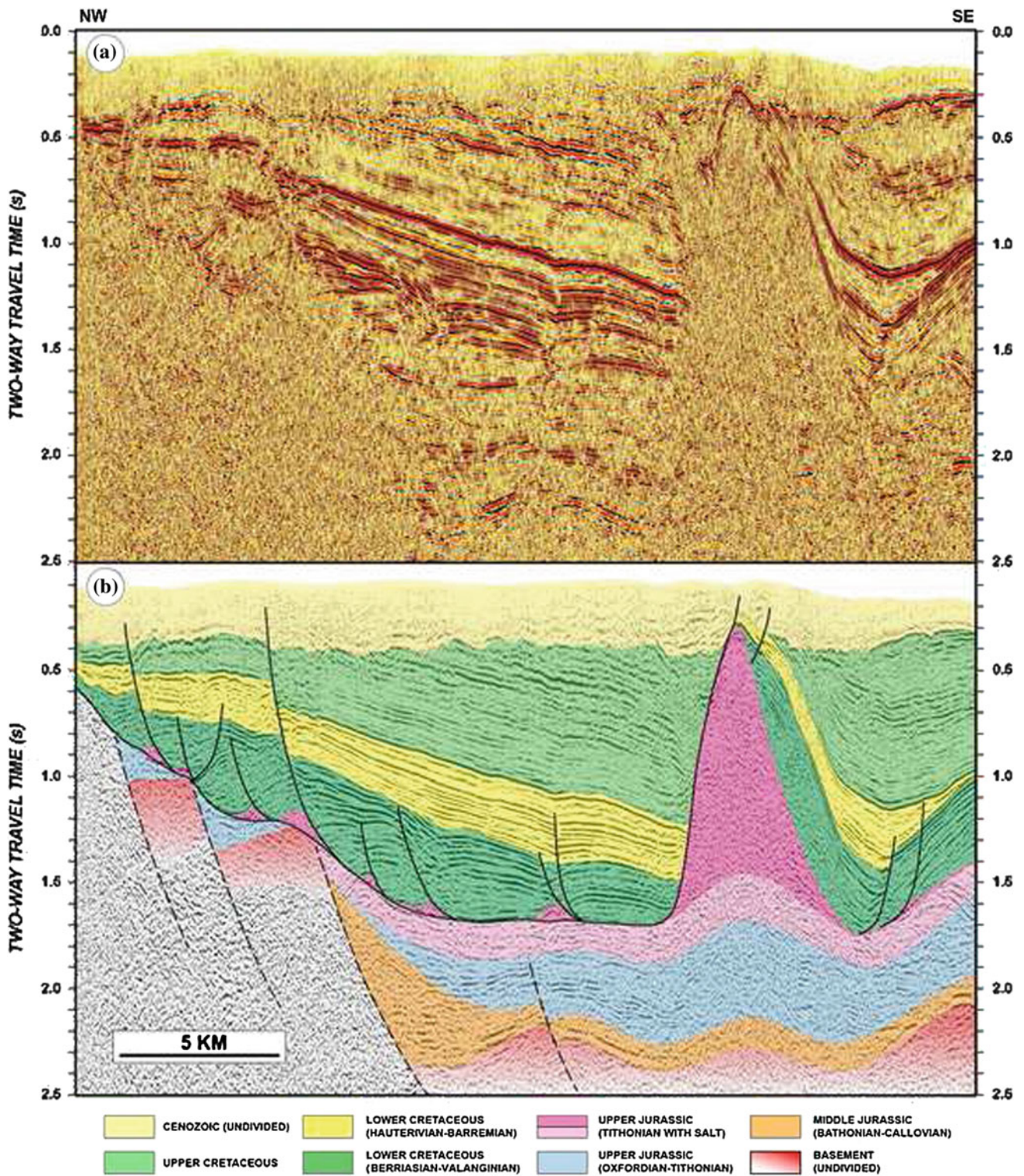


Fig. 14 a Sub-regional 2D seismic section located in the Al Uqlah subbasin of the Sab'atayn Basin (see Fig. 8 for location). b Interpretation of the seismic data, with emphasis on the salt highlighted in magenta. Salt tectonics in this segment of the basin formed “early” salt-rollers involving the Berriasian-Valanginian strata but there some much larger “late” salt rollers as well which formed at the end of

Cretaceous. The large diapir, similarly to the example of Fig. 12, has a marked asymmetry, the northwestern flank being controlled by a major normal fault. The reflection termination of the Upper Cretaceous Tawilah sequence at the base Cenozoic angular unconformity (see Fig. 3) indicates the erosional removal of large portions of the Upper Cretaceous strata

in this segment of the basin formed “early” salt-rollers involving the Berriasian-Valanginian strata. In this example, there is a growth sequence associated with some of the listric faults suggesting ongoing extension during the deposition of the Nayfa in this part of the basin. The larger “late” salt rollers, which formed at the end of Cretaceous, are not as prominent as the ones shown on Fig. 11.

Finally, the salt diapir wall in the southwestern part of the study area (Fig. 8) shows a particular geometry (Fig. 15) suggesting ‘flip-flop’ salt tectonics (sensu Quirk and Pilcher 2012). This particular salt tectonics style refers to salt structures starting out as salt rollers associated with a normal fault detaching down one flank. Then they evolve into asymmetric salt walls when a new fault forms on the opposite flank. In the case of the salt wall shown in Fig. 15, it initially developed as a salt roller with a normal fault on the NE flank. The upper part of this NE-dipping fault can be seen below the intra-Cretaceous unconformity on the SW side of the diapir, in what was originally the footwall. Then, at the end of the Cretaceous, the polarity of the structure

dramatically flipped when a new SW-dipping normal fault formed along the northwestern flank of the diapir so that this side became the hangingwall (Tari et al. 2014).

Map-View Distribution of Salt Tectonics Styles

The observations made on the above described representative seismic sections are summarized in a map-view sense (Fig. 16) using the same top salt time structure map as shown in Fig. 8. Note that the top salt seismic horizon was extended beyond the actual extent of the mobile salt in the basin correlating the age equivalent stratigraphic horizon onto the basement highs around the basin. Therefore the top salt time structure map is also a good regional-scale approximation of the underlying syn-rift structure in this part of the Sab’atayn Basin.

The salt basin is bound by a ca. 80 km long ENE-WSW trending basement fault zone on the north and an almost equally long E-W trending basement fault zone in the south.

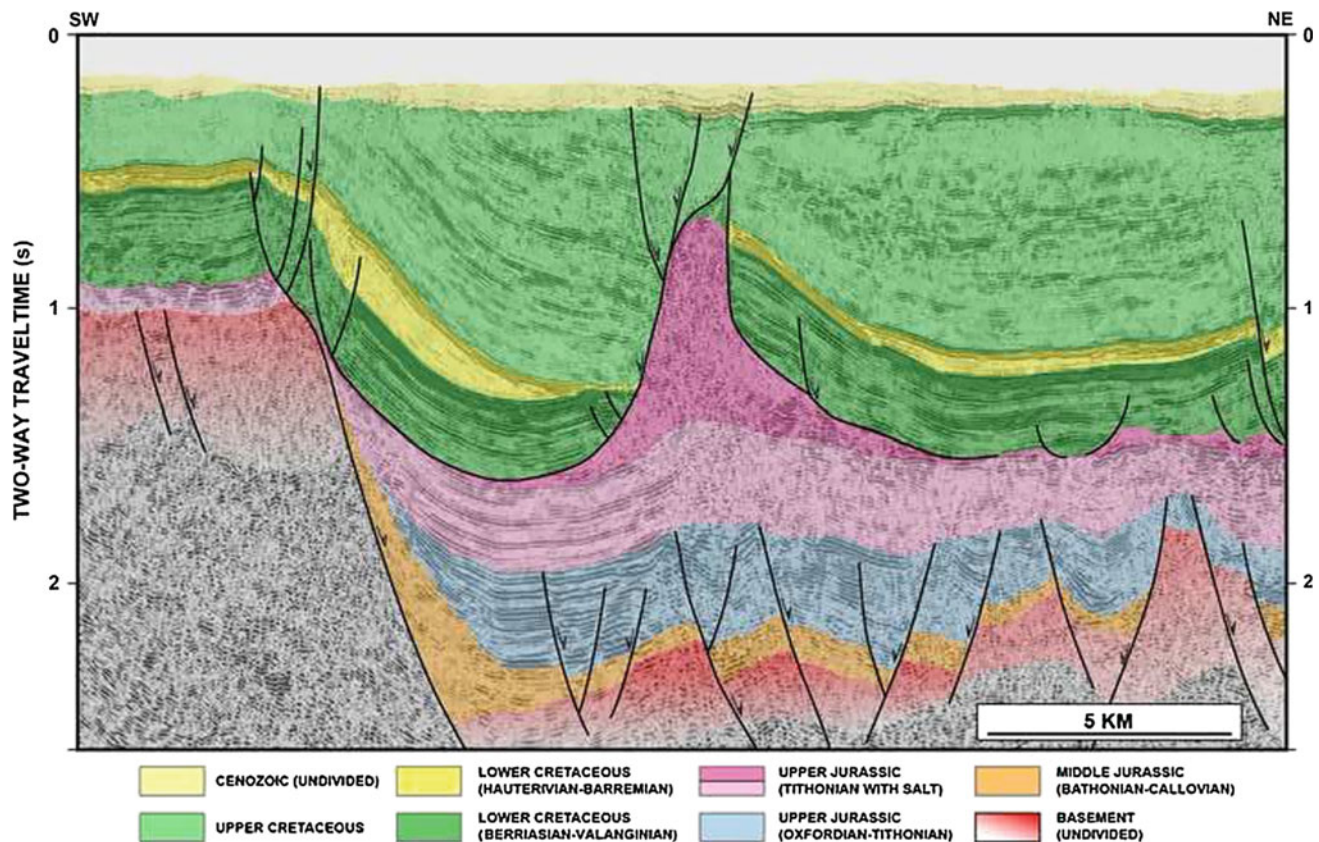


Fig. 15 Sub-regional 2D seismic section located in the Al Uqlah subbasin of the Sab’atayn Basin (see Fig. 8 for location), slightly modified from Tari et al. (2014). The salt diapir has faults detaching on

its flanks suggesting ‘flipflop’ tectonics (sensu Quirk and Pilcher 2012), see text for detailed description

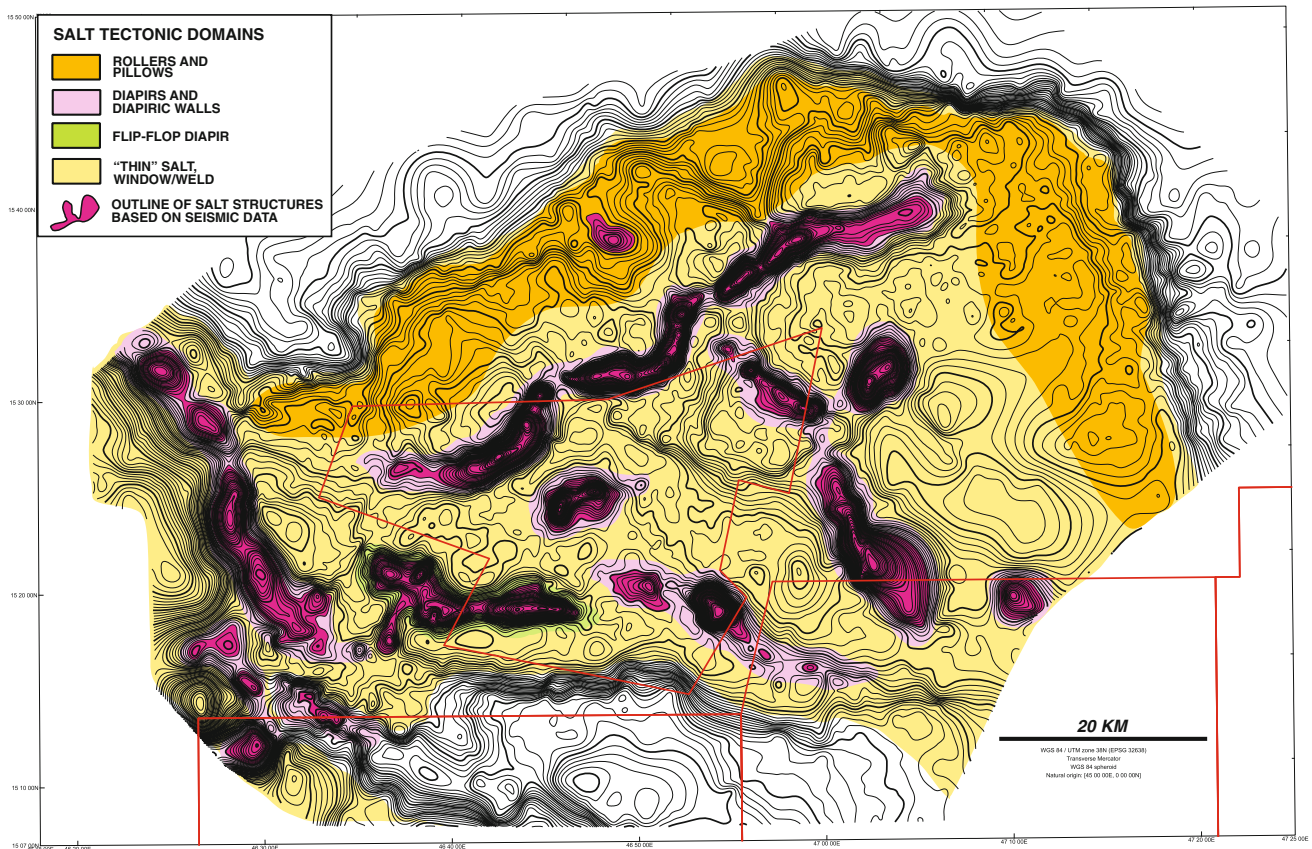


Fig. 16 Simplified salt tectonic domains in the central part of the Sab'atayn Basin. For detailed discussion see text

To the west, there seems to be a connection to the deeper Marib segment of the Sab'atayn Basin. Similarly, the salt seems to be unconfined to the SE (Fig. 16). The salt basin in the study area is segmented into smaller sub-basins which are set up by underlying large normal faults with kilometer-scale offsets at the level of the basement (cf. Fig. 4). The NW-SE to WNW-ESE trending diapiric salt walls appear to follow this underlying structural grain, like in most segments of the Shabwah segment of the Sab'atayn Basin (Fig. 4).

However, roughly perpendicularly, three diapiric walls are lined up in a single ENE-WSW trend in the northern part of the salt basin (Fig. 16). In addition, there are at least three isolated diapirs in the basin which are not part of salt walls.

The salt rollers are distributed along the northern perimeter of the basin and appear to be missing in the southern part. As to the areal extent of thin salt versus the large inflated salt features, the salt windows cover about 90 % of the salt basin (Fig. 16). This illustrates the scale of salt remobilization in the basin from an original salt layer of relatively uniform thickness, given its post-rift character (Tari et al. 2014). Our approximate estimation of the original depositional salt thickness in the central part of the Sab'atayn Basin, using the isochron map of the salt, is about

200 m, slightly less than the 300 m estimation given by Seaborne (1996) for a larger segment of the Sab'atayn Basin.

Temporal Evolution of Salt Tectonics

The following cartoonish description of the evolution of the flip-flop diapiric wall (Tari et al. 2014) in the southern part of the basin (Fig. 15) is intended to illustrate the structural evolution of the basin expressed by the changing styles of salt tectonics (Figs. 17 and 18).

The E-W trending major syn-rift fault, bounding the Central High on its northern flank in the Shabwah Basin (Fig. 4), started to develop as early as the Middle Jurassic (Bathonian-Callovian) shedding coarse continental clastics (Kuhlan Formation) into the basin (Fig. 17). As the basin deepened, the continental clastics were quickly replaced by the marine limestones of the Shuqra Formation, followed by the deeper marine Madbi Formation with its interbedded sandstones in a shale-dominated sequence (Fig. 3). Based on the many 2D reflection seismic examples shown in this paper (Figs. 10–15) the major phase of rifting ceased in the basin before the latest Jurassic as the syn-rift faults typically do not extend up the base of the salt. Tithonian marine shales

Fig. 17 Cartoonish summary of the temporal evolution of salt tectonics in the central part of the Sab'atayn Basin during the Late Jurassic syn-rift and the Early Cretaceous post-rift periods. For detailed discussion see text

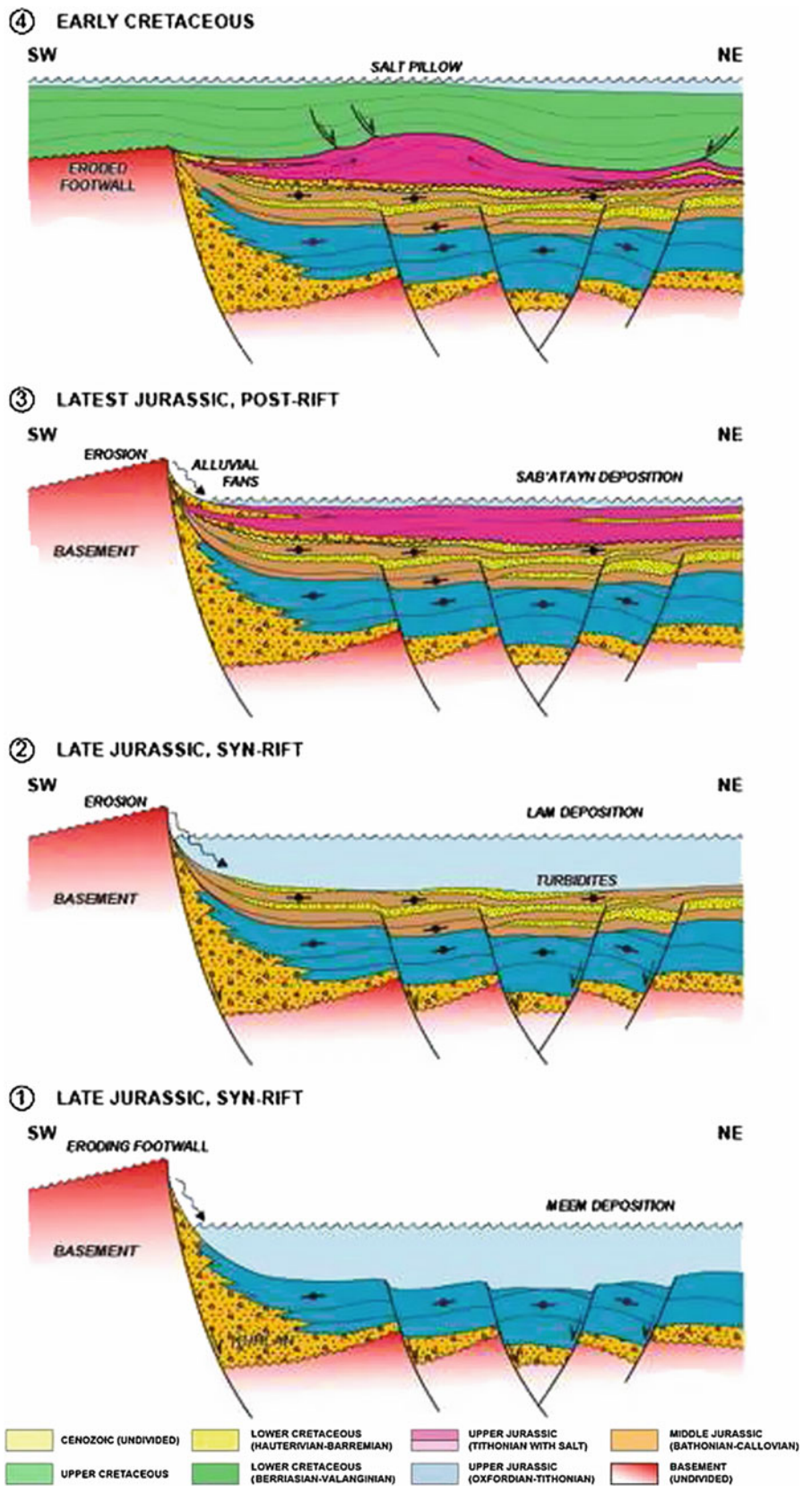
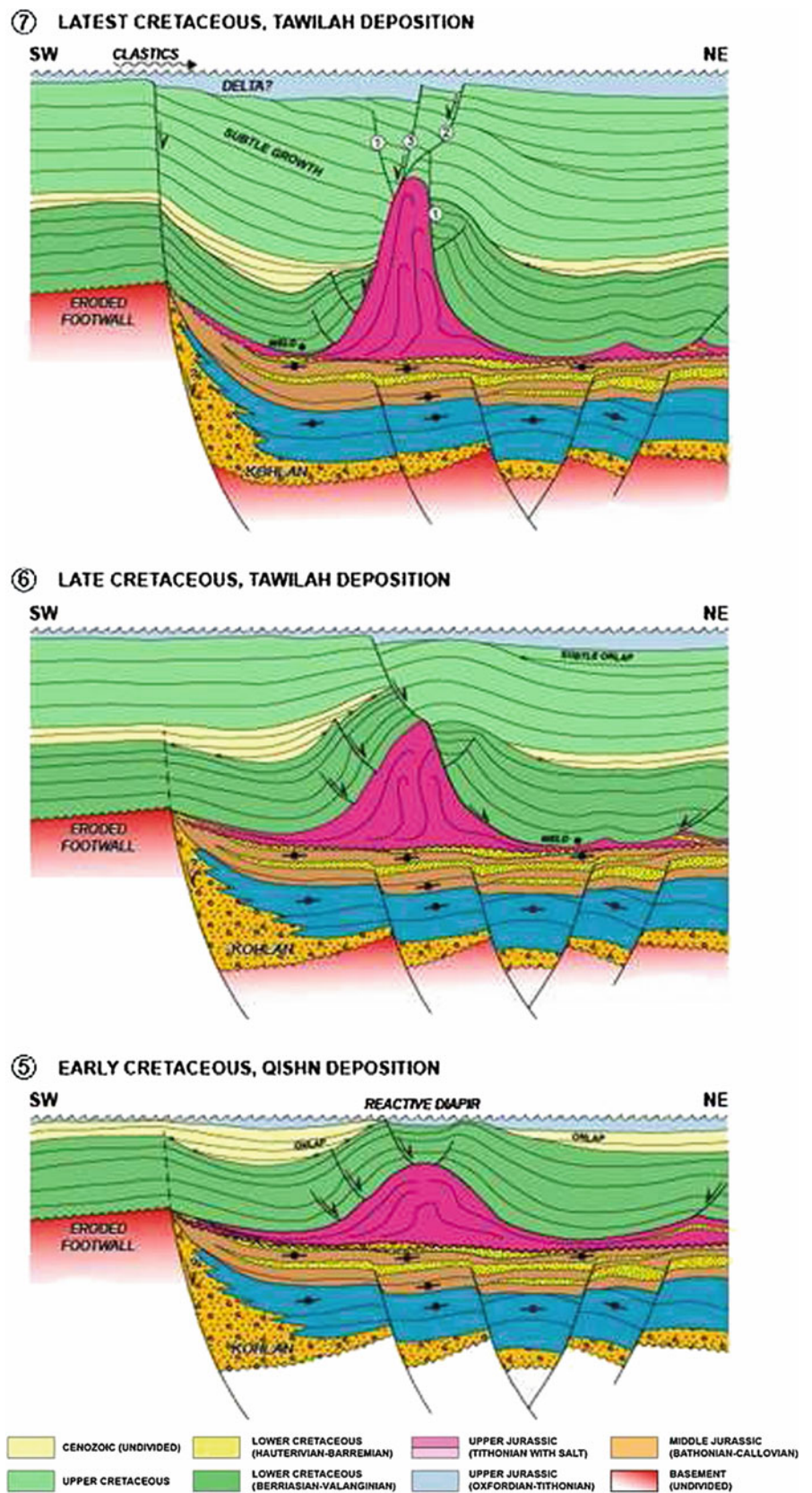


Fig. 18 Cartoonish summary of the temporal evolution of salt tectonics in the central part of the Sab'atayn Basin during the Early and Latest Cretaceous post-rift periods. For detailed discussion see text



were overlain by a sequence of salt and evaporites deposited in salinas during the early post-rift stage (Fig. 3). As the footwall of the large basin-bounding fault was subaerially exposed, large amounts of non-evaporitic materials were intercalated in the evaporites producing a basinwide “dirty” salt sequence, originally 200 m thick, on average.

By the end of the Valanginian, salt rollers and salt pillows started to develop across the basin, as the result of renewed, but low-strain extension during the deposition of the Nayfa and Sa’ar Formations (Fig. 3).

The continuing growth of the initial salt pillows is best recorded by the onlaps of the Qishn sequence (Fig. 18) seen on many seismic examples (e.g. Fig. 15). The salt pillow evolved to a reactive diapir during this time recording ongoing extension across the basin. The passively rising diapir then developed a large normal fault detaching on its basinward flank during the early Tawilah deposition creating a slightly asymmetric salt feature. When a new fault formed on the opposite flank of the diapir during the latest Tawilah deposition, the polarity of the salt diapir flipped (Tari et al. 2014). Note that this last extensional deformation episode also reactivated the large boundary syn-rift fault. As to its overall impact on salt tectonics in the basin, the extensional period at the very end of the Cretaceous (or early Cenozoic?) appears to be the most important.

There is clear seismic evidence for significant erosion of the Tawilah Group in the study area (Tari et al. 2014) as thick packages of parallel reflectors of the Upper Cretaceous strata terminate against the base Cenozoic angular unconformity (Fig. 18). The magnitude of missing Cretaceous section could be at least as much as 500 m based on the truncated geometry of the reflectors. Interestingly, to the NW of the study area, in the Marib segment of the Sab’atayn Basin (Fig. 2) Mitchell and Galbiati (1995) reported uplift and erosion of a *circa* 1000 m thick Cretaceous and Cenozoic sequence due to the Miocene opening of the Red Sea.

Record of Extensional Deformational Stages in the Basement

As the various salt tectonics styles described above are the results of distinct basin-scale extensional periods, the record of the corresponding deformational periods should be found in the basement, below the salt basin. Le Garzic et al. (2011) analysed the scale and geometric properties of extensional fracture systems in basement outcrops to the SE from our study area, in the Mukalla High (Fig. 2). Based on automatically extracted faults in a multi-azimuth 3D seismic cube, derived by an ant-tracking workflow in the Habban Field area (Figs. 4 and 5), Angerer et al. (2011) recognized two major fault sets at the top of the basement (Fig. 19a).

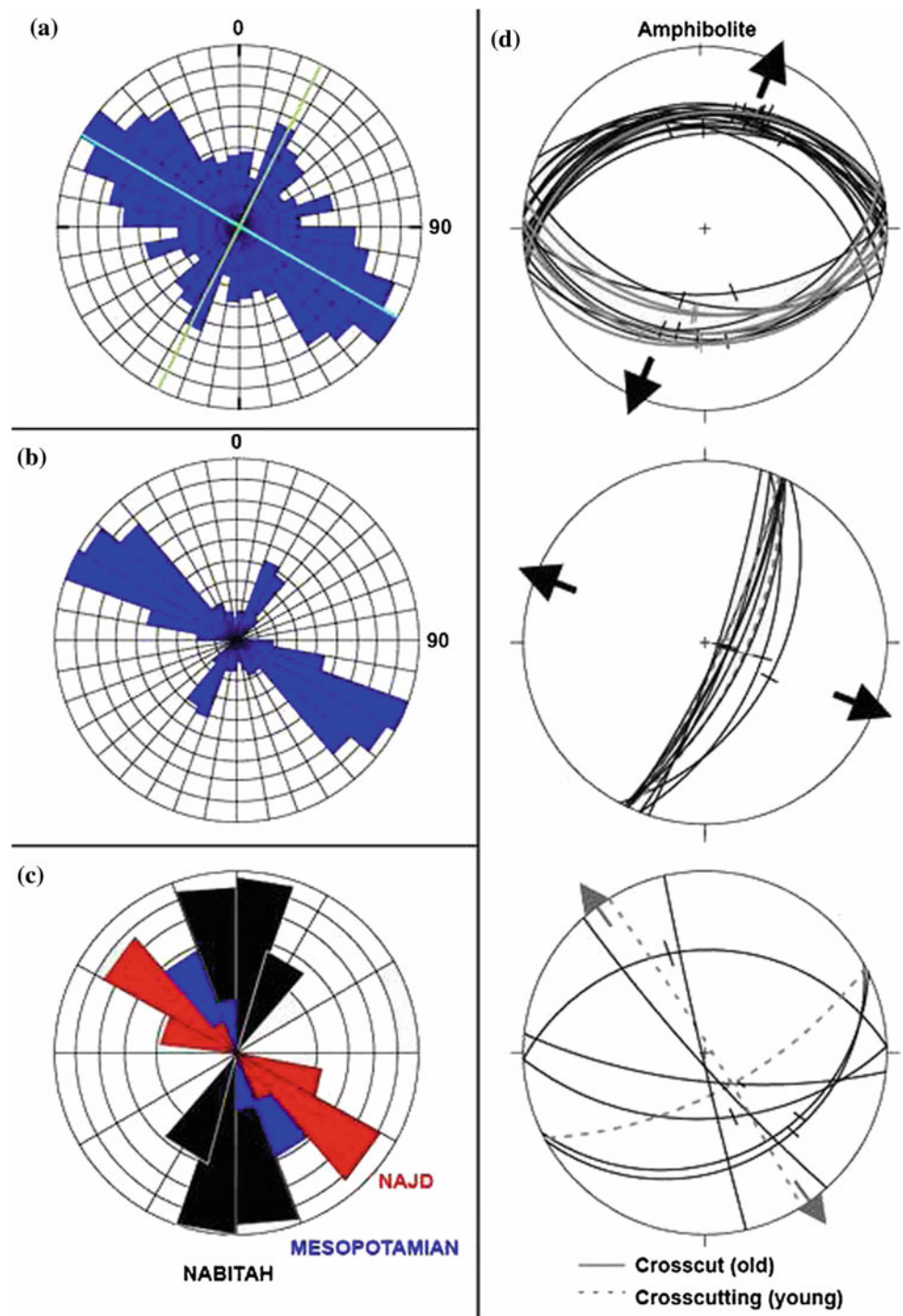
The dominant trend oriented NW-SE could be detected easily whereas the NE-SW trend was often detected at the limit of seismic resolution. Moreover, the NE-SW trend was interpreted by Angerer et al. (2011) as being younger and also aligned with the present-day stress field observed in borehole breakouts. A similar analysis of the same data set integrated more with observations made on drill-cores by Legrand et al. (2011) provided almost identical results (Fig. 19b). Ghiglione and Iftikhar (2012) named the NW-SE trend as the Najd trend and the NE-SW the Hadramawt trend in the Habban Field area.

Interestingly, on the scale of the entire Arabian Peninsula, Zampetti et al. (2009) defined three major fault trends, the N-S “Nabitah”, the WNW-ESE to NW-SE “Najd” and the NW-SE to NNW-SSE “Mesopotamian” trends (Fig. 19c). The Nabitah lineaments were attributed by Zampetti et al. (2009) to N-S trending Neo-Proterozoic (~800–520 Ma) Pan-African shear zones generally younging to the East. The “Najd Event” is understood as a major, Gondwana-scale continental shearing event during the latest Neo-Cambrian to Early Cambrian (e.g. Stern and Johnson 2010). The prevailing steep dips of the Najd structures played a very important role in the subsequent evolution of the Arabian Plate. Oversteps between Najd shear zones formed pull-aparts and pop-ups at many scales, mainly relaying over the NW-SE trending Mesopotamian trends.

At a markedly different scale of observations, i.e. by measuring fractures and foliations in basement drill cores from key wells in the Habban area, Veeningen et al. (2013, 2015) distinguished three deformational episodes (Fig. 19d). The oldest, ductile to brittle deformation (D1), resulting in the cataclastic bands is the oldest deformation feature must have occurred during the Late Ediacaran, at the latest stage or shortly after the Pan-African Orogeny. The timing and the orientation of the cataclasites suggest a close relationship with the NW-SE oriented Najd Fault system of the Arabian Peninsula (Fig. 19c) that was either reactivated or was still active at the time of the cataclastic formation.

The first major purely brittle deformation event (D2) that affected the basement after the Pan-African orogeny occurred during the Late Jurassic. It is characterized by multi-stage extension sub-parallel to the Najd Fault system, forming the Sab’atayn Basin. On the macro-scale (i.e. seismic to outcrop scale) Mesozoic WNW-ESE oriented extensional D2 structures are easy to observe, as they outline the horst-and-graben structure of the Sab’atayn Basin (Fig. 4). On the core scale, D2 is best recognized as faults with NNE and SSW oriented slickensides, suggesting NNE-SSW oriented extension (Fig. 19d). A significant part of the observed fractures in the basement cores displays a spread in orientations which could be due to the multiple pulses of extension which shifted from NNE-SSW (Kimmeridgian) to NE-SW (Tithonian, e.g. Beydoun 1997).

Fig. 19 Comparison of seismic- and core-scale fracture sets in the central part of the Sab'atayn Basin with the regional structural fabric of the Arabian Peninsula. **a** Seismic-scale fault sets at the top of the basement in the Habban Field area based on automatically extracted faults in a multi-azimuth 3D seismic cube, derived by an ant-tracking workflow (Angerer et al. 2011). **b** Seismic-scale faults analysis in the Habban Field area integrated with observations made on drill-cores (Legrand et al. 2011; see also Ghiglione and Iftikhar 2012). **c** Rose diagram showing the three main regional basement fabrics of the Arabian Peninsula: the N-S Nabitah (black), the WNW-ESE to NW-SE Najd (red) and the NW-SE to NNW-SSE Mesopotamian (blue) trends (Zampetti et al. 2009). **d** Fracture and vein orientation data for amphibolite basement cores in the Habban Field area showing three extensional deformation episodes. All data is plotted in a lower hemisphere, equal angle projection (Veeningen et al. 2013, 2015)



The most recent extensional related structures (D3), partially reactivating the older Late Jurassic fractures and generating new fractures in the younger Post-Jurassic rift sediments, were interpreted by Veeningen et al. (2013, 2015) as the expression of the Miocene to Recent opening of the

Red Sea. Within the amphibolite basement core sample (Fig. 19d) D3 forms a set of steeply dipping and foliation parallel fractures and veins that indicate WNW-ESE extension. The fractures locally crosscut structures formed during D2.

Discussion

Our systematic interpretation of salt tectonic styles using the large vintage 2D seismic data sets in the Sabwah segment of the Sab'atayn Basin revealed salt structures which formed as a response to basinwide extension during the Cretaceous. Extensional reactivation of pre-existing Jurassic graben systems are well known from East Africa (e.g. Bosworth 1992; Guiraud et al. 2005). Note that it is the Late Jurassic rifting which is primarily responsible for the formation of the Sab'atayn Basin (Figs. 1 and 2) and the subsequent Cretaceous extensional periods only re-used and modified the pre-existing structural fabric. As of today, there is no quantitative estimation of the relative proportions of Jurassic versus Cretaceous extensional strain across this basin system. However, the various structural observations pertinent to the syn-rift fabric of the Jurassic Sab'atayn Basin (Fig. 19) indicate an NNE-SSW to NE-SW directed extensional stress field shortly before the deposition of the Tithonian evaporite sequence of the Sab'atayn Formation (Fig. 20).

Seismic data shows (Fig. 10) that early salt rollers started to form very shortly after the salt deposition, as early as the Berriasian, due to diminishing extension in the basin. Salt pillows were forming in the more basinward segments of the basin (Fig. 20).

It is not clear whether the extension driving halokinetics in the basin occurred in distinct successive episodes or it was a continuously diminishing process during the Early Cretaceous. The unconformities on top of the Sa'ar and the Qishn Formations, respectively, may reflect the interplay of regional tectonism and global eustatic sea-level changes. On the conjugate margin of the Gulf of Aden, a major pre-Aptian deformational event has been documented (e.g. Ali 2015; Ali and Watts 2015) which caused the absence of the entire Neocomian-Barremian interval. The geodynamics of this event has not been fully understood yet.

The onlaps of the Qishn Formation onto salt pillows and reactive diapirs indicate some extensional deformation across the basin. However, the orientation of the corresponding extensional stress field is somewhat elusive, as the strike of normal faults bounding the early and late salt rollers was determined by the local paleo-slope dipping towards the basin center. Regardless, some of the reactive diapirs evolved into active diapirs and diapiric walls during the early deposition of the Tawilah Group (Fig. 20).

The overall extensional stress field during the Jurassic and Cretaceous seems to be interrupted briefly by a compressional event. There is some evidence for an episode of shortening in the basin during the late Cretaceous (Tari et al. 2014). The present-day geometry of the salt rollers situated above the basin-bounding fault system (Fig. 11) suggests an element of shortening as their crests do not fall below the top

Qishn Formation regional seismic marker horizon (cf. Tari et al. 2014, their Fig. 8). If correct this may be the signature of the intra-Santonian period of regional compression in Africa (Guiraud and Bosworth 1997; Guiraud et al. 2005) in the central part of the Sab'atayn Basin (Fig. 20). The definitive age-dating of salt tectonics during the Late Cretaceous is limited by the fact that the subsurface continental clastics within Tawilah Group, spanning the entire Albian to Maastrichtian interval (Fig. 2), cannot be more precisely subdivided in the study area at present.

Given the falling diapiric wall (Fig. 13), the large normal faults detaching on the flanks of diapiric salt walls (Fig. 12), including the flip-flop diapir wall itself (Fig. 15) the most important extensional period recorded by the salt tectonics in the basin is interpreted as uppermost Senonian in age (Fig. 20).

In Syria, major NW to WNW-oriented Senonian grabens are known, e.g. the Euphrates Trough (e.g. Barrier et al. 2014). The main pulse of rifting in these Syrian basins is reported to be Campanian in age. This regional extensional tectonics was coeval with the obduction of the Neo-Tethyan ophiolites onto the Northern Arabian platform and, as a far-field effect, it could have been responsible for the observed drastic change in salt tectonics in the study area at the southern part of the Arabian Plate.

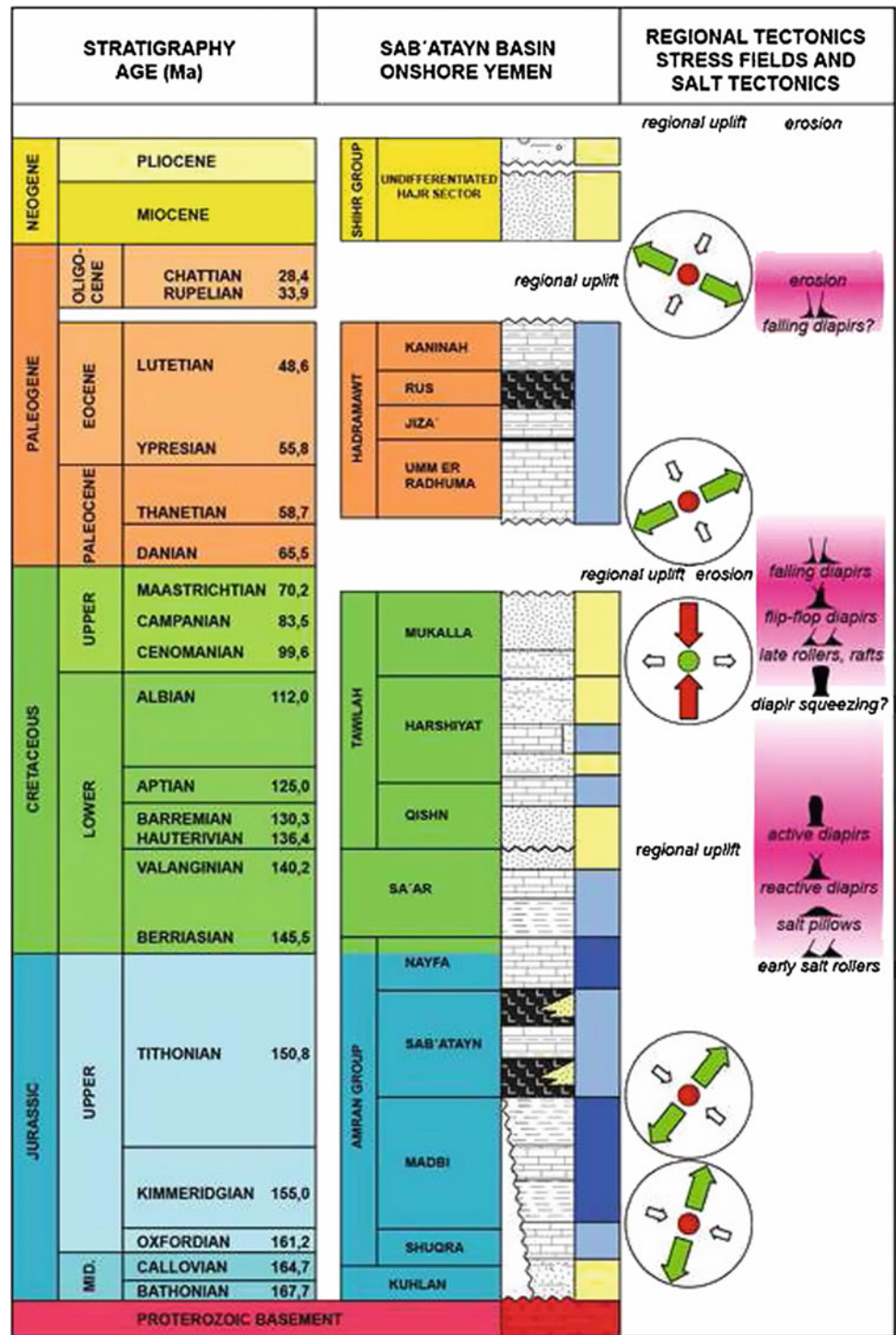
Finally, a different challenge is posed by the general lack of seismically resolved subsurface Cenozoic sediments in the study area leaving the post-Cretaceous evolution of salt structures unconstrained. It is likely that additional extensional episodes reactivated the Sab'atayn salt basin during the Cenozoic (Fig. 20). For example, the NE-SW trending diapir salt wall bounded by large concave-to-the-NW fault segments detaching on its northwestern flank (Figs. 8 and 14) might have been reactivated during the Oligocene as the result of the initial rifting in the Red Sea area (Bosworth et al. 2005). The geometries observed on some of the seismic sections (e.g. Fig. 12) and at the outcropping salt diapirs (Figs. 6 and 7) suggest considerable amount of erosional truncation of the diapirs, perhaps during the Pliocene to Quaternary (Fig. 20).

Conclusions

Numerous salt tectonic features can be interpreted on 2D seismic reflection data in the Sabwah segment of the Sab'atayn Basin of western Yemen. The early post-rift Tithonian Sab'atayn Formation shows a range of salt tectonic styles ranging from salt rollers, salt pillows, reactive, flip-flop, active and falling diapirs and diapiric walls.

Halokinetics driven by renewed extension began as soon as the early Cretaceous, pre-dating the basinwide top Valanginian unconformity. This extensional period is

Fig. 20 Summary of the temporal evolution of salt tectonics in the central part of the Sab'atayn Basin during the Jurassic syn-rift and the Cretaceous/Cenozoic post-rift periods. The stratigraphic synopsis on the left is adapted from As-Saruri and Sorkhabi (2014), for lithologic legend see Fig. 3. The inferred stress regimes are illustrated by using the subdivision of Delvaux et al. (1997), i.e. the length and colour of arrows symbolise the horizontal deviatoric stress magnitude, relative to the isotropic stress. *Green outward arrows*: extensional deviatoric stress, *red inwards arrows*: compressional deviatoric stress. We infer the presence of extensive to transpressive stress fields during the post-middle Jurassic development of the Sab'atayn Basin, triggering and driving salt tectonics, like in many other salt basins of the world (Vendeville and Jackson, 1992a, b). The only compressional episode shown is the regional "intra-Santonian event" (Guiraud and Bosworth, 1997; Guiraud et al. 2005). See text for a detailed discussion



regionally correlated with rifting in East Africa, including Sudan, Ethiopia and Somaliland. Even though the regional extension was of a low-strain type, only slightly reactivating the Jurassic structural fabric, it triggered the formation of salt rollers in the northern part of the study area. The overlying Qishn Formation recorded further growth of salt pillows, reactive and active diapirs due to ongoing extension in the

basin. A major pulse of basin-wide extension at the end of the Cretaceous had a major impact on the existing salt features in the basin forming diapiric salt walls with detached normal faults on their updip flanks. As to its overall impact on salt tectonics in the basin, this poorly dated latest Cretaceous to earliest Cenozoic extensional period appears to be the most important in the Sab'atayn Basin.

Acknowledgments The Petroleum Exploration and Production Authority of Yemen (PEPA) is acknowledged for the permission to publish this work. We appreciate the editorial patience of Francois Roure and the helpful and detailed reviews by two anonymous reviewers and Mustafa As-Saruri. The seismic interpretation technique named “Napoleon’s hat” was coined by Albert Bally and it was introduced to the first author of this paper in the late 1980s, in the context of mapping salt detachments in thrust-fold belts. Conversations about the pre-salt prospectivity of the Sab’atayn Basin with Alan Holmes, Michael Bierbaumer, Isabella Zabalza, Pascal Neff, Erika Angerer, Robert McDonald, Leo Kreczy and Shaista Sultan were helpful. DigitalGlobe is thanked for providing the high-resolution satellite image shown in Fig. 6. Peter Pernegr is thanked for drafting most of the figures.

References

- Ahlbrandt TS (2002) Madbi Amran/Qishn total petroleum system of the Ma’Rib–Al Jawf/Shabwah, and Masila-Jeza Basins, Yemen. *U. S. Geol Surv Bull* 2202-G:28 p
- Ali MY (2015) Petroleum geology and hydrocarbon potential of the Guban Basin, northern Somaliland. *J Petr Geol* 38:433–457
- Ali MY, Watts AB (2015) Tectonic evolution of sedimentary basins of northern Somalia. *Basin Res* 27:1–25
- Alsharhan AS, Nairn AEM (1997) Sedimentary basins and petroleum geology of the Middle East. Elsevier, 843 p
- Angerer E, Neff P, Abbasi I, Ghiglione G (2011) Integrated reservoir characterization of a fractured basement reservoir. *Lead Edge* 30:1408–1413
- As-Saruri M, Sorkhabi R, Baraba RS (2010) Sedimentary basins of Yemen: their tectonic development and lithostratigraphic cover. *Arab J Geosci* 3:515–527
- As-Saruri MA, Sorkhabi R (2014) Petroleum systems and basins of Yemen. In: Marlow L, Kendall C, Yose L (eds) *Petroleum systems of the Tethyan region*. AAPG Memoir, vol 106, pp. 757–780
- Autin J, Bellahsen N, Leroy S, Husson L, Beslier MO, d’Acremont E (2013) The role of structural inheritance in oblique rifting: insights from analogue models and application to the Gulf of Aden. *Tectonophysics* 607:51–64
- Barrier E, Machhour L, Blaizot M (2014) Petroleum systems of Syria In: Marlow L, Kendall C, Yose L (eds) *Petroleum system of the Tethyan Region*. AAPG Memoir, vol 106, pp. 335–378
- Beydoun, ZR (1964) The stratigraphy and structure of Eastern Aden Protectorate Overseas Geology. In: *Overseas geology and mineral resources*, supplementary series, Bulletin Supplement, vol 5. HMSO, London, pp. 1–107
- Beydoun ZR (1997) Introduction to the revised Mesozoic stratigraphy and nomenclature for Yemen. *Mar Pet Geol* 14:617–629
- Beydoun ZR, As-Saruri ML (1998) Phanerozoic depositional basins and inter-basinal highs of Yemen: their structural framework and sedimentary cover. *Zeitschrift für Geologische Wissenschaften* 26:517–529
- Beydoun ZR, As-Saruri ML, Baraba’ RS (1996) Sedimentary basins of the Republic of Yemen: their structural evolution and geological characteristics. *Revue de l’Institute Francais du Petrole* 51:763–775
- Beydoun ZR, As-Saruri MAL, El-Nakhal H, Al-Ganad IN, Baraba RS, Nani ASO, Al-Aawah MH (1998) International lexicon of stratigraphy, Volume III, Republic of Yemen, 2nd edn. In: *International union of geological sciences and ministry of oil and mineral resources*, vol 34. Republic of Yemen Publication, 245 p
- Bosence DWJ (1997) Mesozoic rift basins of Yemen. *Mar Pet Geol* 14:611–616
- Bosworth W (1992) Mesozoic and early Tertiary rift tectonics in East Africa. *Tectonophysics* 209:115–137
- Bosworth W, Huchon P, McClay K (2005) The red sea and gulf of aden basins. *J African Earth Sci* 43:334–378
- Brannan J, Sahota G, Gerdes KD, Berry JAL (1999) Geological evolution of the central Marib-Shabwa Basin, Yemen. *GeoArabia* 4:9–34
- Csato I (2005) Extensional tectonics and salt structures, Marib-Shabwa Basin, Yemen. Search and discovery Article # 30030
- Csato I, Habib A, Kiss K, Koncz I, Kovacs Z, Lorincz K, Milota K (2001) Play concepts of oil exploration in Yemen. *Oil Gas J* 99:68–74
- Davison I, Al-Kadasi M, Al-Khribash S, Al-Subbary AK, Baker J, Blakey S, Bosence D, Dart C, Heaton R, McClay K, Menzies M, Nichols G, Owen G, Yelland A (1994) Geological evolution of the southeastern Red Sea rift margin, Republic of Yemen. *Geol Soc America Bull* 106:1474–1493
- Davison I, Bosence, DWJ, Alsop GI, Al-Aawah MH (1996) Deformation and sedimentation around active Miocene salt diapirs on the Tihama plain, northwest Yemen. In: Alsop GI, Blundell DJ (eds) *Salt tectonics: geological society, London, Special Publication*, vol 100, pp. 23–39
- Delvaux D, Moeys R, Stapel G, Petit C, Levi K, Miroshnichenko A, Ruzhich V, San’kov V (1997) Paleostress reconstructions and geodynamics of the Baikal region, central Asia, Part 2. Cenozoic rifting. *Tectonophysics* 282:1–38
- Duval B, Cramez C, Jackson MPA (1992) Raft tectonics in the Kwanza basin. *Angola Mar Petr Geol* 9:389–404
- El-Anbaawy MIH, Al-Awaah MH, Al-Thour KA, Tucker M (1992) Miocene evaporites of the Red Sea rift, Yemen Republic: sedimentology of the Salif halite. *Sed Geol* 81:61–71
- Ellis AC, Kerr HM, Cornwell CP, Williams DO (1996) A tectonostratigraphic framework for Yemen and its implications for hydrocarbon potential. *Petrol Geosci* 2:29–42
- Fairchild R (1992) Yemen oil hunt—a gift from the gods. In: Hatley AG Jr (ed) *The oil finders*. American Association of Petroleum Geologists Special Publication, pp. 127–134
- Fournier M, Chamot-Rooke N, Petit C, Huchon P, Al-Kathiri A, Audin L, Beslier MO, d’Acremont E, Fabbri O, Fleury JM, Khanbari K (2010) Arabia-Somalia plate kinematics, evolution of the Aden-Owen-Carlsberg triple junction, and opening of the Gulf of Aden. *J Geophys Res: Solid Earth* 115(B4)
- Ghiglione G, Iftikhar A (2012) Tectonic discontinuities analysis using seismic and well datasets in a fractured basement reservoir. In: Abu Dhabi international petroleum conference and exhibition. Society of Petroleum Engineers, SPE 162399
- Granath JW (2001) The Nogal rift of northern Somalia: Gulf of Aden, reactivation of a Mesozoic rift. *Mémoires du Muséum national d’histoire naturelle* 186:511–527
- Guiraud R, Bosworth W (1997) Senonian basin inversion and rejuvenation of rifting in Africa and Arabia: synthesis and implications to plate-scale tectonics. *Tectonophysics* 282:39–82
- Guiraud R, Bosworth W, Thierry J, Delplanque A (2005) Phanerozoic geological evolution of Northern and Central Africa: an overview. *J Afr Earth Sci* 43:83–143
- Hakimi MH, Abdullah WH (2013) Geochemical characteristics of some crude oils from Alif Field in the Marib-Shabowah Basin, and source-related types. *Mar Pet Geol* 45:304–314
- Hakimi MH, Abdullah WH, Shalaby MR (2011) Organic geochemical characteristics and depositional environments of the Jurassic shales in the Masila Basin of Eastern Yemen. *GeoArabia* 16:47–64
- Hall DM, Le Nen P (2014) Subsalt exploration for fractured basement play in Sabatayn Basin, Yemen. In: *Third EAGE exploration workshop*, Abu Dhabi, United Arab Emirates, 6–9 April 2014, extended abstract EW08

- Heathon RC, Jackson MPA, Bamahmoud M, Nani ASO (1996) Superposed neogene extension, contraction, and salt canopy emplacement in the Yemeni Red Sea. In: Jackson MPA, Roberts DG, Snelson S (eds) Salt tectonics: a global perspective: AAPG memoir, vol 65, pp. 333–351
- Huchon P, Jestin F, Cantagrel JM, Gaulier JM, Al Khirbash S, Gafaneh A (1991) Extensional deformations in Yemen since Oligocene and the Africa-Arabia-Somalia triple junction. *Ann Tectonicae* 5:141–163
- Jungwirth J, As-Saruri ML (1990) Structural evolution of the platform cover on Southern Arabian Peninsula. *Z Geol Wiss* 18:505–514
- Le Garzic E, De L'hamaide T, Diraison M, Geraud Y, Sausse J, De Urreiztieta M, Hauville B, Champanhet J-M (2011) Scaling and geometric properties of extensional fractures systems in the Proterozoic basement of Yemen. Tectonic interpretation and fluid flow implications. *J Struct Geol* 33:519–536
- Leckie DA, Rumpel T (2003) Tide-influenced sedimentation in a rift basin—Cretaceous Qishn formation, Masila Block, Yemen: a billion barrel oil field. *Am Assoc Petrol Geol Bull* 87:987–1013
- Legrand N, De Kok J, Neff P, Clemens T (2011) Recovery mechanisms and oil recovery from a tight, fractured basement reservoir, Yemen. *SPE Reservoir Eval Eng* 14:473–484
- Leroy S, Razin P, Autin J, Bache F, d'Acremont E, Watremez L, Robinet J, Baurion C, Denèle Y, Bellahsen N, Lucazeau F (2013) From rifting to oceanic spreading in the Gulf of Aden: a synthesis. In: Al Hosani K, Roure F, Ellison R, Lokier S (eds) Lithosphere dynamics and sedimentary basins: the Arabian plate and analogues. Springer, Berlin Heidelberg, pp. 385–427
- McDonald R (2005) Reservoir potential and facies distribution of the Upper Jurassic Lam Member, Yemen. MSc thesis, Department of Geology, Royal Holloway, University of London, 67 p
- Mitchell G, Galbiati LD (1995) Tectonic and stratigraphic framework of the Marib-Jawf Basin, Yemen. In: Bosence DWJ (ed) Rift sedimentation and tectonics in the Red Sea-Gulf of Aden region, Abstract volume. Sana'a, Yemen, p. 43
- Quirk DG, Pilcher RS (2012) Flip-flop salt tectonics. *Geol Soc, London, Spec Publ* 363:245–264
- Redfern P, Jones JA (1995) The interior rifts of the Yemen—analysis of basin structure and stratigraphy in a regional plate tectonic context. *Basin Res* 7:337–356
- Sachsenhofer RF, Bechtel A, Dellmour RW, Mobarakabad AF, Gratzner R, Salman A (2012) Upper Jurassic source rocks in the Sab'atayn Basin, Yemen: depositional environment, source potential and hydrocarbon generation. *GeoArabia* 17:161–186
- Schull TJ (1988) Rift basins of interior Sudan: petroleum exploration and discovery. *AAPG Bull* 72:1128–1142
- Seaborne TR (1996) The influence of the Sabatayn evaporites on the hydrocarbon prospectivity of the Eastern Shabwa Basin, Onshore Yemen. *Mar Petr Geol* 13:963–972
- Stern RJ, Johnson P (2010) Continental lithosphere of the Arabian Plate: a geologic, petrologic, and geophysical synthesis. *Earth Sci Rev* 101:29–67
- Tari G, Dellmour R, Rodgers E, Sultan S, Al Atabi A, Daud F, Salman A (2014) Seismic expression of salt tectonics in the Sab'atayn Basin, onshore Yemen. *Interpretation* 2:SM91–SM100
- Towner B, Lindsay R (2000) Subsalt success in the Republic of Yemen, using 3-D AVO and integrated exploration. *Lead Edge* 19:1064–1142
- Veeningen R, Rice H, Schneider D, Grasemann B, Decker K (2013) Structural analysis of a fractured basement reservoir, central Yemen. *EGU Gen Assembly Conf Abstr* 15:4464
- Veeningen R, Rice AHN, Schneider DA, Grasemann B (2015) Thermochronology and geochemistry of the Pan-African basement below the Sab'atayn Basin, Yemen. *J African Earth Sci* 102:131–148
- Vendeville BC, Jackson MPA (1992a) The rise of diapirs during thin-skinned extension. *Mar Petr Geol* 9:331–353
- Vendeville BC, Jackson MPA (1992b) The fall of diapirs during thin-skinned extension. *Mar Petr Geol* 9:354–371
- Watchorn F, Nichols GJ, Bosence DWJ (1998) Rift-related sedimentation and stratigraphy, southern Yemen (Gulf of Aden). In: Purser BH, Bosence DWJ (eds) Sedimentation and tectonics of rift basins: Red Sea-Gulf of Aden. Chapman and Hall, London, pp 165–189
- Zabalza IA, Legrand N, Neff P (2012) An integrated history matching approach of a fractured basement reservoir-block S2, Yemen. In: Abu Dhabi international petroleum conference and exhibition. Society of Petroleum Engineers, SPE 162398-PP
- Zampetti V, Borkhataria R, Koopman A, Vroon M, van Oosterhout C (2009). Structural control on permo-triassic deposition in the Central Arabian Plate: a multi-scale approach. In: IPTC 2009: international petroleum technology conference, IPTC 13686
- Ziegler MA (2001) Late Permian to Holocene paleofacies evolution of the Arabian Plate and its hydrocarbon occurrences. *GeoArabia* 6:445–504

The Effect of the Palmyra Trough and Mesozoic Structures on the Levant Margin and on the Evolution of the Levant Restraining Bend

Ramadan Galhyani, Jean-Marc Daniel, Catherine Homberg, Fadi Henri Nader, Romain Darnault, Jean-Marie Mengus, and Eric Barrier

Abstract

The central Levant margin is characterised today by a restraining bend, part of the Levant Fracture System (LFS) delineating the north-western boundary of the Arabian Plate. This area has been affected throughout geological times by several tectonic events, resulting, in particular, in deep crustal faults oriented oblique to the main NNE trending sinistral strike-slip plate boundary. These faults, together with other structures along the Levant margin, are similar to those found eastward in the Palmyra Basin. In this study, we tested the hypothesis that the Palmyra Basin extends westward to the Levant margin through sandbox analogue modelling. We examined the role of pre-existing oblique structures, believed to be part of the Palmyra Basin, on the development of the Levant restraining bend. Results indicated a similarity between the model and the natural example asserting the effect of the pre-existing structures on the growth of the restraining bend. Consequently, the pre-existing structures, which are believed to be part of the Palmyra basin structural system, attest that the latter extends westward to the Levant margin forming its westward termination. The evolution and propagation of the LFS were thus impacted by the presence of the Palmyra Basin and the resulting crustal thickness variations, bending the LFS and creating three different segments along its path.

Keywords

Levant Fracture System • Palmyra Basin • Mount Lebanon • Analogue modelling

Introduction

The Levant margin runs from Sinai to North-west Syria and is located between three large geological elements: the Levant Basin, the Palmyra Basin and the Levant Fracture System (LFS) (Fig. 1). The latter is a major sinistral

transform plate boundary forming the northwest limit of the Arabian plate (Dubertret 1955; Quennell 1958). In this paper we discuss primarily its central segment with its respective central Levant margin. The Palmyra Basin is an intracratonic Mesozoic basin found eastward of the LFS, which accumulated a great thickness of Mesozoic sediments (Chaimov et al. 1992; Searle 1994; Brew et al. 2001b). The rifting event that was responsible for the creation of Palmyra has also resulted in numerous NE trending normal faults found in the entire Levant region in Palmyra, across the Levant margin and in Egypt (Fig. 2).

The establishment of the LFS during the Late Miocene/Pliocene and the creation of a restraining bend along the central Levant margin is the most recent tectonic event in this region (Quennell 1958, 1984; Ben-Avraham

R. Galhyani (✉) · C. Homberg · E. Barrier
Sorbonne Universités, UPMC Univ Paris 06,
UMR 7193, ISTeP, 75005 Paris, France
e-mail: Ramadan.ghalayini@ifpen.fr

R. Galhyani · C. Homberg · E. Barrier
CNRS, UMR 7193, ISTeP, 75005 Paris, France

R. Galhyani · J.-M. Daniel · F.H. Nader · R. Darnault ·
J.-M. Mengus
Geosciences, IFPEN, 1–4 Avenue de Bois-Préau,
92852 Rueil-Malmaison Cedex, France

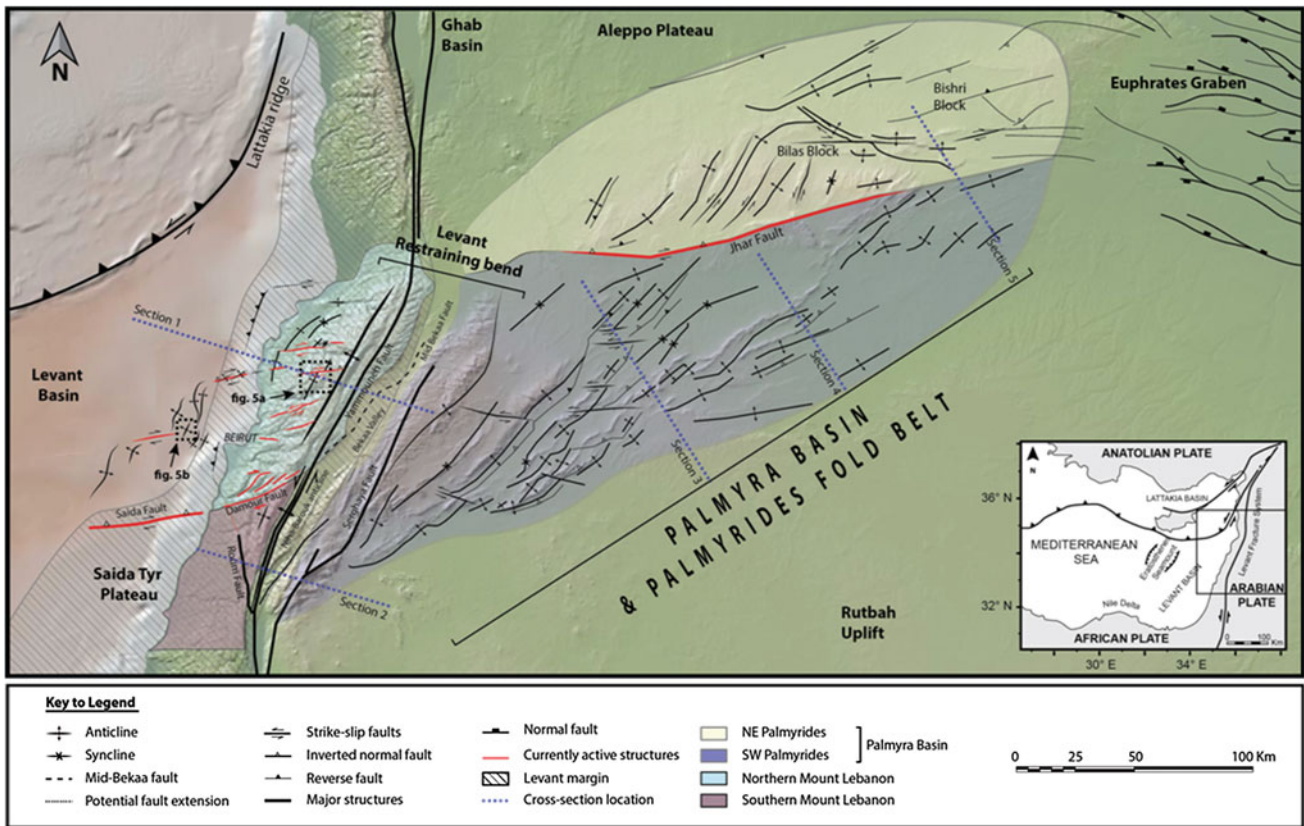
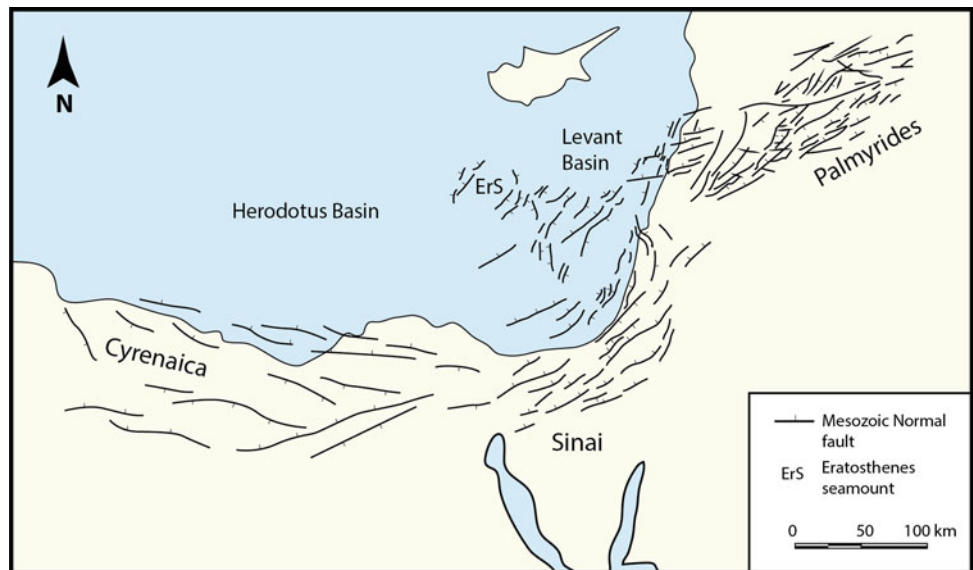


Fig. 1 Map showing the structural elements of the Levant region and the current geographic delineation of the Palmyra Basin with its separation into a north-eastern and a south-western part, together with the adjacent northern and southern Mount Lebanon. The Levant

Margin is shown to the west, encompassing Mount Lebanon and part of the Yammouneh Fault. Map compiled from Ghalayani et al. 2014, Brew et al. 2001a, b, Walley 1998, Searle 1994 and Dubertret 1955

Fig. 2 Map showing the location of the Mesozoic extensional structures found, from west to east, in the Cyrenaica, Egyptian western desert, Sinai, the Levant Margin and the Palmyra Basin. Map compiled from Walley 1998, Gardosh et al. 2010, Frizon de Lamotte et al. 2011 and Arsenikos et al. 2013



1978; Hancock and Atiya 1979; Gomez et al. 2006). The Levant restraining bend is compartmentalised with latitudinal faults separating structurally different blocks (Hancock and Atiya 1979; Walley 1998). The northern Mount

Lebanon is similar to a symmetric box-fold anticline cross-cut by a number of ENE-WSW dextral strike-slip faults (Dubertret 1955; Walley 1998). It is separated from the southern Mount Lebanon by the Damour fault, a deep

fault zone, currently active, consisting of ENE-WSW trending nearly vertical dextral strike-slip faults (Hancock and Atiya 1979) (Fig. 1). These ENE-WSW latitudinal faults are believed to be old Mesozoic rift structures currently active as a dextral strike-slip (Dubertret 1955; Sabbagh 1961; Ghalayini et al. 2014).

The variation in structural styles along strike in Mount Lebanon is in fact intriguing. In an effort to explain this, Walley (1998) makes an analogy between the different compartments along Mount Lebanon with the southern and northern Palmyrides without proposing a mechanical model to explain such variability. He attributes the structural styles along the Levant restraining bend to be an extension of the Palmyrides fold belt into Lebanon, making northern Mount Lebanon part of the northern Palmyrides, while southern Mount Lebanon is part of the southern Palmyrides. It is very likely that Mount Lebanon is affected by the pre-existing Mesozoic structures of the greater Palmyra basin, the latter having a strong impact on its geometry and evolution, similarly to the Palmyrides fold belt.

Large uncertainties prevail today regarding the growth and evolution of the central segment of the LFS. They involve mainly the initial timing of structuration, the role of pre-existing structures, notably the adjacent Palmyra Basin. A number of authors insinuate that the Palmyra Basin stops near the political boundary between Lebanon and Syria (Hancock and Atiya 1979; Butler and Spencer 1999; Elias et al. 2007; Carton et al. 2009), and advocate that the present day Levant margin and its restraining bend in Lebanon are recent structures acting independently of the Palmyrides fold belt or pre-existing structures. However, the similarity of structures along the Levant Margin and the Palmyra Basin argue for a common geologic history (Fig. 2).

In this paper, we acknowledge the role of older tectonic episodes and examine the effect of pre-existing structures on the evolution of the central Levant margin through analogue modelling. Few studies were targeted to understand the evolution of the LFS through modelling, in particular the strain partitioning and efficiency of the Levant restraining bend (Hatem et al. 2015), the rift-like morphology of the southern segment in light with plate kinematics (Smit et al. 2010), the propagation of the LFS simultaneously from the north and the south (Hardy 2009) and the effect of NW oblique structuration on the nucleation and propagation of the initial southern segment of the LFS (Segev et al. 2014).

We emphasize in this study on a particularly important set of structures consisting of currently active ENE-WSW dextral strike-slip faults found onshore and offshore (Fig. 1). The implications of the modelling performed in this study is important, as few authors tried to extend the Palmyra Basin westward to Lebanon (e.g. Searle 1994; Walley 1998; Beydoun 1999; Nader 2011) while most of the authors prefer to separate Lebanon from the Palmyra Basin. The pre-existing

structures must have played an important role in affecting the style of deformation along the central margin, and resulted in the complex structural setting of the Levant region. The southern margin in Israel has been similarly affected by the northwest propagating Azraq-Sirhan graben resulting in right-stepping fault segments formed on the northern side of the pre-existing weak zone (Segev et al. 2014). We propose in this study that the compartmentalisation, or segmentation of the Levant restraining bend with variable structural styles in northern and southern Mount Lebanon is attributed to decoupling along ENE-WSW oblique faults, which reactivated deeper structures interpreted as the westward continuation of the larger Mesozoic Palmyra basin below the present day Levant margin.

The outline of this paper consists of a review of the regional geology discussing the evolution of the central Levant margin and the Palmyra Basin. Results of recent analogue modelling are then presented, aiming to test the role of pre-existing structuration with respect to the development of restraining bends. Consequently, we propose a common geologic history for the Palmyra Basin and the central Levant margin.

Regional Geology

Main Tectonic Provinces

The NW Arabian Plate is located close to the intersection with the Arabian-African plate boundary along the LFS and the Arabian-Anatolian plate boundary along the Taurus Mountains. Important structures are found in this domain, namely the Palmyrides ranges, the Jhar fault, the LFS, Lebanese mountain ranges, the Rutbah uplift, Aleppo high and the Euphrates graben (Fig. 1). In this paper, we are interested mainly in the Palmyrides and the central LFS including the Lebanese ranges, which will be discussed below.

Palmyrides Ranges

The Palmyrides ranges are separated into a NE and a SW part with a strong along-strike structural variations as thrust faulting becomes less pronounced toward the northeast. The SW Palmyrides are dominated by a series of narrow, en echelon, short SE verging asymmetric folds controlled by reverse faults with cretaceous outcrops at their crest (Chaimov et al. 1992; Brew et al. 2001b) (Fig. 3). Short-wavelength anticlines (10–20 km) have steeply dipping forelimbs and shallowly dipping backlimbs, steeper toward the southwest, and are the result of fault-propagation folding linked by sinistral transfer faults as evidenced in seismic data (Chaimov et al. 1993). A locally developed Triassic detachment level can accommodate the fault-bend fold formation. It was mapped by Chaimov et al. (1993) and probably effective in the northern part of SW Palmyrides.

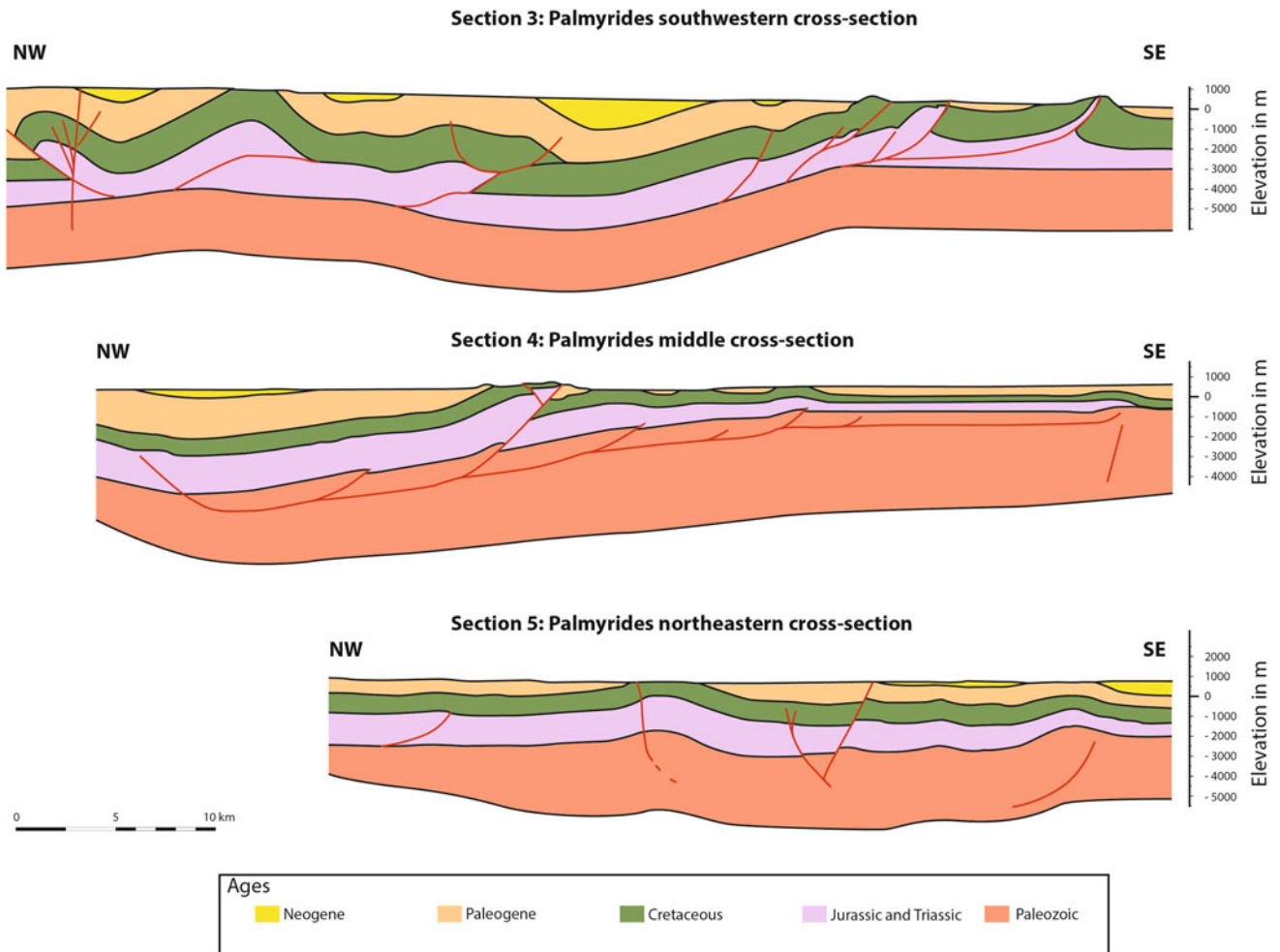


Fig. 3 Cross-sections across the south western, central and north eastern Palmyrides showing their relative structural style. Modified from Chaimov et al. (1993)

Another Upper-Cretaceous and lower Paleogene detachment is also mapped by Chaimov et al. (1993). To the west, the Palmyrides folds reoriented from NE to NNE connect with the Mount Lebanon through Anti-Lebanon.

The NE Palmyrides are dominated by complex folding, sometimes resembling box-folds, above an upper Triassic detachment with minor reverse faulting (Searle 1994) (Fig. 3). The Bilas and Bishri blocks (Fig. 1) are larger-wavelength anticlinoria with Cretaceous exposure, forming the central highlands of the NE Palmyrides. Deformation in the Bilas block is dominated by strike-slip duplexing where large, relatively undeformed anticlines are bound by steep faults that show very little shortening, smaller than the SE Palmyrides one (Chaimov et al. 1990). It is separated from the Bishri block by the right lateral Bishri strike-slip fault. NE-striking Mesozoic normal faults were more active in the Bishri Block than in other parts of the

Palmyrides, particularly in Jurassic and Late Cretaceous times (Brew et al. 2001b).

Jhar Fault

The Jhar fault separates the NE Palmyrides from its SW counterpart (Fig. 1). This fault is a deep crustal structure probably dating back to the suturing of Arabia and trends E-W to WSW–ENE across central Syria. It has been traced for 200 km and shows an average of 1000 m of uplift on its northern side. It is believed to be an active extensional fault since at least the Jurassic based on well data (Al-Saad et al. 1992; Brew et al. 2001b) with significant recent dextral strike-slip movement (Al-Saad et al. 1992; Searle 1994). Its length might probably be much longer and its western continuation is not well known. Evidence for active deformation on the Jhar Fault includes small Quaternary offsets (Ponikarov 1966) and seismicity.

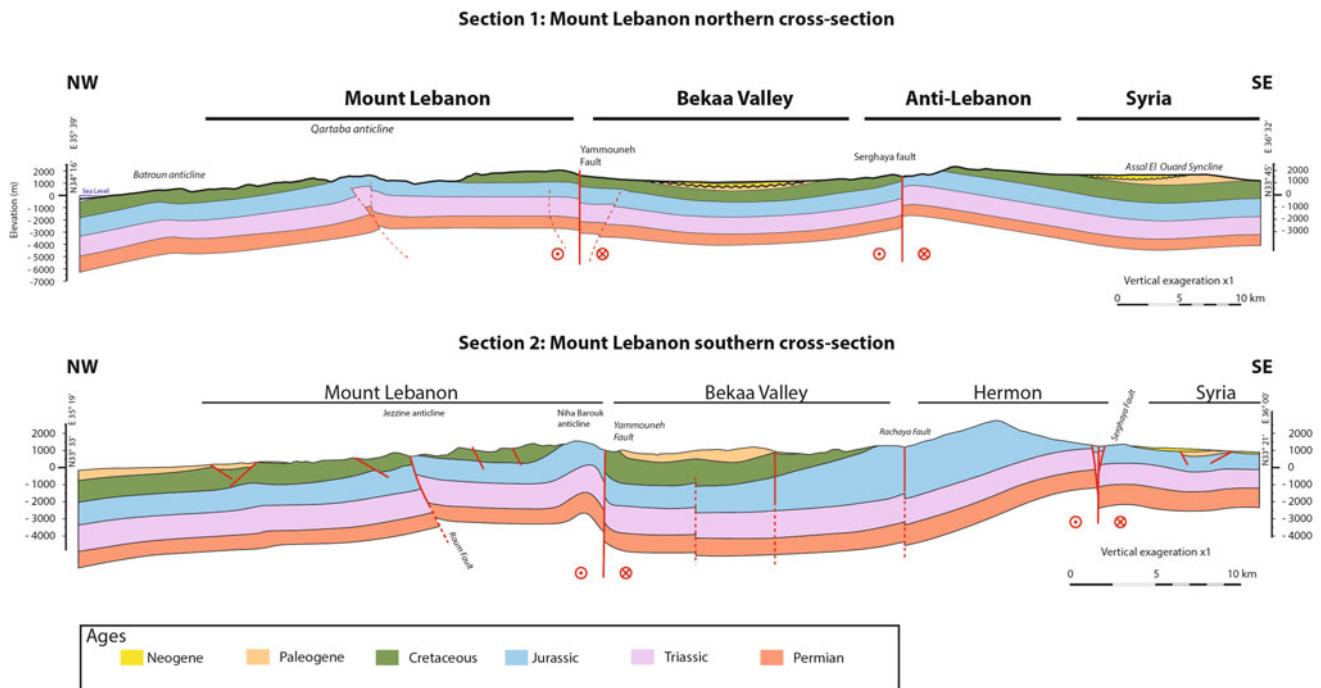


Fig. 4 Cross-sections across the southern and northern Mount Lebanon, their relative structural style. Modified from Sabbagh (1962)

The Central Levant Margin

The central Levant margin onshore is marked by Mount Lebanon, a major NNE trending anticlinorium with Jurassic limestone at its core (Dubertret 1955) (Fig. 4). It has been long considered as a complex structure with significant along-strike structural variations. Northern Mount Lebanon consists of a broad and symmetric box-fold anticline, probably affected by a Triassic detachment surface (Renouard 1955; Beydoun and Habib 1995), while southern Mount Lebanon is topographically lower and the deformation zone includes several shorter wavelength folds including a tight SE verging overfold termed the Niha-Barouk anticline (Figs. 1, 2 and 4) (Dubertret 1955; Walley 1998). Mount Lebanon is thus divided into two compartments of variable styles.

This separation takes place through a zone of ENE-WSW trending nearly vertical dextral strike-slip faults (Hancock and Atiya 1979). They constitute a larger zone of deformation termed the Damour Fault zone that is believed to be an ancient deep crustal fault originated from the Mesozoic rifting. It continues westward to the offshore Levant Basin to form the Saida fault, which consists of a deep crustal structure oriented ENE-WSW separating the deep Levant Basin at its north from an elevated Mesozoic plateau at its south (Ghalayini et al. 2014). At a larger scale, the central Levant margin contains a multitude of currently active E-W to ENE-WSW dextral strike-slip faults (Fig. 5), forming

what is believed to be an ancient horst and graben structure prior to the folding of Mount Lebanon and the development of the restraining bend (Collin et al. 2010; Ghalayini et al. 2014). These faults contain Jurassic basalt in their fault plane and Jurassic/Cretaceous units exhibit thickness variations across those faults (Dubertret 1955; Homberg et al. 2009; Collin et al. 2010). They are part of the extensional Mesozoic rifting structures found all over the Levant region, Sinai and Egypt (Fig. 2) and were reactivated in the Late Miocene due to the transpressive activity of the LFS.

The Yammouneh Fault (Figs. 1 and 4) passes through Mount Lebanon is the only structural link between the southern LFS in Israel and the northern LFS in NW Syria. Its 160 km long surface trace is sharp and clear in the topography. The Yammouneh Fault generally bounds the east side of southern Mount Lebanon, while it lies adjacent to the eastern flank of northern Mount Lebanon. Displaced landforms, such as faulted alluvial fans and wind gaps (Dubertret 1955; Daëron et al. 2004; Gomez et al. 2007b), demonstrate that the Yammouneh Fault has experienced only strike-slip movements during the Late Quaternary (Daëron et al. 2004; Gomez et al. 2006), with no evidence of recent or active dip-slip along it (Gomez et al. 2007b). The Serghaya Fault (Fig. 1, 2, 3 and 4) is another major sinistral strike-slip fault branching from the southern LFS in the Golan Heights. It can be traced approximately 125 km through the Anti-Lebanon Mountains to the eastern edge of the Bekaa

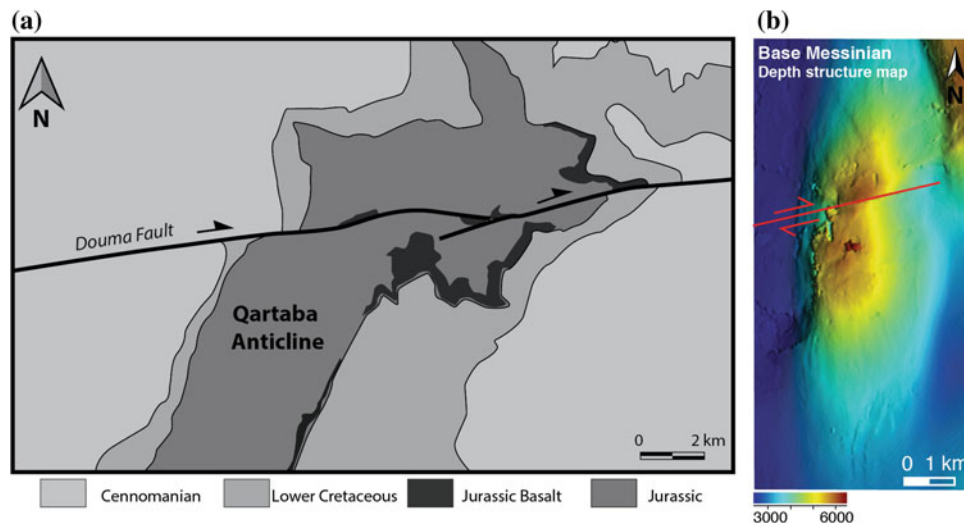


Fig. 5 **a** Simplified geologic map showing the passage of the Douma fault, a ENE-WSW dextral strike slip fault, displacing the Qartaba structure 1–2 km to the east. **b** Base Messinian depth structure map of a NNE trending anticline in the Levant Basin offshore Lebanon. Its

anticlinal axis is displaced by one dextral strike-slip fault for about 500 m. For location see Fig. 1. Modified from Ghalayini et al. (2014) and the 1/50000 map of Qartaba

Valley. It is associated with many pull-apart basins (Gomez et al. 2001, 2003) and shows a small dip-slip component of about 20–25 % (Gomez et al. 2001).

Current Crustal Configuration

The crust in the Levant region exhibits variations in its thickness along a N-S direction from Gaza to Lebanon and along an E-W direction from the Arabian plate to the Levant Basin. In the Palmyrides, the depth to Moho varies along the Palmyrides trend reaching 44 km in the SW Palmyrides and 31 km in the NE Palmyrides (Brew et al. 2001a, b). This difference in crustal thickness could indicate that the northern and southern Palmyrides are two different crustal blocks sutured along the Jhar fault, as a result of old Proterozoic sutures and shear zones (Brew et al. 2001a, b). Today the Palmyrides blocks are likely acting as a single block part of the Arabian plate. The thickness of the crust gradually decreases westward to the Levant Basin, with ~35 km beneath the anti-Lebanon ranges, ~27 km beneath Mount Lebanon (Khair et al. 1993) and ~20 km beneath the Levant Basin (Hirsch et al. 1995; Khair and Tsokas 1999; Ben-Avraham et al. 2002). Thus, it is likely that the rest of the Levant region, including Lebanon and Israel, is exhibiting an older architecture controlling the style and the location of Phanerozoic deformation, hence explaining the N-S crustal thickness variation along Judea similarly to the Palmyrides. Along the margin offshore Lebanon, the elevated Tyr-Saida plateau is suggested to overly a crust thicker than the one of the Levant Basin (Ghalayini et al. 2014). Its

northward bounding Saida Fault might thus be similar to the Jhar fault in the sense that it separates two different crustal blocks.

Refraction profiles along the Eastern Mediterranean (Makris et al. 1983; Ben-Avraham et al. 2002; Netzeband et al. 2006) indicate an 8–10 km crustal thickness suggesting the presence of a thinned continental crust beneath the Levant basin (Hirsch et al. 1995; Vidal et al. 2000; Gardosh et al. 2006). This westward thinning of the crust beneath onshore Lebanon, Syria and Israel (Beydoun 1977; Makris et al. 1983; Khair et al. 1997; Netzeband et al. 2006) indicates a transition between a crust of continental type east of the Levant margin, transitioning to a thinned continental crust beneath the Levant Basin.

Tectono-Stratigraphic Evolution

In this section we review the Mesozoic–Cenozoic tectono-stratigraphic evolution of the Levant region as it is well documented (Fig. 6). Available field and subsurface data allow reasonably accurate reconstruction since Late Paleozoic times in Syria and to the base Jurassic in Lebanon (Fig. 7).

Pre-Neogene History of the Levant Region

The Levant region was formed by the breakup of Gondwana and Eurasia during the Late Palaeozoic to Early Mesozoic period in different pulses (Garfunkel and Derin 1984; Robertson 1998a). This was accompanied by continental breakup, rifting and drifting of various micro-continental

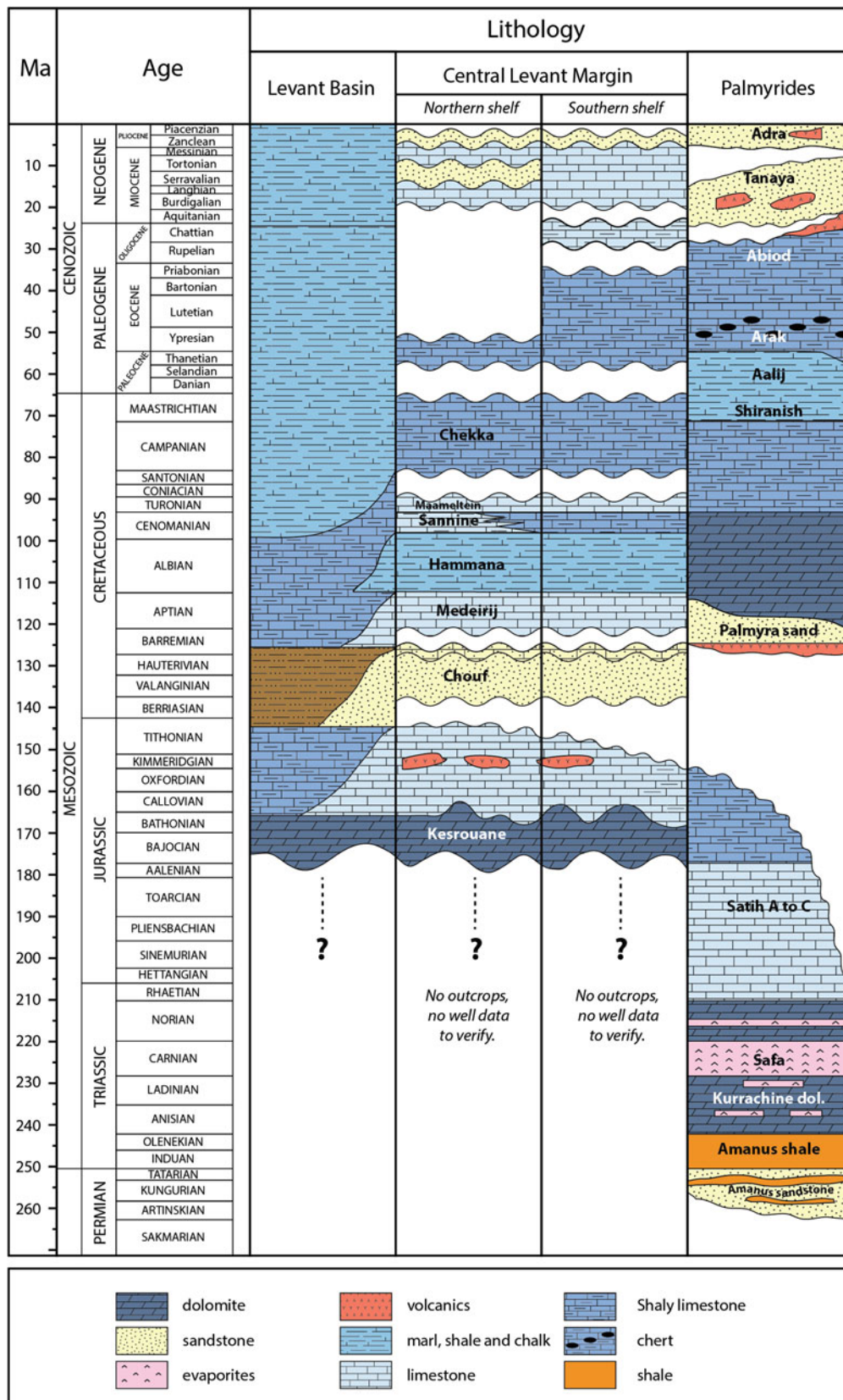


Fig. 6 Schematic chronostratigraphy of the Palmyrides, the central Levant margin and the Levant Basin. Modified from Hawie et al. 2013, 2014, Barrier et al. 2014

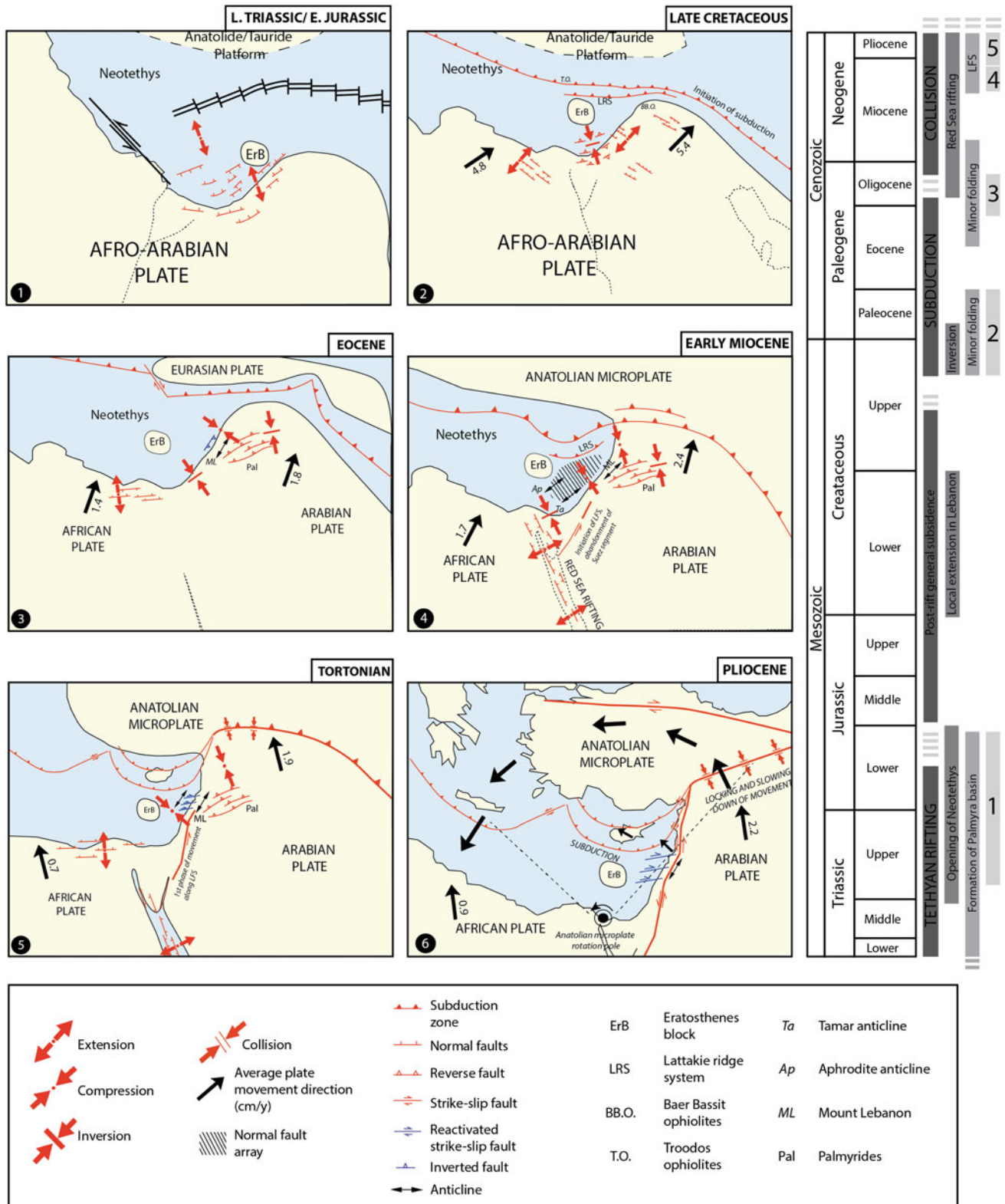


Fig. 7 Paleogeographic maps of the Levant region summarising the tectonic evolution of this area. (1) refers to the Mesozoic rifting event, (2 & 3) refers to the start of closure of Neotethys and convergence tectonics, (4) the initial structuration and folding along the Levant margin and Palmyra, (5) 1st stage of LFS movement and establishment

of the restraining bend in Lebanon, and (6) 2nd stage of LFS movement and rapid uplift of the Levant margin. Compiled from Brew et al. (2001b), Barrier and Vrielynck (2008), Gardosh et al. (2010), Hardy et al. (2010), Ghalayini et al. (2014, 2016)

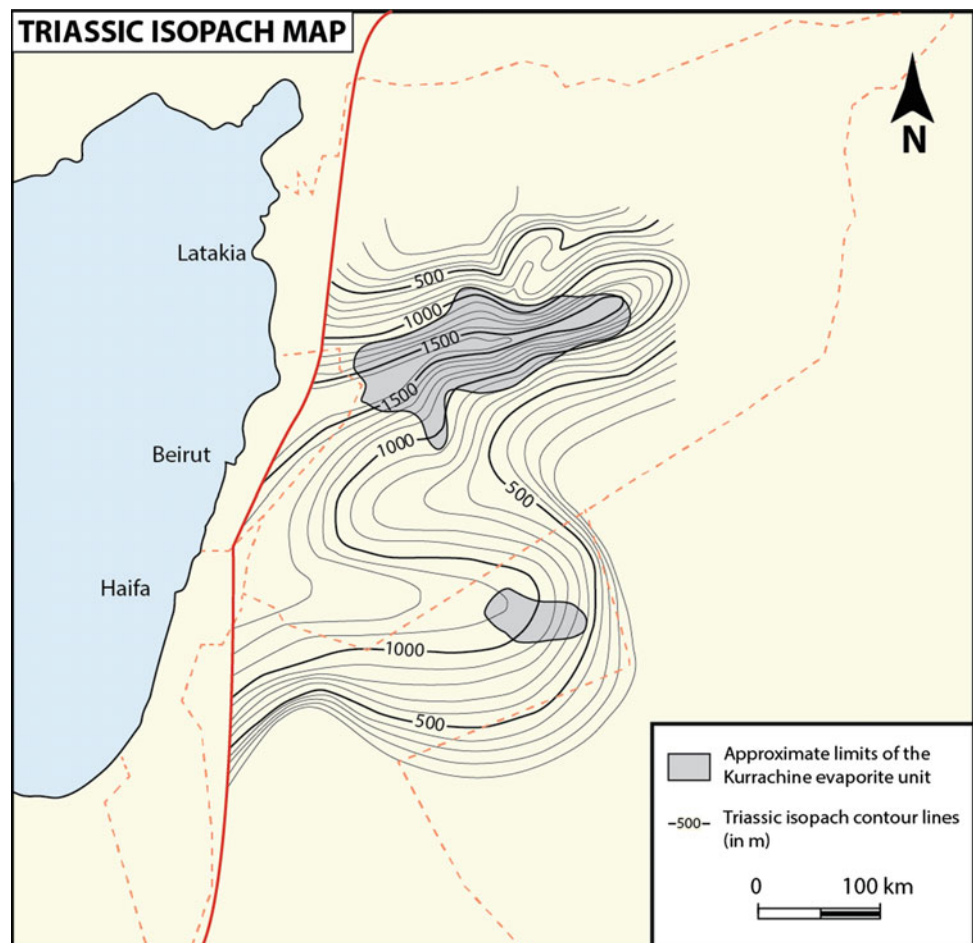
blocks (Robertson and Dixon 1984; Garfunkel 1998; Robertson 1998b, 2007) (Fig. 7). Although the exact timing and location of rifting are still under debate (Robertson and Mountrakis 2006), there is a general consensus that the most important rifting stage took place in the Early Jurassic (Ben-Avraham et al. 2002). This has resulted in NW-SE trending extensional structures preserved and documented throughout the Levant region from the Palmyra area in central Syria to the Egyptian western desert (Freund 1965; Druckman 1984; Garfunkel and Derin 1984; Guiraud and Bosworth 1997, 1999; Garfunkel 1998; Brew et al. 2001b; Sawaf et al. 2001; Gardosh et al. 2010) (Fig. 2).

This Mesozoic rifting transformed the east-facing Paleozoic margin into a west-facing Mesozoic Margin. The continental deposits of Permian age were first introduced as the "Amanus Sand," mainly consisting of shales interbedded with channel sandstones and siltstone beds (Fig. 6) (Barrier et al. 2014). These Permian continental deposits belong to the Permian to Lower Triassic clastic sequence of the Amanus Group, including the Permian Amanus Sandstone and Amanus Shale Formations, Permian and Early Triassic in age respectively.

The most complete Triassic sequence is known in Central Syria where the Permian to Middle Triassic sequence is conformable. Isopach maps show that there is a westward thickening of Triassic sediments into Lebanon (Beydoun 1981) (Fig. 8). Based on regional facies correlation, it is proposed that a Late Permian-Triassic succession with an estimated thickness of 2000 m is present in Lebanon (Beydoun and Habib 1995) (Fig. 8). Geophysical data confirm the existence of evaporites, believed to belong to the Kurrachine formation, along the central Levant margin (Renouard 1955; Beydoun and Habib 1995; Nader and Swennen 2004).

Between the end of Triassic to the Early Jurassic, marine transgression covered most of Syria. The Palmyra basin has witnessed deposition of Jurassic sediments characterised by deeper-water carbonate facies and a typical west-facing configuration with a thickening toward the west (Barrier et al. 2014). Similarly, in the western extension of the Palmyrides in Anti-Lebanon, (Mount Hermon) deeper facies progressively replaced the Triassic lagoonal-evaporitic deposition. In Mount Hermon and Mount Lebanon, up to 1800 m of carbonate Jurassic sediments were deposited

Fig. 8 Isopach map of the Triassic unit in Syria showing westward thickening toward Lebanon and indicating a continuous basin throughout the Triassic times. Modified from Beydoun and Habib (1995)



(Dubertret 1955; Walley 1998; Collin et al. 2010). In the Late Jurassic a large epicontinental shelf with shallow environments developed all over Lebanon and Anti-Lebanon, while deeper sediments deposited in the Palmyra Basin (Dubertret 1955).

Extensional activity in the Levant ceased during the Middle to Late Jurassic. The Bajocian-Oxfordian and the younger, Cretaceous section in the inner part of the Levant show minor thickness variations indicating tectonic quiescence (Gardosh et al. 2010). However, in onshore Lebanon, extensional geometries within the Kesrouan Formation are documented (Late Bathonian to Early Kimmeridgian) and are characterized by the creation of tilted fault blocks corresponding to the initiation of an extensional phase in conjunction with intra-plate volcanism during the Kimmeridgian (Collin et al. 2010). Similarly, broad subsidence and normal faulting are documented in the Palmyra basin during the Late Jurassic and Early Cretaceous (Best et al. 1993).

Following the rifting event, the Late-Cretaceous times witnessed the progressive closure of the Neo-Tethys ocean (Beydoun 1988; Stampfli and Hochard 2009; Frizon de Lamotte et al. 2011) (Fig. 7). Most areas remained under marine conditions with pelagic deposition. This major geodynamic event caused the contraction of the Levant basin and margin and the subsequent initiation of an arcuate fold belt, the Palmyrides in Syria, folds in Lebanon, Israel and Sinai, collectively termed the “Syrian Arc” (Walley 1998). This results from inversion of Early Mesozoic extensional structures whereby pre-existing normal faults became reverse faults, and the Jurassic and Early Cretaceous synclines became Late Cretaceous anticlines (Druckman 1981; Chaimov et al. 1990, 1993; Best et al. 1993; Druckman et al. 1995). The inversion took place in three distinct time periods (Chaimov et al. 1992) (Table 1).

In the central Levant margin, the Palmyra region and NW Syria, the Late-Oligocene/Early Miocene NW-SE compression is the major regional tectonic event associated with folding and thrusting. It has created the NE-SW trending intra-platform Lattakia thrust as well as the regional NE-SW folding in the Palmyrides (Sawaf et al. 2001). This tectonic phase is associated with a significant uplift and a strong erosion of the Mesozoic to Palaeogene sequence of the

Palmyrides and the central Levant margin (Brew et al. 2001b).

An ancient structuration of the Levant margin was proposed by Dubertret (1955) and more recently by Hawie et al. (2014) who proposed that the Levant margin has been subject to minor uplift in the Oligocene and early Miocene times. This hypothesis is based on detailed micropalaeontology and investigation of the Tertiary sedimentary facies. Indeed, the presence of open marine Miocene facies along the margin in contrast with restricted and continental Miocene facies in the Bekaa valley east of Mount Lebanon, indicate that there must have been a topographic barrier between the margin and the inner shelf (modern Bekaa valley and inland Syria) to explain the facies differentiation during the Miocene. Similarly, the modest, angular unconformity between Lutetian and Burdigalian in northern Lebanon and erosion of the majority of the Oligocene unit in Lebanon (Boudagher-fadel and Clark 2006; Homberg et al. 2010; Müller et al. 2010; Hawie et al. 2014) also attest to a minor orogenic phase during the Oligocene.

These observations point that the central Levant margin has been uplifted and deformed prior to the onset of the Levant Fracture System synchronously with the major deformation time in the Palmyrides (Chaimov et al. 1992; Brew et al. 2001b) and the Levant Basin (Montadert et al. 2014). In conclusion, the Palmyra basin and the central Levant margin share the same geologic history since at least the Permian.

Neogene History of the Levant Region

The Neogene tectonic history of the Levant region is dominated by the establishment and evolution of the LFS, a 1000 km long transform fault comprising three segments passing through Jordan, Israel, Lebanon and Syria (Quennell 1958, 1984; Freund 1965; Dubertret 1972): the 400 km long southern part from the gulf of Aqaba to the Dead Sea in Jordan in a N005E trend, the 180 km long central part in Lebanon where the transform bends to N030E and the motion becomes transpressive creating some restraining bends, and the northern 250 km long part in Syria with a

Table 1 Table showing the three periods of inversion documented in the Palmyrides and Lebanon as a result of the closure of Neo-Tethys

Time	Effect in the Palmyrides	Effect in Lebanon
Late Cretaceous	Minor, caused slight uplift of the SE Palmyrides	No evidence documented
Middle Eocene	Minor, caused some Paleogene thickness variations	Minor, caused some facies differentiation
Late Oligocene-Early Miocene	Major, responsible for the uplift and erosion of the Palmyrides	Major, responsible for initial folding and uplift of Mount Lebanon

N005E trend abutting the Taurus mountains in the Anatolian microplate. We primarily focus on the central part in this paper.

At the southern part of the LFS from the Gulf of Aqaba to the Dead Sea basin, the LFS cross-cuts quaternary sediments of the Arava Valley. In Israel, the left-lateral movement along the left-stepping LFS led to the development of several pull-apart basins, with the largest ones in the Gulf of Aqaba, the Dead Sea, Sea of Galilee and Hula basins along the Jordan valley (Garfunkel 1981; Garfunkel and Freund 1981). The LFS is almost purely strike-slip in this section and is composed of linear segments several tens of kilometers long connected either by compressive or extensive jogs that form, respectively, small-scale push-ups or basins (Garfunkel and Freund 1981). Linking the southern and the northern parts, the LFS bifurcates in Lebanon into a series of structures and displays a braided fault system (Walley 1988). Here, a restraining bend dominates the landscape due to the bending of the main sinistral strike-slip fault making the motion transpressive along this segment. The northern segment of the LFS cuts through the eastern margin of the Syrian coastal ranges with a NS trend into the Al-Ghab basin where the fault bifurcates into a dominant eastern branch (Al Ghab fault) which has a throw down to the west of up to 1000 m and a western branch that shows a throw down to the East of about 1500–2000 m. Between these two faults, the 15 km wide, 60 km long Pliocene-recent Al-Ghab depression forms a pull-apart basin similar to the Dead Sea (Brew et al. 2001a).

The total displacement recorded along the southern LFS leads to an estimated 107 km taken place in two stages; 62 km in the Miocene and 45 km in the Pleistocene based on stratigraphic markers (Quennell 1958; Freund 1965; Freund et al. 1970). Nevertheless, this value is contested especially along the central segment in Lebanon as there is no evidence to support more than 40 km of lateral displacement (Dubertret 1955; Walley 1998; Beydoun 1999; Gomez et al. 2007b), and also in the northern Ghab segment where only 30–40 km are documented (Al Abdalla et al. 2010). Dubertret (1972) found invoking large scale horizontal displacement is totally inconsistent with the detail of stratigraphy and structural block relationships in Lebanon. He envisaged minor horizontal displacement amounting to a maximum of 30–40 km, shared amongst the other branches of the Lebanese faults that make up the Levant Fracture System, in a strain-partitioning model. In Israel, transform activity postdates the 22 my old diabase dykes of Eyal et al. (1981) and has most likely initiated during the Early Miocene (Freund et al. 1970; Steckler and ten Brink 1986). The question on the timing of folding along the central Levant margin in Lebanon has also been fostering debates for a long time. As stated earlier, several authors link the uplift and folding of Mount Lebanon to the transpressive activity along

the LFS during Late Miocene times (Hancock and Atiyah 1979; Daeron 2005; Gomez et al. 2006; Elias et al. 2007; Homberg et al. 2010) while others argue for an older folding time, of Early Miocene or before (Renouard 1955; Dubertret 1972; Walley 1998; Beydoun 1999). The controversy is caused by the lack of data and unclear knowledge of the subsurface due to its complexity.

Walley (1998) provides a series of field observations to prove that the Lebanese ranges predate the LFS and were folded as part of the Syrian arc episodes. The hypothesis of Walley (1998) is coherent in terms of linking the Lebanese ranges with the regional deformation in northern Arabia and even argues for strain partitioning between the LFS structures and those of the Palmyrides. This idea of strain partitioning was fully developed and proposed by Gomez et al. (2007a, b), arguing that the deformation was characterised by distribution and partitioning of strain between all the structures of the Lebanese restraining bend and the Palmyrides based on recent seismogenic data, geodesy and satellite imagery.

As the shortening is partitioned between the Palmyrides and the structures of the central Levant margin, Gomez et al. (2007a, b) propose that part of the shortening should be accommodated offshore. This idea, however, was refuted by Ghalayini et al. (2014) who argue that no significant shortening has taken place during the Neogene offshore Lebanon, but only ENE-WSW dextral strike-slip faults are active today. These observations also discard the presence of an offshore fold and thrust belt part of the restraining bend (Elias et al. 2007; Carton et al. 2009).

In summary, the evolution of the central Levant margin in Lebanon and the central LFS segment is still a matter of controversy despite few decades of scientific work undertaken in this region. Today, there is a growing knowledge of Mesozoic inherited faults along the entire Levant margin without a clear understanding of their effect on the overall evolution of the central LFS segment.

Analogue Models

We used sandbox analogue modelling with brittle and ductile materials to test the effect of variable parameters on the evolution of restraining bends. These parameters include the effect of pre-existing structures, their angle relative to the main strike-slip fault and the style and velocity of deformation.

Materials and Scaling

The performed experiments investigate strike-slip tectonics by deformation from a reactivated, straight, and vertical

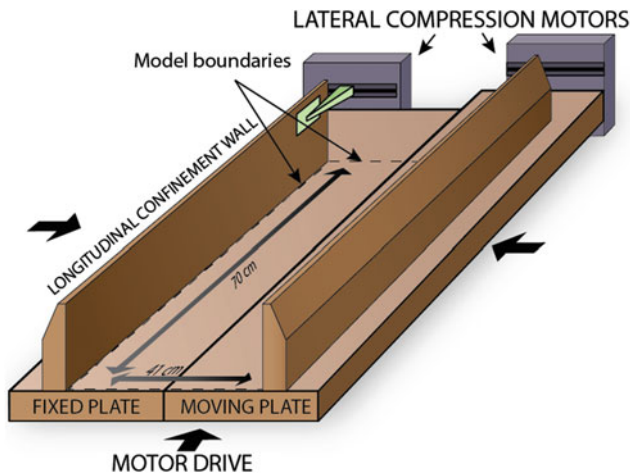


Fig. 9 The experimental setup consisted of a 70 × 41 cm wooden box bordered by two longitudinal confinement walls. The different parts of the box are moved by stepper motors

basement fault into an overburden. The experimental setup consisted of a wooden box with two overlapping plates

(Figs. 9 and 10). One of these plates is movable, driven by stepper motors, whereas the other is fixed (Figs. 9 and 10). The overlapping plates simulate basement master faults in which two parallel strike-slip faults are connected by a 45° oblique bend (Fig. 10). This is in order to simulate a restraining bend similarly to the one observed at the modern Levant margin. The stepover size is 9 × 3 cm in all experiments.

The wooden box is bordered by two mobile longitudinal confinement walls (Fig. 9), which are also controlled by stepper motors. The movable confinement walls simulate lateral compression in these experiments. Thus, transpression (or oblique shortening) could be achieved by combining the basal strike-slip shear component of the overlapping plates and the transverse shortening by the longitudinal confinement walls.

The original configuration of each model before deformation is shown in Fig. 10. The base of each analogue model consisted of a silicone layer (PDMS), 1 cm thick placed directly over the plates and representing the ductile behaviour of weak layers within the brittle upper crust.

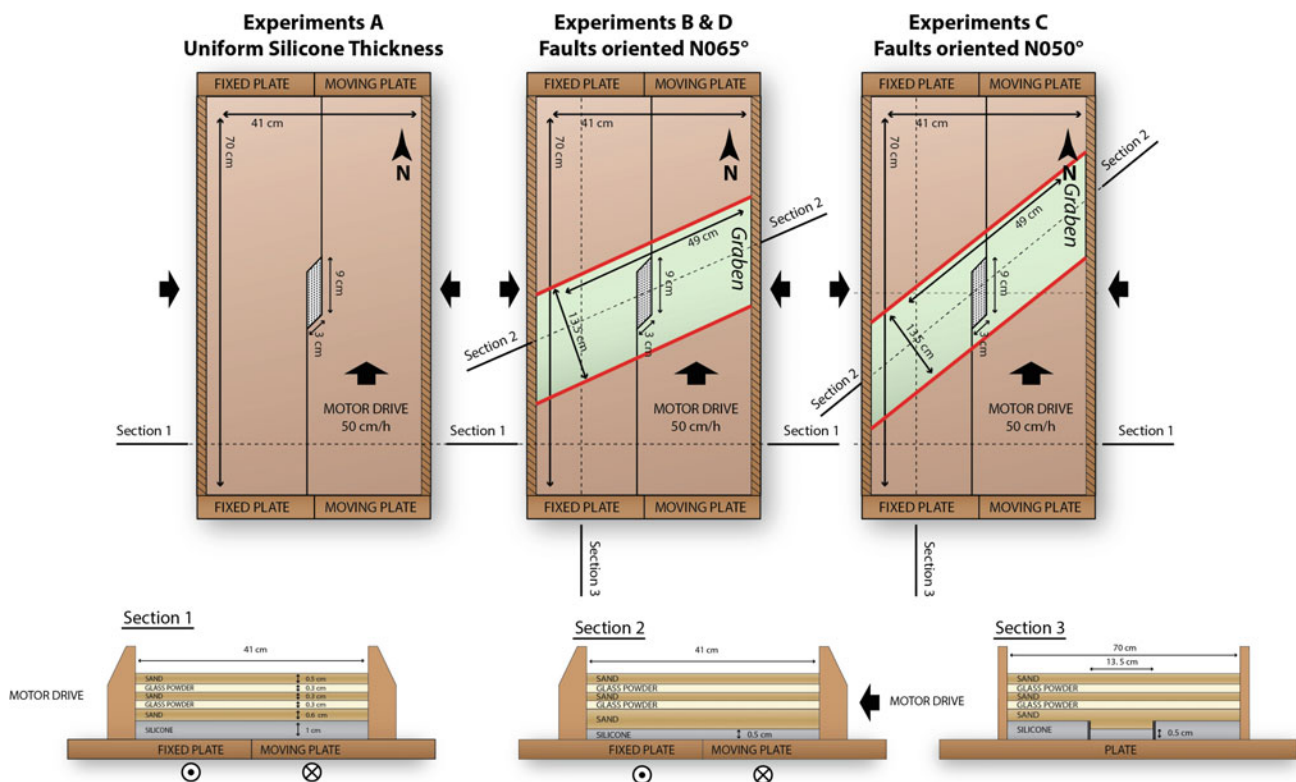


Fig. 10 Modelling parameters in experiments A, B, C and D. Experiment A consists of a uniform 1 cm silicone thickness across the entire box overlain by 2 cm thick layer of alternating quartz sand and glass-powder (Pyrex). In contrast, in experiment B, C and D, a graben was simulated oblique from the bend in the basement faults

whereby the thickness of the silicone was reduced from 1 cm across the box to 0.5 cm inside the graben only. Bordering the graben, two faults were created in the silicone and their planes filled with microbeads. In experiment B and D the orientation of these faults is N065°E while in experiment C it is N050°E

The PDMS behaves nearly as a Newtonian fluid, with a density of 0.965 g cm^{-3} , a viscosity of $2.5 \times 10^4 \text{ Pa s}$ at room temperatures (Weijermars 1986) and strain rates below $3 \times 10^{-3} \text{ s}^{-1}$. The sedimentary brittle rocks were simulated by quartz sand sifted on top of the silicone unit (Fig. 10). This layer equals to 2 cm thick layer of alternating quartz sand and glass-powder. Both materials are well sorted and have a mean grain size of $115 \mu\text{m}$. The sand has a low/negligible cohesion, an angle of internal friction of 30° , and a density ranging from 1400 to 1600 kg m^{-3} . The glass powder acted as a stratigraphic marker, thus allowing the identification of structures on cross-sections due to contrasting densities during scanning.

The models were scaled for length and time following the basic principles of Hubbert (1937) and Ramberg (1967). The length ratio, or geometric scale, between the natural example and the model is in the order of 10^{-6} , i.e. every 1 cm in the model equals 10 km in nature. The chosen time scaling factor depended on the deformation velocity chosen and is thus around 5×10^{-11} in the experiments (every 1 min of deformation in the model represents 1 My in the natural example). It is important to keep in mind that some geological parameters such as temperature evolution through time and effects of pore pressure on sediment rheology could not be taken into account as in most analogue modelling studies due to the related technical difficulties.

At the end, the models were gridded by $5 \times 5 \text{ cm}$ grid at the surface in order to measure and quantify surface deformation using a camera and scanned by X-ray computerized tomography using a General Electric CT-scanner. This technique is non-destructive and generates 3D cross-sectional images through the models (Hounsfield 1973; Colletta et al. 1991). The model was scanned before and during deformation at every 1 cm of strike-slip movement while simultaneously taking surface pictures using a camera. For practical reasons, the north direction within the models is taken as indicated in Fig. 10.

Modelling Parameters

More than 40 experiments were undertaken in the course of this study to choose the most convenient modelling parameters and calibrate the results. Only four experiments are discussed in this study and compared, experiment A, B, C and D with their characteristics explained in Table 2. These experiments were chosen because they yielded the best results.

In all the experiments, the same materials and thicknesses discussed above are used. Experiment A simulates a classical restraining bend without any oblique pre-existing structure. In experiment B, C and D, oblique inherited structures were simulated by creating two parallel faults oriented $\text{N}065^\circ\text{E}$, $\text{N}050^\circ\text{E}$ and $\text{N}065^\circ\text{E}$ respectively (Fig. 10). They were cut through the silicone and filled with microbeads to decrease friction along fault planes and prohibit the silicone to amalgamate. Between the two faults, the silicone thickness was reduced to 0.5 cm (Fig. 10). The end result setup represented an oblique graben structure (with respect to the strike slip system) bordered by faults. The thickness of the silicone varied across the modelled graben. In the natural example, several crustal faults are observed along the margin creating horst and graben structures, but we have chosen to only model two faults bordering a single graben for simplicity. Once the faults were cut, the sand was sifted uniformly on top of the silicone and was thus considered as undeformed. In experiment D, the initial configuration of the pre-existing faults is similar to experiment B but the compression velocity was decreased to 6.25 cm/h instead of 12.5 cm/h .

Results

Simple Transpressive Experiment

Experiment A shows a restraining bend observed on the surface of the model resembling the classical ones

Table 2 Properties of the experiments described in this work

	Material thickness	Deformation velocity	Characteristics
Experiment A	Sand 2 cm Silicone 1 cm	Strike-slip 50 cm/h Compression 12.5 cm/h	Simple restraining bend, no pre-existing structures
Experiment B	Sand 2 cm Silicone 1 cm	Strike-slip 50 cm/h Compression 12.5 cm/h	Pre-existing structures modelled by two faults bordering a graben in the silicone oriented $\text{N}065^\circ\text{E}$
Experiment C	Sand 2 cm Silicone 1 cm	Strike-slip 50 cm/h Compression 12.5 cm/h	Pre-existing structures modelled by two faults bordering a graben in the silicone oriented $\text{N}050^\circ\text{E}$
Experiment D	Sand 2 cm Silicone 1 cm	Strike-slip 50 cm/h Compression 6.25 cm/h	Compression velocity reduced, Pre-existing structures oriented $\text{N}065^\circ\text{E}$

described by previous studies (Mcclay and Bonora 2001; Mitra and Paul 2011; Dooley and Schreurs 2012). It consists of 15 cm long and 10 cm large symmetric pop-up (Fig. 11). It is bordered by two thrust faults roughly parallel to the main trace length of the basement strike-slip fault. Outside the pop-up, the strike-slip segment that are accommodated by en echelon R shears show a small uplift and folding, due to compression. In all experiments, en echelon R shears striking at around 17° – 20° to the trace of the main sinistral basement fault are observed away from the pop-up (Fig. 11).

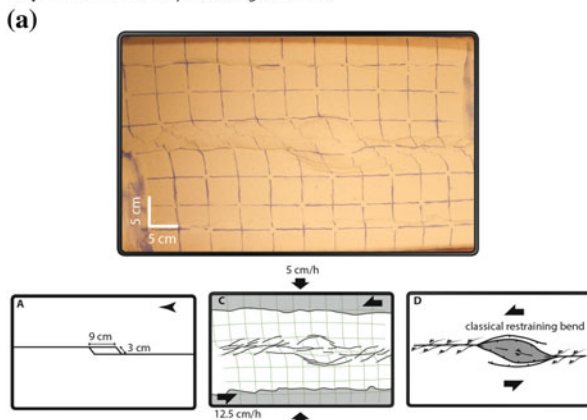
Cross-section of the restraining bend in experiment B (Fig. 12) show that the latter has the shape of a classical pop-up structure (e.g. Mcclay and Bonora 2001). It resembles

a positive flower structure with a symmetric box-shaped uplift bounded by reverse faults with moderate dips of 30° . The pop-up uplift amounts to 2 cm. The centre of the pop-up is crosscut by near-vertical faults. All faults are dying out at the silicone level and cannot be mapped all the way down to the presumed basement fault. They have a maximum vertical displacement of 5 mm.

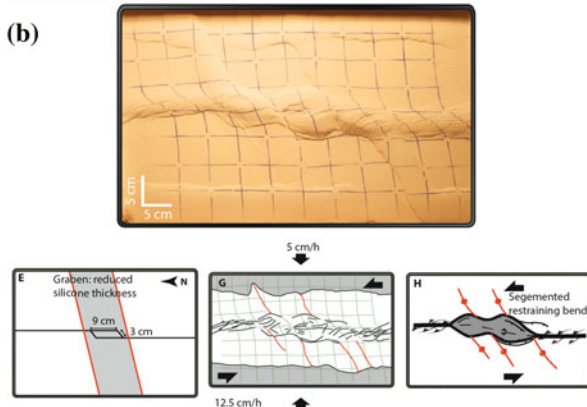
Experiments with Pre-existing Faults

Experiment B, C and D show the effect of pre-existing faults on the evolution of the restraining bend. In these three experiments, an asymmetric and segmented pop-up is observed when an oblique graben in silicone was introduced (Fig. 11). This asymmetry is variable and is more

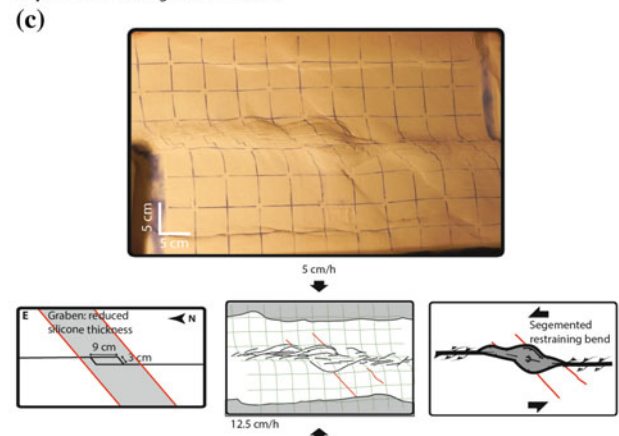
Experiment A without pre-existing structures



Experiment B with graben in silicone



Experiment C with graben in silicone



Experiment D with graben in silicone reduced compression

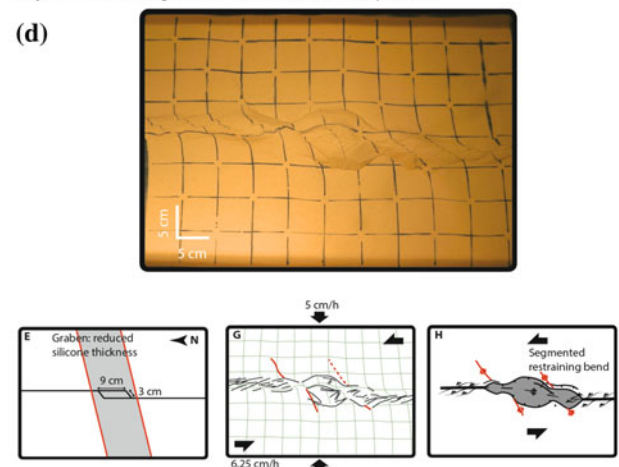


Fig. 11 Comparison between experiments without pre-existing structures (experiment A) and those with in silicone (experiment B, C and D). In experiment B the overlying sand package was cross-cut by dextral strike-slip faults parallel and aligned with the faults in the silicone. The resulting pop-up was also segmented into at least two compartments. In contrast, the experiment without inherited deformation results in a classical restraining bend showing symmetry in its

geometry. In experiment C, no strike-slip faults are seen on the surface of the model, while in experiment D a very small displacement of <0.2 mm is seen on one strike-slip fault. Total strike-slip movement was 9 cm in both experiments and total compression was 4.5 cm (2.25 cm on every side) in experiment A, B and D and 2.25 cm (1.125 cm on every side) in experiment C

pronounced when the pre-existing faults are N065°E (i.e. 25° to the compression direction).

In experiment B, the central popup is composed of primarily three compartments (Fig. 11). The middle one is 12.5 cm long and 8 cm wide while the lateral ones are 6 cm long and 7.5 cm wide. They are all bordered by thrust faults. Within the central popup, 20°–35° counter clockwise rotation is observed. The striking observation in this experiment is the presence of dextral strike-slip faults oriented around N065°E (Fig. 11). These structures are aligned with the faults created in the silicone. The horizontal displacement along these faults ranges between 0.2 mm and 1 cm. Segmentation of the popup into three compartments is controlled by these oblique strike-slip faults as the fault location coincides with the different boundaries of the popup compartments. Away from the popup and the main sinistral strike-slip fault, the horizontal displacement along the pre-existing faults is gradually reduced.

Cross-section of the central compartment in experiment B (Fig. 12) shows that the latter has the shape of a classical popup structure (e.g. McClay and Bonora 2001) very similar to the one in experiment A. It also exhibits a symmetric box-shaped uplift bounded by reverse faults with moderate dips of 30°. The centre of the popup is crosscut by near-vertical faults. All faults are dying out at the silicone level and cannot be mapped all the way down to the presumed basement fault. They have a maximum vertical displacement of 5 mm.

Vertical sections across the three compartments reveal the changing geometry along strike (Figs. 12 and 13).

Section AA' intersects the passage of the oblique dextral strike-slip fault with the trace of the basement fault. The popup in this location is different than the one in Fig. 12 and has an asymmetric cross-sectional geometry. It consists of an overturned fold trending 22° from the main basement fault. It exhibits a major reverse fault rooted in the silicone with a dip of 30° and a displacement of 5 mm, and smaller antithetic reverse faults with 2 mm maximum displacement. These two differing geometries characterise the resulting segmented popup. The central popup thus consists of a symmetric box-fold, and at the contact with the pre-existing basement faults the popup changes its structural character to appear as an asymmetric overturned fold. 19 % total shortening is attested in the central popup while 23 % shortening is observed in the lateral popups at the intersection with the pre-existing faults in silicone.

Section BB' (Fig. 13) is at right angle to the graben created in the silicone in experiment B. It shows that the faults were not reactivated into a single vertical strike-slip fault. Instead, localised reverse faulting is observed in the sand package, with 4 mm of vertical displacement. Antithetic reverse faults are also seen in some instances, resulting in double dextral strike-slip faults at the surface (Fig. 11). These observations indicate that the pre-existing normal faults were not reactivated, but have localised new structures on their crest. They consist of strong reverse faults with a mild dextral strike-slip component at surface. It is likely that this reverse movement is intensified at the intersection with the main basement sinistral strike-slip fault, resulting in an asymmetric fold in the popup (Fig. 13).

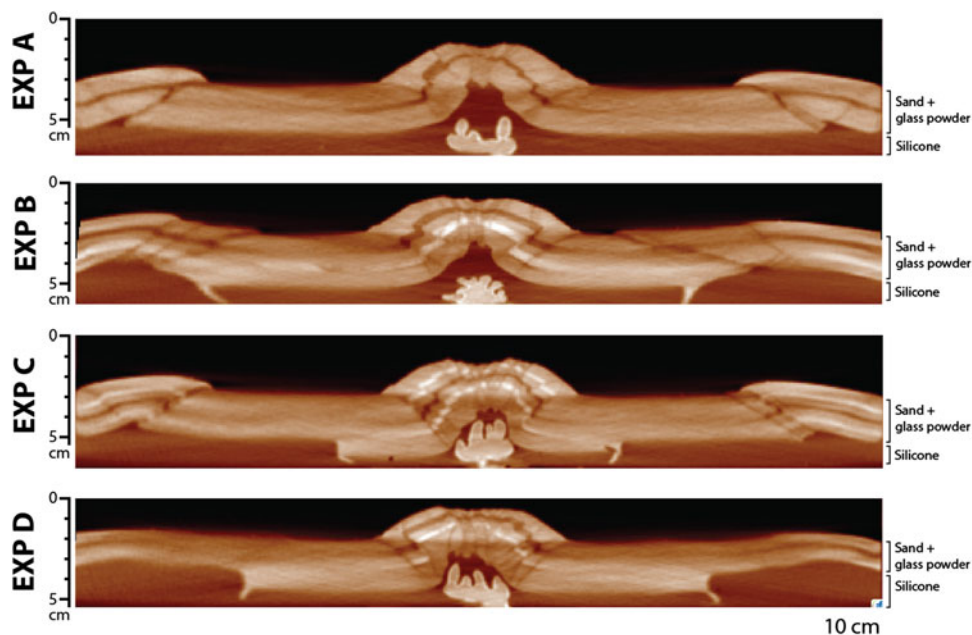


Fig. 12 Sections along experiment A, B, C and D showing the structural style of the central popup. All experiments exhibit a symmetric box-fold anticline

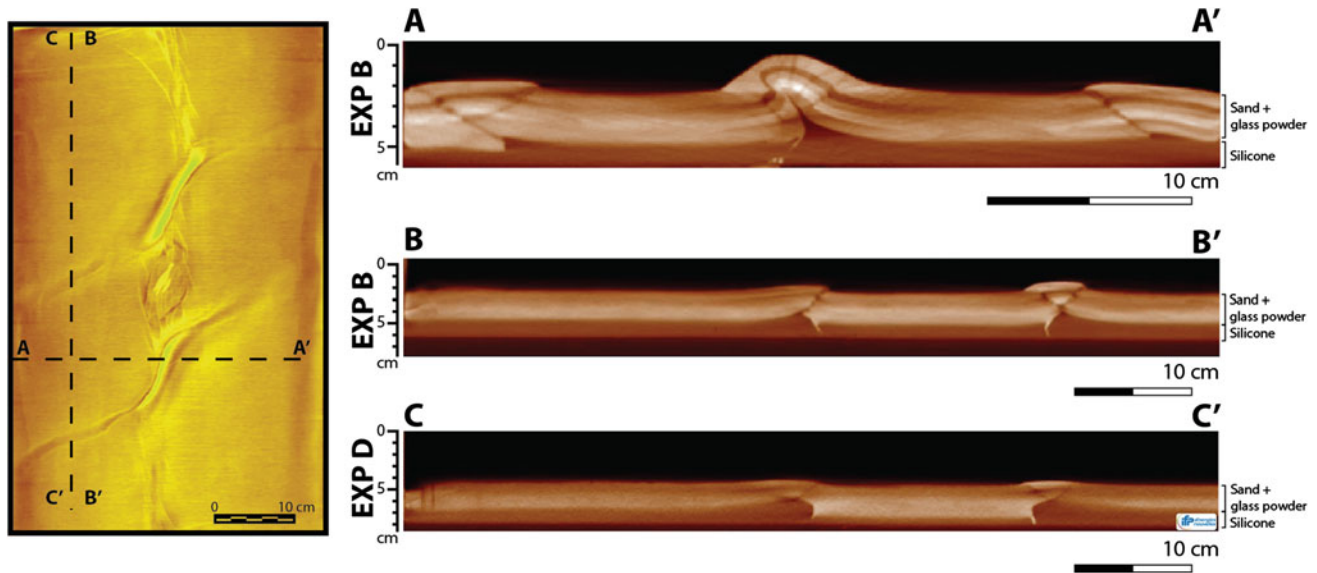


Fig. 13 Sections along experiment B and D. Section AA' in experiment B shows an asymmetric fold at the intersection between the main basement strike-slip fault with the introduced pre-existing faults. Section BB' in experiment B shows the geometry of the reactivated pre-existing faults and how they preferentially localise deformation at

their top. Section CC' in experiment D is taken at the same location as section BB' and shows that the pre-existing faults exhibit a smaller reverse movement than experiment B. The *top view* in **a** is a horizontal slice taken near the surface of the model

In experiment C, the angle of the two pre-existing faults was changed to N050°E. As stated before, the resulting restraining bend looks closer to experiment A than B with a minor amount of asymmetry (Fig. 11). The middle compartment is 12.5 cm long and 7.5 cm wide while the lateral ones are 5 cm long and 4 cm wide. The central popup is bordered by thrust faults. Within the central popup, 20°–35° counterclockwise rotation is also observed. In this experiment, the pre-existing faults do not show any strike-slip movement on the surface of the model. As it is very challenging to quantify strike-slip movement inside the models, we argue that these faults did not accommodate any lateral movement. They do however show reverse faulting similarly to experiment B (Fig. 11).

In experiment D, the velocity of compression was reduced to 6.25 cm/h while keeping the original N065°E orientation of the pre-existing structures. The middle compartment is 14 cm long and 8 cm wide while the lateral ones are 9 cm long and 6 cm wide. The central popup is bordered by thrust faults. Within the central popup, 20°–35° counterclockwise rotation is observed. In this experiment, the pre-existing faults show a strike-slip movement on the surface of the model of less than 0.2 mm, much smaller than

experiment B. Cross-section at a right angle to the pre-existing faults in silicone shows that the faults have localised a small reverse component of less than 1 cm, much smaller than the 2 cm reverse movement recorded at the same faults in experiment B (Fig. 13).

Discussion

Reactivation of Pre-existing Structures

Inversion of structures in analogue models of strike-slip fault systems was investigated by Mattioni et al. (2007) who applied transpression and oblique shortening after exerting extension to an undeformed silicone/sand model. Their final model showed that the orientation of existing extensional structures had affected the resulting stress field with respect to the applied simple shear component of the transpression, and hence strongly affected the geometry of a succeeding strike-slip system. In contrast to their experiment, we tested the effect of a graben in an undeformed silicone/sand model lying obliquely to the direction of simple shear, while they tested the effect of grabens in a deformed silicone/sand

model lying parallel to the direction of simple shear. In all cases, the results show that existing structures, affect the resulting restraining bend depending on their orientation relative to the compression direction.

In our experiments, we have placed two pre-existing faults bordering a graben in the silicon prior to deformation and not in the sand in order to simulate deep crustal faults. Faults created in undisturbed zones have a friction angle 20 % lower than the homogeneous sand (Sassi et al. 1993) and for this reason it's easier to reactivate these faults during deformation. But when we attempt to create faults in the silicone, the result will be strong mechanical discontinuities between the sand and the silicone instead of a true fault. The faults bordering the graben lying obliquely to the direction of simple shear, have localised deformation by having thrust faults nucleating directly above their initial location. They have propagated upward with a dextral strike-slip component as observed at the surface of the model (Figs. 11 and 13). Their maximum horizontal displacement (ca. 2 mm) amounts to 2 km in nature if scaling rules apply.

Several experiments were targeted to understand the inversion of extensional fault patterns by using analogue modelling, such as reactivation of a simple listric normal faults or tilted fault blocks (e.g. McClay 1989, 1996; Mitra 1993; Sassi et al. 1993; Eisenstadt and Withjack 1995; Viola et al. 2004). These studies indicate how the orientation of old faults relative to the stress field strongly affects the rate and degree of reactivation. Brun and Nalpas (1996) show that the angle between compression and fault trend should be $<45^\circ$ in their experiments in order for faults to be reactivated in oblique slip mode, and when larger than 45° they will be active as strike-slip faults while oblique displacement is accommodated by newly formed thrust faults. In our models, the graben oriented $N050^\circ E$ (i.e. at 40° from the direction of compression) only exhibited a reverse component with no visible sign of strike-slip movement at the surface while faults oriented $N065^\circ E$ (i.e. at 25° from the direction of compression) showed clear strike-slip movement at the surface with a strong component of reverse in cross-section. When the compression rate was reduced in experiment D, the pre-existing faults showed considerably less strike-slip movement along the surface. Thus, it is likely that the difference between our models and those of Brun and Nalpas (1996) is caused by activity of the main N-S strike-slip faults that is affecting the pre-existing structures and causing strike-slip movement along these fault observed at the surface. The horizontal displacement reduction along the pre-existing faults away from the main N-S strike-slip faults further asserts this relationship.

In addition to the effect of the angle of pre-existing faults, our experiments showed that the rate of compression also impacts fault inversion. Decreased compression velocity has

resulted in smaller fault inversion in experiment D. The pre-existing faults were reactivated and show a very small amount of strike-slip at the surface. Similarly, they do show a smaller degree of reverse faulting compared to the other experiments described herein. The resulting restraining bend is also slightly segmented, probably due to the effect of the small pre-existing fault reactivation. This is due to the fact that the decreased velocity of compression has affected the viscosity of the silicone making it more ductile.

Comparison with the Central Levant Margin

Comparison between the experiments undertaken in this study and the natural example yields results with a certain similarity. The introduced pre-existing faults in the model represent the numerous ENE-WSW inherited normal faults found along the Levant margin. We only introduced two faults in the model for simplicity although the margin is cross-cut by tens of latitudinal faults.

Experiment B yields results that are the closest and most comparable with the natural example. In this experiment, the pre-existing faults have almost the same orientation as the faults along the margin. In the model, the pre-existing faults exhibited strike-slip movement at the surface, amounting to 1–2 km of displacement after scaling, in a very similar way to the faults along the central Levant margin. Similarly, the resulting model was compartmentalised at the intersection between the main sinistral strike-slip fault and the reactivated dextral strike-slip faults having a reverse component in section view. The compartmentalisation of the Levant restraining bend is documented in literature (e.g. Dubertret 1955; Hancock and Atiya 1979; Walley 1998) but no study have discussed the role of these latitudinal faults in this compartmentalisation. The northern Mount Lebanon is separated from its southern counterpart by the Damour fault, a fault zone that is currently active. According to our model, it is likely that the Damour fault zone corresponds to a deep crustal fault that is affecting the style of the restraining bend by creating two different compartments with markedly different structural styles. The model is different as it exhibits three compartments separated by two major crustal faults. In this sense, the smaller ENE-WSW latitudinal faults along Mount Lebanon might correspond either to smaller crustal faults or have some other mechanical control over their reactivation, because they were not affecting the growth and segmentation of the restraining bend in the same degree as the Damour fault. The modelling parameters could not take into account the variety of faults with their respective size and distribution and for this reason we opted for only two large faults bordering a graben. The model shows however, that crustal faults will be reactivated during transpression.

Other similarities between the model and the natural example include the counter-clockwise rotation in the central pop-up. This rotation amounts to 18° in Pliocene times and 28° in total since Late Cretaceous (Henry et al. 2010). Slightly larger values of 20° – 30° is observed in the analogue model described in this work and in other experiments (e.g. Mitra and Paul 2011) making block rotation a primary feature of restraining bends. The pre-existing faults thus serve as weak planes to localise compression and to help counter-clockwise rotation of the Levant margin (Ron et al. 1984; Ghalayini et al. 2014) in later stages of transpression following the model of Jackson (1987).

The Relationship Between the Palmyrides and the Levant Margin

The pre-existing faults in the model simulate structures along the central Levant Margin that are most likely part of the Palmyra Basin extending to Lebanon and responsible of establishing a pre-existing fabric. This is not surprising since the Palmyra Basin contains similar structures, is bordering the central Levant margin and the Palmyrides ranges are considered to extend to Lebanon encompassing the Anti-Lebanon ranges (Searle 1994; Brew 2001). Therefore, it is very likely that the central Levant margin constitutes the western continuation of the Palmyra Basin, given that the modelled faults in the analogue experiment yielded results very similar to observations along the Levant restraining bend upon its deformation and inversion.

Such hypothesis points to a common geologic history between the Levant margin in Lebanon and the Palmyra Basin. Both witnessed similar tectonic events with rifting and inversion. Several arguments, discussed in previous sections, point that the Levant margin was deformed and uplifted in the Neogene similarly to the Palmyrides ranges. The crust is thinning to the west, indicating continuity in the Palmyrides trend toward the Levant Basin with no abrupt crustal variation. Thus, it is most likely that the Palmyra Basin extends westward to Lebanon whereby its pre-existing structures must have played an important role in affecting the style of deformation along the central margin, in a similar way to the Palmyrides ranges.

Impact on the Evolution of the LFS

Reconstruction of the Palmyra Basin prior to the onset of the LFS brings the Jhar fault closer to the Saida and Damour faults in Lebanon (Fig. 14). Today they are separated from the Jhar by ~ 85 km of horizontal displacement, and when the 20 km of shortening in the Palmyrides are taken in the calculation (Chaimov et al. 1990), the total displacement will

add up to ~ 107 km as proposed for the southern LFS (Quennell 1958). The three faults have the same trend, they are deep faults active since at least the Mesozoic and both separate two different crustal blocks (see fault F1 in Ghalayini et al. 2014). Thus it is very likely that the Saida, Damour and the Jhar faults are in fact the same structure but today they are displaced by the LFS.

However, the total 107 km LFS displacement is contested along its central segment in Lebanon with only a maximum of 30 or 40 km of displacement mapped (see section above). This variation in lateral displacement has been the focus of many debates during the last century (for a review refer to Beydoun 1999). Since it is agreed that the LFS is considered as a large transform system linking rifting in the Red Sea with collision in the Taurus (Freund et al. 1970), one can argue that such transform has variable displacement along its path, becoming less pronounced in the north when reaching the Taurus collision zone. Nevertheless, the GPS data does not show any decrease in motion in NW Syria relative to the southern LFS segment (Reilinger et al. 2006; Gomez et al. 2007a) refuting such hypothesis. An alternative solution, proposed by Hardy et al. (2010) states that the Lebanese restraining bend is a relay between two strike-slip faults, forming at a later stage. As much as this model seems likely, the difficulty in finding supportive evidence is persistent. For example, the northern Ghab segment shows only 30–40 km displacement (Al Abdalla et al. 2010), significantly less than the one measured along the Dead Sea segment but similar to the one documented in Lebanon (Dubertret 1972; Walley 1998). Furthermore, it is documented that the the LFS in north Syria formed during the Messinian or Pliocene (Searle et al. 2010), later than or synchronous with the proposed Late Miocene/Pliocene time for the Lebanese restraining bend (e.g. Gomez et al. 2007b; Homberg et al. 2010).

We propose what could be a likely model for the propagation of the LFS related to heterogeneities in crustal strength along its path. The location of the LFS parallel to the coast of the Levant margin has been established preferentially in the continental crust close to the thinned continental crust situated to the west (e.g. Vink et al. 1984; Lyakhovskiy et al. 2012). According to Steckler and Ten Brink (1986) this intersection is considered as being the weakest zone and thus the mechanically easiest place to initiate a plate boundary. It is likely that the northward propagation of the LFS was initially halted at the latitude of the Palmyra Basin (Fig. 15). Here, the N-S variation in crustal thickness, decreasing from 36 km in Israel to 20 km in Lebanon (Netzeband et al. 2006), the presence of the Palmyrides structures (including Mount Lebanon) and a thicker sedimentary cover have all contributed to bending of the LFS due to lithospheric strength variations (Steckler and ten Brink 1986). In the southern LFS segment, the interaction between the propagating strike-slip fault and the

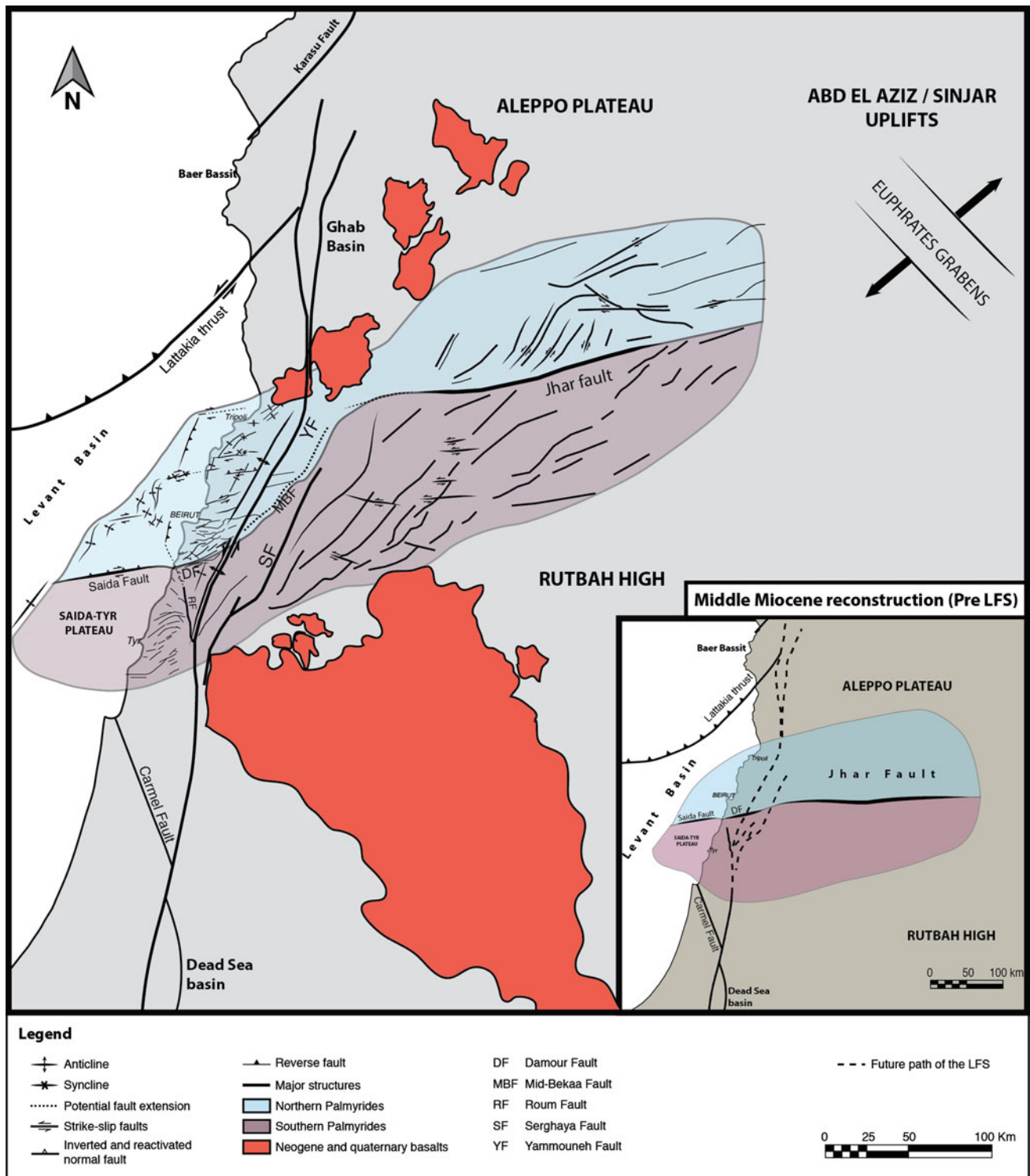


Fig. 14 Map showing the proposed extension of the Palmyra basin westward into the Levant margin. Thus, northern Mount Lebanon corresponds to the northern Palmyrides while the southern Mount Lebanon corresponds to the southern Palmyrides. The Saida fault and the Damour fault are likely the westward continuation of the Jhar fault as they show a displacement of ~85 km and separate blocks that are structurally different. The Mid-Bekaa Fault might also be the link

between the Jhar and the Damour fault. The small map on the right is a simple reconstruction of the initial geometry of the Palmyra basin prior to the activity of the LFS. Note that during this time, it is very likely that the Levant margin was already structured and Mount Lebanon in place. Map compiled from Ghalayini et al. (2014), Brew et al. (2001a, b), Walley (1998), Searle (1994), Dubertret (1955)

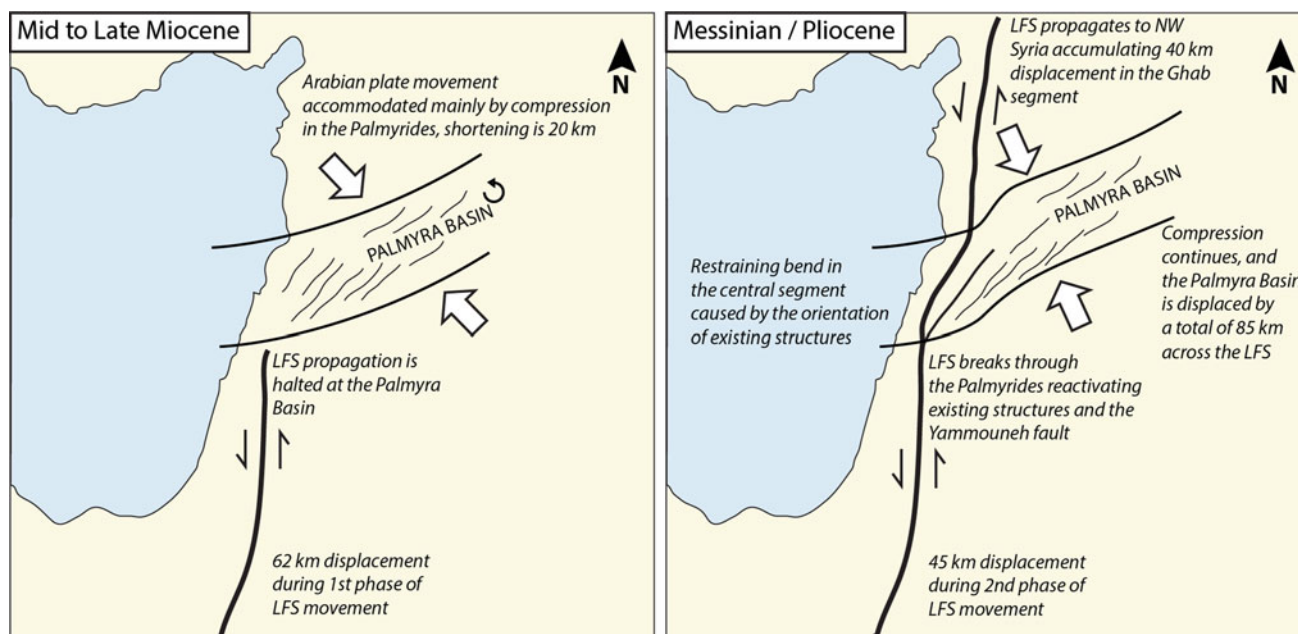


Fig. 15 Map showing the evolution of the Levant Fracture System through time. The LFS has initiated during the Mid to Late Miocene in the Dead Sea Segment in Israel. Its northward propagation was halted by the deformed Palmyra Basin and because of lithospheric strength variations. Thus the northward movement of Arabia was mostly accommodated by folding and compression in the Palmyra Basin and Lebanon amounting to 20 km of shortening. In the Messinian and Pliocene, the LFS propagated northward reactivating existing structures in the Palmyra such as the Yammouneh fault and continued its way

northward along the Ghab segment in NW Syria. The movement of the LFS during this time was mostly accommodated by strike-slip faulting and compression in the Palmyra region where it has accumulated 45 km in its southern segment and around 30–40 km in its central segment in Lebanon. The remaining displacement is most likely accommodated through strain partitioning along the structures of the Palmyrides. The stress field has changed from compressive NW-SE direction in the Mid to Late Miocene to compressive NNW-SSE in the Pliocene and recent times

pre-existing Azraq-Sirhan Graben has affected the propagation of the transform and resulted in right stepping fault segments of the LFS (Segev et al. 2014). It is thus very likely that the interaction between the Palmyra Basin and the northward propagating LFS has affected the geometry of the fault making it easier for the LFS to bend rightward, reactivate and amplify existing structures, such as the Yammouneh and Serghaya fault, rather than creating new ones.

This process must have happened during the two documented stages of the LFS movement (Quennell 1958; Freund et al. 1970). During the first phase in the Late Miocene, 62 km displacement was recorded in southern Israel and as the LFS could not propagate through the Lebanese segment of the Palmyrides, the accommodation of movement was most probably taking place through shortening, folding and counter-clockwise rotation (Henry et al. 2010) (Fig. 15). This shortening should have amounted to a maximum of 20 km in the Palmyrides and Lebanon, since the Jhar fault is separated from its Lebanese counterpart by 85 km, pointing that ~20 km of shortening was accommodated through folding. According to Chaimov et al. (1993) and Henry et al.

(2010) the Palmyrides and Lebanon exhibit 20 and ~25 km of shortening respectively. Similarly, Ghalayini et al. (2014) proved that shortening in the Levant basin offshore Lebanon has only taken place prior to the Pliocene.

It is only during the second phase in the Late Messinian and Pliocene that the LFS has propagated into the Palmyrides and large-scale strike-slip movement on the Yammouneh and Serghaya faults have taken place with the displacement significantly accelerating. It is during this phase that the ~30–40 km horizontal displacement measured in Lebanon must have been taking place. Synchronously, the northern Ghab segment must have been activated during this time and accumulated the same 30–40 km displacement. In the Levant Basin, these two stages are well recorded and affect all the offshore structures accordingly (Ghalayini et al. 2014). In conclusion, the total horizontal displacement should have been accommodated by 20 km shortening in the Palmyrides and the Lebanese blocks, while the remaining 85 km partitioned among all the structures of the Palmyrides, including the Lebanese structures. For this reason, the Jhar fault is separated from its Damour-Saida counterparts by 85 km.

Conclusion

The review of the evolution of the Levant region concur that the current structural setting observed in the Levant is profoundly impacted by pre-existing structures. This hypothesis was tested by means of analogue modelling performed in this study, to particularly investigate the effects of the intersected Palmyra/Levant on the growth of the Levant Fracture System. Results indicated geometrical similarities between the Levant restraining bend and that of the model, emphasizing the role of oblique existing structures on the evolution of the restraining bend, mainly causing its segmentation. ENE-WSW ancient extensional structures are found along the Levant margin both offshore and onshore, along the restraining bend and in the Palmyra Basin. There is a certain similarity between these structures, namely in their comparable size, strike, and inheritance from the Mesozoic rifting event. Similarly, no abrupt crustal boundary between Lebanon and the Palmyrides exists. Such observations indicate that it is very likely that the observed pre-existing structures are part of the Mesozoic Palmyra Basin, which extends westward into the Levant margin.

The evolution and propagation of the LFS was strongly affected by the Palmyra Basin and the associated crustal thickness variations. Thus, the location of the LFS is not random but follows instead crustal weaknesses in the lithosphere caused by the N-S and E-W crustal thickness variations. We have proposed a model that likely explains the evolution of the region taking into account the total displacement along the LFS and the spacing between the Jhar and its corresponding extension in Lebanon to join the Damour and Saida faults. Today they are separated by around 85 km of displacement, indicating that 20 km shortening in the Palmyrides was responsible for accommodating part of the total displacement while the remaining 85 km is displayed through horizontal displacement.

Initial structuration has important effects on the geometry of the popup. The orientations of existing structures play a key role in controlling whether the structures will be reactivated or not. The modelling performed in this study investigated the effect of oblique structuration instead, and revealed to which degree they might affect the restraining bend. A future study should test the effect of existing folds and whether they impact the final geometry of the popup, and include the mantle in the modelling parameters.

Acknowledgments The authors would like to acknowledge TOTAL, IFPEN, and UPMC, for funding this project. The Lebanese Ministry of Energy and Water and the Lebanese Petroleum Administration are thanked for their support. Marie-Claude Lynch is greatly acknowledged for her help scanning the models. Editor Francois Roure, Bernard Colletta and an anonymous reviewer are greatly acknowledged for their detailed and constructive reviews, which helped focus the manuscript.

References

- Al Abdalla A, Barrier É, Matar A, Müller C (2010) Late Cretaceous to Cenozoic tectonic evolution of the NW Arabian platform in NW Syria. In: Homberg C, Bachmann M (eds) Evolution of the Levant margin and western Arabia platform since the Mesozoic, vol 341. Geological Society Special Publications, London, pp 305–327
- Al-Saad D, Sawaf T, Gebran A, Barazangi M, Best JA, Chaimov TA (1992) Crustal structure of central Syria: the intracontinental Palmyride mountain belt. *Tectonophysics* 207(3–4):345–358. doi:[10.1016/0040-1951\(92\)90395-M](https://doi.org/10.1016/0040-1951(92)90395-M)
- Arsenikos S, Frizon De Lamotte D, Chamot-Rooke N, Mohn G, Bonneau MC, Blanpied C (2013) Mechanism and timing of tectonic inversion in Cyrenaica (Libya): integration in the geodynamics of the East Mediterranean. *Tectonophysics* 608:319–329. doi:[10.1016/j.tecto.2013.09.025](https://doi.org/10.1016/j.tecto.2013.09.025)
- Barrier É, Vrielynck B (2008) Paleotectonic maps of the Middle East: tectono-sedimentary-palinspatic maps from Late Norian to Pliocene, 14 maps, Comm. la Cart. Geol. du monde
- Barrier E, Machhour L, Blaizot M (2014) Petroleum systems of Syria. In: Marlow L, Kendall C, Yose L (eds) Petroleum systems of the Tethyan region: AAPG Memoir 106, pp 335–378
- Ben-Avraham Z (1978) The structure and tectonic setting of the Levant continental margin, eastern Mediterranean. *Tectonophysics* 46:313–331
- Ben-Avraham Z, Ginzburg A, Makris J, Eppelbaum L (2002) Crustal structure of the Levant Basin, eastern Mediterranean. *Tectonophysics* 346(1–2):23–43. doi:[10.1016/S0040-1951\(01\)00226-8](https://doi.org/10.1016/S0040-1951(01)00226-8)
- Best JA, Barazangi M, Al-Saad D, Sawaf T, Gebran A (1993) Continental margin evolution of the Northern Arabian Platform in Syria. *Am Assoc Pet Geol Bull* 77(2):173–193
- Beydoun ZR (1977) Petroleum prospects of Lebanon: reevaluation. *Am Assoc Pet Geol Bull* 61(1), 43–64. doi:[10.1306/C1EA3BF4-16C9-11D7-8645000102C1865D](https://doi.org/10.1306/C1EA3BF4-16C9-11D7-8645000102C1865D)
- Beydoun ZR (1981) Some open questions relating to the petroleum prospects of Lebanon. *J Pet Geol* 3:303–314. doi:[10.1306/BF9AB5CA-0EB6-11D7-8643000102C1865D](https://doi.org/10.1306/BF9AB5CA-0EB6-11D7-8643000102C1865D)
- Beydoun ZR (1988) The Middle East: regional geology and petroleum resources. Scientific Press, Beaconsfield
- Beydoun ZR (1999) Evolution and development of the Levant (Dead Sea Rift) transform system: a historical-chronological review of a structural controversy. In: Mac Niocail C, Ryan PD (eds) Continental tectonics, vol 164. Geological Society Special Publications, London, pp 239–255
- Beydoun ZR, Habib JG (1995) Lebanon revisited: new insights into Triassic hydrocarbon prospects. *J Pet Geol* 18(1):75–90
- Boudagher-fadel M, Clark GN (2006) Stratigraphy, paleoenvironment and paleogeography of Maritime Lebanon: a key to Eastern Mediterranean Cenozoic history. *Stratigraphy* 3(2):1–38
- Brew GE (2001) Tectonic evolution of Syria interpreted from integrated geophysical and geological analysis. Cornell University
- Brew GE, Lupa J, Barazangi M, Sawaf T, Al-Imam A, Zaza T (2001a) Structure and tectonic development of the Ghab basin and the Dead Sea fault system, Syria. *J Geol Soc London* 158(4):665–674. doi:[10.1144/jgs.158.4.665](https://doi.org/10.1144/jgs.158.4.665)
- Brew GE, Barazangi M, Al-Maleh AK, Sawaf T (2001b) Tectonic and geologic evolution of Syria. *GeoArabia* 6(4):573–616
- Brun J, Nalpas T (1996) Graben inversion in nature and experiments. *Tectonics* 15(2):677. doi:[10.1029/95TC03853](https://doi.org/10.1029/95TC03853)
- Butler RWH, Spencer S (1999) Landscape evolution and the preservation of tectonic landforms along the northern Yammouneh Fault, Lebanon. *Geol Soc Lond Spec Publ* 162(1):143–156. doi:[10.1144/GSL.SP.1999.162.01.12](https://doi.org/10.1144/GSL.SP.1999.162.01.12)

- Carton H et al (2009) Seismic evidence for Neogene and active shortening offshore of Lebanon (Shalimar cruise). *J Geophys Res* 114:15–18. doi:[10.1029/2007JB005391](https://doi.org/10.1029/2007JB005391)
- Chaimov TA, Barazangi M, Al-Saad D, Sawaf T, Gebran A (1990) Crustal shortening in the Palmyride fold belt, Syria, and implications for movement along the Dead Sea fault system. *Tectonics* 9:1369–1386
- Chaimov TA, Barazangi M, Al-Saad D, Sawaf T, Gebran A (1992) Mesozoic and Cenozoic deformation inferred from seismic stratigraphy in the southwestern intracontinental Palmyride fold-thrust belt, Syria. *Geol Soc Am Bull* 104(6):704–715. doi:[10.1130/0016-7606\(1992\)104<0704:MACDIF>2.3.CO;2](https://doi.org/10.1130/0016-7606(1992)104<0704:MACDIF>2.3.CO;2)
- Chaimov TA, Barazangi M, Al-Saad D, Sawaf T, Khaddour M (1993) Seismic fabric and 3-D structure of the southwestern intracontinental Palmyride fold belt, Syria. *Am Assoc Pet Geol Bull* 77 (12):2032–2047
- Colletta B, Bale P, Ballard JF, Letouzey J, Pinedo R (1991) Computerized X-ray tomography analysis of sandbox models: examples of thin-skinned thrust systems. *Geology* 19:1063–1067
- Collin PY, Mancinelli A, Chiocchini M, Mroueh M, Hamdan W, Higazi F (2010) Middle and Upper Jurassic stratigraphy and sedimentary evolution of Lebanon (Levantine margin): palaeoenvironmental and geodynamic implications. In: Homberg C, Bachmann M (eds) *Evolution of the Levant margin and western Arabia platform since the Mesozoic*, vol 341. Geological Society Special Publications, London, pp 227–244
- Daeron M (2005) comportement sismique à long terme de la faille de Yammoûneh. PhD thesis, Institut du Physique du Globe de Paris
- Daëron M, Benedetti L, Tapponnier P, Sursock A, Finkel RC (2004) Constraints on the post ~25-ka slip rate of the Yammoûneh fault (Lebanon) using in situ cosmogenic ³⁶Cl dating of offset limestone-clast fans. *Earth Planet Sci Lett* 227(1–2):105–119. doi:[10.1016/j.epsl.2004.07.014](https://doi.org/10.1016/j.epsl.2004.07.014)
- Dooley TP, Schreurs G (2012) Analogue modelling of intraplate strike-slip tectonics: a review and new experimental results. *Tectonophysics* 574–575:1–71. doi:[10.1016/j.tecto.2012.05.030](https://doi.org/10.1016/j.tecto.2012.05.030)
- Druckman Y (1981) Comments on the structural reversal model as a factor of the geological evolution of Israel. *Isr J Earth Sci* 30:44–48
- Druckman Y (1984) Evidence for Early-Middle Triassic faulting and possible rifting from the Helez Deep Borehole in the coastal plain of Israel. In: Dixon JE, Robertson AHF (eds) *The geological evolution of the Eastern Mediterranean*, vol 17. Geological Society Special Publications, London, pp 203–212
- Druckman Y, Buchbinder B, Martinotti GM, Siman Tov R, Aharon P (1995) The buried Afiq Canyon (eastern Mediterranean, Israel): a case study of a Tertiary submarine canyon exposed in Late Messinian times. *Mar Geol* 123:167–185
- Dubertret L (1955) Carte Géologique du Liban au 1/200000, 74
- Dubertret L (1972) Sur la dislocation de l'ancienne plaque sialique afrique sinai peninsula arabeque.pdf, Notes Mem. sur le Moyen. Orient 12(2):227–243
- Eisenstadt G, Withjack MO (1995) Estimating inversion: results from clay models. In: Buchanan JG, Buchanan PG (eds) *Basin inversion*, vol 88. Geological Society Special Publications, London, pp 119–136
- Elias A et al (2007) Active thrusting offshore Mount Lebanon: source of the tsunamigenic A.D. 551 Beirut-Tripoli earthquake. *Geology* 35(8):755. doi:[10.1130/G23631A.1](https://doi.org/10.1130/G23631A.1)
- Eyal M, Eyal Y, Bartov Y, Steinitz G (1981) The tectonic development gulf of elat (aqaba) rift of the western margin of the Gulf of Elat (Aqaba) rift. *Tectonophysics* 80:39–66
- Freund R (1965) A model of the structural development of Israel and adjacent areas since Upper Cretaceous times. *Geol Mag* 102(3)
- Freund R, Garfunkel Z, Zak I, Goldberg M, Weissbrod T, Derin B, Bender F, Wellings FE, Girdler RW (1970) The shear along the Dead Sea Rift [and Discussion]. *Philos Trans R Soc Math Phys Eng Sci* 267(1181):107–130. doi:[10.1098/rsta.1970.0027](https://doi.org/10.1098/rsta.1970.0027)
- Frizon de Lamotte D, Raulin C, Mouchot N, Christophe J, Daveau W, Blanpied C, Ringenbach JC (2011) The southernmost margin of the Tethys realm during the Mesozoic and Cenozoic: initial geometry and timing of the inversion processes. *Tectonics* 30:1–22. doi:[10.1029/2010TC002691](https://doi.org/10.1029/2010TC002691)
- Gardosh M, Druckman Y, Buchbinder B, Rybakov M (2006) The Levant basin offshore Israel: stratigraphy, structure, tectonic evolution and implications for hydrocarbon exploration
- Gardosh M, Garfunkel Z, Druckman Y, Buchbinder B (2010) Tethyan rifting in the Levant Region and its role in Early Mesozoic crustal evolution. In: Homberg C, Bachmann M (eds) *Evolution of the Levant margin and western Arabia platform since the Mesozoic*, vol 341. Geological Society Special Publication, London, pp 9–36
- Garfunkel Z (1981) Internal structure of the Dead Sea leaky transform (rift) in relation to plate kinematics. *Tectonophysics* 80:81–108. doi:[10.1016/0040-1951/81/90143-8](https://doi.org/10.1016/0040-1951/81/90143-8)
- Garfunkel Z (1998) Constrains on the origin and history of the Eastern Mediterranean basin. *Tectonophysics* 298(1–3):5–35. doi:[10.1016/S0040-1951\(98\)00176-0](https://doi.org/10.1016/S0040-1951(98)00176-0)
- Garfunkel Z, Derin B (1984) Permian-early Mesozoic tectonism and continental margin formation in Israel and its implications for the history of the Eastern Mediterranean. In: Dixon RJ, Robertson AHF (eds) *The geological evolution of the Eastern Mediterranean*, vol 17. Geological Society Special Publications, London, pp 187–201
- Garfunkel Z, Freund R (1981) Active faulting in the Dead Sea rift. *Tectonophysics* 80:1–26
- Ghalayini R, Daniel J-M, Homberg C, Nader FH, Comstock JE (2014) Impact of Cenozoic strike-slip tectonics on the evolution of the northern Levant Basin (offshore Lebanon). *Tectonics* 33(11):2121–2142. doi:[10.1002/2014TC003574](https://doi.org/10.1002/2014TC003574)
- Ghalayini R, Homberg C, Daniel J-M, Nader FH (2016) Growth of layer-bound normal faults under a regional anisotropic stress field. *Geol Soc Lond Spec Publ* 439. doi:[10.1144/SP439.13](https://doi.org/10.1144/SP439.13)
- Gomez F, Meghraoui M, Darkal AN, Sbeinati R, Darawcheh R, Tabet C, Khawlie M, Charabe M, Khair K, Barazangi M (2001) Coseismic displacements along the Serghaya fault: an active branch of the Dead Sea fault system in Syria and Lebanon. *J Geol Soc Lond* 158:405–408
- Gomez F, Meghraoui M, Darkal AN, Hijazi F, Mouty M, Suleiman Y, Sbeinati R, Darawcheh R, Al-Ghazzi R, Barazangi M (2003) Holocene faulting and earthquake recurrence along the Serghaya branch of the Dead Sea fault system in Syria and Lebanon. *Geophys J Int* 153(3):658–674. doi:[10.1046/j.1365-246X.2003.01933.x](https://doi.org/10.1046/j.1365-246X.2003.01933.x)
- Gomez F, Khawlie M, Tabet C, Darkal AN, Khair K, Barazangi M (2006) Late Cenozoic uplift along the northern Dead Sea transform in Lebanon and Syria. *Earth Planet Sci Lett* 241(3–4):913–931. doi:[10.1016/j.epsl.2005.10.029](https://doi.org/10.1016/j.epsl.2005.10.029)
- Gomez F, Karam G, Khawlie M, McClusky S, Vernant P, Reilinger R, Jaafar R, Tabet C, Khair K, Barazangi M (2007a) Global Positioning System measurements of strain accumulation and slip transfer through the restraining bend along the Dead Sea fault system in Lebanon. *Geophys J Int* 168(3):1021–1028. doi:[10.1111/j.1365-246X.2006.03328.x](https://doi.org/10.1111/j.1365-246X.2006.03328.x)
- Gomez F, Nemer T, Tabet C, Khawlie M, Meghraoui M, Barazangi M (2007b) Strain partitioning of active transpression within the Lebanese restraining bend of the Dead Sea Fault (Lebanon and SW Syria). In: Cunningham WD, Mann P (eds) *Tectonics of strike-slip restraining and releasing bends*, vol 290. Geological Society Special Publications, London, pp 285–303
- Guiraud R, Bosworth W (1997) Senonian basin inversion and rejuvenation of rifting in Africa and Arabia: synthesis and

- implications to plate-scale tectonics. *Tectonophysics* 282(1–4):39–82. doi:[10.1016/S0040-1951\(97\)00212-6](https://doi.org/10.1016/S0040-1951(97)00212-6)
- Guiraud R, Bosworth W (1999) Phanerozoic geodynamic evolution of northeastern Africa and the northwestern Arabian platform. *Tectonophysics* 315:73–108
- Hancock PL, Atiya MS (1979) Tectonic significance of mesofracture systems associated with the Lebanese segment of the Dead Sea transform fault. *J Struct Geol* 1(2):143–153. doi:[10.1016/0191-8141\(79\)90051-8](https://doi.org/10.1016/0191-8141(79)90051-8)
- Hardy C (2009) Evolution tectonique du domaine Levantin depuis le Mésozoïque. Université Pierre et Marie Curie
- Hardy C, Homberg C, Eyal Y, Barrier É, Müller C (2010) Tectonic evolution of the southern Levant margin since Mesozoic. *Tectonophysics* 494(3–4):211–225. doi:[10.1016/j.tecto.2010.09.007](https://doi.org/10.1016/j.tecto.2010.09.007)
- Hatem AE, Cooke ML, Madden EH (2015) Evolving efficiency of restraining bends within wet kaolin experiments. *J Geophys Res Solid Earth* 120:1975–1992. doi:[10.1002/2014JB011735](https://doi.org/10.1002/2014JB011735). Received
- Hawie N, Gorini C, Deschamps R, Nader FH, Montadert L, Granjeon D, Baudin F (2013) Tectono-stratigraphic evolution of the northern Levant Basin (offshore Lebanon). *Mar Pet Geol* 48:392–410. doi:[10.1016/j.marpetgeo.2013.08.004](https://doi.org/10.1016/j.marpetgeo.2013.08.004)
- Hawie N, Deschamps R, Nader FH, Gorini C, Müller C, Desmares D, Hoteit A, Granjeon D, Montadert L, Baudin F (2014) Sedimentological and stratigraphic evolution of northern Lebanon since the Late Cretaceous: implications for the Levant margin and basin. *Arab J Geosci* 7(4):1323–1349. doi:[10.1007/s12517-013-0914-5](https://doi.org/10.1007/s12517-013-0914-5)
- Henry B, Homberg C, Mroueh M, Hamdan W, Higazi F (2010) Rotations in Lebanon inferred from new palaeomagnetic data and implications for the evolution of the Dead Sea Transform system. In: Homberg C, Bachmann M (eds) vol 341. Geological Society Special Publications, London, pp 269–285
- Hirsch F, Flexer A, Rosenfeld A, Yellin-Dror A (1995) Palinspastic and crustal setting of the eastern Mediterranean. *J Pet Geol* 18(2):149–170
- Homberg C, Barrier É, Mroueh M, Hamdan W, Higazi F (2009) Basin tectonics during the Early Cretaceous in the Levant margin, Lebanon. *J Geodyn* 47(4):218–223. doi:[10.1016/j.jog.2008.09.002](https://doi.org/10.1016/j.jog.2008.09.002)
- Homberg C, Barrier É, Mroueh M, Müller C, Hamdan W, Higazi F (2010) Tectonic evolution of the central Levant domain (Lebanon) since Mesozoic time. In: Homberg C, Bachmann M (eds) Evolution of the Levant margin and western Arabia platform since the Mesozoic, vol 341. Geological Society, London, pp 245–268
- Hounsfield GN (1973) Computerized transverse axial scanning (tomography). *Br J Radiol* 46:1016–1022
- Hubbert MK (1937) Theory of scale models as applied to the study of geologic structures. *Geol Soc Am Bull* 48:1459–1520
- Jackson JA (1987) Active normal faulting and crustal extension. In: Coward MP, Dewey JF, Hancock PL (eds) Continental extensional tectonics, vol 28. Geological Society Special Publications, London, pp 3–17
- Khair K, Tsokas GN (1999) Nature of the Levantine (eastern Mediterranean) crust from multiple-source Werner deconvolution of Bouguer gravity anomalies. *J Geophys Res* 104(B11):25469–25478. doi:[10.1029/1999JB900228](https://doi.org/10.1029/1999JB900228)
- Khair K, Khawlie M, Haddad F, Barazangi M, Seber D, Chaimov TA (1993) Bouguer gravity and crustal structure of the Dead Sea transform fault and adjacent mountain belts in Lebanon. *Geology* 21:739–742
- Khair K, Tsokas GN, Sawaf T (1997) Crustal structure of the northern Levant region: multiple source Werner deconvolution estimates for Bouguer gravity anomalies. *Geophys J Int* 128(3):605–616. doi:[10.1111/j.1365-246X.1997.tb05322.x](https://doi.org/10.1111/j.1365-246X.1997.tb05322.x)
- Lyakhovsky V, Segev A, Schattner U, Weinberger R (2012) Deformation and seismicity associated with continental rift zones propagating toward continental margins. *Geochem Geophys Geosyst* 13(1):1–21. doi:[10.1029/2011GC003927](https://doi.org/10.1029/2011GC003927)
- Makris J, Ben-Avraham Z, Behle A, Ginzburg A, Giese P, Steinmetz L, Whitmarsh RB, Eleftheriou S (1983) Seismic refraction profiles between Cyprus and Israel and their interpretation. *Geophys J Int* 75:575–591
- Mattioni L, Sassi W, Callot J (2007) Analogue models of basin inversion by transpression: role of structural heterogeneity. In: Ries AC, Butler RWH, Graham RH (eds) Deformation of the continental crust: the legacy of Mike Coward, vol 272. Geological Society Special Publications, London, pp 397–417
- McClay KR (1989) Analogue models of inversion tectonics. In: Cooper MA, Williams GD (eds) inversion tectonics, vol 44. Geological Society Special Publications, London, pp 41–59
- McClay KR (1996) Recent advances in analogue modelling: uses in section interpretation and validation. In: Buchanan PG, Nieuwland DA (eds) Modern developments in structural interpretation, validation and modelling, vol 99. Geological Society Special Publications, London, pp 201–225
- McClay KR, Bonora M (2001) Analog models of restraining stepovers in strike-slip fault systems. *Am Assoc Pet Geol Bull* 85(2):233–260
- Mitra S (1993) Geometry and kinematic evolution of inversion structures. *Am Assoc Pet Geol Bull* 77(7):1159–1191
- Mitra S, Paul D (2011) Structural geometry and evolution of releasing and restraining bends: insights from laser-scanned experimental models. *Am Assoc Pet Geol Bull* 95(7):1147–1180. doi:[10.1306/09271010060](https://doi.org/10.1306/09271010060)
- Montadert L, Nicolaidis S, Semb PH, Lie O (2014) Petroleum systems offshore Cyprus. In: Marlow L, Kendall C, Yose L (eds) Petroleum systems of the Tethyan region. AAPG special publication, Tulsa, pp 301–334
- Müller C, Higazi F, Hamdan W, Mroueh M (2010) Revised stratigraphy of the Upper Cretaceous and Cenozoic series of Lebanon based on nannofossils. In: Homberg C, Bachmann M vol 341. Geological Society Special Publications, London, pp 287–303
- Nader FH (2011) The petroleum prospectivity of Lebanon: an overview. *J Pet Geol* 34(April):135–156
- Nader FH, Swennen R (2004) The hydrocarbon potential of Lebanon: new insights from regional correlations and studies of Jurassic dolimitization. *J Pet Geol* 27(3):253–275
- Netzeband G, Gohl K, Hübscher C, Ben-Avraham Z, Dehghani GA, Gajewski D, Liersch P (2006) The Levantine Basin—crustal structure and origin. *Tectonophysics* 418(3–4):167–188. doi:[10.1016/j.tecto.2006.01.001](https://doi.org/10.1016/j.tecto.2006.01.001)
- Ponikarov VP (1966) The geological map of Syria scale 1:1000000 explanatory notes. Syrian Arab Republic Ministry of Industry, Damascus
- Quennell AM (1958) The structural and geomorphic evolution of the Dead Sea Rift. *Q J Geol Soc* 114(1–4):1–24. doi:[10.1144/gsjgs.114.1.0001](https://doi.org/10.1144/gsjgs.114.1.0001)
- Quennell AM (1984) The Western Arabia rift system. In: Dixon RJ, Robertson AHF (eds) The geological evolution of the Eastern Mediterranean, vol 17. Geological Society Special Publications, London, pp 775–788
- Ramberg H (1967) Gravity, deformation and the earth's crust. Academic Press, New York
- Reilinger R et al (2006) GPS constraints on continental deformation in the Africa-Arabia-Eurasia continental collision zone and implications for the dynamics of plate interactions. *J Geophys Res* 111(B5):B05411. doi:[10.1029/2005JB004051](https://doi.org/10.1029/2005JB004051)

- Renouard G (1955) Oil prospects of Lebanon. *Am Assoc Pet Geol Bull* 39(11):2125–2169
- Robertson AHF (1998a) Mesozoic-Tertiary tectonic evolution of the Easternmost Mediterranean area: integration of marine and land evidence. *Proc Ocean Drill Program Sci Results* 160
- Robertson AHF (1998b) Tectonic significance of the Eratosthenes Seamount: a continental fragment in the process of collision with a subduction zone in the eastern Mediterranean (Ocean Drilling Program Leg 160). *Tectonophysics* 298(1–3):63–82. doi:[10.1016/S0040-1951\(98\)00178-4](https://doi.org/10.1016/S0040-1951(98)00178-4)
- Robertson AHF (2007) Overview of tectonic settings related to the rifting and opening of Mesozoic ocean basins in the Eastern Tethys: Oman, Himalayas and Eastern Mediterranean regions. In: Karner GD, Manatschal G, Pinheiro LM (eds) *Imaging, mapping and modelling continental lithosphere extension and breakup*, vol 282. Geological Society Special Publications, London, pp 325–388
- Robertson AHF, Dixon JE (1984) Introduction: aspects of the geological evolution of the Eastern Mediterranean Introduction: aspects of the geological evolution of the Eastern Mediterranean. In: Robertson AHF, Dixon JE (eds) *the geological evolution of the Eastern Mediterranean*, vol 17. Geological Society Special Publications, London, pp 1–74
- Robertson AHF, Mountrakis D (2006) Tectonic development of the Eastern Mediterranean region: an introduction. In: Robertson AHF, Mountrakis D (eds) *Tectonic development of the Eastern Mediterranean region*, vol 260. Geological Society Special Publications, London, pp 1–9
- Ron H, Freund R, Garfunkel Z, Nur A (1984) Block rotation by strike-slip faulting: structural and paleomagnetic evidence. *J Geol Res* 89(B7):6256–6270
- Sabbagh G (1961) *Stratigraphie et tectonique du liban generalites: exemple de deux structures anticlinales*. Memoire de these, Faculte de Science de Grenoble
- Sabbagh G (1962) Geological cross-section across northern and southern Mount Lebanon. *Am Univ Beirut Arch*
- Sassi W, Colletta B, Bale P, Paquereau T (1993) Modelling of structural complexity in sedimentary basins: the role of pre-existing faults in thrust tectonics. *Tectonophysics* 226:97–112
- Sawaf T, Brew GE, Litak RK, Barazangi M (2001) Geologic evolution of the intraplate palmyride basin and euphrates fault system syria. In: Ziegler PA, Cavazza W, Robertson AHF, Crasquin-Soleau S (eds) *Peri-Tethys Memoir 6: Peri-Tethyan rift/Wrench basins and passive margins*. Memoire du Museum national d'histoire naturelle, Paris, pp 441–467
- Searle MP (1994) Structure of the intraplate eastern Palmyride fold belt, Syria. *Geol Soc Am Bull* 106:1332–1350. doi:[10.1130/0016-7606\(1994\)106<1332](https://doi.org/10.1130/0016-7606(1994)106<1332)
- Searle MP, Chung S-L, Lo C-H (2010) Geological offsets and age constraints along the northern Dead Sea fault, Syria. *J Geol Soc Lond* 167(5):1001–1008. doi:[10.1144/0016-76492010-009](https://doi.org/10.1144/0016-76492010-009)
- Segev A, Lyakhovsky V, Weinberger R (2014) Continental transform-rift interaction adjacent to a continental margin: the Levant case study. *Earth-Sci Rev* 139:83–103. doi:[10.1016/j.earscirev.2014.08.015](https://doi.org/10.1016/j.earscirev.2014.08.015)
- Smit J, Brun J-P, Cloetingh S, Ben-Avraham Z (2010) The rift-like structure and asymmetry of the Dead Sea Fault. *Earth Planet Sci Lett* 290(1–2):74–82. doi:[10.1016/j.epsl.2009.11.060](https://doi.org/10.1016/j.epsl.2009.11.060)
- Stampfli GM, Hochard C (2009) Plate tectonics of the Alpine realm. In: Murphy JB, Keppie JD, Hynes AJ (eds) *Ancient orogens and modern analogues*, vol 327. Geological Society Special Publication, London, pp 89–111
- Steckler MS, ten Brink US (1986) Lithospheric strength variations as a control on new plate boundaries: examples from the northern Red Sea region. *Earth Planet Sci Lett* 79(1–2):120–132. doi:[10.1016/0012-821X\(86\)90045-2](https://doi.org/10.1016/0012-821X(86)90045-2)
- Vidal N, Alvarez-Marron J, Klaeschen D (2000) Internal configuration of the Levantine Basin from seismic reflection data (eastern Mediterranean). *Earth Planet. Sci Lett* 180:77–89
- Vink GE, Morgan WJ, Zhao W-L (1984) Preferential rifting of continents a source of displaced terrains. *J Geol* 89(B12):10072–10076
- Viola G, Odonne F, Mancktelow N (2004) Analogue modelling of reverse fault reactivation in strike-slip and transpressive regimes: application to the Giudicarie fault system, Italian Eastern Alps. *J Struct Geol* 26(3):401–418. doi:[10.1016/j.jsg.2003.08.014](https://doi.org/10.1016/j.jsg.2003.08.014)
- Walley CD (1988) A braided strike-slip model for the northern continuation of the Dead Sea Fault and its implications for Levantine tectonics. *Tectonophysics* 145(1–2):63–72. doi:[10.1016/0040-1951\(88\)90316-2](https://doi.org/10.1016/0040-1951(88)90316-2)
- Walley CD (1998) Some outstanding issues in the geology of Lebanon and their importance in the tectonic evolution of the Levantine region. *Tectonophysics* 298(1–3):37–62. doi:[10.1016/S0040-1951\(98\)00177-2](https://doi.org/10.1016/S0040-1951(98)00177-2)
- Weijermars R (1986) Flow behaviour and physical chemistry of bouncing putties and related polymers in view of tectonic laboratory applications. *Tectonophysics* 124:325–358

Tectonic Style and Structural Features of Alpine-Himalayan Orogeny in Central Arabia

Abdullah O. Bamousa, Abdullah M. Memesh, Saleh M. Dini,
and Ali A. Al-Zahrani

Abstract

Mesozoic rocks of the Interior Homocline and overlying Early Paleogene rocks in Central Saudi Arabia were investigated via detailed geologic and structural mapping, image interpretation and GIS compilation of geological and remote sensing data. These rocks were deformed by several large-scale tectonic and structural features. The main tectonic feature is related to the East Arabian Block, which is bounded by three large-scale structures. The northern margin of the East Arabian Block is outlined by Wadi Al Batin Dextral Fault. The western margin of the block is related to the Az Zulfi Lineament, whereas the southern boundary of the block corresponds to Dhurma-Nisah-Sahba Sinistral Fault zone, also known as the Central Arabian graben. The East Arabian Block includes several large-scale features, such as N-S Artawiyah Depression, which is a geomorphic feature reflecting inversion and reactivation of the Proterozoic Al Amar fault that extends below the Phanerozoic rocks from easternmost Arabian Shield up to Iraq. Structural features include the NNW-SSE Majma'ah Sinistral Fault Zone, and the NNW-SSE fault-related Majma'ah anticline, as well as other NNW-SSE anticlines, such as Al Jinadriyah and Jabal Al Jubayl anticlines. The NNW-SSE Majmaah fault zone and fault-related fold deformed Paleogene beds and older rock units. Therefore, these various structural features suggest a first episode of inversion during the Eocene, which occurred synchronously with the Alpine-Himalayan Orogeny. However, these tectonic features still control local depressions, developed during the Pleistocene, which have accommodated sedimentation and deposition of Pliocene rocks and Pleistocene sediments. E-W and NE-SW trending structural features such as E-W sinistral fault zones, the NE-SW Wadi Al-Batin strike-slip fault, and minor NE-SW en echelon strike-slip faults and folds dissected the former N-S structural features in Central Arabia. These younger features developed during the Pleistocene, accounting for a second phase of foreland inversions, and are still related to the Alpine-Himalayan Orogeny. This recent deformational event includes disharmonic folds, formed by detachment folding and layer-parallel shortening of the Late Jurassic to Early Cretaceous strata of the Sulaiy Formation. The detachment folding event may be part of a decollement zone, responsible for the overall basin-and-dome out crop pattern of the Sulaiy Formation. The cross-cutting relationship between the NNW-SSE structures and the NE-SW fractures and folds suggest a main NE-SW regional tectonic stresses, developed by Zagros Mountain fold-and-thrust belt in its adjacent foreland. The

A.O. Bamousa (✉)
Geology Department, Taibah University, Madinah, Saudi Arabia
e-mail: abamousa@taibahu.edu.sa; aobamousa@gmail.com

A.M. Memesh · S.M. Dini · A.A. Al-Zahrani
Saudi Geological Survey, Jeddah, Saudi Arabia

© Springer International Publishing AG 2017
F. Roure et al. (eds.), *Lithosphere Dynamics and Sedimentary Basins of the Arabian Plate and Surrounding Areas*, Frontiers in Earth Sciences, DOI 10.1007/978-3-319-44726-1_8

Zagros Mountain fold-and-thrust belt represents the easternmost margin of the East Arabian Block.

Keywords

Central Arabia plate • East Arabian Block • Zagros Mountain • Alpine-Himalayan orogeny • Fault-related folds • Layer-parallel shortening • Late Eocene • Inversion

Introduction

Central Arabia is part of the Arabian Platform (shelf), which occupies 2/3 of the Arabian Plate; the other 1/3 is occupied by the Arabian Shield (e.g. Powers et al. 1966). The main geomorphic feature in Central Arabia is the Interior Homocline, formed by Paleozoic-Mesozoic rock units that crop out as an arcuate belt, binding the Arabian Shield to the east (Fig. 1). The Phanerozoic and Mesozoic beds dip gently, 1 degree to the east. The Interior Homocline is bounded to the east by flat beds of Paleogene rocks (Fig. 2). Two major tectonic regimes are dominant in the Arabian Plate, the Red Sea rifting event to the west of Arabia, and the Alpine-Himalayan Orogenic belt (Zagros Mountains) to the east of Arabia. The Red Sea Rifting event started to develop in the Oligocene time and is still active (e.g. Reilinger et al. 2015), whereas numerous compressional episodes have been recorded in the Zagros Mountains during the Paleogene and the Neogene. These two stress regimes have interrupted the gently dipping Mesozoic and overlying Tertiary beds in the Arabian foreland, forming different shearing (strike-slip) structures, associated with local contractional and extensional features, which are superimposed on the Interior Homocline in Central Arabia.

Central Arabia comprises a major tectonic feature, the East Arabian Block, which is bounded by the E-W Dhurma-Nisah-Sahba strike-slip fault to the south, the ENE-WSW Wadi Al Batin strike-slip fault to the north and the Az Zulfi Lineament to the west (Hancock and Al-Khadi 1978; Al-Sawari 1980; Hancock et al. 1981; Weijermars 1998). It is interesting to note that most of the oil fields of Saudi Arabia are found within the East Arabian Block, including the southernmost part of Gawar oil field, which is cut by the Nisah-Sahba portion of the Dhurma-Nisah-Sahba fault zone. Moreover, half of the oil fields in the world are found within Mountain Zagros Belt, which represents the easternmost boundary of the East Arabian Block (Fig. 1). Thus, studying these exposed tectonic features allows a better understanding of subsurface structures that accommodate most of oil fields in the world (Fig. 3).

The main aim of this study is to find out when structural features were developed, and what is their overall tectonic setting. This paper focus on the structural style and local tectonic features observed in the Arabian foreland, that took

place from Himalayan Mountains in Central Asia to Alpine Mountains in West Europe, after the closure of the former Tethyan oceanic realm.

Geologic Setting

Rock units of the study area form an arcuate belt of Phanerozoic rocks, known as the Interior Homocline that overlies the eastern flank of the Proterozoic Arabian Shield along an angular unconformity (Fig. 4). The Cambro-Ordovician clastic rocks of Saq Formation unconformably overly a small part of the Arabian Shield, which is in turn overlain mainly by Permian rock units, in the southwestern part of the study area (Manivit et al. 1985b). Late Carboniferous to Middle Permian Unayzah and Early Triassic to Middle Permian Khuff formations are overlain to the east by Early, Middle and Late Triassic Sudair, Minjur and Jilh formations, in which Permian-Triassic formations form the Buraydah Group (Manivit et al. 1985b; Vaslet et al. 1985). The Shaqra Group (Middle to Late Jurassic) overlies the Buraydah Group, consisting of the Marat, Dhurma, Tuwaiq, Hanifah, Jubailah, Arab, and Hit formations in ascending order (Vaslet et al. 1985; Manivit et al. 1985a; Vaslet et al. 1988, 1991). The Shaqra Group is a sequence of continental and near-shore clastic rocks at the base, overlain by near-shore, shallow-marine carbonate and fine-grained detrital deposits, and an alternating carbonate and evaporite cyclic sequence at the top (Vaslet et al. 1988; Memesh et al. 2010). The anhydrite is commonly hydrated to gypsum near the surface, within the Arab Formation. Anhydrite of the Hit Formation is not exposed due to near surface dissolution processes. However, in one famous sinkhole, south of Riyadh, known as Dahl Hit, the Jurassic evaporite crops out below the Cretaceous Sulaiy Formation along the wall of the sinkhole (Vaslet et al. 1991).

Unconformably above the Shaqra Group is the Thumamah Group (Late Jurassic? to Lower Cretaceous). It consists of the Sulaiy, Yamamah, Buwaib, and Biyadh formations, in ascending order (Vaslet et al. 1988; Memesh et al. 2010; Memesh et al. in-press, in-prep.). It begins with argillaceous limestone at the base, and clastic rocks at the top. The lower Sulaiy Formation forms a prominent topographic basin-and-dome surface and is dominated by

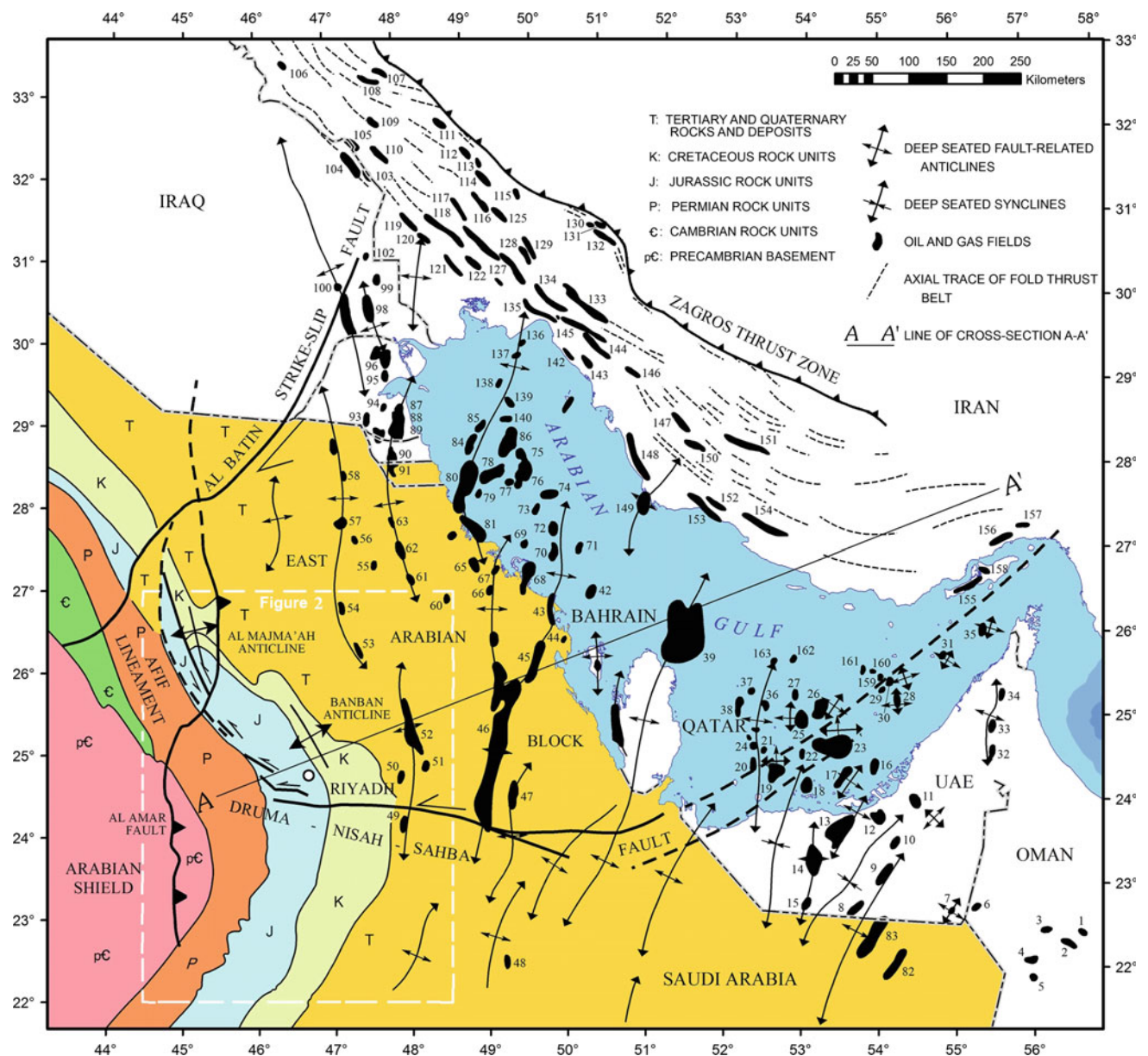


Fig. 1 Tectonic map of the Central Arabia, showing deep-seated fault-related folds and associated oil and gas fields (Al-Sharhan and Nairn 1989); the Precambrian basement (Arabian Shield) boundary and major overlying Phanerozoic units, with respect to the East Arabian

Block (Weijermars 1998); major structural elements, mentioned in the text, mapped by Vaslet et al. (1988), Bamousa et al. (2014a) and Memesh et al. (in-prep.). Cross-section A-A' is shown in Fig. 3

brecciated limestone (Memesh et al. 2010; Bamousa et al. 2014a, b). Caves are common in the lower part of the lower member. Undulating beds of the lower member formed during roof collapse of voids that resulted from dissolution of the underlying Hit Formation. To a lesser extent than Sulaiy Formation, the Yamamah and Buwaib formations are also disrupted by dissolution-collapse structures that filled the voids left from dissolution of evaporite beds in the Arab and Hit formations (Memesh et al. 2010). The Wasia and Aruma formations (Upper Cretaceous) disconformably

overlie the Thumamah Group. The Buraydah, Shaqra and Thumamah groups form the Diriyah Supergroup.

The Upper Cretaceous rock units are unconformably overlain by the Umm Radhamah Formation (Early Paleocene to Early Eocene). The Cretaceous units are bounded to the east by the Umm Radhamah Formation, which is in turn bounded by the Neogene rocks to the east. Most of the Neogene rocks and deposits in the eastern part of the map area are undifferentiated. However, there are several formations mapped, such as the Umm Ash Sha'al (Pliocene),

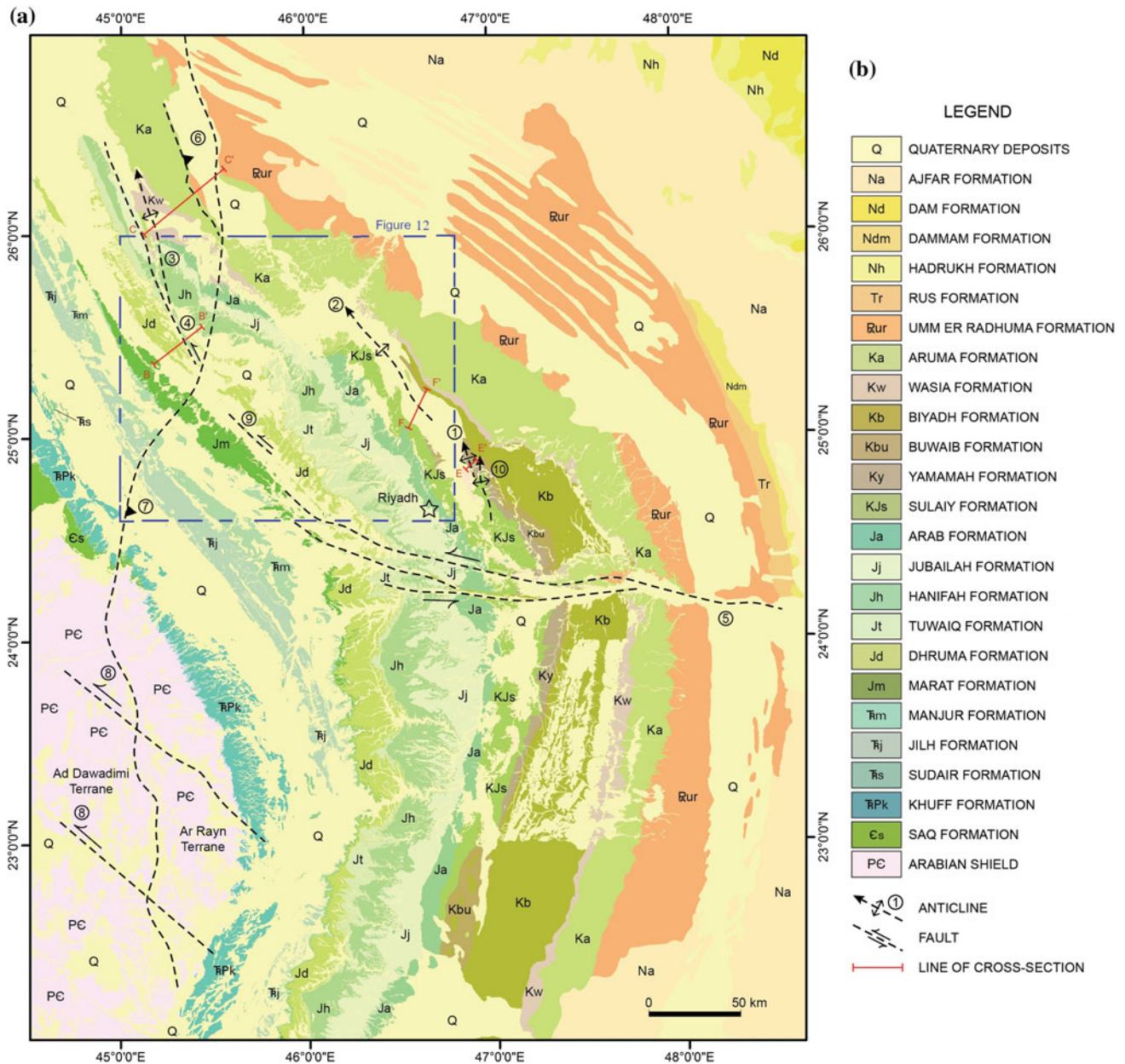


Fig. 2 a Geologic map of the study area, showing most of stratigraphic units of the study area; paleozoic, mesozoic and tertiary units, undifferentiated neogene deposits and quaternary gravels, sand and sabkha deposits. The map also showing major structural elements: Al Jinadriyah anticline (1), Banban anticline (2), Majma'ah anticline (3), Majma'ah strike-slip fault zone (4), Druma-Nisah-Sahba strike-slip fault, also known as Central Arabian graben (5), Al Artawiyah

depression, bound to the east by reactivated Al Aamr fault, near Al Majma'ah town (6), Al Amar fault, where it is exposed in the Arabian Shield, separating Al Amar from Ad Dawadimi terranes of the Arabian Shield (7), late Precambrian Najd strike-slip faults (8), Barrah sinistral fault zone (9) and Jabal Al Jubayl anticline (10). A star, showing location of Riyadh, the capital of Saudi Arabia. **b** Legend of the map

Hadrukh, Dammam, Dam and Ajfar formations. They form mesas, and fill shallow depressions within Mesozoic rocks. Their main components are sandstone, conglomerate, siltstone, claystone, limestone, gypsum and marl. Their age may be Pliocene (Vaslet et al. 1991). The Ar Rufa Formation (Middle to Late Pleistocene) unconformably overlies the

Umm Ash Sha'al Formation, and consists of conglomerate at the base, gavelly sand, clayey sand and sandy gypsum, and lacustrine limestone at the top. Quaternary deposits consist of alluvium wadi deposits, sand dunes, khabra and sabkha deposits which unconformably overlay the Ar Rufa' Formation.

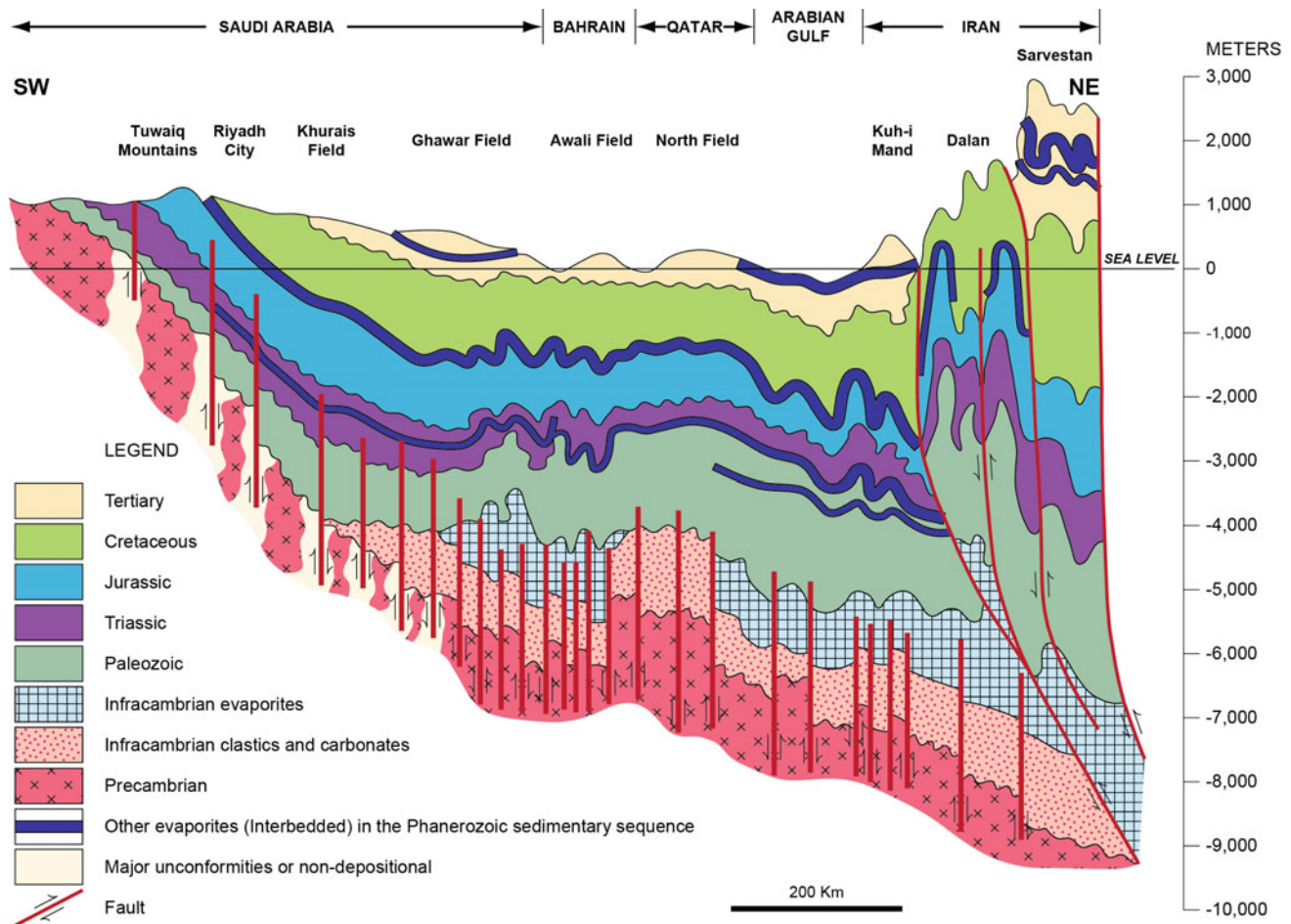


Fig. 3 Cross-section A-A' from Zagros Mountain thrust belt in the east to Central Arabia to the west, showing formation of deep-seated structures and oil field traps, inversion and development of the

fault-related folds, during Zagros Mountain development. Adapted from (Peterson and Wilson 1986)

Methodology

Geologic mapping has been conducted since 2010 for different 1:250,000 quadrangles that cover most parts of Central Arabia (Fig. 1). It includes the Artawiyah (Memesh et al. in-prep.), Rumah (Memesh et al. in-prep.), and Layla (Al-Zahrani et al. in-prep.) 1250:000 quadrangles, which were combined with previously published work of the Wadi Ar Rayn (Vaslet et al. 1983), Darma' (Manivit et al. 1985a), Wadi Al Mulayh (Manivit et al. 1985b), Shaqra (Vaslet et al. 1988), Riyadh (Vaslet et al. 1991) and Hawtat Bani Tamim (Memesh et al. 2010) 1:250,000 quadrangles. These 9 maps were combined into a single geological map, using a Geographic Information System (GIS) package. Base maps of geological mapping were 1:100,000 topographic maps and ETM + satellite bands of the 7-4-2 composite on Red Green Blue, forming a false colour composite images for several

smaller areas with 1:100,000 scale for the recent 1:250,000 quadrangles. Structural analysis and regional synthesis was performed for complex areas for detailed structural work purposes. The data collected in the field provided also interesting hypotheses for further research and academic work.

Results

The main recognized structural features, related to Cenozoic tectonic event, are closely associated to the East Arabian Block, which was identified first by aerial photographs and remotely sensed data (Hancock et al. 1981). The East Arabian Block includes several large-scale features such as Majma'ah fault zone and NW-SE major (Banban, Jabal Al Jubayl, Al Jinadriyah and Majma'ah) anticlines that represent fault-related folds. It also includes the Artawiyah

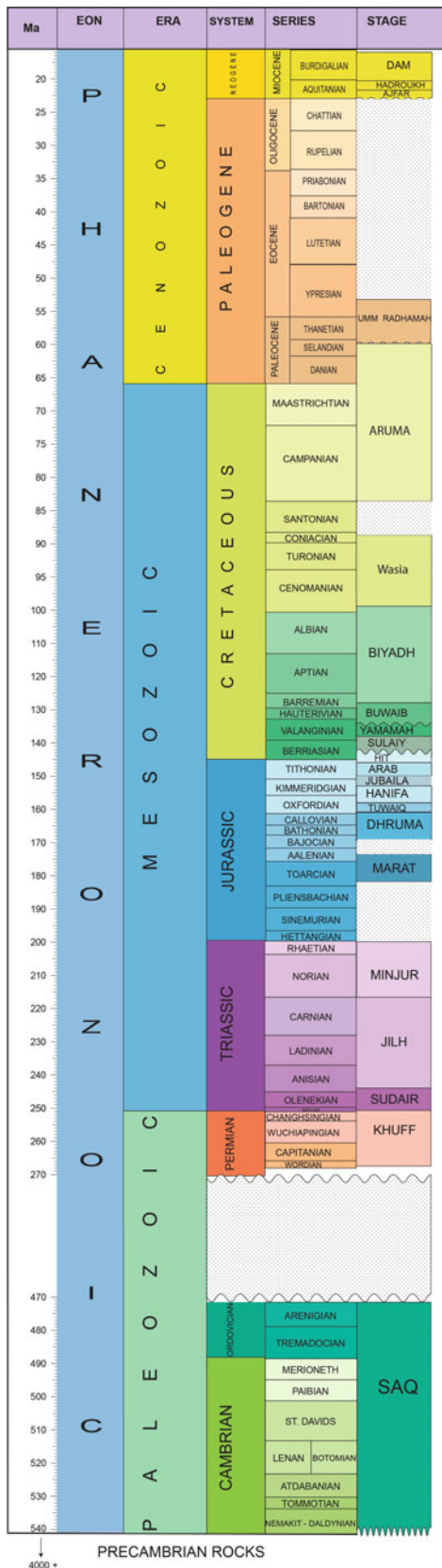


Fig. 4 Stratigraphic column of the Arabian platform, from older to younger. Adapted from Bilal and Al-Qahtani (2005), and Al-Laboun (2009)

Depression, and the pervasive basin-and-dome style of the Sulaiy Formation.

The East Arabian Block

The western boundary of the East Arabian Block is also identified as the Az Zulfi lineament, which is covered by sediments, with no evidence for any kinematic indicators that would help interpreting its role. However, it might be a reverse fault that bounds the block to the west (Weijermars 1998). The Dhurma-Nisah-Sahb (DNS) represents the southern boundary of the East Arabian Block, which was mapped in-details by Vaslet et al. (1991), and was previously mapped as the Central Arabian graben by Hancock and Al-Kadhi (1978). The DNS fault is a large-scale sinistral fault zone, associated with pull-apart basins and pop-up structures (Figs. 1 and 2). The DNS fault is believed to be continuous further to the east, cutting features within the Arabian Gulf (Fig. 1). Therefore, it suggests that it is an active fault. The northern boundary of East Arabian Block is outlined by the ENE-WSW Wadi Al Batin lineament, cutting through Cenozoic deposits, east of the Al Majma'ah fault zone. Several wadis are cross-cut by the fault suggesting that it is a dextral fault, younger than Neogene deposits. The DNS Fault and Wadi Al Batin strike-slip faults cut through Quaternary valleys and deposits and recent sand dunes, suggesting development during Pleistocene time (Vaslet et al. 1991; Weijermars 1998). Figure 3 shows a cross-section of the East Arabian Block, bounded to the east by the Zagros Mountain, and deep-seated structures that trap oil fields, below the surface.

Majma'ah Fault Zone

To the east of Az Zulfi lineament, a graben system, known as Majma'ah Graben was mapped (Vaslet et al. 1988). However, more recent studies showed that the Majma'ah structure extends to the north, and is associated with pop-up inversion structures, as well as with the Majma'ah anticline that extends parallel to the fault zone (Memesh et al. in-prep.; Bamoussa et al. 2014b). This suggests that the Majma'ah Fault is a sinistral fault zone, associated with pull-apart basins (graben systems) in the south (Fig. 5), and pop-up structures in the north (Fig. 6). Al Majma'ah fault zone developed during Early Paleogene (Eocene) as suggested by deformation of the Late Cretaceous Arumah Formation, and faulting against series of the Wasia Formation, the later being older than the Arumah Formation (Fig. 7). Thus, the Majma'ah fault zone and the Artawiyah Depression constitute two Key areas for identifying the age of deformation events in the Arabian foreland.

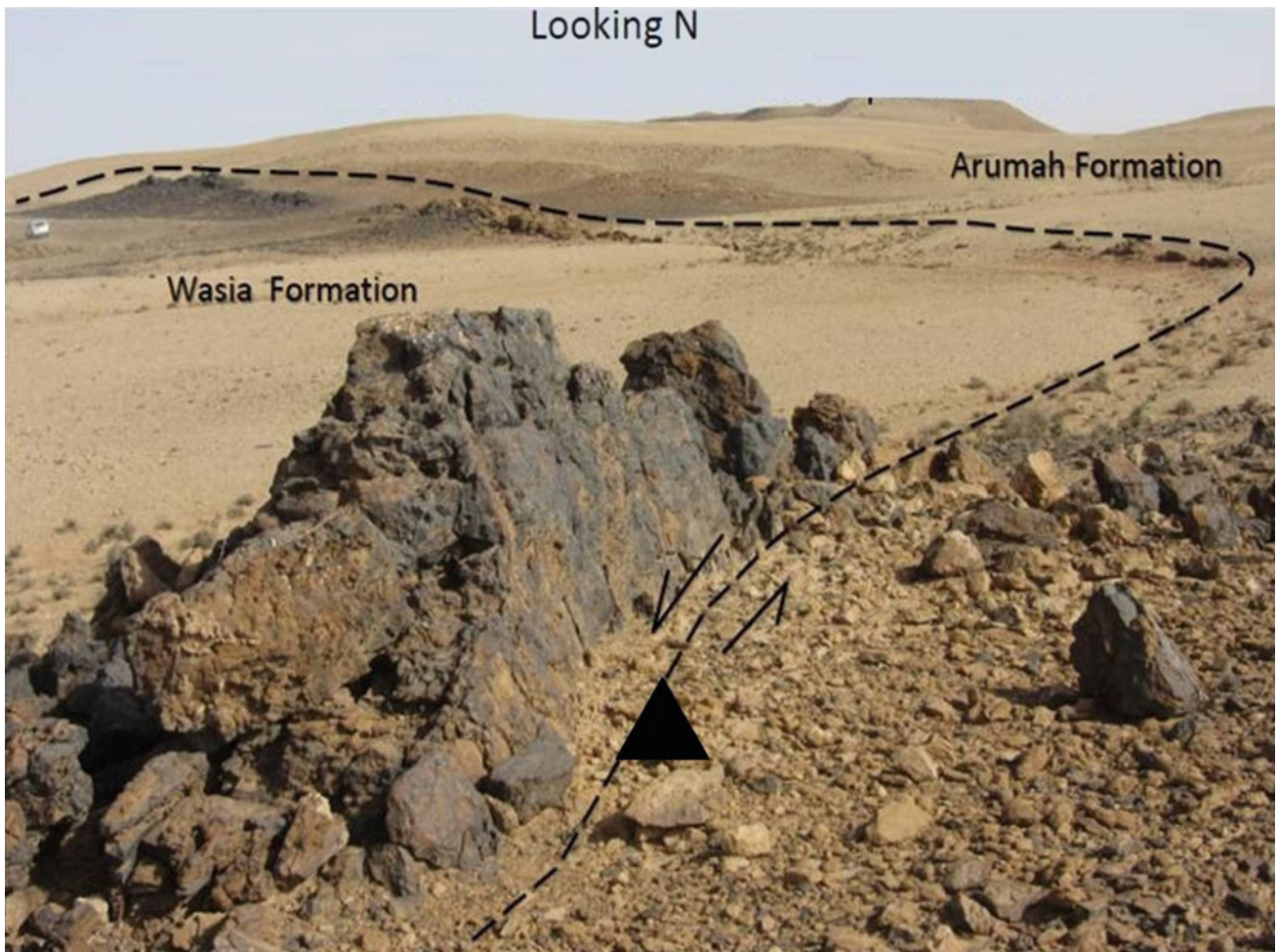
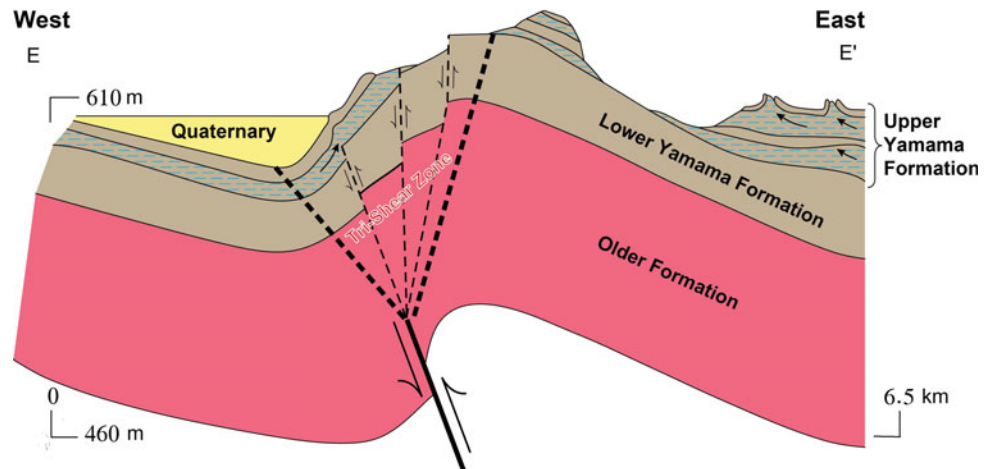


Fig. 7 Picture showing a fault contact between the Arumah and Wasia formations. Slickensides on the Wasia rocks (*dark color*) suggest a reverse component of the fault, shown on the cross-section (Fig. 6)

Fig. 8 Generalized cross-section E-E' of Al Jinadriyah anticline, based on seismic lines. Adapted from (Al-Mahmoud et al. 2009). See Fig. 2 for location



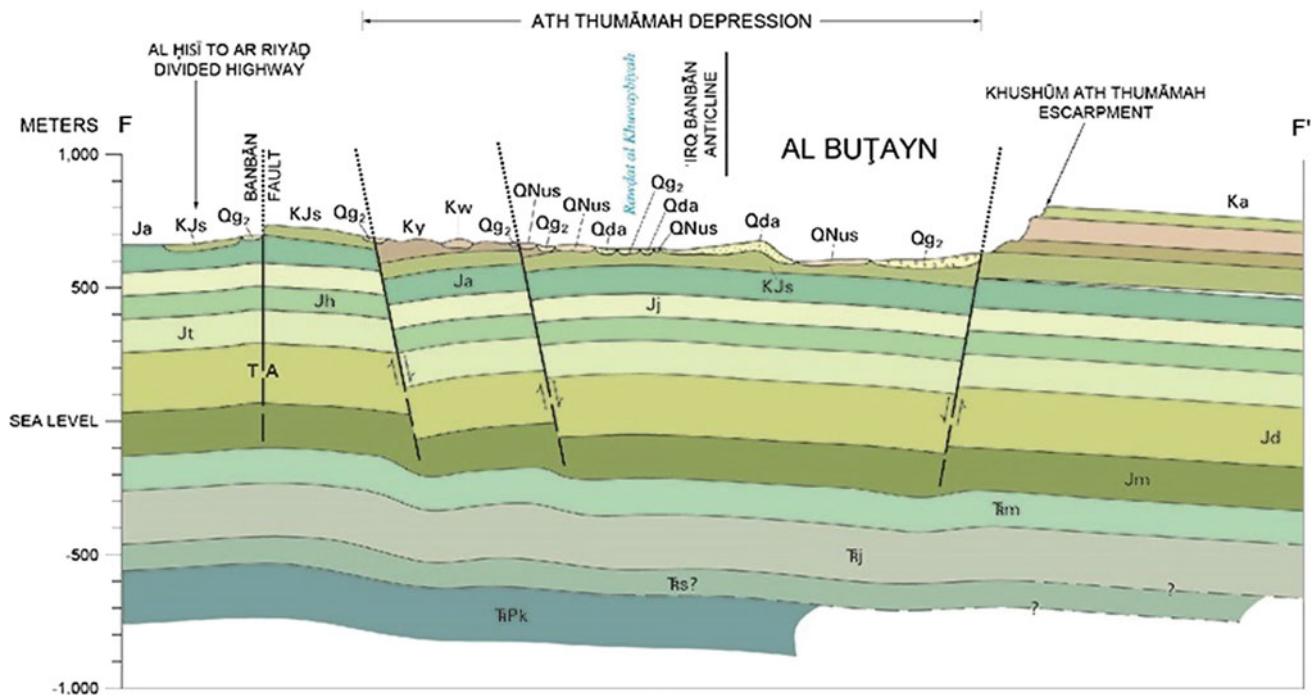


Fig. 9 Geological cross-section F-F' across the Banban fold, adapted from Memesh et al. (in-press). See Fig. 2 for location

Basin-and-Dome of the Sulaiy Formation

Sulaiy Formation show basin-and-dome structures throughout the study area. At the key locality known as Wadi Nisalah, in the southern part of the study area, south of Hawtah Bani Tamim Town, the Sulaiy Formation shows detachment folds, which are an evidence for a decollement zone within lower part of Sulaiy Formation (Fig. 10). This structural feature was found southwest of the DNS fault zone (Memesh et al. 2010). Kinematic indicators suggest SW-directed transport, implying that these basin-and-dome structures are developing above a thin-skinned decollement zone. Therefore, the pervasive basin-and-dome style of the Sulaiy Formation may be related to development of disharmonic (non cylindrical) folds, detached at the base along a decollement zone (Fig. 11). The disharmonic folds are also associated with local reverse faults, suggesting a similar style mode of folding as in the Zagros Mountains folds and thrust belt. The decollement zone in the lower part of the Sulaiy Formation, may dip towards the east, forming a tectonic wedge beneath the Arab Formation (Fig. 3). Figure 3 also shows a box structure above the deep-seated faults of the Gawar Anticline, which is cored by evaporites. This decollement zone may also account for deep-seated structures below the surface.

Fracture Analysis and Stresses

Camran (1996) defined a principal maximum stress field orientation of N040–N050, onshore Kuwait. Saner et al. (2005) suggested N035 maximum stresses, based on Landsat image analysis of lineaments locally, outlined by the Gawar anticline and other surface expressions. Thus, it is consistent with the regional trends of Zagros Mountain orogeny (Jorgensen et al. 1994). Al-Mahmoud et al. (2009) reported that the maximum stress field in the Arabian foreland ranges between N030 and N090.

In this study, the NNW-SSE large-scale Majma'ah fault zone and anticline were interrupted by an echelon strike-slip faults and minor folds that trend NE-SW in the Majma'ah area. Banban anticline is a NW-SE fold, bounded by a NE-SW Wadi Al Atk lineament to the north, which was mapped by Vaslet et al. (1988). The Wadi Al Atk Lineament is affecting the N-S Al Amar Fault, suggesting a dextral sense of shear. It is binding the NW-SE Banban anticline to the north. The NE-SW large-scale Wadi Al Batin dextral fault (Fig. 1) cuts the older NW-SE structures and outcrops, with similar setting. According to the Anderson theory of stresses, the cross-cutting relationship of the two (NE-SW) and (NW-SE) polarities suggest a ENE-WSW maximum stress (Fig. 12).



Fig. 10 Interpreted outcrop picture documenting kinematic analysis of the lower Sulaiy decollement zone, suggesting SW-directed sense of shear

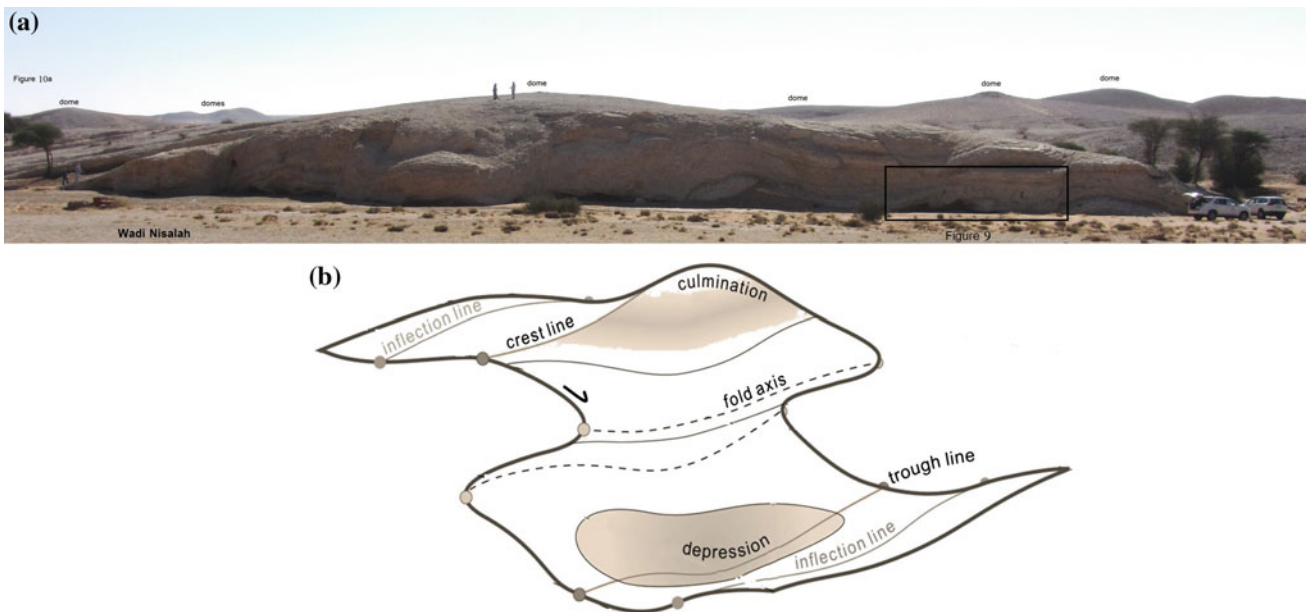


Fig. 11 **a** Outcrop picture showing basin-and-dome pattern of the Sulaiy formation. **b** Possible interpretation of the basin and dome geomorphology, formed by non cylindrical folds, due to layer-parallel shortening and detachment on a decollement zone, modified after (Burg 2013)

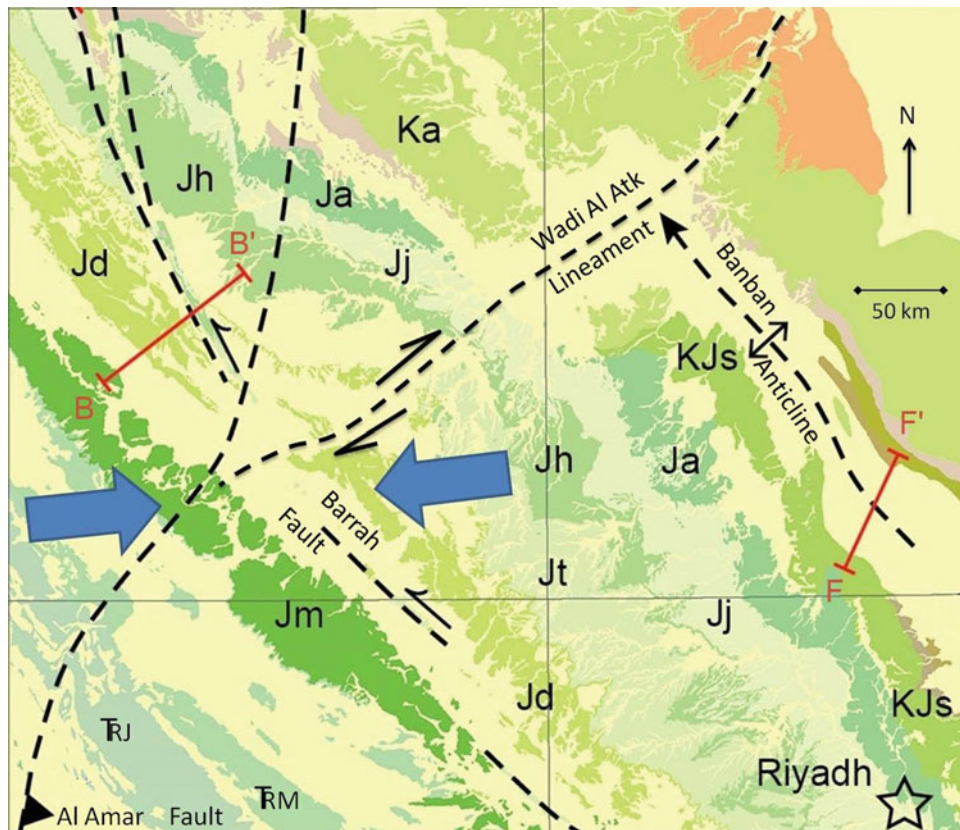


Fig. 12 Geologic map showing the main structural features of the study area. Notice the NE-SW Wadi Al Atk Lineament, cross-cutting

NW-SE Barrah sinistral fault and Banban Anticline, suggesting NE-SW stresses, (modified after Fig. 2)

Discussion

Three compressional tectonic events between Arabian and Eurasian plates played a significant role in developing the fault-related anticlinal structures, observed in the study area and known to host major oil fields mainly within the East Arabian Block (Hancock et al. 1981; Beydoun 1991; Edgell 1992; McGillivray and Hussein 1992; Weijermars 1998; Al-Amri 1999; Jolivet and Faccenna 2000; Konert et al. 2001; Ziegler 2001; Alsharhan and Nairn 2003; Agard et al. 2005; Saner et al. 2005; Allen and Armstrong 2008; Fakhari et al. 2008; Horton et al. 2008; Vincent 2008; Al-Mahmoud et al. 2009; Ballato et al. 2011; Mouthereau et al. 2012; McQuarrie and Hinsbergen 2013; Ahmadian et al. 2014; Bamousa et al. 2014b). The first of these three tectonic events was associated with the Hercynian Orogeny being restricted to Paleozoic series, whereas the two others are quite younger and associated with the main episodes of mountain building processes in the Zagros fold-and-thrust belt, i.e. the early Alpine-Himalayan Orogeny (late Cretaceous to early Tertiary) and finally late Alpine-Himalayan Orogeny (late Eocene to Pliocene).

Deep-seated basement faults were firstly reactivated during the Devonian to early Triassic Hercynian Orogeny, forming horst and graben structures at depth (Fig. 3). This event probably initiated the uplift of Central Arabian, where the beds of the Permian Khuff Formation beds are lying unconformably above Precambrian Basement rocks west of Riyadh. From Late Cretaceous onward, basement faults of Jurassic and younger systems were progressively inverted towards the west, and related folds were started to grow. Oil and gas were trapped in the Arabian foreland mainly when early Alpine-Himalayan Orogeny was taking place, i.e. during Late Cretaceous to middle Eocene (85–40 Ma), with localized inversion features within the Arabian Plate being associated with the late stages of subduction of the former Tethyan ocean.

Foreland deformation and inversions occurred also from late Eocene (35 Ma) to Pliocene, during the subsequent collision between the Arabian and Eurasian plates near the plate boundary in the Zagros fold-and-thrust belt, at a time when the foreland lithospheric flexure impacted the Arabian Plate as a whole. This later period corresponds to the late Alpine-Himalayan Orogeny in Europe. It was the time when Central Arabia was uplifted and tilted. Fault-related folds

resuming their growth, developing further shallower structures around Riyadh, such as Al Jinadriyah and Majma'ah anticlines. At a later stage, between Pleistocene and recent, E-W trending strike-slip Nisah and Wadi Al-Batin faults, and final decollement zone within the lower part of the Sulaiy Formation developed, forming the basin-and-domes structures.

Conclusion

The structural features described in this paper suggest that local inversion tectonics occurred in Central Arabia, in which younger rocks, mainly Late Cretaceous, were faulted against Lower Paleogene, mainly Paleocene rocks. Moreover, this event formed local and structurally controlled depressions or small depositional basins, such as the Artawiyah Depression, that accommodated Neogene (Pliocene) rocks and recent sediments. Timing of these events corresponds most-likely to the late collisional period of the Alpine-Himalayan Orogeny during late Eocene, most of the anticlinal structures being probably reactivated during to Pleistocene time. Neotectonics are still active in the East Arabian Plate, probably due to Red Sea rifting and still ongoing northward motion of Arabia towards Eurasia.

The late Alpine-Himalayan orogeny can be subdivided into two distinct stages, the first stage being late Eocene in age, developing N-S structures such as the Majma'ah fault zone and the N-S fault-related Majma'ah Al Jinadriyah anticlines. The second stage was Pleistocene in age, accounting for the major and minor E-W lateral offset structures, which cross-cut N-S structures. The East Arabian Block developed during these two stages. It is probably the largest tectonic feature related to the late Alpine-Himalayan orogeny in Central Arabia. The E-W strike-slip faults and bounded block may represent escape structures that formed during last stage of collision.

Acknowledgments The authors would like to thank Saudi Geological Survey President Dr. Zuhair Nawab, for his permission and support. Thanks to SGS staffs of remote sensing and GIS departments, for their efforts on producing geologic map and remotely sensed data. Great thanks to editors for their advises and help in the script. The authors would like to thank Mr. George Certeza for his cartographic work.

References

- Agard P, Omrani J, Jolivet L, Mouthereau F (2005) Convergence history across Zagros (Iran): constraints from collisional and earlier deformation. *Int J Earth Sci* 94:401–419
- Ahmadian J, Murata M, Nadimi A, Ozawa H, Kozai T (2014) Active tectonics of Iran deduced from earthquakes, active faulting and GPS evidences. *Bull Center Collab Community Naruto Univ Educ* 28:11–22
- Al-Amri A (1999) The crustal and upper mantle structure of the interior Arabian platform. *Geophys J Int* 136:421–430
- Al-Laboun AA (2009) Lithostratigraphy of Saudi Arabia, 9th meeting of the Saudi society of geosciences. Ibn LABoun Publisher Riyadh, Riyadh
- Allen MB, Armstrong HA (2008) Arabia-Eurasia collision and the forcing of mid-cenozoic global cooling: palaeogeography. *Palaeoclimatol Palaeoecol* 265:52–58
- Al-Mahmoud MJ, Mesbah KH, Moustafa AR (2009) The Jinadriyah anticlines: a surface model for oil fields in eastern Saudi Arabia. *Arab J Geosci* 2(3):213–234
- Al-Sawari AM (1980) Tertiary faulting beneath Wadi Al-Batin (Kuwait): Geological Society American. *Geol Soc Am Bull* 91 (10):610–618
- Al-Sharhan AS, Nairn AEM (1989) Cretaceous rudist buildup forms giant fields in Arabian Gulf. In: 28th International geological congress, Washington (Abs.), vol 1, p. 35
- Al-Sharhan AS, Nairn AEM (2003) Sedimentary basins and petroleum geology of the Middle East, 2nd edn. Elsevier, Amsterdam 942 p
- Al-Zahrani AA, Memesh AM, Dini SM, Bamoussa AO (in-prep) Explanatory notes to the geologic map of the Layla Al Aflaj Quadrangle, sheet 24H, Kingdom of Saudi Arabia. Ministry of Petroleum and Mineral Resources, Saudi Geological Survey, GM-148C, 1:250,000
- Ballato P, Uba CE, Landgraf A, Strecker MR, Sudo M, Stockli DF, Friedrich A, Tabatabaei SH (2011) Arabia-Eurasia continental collision: insights from late tertiary forelandbasin evolution in the Alborz Mountains, northern Iran. *Geol Soc Am Bull* 123:106–131
- Bamoussa AO, Memesh A, Dini S (2014a) Morphostructural evolution of Ath Thumamah depression, north Riyadh, Saudi Arabia. *Carbonates Evaporites* 29:65–72
- Bamoussa AO, Memesh AM, Dini SM (2014b) Evidences for inversion and strike-slip structures in Al Majma'ah fault zone, northern part, northwest of Al Majma'ah city, Central Saudi Arabia (abs). In: 11th Middle East geosciences conference and exhibition, Bahrain
- Beydoun ZR (1991) Arabian plate hydrocarbon geology and potential—a plate tectonic approach. *AAPG Stud Geol* 33:77
- Bilal HU, Al-Qahtani A (2005) Phanerozoic cycles of sea-level change of the Arabian platform. *GeoArabia* 10(2):127–160
- Burg JP (2013) Folds. Geologic Institute, ETH Zurich, University of Switzerland <http://www.files.ethz.ch/structuralgeology/jpb/files/English/8folds.pdf>
- Carman GJ (1996) Structural elements of onshore Kuwait. *GeoArabia* 1 (2):239–266
- Edgell HS (1992) Basement tectonics of Saudi Arabia as related to oil structures. In: Rickard MJ et al (eds) *Basement tectonics*. Kluwer Academic Publishers, Dordrecht, pp 169–193
- Fakhari MD, Axen GJ, Horton BK, Hassanzadeh J, Amini A (2008) Revised age of proximal deposits in the Zagros foreland basin and implications for cenozoic evolution of the High Zagros. *Tectonophysics* 451:170–185
- Hadley D, Focke J (1991) Old sandstone horizons. *Middle East Well Eval Rev* i(11):10–26
- Hancock PL, Al-Kadhi A (1978) Analysis of mesoscopic fractures in the Dhurma-Nisah segment of the central Arabian graben system. *Geol Soc Lond* 135(3):339–347
- Hancock PL, Al-Khatieb SO, Al-Kadhi A (1981) Structural and photogeological evidence for the boundaries to an East Arabian block. *Geol Mag* 118:533–538
- Horton BK, Hassanzadeh J, Stockli DF, Axen GJ, Gillis RJ, Guest B, Amini A, Fakhari MD, Zamanzadeh SM, Grove M (2008) Detrital zircon provenance of neoproterozoic to cenozoic deposits in Iran:

- implications for chronostratigraphy and collision tectonics. *Tectonophysics* 451:97–122
- Johnson PR, Stewart ICF (1995) Magnetically inferred basement structure in central Arabia. *Tectonophysics* 245:37–52
- Jolivet L, Faccenna C (2000) Mediterranean extension and the Africa-Eurasia collision. *Tectonics* 19:1095–1106
- Jorgenson LN, Brown AA, and Redekop GE (1994) Stress field orientation and fault trends offshore Qatar. In: Husaini MI (ed) Middle East petroleum geosciences, GEO'94, vol 2. Gulf Petrolink, Bahrain, pp 561–570
- Jorgenson LN, Brown AA, Redekop GE (1995) Stress field orientation and fault trends offshore Qatar. In: Husaini MI (ed) Middle East petroleum geosciences, GEO'94, vol 2. Gulf Petrolink, Bahrain, pp 561–570
- Konert G, Afif AM, Al-Harjri SA, Droste HJ (2001) Paleozoic stratigraphic and hydrocarbon habitat of the Arabian plate. *GeoArabia* 6:407–442
- Manivit J, Pellaton C, Vaslet D, Le Nindre YM, Brosse JM, Breton JP, Fourniguet J (1985a) Geologic map of the Darma' Quadrangle, sheet 24H, Kingdom of Saudi Arabia. Saudi Arabian Deputy Ministry for Mineral Resources, GM-101C, scale 1:250,000 with accompanied report, 33 p
- Manivit J, Pellaton C, Vaslet D, Le Nindre YM, Brosse JM, Fourniguet J (1985b) Geologic map of the Wadi Al Mulayh Quadrangle, sheet 22H, Kingdom of Saudi Arabia. Ministry of Petroleum and Mineral Resources, GM-92C, scale 1:250,000 with accompanied report, 32 p
- Mcgillivray JG, Hussein MI (1992) The paleozoic petroleum geology of Central Arabia. *AAPG Bull* 76(10):1473–1490
- McQuarrie N, Hinsbergen DJJ (2013) Retrodeforming the Arabia-Eurasia collision zone: age of collision versus magnitude of continental subduction. *Geology* 41:315–318
- Memesh AM, Dini SM, Al-Amoudi SM, Wallace CA, Sobhi SA, Al-Juaid AJ (2010) Explanatory notes to the geologic map of the Hawtat Bani Tamim Quadrangle, sheet 23I, Kingdom of Saudi Arabia. Ministry of Petroleum and Mineral Resources, Saudi Geological Survey, GM-143C, with accompanied report, 64 p
- Memesh AM, Dini SM, Bamousa AO, Al-Amoudi SM, Al-Juaid AJ (in-press) Explanatory notes to the geologic map of the Rumah Quadrangle, sheet 25I, Kingdom of Saudi Arabia. Ministry of Petroleum and Mineral Resources, Saudi Geological Survey, GM-145C, with accompanied report
- Memesh AM, Dini SM, Bamousa AO, Tasan AA, Al-Zahrani AA (in-prep) Explanatory notes to the geologic map of the Al Artawiyah Quadrangle, sheet 26H, Kingdom of Saudi Arabia. Ministry of Petroleum and Mineral Resources, Saudi Geological Survey, GM-146C, with accompanied report
- Mouthereau F, Lacombe O, Vergés J (2012) Building the Zagros collisional orogen: timing, strain distribution and the dynamics of Arabia/Eurasia plate convergence. *Tectonophysics* 532–535:27–60
- Peterson JA, Wilson JL (1986) Petroleum stratigraphy of the Northeast Africa-Middle East region. U.S. geological survey open-file report 87–85, 43 p
- Powers RW, Ramirez LF, Redmond CD, Elberg EL Jr (1966) Geology of the Arabian Peninsula—sedimentary geology of Saudi Arabia. U. S. geological survey professional paper 560-D, 147 p
- Reilinger R, McClusky S, ArRajhi A (2015) Geodetic constraints on the geodynamic evolution of the Red Sea. In: Rasul NMA, Stewart ICF (eds) *The Red Sea: the formation, morphology, oceanography and environment of a young ocean basin*. Springer, London, pp 135–149
- Saner S, Al-Hinai K, Perincek D (2005) Surface expressions of the Ghawar structure, Saudi Arabia. *Mar Pet Geol* 22:657–670
- Vaslet D, Manivit J, Le Nindre YM, Brosse JM, Fourniguet J, and Delfour J (1983) Geologic map of the Wadi Ar Rayn Quadrangle, sheet 23H, Kingdom of Saudi Arabia: Deputy Ministry for Mineral Resources, Ministry of Petroleum and Mineral Resources, GM-63C, scale 1:250,000, with accompanied report, 46 p
- Vaslet D, Pellaton C, Manivit J, Le Nindre YM, Brosse JM, Fourniguet J (1985) Geologic map of the Sulayyimah Quadrangle, sheet 21H, Kingdom of Saudi Arabia. Saudi Arabian Deputy Ministry for Mineral Resources, GM-121, scale 1:250,000, with accompanied report, 54 p
- Vaslet D, Brosse JM, Breton JP, Manivit J, Le Strat P, Fourniguet J, Shorbaji H (1988) Geologic map of the Shaqra' Quadrangle, sheet 25H, Kingdom of Saudi Arabia. Saudi Arabian Deputy Ministry for Mineral Resources, GM-120C, scale 1:250,000, with accompanied report 29 p
- Vaslet D, Al-Muallem MS, Maddah SS, Brosse JM, Fourniguet J, Breton JP, Le Nindre YM (1991) Geologic map of the Ar Riyadh Quadrangle, sheet 24I, Kingdom of Saudi Arabia. Saudi Arabian Deputy Ministry for Mineral Resources, GM-121, scale 1:250,000, with accompanied report 54 p
- Vincent P (2008) Saudi Arabia: an environmental overview. Taylor and Francis, The Netherlands, p 332
- Weijermars R (1998) Plio-quadernary movement of the East Arabian block. *GeoArabia* 3:509–540
- Ziegler MA (2001) Late permian to holocene paleofacies evolution of the Arabian Plate and its hydrocarbon occurrences. *GeoArabia* 6 (3):445–504

Fast-Track 2D Seismic Processing While Drilling to Ameliorate Foothills Exploration and Optimize Well Trajectory: An Example from the Central Kurdistan Region of Iraq

François Sapin, Hassan Allouche, Grégoire Sterbecq, Bertrand Chevallier, and Boerre Eriksen

Abstract

Complex mechanical stratigraphy and misplaced formation tops often make petroleum exploration of foothills domains extremely challenging. As a consequence, proper seismic imaging, as well as good geological knowledge, are mandatory to optimize a well trajectory that is suited for all the targeted objectives. Although the stratigraphy of the Kurdistan Region of Iraq, is relatively simple, the tightening of the structures often leads to the activation of internal mechanical discontinuities and a shift of the main objectives. As a result, as is typically the case in foothills, side-tracked wells have to be carefully planned. In this case study, the first leg of the well demonstrated that the current seismic image was structurally incorrect and would not allow penetration of the deepest objectives. As consequence side-track was planned. A fast-track processing on the closest 2D line was performed to correct the dips of the drilled formations. The output helped optimize the side track trajectory and to drill ahead with better constraints.

Keywords

Foothills • Seismic imaging • Seismic interpretation

Introduction

Seismic acquisition and processing are crucial techniques in petroleum exploration. Firstly for geometrical evaluation of a prospect and to estimate hydrocarbon impregnated volumes of rock. Secondly, they play a major role in the design of exploration wells. In foothill domains, the correct positioning of exploration wells remains a significant challenge. Surface conditions (topography, rapid lateral change of surface geology) as well as subsurface structural complexity

often led to poor seismic imagery. In these conditions, it becomes a real challenge to achieve optimal location of wells targeting different objectives, especially in places where there are several mechanical discontinuities in the stratigraphy. These mechanical discontinuities may induce changes in structural shape at depth. As a consequence, seismic imaging and a good geological knowledge are mandatory.

The association of poor quality seismic with areas of rough topography is well documented. Indeed, topography-related phenomena are often cited as the first order problem. Energy traveling away from the seismic source is scattered back into the recording spread, when an abrupt change in topography is encountered (Hudson 1967; Palaz and Marfurt 1997; Tarras et al. 2010). In addition, when this backscattered energy is strong and interferes with primary reflections, de-noising becomes very challenging. Finally, complex ground-roll propagation including mode conversion between surface waves and body waves results in very noisy field seismograms where primary reflections can be barely seen.

F. Sapin (✉) · H. Allouche · G. Sterbecq · B. Chevallier
Total E&P Exploration Mena Hub-Dubai, The H-Dubai Office
Tower, 24th Floor, 1 Sheikh Zayed Road, P.O. Box 116538
Dubai, United Arab Emirates
e-mail: francois.sapin@total.com

B. Eriksen
Marathon Oil Company, Corporate Headquarters, 5555 San Felipe
Street, Houston, TX 77056-2723, USA

© Springer International Publishing AG 2017

F. Roure et al. (eds.), *Lithosphere Dynamics and Sedimentary Basins of the Arabian Plate and Surrounding Areas*, Frontiers in Earth Sciences, DOI 10.1007/978-3-319-44726-1_9

187

In complex geological areas, a secondary problem is caused by highly dipping strata which are very difficult to properly illuminate, and image with conventional 2D seismic.

Generally, in foothills, *a priori* geological information, such as formation depth and mechanical stratigraphy, plays a critical role in the seismic interpretation. Field mapping and well penetrations are crucial to develop this knowledge and each improvement in this domain may have an impact on seismic imaging. Better geological control not only helps in calibrating the seismic processing but also in better defining acquisition parameters in the case of a new seismic campaign design. Considering this, each major step in the geological appreciation of an area should be followed by tests of seismic reprocessing to evaluate the impact on the imaging quality.

The Kurdistan Region of Iraq has been extensively explored in the last 10 years. After several field and drilling campaigns, it was decided to drill an undrilled structure in Central KRI. The drilling plan for this well comprised two side-track trajectories in order to maximize penetration of the different objectives. During drilling, it was decided to re-process the nearest 2D seismic line to the well in order to optimize the side-track trajectory of the first leg and to clarify different drilling scenarios for the second well leg.

Geological Setting

The drilled structure is located in Central Kurdistan Region of Iraq Foldbelt (Fig. 1). The Kurdistan Foldbelt is the northwestern extension of the Zagros Foldbelt, a wide collision related compression zone mainly located in Iran (Allen et al. 2004; Agard et al. 2005, 2011; Vergés et al. 2011; Mouthereau et al. 2012). The Kurdistan Region of Iraq (KRI) Foldbelt is usually divided into three structural domains (Buday and Jassim 1987; Jassim and Buday 2006a, b; Aqrabi et al. 2010; Fig. 1):

- The Nappes domain (or Thrust Zone) is a narrow belt (25–50 km) along the border between Iraq and Iran. It is characterized by intensively, sometime with evidence of metamorphism (Penjwin Metamorphics with marbles and metapphyllite), folded Cretaceous and Tertiary deepwater sediments thrust over the Arabian Platform in front of Cretaceous Ophiolites;
- The Foldbelt domain (or High Folded Zone, or Mountain Foothills) is characterized by outcropping of Mesozoic sediments. It is an arc-shape belt containing imbricate thrust sheets and faulted folds (Ameen 1991). It can be sub-divided into two areas, the Internal Foldbelt where

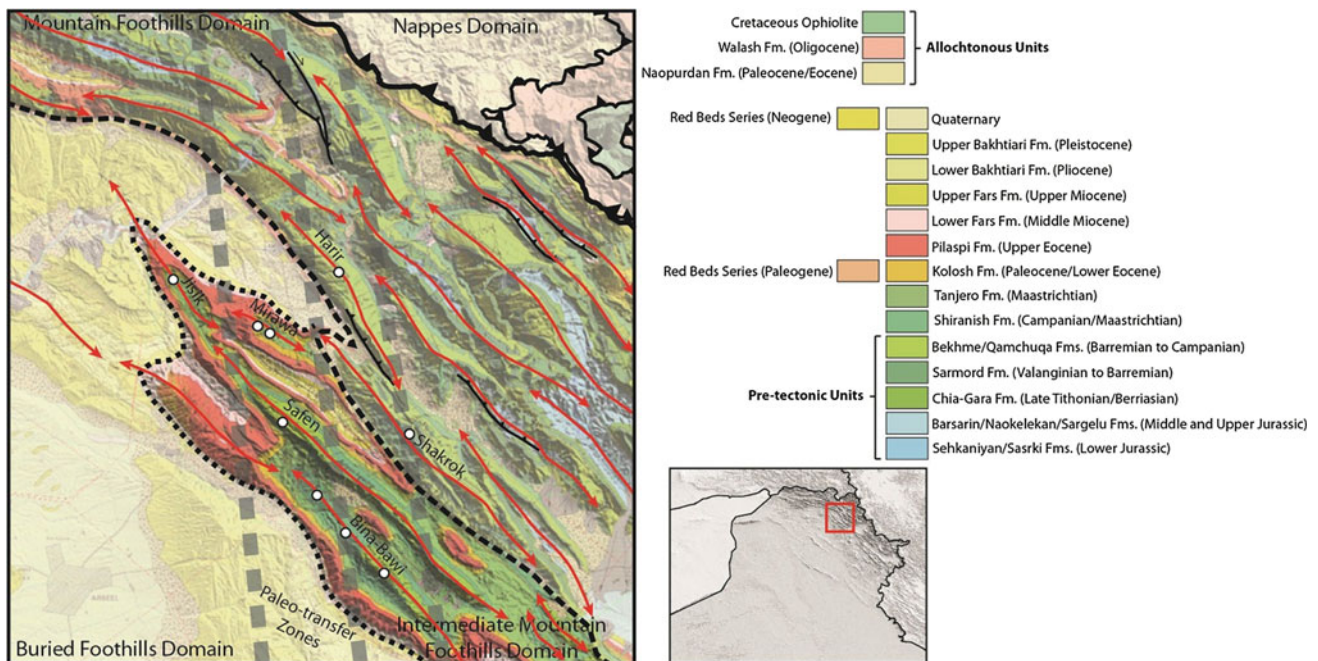


Fig. 1 Central Kurdistan Region of Iraq geological setting and well database localization. The well studied is located in the Frontal Foldbelt of the Kurdistan Zagros, in Central KRI. This area is

characterized by series of anticlines cored by Paleocene/Cretaceous formations

most of the anticlines are cored by Jurassic to Triassic formations and the Frontal Foldbelt where anticlines are cored only by Cretaceous formations;

- The Broken Foreland Domain (or Low Folded Zone, or Buried Foothills) is a wide (150–175 km), slightly folded belt where anticlines are cored by Tertiary formations.

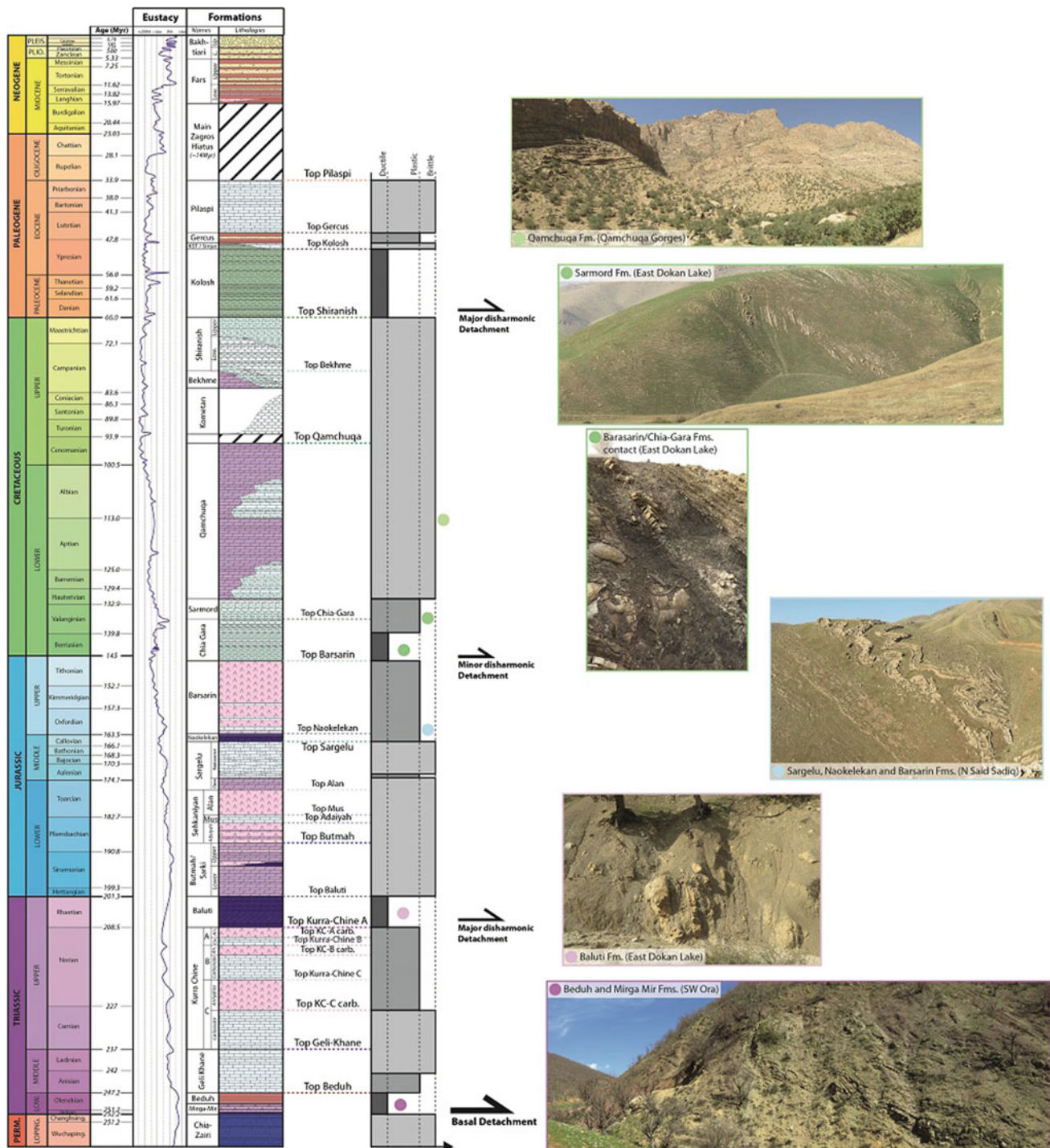


Fig. 2 Central Kurdistan Region of Iraq stratigraphy and associated mechanical stratigraphy. The Central KRI stratigraphy is mainly driven by the deposition of low energy inner shelf carbonate platform throughout the Mesozoic. In the Latest Cretaceous and Tertiary it was subjected to two compression episodes that interrupted the depositional

continuity. This stratigraphic sequence acts mechanically as a single unit above the Beduh and Mirga-Mir shaly detachment. Shale units deposited during occasional periods of regional drowning act as disharmonic detachments

This domain includes most of the major oil fields of northern Iraq (Kirkuk, Bai Hassan, Jambur, etc.).

The stratigraphy of the area is characterized by a thick carbonate sequence (Fig. 2) associated with the drowning of the Arabian Platform after the rifting of the Neo-Tethys Ocean in the Lower Triassic (van Bellen et al. 1959; Fontaine et al. 1989; Aqrabi et al. 2010). From Middle Triassic to Late Jurassic, the depositional environment alternates between semi-restricted platform and evaporitic lagoon (van Bellen et al. 1959; Aqrabi et al. 2010).

In the Cretaceous, following an significant drowning event in the Latest Tithonian, the depositional environment is more open (van Bellen et al. 1959; Aqrabi et al. 2010) with the development of a thick sequence of dolomitic limestone rich in fossils (Qamchuqa Fm.; Fig 2).

In the Campanian tectonic related drowning of this quiet passive margin created a foredeep basin (van Bellen et al. 1959; Karim and Surdady 2005; Aqrabi et al. 2010). This episode mainly affects the SE KRI and the northern part of Central KRI. In the study area, the sediments record the drowning (transgressive sequence of the Bekhme and Aqra Formations) of the Arabian Platform but in shallow water, fossil-rich environment (van Bellen et al. 1959; Ameen and Karim 2008; Aqrabi et al. 2010). The effect of the tectonic load related to this compressive episode continued throughout the Paleocene and Eocene with the development of the syn-tectonic clastic shallow (deltaic) to deep water Kolosh formation (van Bellen et al. 1959) which is terminated by carbonate sequences (Pilaspi formation; Fig. 2).

In the study area, there is a major hiatus due to non-deposition during the whole Oligocene and the Lower Miocene. The sedimentation resumed with the onset of the second major tectonic phase, the Zagros collision (Allen et al. 2004; Agard et al. 2005, 2011; Vergés et al. 2011; Mouthereau et al. 2012). Currently still active, it is characterized by the deposition of thick shallow marine to continental clastic-rich formations typical of foreland basins (van Bellen et al. 1959; Aqrabi et al. 2010; Fig. 2).

The deformation in foothills is strongly controlled by the sensitivity of the deformed stratigraphic sequence to the compressive stress. Several types of deformation can be described within this section (ductile, plastic, brittle, etc.) and summarized in a mechanical stratigraphic chart (Fig. 2). This helps to propose deformation models to explain observed fold geometries.

In terms of mechanical stratigraphy (Fig. 2), well penetrations and outcrops analyses show that the whole stratigraphic sequence can be considered as one unit in the Foldbelt domain. The basal detachment is the Beduh/Mirga-Mir shale/evaporitic interval in the Lower

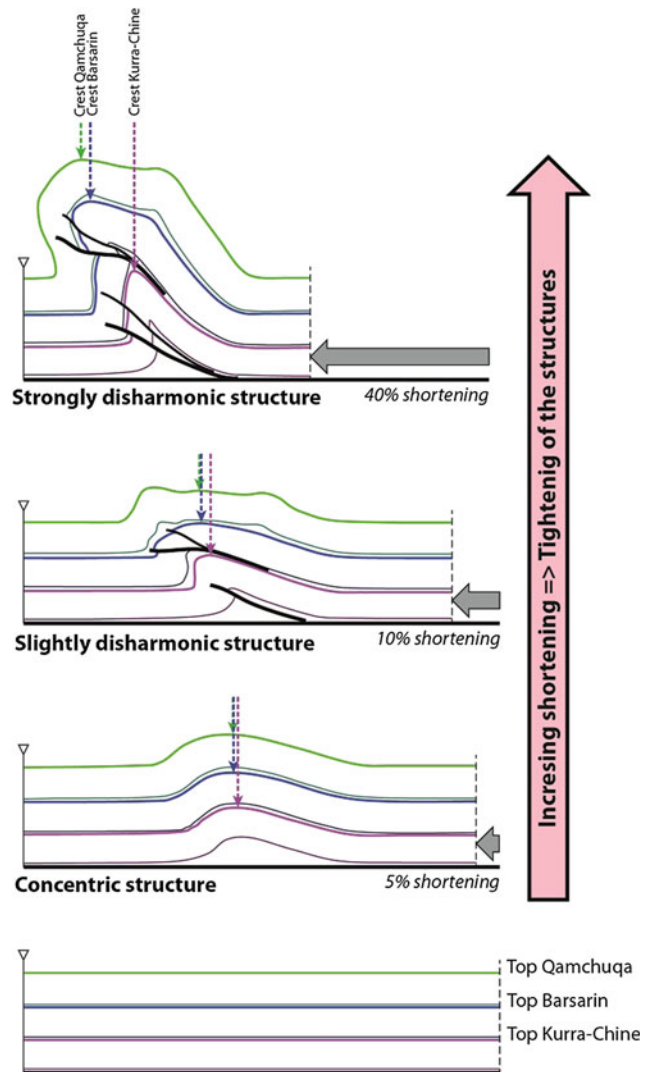


Fig. 3 Mechanical behavior of the Central Kurdistan folds. The Kurdistan Foldbelt exhibits mainly detachment folds over the Beduh/Mirga-Mir formations. With the growth of the fold, internal disharmonies may be expressed because of the presence of several minor detachments. In consequence, the more a structure accumulates shortening, the more important is the risk to have strong disharmonies between petroleum objectives

Triassic. However, based on the same data, three other minor detachments exist: the Baluti Shales, The Chia-Gara Hot Shales and the Kolosh Shales. The presence of these detachments may induce slight disharmonies that need to be considered in the building of the seismic interpretation to account for possible lateral shift of the structure shape in depth (Fig. 3).

Folds in the Central KRI Foldbelt are detachment folds which may evolve into faulted folds with increasing shortening as evident in other basins (Ameen 1991; Poblet and

McClay 1996; Mitra 2002). Activation of the internal detachments with increase of shortening is particularly well expressed in the Baluti Shales (Fig. 3). Several wells drilled in the area have shown major bedding dips change while drilling this interval. Moreover, it is frequent to find repeated sections in the Jurassic, evidencing thrusts, while it is rare in the Triassic. As a consequence, it can be difficult, with a vertical well, to drill through the main petroleum objectives (Fig. 3).

Building this geological model using field campaigns observations and previous drilling results is key for seismic interpretation and thus for location of a new well. This geological knowledge is also used to process the seismic data in the most accurate way.

Pre-Drill Seismic Processing and Interpretation

The original seismic dataset for our petroleum exploration in this area was acquired in 2011 by Global Geophysical Services. The parameters that were utilized are typical of modern land seismic acquisition and enable convenient sampling of the reflected wave field:

Receiver Group Interval:	20 m
Source Type:	Vibroseis/Dynamite
Source Interval:	40 m for Vibroseis/80 m for Dynamite
Min/Max Offsets:	30 m/6010 m Split Spread
Recording Length:	6 s
Vibro Sweep Length:	12 s
Sweep Frequency:	6–80 Hz Linear
Charge Mass:	2 kg
Hole Depth:	10 m

The processing was done with a standard workflow (Yan and Rines 2001; Yilmaz 2001; Dell'Aversana et al. 2003; Jaiswal et al. 2008) comprising noise reduction, statics correction using refraction tomography, velocity analysis and pre-stack time and depth migrations. A second infill set of lines was acquired in 2012 and processed with the same parameters. At that time, little structural information was available to the image processor, and the imaging parameters were not optimized to allow imaging of possible steep dips. In particular, dip limit parameter and aperture were limited to 45° and 4000 m respectively. The studied structure appeared then as a smooth fold with little internal complexity (Fig. 4).

The interpretation used 2D seismic time and depth data from both surveys acquired in 2011 and 2012. Initial mapping was done using the fast track Post-Stack Time Migration (PSTM). Subsequent interpretation used anisotropic

Pre-Stack Depth Migration (PSDM) data for detailed prospect mapping of key stratigraphic horizons and faults. Nearby well data, Zero-Offset Vertical Seismic Profile (VSP) (velocity data as well as check shot) and synthetic seismograms were integrated into the seismic interpretation to calibrate the acoustic response of the key seismic markers (Fig. 5).

The proposed interpretation of the structure, from Tertiary to Triassic levels, was a simple anticline (box fold) faulted toward the NE with a slight disharmony in the Baluti Shale at the base of the Jurassic sequence.

First Well Leg Drilling

The well was planned as a vertical exploration well to target the prognosed Cretaceous, Jurassic and Triassic structural apices within the NW-SE trending four-way dip closure. Based on the seismic image, the stratigraphic units appeared to be of relatively uniform thickness across the structure except in the detachment levels where some lateral thickening may occur as a result of folding or faulting. Due to the geometry of the fold, shortening and degree of complexity were thought to increase with depth accordingly to the mechanical model described above.

The well was drilled to a total depth (TD) of 4511mMD/RT in the main hole. Extensive open-hole logging was conducted through the Cretaceous, Jurassic and Triassic sections. The 26" and 17 1/2" sections penetrated the Tertiary and Cretaceous formations and encountered the tops in a range of ±15 m compared with the well prognosis. The 17 1/2" phase ended in first meters of the Barsarin Fm. anhydritic levels. No formation imager tools were ran in these sections.

The Jurassic Section—12 1/4" Phase

The 12 1/4" phase penetrated the entire Jurassic section with a measured depth thickness (MD) of 1500 m measured depth and terminated in the top few meters of the Kurra-Chine A Fm. anhydrite (Fig. 6).

The 12 1/4" phase may be divided into four main structural intervals (Fig. 6):

- The first 400 m encountered formations approximately in agreement with the well prognosis, with only a downward shift of just under 50 m. The Barsarin, Naokelekan, Sargelu and Alan formations all slightly dipped slightly toward the SW;
- In contrast the next 250 m dipped to the NE. The sharp change of dip direction from SW to NE was associated

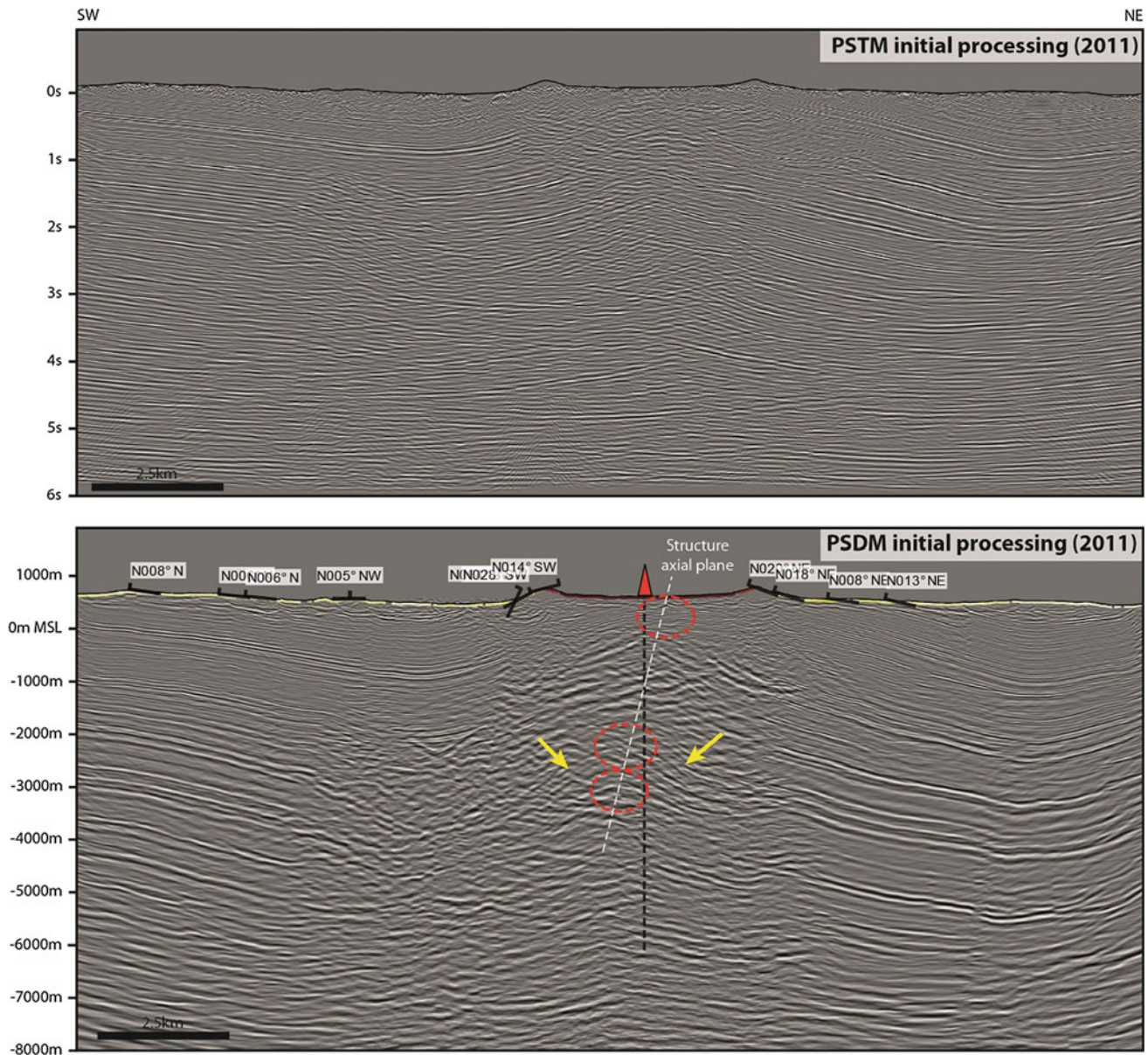


Fig. 4 Legacy image running through the prognosed position of our well in PSTM (*top*) and PSDM (*bottom*). The *yellow arrows* points at the areas where the dips reach the dip limit entered in the processing (45°). *Red circles* locate areas with clear structural apices. The PSDM

image interpretation led to consider this structure as a rather simple detachment fold slightly verging toward the NE with no evidence of clear internal disharmonies

with a fault in the middle part of the Alan Fm. Despite the change in dip the tops of Mus, Adaiyah and Butmah formations were encountered less than 50 m below the prognosed depth;

- In the next 100 m, the well drilled through a repetition of the lower part of the Adaiyah formation. This segment, comprised between two faults, was found to be dipping quite strongly toward the NE;
- The last 750 m to the 12 1/42 TD penetrated the Butmah and Baluti. It began with low bedding dips toward the north which increased to quite strong dips toward the NE.

Compared to the well prognosis, there was a significant difference in both fold domain and formation tops depth predictions.

The prognosed structure was a NE verging fold with some thrusting excepted in the lower part of the section (basal Butmah or Baluti Fms.; Fig. 6 left). The updated structural interpretation following the drilling and imagery logging of the 12 1/4" phase confirmed the structural hypothesis. However, structural data demonstrated that instead of drilling the structure on the upper part of the

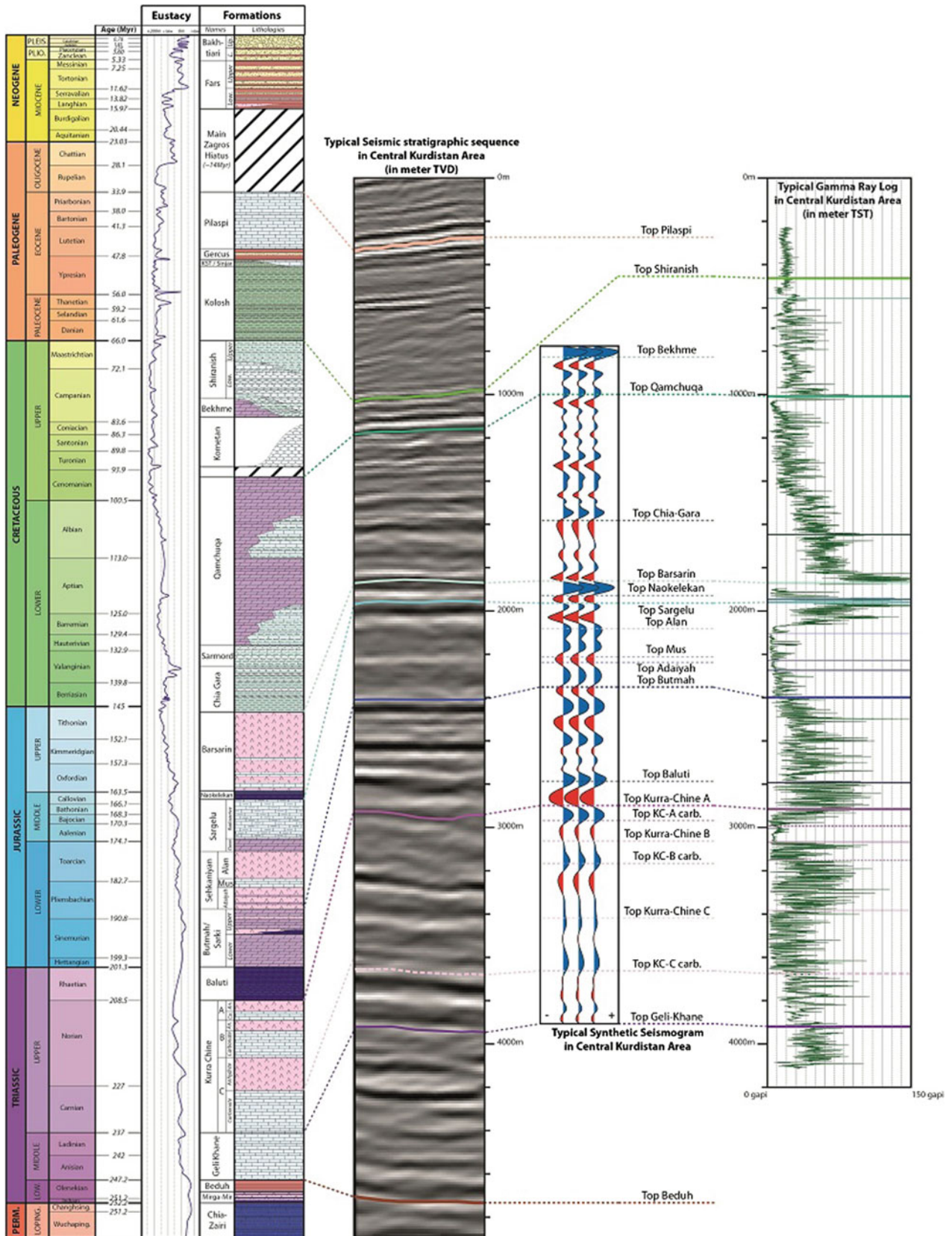


Fig. 5 Typical seismic facies (*left*), synthetic seismogram (*middle*) and Gamma-Ray log (*right*) of Central KRI stratigraphic sequence. Knowledge acquired during exploration of Central KRI allows a good calibration of the seismic facies where seismic imaging is of good quality. Typical seismic response can be used to identify key stratigraphic surfaces and helped seismic interpretation

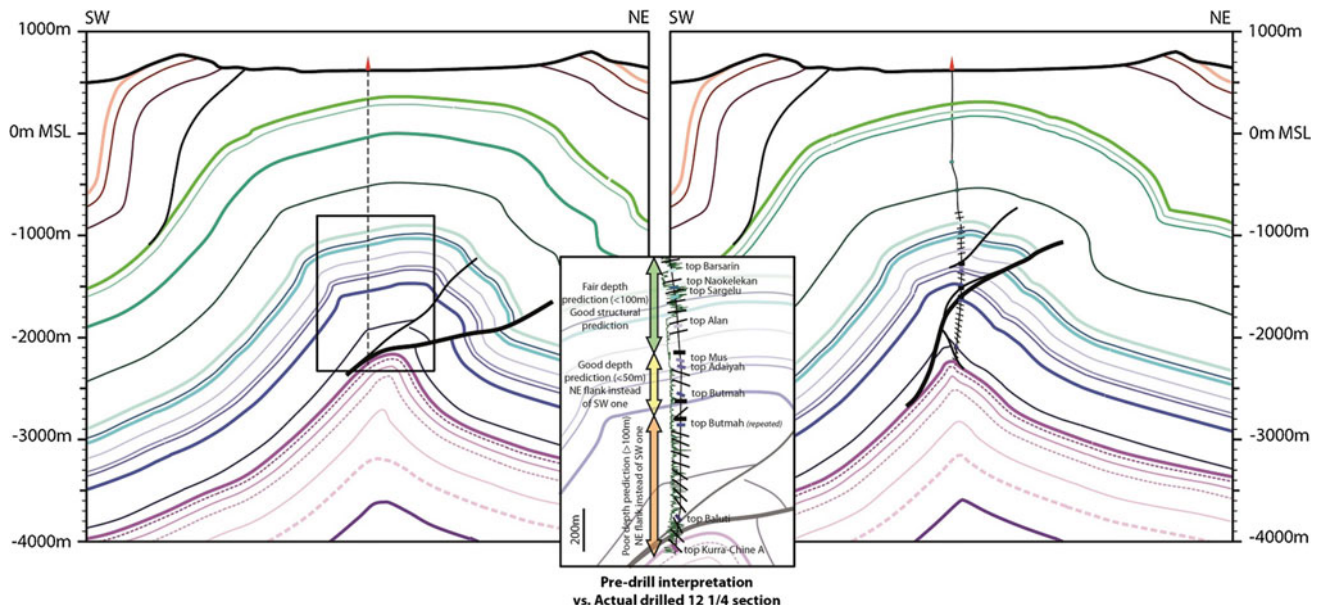


Fig. 6 Prognosed (left) versus actual (right) 12 ¼" phase geological sections. As expected the 12 ¼" section entered the fold in its southwestern flank. However, after passing through some faults, the well entered the northeastern flank of the structure with a sharp bedding

dip direction change around 750m after the beginning of the phase suggesting a major fault. This phase confirmed the northeastward direction of the thrusting

southwestern flank, the location was on the crest the structure passing downwards to mainly penetrate the north-eastern flank. In consequence, the new interpretation made with the new data preserved the global shape of the structure, it is only slightly tightened (Fig. 6 right).

The Triassic Section—8 ½" Phase

The 8 ½" phase penetrated 1600 m (MD) of the upper part of the Triassic section terminating in the first meters of the Kurra-Chine B Fm. carbonates (Fig. 7). The 8 ½" phase may be divided into two main structural intervals (Fig. 7):

- The first 400 first meters penetrated the Kurra-China A and B formations, with bedding of around 30° to the NE and in line with the prognosis;
- During the remaining 1200 m the well clearly entered into the southwestern flank of the structure which was associated with a sharp change from low dips toward the NE to high/vertical to nearly overturned dipping beds toward the SW. In the last 650 m, the bed dips decreased to 50° to the SW and the well re-entered the an inverted sequence of Kurra-Chine B carbonates and then anhydrites suggesting the well drilled through a highly dipping southwestward syncline.

The broad NE verging structure expected in the Triassic, as interpreted from the seismic image, appeared to be

incorrect. Structural information gathered during the 8 ½" phase and well logs interpretation suggested a tight south-westward fold in the Triassic formations (Fig. 7 right).

Considering these data and their interpretation, it was clear that the deeper Triassic targets were missed and a decision to side-track was made. Due to the tight geometry of the structure, the possibility of improving the seismic imaging was urgently evaluated in order to clarify different side-track trajectory scenarios and provide the basis for reacting quickly if needed during the drilling.

Seismic Re-Processing and Re-Interpretation

Following the acquisition of FMI data at the end of first leg, an in-house reprocessing (in collaboration with GEOTOMO) of the 2011 legacy data was launched on the nearest 2D line. As this line was located 3 km away from the well, the seismic processing improvements were qualitative by nature. The main objective was to improve the image of the core and the flanks of the anticline at the Triassic level. Efforts were therefore put forth onto two key steps: the first one was data preprocessing to enhance the signal to noise ratio (solving noise and near surface perturbation issues; Mardsen 1993) and imaging, that could be now driven by a robust geological a priori based on well data and surface geology.

The reprocessing sequence was launched with a constant interaction between the processing group, the interpreters

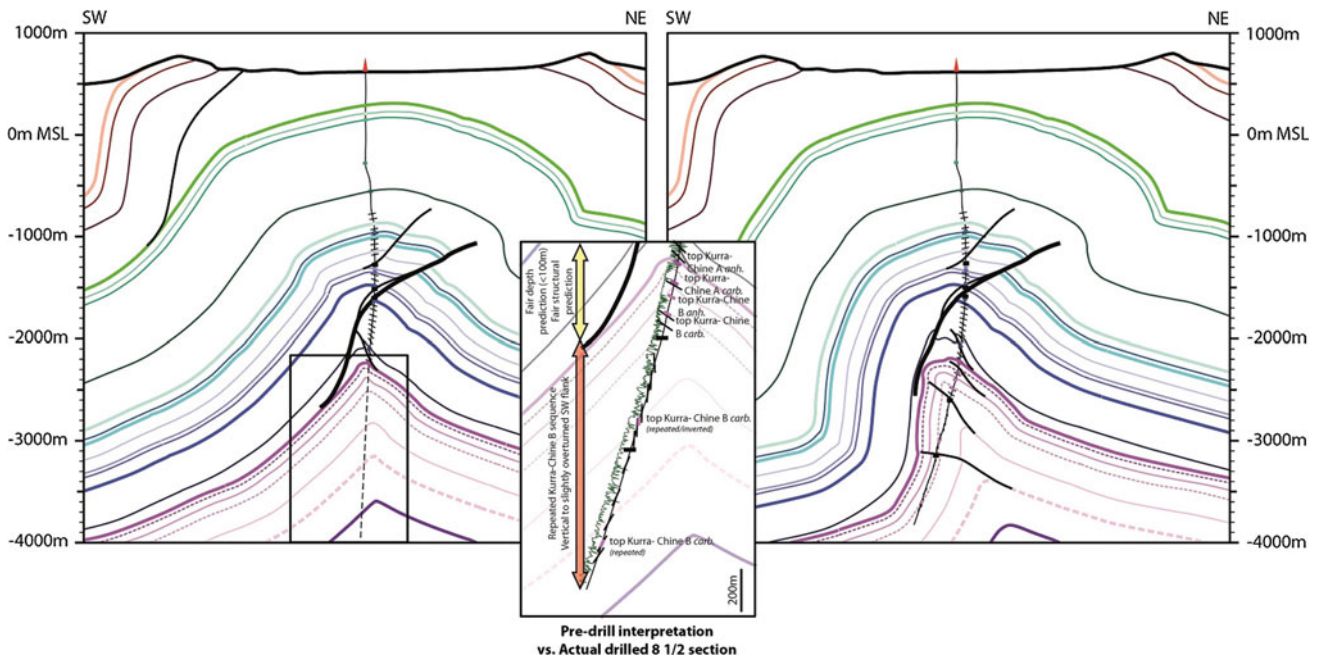


Fig. 7 Prognosed (*left*) versus actual (*right*) 8 1/2" phase geological sections. Globally, the well drilled through a highly dipping SW flank suggesting a difference of fold vergency between the Jurassic (NE vergency) and the Triassic (SW vergency) objectives. The updated interpretation considered a tighter fold than expected

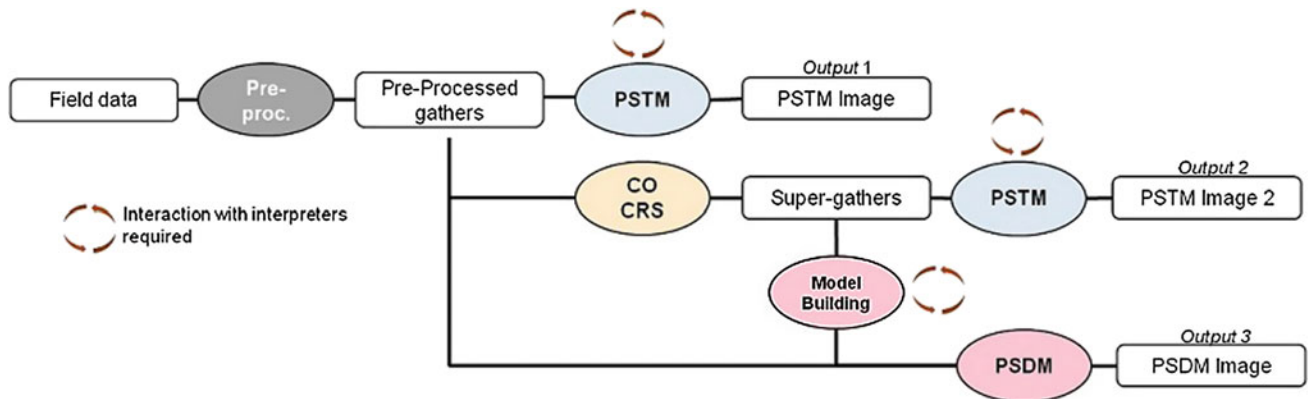


Fig. 8 2D seismic data processing workflow used internally (Allouche et al. 2015). From the field data to the final images (both PSTM and PSDM) four steps of processing were applied with a constant implication of the interpreters/geologists to help the processing team to get the best image with the current knowledge

and the geologists to end up with the best imaging of the structure. This sequence can be summarized in the following four main steps (Fig. 8):

- First, by performing a non linear tomography of first arrival times, and building a near surface model to correct for near surface perturbations. The quality of first-break picking is of utmost importance. Manual picking, though time-consuming, is a must;
- Second, image based RMS velocity estimation was performed to obtain an image from Pre-Stack Time

Migration (PSTM) of shot/receiver gathers, from a floating datum. Having in mind the poor data quality at target level, the classical “gather flatness” criterion alone failed to provide a robust model. Velocities were mostly picked using constant velocity scans, allowing velocity values to be chosen based of the migrated image itself, ensuring a geologically sound velocity model;

- Third, a velocity field is built layer-by-layer to obtain a Pre-Stack Depth Migration (PSDM) image from floating datum. The near surface model derived from step 1 is the starting point; below the depth of investigation of

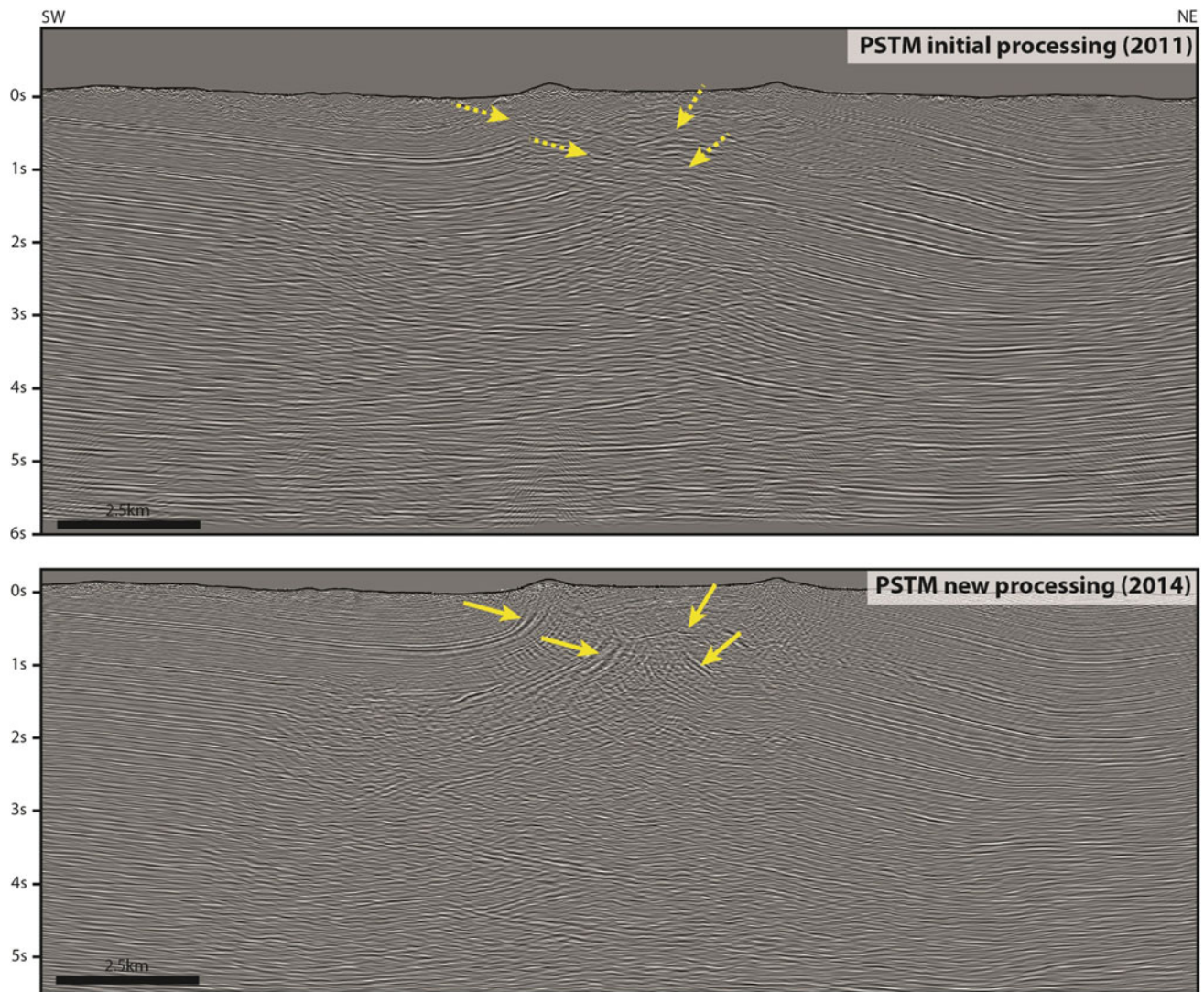


Fig. 9 Legacy PSTM image (*top*) comparison with the reprocessed PSTM image (*bottom*). The *yellow arrows* points at the areas of major

improvement in the structural imaging. The presence of steep dip flanks in the Triassic became clearer

the latter (typically of the range of 500–1000 m), the model is updated iteratively layer by layer (layer-stripping) down to the depth of interest. Each layer is bounded by seismic horizons that are meaningful in terms of velocity contrast (e.g. Cretaceous—Jurassic interface), consistency from line to line also has to be assured.

- Lastly, as shown on the diagram below, the CRS (Common Reflection Surface Stack; Civello et al. 2015) tool was used as a signal enhancement technique; it provides cleaner gathers to feed the velocity building process. The CRS gathers are also migrated to provide alternative images.

The quality of the final image is equally sensitive to every step (Allouche et al. 2015); therefore each one should be

carried out very carefully. In all three final steps, interaction between interpreters and the processing team is essential.

The resulting image showed clear improvements in the deep as well as in the shallow parts, and showed more consistency with the geological model. In PSTM image (Fig. 9), steep dips became to appear both in shallow and deep levels.

In addition to these less restrictive migration parameters, a fine-tuning of the velocity model was performed (Fig. 10; Wu et al. 1998; Le Begat et al. 2004; Jaiswal and Zelt 2008). As a result nearly vertical beds begin to appear in the PSDM image (Fig. 11). The quality of imaging shows that the structural apexes are probably off-set with depth indicating internal disharmony in the fold in which the shallower levels (Cretaceous and Jurassic) are folded toward the NE and the deeper ones (Triassic) toward the SE.

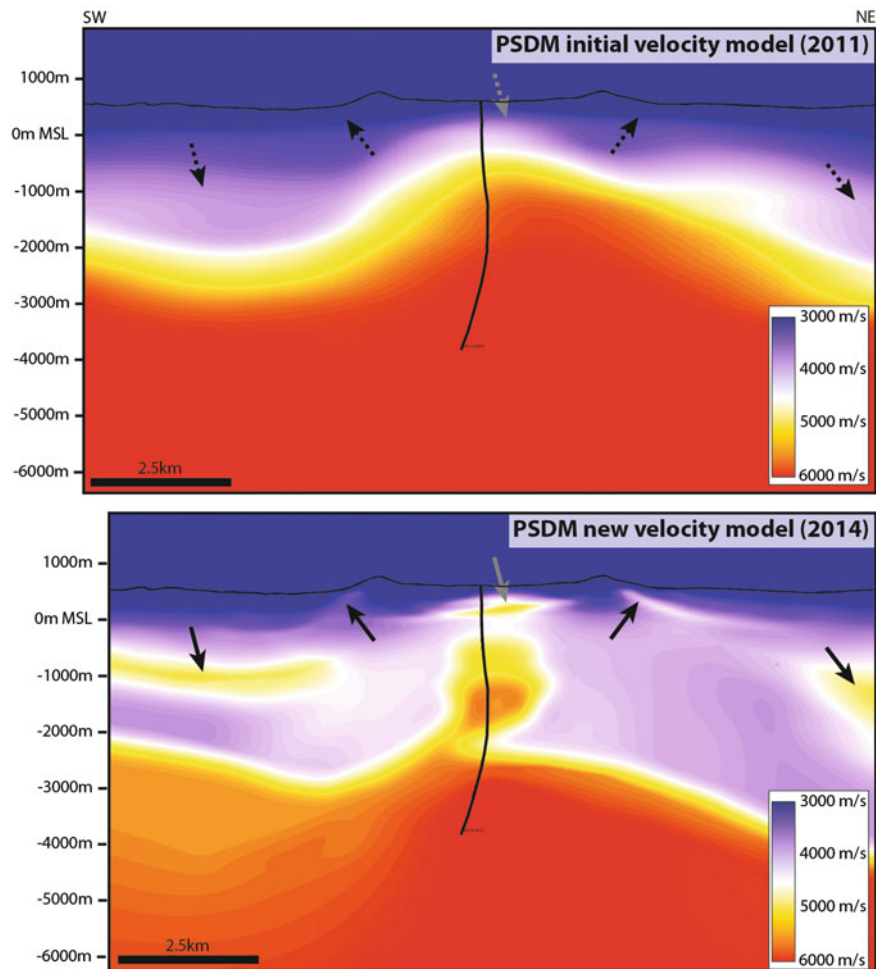


Fig. 10 Legacy PSDM Velocity model image (*top*) comparison with the reprocessed PSDM model (*bottom*) and the well trajectory (first leg). The reprocessed model exhibits a richer content. The shallow high velocity anomalies are retrieved from Refraction Tomography.

These anomalies correspond to real geological features such as the Pilaspi Fm. carbonates black (*black arrows*) or the Cretaceous carbonates (*grey arrow*), and are crucial to the image quality in the deeper section

In the re-processed image the steep dips, and the tightness of structure is can be clearly seen (Fig. 11). The revised interpretation made for the Triassic, using these new data comprised a very pinched fold, verging toward the SW, with a relatively important disharmony in the Baluti shale, sufficient to allow a change of vergency. The remaining uncertainty was on the NE flank of the Triassic fold to know whether it is quite smooth (30–50° to the NE) or more pinched (70° to the NE).

Second Well Leg Drilling

Unfortunately, no VSP was acquired after the first leg. This could have helped to improve the image in the vicinity of the borehole and provide a valuable guide in defining the side-track trajectory. Nevertheless the recognition from the new processing of the possible strongly tightened structure in the

Triassic, led to the proposal of two options for the side-track trajectory (Fig. 12):

- A tight structure interpretation (option 1, Fig. 12 top left). This option suggests that to drill the Kurra-Chine C carbonates, a S-shape side track trajectory would be required;
- A wider structure interpretation (option 2, Fig. 12 top right). This option suggests that a J-shape trajectory would be sufficient to drill down to the Kurra-Chine C carbonates.

Based on these two end-member options, an intermediate point for structural logging was chosen in order to discriminate between the two options before a possible drop-off point in the side-track trajectory. The actual section and associated trajectory was finally in between the two options (Fig. 12 bottom).

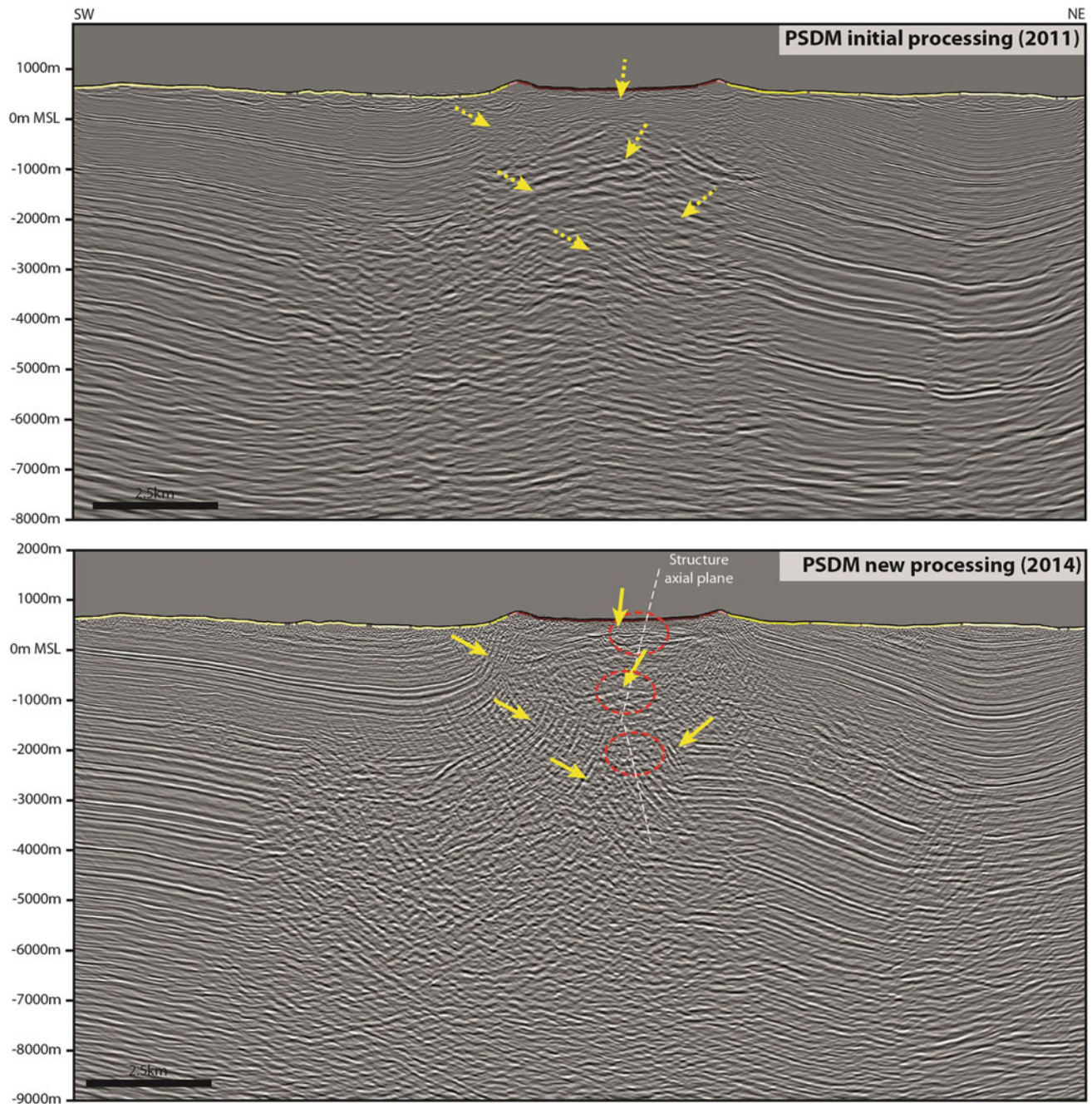


Fig. 11 Legacy PSDM image (*top*) comparison with the reprocessed PSDM image (*bottom*). The *yellow arrows* points at the areas of major improvement in the structural imaging. *Red circles* locate areas with

clear structural apices. The PSDM image shows clear nearly vertical SW flank. The image evidence the possibility of having internal disharmonies in the deep levels of the structure

The 8 ½" phase of the well side-track drilled through 1050 m (MD) of the Upper Triassic formations terminating in the middle of the Kurra-Chine C Fm. anhydrites (Figs. 12 and 13). Consistent with the revised prognosis, the side-tracked well leg drilled the Kurra-Chine A, B and C-Anhydrite with increasing bed dips from 30–50° to the NE (Fig. 13). Significant thickening was found in the Kurra-Chine C anhydrites suggesting ductile flow of these

plastic rocks into the core of the anticline. The drilling stopped here for technical reasons.

The good prediction of the formation tops depth and structural domain in this side-track (Fig. 12) shows the importance of the integration of the geological data acquired while drilling within the seismic processing. This leads to better seismic imaging that helped considering different options for the side-track and better react while drilling.

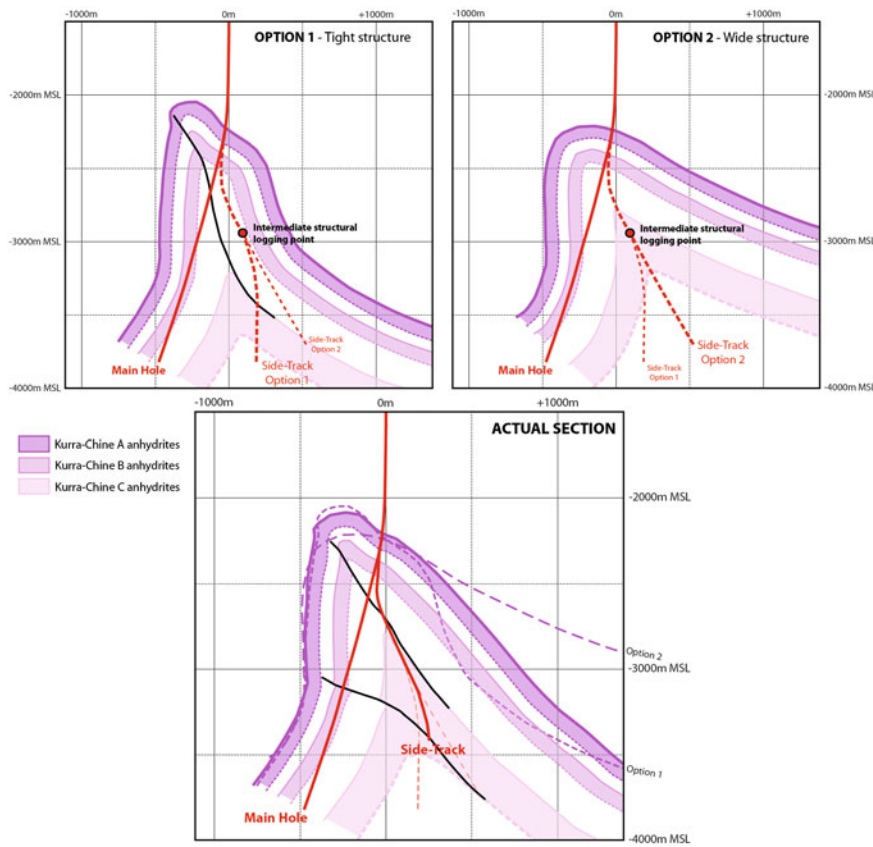


Fig. 12 Side-track trajectory options (*top left and right*) depending on the structural interpretations suggested by the first well leg results and new seismic processing and actual realized side-track trajectory (*bottom*). The new seismic processing suggested clearly the possibility

to have a tight structure in the Triassic. Considering this possibility, two end-member structural scenarios were envisaged, a tight structure (*top left*) and a wide structure (*top right*). These scenarios were used to design the side-track trajectory

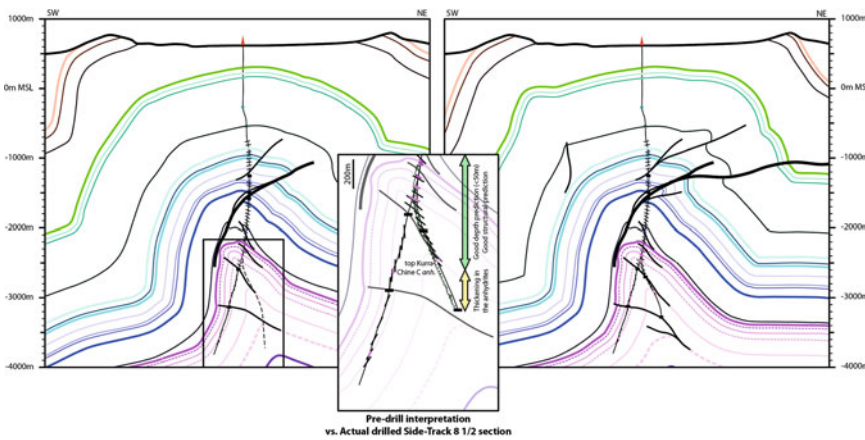


Fig. 13 Prognosed (*left*) versus actual (*right*) 8 1/2" phase of the side-track geological sections. The drilled section was in line with the prognosis in both depth and structural position predictions. A thickening of the Kurra-Chine C anhydritic sequence was found at the *bottom*

of the phase suggesting possible bourrage (ductile flow) of these plastic levels into the core of the anticline which may lead to more structural disharmony between the *upper part* of the Kurra-Chine formation and its *Lower part* and Geli-Khane formation

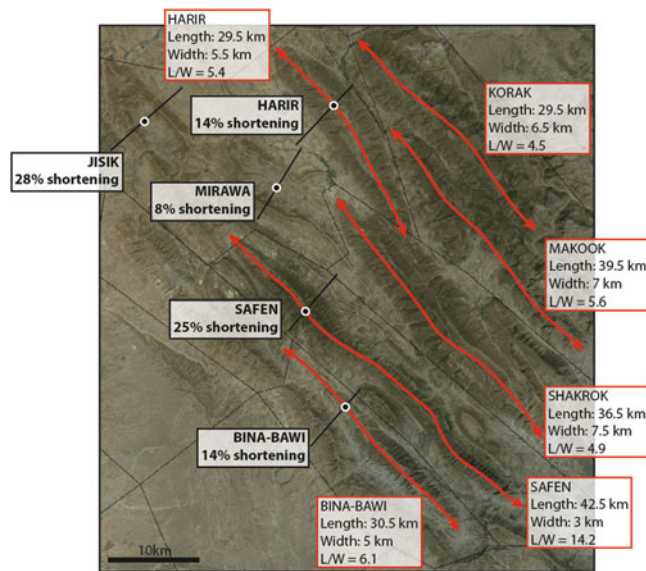


Fig. 14 Central KRI major folds Length/Width ratios and associated shortening calculated along well-calibrated sections. The Safen Anticline presents an anomalously high L/W ratio compared to other structures in Central KRI. In trend of Safen Structure, the Jisik Structure presents, together with Safen Anticline, high shortening rates

Discussion

This paper stresses the impact of the geological knowledge on the processing of seismic data in foothills domain and the possibilities it offers to enhance the design of a well trajectory. In this case study, the question of the place of the seismic re-processing workflow in the exploration sequence was raised.

Seismic processing workflow and its place in foothills exploration sequence

This experience shows that the seismic re-processing in foothills represents a valuable, cost-effective exploration tool that can be used at any moment of the prospect history (initial well planning but also, while drilling). We also showed with this example that reprocessing of such complex data should not be done by strongly constraining the processing parameters from start (in particular dip and aperture). Limiting these two parameters in foothills exploration in order to filter the noise and trying to enhance the signal/noise ratio could result in filtering more signal than noise. Interpreters, from their experience (field campaigns, drillings) are the most appropriate persons to choose which seismic event should be enhanced.

Close co-operation between the processing team and the interpreters/geologists is essential. In the event of a major breakthrough in the geological understanding of the area, a

re-processing of one or several 2D lines should be done to calibrate the impact on seismic imaging. In this case example, the re-processing was done too late and a side-track was needed to drill through deep objectives.

Despite apparently good geological knowledge of an area, surprises often happen in foothills exploration. It is therefore important to plan side-track options in advance and keep an open mind on different interpretation scenarios. During the preparation and drilling of the well, the very high dips to vertical beds were not anticipated despite the good geological a priori understanding.

Intense and Localized Shortening

The type of fold found in the well in this case example is usually associated with significant shortening. Calculated on the top of Cretaceous surface, the degree shortening (initial length—final length)/initial length on this structure is above 20 %. This value is quite high compared to on-trend structures for which shortenings of 8–14 % were calculated (Fig. 14).

Furthermore, the length/width ratio calculated for all structures cored by at least Cretaceous formation (Fig. 13) shows that the Safen Anticline ($L/W = 14.2$) is anomalous compared to what is usually found in Central KRI (L/W comprised between 4.5 and 6.1). Both of these observations show an important shortening, localized onto the Jisik-Safen trend, leading to strongly dipping SW flanks.

Accumulation of shortening along a single structure is often related to a change in the behavior of the detachment level (Schott and Koyi 2001; Lujan et al. 2003). In this area, the changes of thickness or global rheological properties (lithological variations) of the Beduh/Mirga-Mir basal detachment are poorly known. Only one well in the area succeeded to drill down to this level. However, several basement trends have been described in the literature (Ameen 1992; Bahroudi and Talbot 2003) and may play a role in the detachment level behavior:

- The Nabitah (Idsas) Fault System is a N–S trending system prominent mainly in south and west Iraq. It has also been described in Lurestan (Bahroudi and Talbot 2003). One of its major expression is the Khanaqin Zone at the border between KRI and Iran;
- The Najd Fault System is a major basement trend often delimiting tectonic zones in east and northeast Iraq (Jassim and Buday 2006a). This fault system is trending NW–SE.
- Some minor Transversal Fault Systems are also described (Ameen 1992; Jassim and Buday 2006a). They are E–W to NE–SW trending.

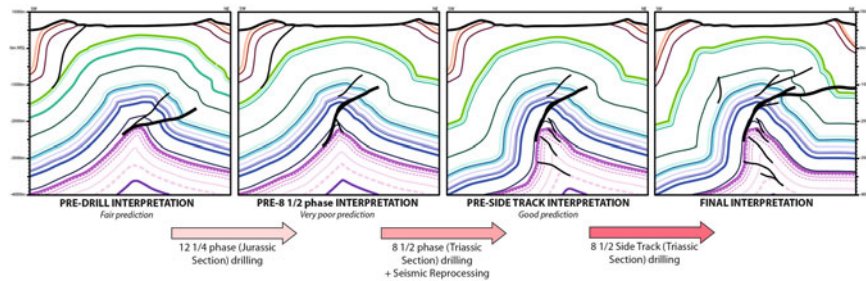


Fig. 15 Steps of the structural interpretation while drilling the studied well. The structural interpretation evolves from a rather simple NE verging fold to a tight disharmonic fold with *upper* level verging to the NE and *lower* ones to the SW. The major breakthrough in the structural

interpretation was the integration of the newly acquired geological knowledge into a re-processing of the seismic data which allows us to be more predictive

In the Central KRI area, the influence of the Nabitah Fault System is evidenced by alignment of folds breaks (Fig. 1). They can be a major controlling factor on the Beduh/Mirga-Mir detachment thickness as they were reactivated during the Tethys rifting (Bahroudi and Talbot 2003) during which these two formations were deposited. However, considering the orientation of the Jisik-Safen trend, the Najd Fault System could be a good candidate if it is proved that it influenced the deposition of the Beduh and Mirga-Mir Fms.

The control of the basement structures within a fold-and-thrust belt is quite common in areas where there are structural anomalies such as changes of fold trend orientations or fold over growth (Wiltschko and Eastman 1983; Woodward 1988; Hinsh et al. 2002).

Conclusion

Following the first series of borehole image logs in the main hole (12 1/4" phase) from the Jurassic to the top of the Triassic (Kurra-Chine Fm.), the interpretation was slightly revised to integrate a slight disharmony observed in the Baluti (rapid change from 50° NE dips in the Butmah/Baluti to 30° NE dips in the uppermost Kurra-Chine A) and a thrust repeating the lower part of the Adaiyah Fm (Fig. 15). Several faults were interpreted, all verging towards the NE, giving more weight to an interpretation of a slightly NE verging box fold.

After drilling of the 8 1/2" phase, it appeared that the well, which was slightly deviated toward the SW, drilled through a pinched anticline penetrating vertical beds in the Kurra-Chine B formation before re-entering the lower part of the section after crossing a reverse section, within the near vertical limb (Fig. 15).

The realization of a fast-track processing following this first well leg, constrained by borehole structural data, helped

us to provide different structural scenarios to design the well side-track trajectory and to choose an intermediate logging point to decide which from a drop-off (S-shape) or a constant angle (J-shape) trajectory will be preferable.

After the side-track was drilled and structural data acquired, the final interpretation did not change drastically from the pre-sidetrack one, giving more constrains on the north-eastern flank (Fig. 15).

As a matter of fact, seismic re-processing in foothills exploration can provide valuable information if the process is fed with relevant structural information. But this requires a closer-than-ever interaction between image processors, interpreters and geologists.

Acknowledgments The authors would like to thanks Marathon Oil Company for agreeing to the publication of this paper. We also are grateful to the Kurdistan Region of Iraq Ministry of Resources for their authorization to publish this paper. We would like to express our deepest thanks to the research team of Sulaimaniya University (Dr. S.H. Ahmed, Dr. S.H.S. Hassan, Dr. I.M.J. Mohialdeen, Dr. F.A. Ameen, Dr. D.H.M. Ameen, Dr. I.M. Ghafor, Dr. F.M. Qader, Dr. A.K.S. Bety, Dr. D.F. Hamamin, Dr. Amanj and Dr. G.A. Hamasur), Dohuk University (Mr. H.S. Shaban and Dr. N.T. Shamoun) and Geological Survey of Sulaimaniya (Dr. N.M. Kadir and Dr. S.F. Ahmad) who helped us greatly in our field campaigns with their knowledgeable advices and enthusiasm. We are also thankful to our reviewers and editor whose constructive remarks and comments helped a lot to improve this paper.

References

- Agard P, Omrani J, Jolivet L, Mouthereau F (2005) Convergence history across Zagros (Iran): constraints from collisional and earlier deformation. *Int J Earth Sci* 94(3):401–419
- Agard P, Omrani J, Jolivet L, Whitechurch H, Vrielynck B, Spakman W, Monié P, Meyer B, Wortel R (2011) Zagros orogeny: a subduction-dominated process. *Geol Mag* 148(5–6):692–725
- Allen M, Jackson JA, Walker R (2004) Late Cenozoic reorganization of the Arabia-Eurasia collision and the comparison of short-term and long-term deformation rates. *Tectonics* 23:16p
- Allouche H, Sapin F, Chevallier B, Brosille E (2015) Seismic imaging in western Zagros and impact on hydrocarbon exploration: a case

- study from Kurdistan Region of Iraq. In: Proceedings of Abu Dhabi international petroleum exhibition and conference. Society of Petroleum Engineers
- Ameen BM, Karim KH (2008) New sedimentologic and stratigraphic characteristics of the upper boundary of the Qamchuqa Formation (Early Cretaceous) at Northwest of Erbil, Kurdistan Region. NE Iraq *Iraqi Bull Geol Mining* 4:1–13
- Ameen MS (1991) Possible forced folding in the Taurus Zagros belt of northern Iraq. *Geol Mag* 128:561–584
- Ameen MS (1992) Effect of basement tectonics on hydrocarbon generation, migration and accumulation in Northern Iraq. *AAPG Bull* 76:356–370
- Agrawi AA, Goff JC, Horbury AD, Sadooni FN (2010) The petroleum geology of Iraq
- Bahroudi A, Talbot CJ (2003) The configuration of the basement beneath the Zagros basin. *J Pet Geol* 26:257–282
- Buday T, Jassim SZ (1987) The regional geology of Iraq, vol 2, tectonism, magmatism and metamorphism
- Civello S, Janiseck JM, Strobbia C (2015) 2D seismic lines reprocessing test using common reflection surface technique. In: Proceedings of offshore mediterranean conference and exhibition, March 25–27th, Ravenna, Italy
- Dell'Aversana P, Colombo D, Buia M, Morandi S (2003) Velocity/interface model building in a thrust belt by tomographic inversion of global offset seismic data. *Geophys Prospect* 51:23–25
- Fontaine J-M, Monod O, Braud J, Perincek D (1989) The Hezan units: a fragment of the south Neo-Tethyan passive continental margin in SE Turkey. *J Petrol Geol* 12:29–50
- Hinsch R, Krawczyk CM, Gaedicke C, Giraudo R, Demuro D (2002) Basement control on oblique thrust sheet evolution: seismic imaging of the active deformation front of the Central Andes in Bolivia. *Tectonophysics* 255:23–39
- Hudson JA (1967) Scattering surface waves from a surface obstacle. *Geophys J* 13:441–458
- Jaiswal P, Zelt CA (2008) Unified imaging of multichannel seismic data: combining travel time inversion and pre-stack depth migration. *Geophysics* 73:269–280
- Jaiswal P, Zelt CA, Bally AW, Dasgupta R (2008) 2-D traveltimes and waveform inversion for improved seismic imaging: Naga Thrust and Fold Belt, India. *Geophys J Int* 173:642–658
- Jassim SZ, Buday T (2006a) Tectonic framework. In: Jassim S, Goff JC (eds) *Geology of Iraq*. pp 45–55
- Jassim SZ, Buday T (2006b) Units of the unstable shelf and the zagros suture. In: Jassim SZ, Goff JC (eds) *Geology of Iraq*. pp 45–55
- Karim KH, Surdasy AM (2005) Tectonic and depositional history of upper Cretaceous Tanjero formation in Sulaimaniya area, NE-Iraq. *J Zankoy Sulaimaniya Univ* 8:47–61
- Le Begat S, Chauris H, Devaux V, Nguyen S, Noble M (2004) Velocity model estimation for depth imaging: comparison of three tomography methods on a 2D real data set. *Geophys Prospect* 52:427–438
- Luján M, Storti F, Balanyá JC, Crespo-Blanc A, Rossetti F (2003) Role of décollement material with different rheological properties in the structure of the Aljibe thrust imbricate (Flysch Trough, Gibraltar Arc): an analogue modelling approach. *J Struct Geol* 25(6):867–882
- Marsden D (1993) Static corrections—a review, part 2. *Leading Edge* 12 (1):43–49
- Mitra S (2002) Fold-accommodation faults. *AAPG Bull* 86:671–693
- Mouthereau F, Lacombe O, Verges J (2012) Building the Zagros collisional orogen: timing, strain distribution and the dynamics of Arabia/Eurasia plate convergence. *Tectonophysics* 532–535:27–60
- Palaz I, Marfurt KJ (1997) Carbonate seismology: an overview. In: Palaz I, Marfurt KJ (eds) *Carbonate seismology*. Geophysical development Series 6, pp 1–8
- Poblet J, McClay K (1996) Geometry and Kinematics of single-layer detachment folds. *AAPG Bull* 80:1085–1109
- Schott B, Koyi HA (2001) Estimating basal friction in accretionary wedges from the geometry and spacing of frontal faults. *EPSL* 194:221–227
- Tarras I, Giraud L, Thore P, Aye F (2010) Modeling of seismic waves propagation in presence of topography. In: Proceedings of SEG annual meeting, October 17–22, Denver, United States of America
- van Bellen RC, Dunnington HV, Wetzel R, Morton DM (1959) *Lexique stratigraphique international, III, Asie, fasc. 10a*, Iraq. Centre National de la Recherche Scientifique, Paris, pp 333
- Vergés J, Saura E, Casciello E, Fernández M, Villaseñor A, Jiménez-Munt I, García-Castellanos D (2011) Crustal-scale cross-sections across the NW Zagros belt: implications for the Arabian margin reconstruction. In: Lacombe O, Grasemann B, Simpson G (eds) *Geodynamic evolution of the Zagros*. *Geol Mag* 148:739–761
- Wiltschko D, Eastman D (1983) Role of basement warps and faults in localizing thrust fault ramps. In: Hatcher JRD, Williams H, Zietz I (eds) *Contribution to the tectonics and geophysics of mountain chains*. Memoir 158. Geological Society of America, Boulder, CO, pp 117–190
- Woodward NB, (1988) Primary and secondary basement controls on thrust sheet geometries. In: Schmidt CJ, Perry Jr W. (eds) *Interaction of the rocky mountain foreland and the cordilleran thrust belt*. Memoir 171. Geological Society of America, Boulder, CO, pp 353–366
- Wu WJ, Lines L, Burton A, Lu HX, Zhu J, Jamison W, Bording RP (1998) Prestack depth migration of an Alberta Foothills data set—the Husky experience. *Geophysics* 63:392–398
- Yan LL, Lines LR (2001) Seismic imaging and velocity analysis for an Alberta Foothills seismic survey. *Geophysics* 66:721–732
- Yilmaz Ö, (2001) *Seismic data Analysis*, vol 2 In: Doherty SM. (ed) SEG